GEOMAR REPORT

KOMEX

KURILE OKHOTSK SEA MARINE EXPERIMENT

CRUISE REPORTS: KOMEX V and VI

RV PROFESSOR GAGARINSKY CRUISE 26
MV MARSHAL GELOVANY CRUISE 1

VLADIVOSTOK - PUSAN - OKHOTSK SEA - PUSAN - VLADIVOSTOK
30 JULY - 5 SEPTEMBER, 1999

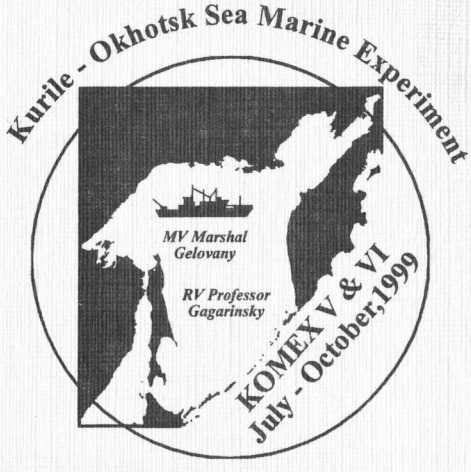

88

GEOMAR REPORT

KOMEX

KURILE OKHOTSK SEA MARINE EXPERIMENT

CRUISE REPORTS: KOMEX V and VI

RV PROFESSOR GAGARINSKY CRUISE 26
MV MARSHAL GELOVANY CRUISE 1

VLADIVOSTOK - PUSAN - OKHOTSK SEA - PUSAN - VLADIVOSTOK
30 JULY - 5 SEPTEMBER, 1999

Edited by
Nicole Biebow, Thomas Lüdmann, Boris Karp and Ruslan Kulinich

The KOMEX V and VI marine expeditions were initialized on responsibility of
the P. P. Shirshov Institute of Oceanology, Moscow,
the Pacific Oceanological Institute (POI), Vladivostok,
and the GEOMAR Research Center for Marine Geosciences, Kiel

GEOMAR
Forschungszentrum
für marine Geowissenschaften
der Christian-Albrechts-Universität
zu Kiel

KIEL 2000

GEOMAR REPORT 88

GEOMAR
Research Center
for Marine Geosciences
Christian Albrechts University
in Kiel

Redaktion dieses Reports:
Nicole Biebow, Thomas Lüdmann, Boris Karp
und Ruslan Kulinich

GEOMAR REPORT
ISSN 0936 - 5788

GEOMAR
Forschungszentrum
für marine Geowissenschaften
Wischhofstr. 1-3
D - 24148 Kiel
Tel. (0431) 600-2555, 600-2505

Editors of this issue:
Nicole Biebow, Thomas Lüdmann, Boris Karp,
and Ruslan Kulinich

GEOMAR REPORT
ISSN 0936 - 5788

GEOMAR
Research Center
for Marine Geosciences
Wischhofstr. 1-3
D - 24148 Kiel
Tel. (49) 431 / 600-2555, 600-2505

PART I: CRUISE REPORT KOMEX VI: SAKURA, 26TH CRUISE OF RV *PROFESSOR GAGARINSKY*, AUGUST-SEPTEMBER 1999

PART II: CRUISE REPORT KOMEX VII: FIRST CRUISE OF MV *MARSHAL GELOVANY*, AUGUST-OCTOBER 1999

PART I:

RV PROFESSOR GAGARINSKY CRUISE 26

CRUISE REPORT KOMEX V:

KOMEX-SAKURA

KURILE-OKHOTSK MARINE EXPERIMENT IN THE SAKHALIN AND KURILE AREAS

VLADIVOSTOK - PUSAN - SEA OF OKHOTSK - PUSAN - VLADIVOSTOK

JULY 30 - SEPTEMBER 9, 1999

1. INTRODUCTION AND BACKGROUND

B. Baranov, T. Lüdmann, B. Karp, and S. Lammers

The 26th Cruise of RV *"Professor Gagarinsky"* (KOMEX 99, SAKURA, Kurile-Okhotsk Marine Experiment in the Sakhalin and Kurile Areas) in the Okhotsk Sea was the final geophysical expedition in the framework of the preliminary and the first stage of KOMEX project. The investigations carried out on this cruise corresponded to the topics of three KOMEX subprojects:

- Tectonic structure and evolution of the Okhotsk Sea
- Recent sedimentation processes and paleo-depo-environment
- Methane monitoring

1.1 Tectonics

During the previous KOMEX cruises (GERDA, GREGORY and INESSA) the investigations were focused on regions of the Okhotsk Sea most important for understanding its tectonic structure and evolution - the Derugin and Kurile Basins. Many authors assume that these two basins were formed as a result of rifting processes. In the Kurile Basin these processes have led to seafloor spreading. Heat flow and seismo-stratigraphic data (Kharakhinov, 1998) suggest that the extensional processes in both basins occur nearly simultaneously in the Oligo-Miocene. But the mode of extension remained unclear before 1995 when the KOMEX project began.

At the stage of preparation of the KOMEX project the tectonic background and during the preliminary stage of the project all available publications on the structure of the Okhotsk Sea were analyzed and a new model of its plate tectonic evolution was proposed (Baranov et al., 1995). Later on, this model served as the theoretical basis of the investigations in the subproject «Tectonic evolution of the Okhotsk Sea» (GERDA, 1995; Nürnberg et al., 1997; Biebow & Hütten, 1999). According to this model, all the extensional structures of the Okhotsk Sea, including the Kurile and Derugin Basins, were formed as the result of a single kinematic process. To a first approximation, it is governed by rotation of the Okhotsk plate. This rotation is related to the relative motions of the surrounding major plates (Amurian, Eurasian, North American and Pacific plates) which are in turn driven by mantle flow.

The mode of Okhotsk plate movement must be recorded in its general tectonic pattern. The orientation of extensional structures must correspond to the vectors of opening and changes from north to south. Thus, the spreading axis in the Kurile Basin must be orthogonal to the general strike of the basin. To verify this statement, the structural patterns in different regions of the sea have to be examined. Corresponding investigations were carried out in the northeastern part of the Derugin Basin (GERDA, 1995) and on the northeastern slope of the Kurile Basin (Nürnberg et al., 1997). They showed that the structural pattern of the northeastern Derugin Basin is represented by a system of grabens and semi-grabens limited by normal faults striking

NE and ENE (Dozorova et al., 1998). In contrast, on the slope of the Kurile Basin, normal faults are oriented in NW and WNW directions. This demonstrates that the structural pattern of the Okhotsk Sea changes from north to south as the proposed model suggests.

The system of normal faults on the slope of the Kurile Basin corresponds to the initial stage of the opening process (Baranov et al., 1999). The character and direction of the later stages of opening may be clarified only by investigating the central part of this backarc basin. So one of the main goals of the present cruise was the study of the morphology of the acoustic basement in the abyssal part of the basin to find structures hitherto unknown which may correspond to spreading centers.

The next important target of the expedition was to investigate the region located north of INESSA and GERDA areas. As mentioned above, the GERDA area is characterized by extensional tectonics, while reverse faults in the INESSA area are indicative of compressional conditions (Baranov et al., 1999). North of this region is the dextral Kashevarov Shear Zone. It is located below 61°N and trends in a northerly direction (Worrall et al., 1996). This shear zone has been considered an extension of the system of dextral shears on Sakhalin Island. According to Kimura & Tamaki (1986), Jolivet et al. (1991) and Fournier et al. (1994), they played an important role in the opening of the Kurile Basin. The Kashevarov Shear Zone is a recent structure which influences the tectonics of the northwestern Okhotsk Sea. Its northern termination is a broad fan of transpressional structures oriented NW-SE. Worrall et al. (1996) assume that this shear zone continues up to the western slope of the Derugin Basin, but evidence for this continuation has not been found in our investigations in the INESSA area (Biebow & Hütten, 1999). Thus, it is very important to study the structure of the area north and northeast of Sakhalin Island. Because different fault systems conjugate here, this zone is also important for an understanding of the geodynamics of the entire Okhotsk region.

Fluid migration is frequently connected with the tectonic regime, therefore a detailed survey of the giant barite field found during cruise 28 of the RV *Akademik Lavrentiev* (Biebow & Hütten, 1999) was carried out in the present cruise.

1.2 Seismo-stratigraphy

The sedimentary cover of the eastern part of the Derugin Basin is divided by two regional unconformities into three seismic sequences: a lower sequence of pre-rift sediments, an intermediate sequence of syn-rift sediments and an upper sequence of post-rift sediments. The thickness of the post-rift sediments averages only 100 m implying that vertical tectonic movements terminated here only recently. Rough estimates based on known rates of sedimentation in this region during the past 300 ka suggest that the largely terrigenous post-rift sediments have an age of ca. 1 Ma. The northern, eastern and southern slopes as well as the eastern part of the Derugin Basin were filled simultaneously from the same sediment source. It is hitherto unclear where this source was located and how long the period of sedimentation was.

The central and western parts of the Derugin Basin are filled by a relatively thick acoustically turbid sequence (turbid facies B2, see Biebow & Hütten, 1999). It was suggested that sequence B2 represents proximal glacial-marine sediments deposited more-or-less close to a glacier front. It is assumed that this facies was deposited during sea-level lowstands in the Pleistocene. During sea-level highstands, the glaciers retreated and hemipelagic to pelagic conditions predominated as indicated by turbiditic layers within the turbid facies. However, the large sediment thickness of over 1,600 m within the northeastern Derugin Basin implies that transported glacial material was not the only source for the turbid facies. The Amur River as an additional source might have played a significant rule in the supply of terrigenous matter. During sea-level lowstands its mouth was possibly close to the northeastern slope of the Derugin Basin and its sediment load was deposited over the entire northern Derugin Basin. One of the important tasks of the present cruise from the seismo-stratigraphic point of view is to verify this idea.

The sedimentary section of the Kurile Basin is divided into two sequences: an upper stratified sequence and a lower semi-transparent sequence (Gnibidenko et al., 1995). The reflectors within the upper sequence are practically horizontal throughout the whole basin. The only exception is the margin adjacent to the Kurile arc where gentle folds were observed. Gnibidenko et al. (1995) proposed that the boundary between these sequences is a subtle unconformity which separates the unit with a compressional wave velocity of 2.4-3.0 km/s from the underlying 4.0-4.3 km/s unit. The upper sequence onlaps the basin slopes and the lower sequence outcrops on these slopes. The existence of an unconformity between the upper and lower sequences and the gradual transition of the lower sedimentary sequence into the basin slopes represent peculiar features of the Kurile Basin, distinguishing it from other marginal seas such as the Japan Sea. Investigation of these phenomena is another seismo-stratigraphic goal of the present cruise.

1.3 Surface water CH_4 and CO_2 concentrations

Methane and carbon dioxide have gained the attention of climatologists and geochemists now for more than two decades because of their significant increase in the global atmosphere and the fact that both are very effective greenhouse gases. Although sources and sinks as well as the geochemical pathways are specific for either gas and their flux rates between geochemical reservoirs vary by several orders of magnitude, both components have important interactions with reservoirs in the oceans and marginal seas. Meanwhile, knowledge on the distribution and dynamics of carbon dioxide and methane in the marine environment has proved crucial to an understanding of how the ocean-atmosphere ecosystem reacts to a global increase in the concentrations of these trace gases in the atmosphere.

Since CH_4 and CO_2 play a major role in diagenetic processes, sediments are their primary reservoirs within the marine environment and global efforts are being made to quantify the re-entry of carbon and other associated elements from these reservoirs into the oceans, usually

summarized under the term "venting" or "seeping". The most promising places to investigate in this respect are tectonically active plate boundaries in regions where sedimentary organic matter accumulates in the sediments, preferably along continental margins and shelves. Areas of active venting may be recognized geophysically, e.g., by the occurrence of gas pockets, gas-flares, pockmark-like structures, and deformations of BSRs, or geochemically, e.g., by anomalously high ambient methane or carbon dioxide concentrations.

In both respects, the Sea of Okhotsk is one of the most promising marginal seas to study and to quantify rates and oscillations of the carbon exchange between lithosphere, hydrosphere and atmosphere, since it features a large variety of organic carbon reservoirs such as gas hydrates, oil and gas, or hydrothermal vents and, because of its climatic conditions, also has a significant influence on the regional oceanography of the North Pacific.

Within the joint Russian-German project KOMEX, subproject 1 undertakes to quantify the temporal variability of vent-compounds in the Sea of Okhotsk. This task includes: (1) frequent observations of CH_4 and CO_2 and their associated parameters (e.g., total inorganic carbon and nutrients) at selected locations; and (2) a quantification of the exchange rates between the sea and the atmosphere. The air-sea measurements accompanied the geophysical surveys on the two KOMEX cruises with RV *Professor Gagarinsky* in the summer of 1998 and 1999, since seismic profiling at a constant speed of 5 knots provides favorable conditions for continuous gas analyses of the surface waters.

Methane

Concentrations of methane in the surface waters of the oceans are largely close to equilibrium with the atmospheric level (currently at a mean of 1.80 ppm). This implies that the partial pressure of methane (pCH_4) is mostly controlled by temperature and salinity. Exceptions are frequently observed in marginal seas and at continental shelves where methane is released by various sources at the bottom and the water is shallow enough for the methane to penetrate oxic water columns, where it provides a valuable energy source for micro-organisms. Reviews of data from methane surveys assess that over 75 % of the global oceanic methane emissions originate from shelf regions (Bange et al., 1994).

In the marine environment, methane is generated mainly through anoxic diagenetic processes in the sediments, i.e., the decomposition of embedded organic matter. Depending on the amount of organic carbon, methane concentrations may even exceed saturation limits and occur as free gas within the sediment column, usually at some tens of meters of sediment depth. In any sedimentary methane reservoir, active vertical transport of pore fluids rather than diffusive processes is required to cause outflows at the sea bottom, which, dependent on their extent and intensity, are mostly referred to as "seeps" or "vents". The driving forces for the upward transport of sedimentary fluids are mostly tectonical, whereas fractures often serve as conduits. These processes are observed worldwide, e.g., on active continental margins, at ocean ridges or in other tectonically active regions on the continental shelves. They are currently being in-

vestigated intensively because of their implications for the global geochemical cycles in the marine environment and also because of their potential contribution to the atmospheric trace gas inventory.

Under certain conditions of temperature and pressure, methane and the associated gases CO_2 and H_2S may form solid, ice-like structures in which the gas molecules are trapped within a cage of water molecules. These clathrates or gas-hydrates are sensitive to changes of either temperature or pressure at which they destabilize and release the gases. Conditions suitable for the formation of gas hydrates are commonly found in the oceans and on high latitude shelves. However, the formation of gas hydrates requires both suitable physical conditions and a source of methane. Presently, gas hydrates are assumed to be the largest marine methane reservoir, even exceeding the total of oil and gas recourses, although systematic investigations have only just begun. As yet, gas hydrate reservoirs appear to be the only source large and potentially unstable enough to release considerable amounts of methane into the atmosphere. Recent reviews and modeling using worldwide carbon and oxygen isotope data have come to the conclusion that a giant blast of methane from marine sources may have caused severe shifts of global atmospheric temperatures, leading to mass extinctions some 55 million years ago (Dickens et al., 1997).

When the fluids enter the oxic water column, the methane contained therein is utilized effectively by micro-organisms, sometimes at the rate of up to 0.15/day, corresponding to a turnover time on the order of one week (De Angelis et al., 1993). Because of this, and because they have no thermohaline buoyancy, methane-plumes emitted from "cold" vents have only a limited ability to penetrate oxic water column to be recognized at the sea surface. Hence, locations of known methane seeps concentrate in shallow waters less than 400 m in depth. Due to the spot-like occurrence and irregular distribution of methane sources at the sea surface, their assessment requires systematic surveying.

The Sea of Okhotsk is known to possess a whole variety of sedimentary methane sources, particularly along the tectonically active coast off Sakhalin, where large gas reservoirs occur and gas hydrates have been recovered (Cranston et al., 1994). This area is therefore the primary region for both the surface and the water column gas surveys of the KOMEX project.

Carbon dioxide

The reservoir of dissolved CO_2 in the oceans is about 50 times larger than its total amount in the atmosphere (Sundquist, 1985). This underscores the significance of transport mechanisms between ocean and atmosphere for the atmospheric level of this gas, which has increased by 35 % since pre-industrial times, mostly for anthropogenic reasons (Keeling et al., 1989). The present increase of CO_2 in the atmosphere of about 0.37 % per year corresponds to the amount of 3 billion tons/a, which is only half of the current emission rate from the combustion of fossil fuels. It is therefore of major importance to find and understand the potential sinks of CO_2 in the

marine environment which apparently buffer the current anthropogenic emissions of CO_2 into the atmosphere.

The major factors controlling the partial pressure of carbon dioxide (pCO_2) in the surface waters of the oceans are temperature and removal of total CO_2 by the biological pump, i.e., uptake by phytoplankton and downward transport (Takahashi et al., 1993). The pCO_2 in ocean surface waters may vary by ±40 % of the saturation pressure, the atmospheric partial pressure being 355 ppm (Tans et al., 1990). A seasonal decrease of pCO_2 is frequently observed in areas north of 40° latitude at the onset of the phytoplankton bloom and continues until the nutrients in the euphotic zone are exhausted. The phytoplankton productivity can be observed as a decrease in surface water pCO_2, since the air-sea exchange rates for CO_2 are much slower than the rate of CO_2 fixation. Exceptions from this rule are regions with a continuous supply of both CO_2 and nutrients by upwelling. A quantification of the biologically pumped CO_2 is therefore crucial to an understanding of the global carbon cycle and the CO_2 partial pressure in the North Atlantic and the North Pacific have been frequently monitored over the last two decades.

The KOMEX project now offers an opportunity to extend the existing systematic records of pCO_2 to the Okhotsk Sea which features extreme seasonal variations, a considerable riverine input and very effective marine currents. A large portion of the North Pacific Intermediate Water originates in the Sea of Okhotsk, thus extending the importance of this marginal sea to the whole of the North Pacific.

2. METHODS AND INSTRUMENTS

T. Lüdmann, B. Karp, A. Sudakov, S. Nikolaev, G. Ion, and S. Lammers

2.1 Geophysical survey

The equipment used during the 1999 cruise of the RV *Professor Gagarinsky* includes:

- a seismic reflection system consisting of a two-GI-gun array, an 8 channel mini-streamer, a multi-channel digital data acquisition system, an air gun trigger unit, a pressurized air distribution board and a linescan recorder. A single-channel digital data acquisition system permits real-time data monitoring (quality control) on screen and profile hard-copy printout on a line printer. The two S.S.I. GI-guns have been used in two different configurations, depending on the study area. For the survey within the deep Kurile Basin, the maximum volume of 3.4 *l* per GI-gun was chosen. This permits a penetration of 2 seconds subbottom. For the high resolution studies at the northern margin of the Kurile Basin and northeast of Sakhalin, a 1.44 *l* gun was combined with a 3.36 *l* GI-gun in the harmonic mode. The two-gun array was pressurized nominally at 150 bar, towed behind the ship and triggered every 25 m along prescribed profiles with pulses generated by a master clock. Each active channel of the GECO PRAKLA 8-channel mini-streamer has a length of 12.5 m.

The operational characteristics of the multi-channel seismic reflection system are summarized in Tab. 2.1.

Tab. 2.1: Operational characteristics of the multi-channel seismic reflection system.

Source	
Type	2 × GI-guns
Pressure	150 bar nominal
Firing interval	25 m
Source depth	4.5 m
Streamer	
Streamer depth	5-10 m
First channel offset	50-250 m
No. of channels	8
Length of active section	12.5 m
Length of inactive section between active sections	25 m
Recording	
Recording length	8 sec
Sampling frequency	1000 Hz
Bandpass analog filter	18-250 Hz

The signals from the eight channels are separately digitized via a PC-based A/D converter board, multiplexed, and written onto high capacity EXABYTE tapes. Back in the home laboratory, the data will be demultiplexed and transformed to the standard SEGY format. Later on it will be processed using the *iXL* seismic processing software package. The main processing steps include sorting, digital filtering, NMO-correction, stacking, deconvolution and migration. Parallel to multi-channel digital recording, the analog signals from the different channels of the streamer are summed, amplified, bandpass filtered (15-350 Hz), and displayed online on an EPC 4800 graphic recorder as well as directed to the single-channel digital data acquisition system for monitoring and data storage.

- a Russian single channel seismic reflection system made up of a 3.4 *l* air gun, a streamer, and a single-channel digital data acquisition system based on a commercial sound card (Sound Blaster 16, 32, Vibra) which writes the analog signal on the harddisk of a Pentium-PC. The recorded traces are displayed on the computer monitor. Backup copies are made on magneto-optical disks. The GPS unit is connected to the serial port of the PC. Recording and adjustment of the dynamic range of the seismic signal are controlled on the PC monitor by software developed for this purpose.

Specification of the single-channel data acquisition system:

- data format: SEG-Y files, 16 bit
- sampling rate: 1 or 2 ms, here: 1 ms
- length of trace: 4. .6 sec
- software: acquisition, filtering, viewing, printing, testing

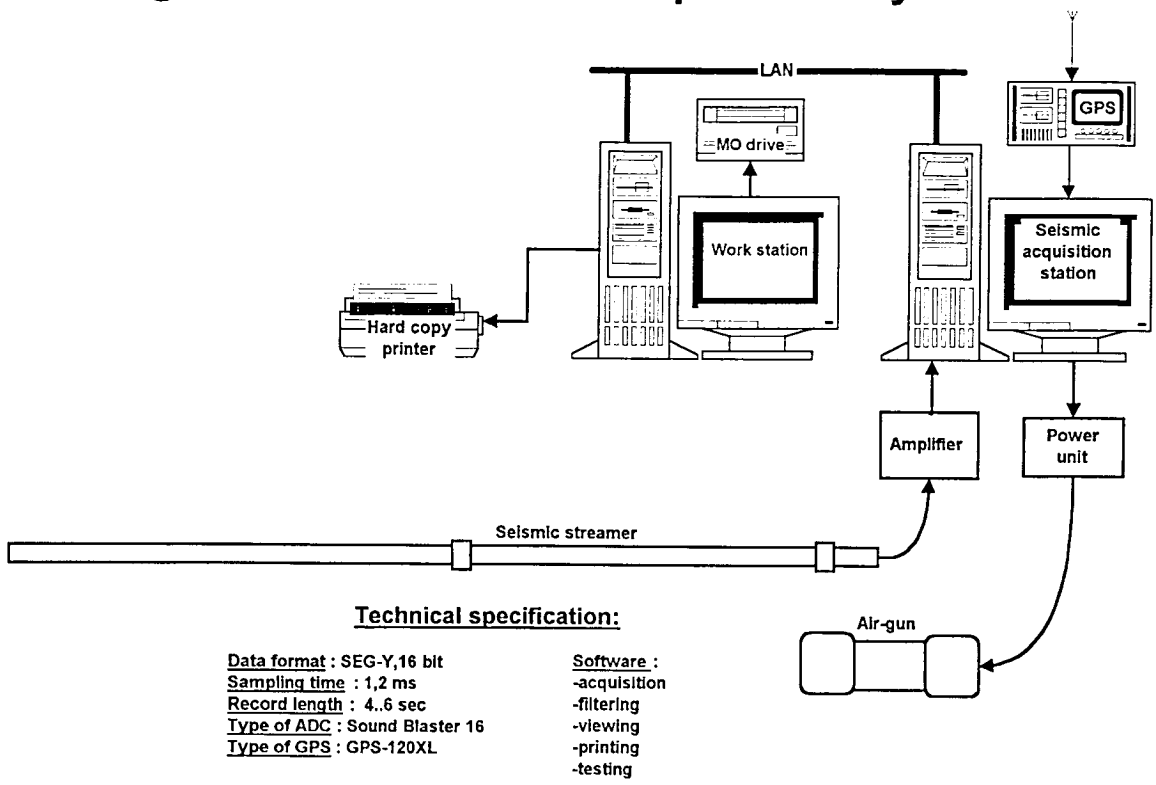

Fig. 2.1: Single channel seismic acquisition system.

- a Russian, surface-towed, MBM-1™ marine proton magnetometer for magnetic total intensity measurements. This magnetometer has a measuring range of 20,000-100,000 nT and an accuracy of 2-4 nT over its entire measuring range. The magnetometer sensor was towed by a non-magnetic cable at a distance of 250 m behind the ship. The magnetic data were written on an analogue recorder for visual display and stored on an IBM PC-386 at a sampling rate of 10 seconds;

- a Russian shipboard gravity meter consisting of four highly-damped, spring-type GMN™ marine gravimeters mounted on GMS-2™ gyro-stabilized platforms installed in a special laboratory on board. The gravimeters achieved an accuracy of 0.8 mgal. In order to reduce cross-coupling errors, a straight-line model of two gravimeters was used. The gravity data were written on an analogue recorder for visual inspection and stored on an IBM PC-386 at a sampling rate of 4 seconds. Gravity observations were started at the pier in Vladivostok at a gravity base station three days before the beginning of the cruise;

- a Russian GEL-3™ wide-beam echo-sounder for bathymetric measurements. This echo-sounder has a measuring range of up to 10 km water depth and operates at a frequency of 12.4 kHz. The water depths were recorded on an analogue echograph which was then sampled manually every 5 minutes;

- a shipboard global positioning system, and
- an "X-STAR full spectrum subbottom profiler" manufactured by EdgeTech from Geoecomar, Romania. This *Chirp* system works within the frequency range of 2 to 16 kHz. The generation of the signal, its modulation, real time processing, data storage and printing is controlled by a SUN Sparc station. The data are stored on EXABYTE cassettes and the processed image printed on an EPC 1086 thermal recorder using 64 gray levels. The actual frequency range used was 2-10 kHz in order to balance between resolution and depth of penetration. The resolution of the system is about 8 cm and the maximum penetration is about 100 m in very fluffy sediments. The towed vehicle was towed at about 4 m below the sea surface.

2.2 Gas survey

Saturation of dissolved methane and carbon dioxide in the surface waters were measured using a flow-through system that maintains equilibrium between continuously pumped surface seawater and air. CH_4 and CO_2 concentrations could be sequentially measured in an equilibrated gas phase as well as in air and, by taking temperature differences into account, the saturation of both species relative to their partial pressures in the ambient atmosphere could be calculated (for further details of the system, see Rehder, 1996).

Sequences of air, equilibrated air, and two different gas standards were sequentially introduced into a two-channel gas-chromatograph (SRI 8610C) and detected by flame-ionisation-detection (FID). A catalytic reduction to CH_4 (by means of a H_2-fed Ni-catalyst at 380° C) made the CO_2 detectable by flame-ionisation. From the multiple gas analyses, standard deviations were found to be less than 1.2% for methane and less than 0.6% for carbon dioxide.

The system was adjusted to record the water values at intervals of 8 minutes, i.e., with a resolution of 0.67 nm at an average speed of 5 knots. The GC analyses were accompanied by sensor recordings of the salinity, temperature, and pH of the supplied seawater. Both data acquisition and system control were performed by the SRI-PeakSimple software installed on a laptop computer.

3. RESULTS

3.1 Bathymetry

B. Baranov, K. Dozorova, and V. Karnaukh

3.1.1 General description

The Okhotsk Sea may be divided in a northeastern and a southwestern part, different in their roughness and depth. The latter is characterized by maximum depths and roughness and includes two deep basins (the Derugin and Kurile Basins). They continue along strike into the Staretsky, Makarov and Atlasov Troughs respectively. The basins are separated from each other by two rises - the Academy of Sciences Rise and the Institute of Oceanology Rise (Fig.

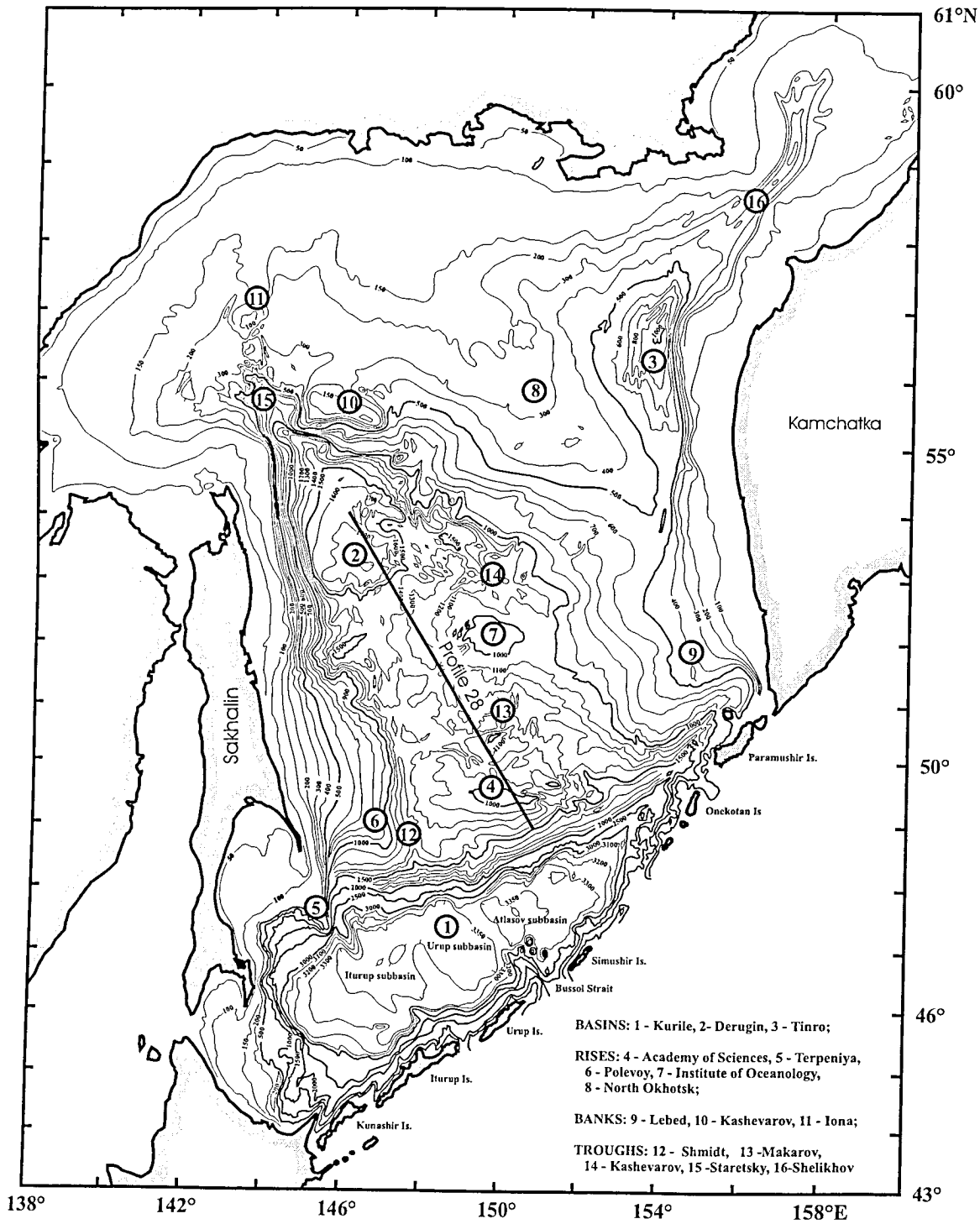

Fig. 3.1.1: *General bathymetry and main morphological features of the Okhotsk Sea. Location of the regional cross-section (profile 28) is shown by a solid line.*

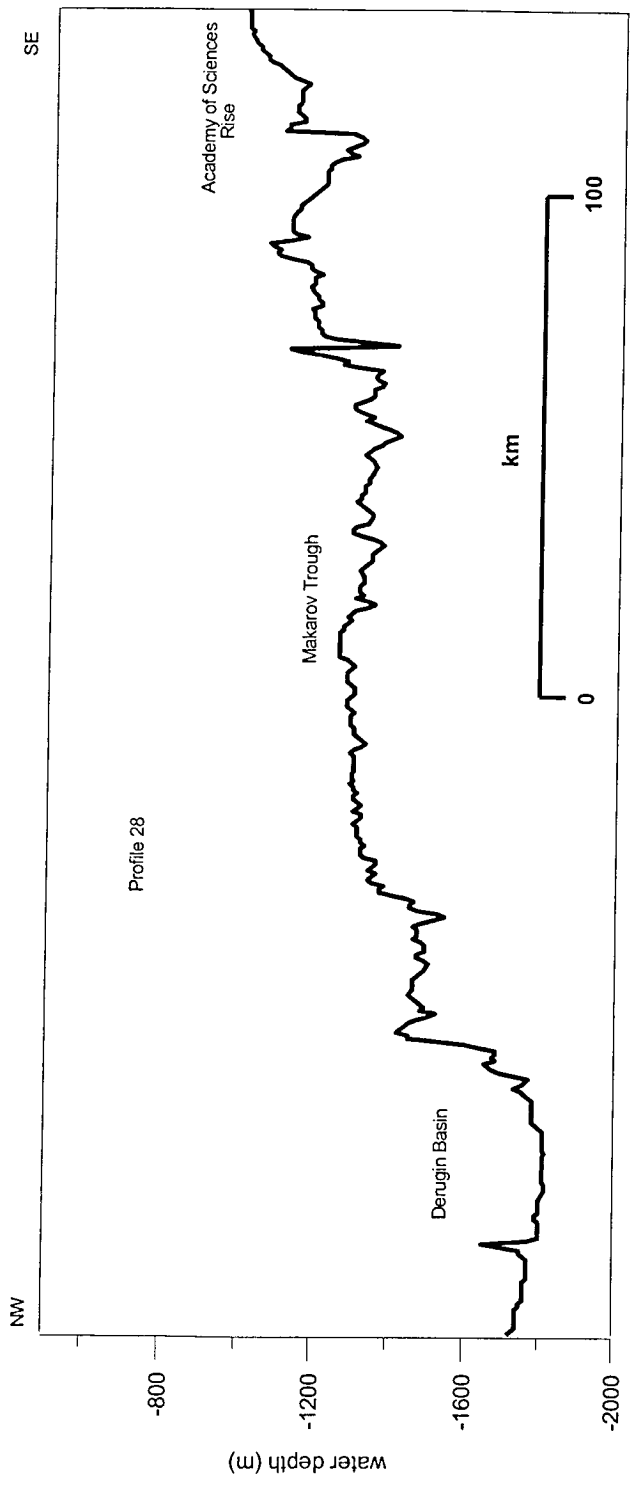

Fig. 3.1.2: *Regional cross-section (profile 28) showing relief features of the Derugin Basin, Makarov Trough and Academy of Sciences Rise. Location is shown in Fig. 3.1.1.*

3.1.1). During cruise 26 of the RV *Professor Gagarinsky* the investigations were carried out in the southwestern area of the sea.

The main morphologic features can be seen on the profile obtained on transit from the northern area of investigation to the southern (Fig. 3.1.2). It crosses the Derugin Basin, Makarov Trough and Academy of Sciences Rise. These structures correspond to different relief levels located at different depths. The Derugin Basin is found at the lowest relief level (depth: 1,700-1,800 m) and is separated from Makarov Trough by two scarps. The Makarov Trough is located at the depth range of 1,300-1,350 m and has the roughest relief. The Academy of Sciences Rise has its base at 1,200-1,110 m. It is characterized by large-scale roughness and the existence of asymmetric highs. Highs of this type are characteristic of the Okhotsk Sea. Seismic data demonstrate that they are widespread throughout the whole sea and correspond to tilted blocks of the acoustic basement (GERDA, 1995; Nürnberg et al., 1997). They are poorly expressed in the bottom relief of basins and troughs filled by thick sediments, but can be distinctly seen on the rises.

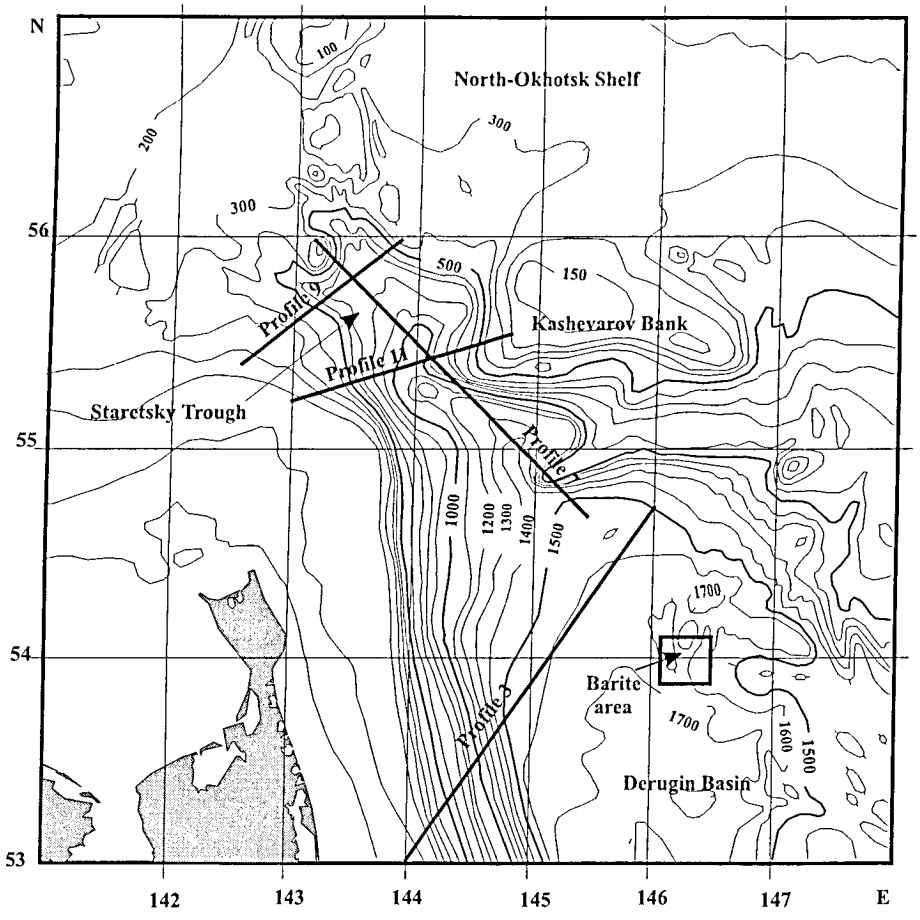

Fig. 3.1.3: Bathymetric map of the northern SAKURA area. Location of profiles 3, 7, 9 and 11 are shown by solid lines. Rectangle indicates area of detailed investigations (barite field in the Derugin Basin). Contour interval is 100 m.

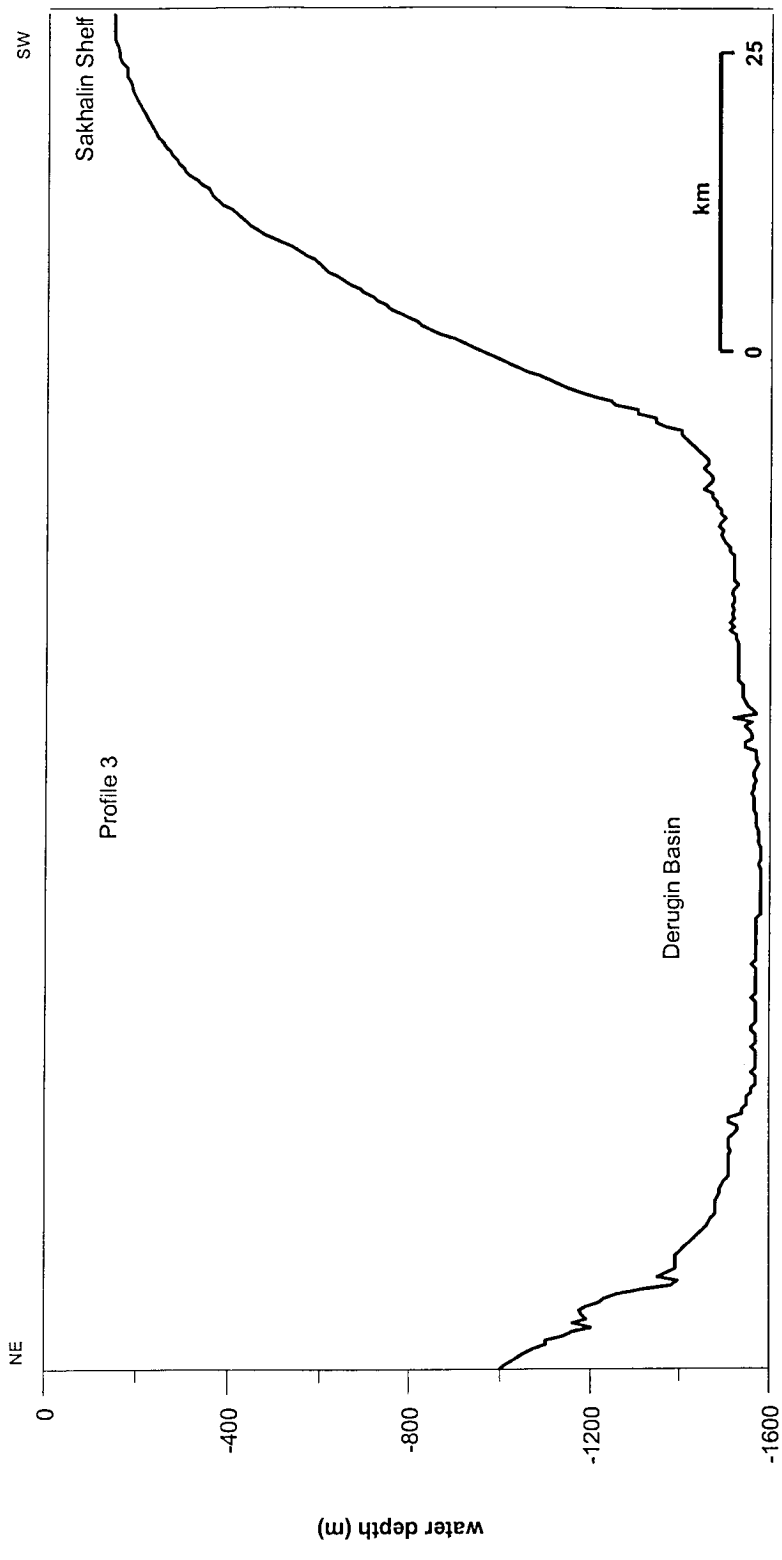

Fig. 3.1.4: *Bathymetric cross-section from the Sakhalin slope (INESSA area) towards the northeastern slope of the Derugin Basin. Small highs of unknown origin occur in the abyssal plain of the Derugin Basin. Location is shown in Fig. 3.1.3.*

Two regions within the southwestern Okhotsk Sea were investigated in the present cruise. The first includes the northwestern Derugin Basin which continues towards the Okhotsk shelf as the Staretsky Trough, and the second comprises the deep part and northern slope of the Kurile Basin.

3.1.2 The northern SAKURA (Sakhalin) area

In this area, four profiles crossing the northwestern slope of the Derugin Basin and the Staretsky Trough were obtained (Fig. 3.1.3). These morphological features are limited to the west by the slope of Sakhalin Island and to the northeast by Kashevarov Bank and the North-Okhotsk shelf. It is possible to distinguish between the morphologic features of the Basin and the Trough (Figs. 3.1.4 and 3.1.5).

In the present cruise, we crossed the Sakhalin slope within the INESSA region between its northern and southern study areas. The slope structure here is simple: a series of highs are observed only near the slope base to the NE (Fig. 3.1.4), while the climb to the Sakhalin shelf is represented by a steep slope. Similar transitions have been described in the INESSA area (Biebow & Hütten, 1999). The shelf break is poorly expressed here, it is distinct only in the northern seepage area (Biebow & Hütten, 1999) and on the southwestern slope of Staretsky Trough (Fig. 3.1.5). Below the shelf break at depths of 370 m (Fig. 3.1.5, profile 9) and 500 m (profile 11), there is a step in the slope relief, after which it becomes more gentle with a rippled surface. The last effect appears to be due to the existence of a series of minor highs with their steep sides facing the slope (in analogy to the INESSA area). The slope transits to the Staretsky Trough with a depth of 700 m to the north and 1,000 m to the south.

The trough bottom is characterized by a relatively smooth surface because of the sediments accumulated. In the Derugin Basin, the smooth seafloor corresponds to abyssal plains which occur from place to place in the deepest parts. Within the main part of the basin, especially near the slopes, many highs with a relief of 50 to 100 m can be observed (Fig. 3.1.4). Their origin is still enigmatic.

On profile 7 along the axis of Staretsky Trough (Fig. 3.1.6), distinct, asymmetric blocks characteristic of the Okhotsk Sea can be recognized. At the beginning of the profile the steep slopes of the tilted blocks face each other to form a graben. Near the base of the blocks, small gullies suggest that strong bottom currents exist in this region. The blocks strike in a north-easterly direction and the height of their tops gradually decreases in the same direction. On the abrasion surface of Kashevarov Bank, their relief becomes negligible.

The block at the end of profile 7 has a very remarkable morphology. Its top is located at 250 m depth and has a sharp form. Since the sea level during the Pleistocene was ca. 100 m lower than now, it is obvious that the top would have been subjected to abrasion. That abrasion is absent suggests that the block has been uplifted rapidly in the Holocene.

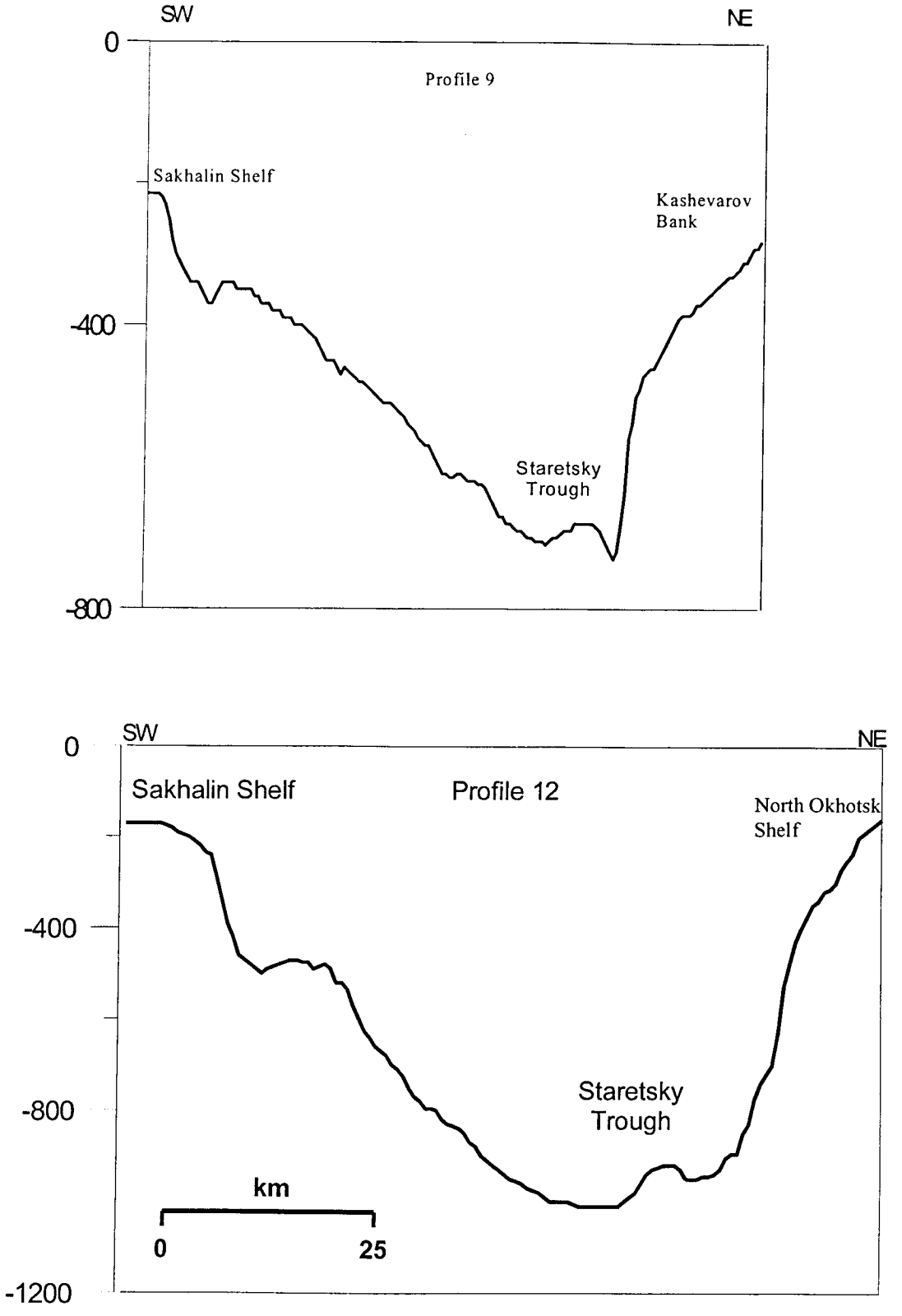

Fig. 3.1.5: *Two bathymetric cross-sections (profiles 11 and 9) across Staretsky Trough. Profile locations are shown in Fig. 3.1.3.*

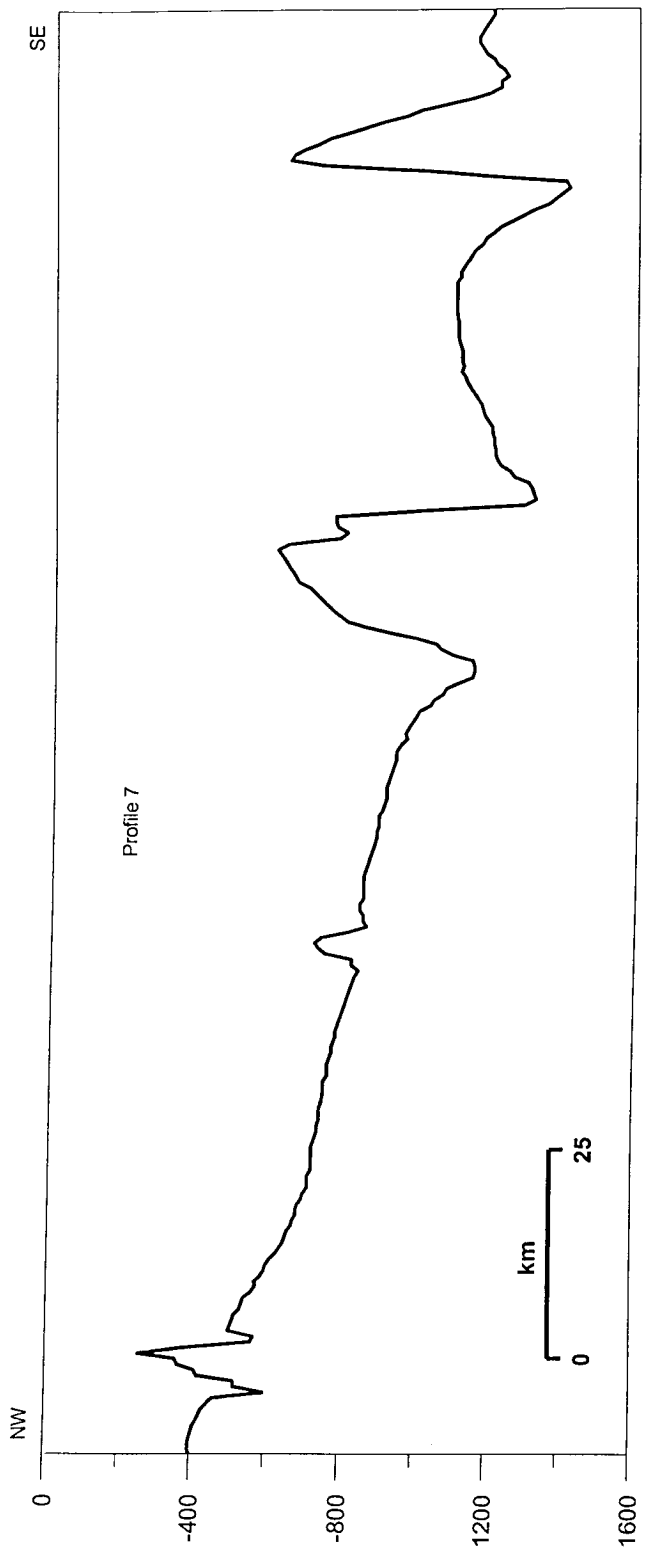

Fig. 3.1.6: *Bathymetric cross-section along the axis of the Staretsky Trough (profile 7). Profile location is shown in Fig. 3.1.3.*

3.1.3 Southern (Kurile) region

In the southern region, studies were carried out on the northern slope of the Kurile Basin and in its central part (Fig. 3.1.7). The Kurile basin is located in the backarc area of the Kurile Arc and strikes parallel to it at a distance of ca. 1,000 km. It has roughly triangular contours, controlled by the strike of Sakhalin-Hokkaido structures to the west, the Academy of Sciences Rise to the northeast and the Kurile Island Arc to the southeast (see Fig. 3.1.1). The maximum width of the Kurile Basin in the southwest is about 300 km. It narrows to the northeast and continues towards Kamchatka as the Atlasov trough. The average depth of the basin is 3,300 m, the maximum depth is about 3,360 m.

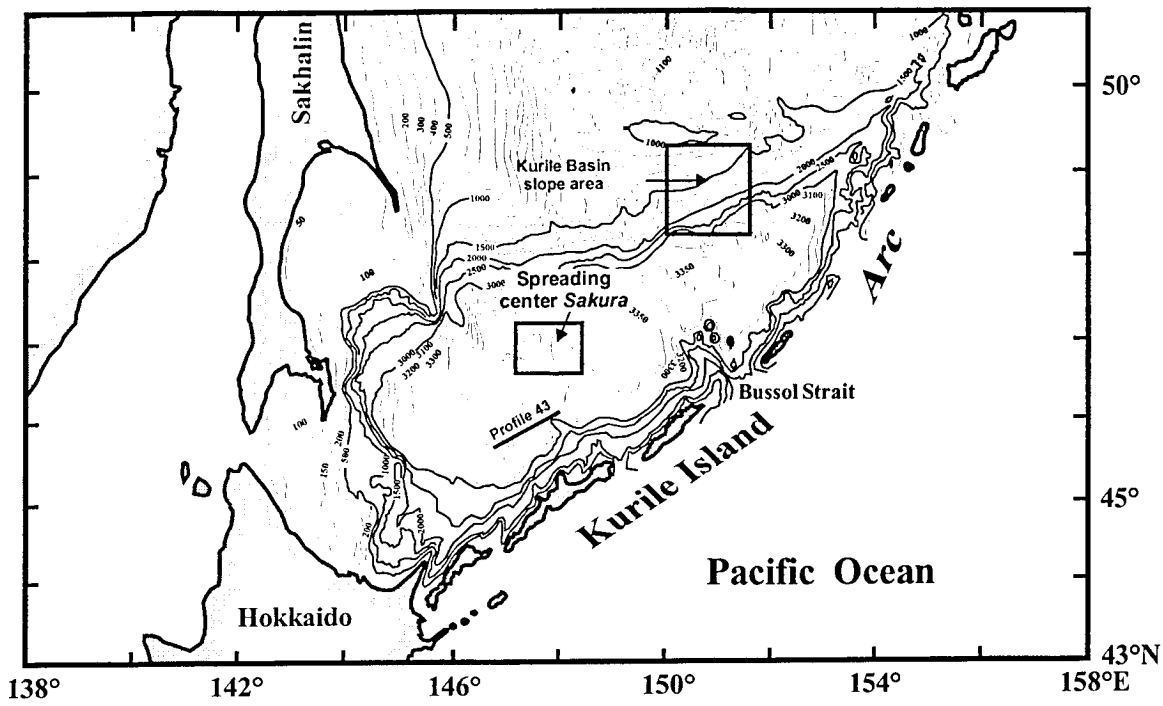

Fig. 3.1.7: Bathymetric map of the Kurile Basin. Location of profile 43 is shown by a solid line; areas of detailed survey are shown by rectangles.

The northern slope of the Kurile Basin compared to the southern slope is structurally relatively simple and is lower because it is limited by the Academy of Sciences Rise whose top is marked by the 1,000 m isobath. The morphology of this region was mapped during the GREGORY expedition (Nürnberg et al., 1997). It was noted that in the lower part of the slope, canyons with a depth of about 200 m are widespread (Fig. 3.1.8). The maximum canyon depth reaches 350 m. The axis of the largest canyon is oriented in NW-SE. This strike is presumably fault-controlled.

The Kurile Basin may be divided into three isolated subbasins with abyssal plains as basin floors lying at depths of about 3,360 m: the Iturup, Urup and Atlasov basins (see Fig. 3.1.1). These subbasins are separated by gentle highs with heights of several tens of meters. The highs

top at ca. 3,350 m and strike in the direction NW-SE orthogonal to the long axis of the Kurile Basin (see Fig. 3. 1.7).

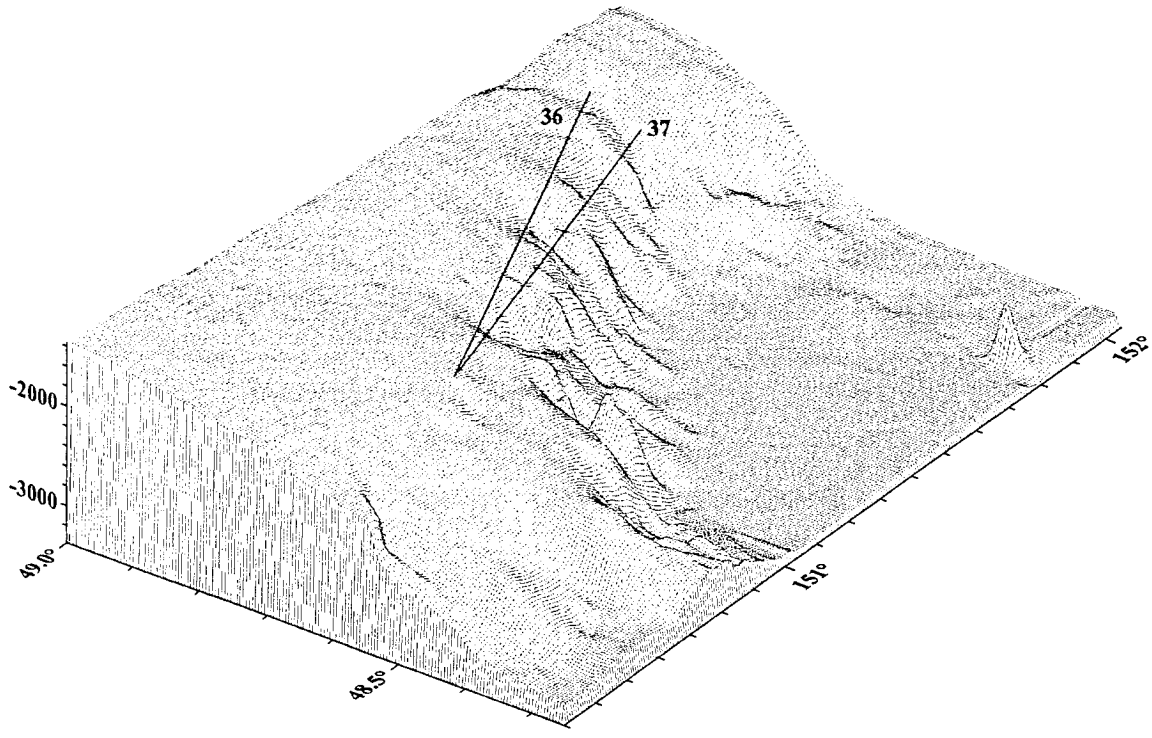

Fig. 3.1.8: Block diagram of the northern slope of the Kurile Basin based on data of the GREGORY and SAKURA expeditions. Locations of profiles 36 and 37 are shown in figure 3.2.2.2.

Although the bottom of the Kurile Basin is generally smooth, linear ridges oriented orthogonal or oblique to the arc occur, especially near the Kurile Arc. Two such ridges were crossed on transit from the northern basin slope to its central part (see Fig. 3.1-9, profile 13). They are distinctly asymmetric and correspond to tilted blocks of the acoustic basement (similarly to the highs on the northern slope).

3.2 Reflection Seismics

3.2.1 Derugin Basin and Staretsky Trough

T. Lüdmann

Reflection seismic profiling were carried out during cruise 26 of the RV *Professor Gagarinsky* in the northern continuation of the INESSA study area (Fig. 3.2.1.1). The main structural elements of this region are the Staretsky Trough and the Kashevarov Bank. A first interpretation of the seismic data shows that of the facies areas mapped during the INESSA cruise, only area III continues into the Sakura area (Fig. 3.2.1.2). It marks the transition zone between the sediments deposited within the Staretsky Trough and in the Derugin Basin. In the northwestern part of the basin, the sediments reach a thickness of at least 1 s TWT. However, the lower boundary of the sedimentary column cannot be determined with certainty because of weak

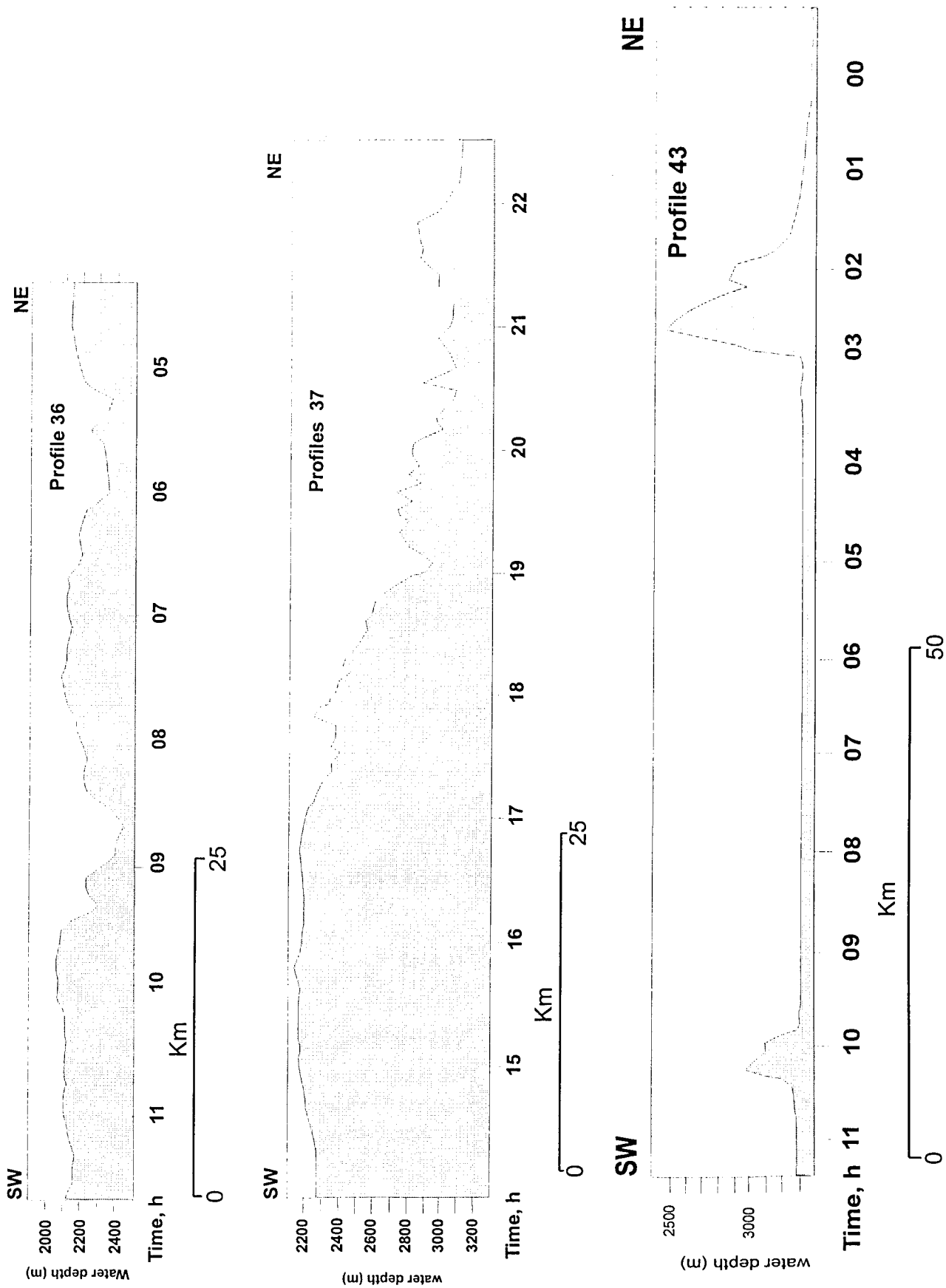

Fig. 3.1.9: *Bathymetric cross-sections along the northern slope of the Kurile Basin (profiles 36 and 37) and within the Kurile Basin abyssal plain (profile 43). Profile locations are shown in Figs. 3.1.8 and 3.1.7 respectively.*

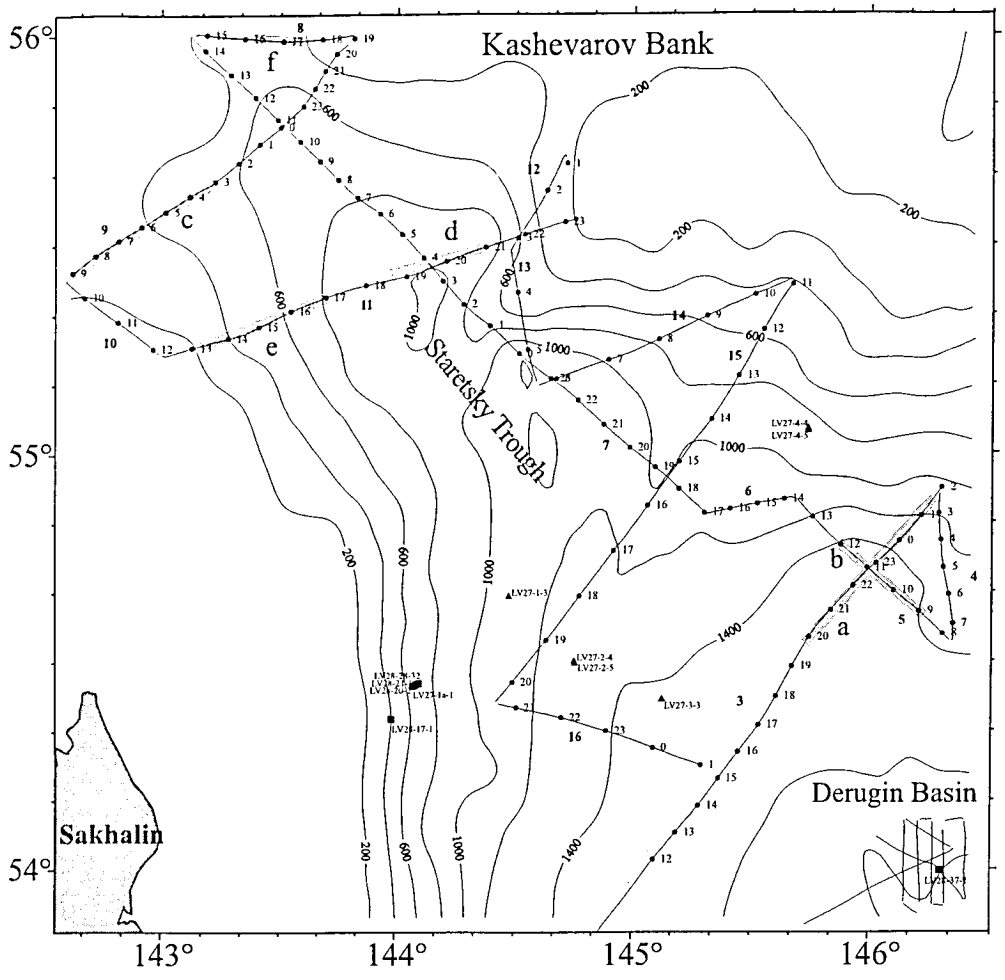

Fig. 3.2.1.1: *Map with SAKURA cruise tracks off northeastern Sakhalin and locations of the example profiles shown (alphabetically numbered). Black triangles and squares indicate gravity core stations of the Lavrentyev cruise 27 (Nürnberg et al., 1997) and LAVRENTYEV cruise 28 respectively (Biebow & Hütten, 1999).*

reflections beneath 1 s TWT. The overall thickness may exceed 2.2 s TWT. The acoustically turbid unit, the main component of area III, is characterized by medium amplitudes and a lack of any significant internal structures. In places, thin layers of well-stratified sediments can be recognized, indicating possible cyclic sedimentation. They cover a more-or-less rough surface within the turbid facies. In the direction of the northern margin of the Derugin Basin, the thickness of these layers increases, while the turbid facies pinches out (Fig. 3.2.1.3). A few thin beds can indeed be traced back to the slope of the Kashevarov Bank. Here, a well-stratified unit comprising continuous reflectors of high amplitude alternating with continuous to discontinuous reflectors of low amplitude dominates (Fig. 3.2.1.4). Occasionally, the stratification is interrupted by transparent zones as can be seen within the eastern part of the Staretsky Trough (facies area V, Fig. 3.2.1.2). Within subbasins of the Trough, a thickness of more than 2 s TWT is arrived at. The external configuration of the stratified unit is mound-like for the younger units (downlap of the reflectors on both sides) and sheet-like for the older

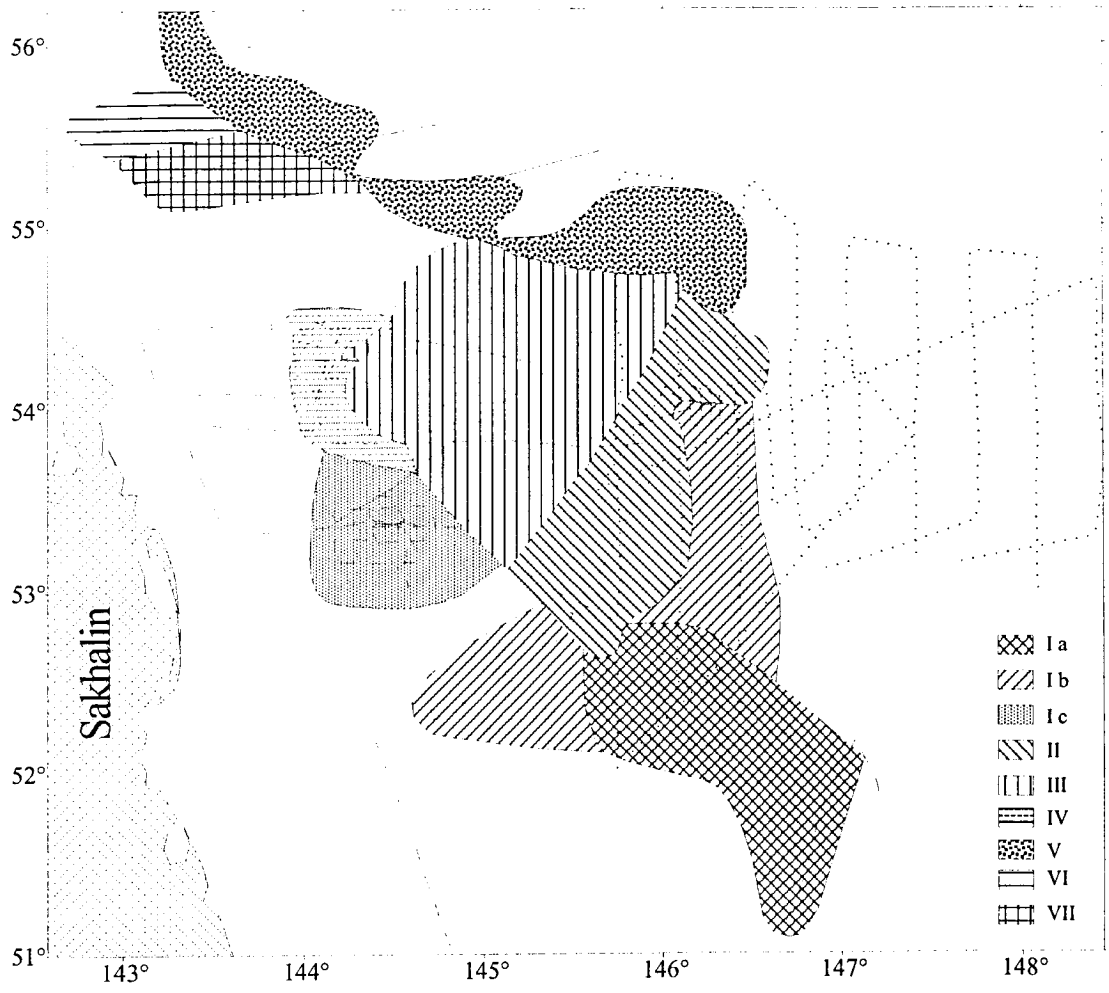

Fig. 3.2.1.2: *Distribution of seismic facies within the study area off northeastern Sakhalin. Continuous lines mark the SAKURA cruise track, dotted lines the GERDA cruise profiles and dashed lines the INESSA cruise profiles. Ia to VII: seismic facies areas (see text for explanation). Thick continuous lines give the location of profiles, present study (SAKURA cruise); dotted lines that of the GERDA cruise and dashed lines that of the INESSA cruise.*

units. The stratification and the external geometry suggest a depo-environment of varying depositional energy leading to an alternation of coarse and fine sediments.

The northwestern part of the Staretsky Trough in the vicinity of the northern Sakhalin slope belongs to seismic facies area VI (Fig. 3.2.1.5). It is dominated by reflectors of high amplitude which can be oblique as well as horizontal and in part chaotic. The external configuration is often mount-like. Typical is a low penetration: below ca. 300 ms TWT reflections are no longer visible, indicating attenuation of the seismic energy by coarse sediments. Father to the west, the seismic unit of facies area VI exhibits parallel to subparallel reflections of high amplitude. Here, this unit terminates downlap on the foot of the northern slope of Sakhalin Island. Southern Staretsky Trough is occupied by facies area VII which is characterized by well-stratified strata of medium reflection amplitude dipping to the southwest (Fig. 3.2.1.6). They are overlain unconformably by a sediment wedge terminating downlap to the northeast.

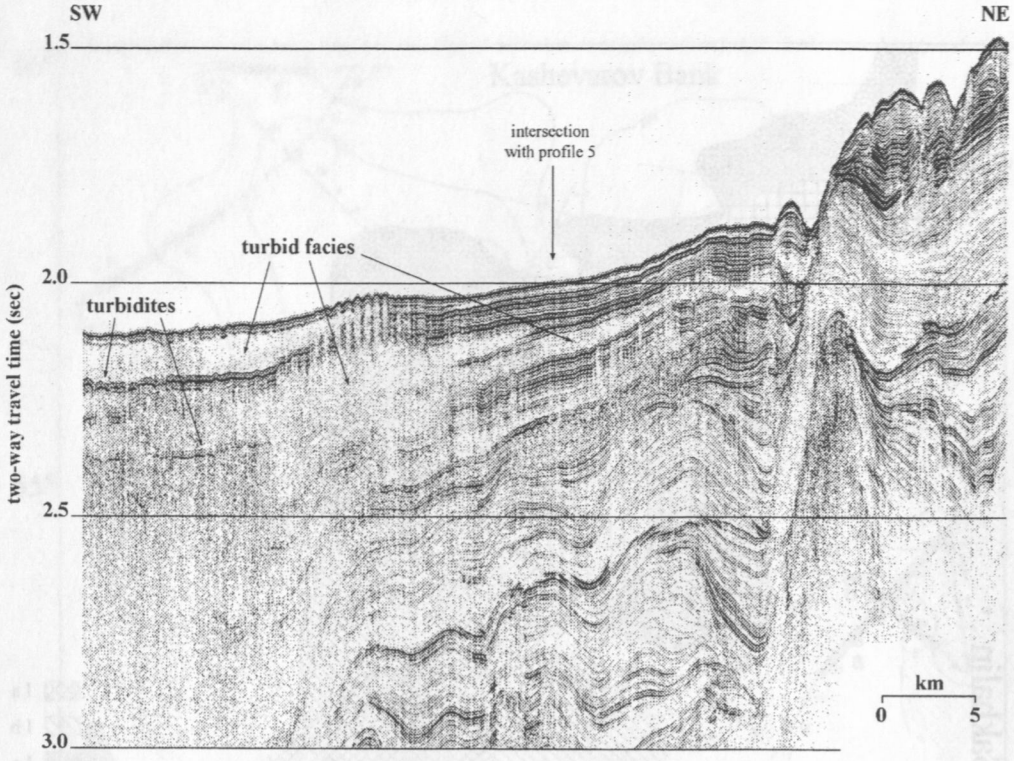

Fig. 3.2.1.3: Part of reflection seismic profile 3 showing interfingering of turbid facies and well-stratified layers. See a in Fig. 3.2.1.1 for profile location.

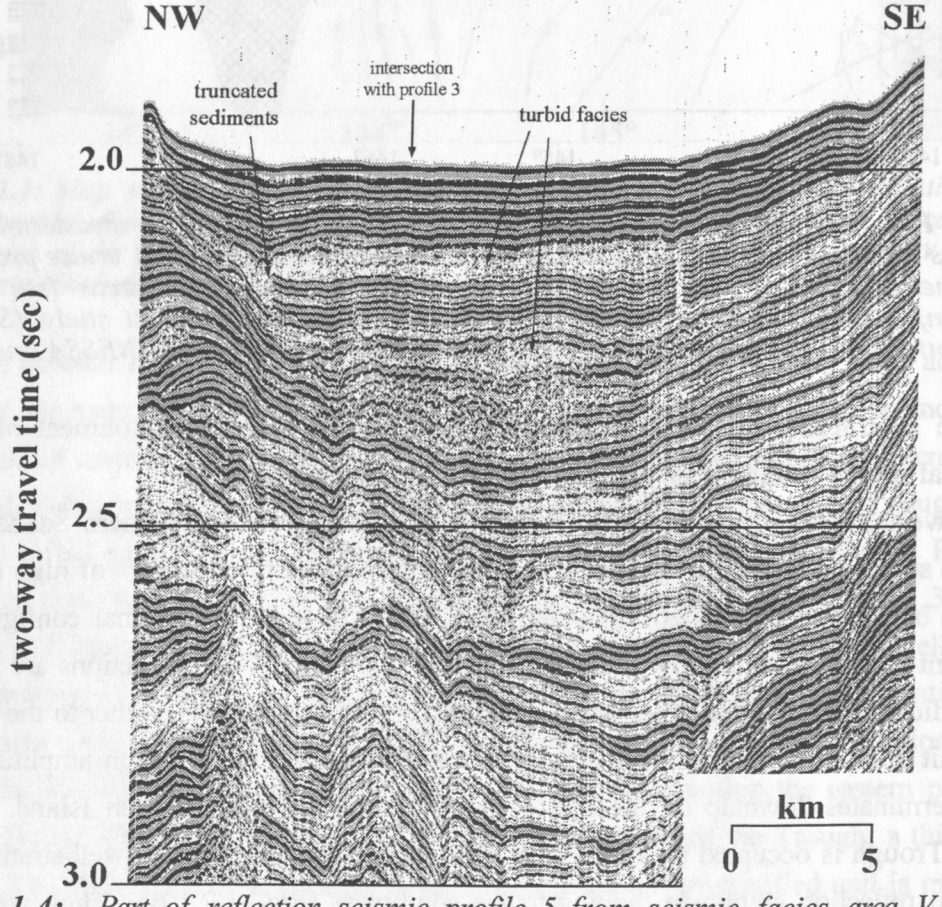

Fig. 3.2.1.4: Part of reflection seismic profile 5 from seismic facies area V. For the distribution of this facies area see Fig. 3.2.1.2 and for profile location see b in Fig. 3.2.1.1.

to the northeast. Incorporated within the wedge are lenticular bodies with either subparallel reflectors, or a turbid internal pattern, or hyperbolic reflections (Fig. 3.2.1.7). The western margin of Staretsky Trough is marked by a prograding wedge overlying the northern Sakhalin shelf and slope. Over the slope, the wedge terminates offlap at its top and downlap on its base. It consists of dipping reflectors of low amplitude (Fig. 3.2.1.7).

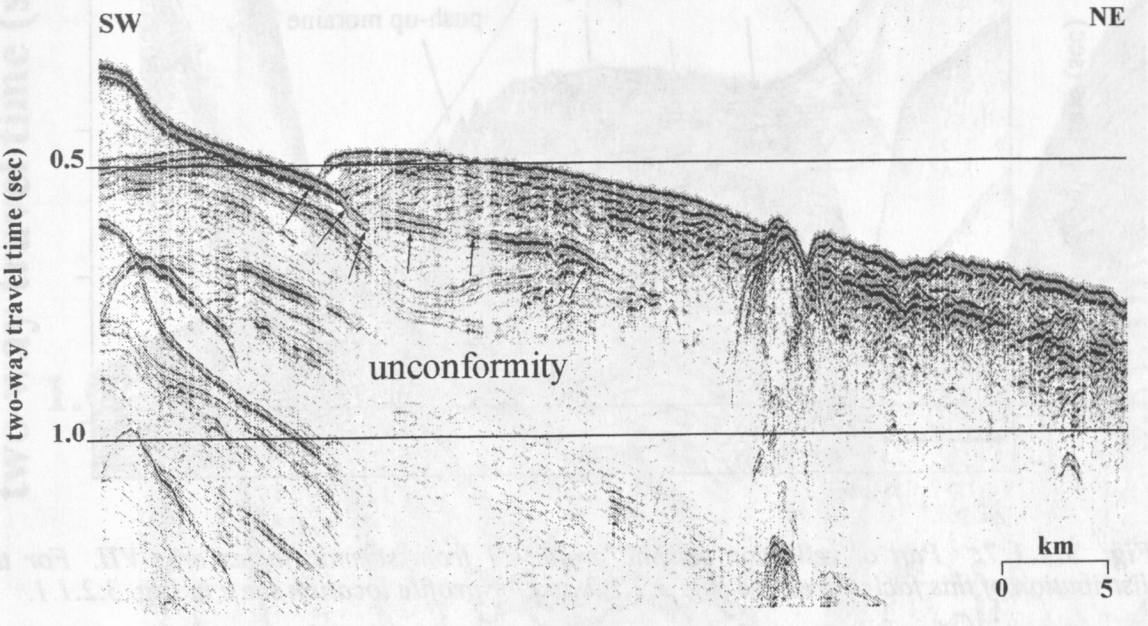

Fig. 3.2.1.5: *Part of reflection seismic profile 9 from seismic facies area VI. For the distribution of this facies area see Fig. 3.2.1.2 and for profile location see c in Fig. 3.2.1.1.*

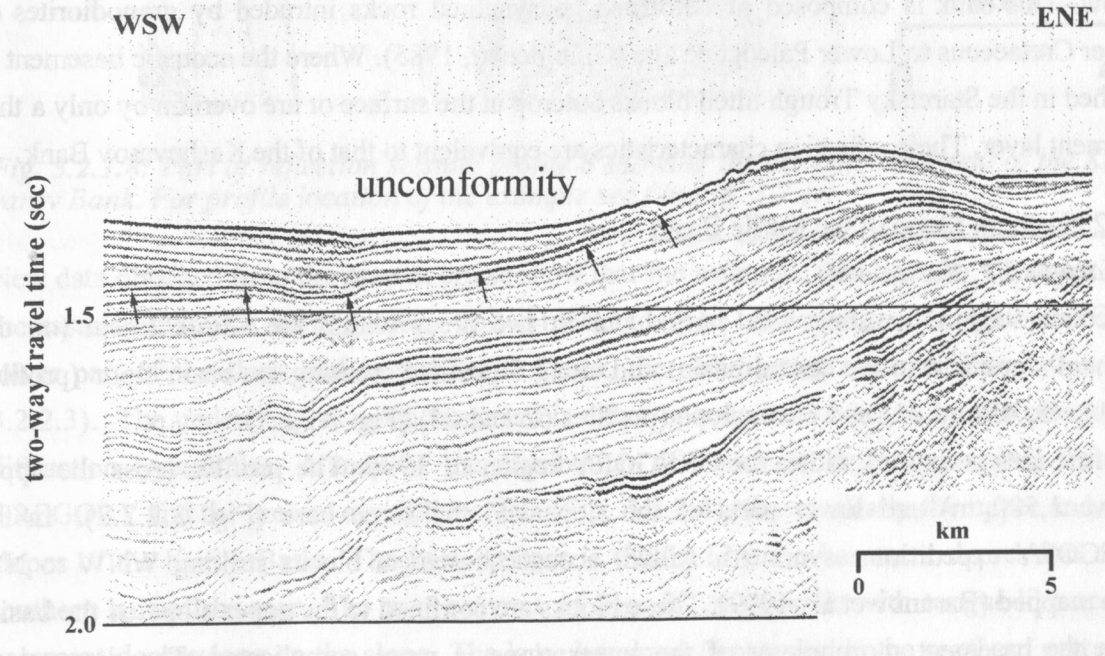

Fig. 3.2.1.6: *Part of reflection seismic profile 11 from seismic facies area VII. For the distribution of this facies area see Fig. 3.2.1.2 and for profile location see d in Fig. 3.2.1.1.*

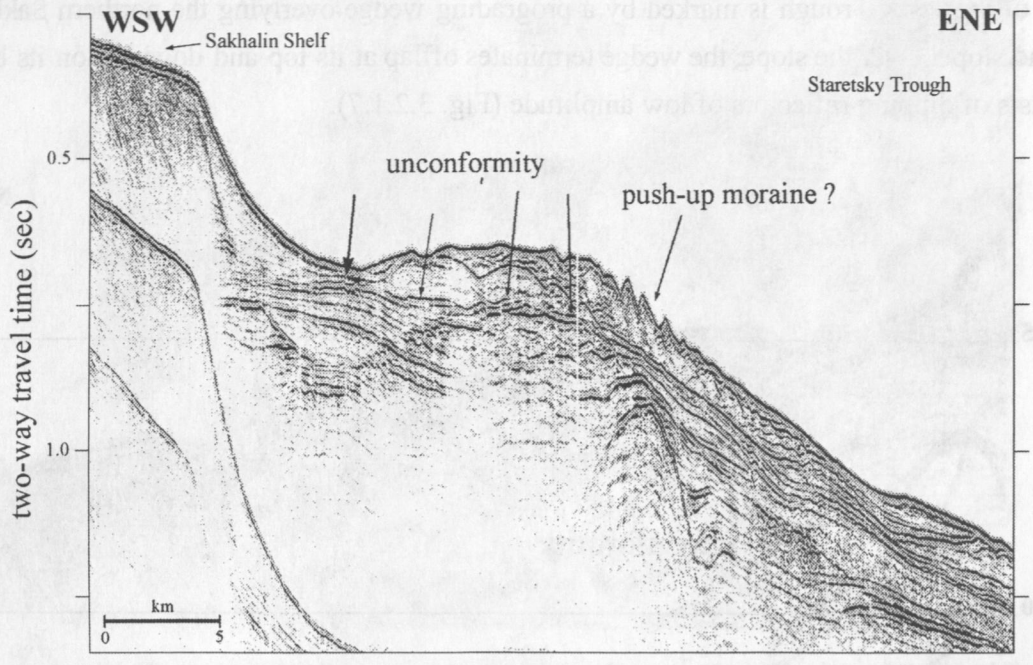

Fig. 3.2.1.7: *Part of reflection seismic profile 11 from seismic facies area VII. For the distribution of this facies area see Fig. 3.2.1.2 and for profile location see e in Fig. 3.2.1.1.*

Within the study area north of Sakhalin Island, different types of acoustic basement occur. Most prominent is the Kashevarov Bank (Fig. 3.2.1.8) which is characterized by a rough surface and chaotic as well as hyperbolic reflections of medium amplitude. Penetration of the seismic energy is low. This bank is composed of deformed geosynclinal rocks intruded by granodiorites of Upper Cretaceous to Lower Paleogene age (Gnibidenko, 1985). Where the acoustic basement is reached in the Staretsky Trough tilted blocks outcrop at the surface or are overlain by only a thin sediment layer. Their reflection characteristics are equivalent to that of the Kashevarov Bank.

3.2.2 Northern Slope of the Kurile Basin

B. Karp and V. Karnaukh

Reflection seismic profiling was carried out in two areas within the Kurile Basin (on the northern slope and in the central basin) and along 7 profiles crossing the basin floor (profiles 39, 41, 43, 45 and 61) and basin slope (profiles 62 and 63) (Fig. 3.2.2.1).

The first area is located within the GREGORY region of 1996. The profiles cross the upper (above 1,500 m) and lower parts of the slope and the slope base (Fig. 3.2.2.2). In the GREGORY expedition, asymmetric (tilted) acoustic basement blocks striking WNW to NW were mapped (Baranov et al., 1999). These blocks are confined to the upper slope of the basin, while the basement morphology of the lower slope is more complicated. The depressions between grabens frequently have a semi-graben form.

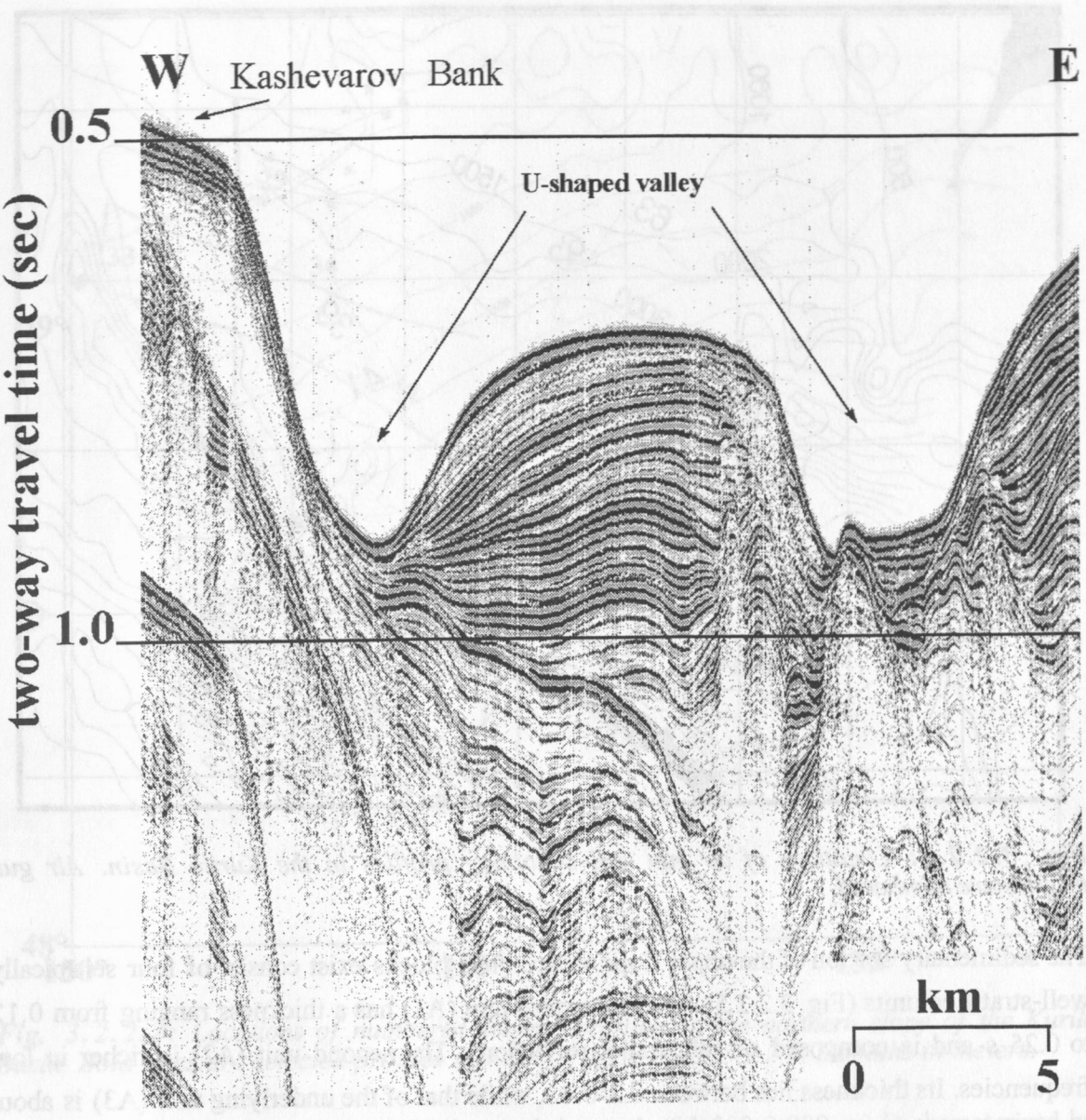

Fig. 3.2.1.8: Part of reflection seismic profile 8 showing the acoustic basement of the Kashevarov Bank. For profile location of the example see f in Fig. 3.2.1.1.

New data obtained from the present cruise show that the sediment thickness on the upper slope increases from 0.15 s above the top of tilted blocks to up to 1.5 s in some semi-grabens. On the lower part of the slope and in the Kurile Basin, the sedimentary cover reaches 2.0 s (Fig. 3.2.2.3). The underlying acoustic basement is either opaque or is marked by the envelope of diffraction hyperbolas. A map of the distribution of basement depths compiled from the GREGORY and the present expeditions data (Fig. 3.2.2.4) shows clearly the upper and lower slopes of the Kurile Basin. The basin proper is outlined by the basement depression on the southern half of the map. The two canyons of Fig. 3.1.8 coincide with tongue-like acoustic basement depressions on the slope. The large basement depression in the southern part of the area is separated from the Kurile Basin floor by a chain of small basement highs.

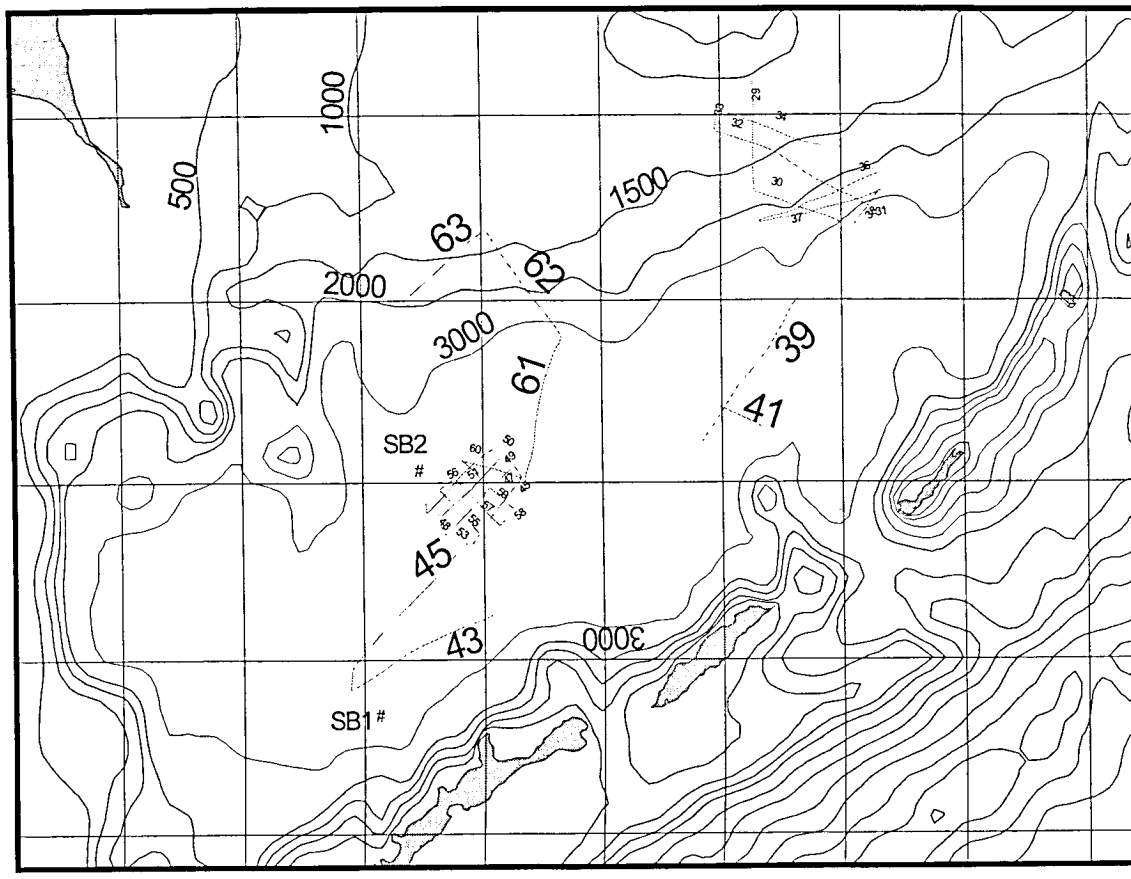

Fig. 3.2.2.1: Locations of air gun and sonobuoy profiles in the Kurile Basin. Air gun profiles are numbered.

The sedimentary section of the upper slope where tilted blocks exist consist of four seismically well-stratified units (Fig. 3.2.2.5). The uppermost unit (A1) has a thickness ranging from 0.12 to 0.25 s and is composed of subparallel reflections. The second unit (A2) is richer in low frequencies. Its thickness lies between 0.3-0.4 s, while that of the underlying unit (A3) is about 0.5 s, and that of the lowermost unit ranges from 0.1 to 0.15 s. These units are separated from each other by unconformities, that between A1 and A2 being an erosional surface. Reflections within the units A1 and A2 are conformal to the seafloor. Reflectors within the unit A3 in some semi-grabens are downdrawn. Thus, it may be assumed that synsedimentary downward tectonic movements occurred, giving rise to this unit. The unit A4 is located on the gentle slopes of tilted blocks and its internal reflections are parallel to the slopes.

Sediments on upper slope of the Kurile Basin can be subdivided into prerift (A4), synrift (A3) and postrift (A1 and A2) units.

The same seismic sequences can be observed on the lower slope of the basin west of 151° 18′. East of this longitude in the extensive depression of the acoustic basement, however, the degree of stratification of the three upper units becomes approximately equal and unit A4 is no longer observable (perhaps due to limited penetration). A new semi-transparent unit with a thickness of 0.5-0.7 s underlies unit A3.

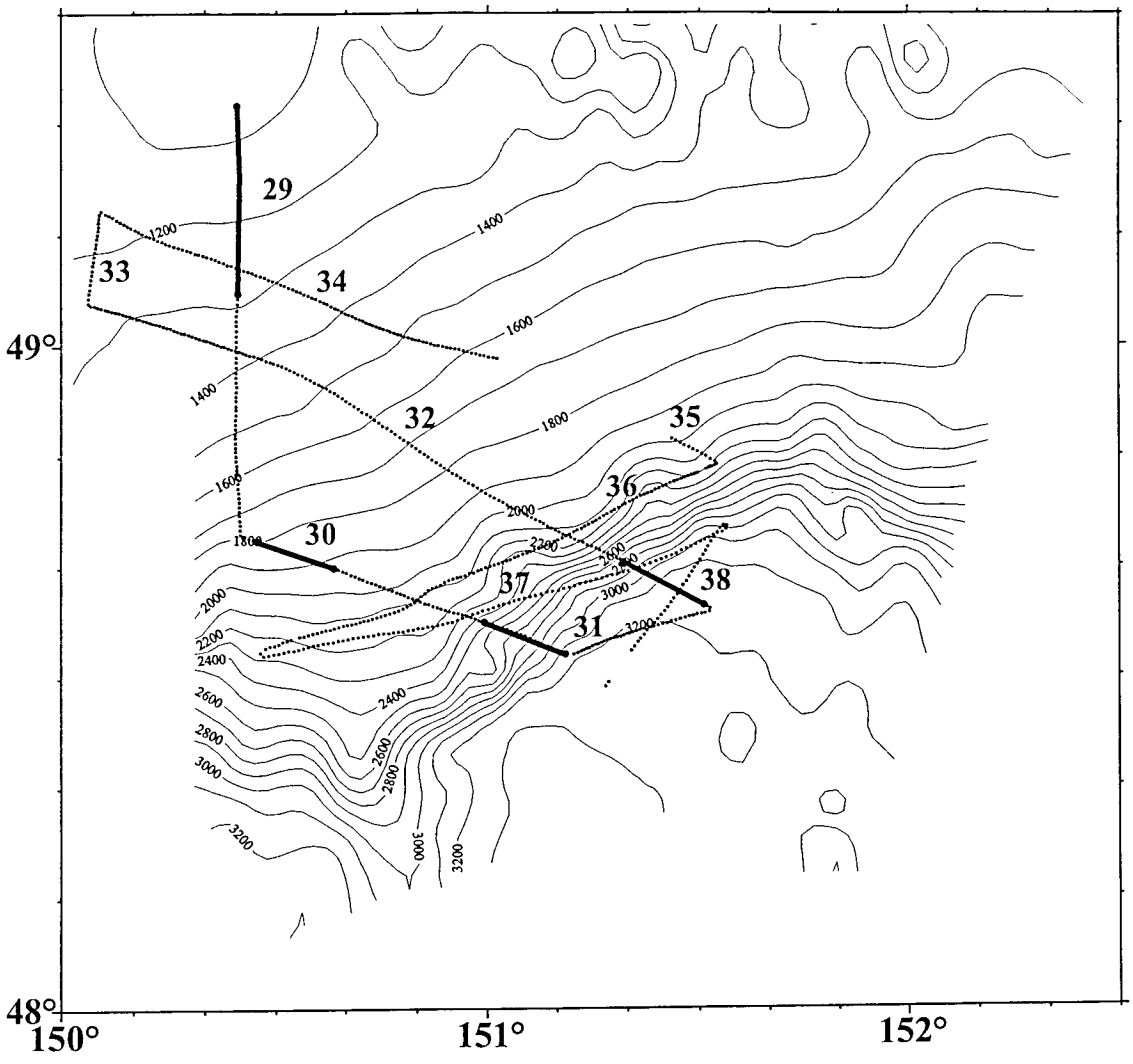

Fig. 3.2.2.2: Locations of numbered seismic profiles on the northern slope of the Kurile Basin. Bold lines are selected profiles shown in Figs. 3.2.2.5-3.2.2.8. Isobaths in meters.

The sedimentary section mid-slope (in the depth interval of 1,500-2,000 m) is characterized by the presence of numerous low amplitude folds. These folds deform mainly the units A2 and A3 (Fig. 3.2.2.6). Where canyons incise the slope, the upper sedimentary layers (with a thickness of up to 0.2 s) are reworked. In the upper part of the sedimentary section, there are chaotic layers (Fig. 3.2.2.7).

Sediments of the Kurile Basin adjacent to the slope are composed of two seismic units: well-stratified in the upper part and semi-transparent in the lower part (Fig. 3.2.2.8). Their internal reflectors are subparallel. The boundary between these units is indistinct. They onlap the slope basement. Several minor unconformities occur within the well-stratified unit. They suggest that this unit is accumulated under conditions of a fluctuating sea level.

Both the Kurile Basin and its northern slope have acoustic basements made up of tilted blocks (profiles 62 and 63; Fig. 3.2.2.1). The sedimentary section crossed by profiles 62 and 63 consists of five units: two well-stratified units, two semi-transparent units and one transparent

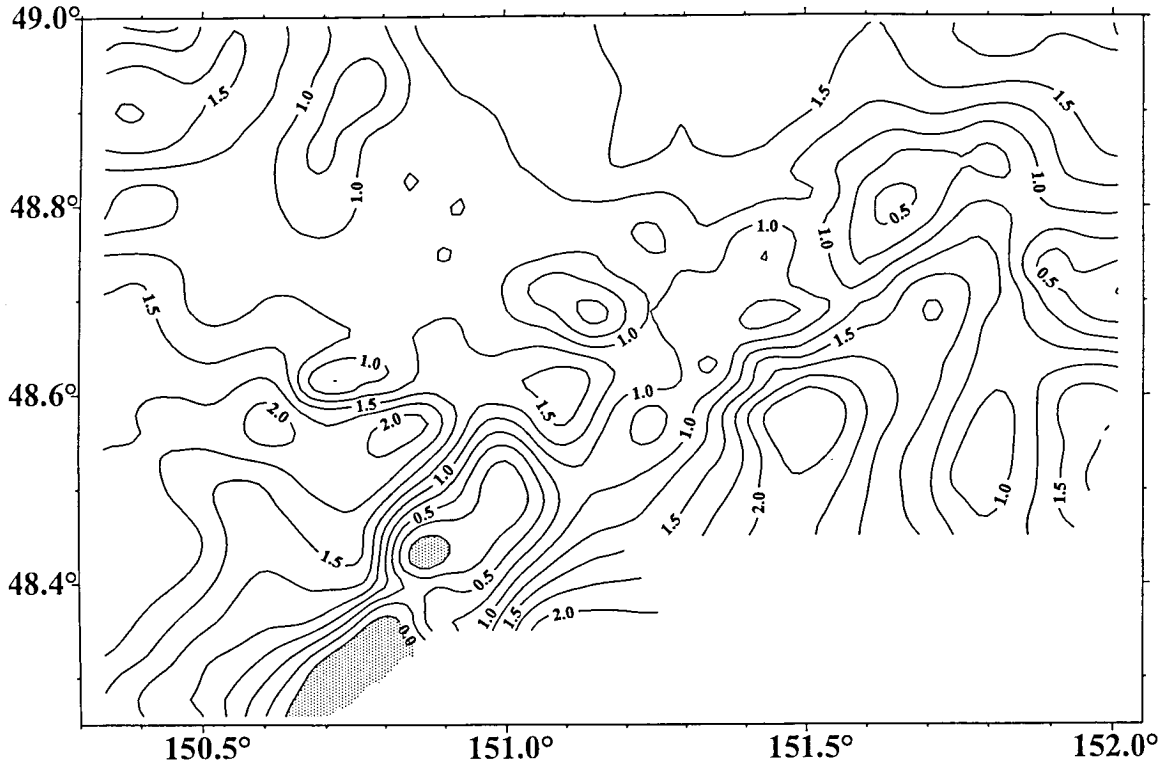

Fig. 3.2.2.3: Isopach map of the sedimentary cover on the northern slope of the Kurile Basin at 0.25 sec TWT intervals. Areas of exposed acoustic basement are shaded.

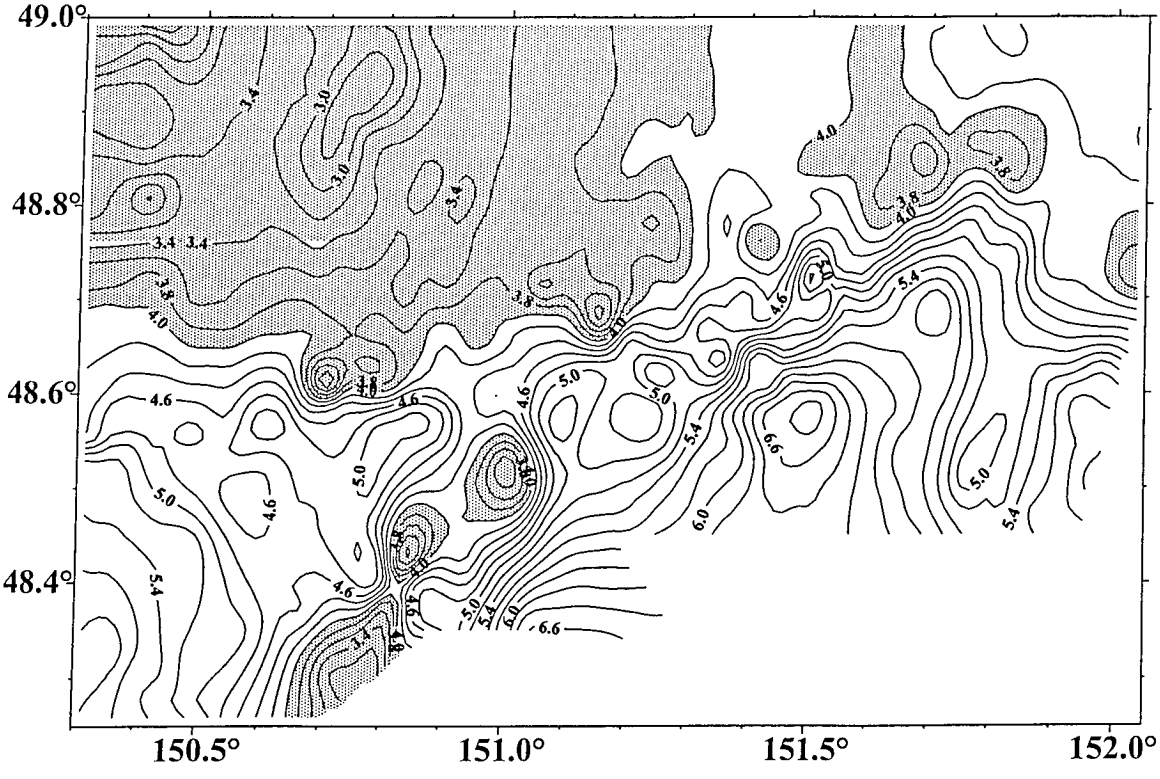

Fig. 3.2.2.4: Distribution of basement depth on the slope of the Kurile Basin in 0.2 sec TWT intervals. Areas with an acoustic basement depth <4.0 sec are shaded.

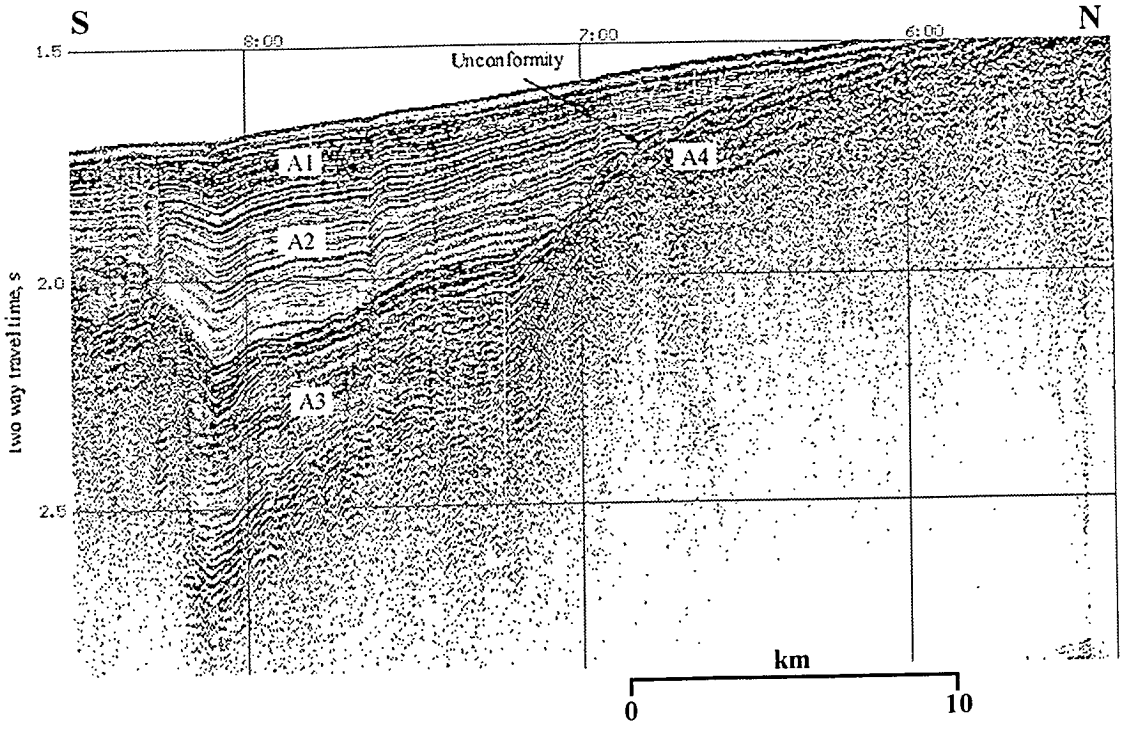

Fig. 3.2.2.5: *Part of reflection seismic profile 29 showing the four seismic sequences recognized (A1 to A4). See Fig. 3.2.2.2 for profile location.*

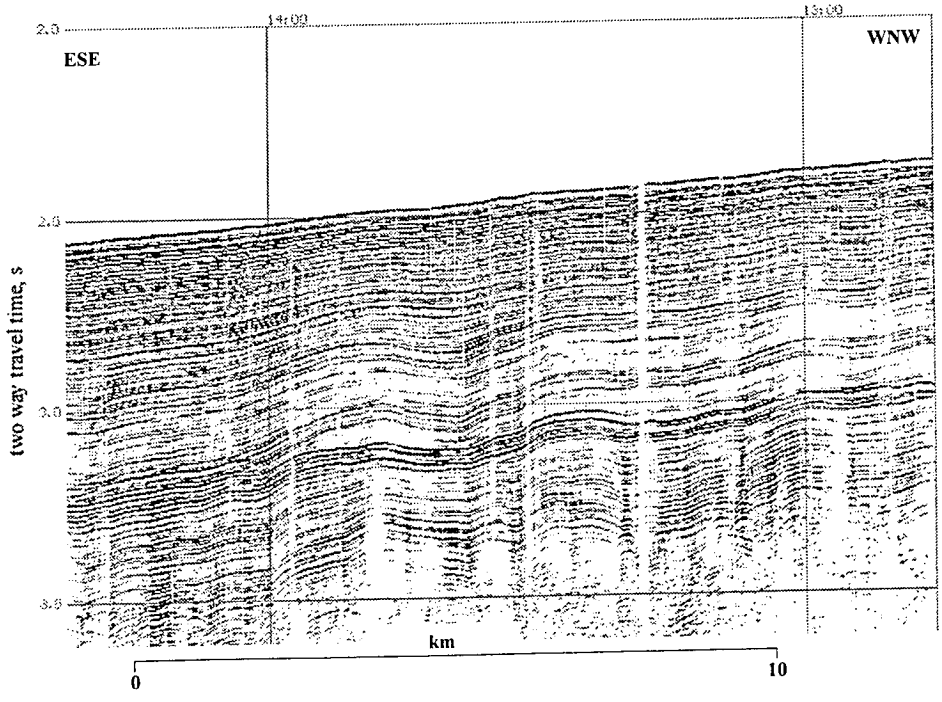

Fig. 3.2.2.6: *Part of reflection seismic profile 30 showing small amplitude folds on the northern slope of Kurile Basin. See Fig. 3.2.2.2 for profile location.*

unit. The upper well-stratified unit with a thickness of 0.2-0.3 s is composed of subparallel reflectors. It is bounded below by an unconformity. The upper semi-transparent unit, 0.3-0.4 s in thickness, is characterized by the existence of a few weak reflecting horizons. It is underlain by a well-stratified unit with a thickness of 0.2-0.3 s. The top of this unit is represented by an erosional unconformity. The lower semi-transparent unit, up to 0.4 s in thickness, exists only in deep semi-grabens between tilted blocks. This is true also for the lowermost transparent unit with a thickness of up to 0.5 s. Internal reflections within the first two units are conformal to the seafloor. They are curved downwards inside the lower well-stratified unit and are deformed into gentle low-amplitude folds in the upper stratified and upper semi-transparent units.

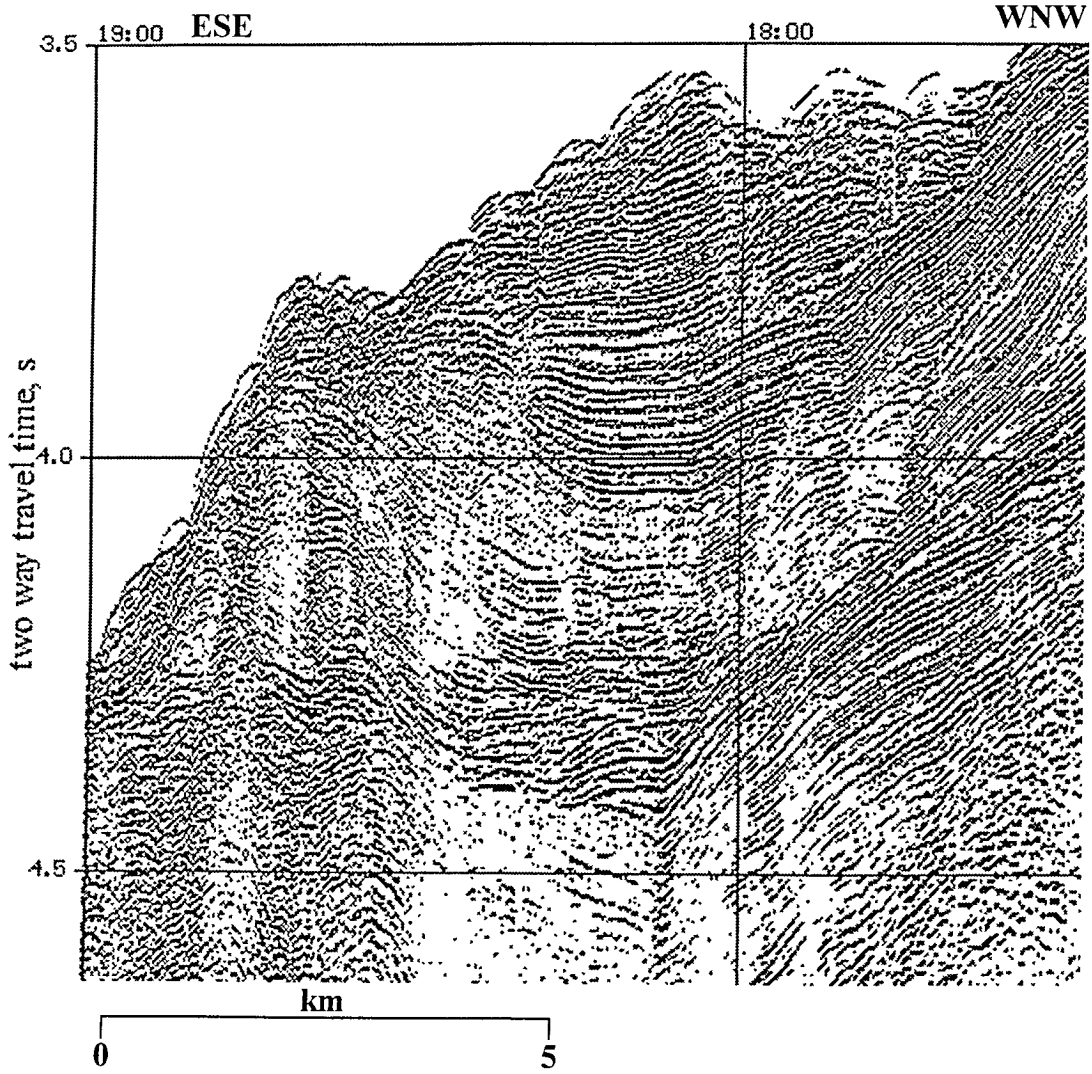

Fig. 3.2.2.7: Part of reflection seismic profile 30 showing the upper seismic sequences in a canyon incised into the northern slope of the Kurile Basin. See Fig. 3.2.2.2 for profile location.

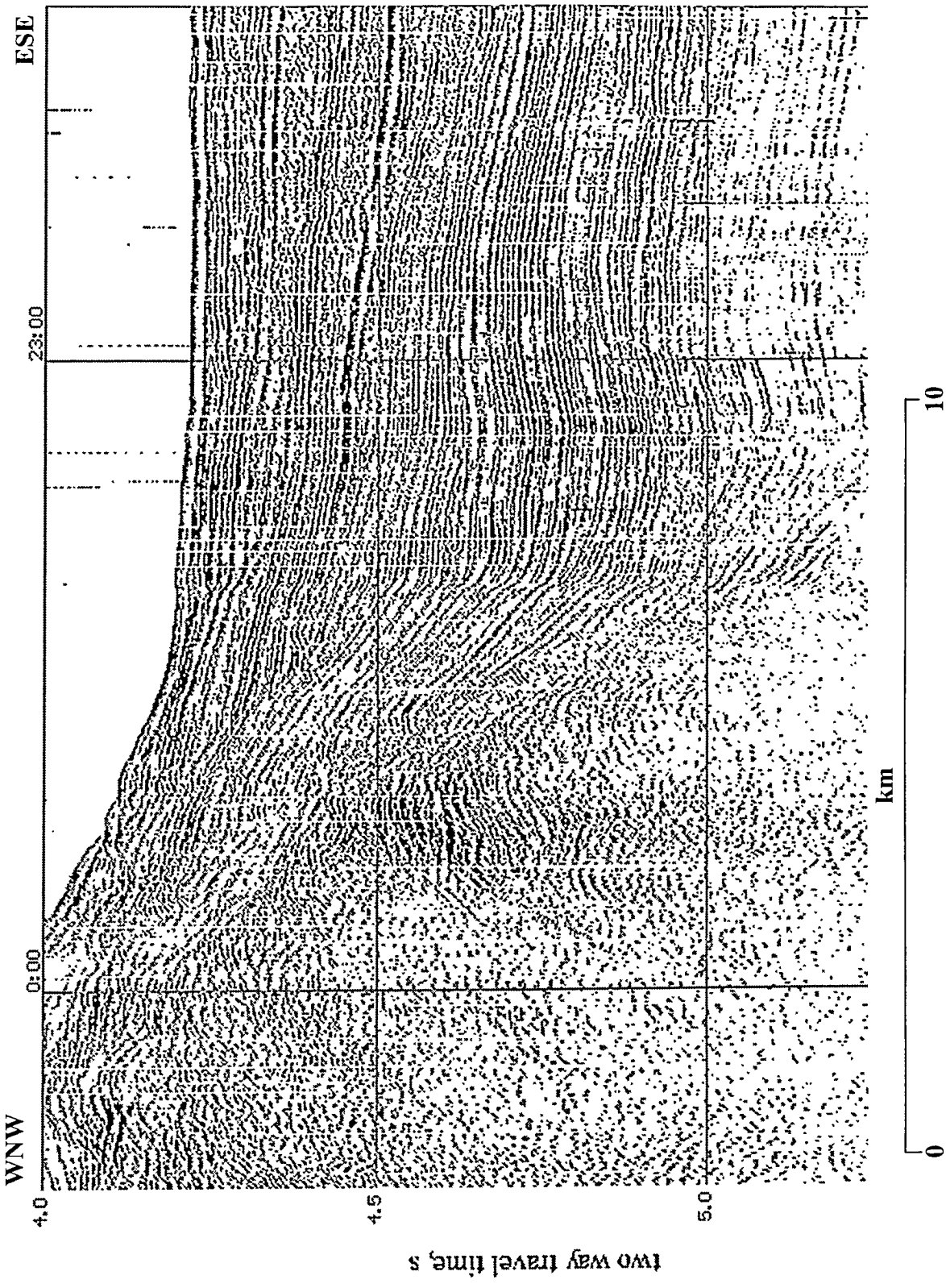

Fig. 3.2.2.8: Part of reflection seismic profile 32 showing seismic sequences at the base of the northern slope of the Kurile Basin. See Fig. 3.2.2.2. for profile location.

3.2.3 Deep Kurile Basin

B. Karp and V. Karnaukh

The study area here is located in the central Kurile Basin within the depth range of 3,350-3,360 m (Fig. 3.2.2.1). The acoustic basement can be followed on all profiles and is represented by an envelope of diffraction hyperbolas. There is a linear basement rise which strikes north-south and widens in the northern direction (Fig. 3.2.3.1). To the west the rise is bounded by a chain of isometric depressions and highs; to the east, there is a linear basement depression. Another smaller isometric high occurs to the north.

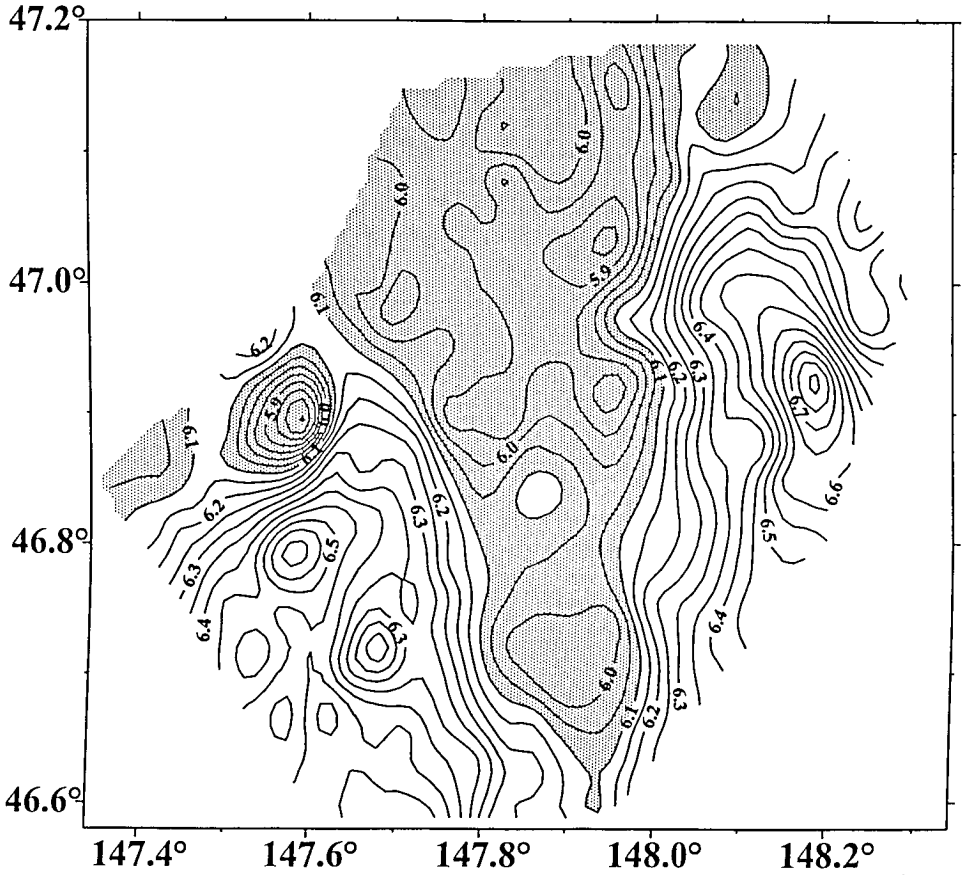

Fig.3.2.3.1: *Basement depth distribution in the study area of the deep Kurile Basin at 0.1 sec TWT intervals. Areas with an acoustic basement depth <6.1 sec are shaded.*

The thickness of sediments above the linear rise does not exceed 1.6 s. However, it reaches 2.3 s (Fig. 3.2.3.2) in the eastern basement depression. To convert thickness in two-way travel times to absolute thicknesses, experimental data on P-wave velocities of the sedimentary layer were used (see section: 3.2.4) (Fig. 3.2.3.3). The sediments thickness above the rise does not exceed 1.8 km, the maximum thickness found in the eastern depression is 3.0 km.

The upper sedimentary layer of the deep basin consists of two sequences: an upper, well-stratified sequence and a lower, semi-transparent sequence (Fig. 3.2.3.4). The thickness of the upper sequence is nearly constant at 0.9-1.1 s. Fluctuations in the general thickness of the sedimentary layer are largely a result of variations in the thickness of the semi-transparent layer.

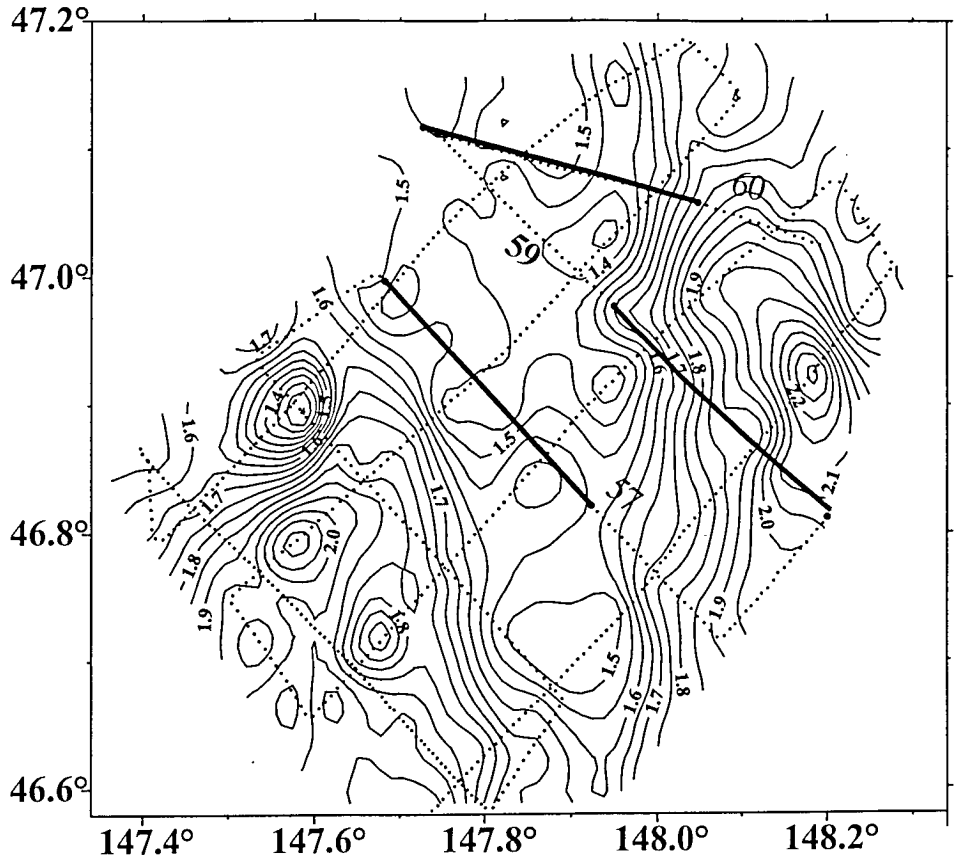

Fig.3.2.3.2: *Isopach map of the sedimentary cover of the study area in the deep Kurile Basin at 0.05 sec TWT intervals. Dotted lines with numbers are seismic profile locations. Bold lines are selected profiles shown in Figs. 3.2.3.4 - 3.2.3.6 and 3.2.3.11.*

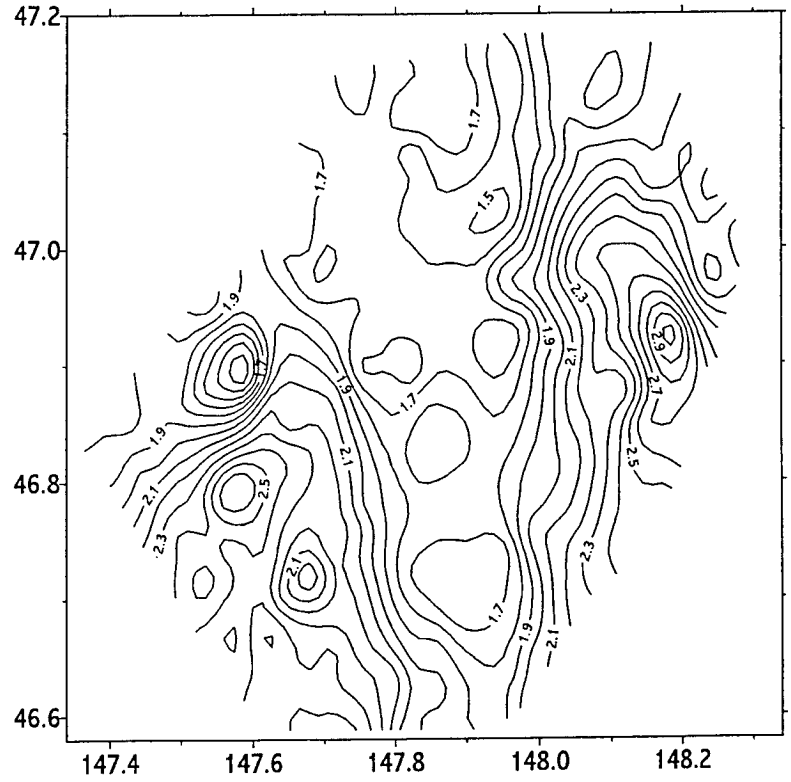

Fig. 3.2.3.3: *Isopach map of the sedimentary layer of the deep Kurile Basin at 0.1 km intervals.*

The well-stratified sequence consists of a series of subparallel, subhorizontal reflectors. In contrast, the semi-transparent sequence comprises only occasional, low-amplitude, continuous reflectors that drape the acoustic basement. On most profiles, the boundary between these two sequences is marked by a high-amplitude, low-frequency reflector.

The well-stratified sequence may be subdivided into four units (B1, B2, B3 and B4) which differ in the thickness of the intercalated transparent layers between reflectors (Fig. 3.2.3.5). Such transparent intercalations represent pelagic to hemipelagic sediments. Thus, it may be postulated that during the sedimentation of the lower-frequency units B2 and B4, the influx of debris into the Kurile Basin was more restricted. This suggests times of sea level highstands.

The upper sedimentary column within the study area is repeatedly interrupted by vertical regions of acoustic turbidity in which diffraction hyperbolas dominate (Fig. 3.2.3.6). Typical are also the accompanying apparent deformations and interruptions of the flat-lying horizons. Seismically turbid areas correlate well with areas having variations in the depth of the acoustic basement.

Since diffraction occurs when seismic waves encounter an abrupt change in reflector geometry (corner points), the turbid zones must mark zones of reflector discontinuity or zones in which the sedimentary column is dissected by numerous vertical fissures. These fissures usually terminate near the base of unit B2.

The seismic characteristics of the sedimentary cover just described persist for approximately 75 km along profile 61. As the slope is approached, both the amplitude and the frequency of the semi-transparent sequence increase. At approximately 70 km from the basin slope, a chaotic layer with a thickness of 0.4-0.45 s representing successive deposition of two fans appears between the upper and lower sequences (Fig. 3.2.3.7). Near the slope base, the seismic section consists of (from top to bottom) an opaque unit, an upper semi-transparent unit, a well-stratified unit, and a lower semi-transparent unit. These units are separated from one another by unconformities. The opaque unit consists mostly of a chaotic facies, while the other units are composed of subparallel reflectors. All units onlap the slope (Fig. 3.2.3.8).

Profiles 39 and 41 located at the center of the Kurile Basin to the east and to the west of our study area show three units: an upper, well-stratified unit, a semi-transparent unit and a lowermost transparent unit. The basement was not reached on these profiles; the total sediment thickness here is > 3.5 s. The upper unit consists of subparallel, subhorizontal reflections, it is about 1 s TWT in thickness. A thin, chaotic layer apparently representing a distal fan is intercalated between the well-stratified and the semi-transparent units on profile 41. The semi-transparent unit is characterized by moderate-amplitude continuous reflectors and a high-amplitude lower boundary. Its thickness is about 1.0 s. The transparent unit, on the other hand, is made up of low-amplitude discontinuous reflectors.

Profile 43 (Fig. 3.2.2.1) crosses two morphological rises which strike NW-SE, stretching from the slope of Iturup Island into the Kurile Basin. Both rises are expressed in basement relief as tilted blocks (Fig. 3.2.3.9). The slopes of these blocks consist of an upper well-stratified

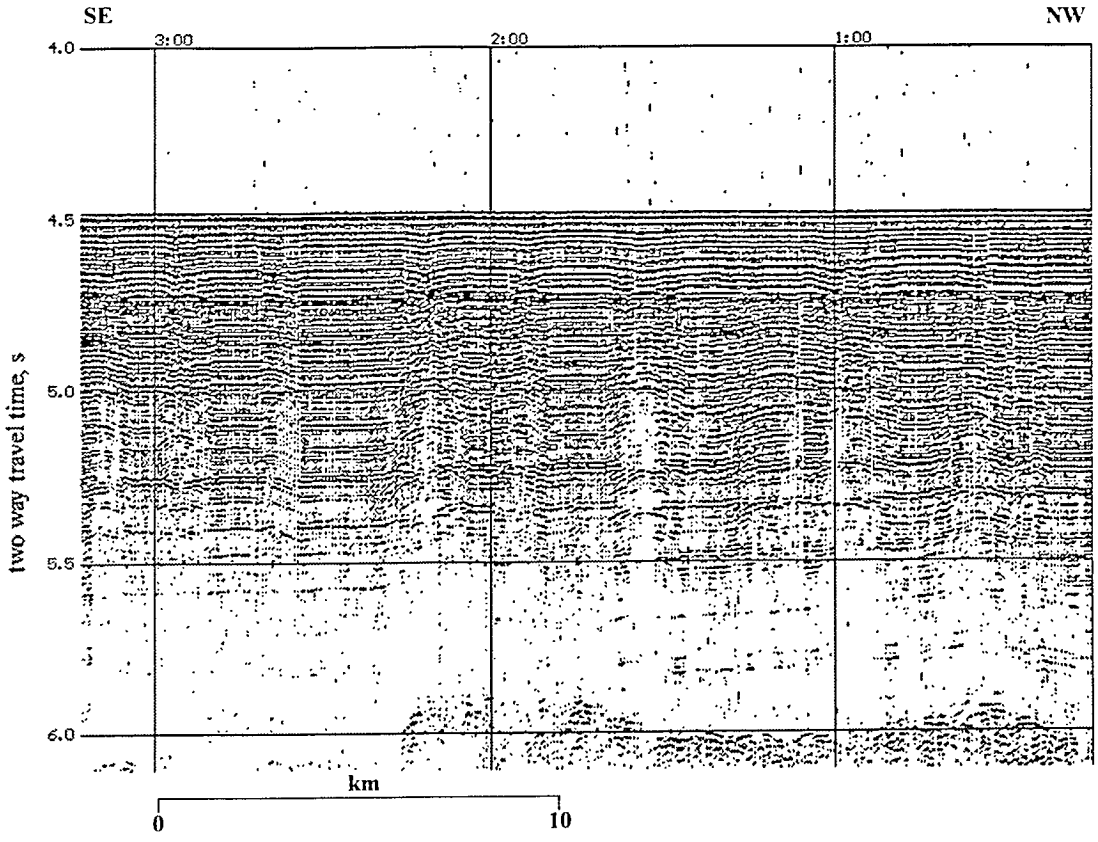

Fig. 3.2.3.4: *Part of reflection seismic profile 57 showing seismic sequences in the Kurile Basin. See Fig. 3.2.3.2 for profile location.*

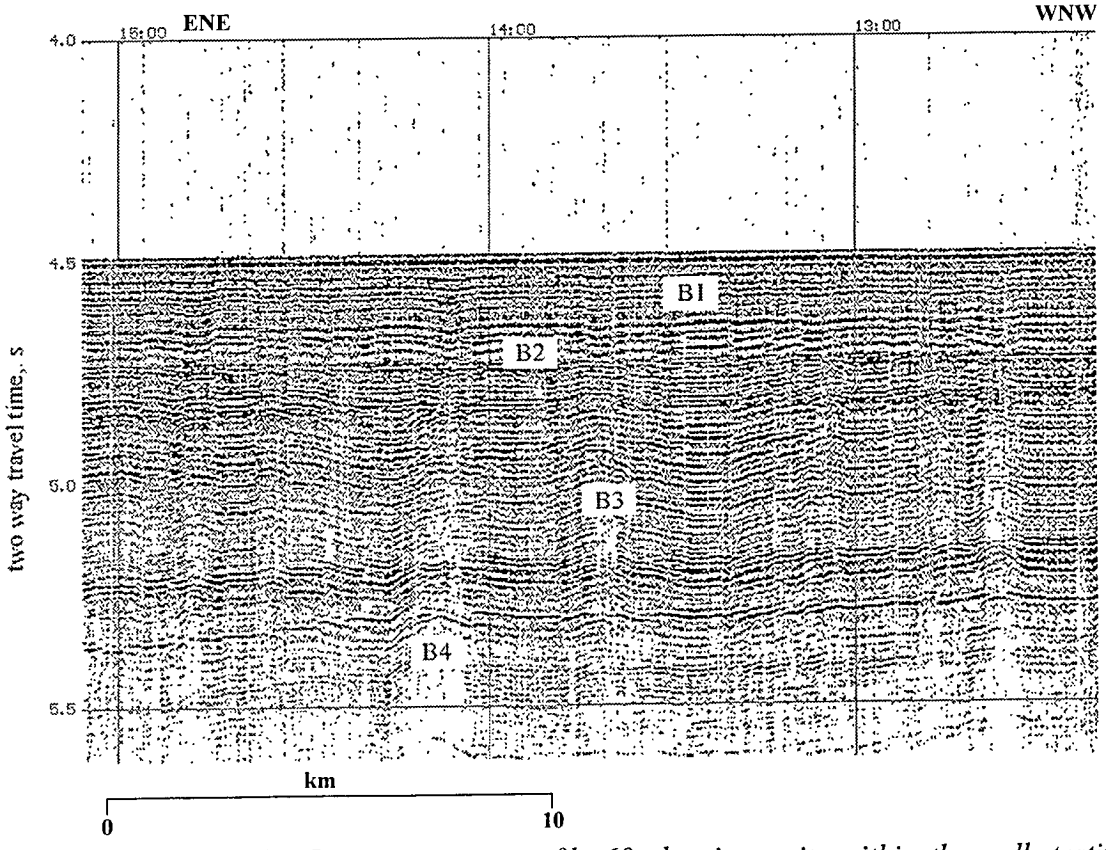

Fig. 3.2.3.5: *Part of reflection seismic profile 60 showing units within the well-stratified sequence of the Kurile Basin. See Fig. 3.2.3.2 for profile location.*

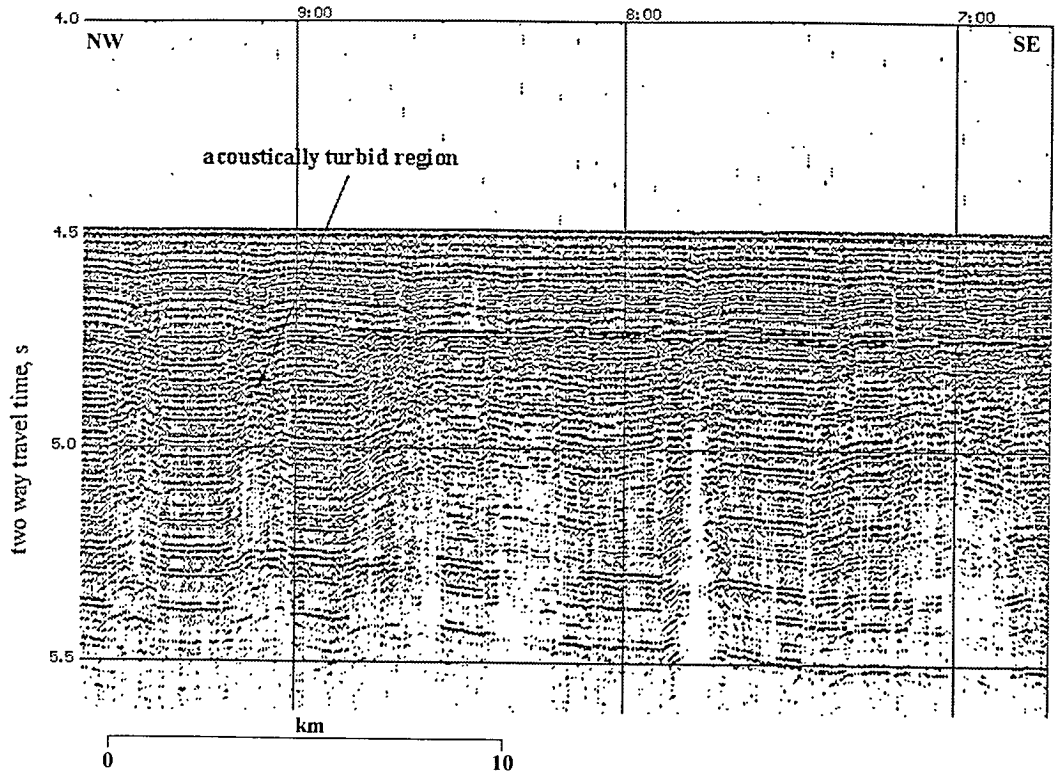

Fig. 3.2.3.6: Part of reflection seismic profile 59 showing vertical acoustically turbid regions within the well-stratified sequence of the Kurile Basin. See Fig. 3.2.3.2 for profile location.

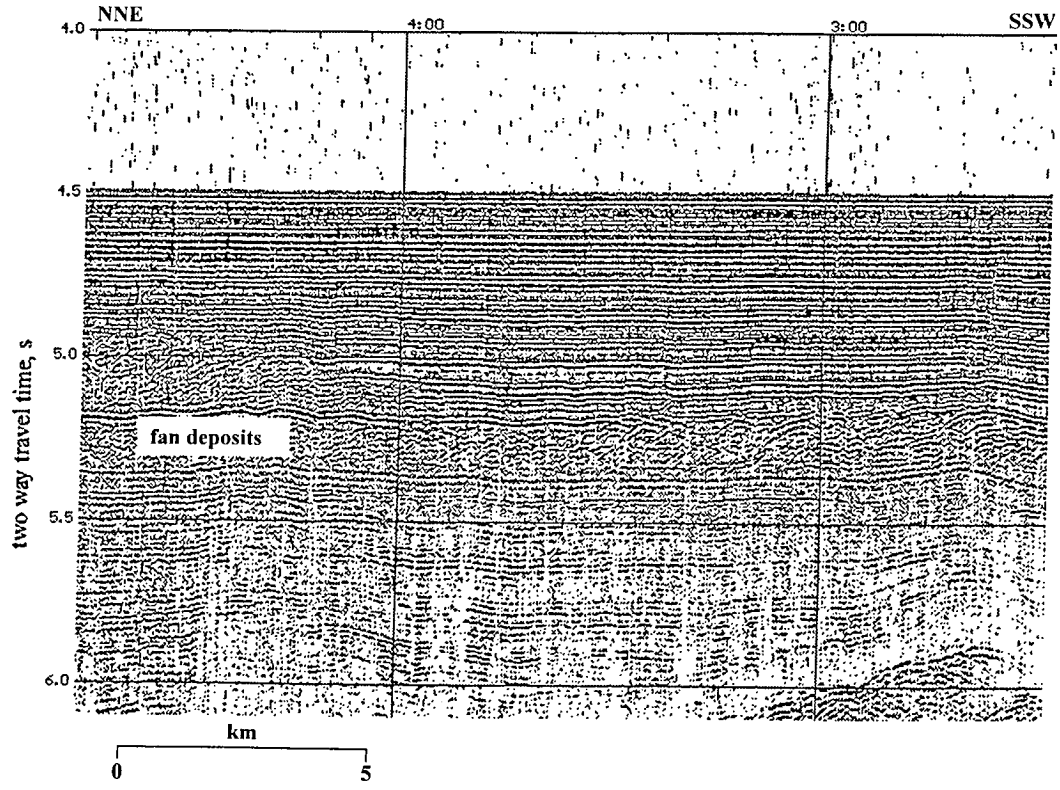

Fig. 3.2.3.7: Part of reflection seismic profile 61 showing fan deposits near the base of the northern slope of the Kurile Basin. See Fig. 3.2.2.1 for profile location.

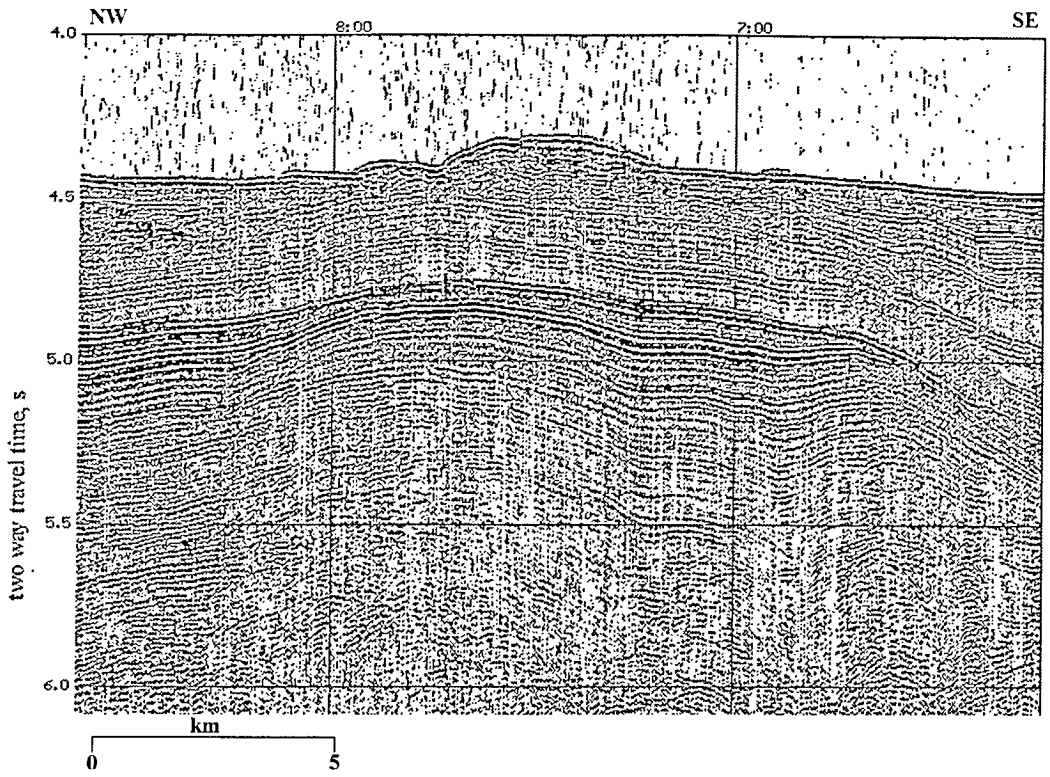

Fig. 3.2.3.8: Part of reflection seismic profile 62 showing seismic sequences at the base of the northern slope of the Kurile Basin. See Fig. 3.2.2.1 for profile location.

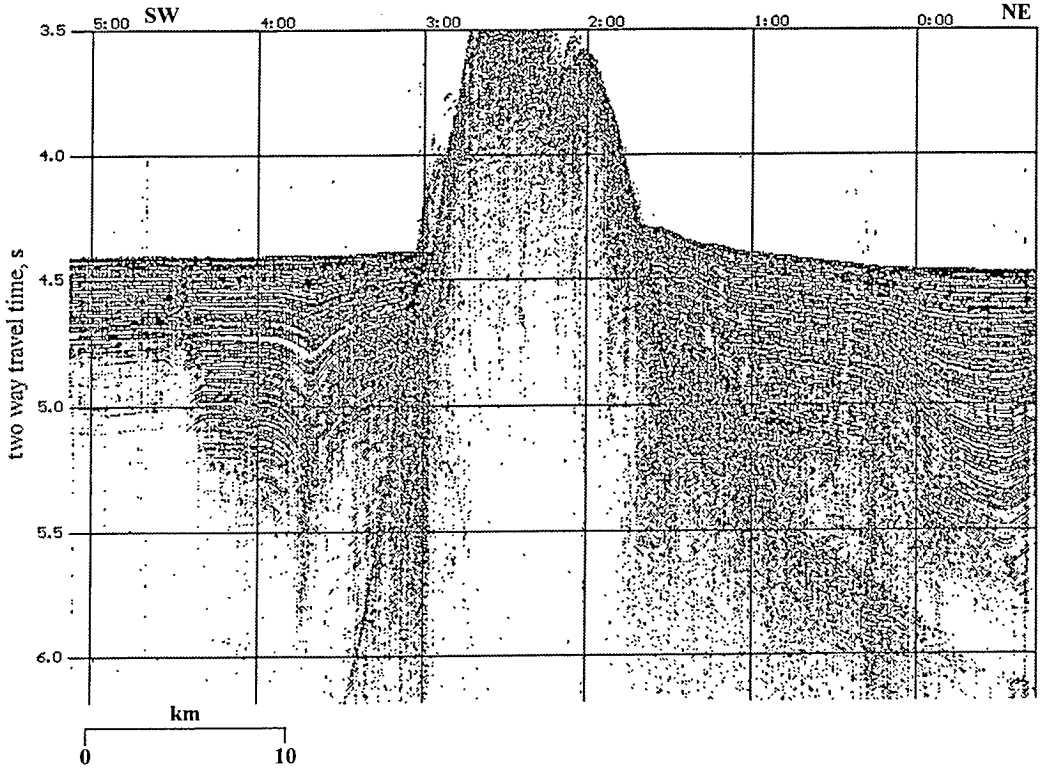

Fig. 3.2.3.9: Part of reflection seismic profile 43 showing a tilted block in the Kurile Basin. See Fig. 3.2.2.1 for profile location and the text for explanations.

unit and a lower acoustically transparent unit (Fig. 3.2.3.10). The stratified unit is subdivided into two parts by an angular unconformity. The reflectors below this unconformity curve downward, suggesting synsedimentary vertical fault movements. Between the two rises, the reflectors in the well-stratified unit are subhorizontal. The thickness of this unit increases gradually in the southwesterly direction from 0.8 to 1.0 s. Because the acoustic basement is not reached here, the thickness of the lower transparent unit is unknown.

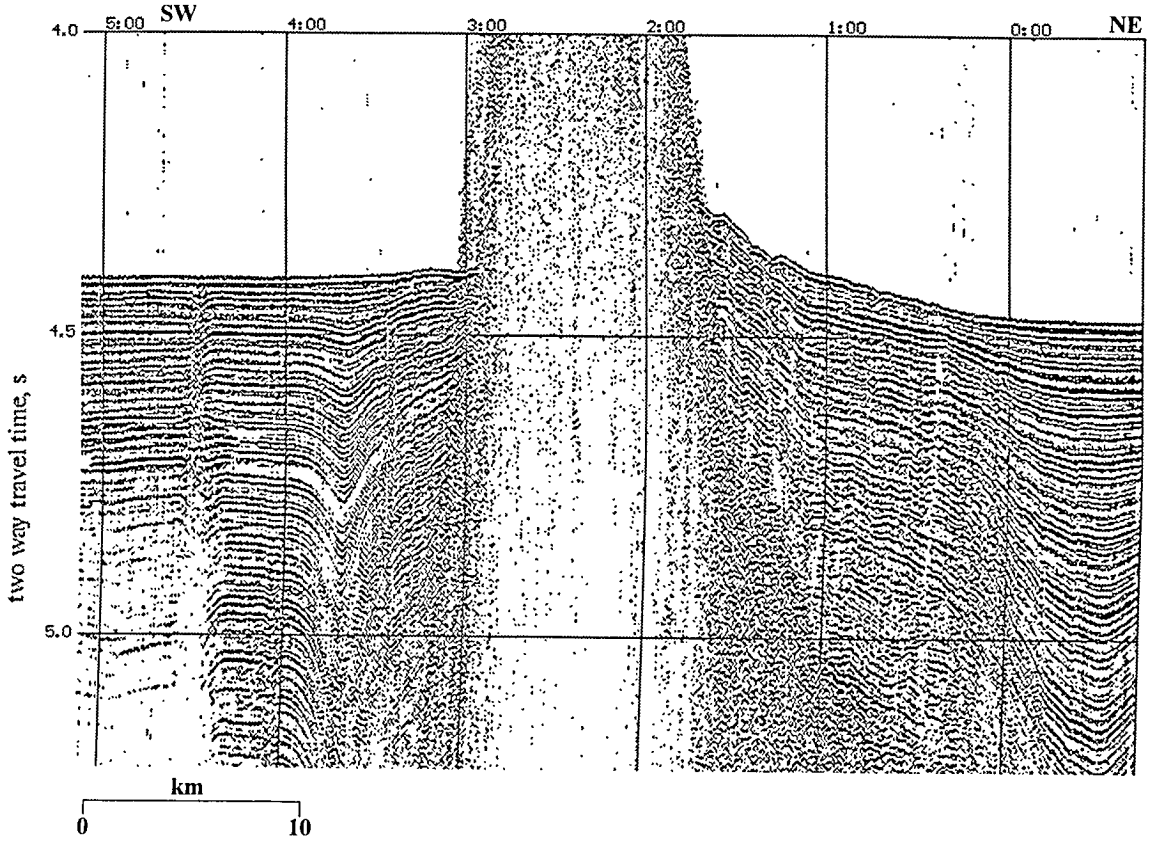

Fig. 3.2.3.10: *Part of reflection seismic profile 43 showing seismic sequences in the vicinity of a tilted block in the Kurile Basin.*

3.2.4 Compressional wave velocities of the sedimentary cover of the deep Kurile Basin

B. Karp and V. Prokudin

There are hitherto very few measurements on seismic velocities within the sedimentary cover of the Kurile Basin. All published velocities were obtained using the refraction method by means of air guns and sonobuoys (Bikkenina et al., 1987; Honza et al., 1978). Honza et al. (1978)

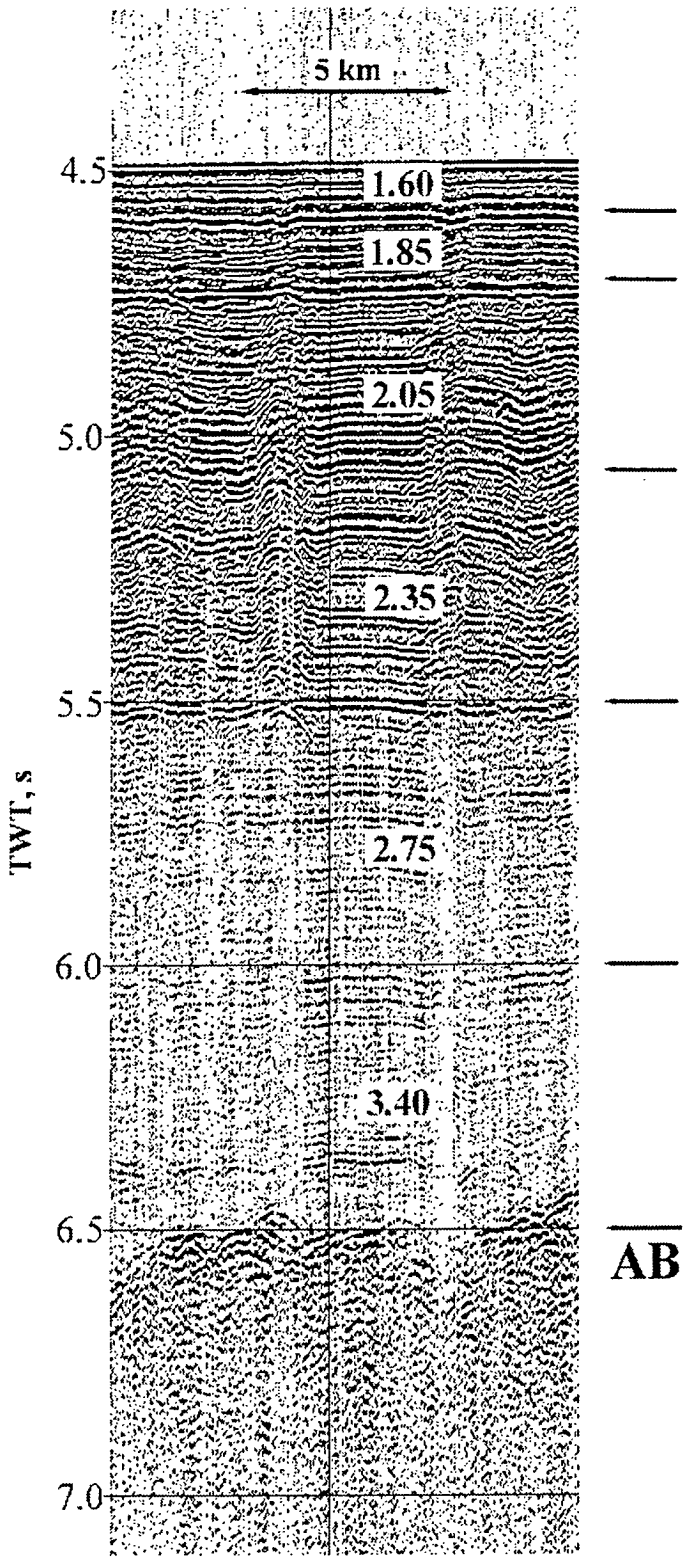

Fig. 3.2.4.1: *Part of reflection seismic profile 58 showing the correlation between sonobuoy and seismic reflection data. Numbers within the seismic section are compressional wave velocities in km/s (SB1: see Table 3.2.4.1, chapter 3.2.4 and Fig. 3.2.2.1 for location). Arrows show locations of reflecting boundaries, AB - acoustic basement. See Fig. 3.2.3.2 for profile location.*

obtained an average velocity of 1.9 km/s for the 2.54 km thick sedimentary layer and a velocity of 4.1 km/s for the acoustic basement. Bikkenina et al. (1987) determined the velocity structure along a profile crossing the western Kurile Basin. Their results from a water depth of 3 km suggest that the 4.2 km thick sediment cover can be divided into three layers with seismic velocities of 1.7, 2.2 and 4.25 km/s respectively. The velocity of the acoustic basement is 5.2 km/s.

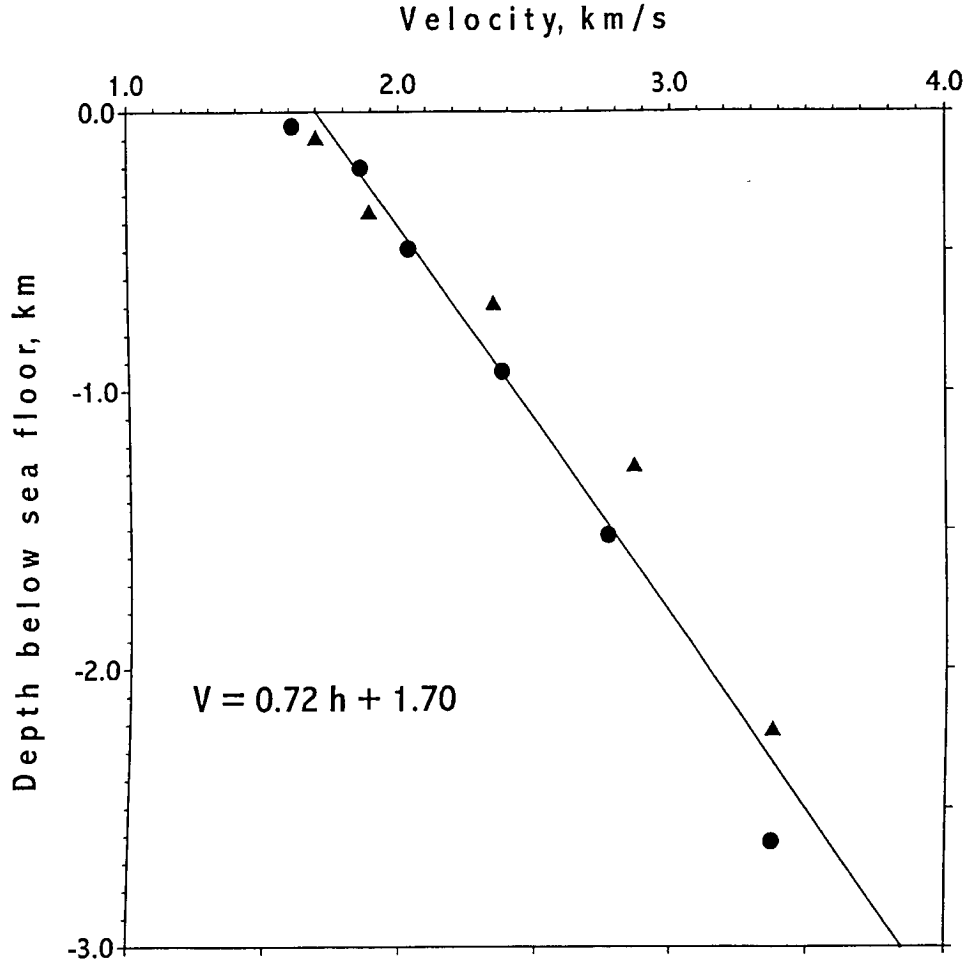

Fig. 3.2.4.2: Compressional wave velocity vs. depth below seafloor in the Kurile Basin.

Scientists of the Pacific Oceanologic Institute measured seismic velocities of the sedimentary cover in the Kurile Basin using the reflection wave method during a cruise of the RV *Professor Gagarinsky* in 1988 (Fig. 3.2.2.1, sonobuoy stations SB1 and SB2) (S. Medvedev & V. Prokudin, unpubl. data). This work was carried out using sonobuoys and an air gun with a volume of 3 *l*. Split travel-time curves were used for the calculation of velocities. The results are shown in Tab. 3.2.4.1. Vertical travel times for waves reflected from the layer boundaries correlate well with seismic profiles obtained during the cruise (Fig. 3.2.4.1). The velocities obtained within the sedimentary cover increase with layer depth (Fig. 3.2.4.2). The linear

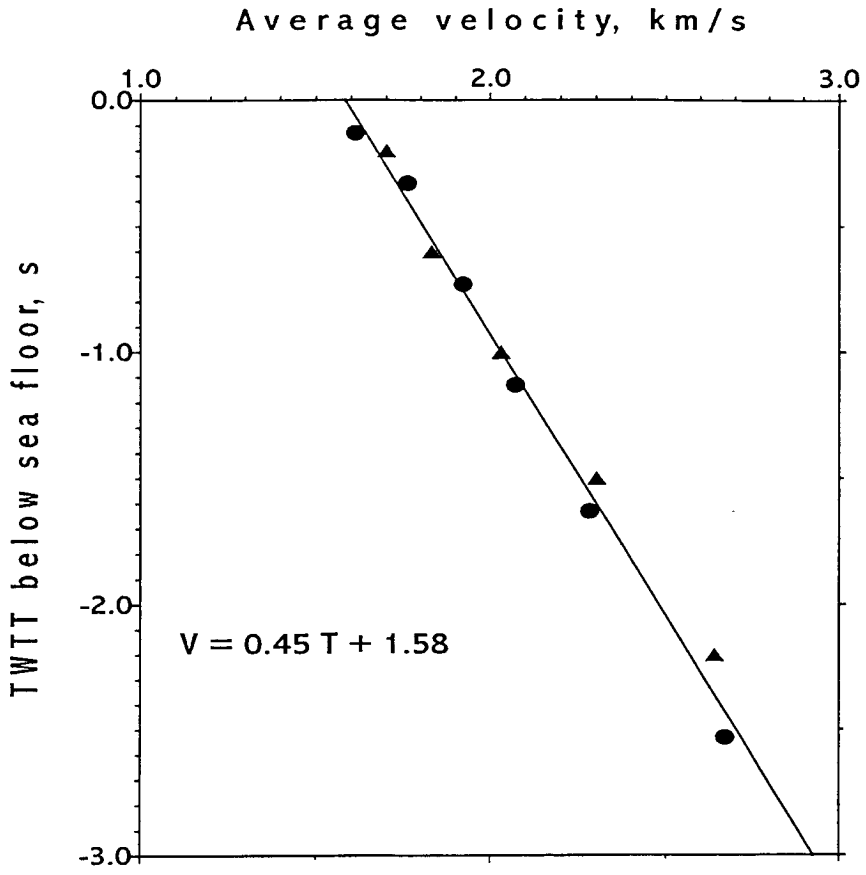

Fig. 3.2.4.3: Average compressional wave velocity vs. two way travel time (TWT) below seafloor in the Kurile Basin.

regression calculated with the minimum root mean square method gives a good fit to the observed data. The average velocity/two-way travel time relationship obtained from the experimental data is shown in Fig. 3.2.4.3.

The depth (h) of the reflecting boundaries recorded on seismic profiles in metric units can be determined from the two-way travel time using the following equation derived from linear regression:

$$h\ (km) = Vt/2 = 0.78\ t + 0.22\ t^2$$

Tab. 3.2.4.1: Seismic velocities of the sedimentary cover in the Kurile Basin (S. Medvedev & V. Prokudin, unpubl. data).

h*, km	To, s*	V, km/s	Δh, km	ΔTo, s	
3.277	4.37				
		1.61	0.1	0.13	
3.377	4.5				
		1.86	0.19	0.2	SB1
3.567	4.7				45° 32.1′ N
		2.05	0.41	0.4	146° 59.6′ E
3.977	5.1				
		2.37	0.47	0.4	
4.447	5.5				
		2.76	0.69	0.5	
5.137	6.0				
		3.37	1.52	0.9	
6.657	6.9				
3.375	4.5				
		1.7	0.17	0.2	
3.545	4.7				
		1.89	0.378	0.4	
3.923	5.1				
		2.34	0.468	0.4	SB2
4.391	5.5				47° 0.3′ N
		2.86	0.71	0.5	147° 22′ E
6.001	6.0				
		3.37	1.18	0.7	
7.181	6.7				

* h: depth of upper boundary of layer; To: two-way travel time of upper boundary of layer

3.3 Gravimetry and magnetics

S. Nikolaev and T. Kolpashikova

Gravity and magnetic measurements were carried out simultaneously with the bathymetric survey in the northern and southern parts of the Okhotsk Sea. They include regional profiles and detailed profiles within the study areas. The regional profiles were oriented in the north-south direction parallel to Sakhalin Island and in the east-west direction along the strike of the Kurile Basin.

A total of 2,256 nautical miles of data were obtained. Magnetic anomalies can be calculated after the regional magnetic field and its temporal variations are subtracted from the measured field values, a process that will take place in the home laboratory in Vladivostok. The gravity anomaly field will be calculated after the gravity observations at the base station in Vladivostok are completed.

Below we present the results of preliminary analyses of data for two profiles: the first in the Kurile Basin (profile 45, Fig. 3.2.2.1) and the second (profile 7) across the Derugin Basin and its northern slope in the SE-NW direction.

A considerably thick sedimentary section and with it a large distance between the source of disturbance of the potential fields and the surface of observation lead to a reduction of the anomaly effects. Consider as an example the profile 45 (Fig. 3.3.1). The large gradients of

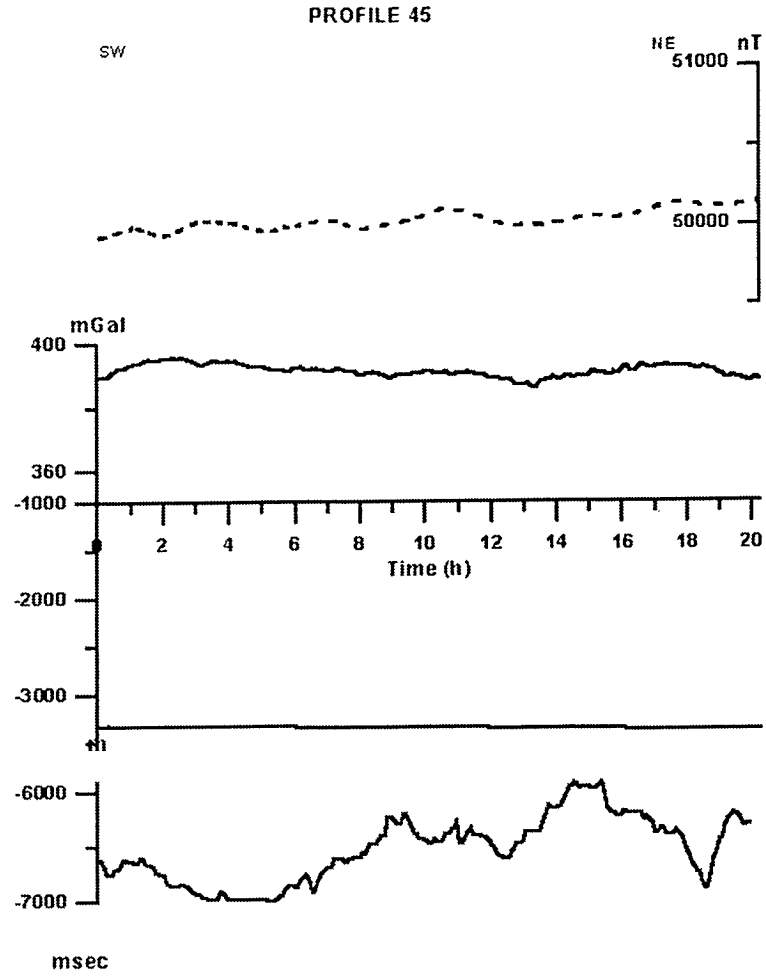

Fig. 3.3.1: Relative values of the gravity (solid line) and magnetic (dashed line) fields along profile 45 (top). Bathymetric and acoustic basement profiles (bottom). See Fig. 3.2.2.1 for profile location.

acoustic basement depths practically do not correlate with anomalies in the potential fields here. In contrast, anomalies of the potential fields on profile 7, where the sedimentary section is considerably thinner, are in good agreement with the relief of the acoustic basement (Fig. 3.3.2). Uplifted and tilted blocks of the acoustic basement are marked by positive local free air gravity anomalies with relative amplitudes of 30-80 mG and by local magnetic anomalies with amplitudes of 100-600 nT. The tilted blocks located on the southeastern part of the profile (at kilometer 20 and 100 from the beginning of profile) are accompanied by positive magnetic anomalies. Blocks located on kilometer 170 and 230 are marked by negative magnetic anomalies. Fig. 3.3.2, in particular, shows that the relationship between relief of the acoustic basement and morphology of the potential fields is rather complicated. To quantify this relationship in the GERDA area, the correlation coefficient between gravity anomalies and depth (from the sea surface) to the acoustic basement as well as between the gravity and magnetic anomalies was calculated. Fig. 3.3.3 shows that the free air anomalies are well correlated with the basement relief, suggesting that the basement is composed of relatively homogeneous rocks.

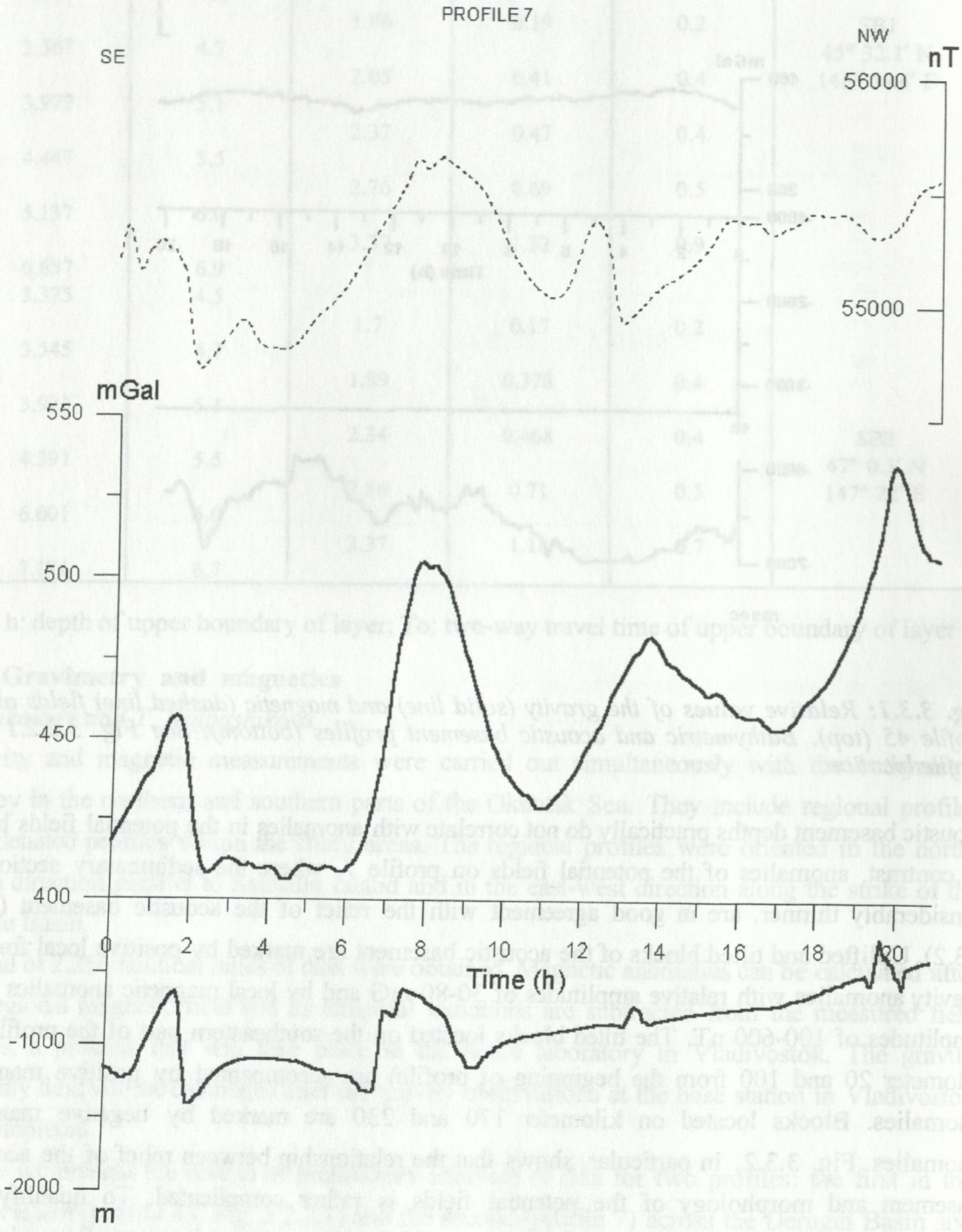

Fig.3.3.2: *Relative values of gravity (solid line) and magnetic (dashed line) fields along profile 7 (top). Acoustic basement profiles (bottom). See Fig. 3.2.1. for profile location.*

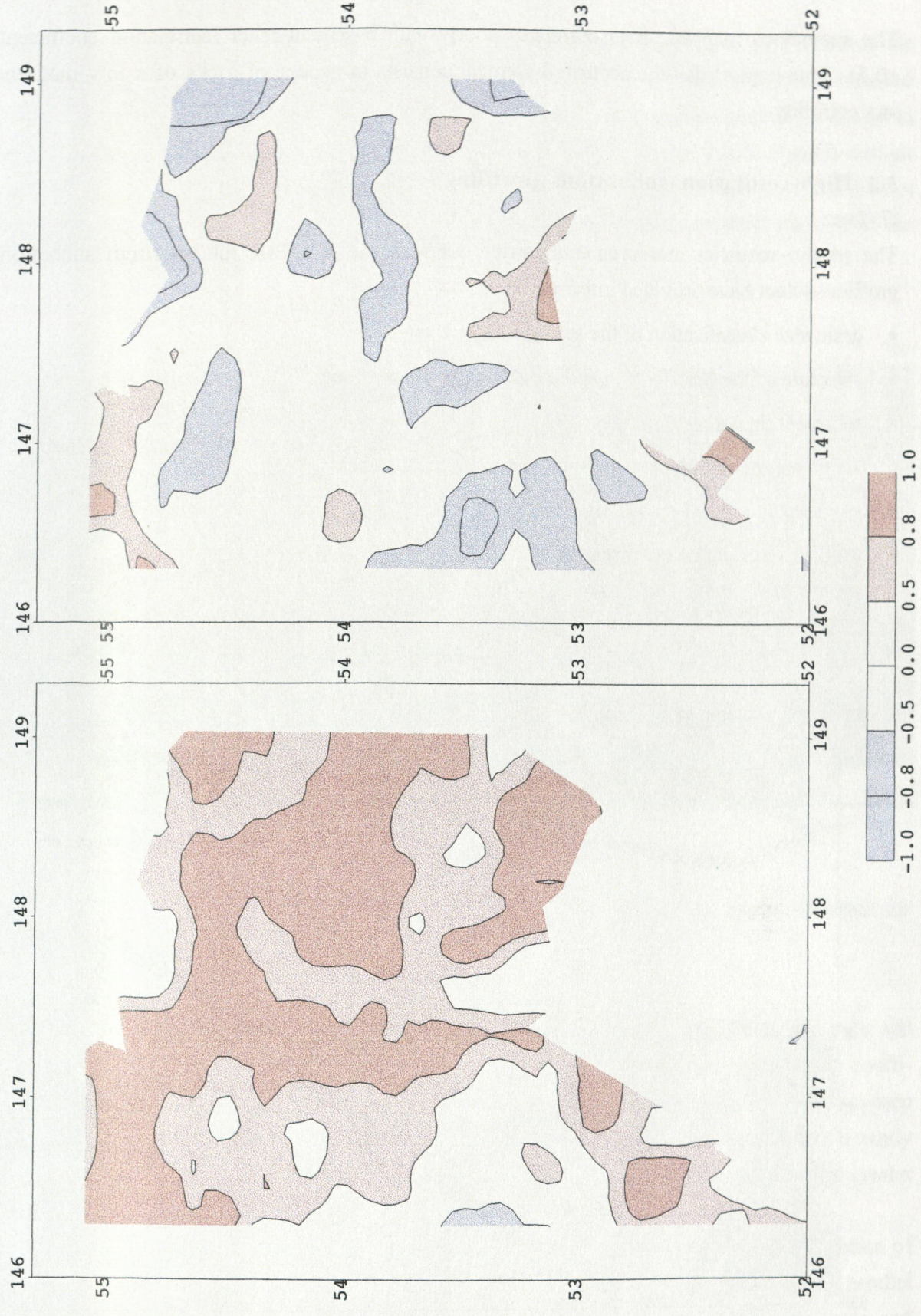

Fig. 3.3.3: *Spatial distribution of the correlation coefficient between free-air gravity anomalies and depth to the acoustic basement (left) and free-air gravity anomalies and magnetic anomalies (right) in the GERDA area.*

The anomalous magnetic field correlates poorly with basement relief (correlation coefficient: ±0.5). This implies that the acoustic basement consists in general of rocks of a low magnetic susceptibility.

3.4 High-resolution subbottom profiling

G. Ion

The seismo-acoustics measurements carried out with the X-STAR full spectrum subbottom profiler system have provided information on:

- grain size classification of the sea bottom;
- structure of the first 40 m of sediments below the seafloor;
- sediment dynamics on slopes;
- active tectonics at the level of the sea bottom to 40 m below;
- gas seep sites; and
- shallow gas hydrate occurrences.

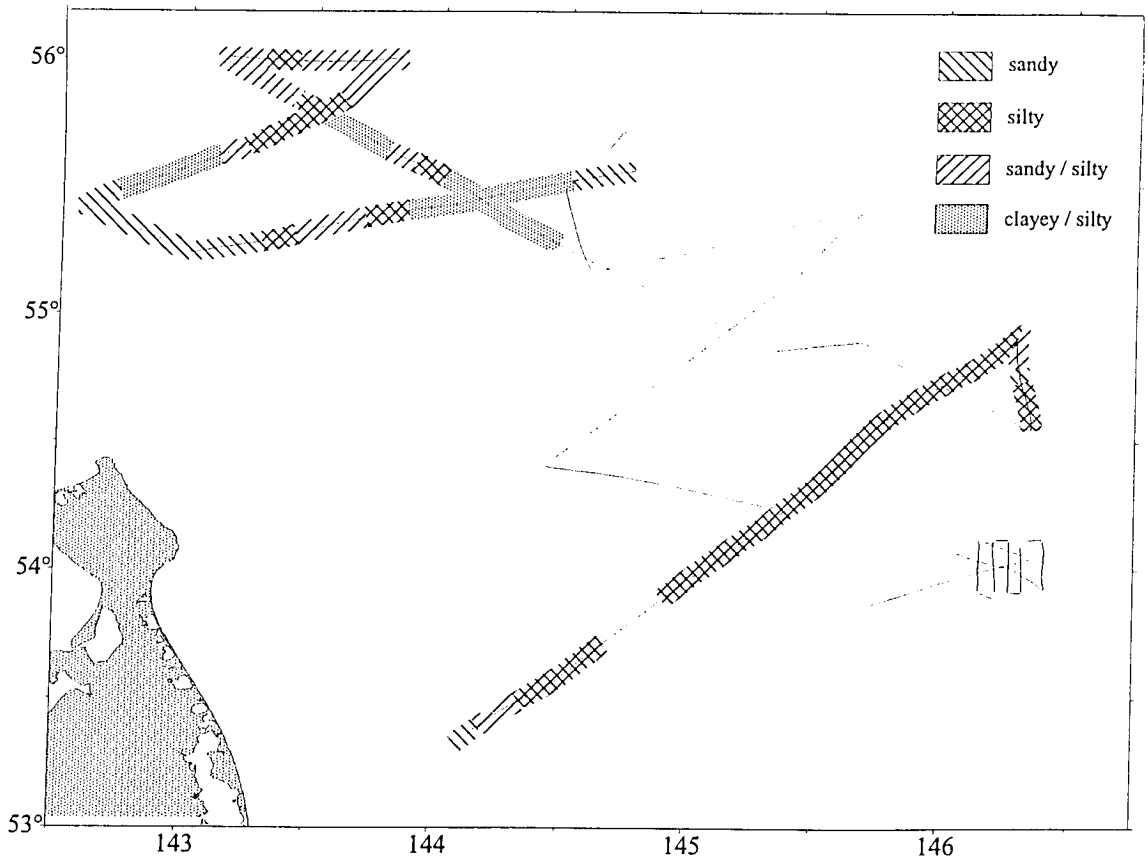

Fig. 3.4.1: *Map of sediment type distribution off northeastern Sakhalin Island based on the attenuation coefficient of the reflected waves recorded by the Chirp system.*

Sea bottom classification in terms of grain size is based on the attenuation coefficient of the reflected wave by tracking the seafloor in a computing window. The amplitude of the received signal at the interface sea water/tracked surface is compared with standard amplitudes stored in the computer. Using these values, it is possible to classify the seafloor in terms of grain size on the profiles 3-11 (Fig. 3.4.1). Unfortunately, the data for grain size classification are not always available, e.g., when bad weather conditions and steep terrain makes continuous tracking of the seafloor impossible.

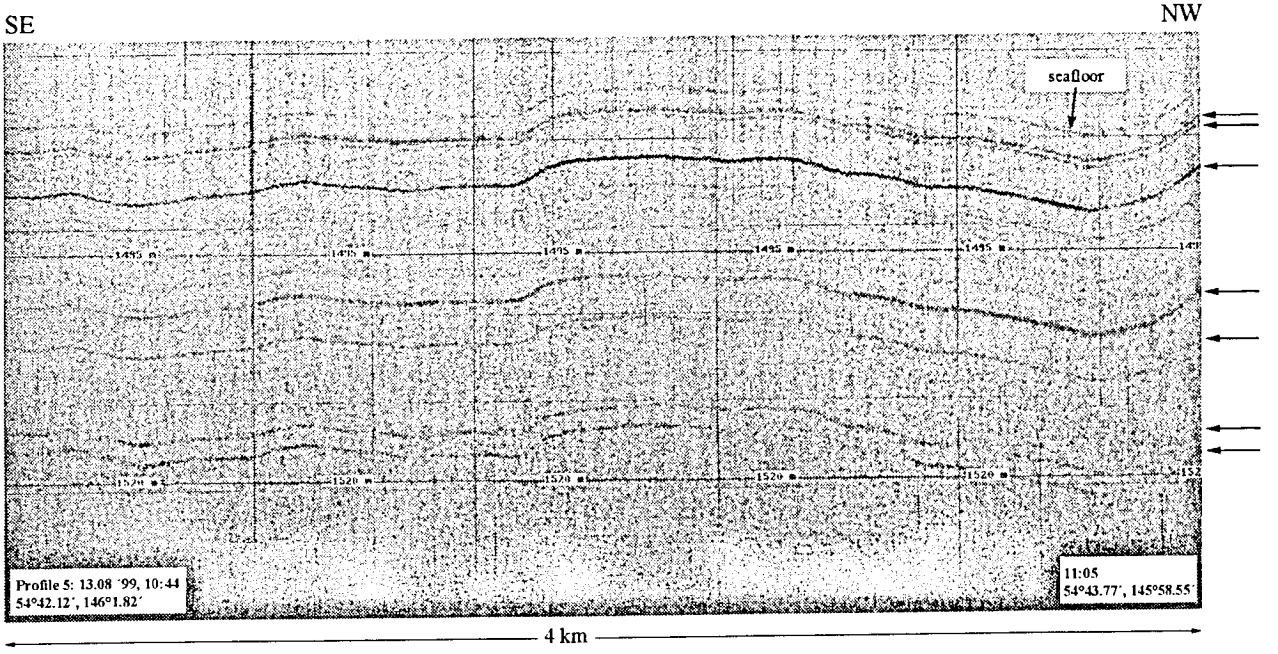

Fig. 3.4.2: Chirp record along profile 5 showing parallel to subparallel layers. See text for further explanations.

From Fig. 3.4.1 it can be inferred that the sandy areas are located generally on the tops and slopes of local highs (tectonic blocks) as well as on terrace-like features. Attenuation coefficients indicative of a silty sea bottom occurred most often. For the areas affected by deep currents, the seafloor is of erosional nature and in terms of coefficient could behave like a sandy bottom. The actual grain size, however, can be silty but more compacted because of its greater age.

The penetration of the subbottom profiler system was between 2 m and 40 m. It is a function of grain size and the degree of compaction. The observed types of structures are: parallel structures, erosional tilted structures, slope structures, tectonically-controlled structures and combined structures.

Parallel or subparallel structures are quite common over large areas and signify a constant depositional energy over a long period of time. An example of a such structure is given in Fig. 3.4.2 in which 5 thin sandy layers depicted in dark gray preceded or are covered by acoustically more transparent beds represented in light gray.

Erosional structures were observed:

- on the Sakhalin Shelf;
- on the slopes of relative highs, and
- on local terrace-like segments of the slope of the Derugin Basin.

Because of the limited coverage of the Sakhalin Shelf, we cannot assert that the entire shelf is erosional in nature. An example suggestive of this type of structure is recorded on profile 11 (Fig. 3.4.3). The Sakhalin Shelf reaches 160 m water depth. The erosional nature of its seafloor could be attributed to subaerial exposure during the sea-level lowstand of the last glaciation, combined with a sediment starvation at the present time or the occurrence of bottom currents which hinder sedimentation. Our interpretation, however, should be confirmed by coring of this very complex Holocene and Pleistocene sedimentary environment.

An erosional sea bottom is also found on quasi-horizontal segments of profiles 4 and 7 on the northern slope of the Derugin basin. The water depth is about 1,420 m and 1,200 m respectively (Figs. 3.4.4 and 3.4.5). The most probable cause for erosion at this water depth is a powerful, descending bottom current which actively erodes the seafloor. However, because of the very complex tectonics of the Sea of Okhotsk, other causes cannot be excluded. Note the breccia-like nature of the seafloor near the shoulder of the tectonic block located on the right of Fig. 3.4.5.

On gentle slopes, some penetration of the subbottom sediments could be achieved and specific structures could be recognized. An example for such a structure is presented in Fig. 3.4.6. The processes responsible are mainly gravitational but there is probably also a significant tectonic control.

Many active tectonic features in the Staretsky Trough and on the northern slope of the Kurile Basin (profiles 4-11) have been mapped. They include active faults reaching the seafloor and their accompanying deformations of the uppermost strata (Figs. 3.4.7, 3.4.8 and 3.4.9).

A very interesting tectonically-controlled structure is recorded on profile 11 over a distance of more than 7 km (Fig. 3.4.10). It is a part of a larger thrust zone characteristic of this part of the Staretsky Trough within the water depth range of 400-1,500 m and probably deeper. Two coring stations have been proposed on this profile.

Other tectonically-controlled features are shown on profile 9 at a water depth of about 490 m (Fig. 3.4.8). Here the seafloor is undulating, dune-like, and obliquely internally bedded. These dune-like features occur in an area of thrusting, although sediment reworking by bottom currents cannot be excluded.

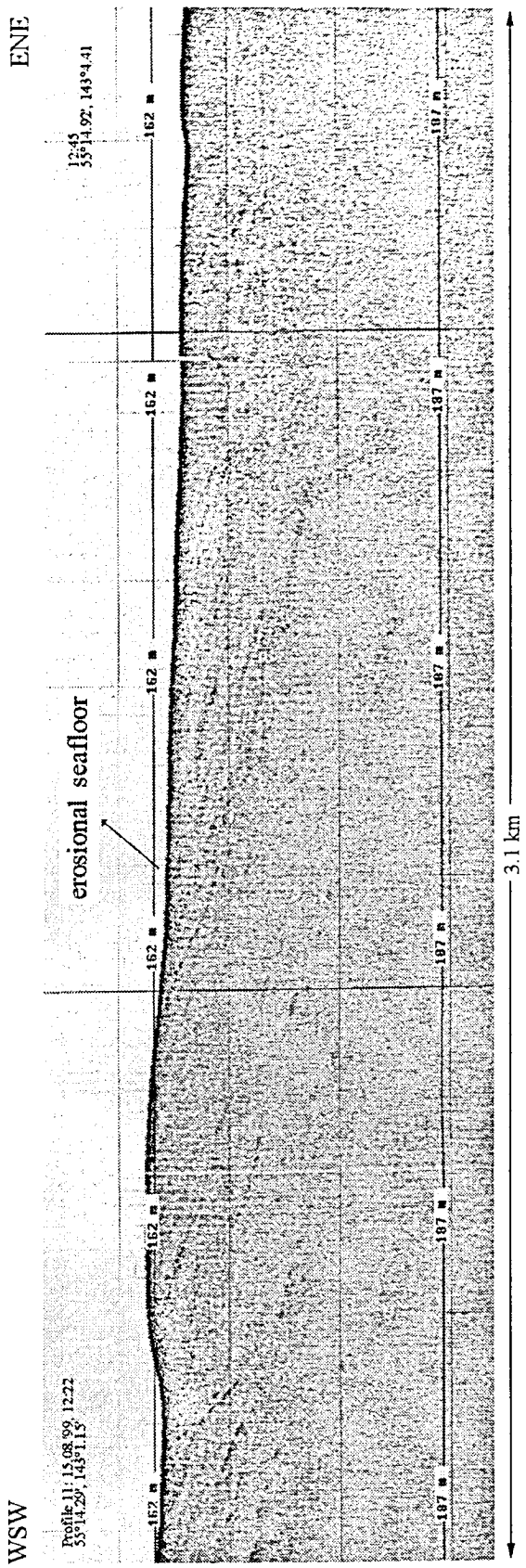

Fig. 3.4.3: *Chirp record along profile 11 showing an eroded seafloor. See text for further explanations.*

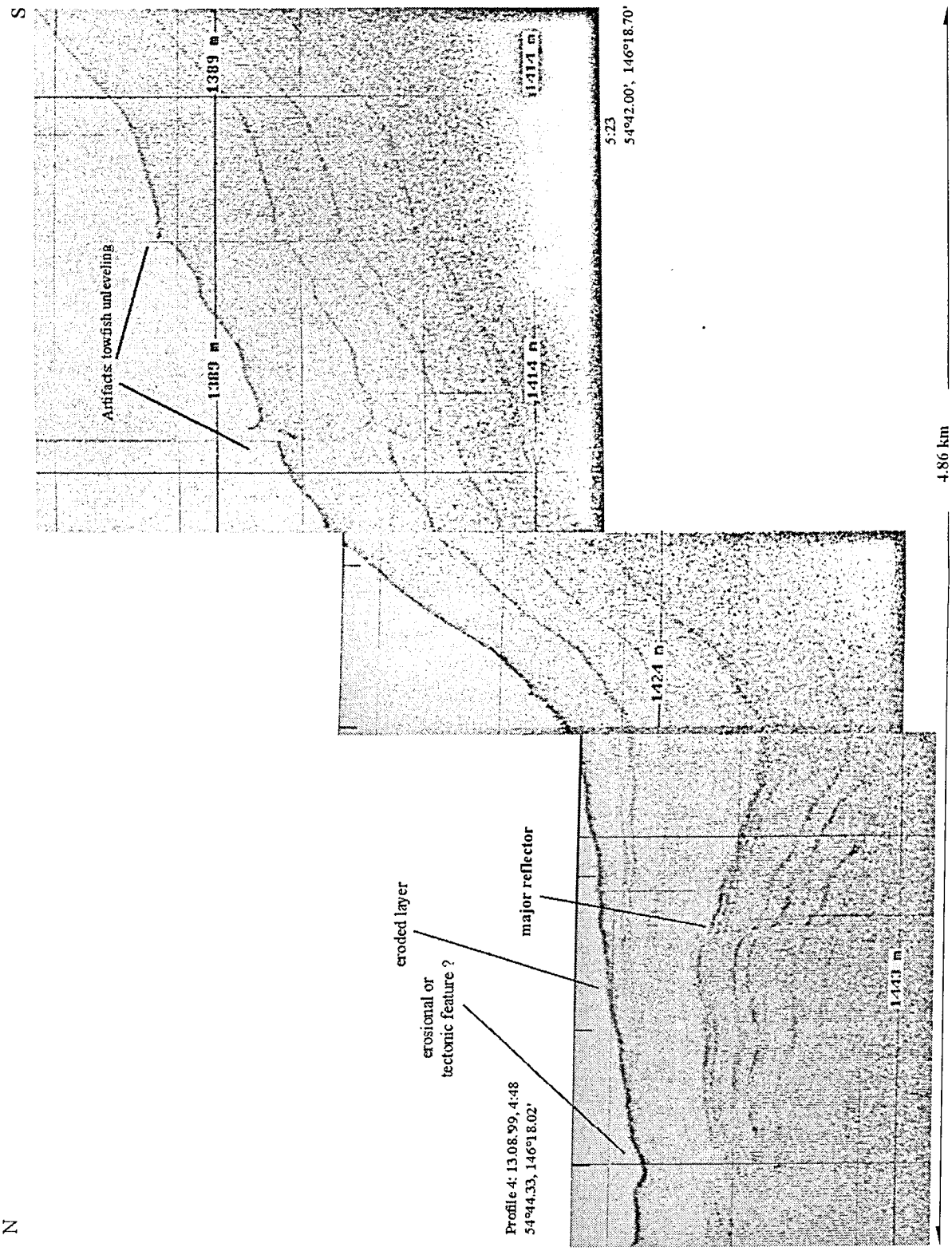

Fig. 3.4.4: Chirp record along profile 4 illustrating truncation of the youngest layers at a water depth of ca. 1,420 m. See text for further explanations.

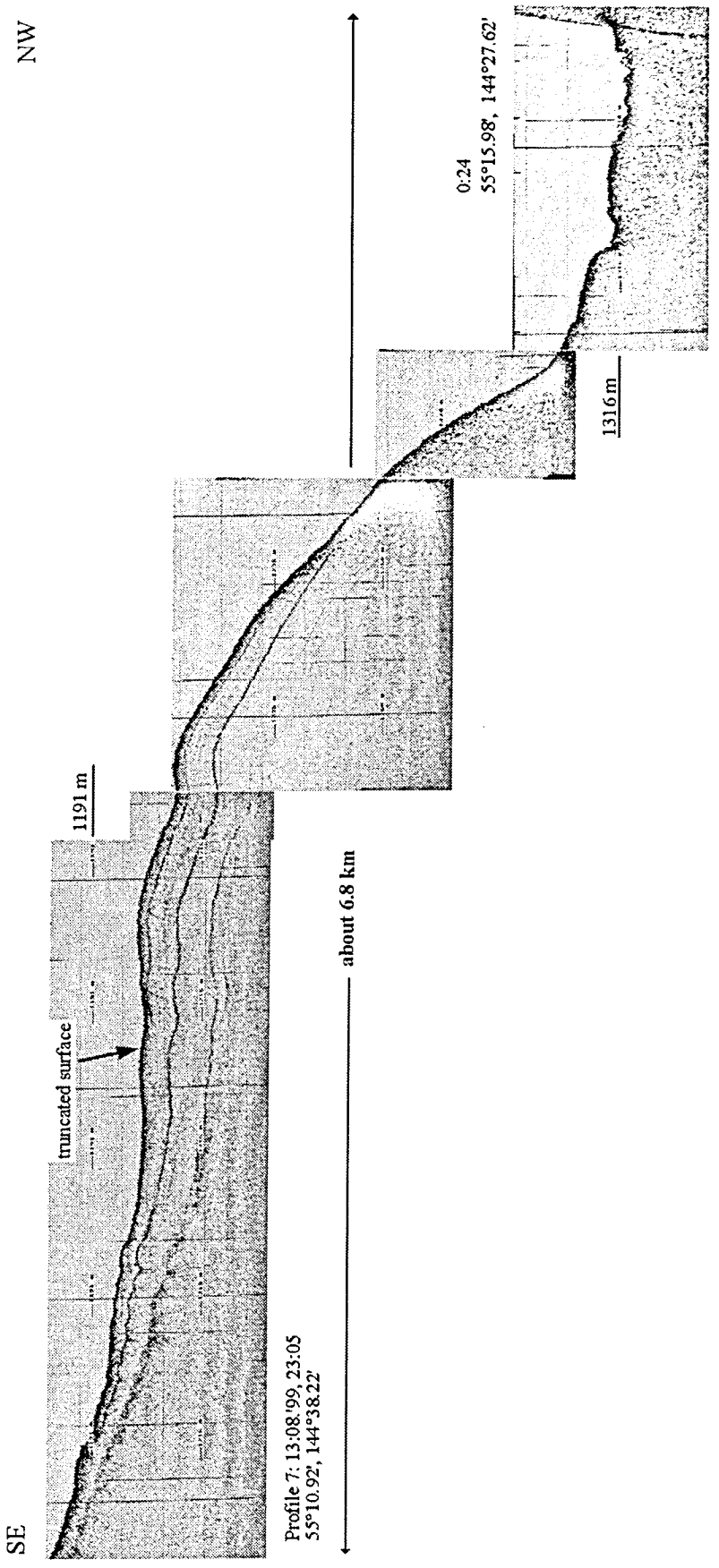

Fig. 3.4.5: *Chirp record along profile 7 showing recent erosion of the uppermost strata at a water depth of 1,200 m. See text for further explanations.*

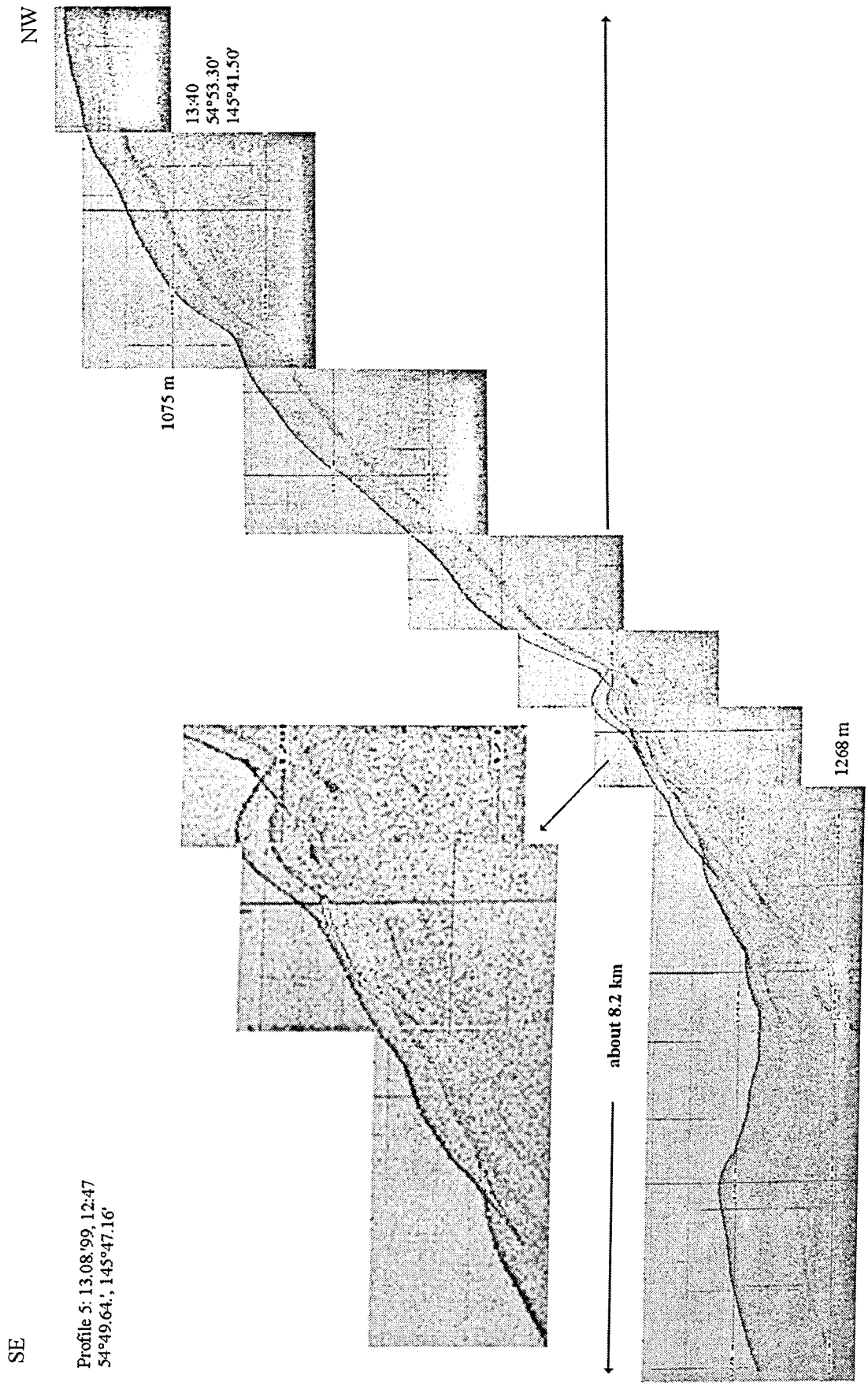

Fig. 3.4.6: *Chirp record along profile 5 showing sediment slumps at the northern slope of the Derugin Basin. See text for further explanations.*

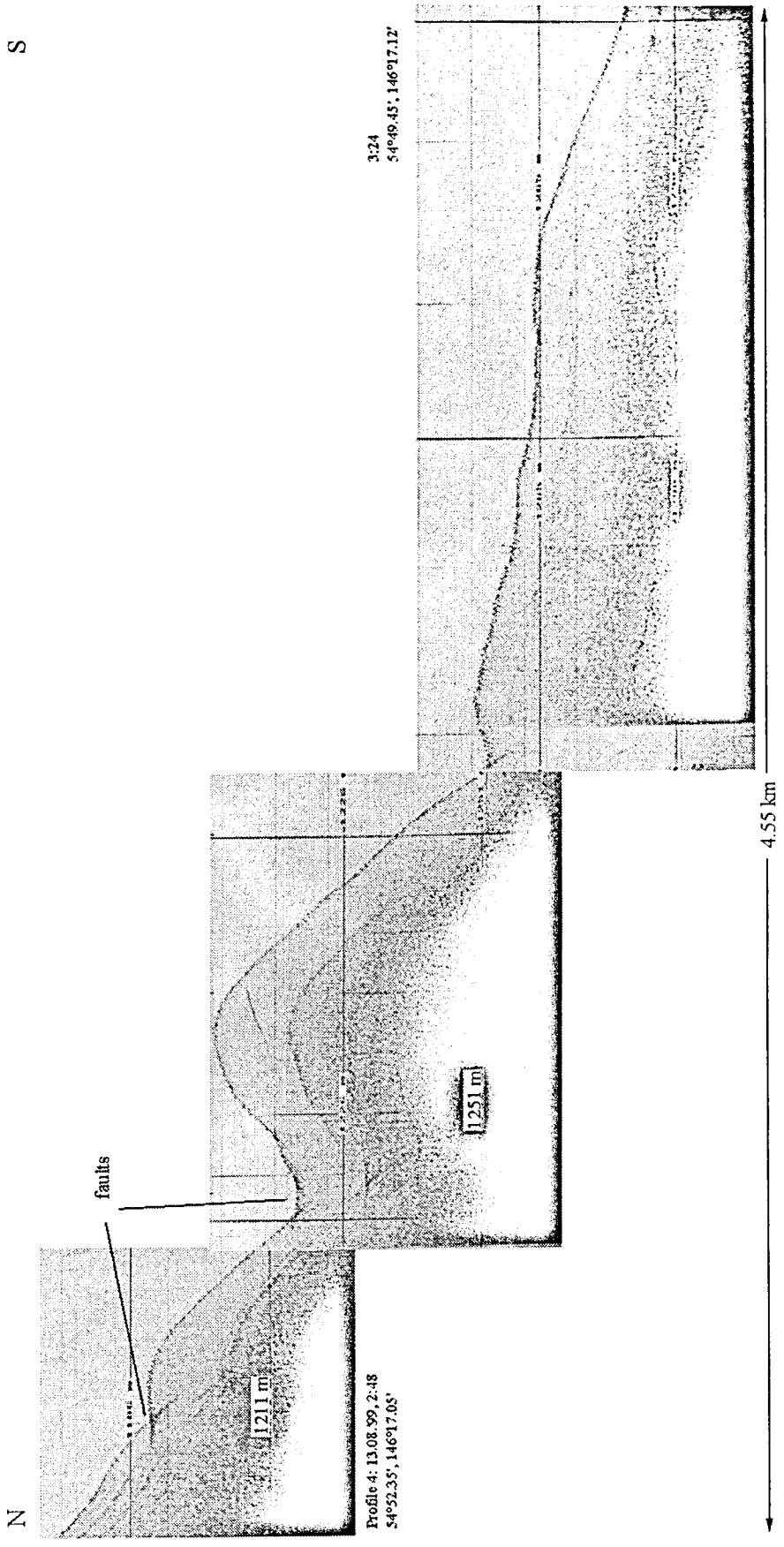

Fig. 3.4.7: Chirp record along profile 4 showing active faulting. See text for further explanations.

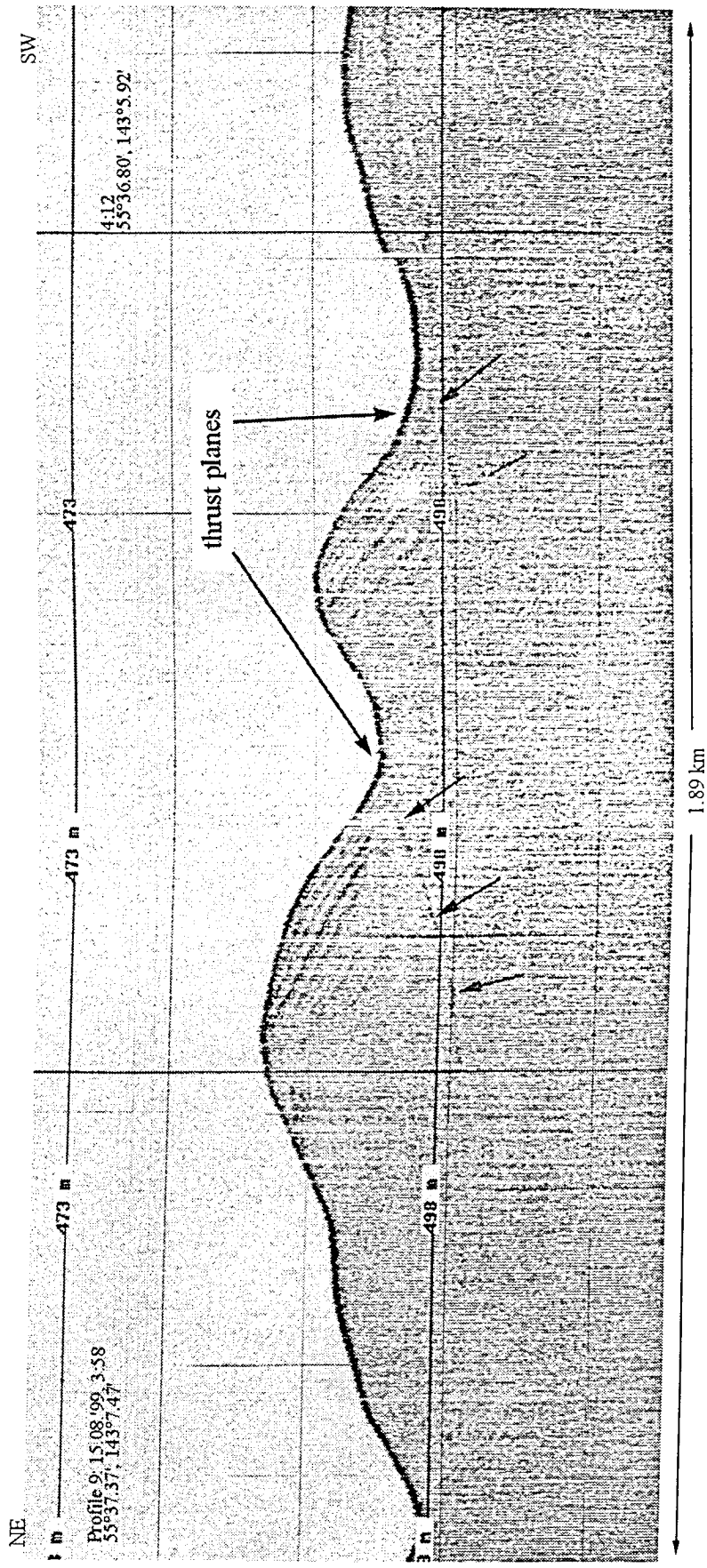

Fig. 3.4.8: Chirp record along profile 9 showing a thrust zone. Fault planes are marked. See text for further explanations.

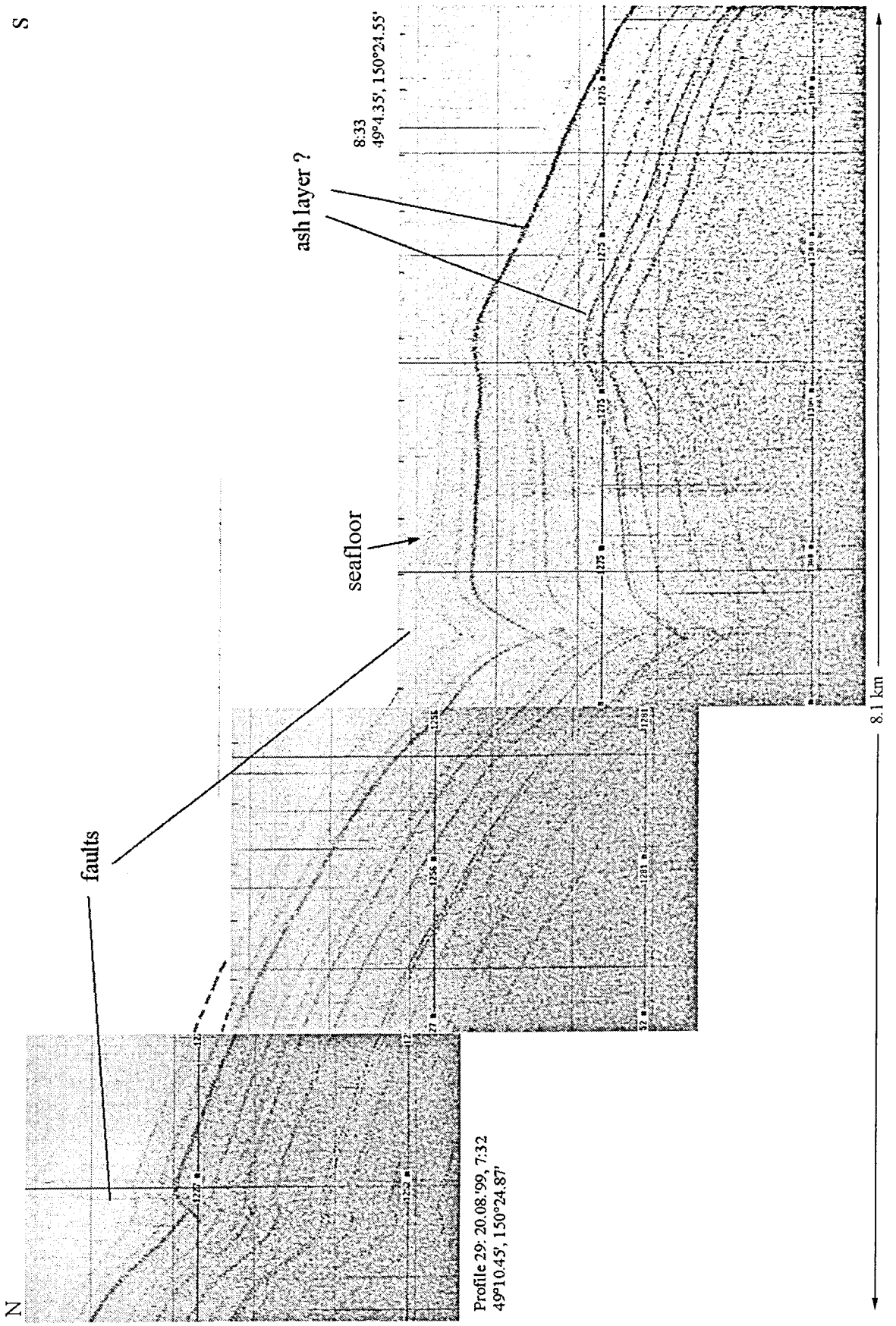

Fig. 3.4.9: *Chirp record along profile 29 showing active faulting at the northern margin of the Kurile Basin. See text for further explanations.*

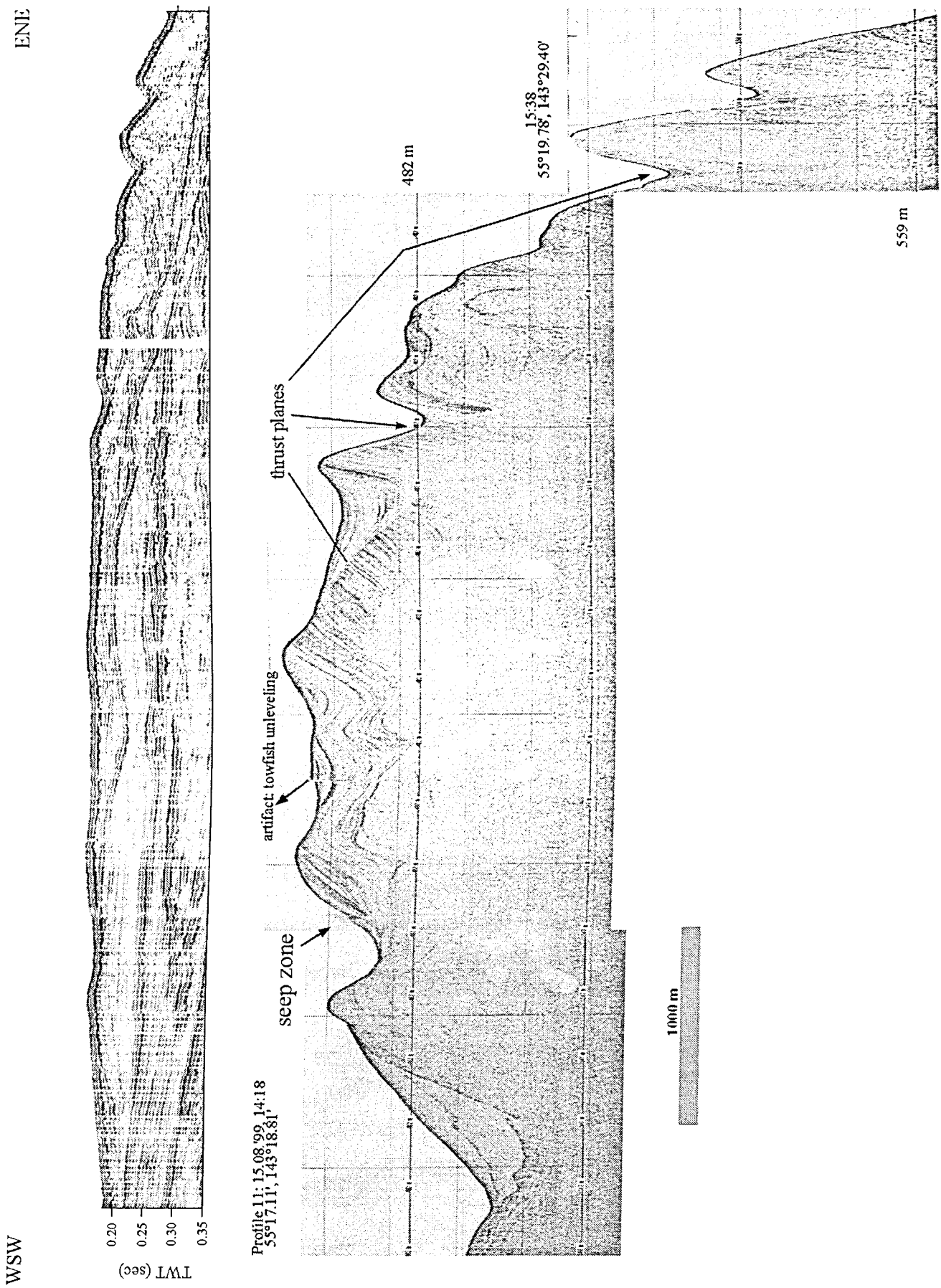

Fig. 3.4.10: Chirp record along profile 11 showing a thrust zone. Above the Chirp image the corresponding reflection seismic profile is shown. See text for further explanations.

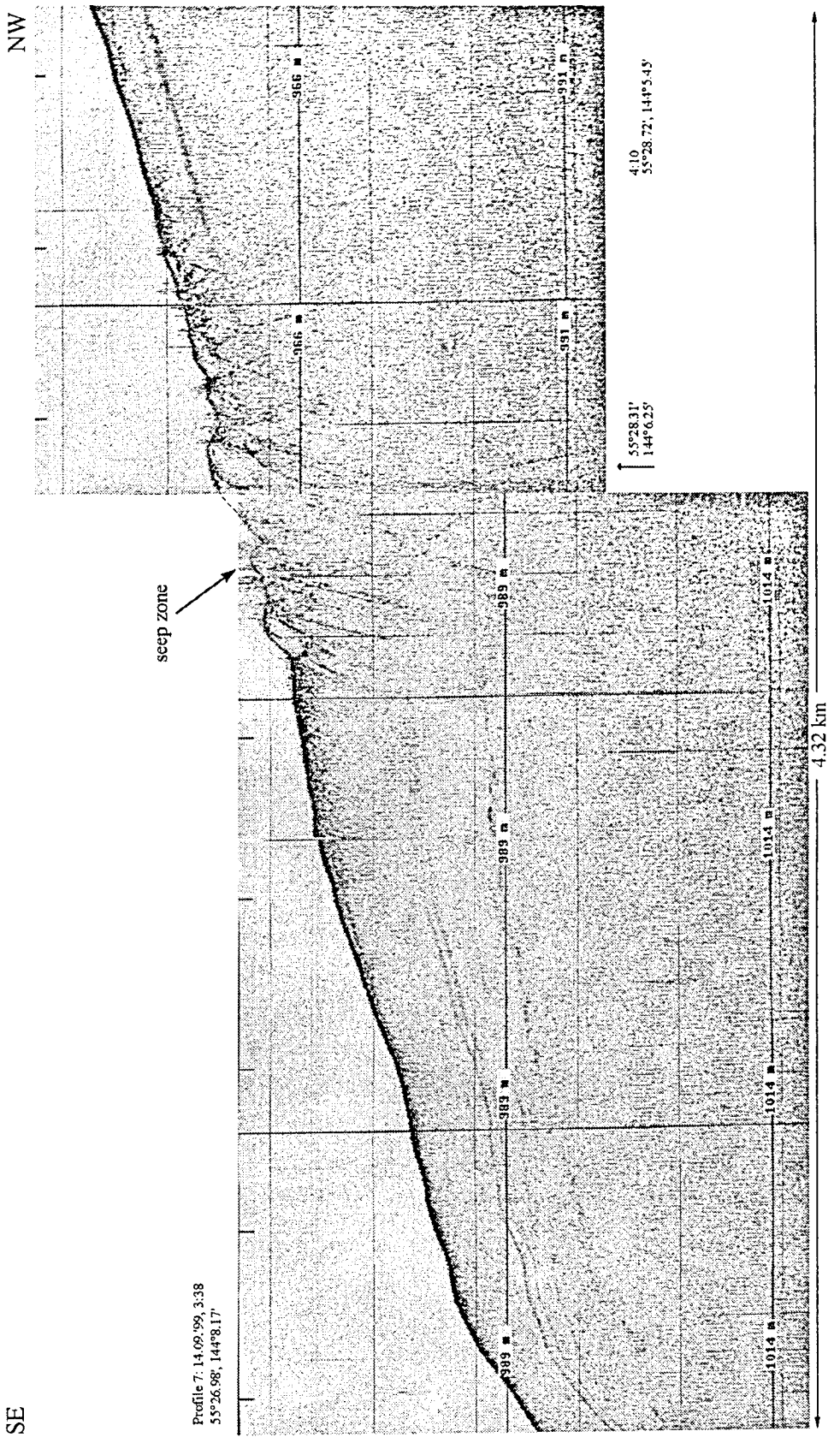

Fig. 3.4.11: Chirp record along profile 7 illustrating a seep zone. See text for further explanations.

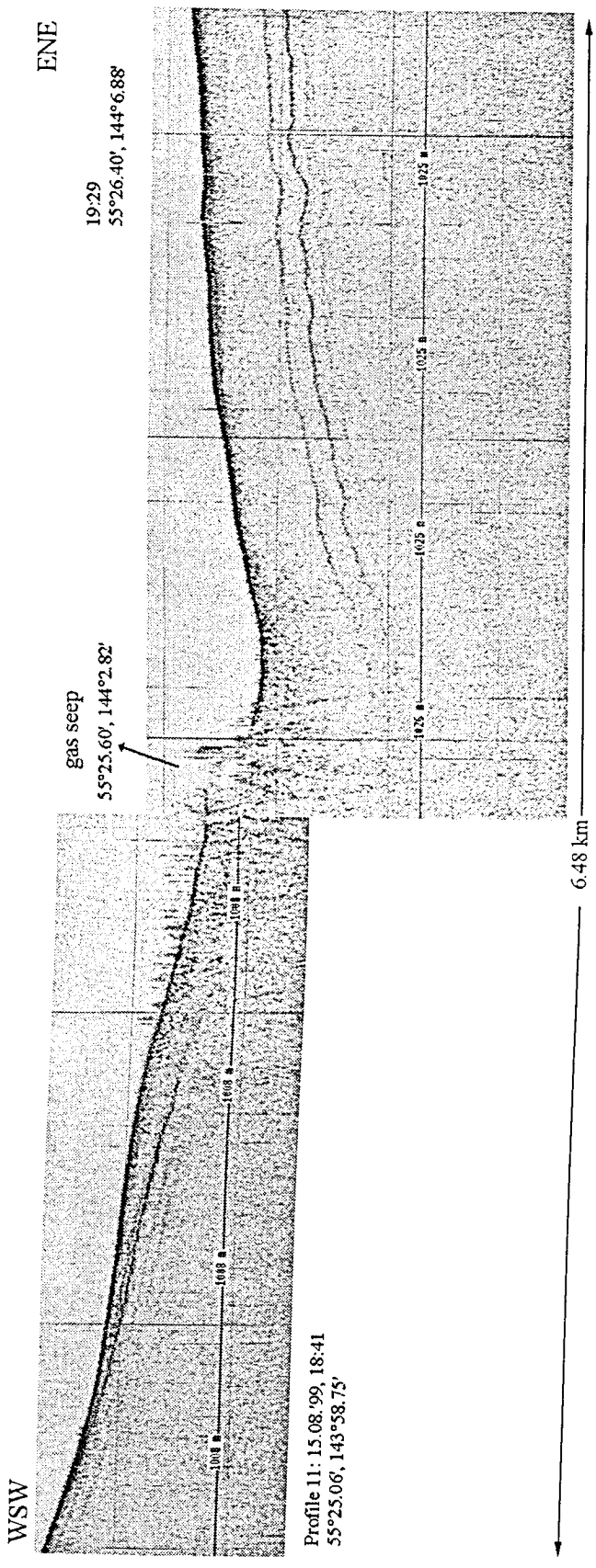

Fig. 3.4.12: Chirp record along profile 11 showing a seep zone. See text for further explanations.

Gas seeps zones were recorded on profiles 7 and 11 at water depths of 960 m, 1,000 m and 470 m respectively. Gas seeps are normally associated with active faulting where faults reach or almost reach the seafloor (Figs. 3.4.11, 3.4.12 and encircled area of Fig. 3.4.10). They represent zones of gas escape along fractures. On profile 9 at a water depth of 360 m, a localized feature (240 m x 240 m), possibly a shallow accumulation of gas hydrates, was mapped (Fig. 3.4.13).

Unequivocal evidence for the occurrence of grounded ice is hard to obtain, in particular because only a small percentage of the profiles are located on the shelf. However, a specific acoustic facies observed on profile 3 (Fig. 3.4.14) and characterized by numerous diffraction hyperbolas originating at a mostly sandy seafloor or directly below may be typical of a glacially-influenced depositional environment. That the seafloor is wavy may be primary or it may be a result of sediment reworking by bottom currents under conditions of sediment starvation.

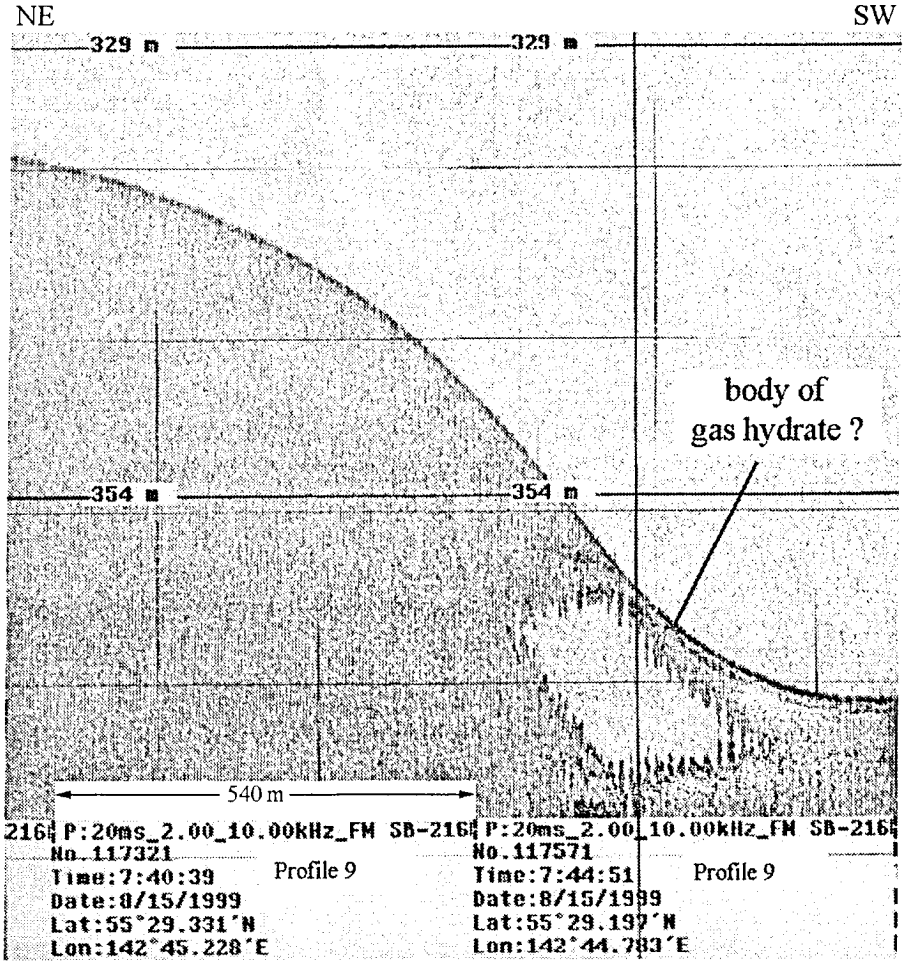

Fig. 3.4.13: *Chirp record along profile 9 showing a possible body of gas hydrates. See text for further explanations.*

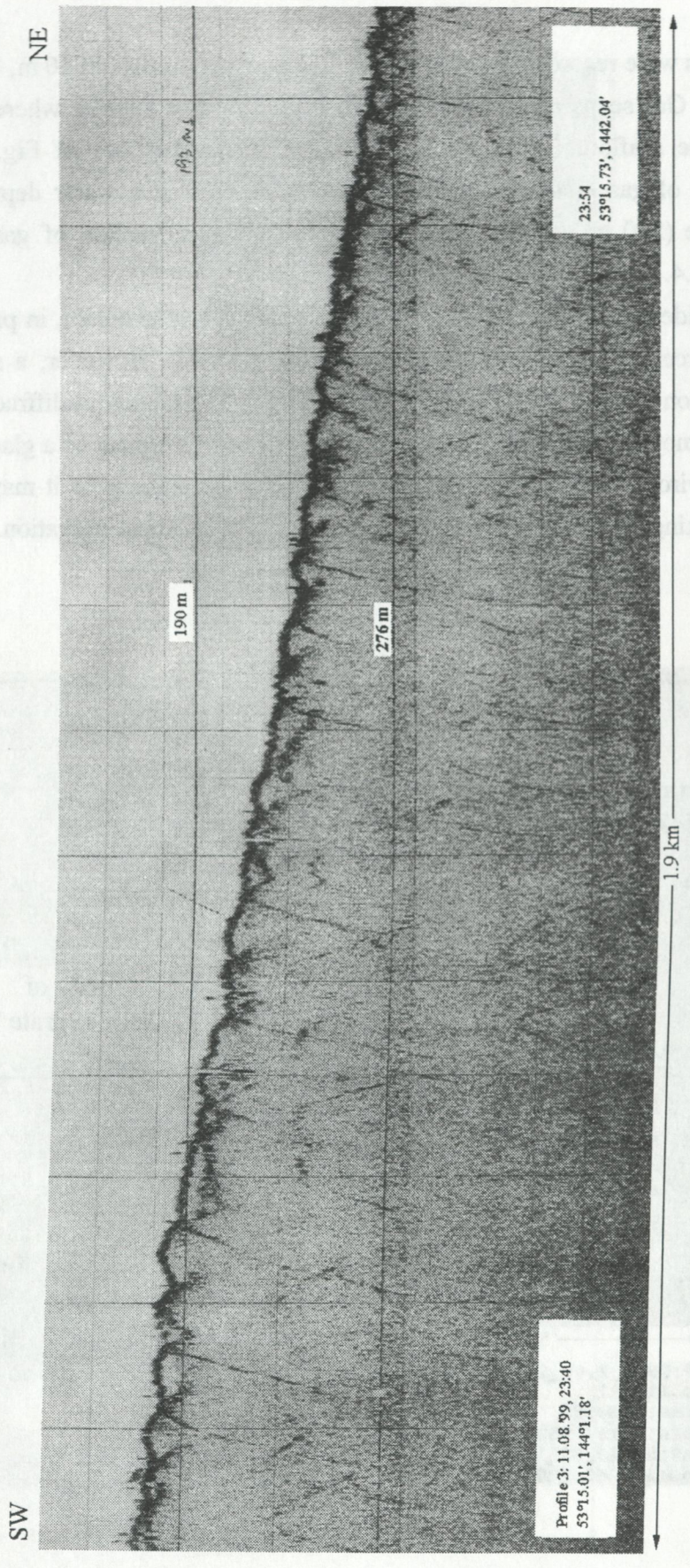

Fig. 3.4.14: *Chirp record along profile 3 showing a strong subbottom reflector and diffraction hyperbolas as indicators for coarse sediments including boulders. See text for further explanations.*

3.5 CH_4 and CO_2 concentrations in surface waters

S. Lammers

During 25 days of continuous survey along all profiles in the Okhotsk Sea, roughly 9,000 analyses of CH_4 and CO_2 were performed, of which 50 % were measurements of the surface water and 25 % of air samples (Fig. 3.5.1). These data (about 360 Mbytes) will require filtering, post-processing and correlation with GPS data prior to detailed evaluation. However, a few preliminary conclusions can already be drawn on the basis of the raw data and by comparison with the 1998 records.

In the following, saturation values are not corrected for variations of the water temperature and refer to an average atmospheric concentration of 1.8 ppm for methane and 355 ppm for carbon dioxide. Hence these values will be subject to modification after re-processing. For the same reason, maps (with the exception of Fig. 3.5.2) could not be produced immediately and will not be presented in this cruise report.

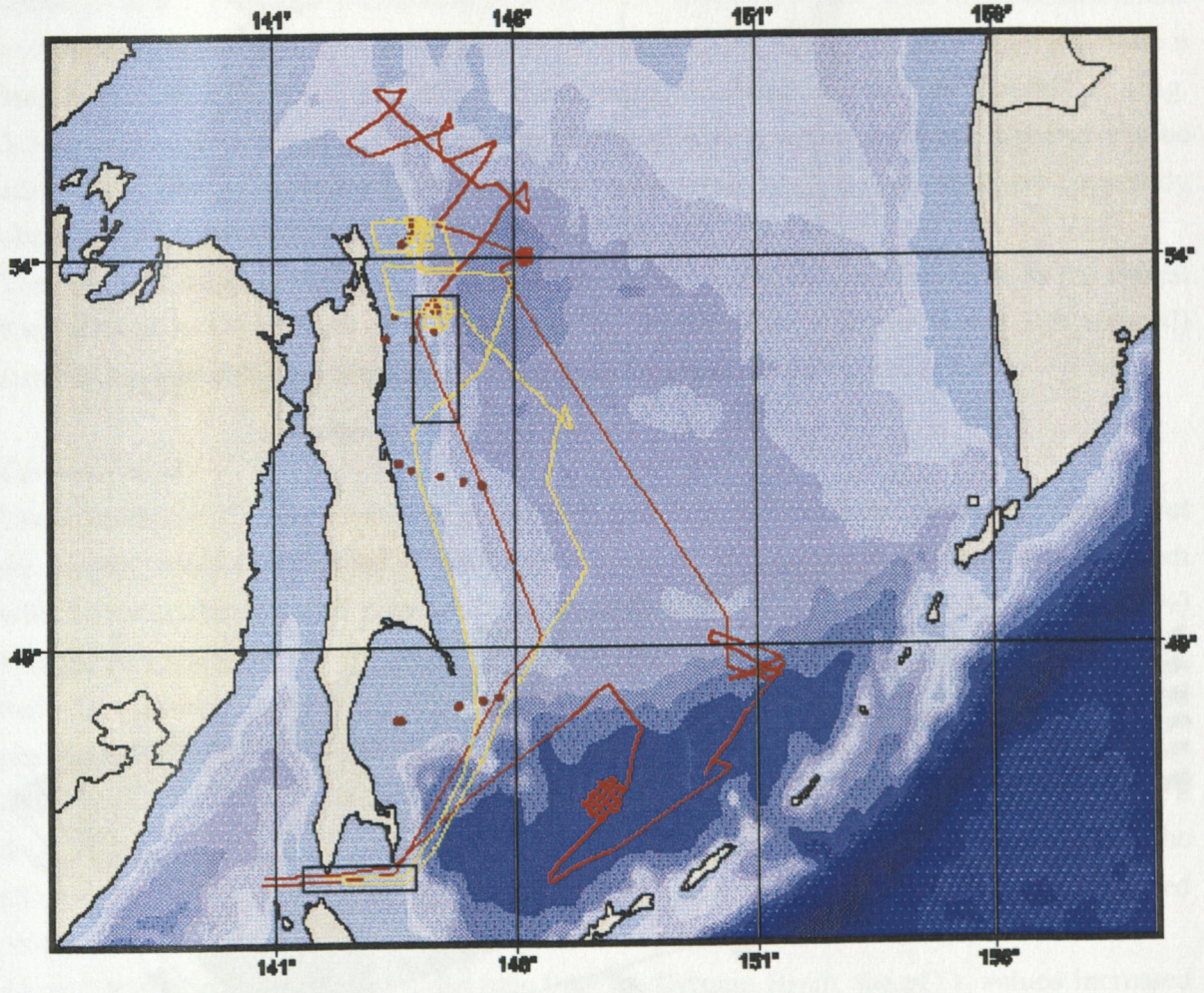

Fig. 3.5.1: *Summary of surveyed routes and stations of KOMEX-Project 1. Yellow tracks: trace gas surveys of Gagarinsky 23 (July 1998); green tracks: Gagarinsky 26 (August 1999); red dots: reference stations for the investigation of seasonal variations in CH_4 and CO_2 distributions.*

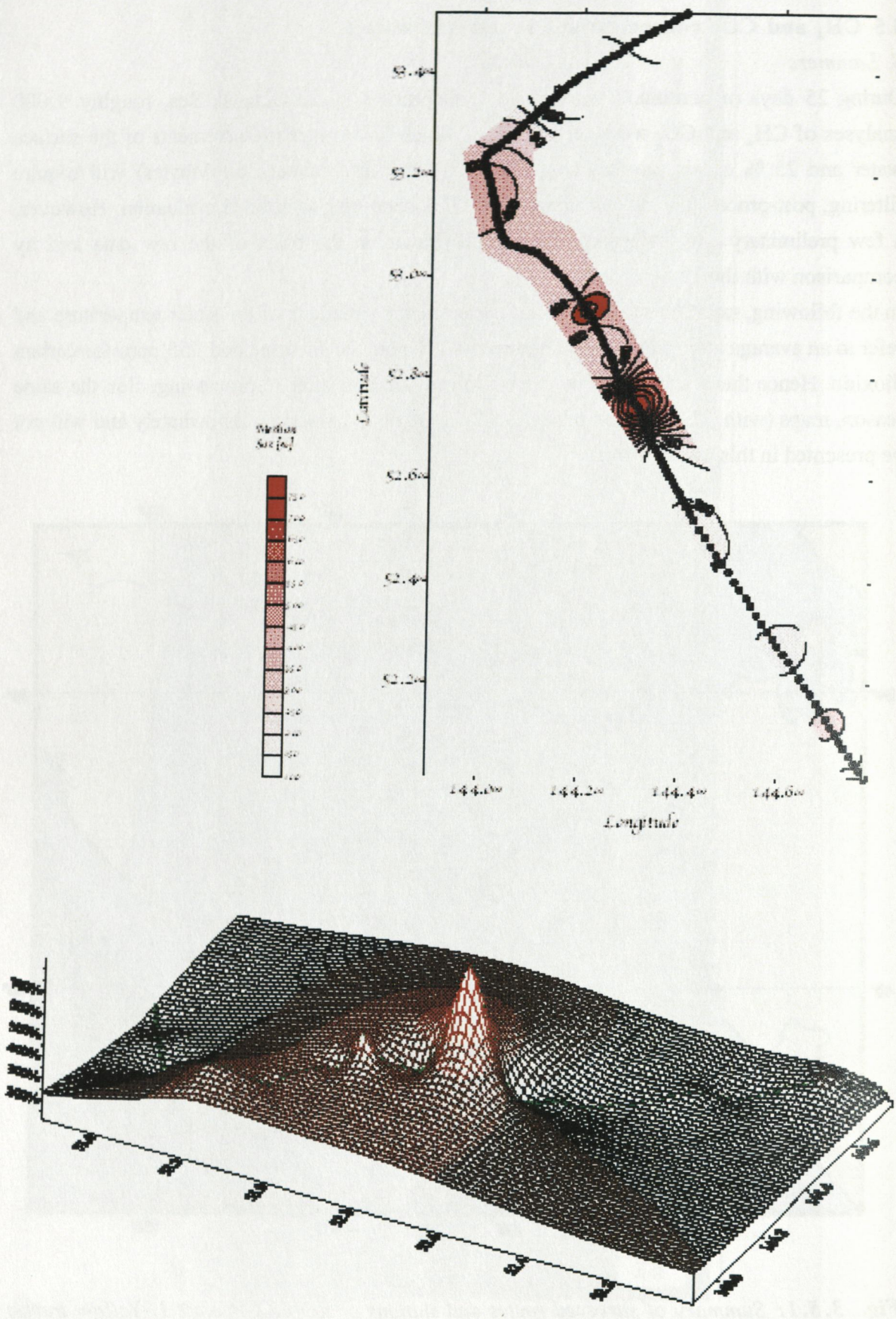

Fig. 3.5.2: *Views of methane saturation (in %) observed in surface water W of the Derugin Basin.*

Methane

The saturation in the surface waters of the survey areas ranged between 100 % and 130 % relative to the average recorded atmospheric CH_4 partial pressure of 1.81 ppm. When not affected by venting of methane-rich fluids from sedimentary sources, surface waters are commonly observed to be close to equilibrium with the atmosphere. Hence, the recorded slight but widespread supersaturations in the SE part of the Okhotsk Sea surveyed is presumably the result of a short-term temperature increase of the surface waters and might reverse on cooling during the autumn months. Final conclusions on the sources are expected from isotope analyses of samples from the consecutive *Marshal Gelovany* expedition.

Two areas of significantly supersaturated surface waters were found south of Sakhalin and along the NE Sakhalin Shelf (see boxes in Fig. 3.5.1). South of Sakhalin between 45°40´N/ 140°40´E and 46°43´N/144°13´E supersaturations between 250 % and 350 % extended over a distance of more than 150 nm. These results correlate with the measurements obtained during cruise 23 of RV *Professor Gagarinsky* in July, 1998. About the same level of supersaturations was recorded in the NE off Sakhalin between 52°0´N/144°46´E and 53°26´N/144°15´E with a local maximum of 750 % saturation at the position 52° 44.681´N and 144° 18.841´E (Fig. 3.5.2). This maximum occurs about 40 nm from the location of the 1998 maxima and can be attributed to another sedimentary source, as plumes released by seeps and vents are frequently observed along these parts of the Sakhalin Self.

The source of another local CH_4 anomaly of more than 1,500 % supersaturation in the central Kurile Basin at 47° 15.532' N and 148° 24.024' E (at a water depth of over 3,500 meters!) remains unclear and must be confirmed by further surveys.

Carbon dioxide

Undersaturation of surface waters between 95 % and 75 % was commonly observed throughout the survey, while the recorded values range between 53 % and 115 % relative to equilibrium with the atmospheric partial pressure of 355 ppm. The lowest series of saturations (53-70 %) was measured between 51° and 53° latitude along the eastern coast of Sakhalin and between 54° and 55° latitude N off Sakhalin. These undersaturations are attributed to enhanced phytoplankton productivity, i.e. the fixation of CO_2 and, in turn, the reduction of pCO_2 in the euphotic zone. On some occasions, the increase of pCO_2 by some 20 % correlated with a decrease in the sea surface temperature, e.g., N of 55° latitude off Sakhalin. Whether this the effect of the temperature dependence of the pCO_2 alone or is also the result of a reduced productivity will be clarified by further evaluation of the data.

Along a transit in the southeastern direction from the Derugin Basin, the pCO_2 values increased and approached equilibrium in the area of the Kurile Basin.

4. DISCUSSION

4.1 Seismic stratigraphy and paleo-depo-environment of the Derugin Basin and Staretsky Trough

T. Lüdmann

A preliminary seismo-stratigraphic interpretation of reflection seismic profiles and high-resolution *Chirp* data within the study area off northeastern Sakhalin shows that most of this area is capped by a thin veneer of Holocene highstand deposits except places surrounding local basement highs where the youngest sediments are winnowed out by currents (Figs. 3.4.5 and 4.1.1). Erosion by strong bottom currents leading to non-deposition or truncation of older sequences is very important. The Holocene sediments are predominantly sandy to clayey as suggested by attenuation coefficients deduced from *Chirp* profiles (Fig. 3.4.1) and shown by sediment cores of the RV *Akademik Lavrentyev* cruise 27 (Nürnberg et al., 1997) and *Lavrentyev* cruise 28 (Biebow & Hütten, 1999) (see Fig. 3.2.1.1 for location). Several cores retrieved within the northwestern Derugin Basin at water depths between ca. 1,100-1,500 m are characterized by a lack of terrigenous components in the surface to near-surface sediments despite the proximity of land and by an abundance of biogenics, in particular of diatoms, mollusks, gastropod shells and carbonaceous shell fragments. The strata are Holocene in age and reach a thickness of up to 4 m, yielding a computed average sedimentation rate of 40 cm/ka, a value consistent with the high bio-productivity. Both seismic and core data suggest that terrigenous material is restricted to river mouths – in particular to that of the Amur River. Coring shows that the abundance of terrigenous components is proportional to core depth, consistent with the progressive dominance of clayey silt (with occasional sand and pebbles) with increasing depth. The maximum core penetration is 738 cm (core LV27-2-4, see Fig. 3.2.1.1 for location) and might have reached the turbid facies in this area (Fig. 3.2.1.2). If this is the case, then the turbid facies is probably made up of homogenous, olive-gray, clayey silt with possibly gas hydrate-filled vacuoles (30 x 40 mm) (Nürnberg et al., 1996).

During the last sea-level lowstand, the slopes of Kashevarov Bank and off northern Sakhalin were areas of erosion and non-deposition. They are bounded by lines along which a pronounced unconformity outcrops. Above this unconformity is the last glacial (Upper Pleistocene) sequence of the Staretsky Trough. Figure 4.1.2 shows a map of the limit of this sequence which includes at its top mound-like structures and a succession of tilted sedimentary blocks separated from one another by thrust folds (Figs. 3.2.1.7, 3.4.8 and 3.4.10). Because the distance between adjacent profiles is very large (ca. 40 km) and there is a lack of swath bathymetric and sidescan data, the strike of these features (NW-SE) can only be inferred. Another prominent feature is the lenticular body located within a trough which rises 110 m above the surrounding seafloor (profile 8, Fig. 3.2.1.8). It terminates downlap at both ends. Slopeward to the south it onlaps thrusted sedimentary bodies of the facies area VI. The shape of the small trough is U-like which might indicate a former glacial valley. The lenticular body may

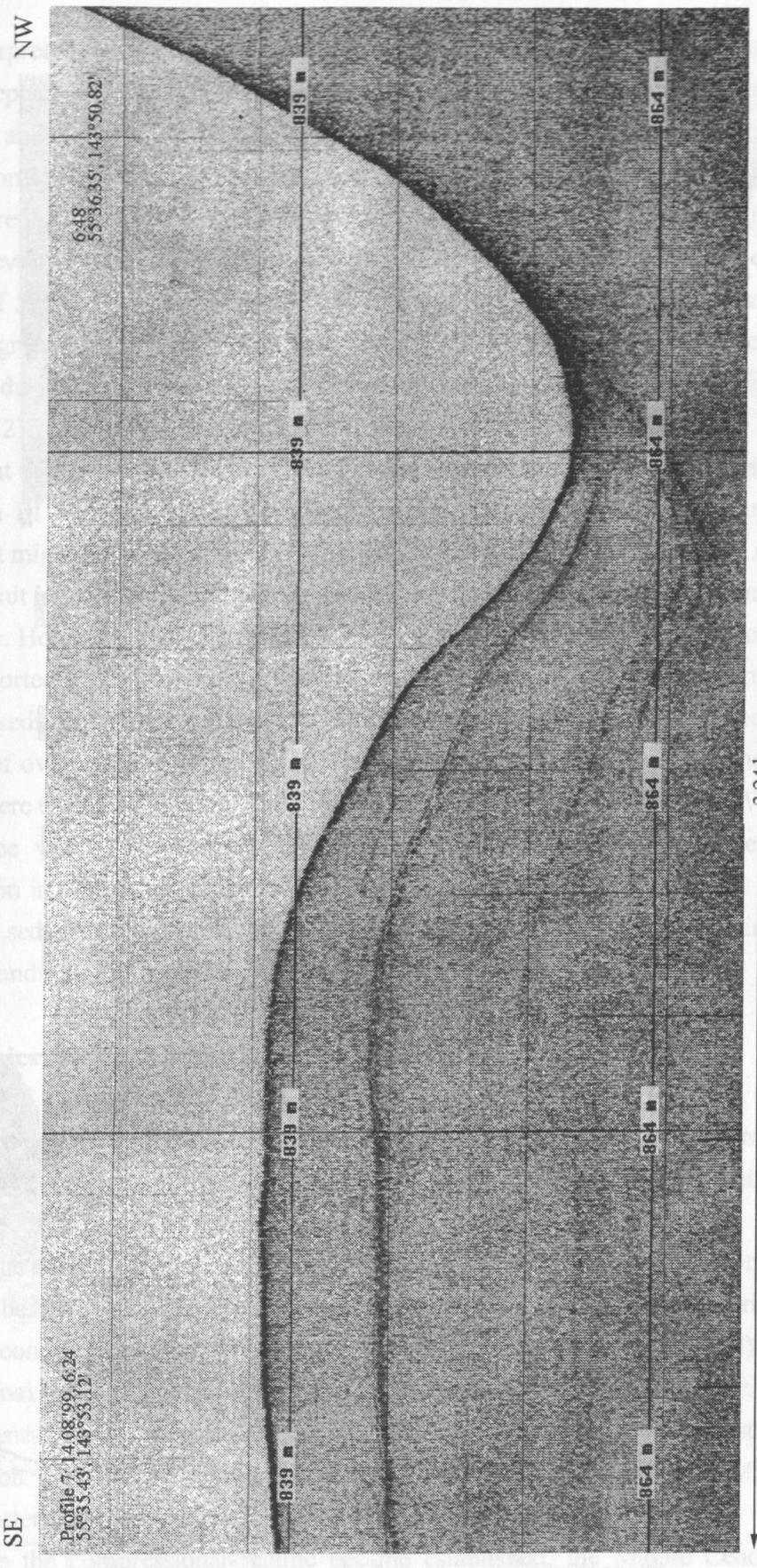

Fig. 4.1.1: *Chirp record along profile 7 showing submarine erosion around a high. See text for further explanations.*

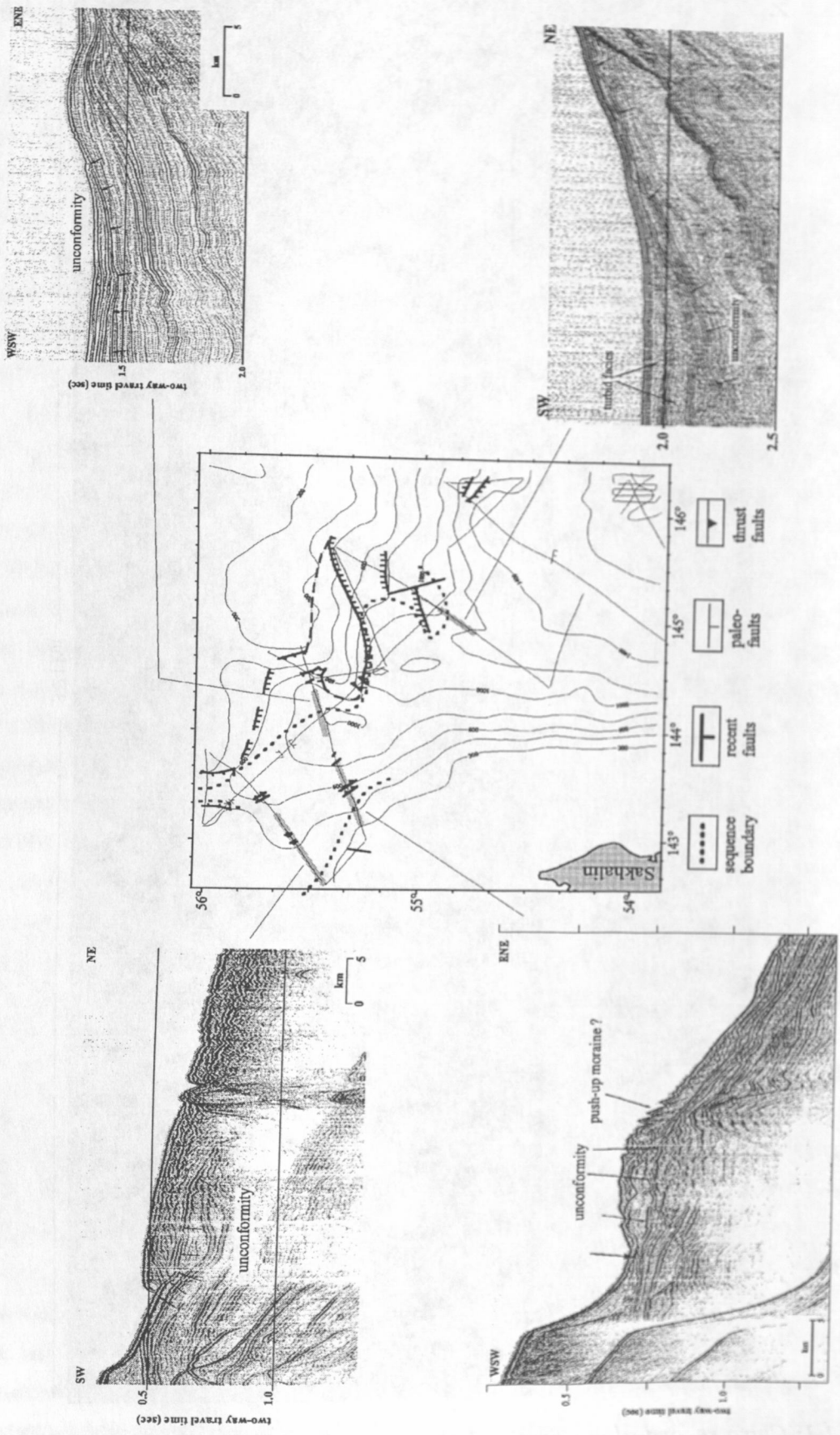

Fig. 4.1.2: *Map showing the limits at the seafloor of deposits of the last glaciation. See text for further explanations.*

then be interpreted to have formed by erosion by ice flow around it or as a remnant of a tunnel valley-fill replaced after retreat of the glacier. The thrusted sediment bodies on profiles 9 and 11 (Figs. 3.4.8 and 3.4.10) at water depths of 650 and 550 m respectively could represent push-up moraines formed during a glacial advance. This interpretation requires the glacier to have crossed Staretsky Trough which has a depth of 710 m on profile 9 and 1,000 m on profile 10. Since sea level was ca. 130 m below present during the last ice age, the glacier must have a thickness of 520-420 m to deposit the moraine and a thickness of 590-880 m to bridge the trough as a grounded ice sheet. An alternative explanation for the thrusted sediments is that they are formed during transpressional tectonic movements along the slope of Sakhalin Island (see section 4.1.2).

Concomitant with the deposition of the uppermost units in the facies areas VI and VII, the turbid unit of area III was laid down. The depo-center of this turbid unit, however, can only be estimated. It might be north of the INESSA study area and south of profile 11 (Fig. 3.2.1.2). Since this unit is both very thick and very widespread, its only source of sediments might be the Amur River. However, profile 3 (Fig. 3.2.1.3) documents that a minor amount of sediment has been transported basinward from the northern and eastern slopes of the Derugin Basin. In addition to sedimentary fans of a turbid facies, turbidites (well-stratified reflectors) overlie a rugged relief over much of the Derugin Basin. Fig. 3.2.1.4 shows that at the basin margin turbidites were truncated and reworked during deposition of the turbid facies. We suggest that the sequence within the northern Derugin Basin may represent a long period of cyclic sedimentation in which turbid deposits are the most prevalent during sea level lowstands and hemipelagic sedimentation combined with mass movements on the slopes dominate during sea level highstands.

4.2 Tectonics of the Okhotsk Sea: extension vs compression

B. Baranov, K. Dozorova, and B. Karp

A preliminary analysis of the data obtained during cruise 26 of the RV *Professor Gagarinsky* suggests that two stages in the tectonic history of the Okhotsk Sea may be distinguished. The first stage is characterized by extension and the second by compression.

The first stage corresponds to the time of formation of the system of semi-grabens, grabens and deep-water basins with a stretched continental crust or an oceanic crust. During this phase, extensional conditions existed over the entire Okhotsk Sea. Kharakhinov (1998) suggested that the extensional process could have begun in the Paleocene, but it was most intensive during the Late Oligocene-Middle Miocene. Although it is highly probable that the main structural pattern of this region was formed during this period, we will refer to it as the Middle Cenozoic structural pattern.

By the time the compressional regime became established, the Middle Cenozoic structural pattern was inherited, but movements on the faults reversed. This reversal could have taken place between the Upper Miocene and the Pliocene (Kharakhinov, 1998). Our data suggest that

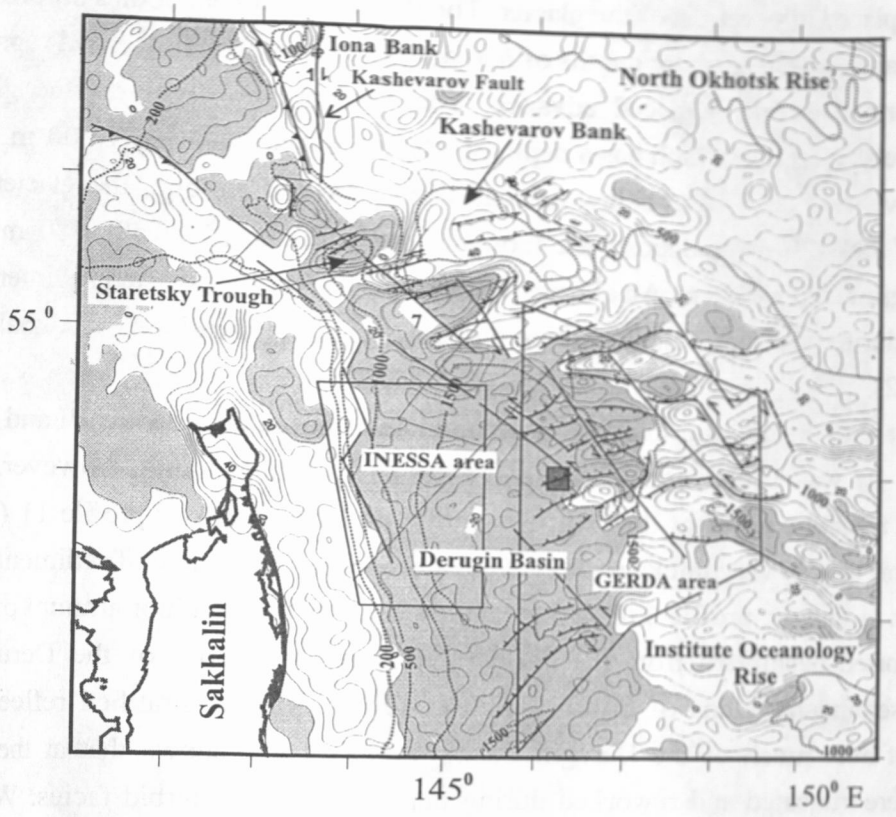

Fig. 4.2.1: *Structural pattern of the northern SAKURA area. Lines with triangles mark reverse faults, with bars: normal faults, and with arrows: strike-slips. Lines without ornament are faults of unknown origin. Dashed lines mark all fault types distinguished on the basis of gravimetry only. Thin lines give gravimetric contours (interval: 10 mG). Areas of negative gravity anomalies are shown in gray. Dotted lines are isobaths. The GERDA and INESSA areas, the barite field (grey rectangle) and the location of seismic profile 7 are also shown. The faults in the northwestern-most corner of the map are from Worrall et al. (1996).*

this compressional regime exists up to the present time, at least in the areas studied. Thus, we shall refer to the corresponding structural pattern as the recent (neotectonic) structural pattern.

4.2.1 Northern SAKURA area

Middle Cenozoic structural pattern

The structural pattern of the northern SAKURA area is shown in Fig. 4.2.1. It is based on data obtained during the present cruise, the GERDA and INESSA expeditions and on the gravimetric map of the Okhotsk Sea. The use of gravimetric data is justifiable because they are well-correlated with the basement relief except in special cases described below in the section on the Southern SAKURA area.

The most remarkable feature of the basement relief in the Northern SAKURA area is the existence of tilted blocks - structural elements characteristic of crustal extension. They are seen most distinctly on seismic records, in basement relief maps and in altimetric maps of the northeastern part of the area (at water depths <1,500 m) (Fig. 4.2.2). In the Derugin Basin

Fig. 4.2.2: *Part of seismic profile 7 showing a graben between two tilted blocks facing each other. See Fig. 4.2.1 for profile location.*

(>1,500 m depth), tilted blocks are well-formed only in the northeast (GERDA area). Compared to their shallow counterparts, they are smaller in dimension, more broken up and have subsided to greater depths. In the central Derugin Basin, the depth to basement is large and the tilted blocks are poorly-expressed, even though they can reach the seafloor (Fig. 3.1.2). On the continental slope (INESSA area), they are absent as the profiles obtained during cruise 22 of the RV *Professor Gagarinsky* testify.

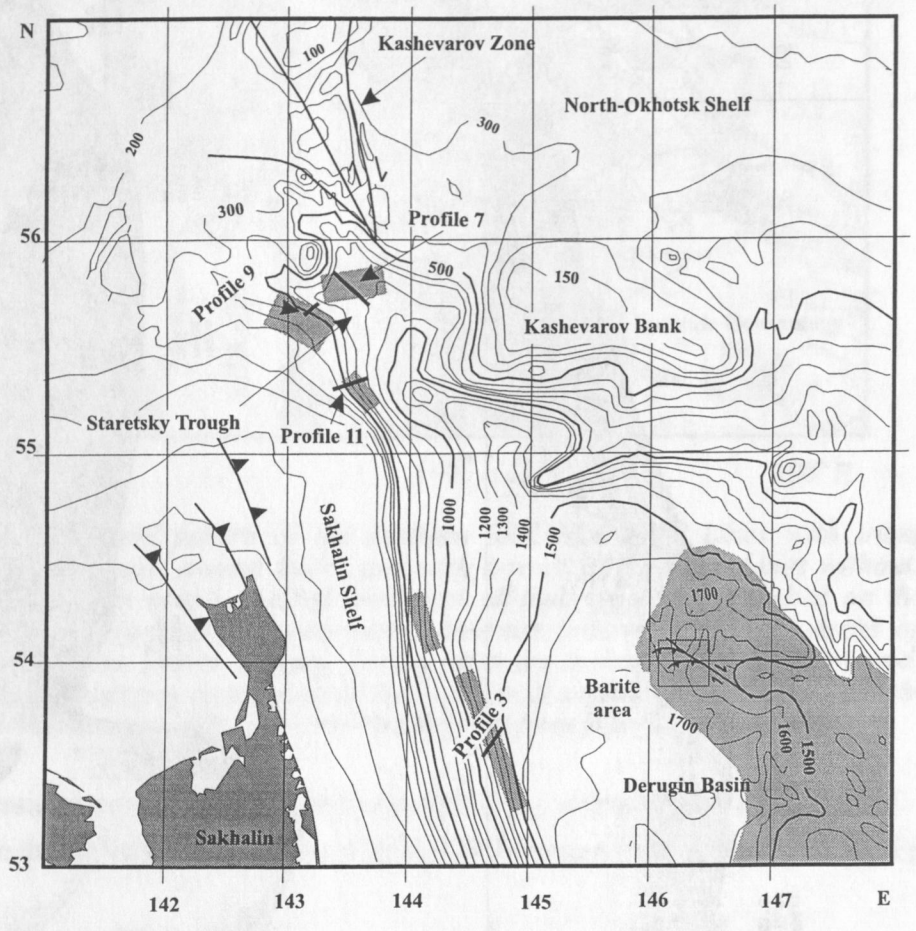

Fig. 4.2.3: *Recent tectonics of the northern SAKURA area. Toothed lines are thrusts. Lines with arrow are strike-slips. Grey areas have a compressive (thrusting/folding) or strike-slip regime. The Kashevarov Zone and the thrusts near northern Sakhalin are from Worrall et al. (1996).*

The strike of the blocks and the normal faults that bound them on one side or on both sides changes from ENE to nearly E-W within the study area (Fig. 4.2.1). A E-W strike dominates the eastern part of the area. It is apparently associated with a minor rotation of the structures from the NW-SE direction. There are relative displacements between and within blocks along northwesterly strike-slip faults. The sense of motion as deduced from cross profiles is left-lateral. In addition, the ENE to E-W orientation of blocks implies that the sense of motion on the conjugate northwesterly strike-slips must also be left-lateral.

Thus, the entire northeastern part of the area from Kashevarov Bank to the Derugin Basin may be regarded as a wide sinistral shear zone, inside which the system of grabens and semi-grabens as well as the Derugin Basin itself were formed. It remains unclear whether this zone continues to the northeast to the North-Okhotsk Rise, because data to answer this question are lacking. Gravimetric data suggest that the blocks are less well-manifested in the basement relief to the north. This may imply that the crust here is stretched to a lesser degree.

The relationship of this zone to the Kashevarov zone is also unclear. The Kashevarov zone according to Worrall et al. (1996) stretches in a N-S direction from the northern coast of the Okhotsk Sea to the western slope of Sakhalin Island (INESSA area). However our present data and data from the INESSA expedition do not give any reliable information on the influence of the Kashevarov zone on the structural pattern of the western part of the Northern SAKURA area. Since the Kashevarov zone is a recent structure (Worrall et al., 1996), we will return to it below in the section on the neotectonic structural pattern.

The Middle Cenozoic structural pattern of the eastern Sakhalin slope and in particular the fault kinematics are also enigmatic. Gnibidenko & Khvedchuk (1982) described a northwestern and a northeastern system of faults for this area without discussing their kinematics. The basement rises have north-northwestern and northeastern strikes on the gravimetric map. Obviously, they must be caused by fault systems oriented in the same directions. Their strikes correspond to the fault network mapped to the east of this area.

Recent structural pattern

It has been noted that the recent structural pattern inherited the existing fault system and is characterized by compression. Evidence for compression are reverse faults and folds in the sedimentary cover observed on the Sakhalin slope, in the Staretsky Trough and in the Derugin Basin. The degree of compression apparently decreases to the northeast. Although the area with compressional structures is larger in the northeastern Derugin Basin (Fig. 4.2.3), these structures are the most distinct on the Sakhalin slope.

The Sakhalin slope

Data from the INESSA expedition (Biebow & Hütten, 1999) and the present cruise show that the recent compressional structures (thrusts and folds) continue along the Sakhalin slope for a distance of at least 200 km (Fig. 4.2.3). They are oriented NW-SE and can be traced from the southern boundary of the INESSA area to the northern. The deformation zones are oriented oblique to the strike of the slope and are found within the depth range of 1,450-1,250 m to the south (Fig. 4.2.4) and 800-600 m to the north within the INESSA area.

Farther to the north, the boundary of the deformation zone is located at shallower depths. On profile 11, the system of recent thrusts exists within the depth interval of 800-500 m. On profile 9, the interval is 670-370 m. Deformation of the sedimentary cover occurs here at two levels. At the lower level, the folds are vergent towards the Sakhalin Shelf or the Staretsky Trough. Their

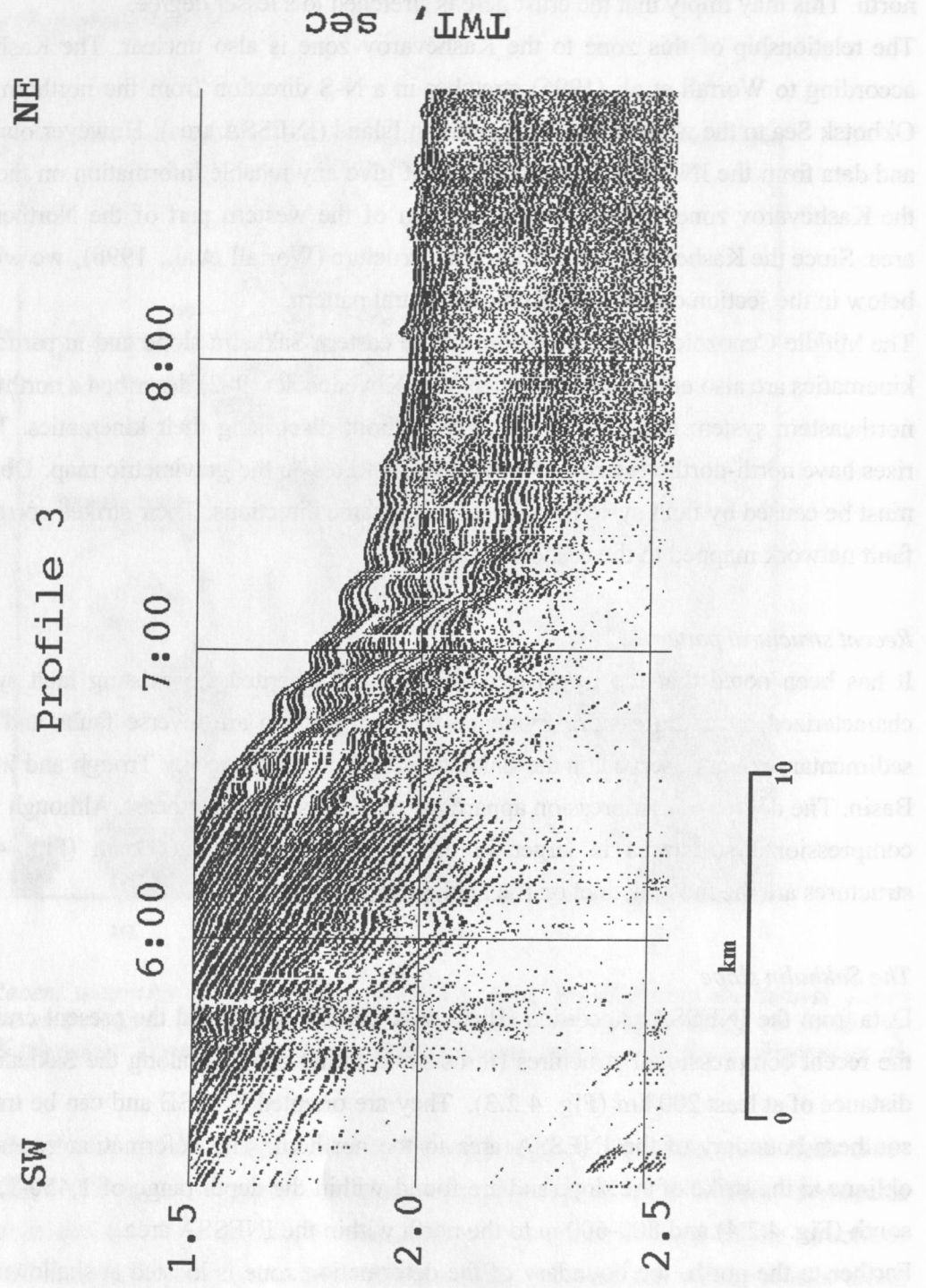

Fig. 4.2.4: *Part of seismic profile 3 showing a system of folds at the base of the Sakhalin slope. See Fig. 4.2.3 for profile location.*

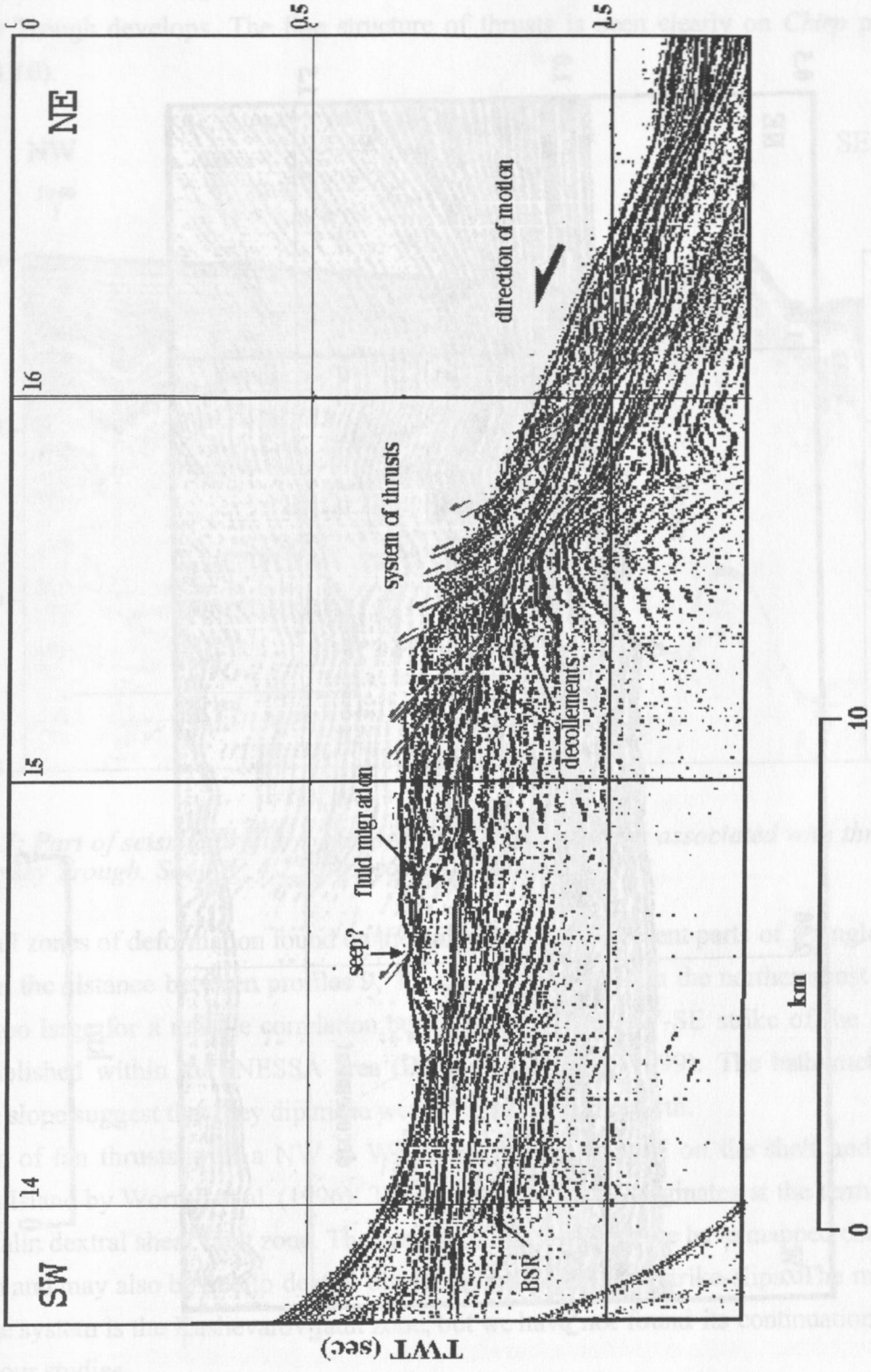

Fig. 4.2.5: *Part of seismic profile 11 showing shallow décollements and a system of thrusts on the Sakhalin slope. See Fig. 4.2.3 for profile location.*

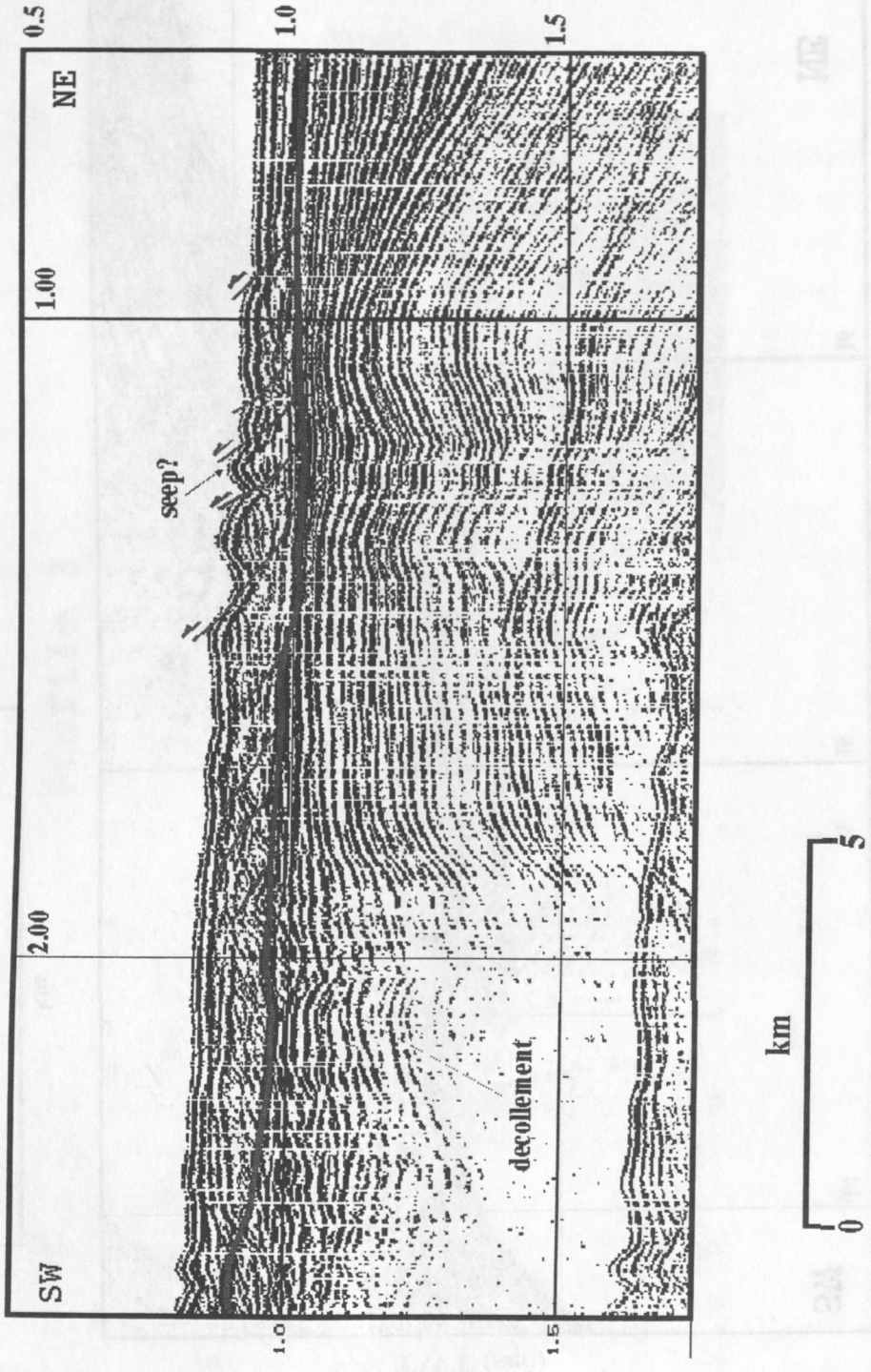

Fig. 4.2.6: *Part of seismic profile 9 showing a shallow décollement and a system of thrusts at the base of the Sakhalin slope. See Fig. 4.2.3 for profile location.*

origin is apparently associated with thrusting at the sediment/basement boundary. The second level of deformation is surficial. Under compression, décollements develop within the sedimentary column at depths of 100-200 m (Figs. 4.2.5 and 4.2.6). The sedimentary sheets move up the Sakhalin slope and in their frontal parts a thrust system dipping towards the Staretsky Trough develops. The fine structure of thrusts is seen clearly on *Chirp* profile 11 (Fig. 3.4.10).

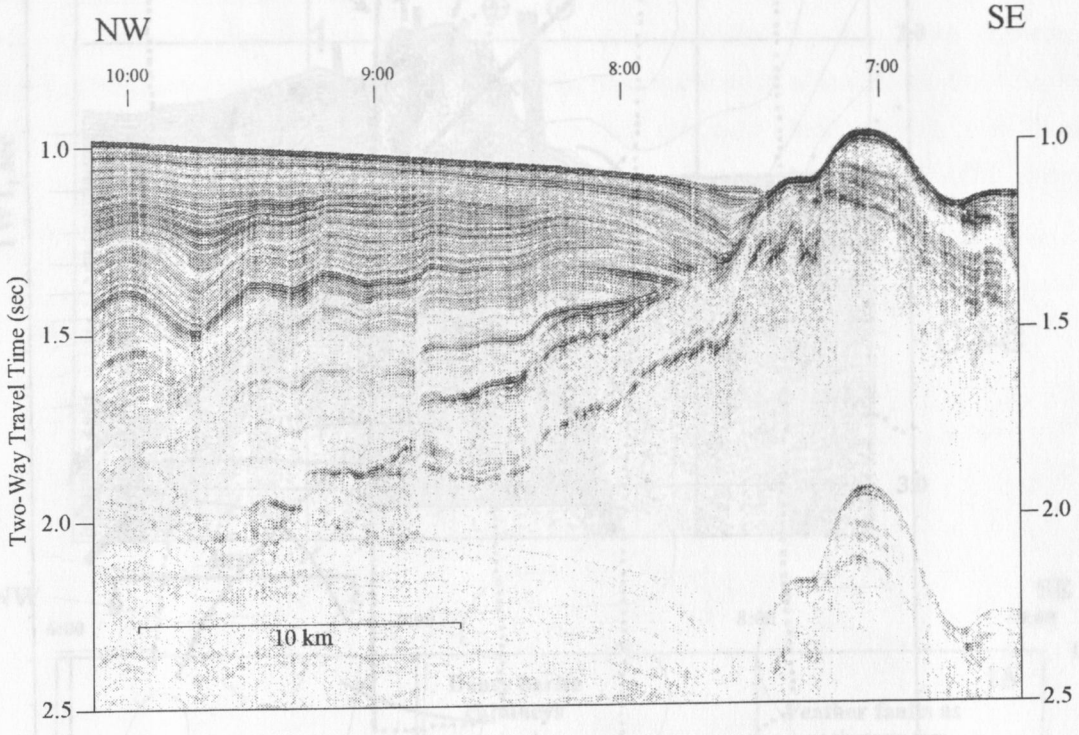

Fig. 4.2.7: *Part of seismic profile 7 showing folded deformations associated with thrusting in the Staretsky Trough. See Fig. 4.2.3 for profile locations.*

Clearly all zones of deformation found on the Sakhalin slope represent parts of a single system. However, the distance between profiles 9, 11 and 28 (the last is in the northernmost INESSA area) is too large for a reliable correlation between them. The NW-SE strike of the thrusts is well-established within the INESSA area (Biebow & Hütten, 1999). The bathymetry of the Sakhalin slope suggest that they dip more westerly farther to the north.

A system of fan thrusts with a NW to WNW strike was mapped on the shelf and slope of Sakhalin Island by Worrall et al. (1996). They postulated that it originates at the termination of the Sakhalin dextral shear fault zone. The system of thrusts which we have mapped continues to the south and may also be due to dextral displacements along N-S strike-slips. The most likely conjugate system is the Kashevarov fault zone, but we have not found its continuation south of 56°N in our studies.

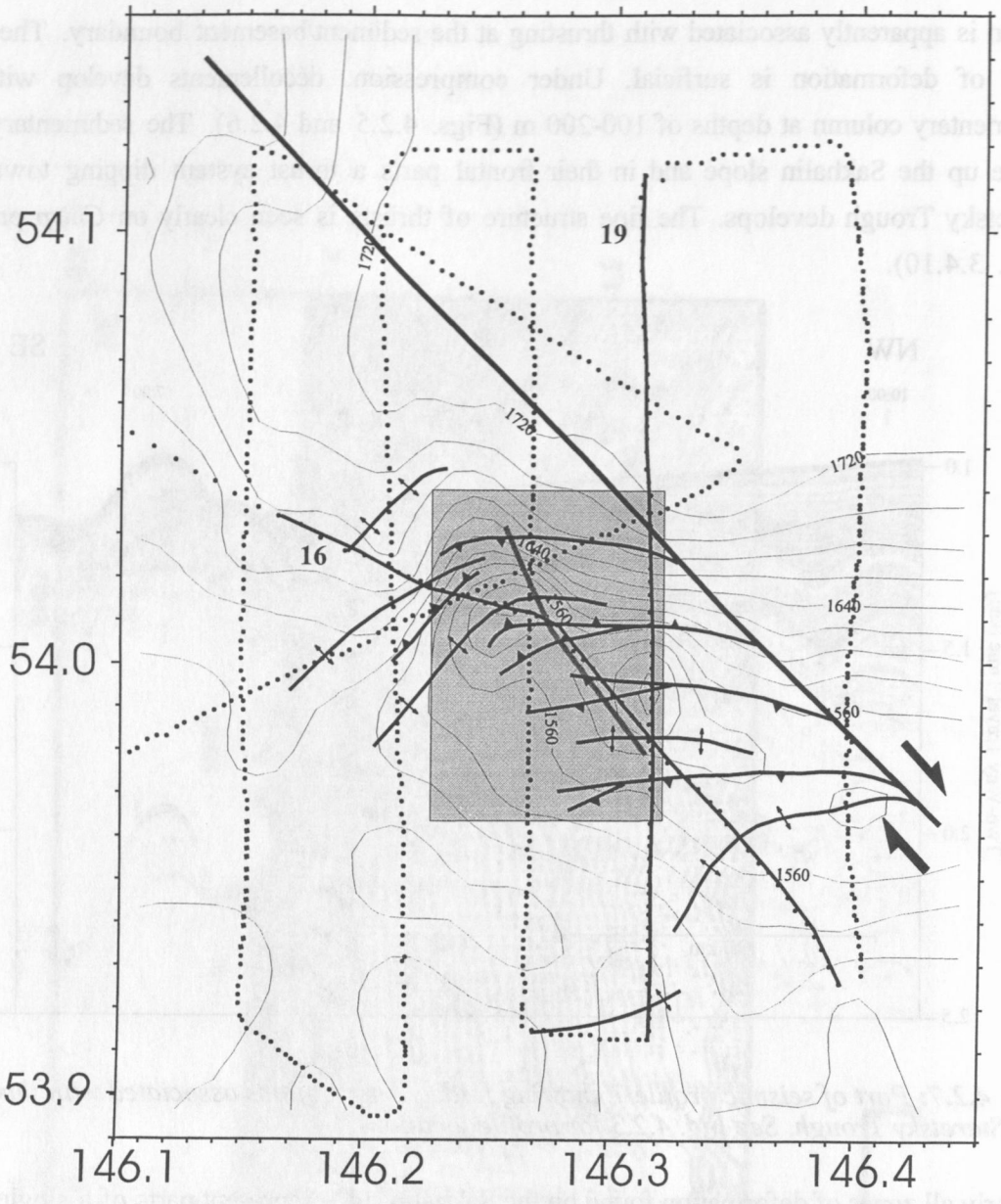

Fig. 4.2.8: *Bathymetry and structure of the barite mineralization area in the Derugin Basin. Lines with triangles indicate thrusts, those with arrows are strike-slips. Lines with double arrows mark fold axes. Grey rectangle and grey line show area mapped by the RV "Akademik Lavrentiev" in 1998 and OFOS track respectively.*

Staretsky Trough and Derugin Basin

Gravimetric data suggest that south of 56°N on the continuation of the Kashevarov zone in the Staretsky Trough, a depression and a basement high oriented in the northeasterly direction exist. There is no evidence that the Kashevarov zone dissected them. The high represents a tilted block formed at the early extensional stage. Now it is undergoing obvious compression. In the sedimentary cover, particularly northwestward of the high, gentle folding apparently associated with thrusting is observed (Fig. 4.2.7). Except for this example, we found no evidence for deformations in the sedimentary cover of the Staretsky Trough. In contrast, thrust and folds are widespread in the northeastern Derugin Basin (Fig. 4.2.3).

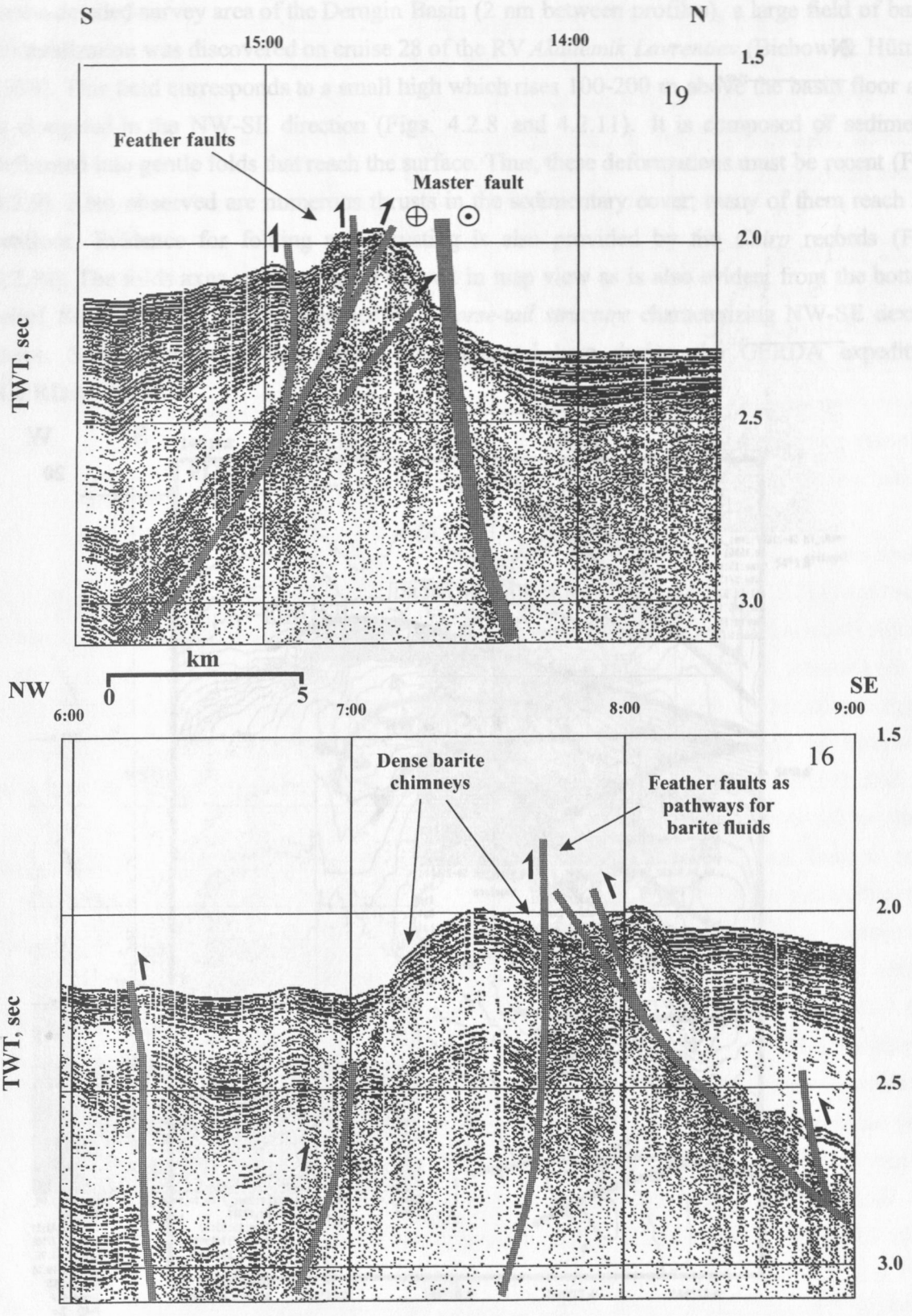

Fig. 4.2.9: *Two seismic cross-sections across the barite field area. Profile 16 at time 08:00 h lies very close to the dense barite chimneys. See Fig.4.2.8 for profile location.*

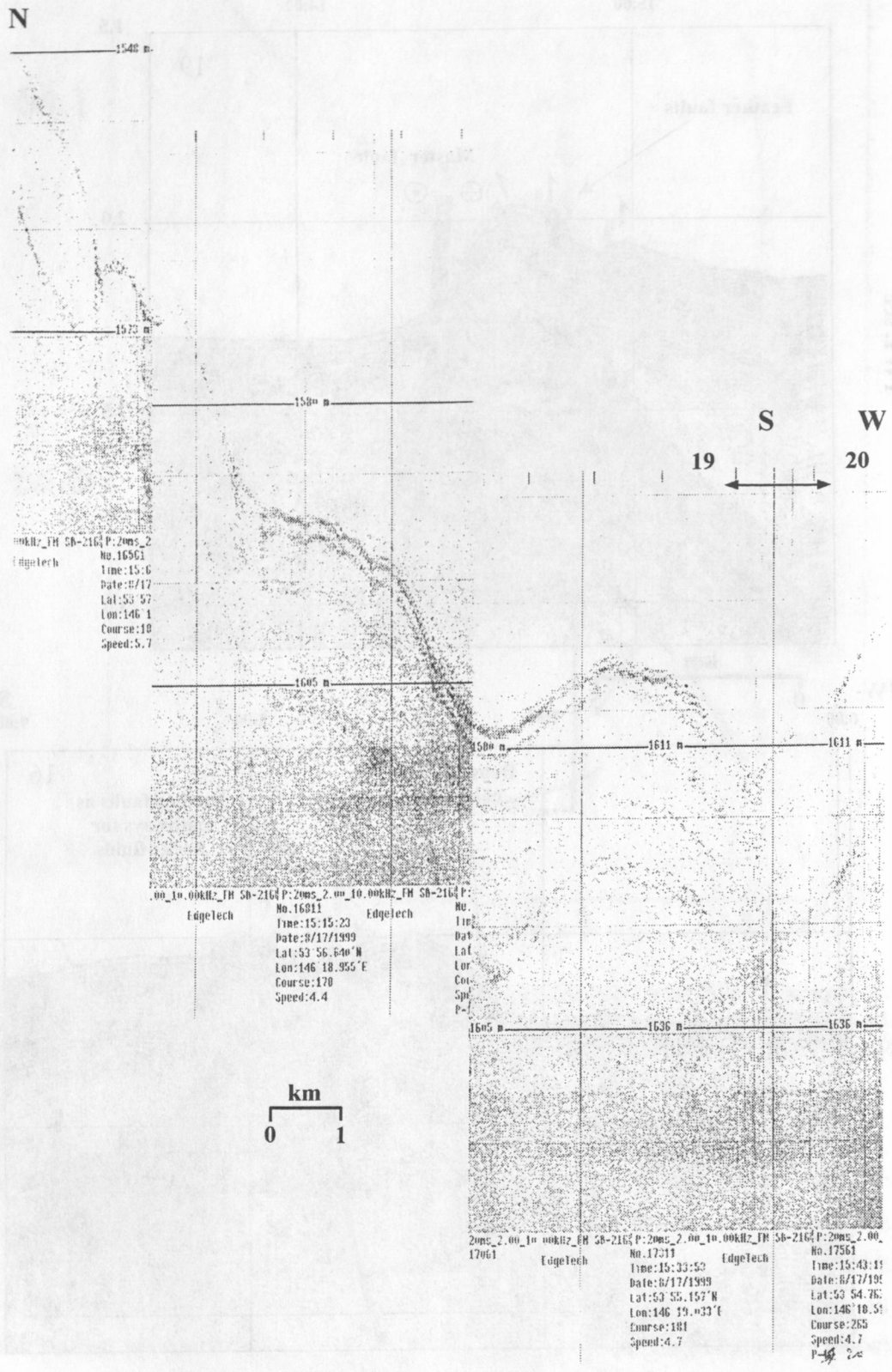

Fig. 4.2.10: *Chirp record showing gently folded sediments and recent thrusts. Part of profile 19 from 15:00 h up to the end of profile.*

The Derugin Basin

In the detailed survey area of the Derugin Basin (2 nm between profiles), a large field of barite mineralization was discovered on cruise 28 of the RV *Akademik Lavrentiev* (Biebow & Hütten, 1999). This field corresponds to a small high which rises 100-200 m above the basin floor and is elongated in the NW-SE direction (Figs. 4.2.8 and 4.2.11). It is composed of sediments deformed into gentle folds that reach the surface. Thus, these deformations must be recent (Fig. 4.2.9). Also observed are numerous thrusts in the sedimentary cover; many of them reach the seafloor. Evidence for folding and thrusting is also provided by the *Chirp* records (Fig. 4.2.10). The folds axes and thrusts are convex in map view as is also evident from the bottom relief. Such a pattern can be regarded as a *horse-tail structure* characterizing NW-SE dextral shear. Strike-slips with such strikes were mapped here during the GERDA expedition (GERDA, 1995).

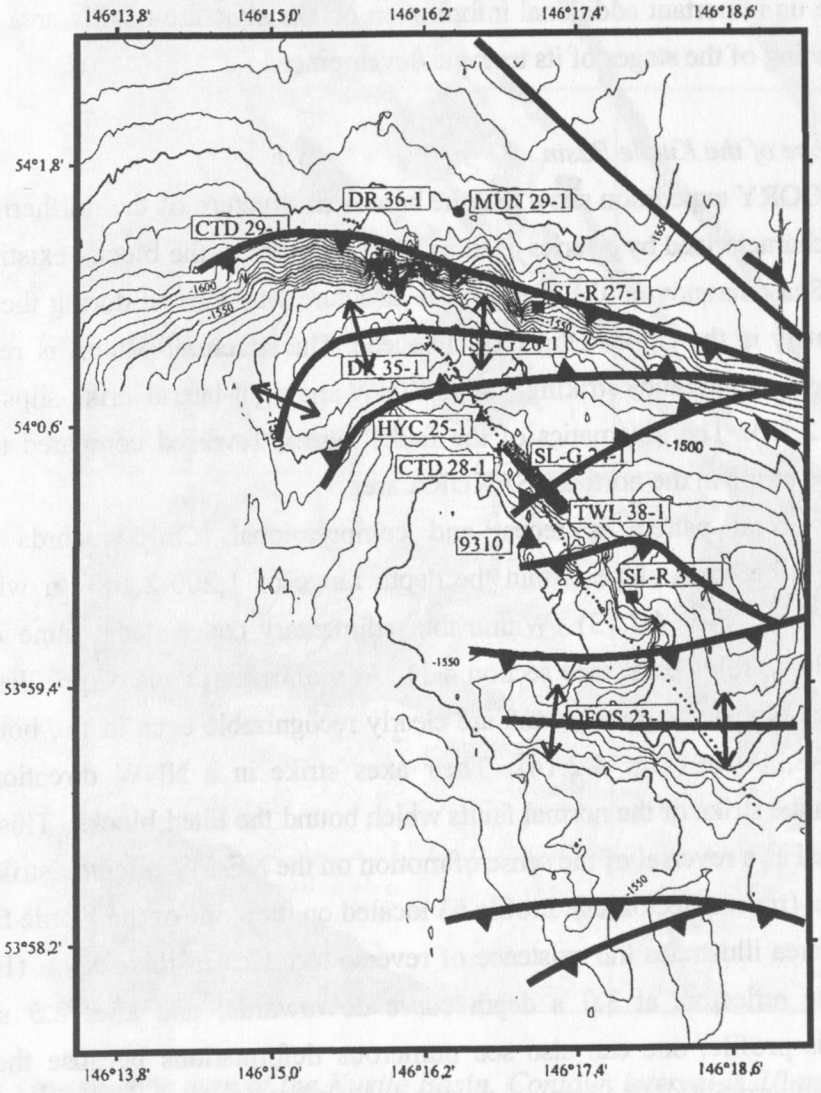

Fig. 4.2.11: *Bathymetric map of the barite field area generated during cruise 27 of the RV "Akademik Lavrentiev" (Biebow & Hütten, 1999). A system of thrusts and folds appears near the strike-slip in a horse-tail pattern.*

The discovery of large barite mineralization fields in this area poses two questions. The first concerns the source of the barite and the second is: Which is the mechanism forcing the barite to rise to the seafloor? Isotopic analyses show that the barite is sedimentary in origin (Derkachev et al., 1999). Our studies suggest that the barite may be squeezed out of the sediments under the existing compressive stress. It then migrates to the surface along the system of thrusts which serve as conduits.

4.2.2 Southern SAKURA area

Studies in the southern SAKURA area were carried out in two regions: the northern slope of the Kurile Basin and the central part of the basin (Fig. 4.2.12). On the northern slope, the profiles were located inside the GREGORY area and they were carried out to provide the necessary site survey for an ODP proposal. Structural analysis was not the main goal. Nevertheless these profiles provide us important additional information on the structure of this area and permit a better understanding of the stages of its tectonic development.

The northern slope of the Kurile Basin

Results of GREGORY expedition show that the basement structure of the northern slope of the Kurile Basin is characterized by a series of tilted blocks similar to the blocks existing elsewhere in the Okhotsk Sea (Baranov et al., 1999). This structure was formed during the first tectonic stage approximately in the Upper Oligocene-Miocene. The structural pattern is represented by two fault systems: normal faults striking NW to WNW and right-lateral strike-slips trending NE to ENE (Fig. 4.2.13). The kinematics of the faults here is reversed compared to that of the faults of the same strike in the northern SAKURA area.

The second structural pattern is recent and compressional. *Chirp* records show many discontinuities on the basin slope within the depth range of 1,200-2,100 m which may be interpreted as thrusts (Fig. 4.2.13). Within the sedimentary cover at the same depth range, gentle low-amplitude folds exist (see section 4.1). At the western ends of profiles 36 and 37, the folds have the highest amplitudes and are clearly recognizable even in the bottom relief at depths of 2,100-2,200 m (Fig. 4.2.14). Their axes strike in a NNW direction, i.e., in a direction close to the strike of the normal faults which bound the tilted blocks. This observation may be interpreted as a reversal of the sense of motion on the NE-SW oriented strike-slips from dextral to sinistral (reverse tectonics). Profile 63 located on the slope of the Kurile Basin west of the GREGORY area illustrates the existence of reverse tectonics in this region (Fig. 4.2.15). Near 21:00 h the reflectors at 3.0 s depth curve downwards, and after 2.5 s they curve upwards. On this profile, one can also see numerous deformations because they reach the seafloor. The southern SAKURA area as well as the GREGORY area belong to the same structural zone, namely the transition zone between the Academy of Sciences Rise and the Kurile Basin. Therefore, although profiles are not available from the area between them, we can assume that the zone of deformation can be traced along the entire slope.

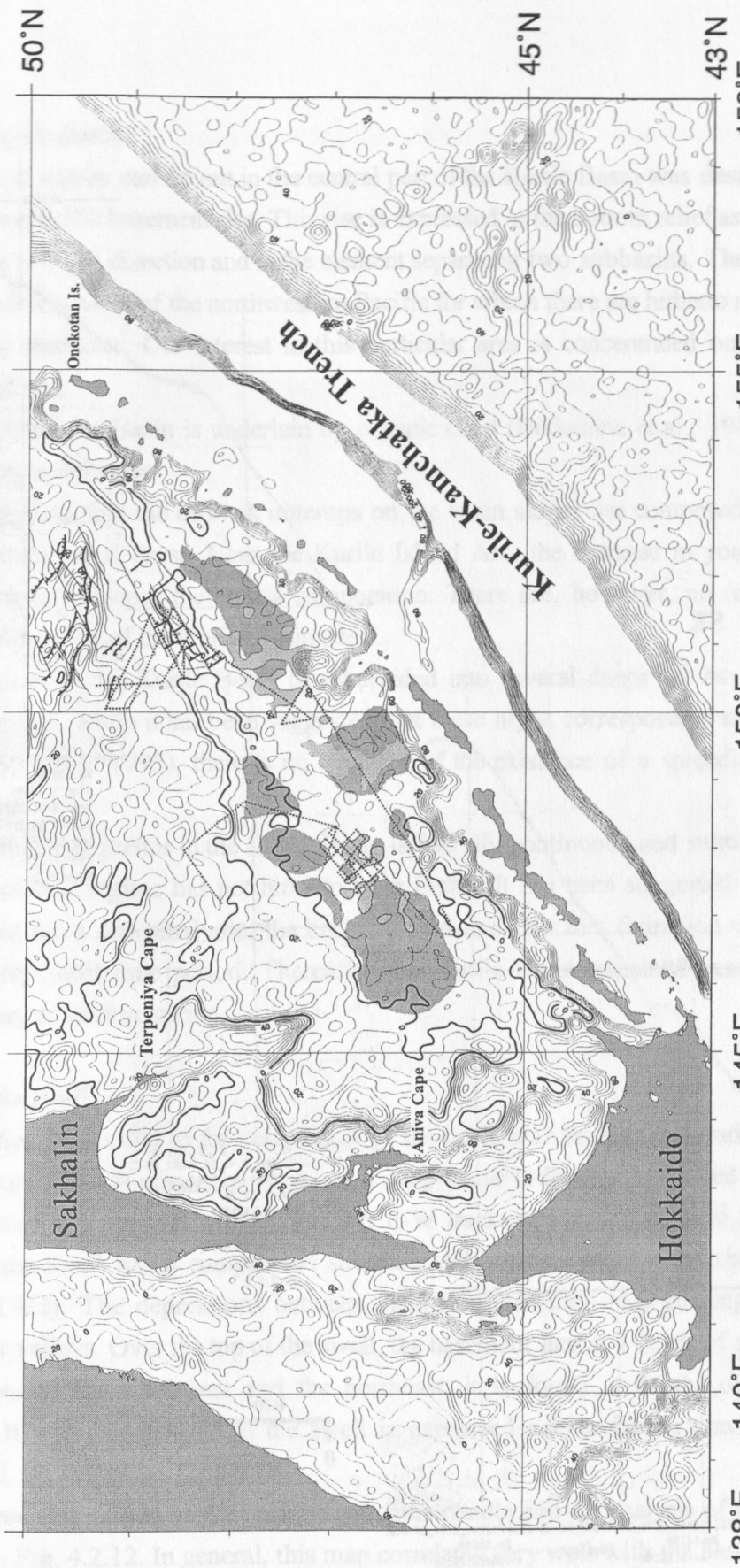

Fig. 4.2.12: *Gravimetric map of the Kurile Basin. Contour interval is 10 mG. The thick line is the zero contour. Dark grey indicates areas with a depth to basement of >7 km. Light grey shows positive anomalies (>20 mG) in the Kurile Basin. Thin lines mark ship's tracks. The system of normal faults and strike-slips on the northern Kurile slope (GREGORY area) and the spreading axis in the central Kurile Basin are also shown.*

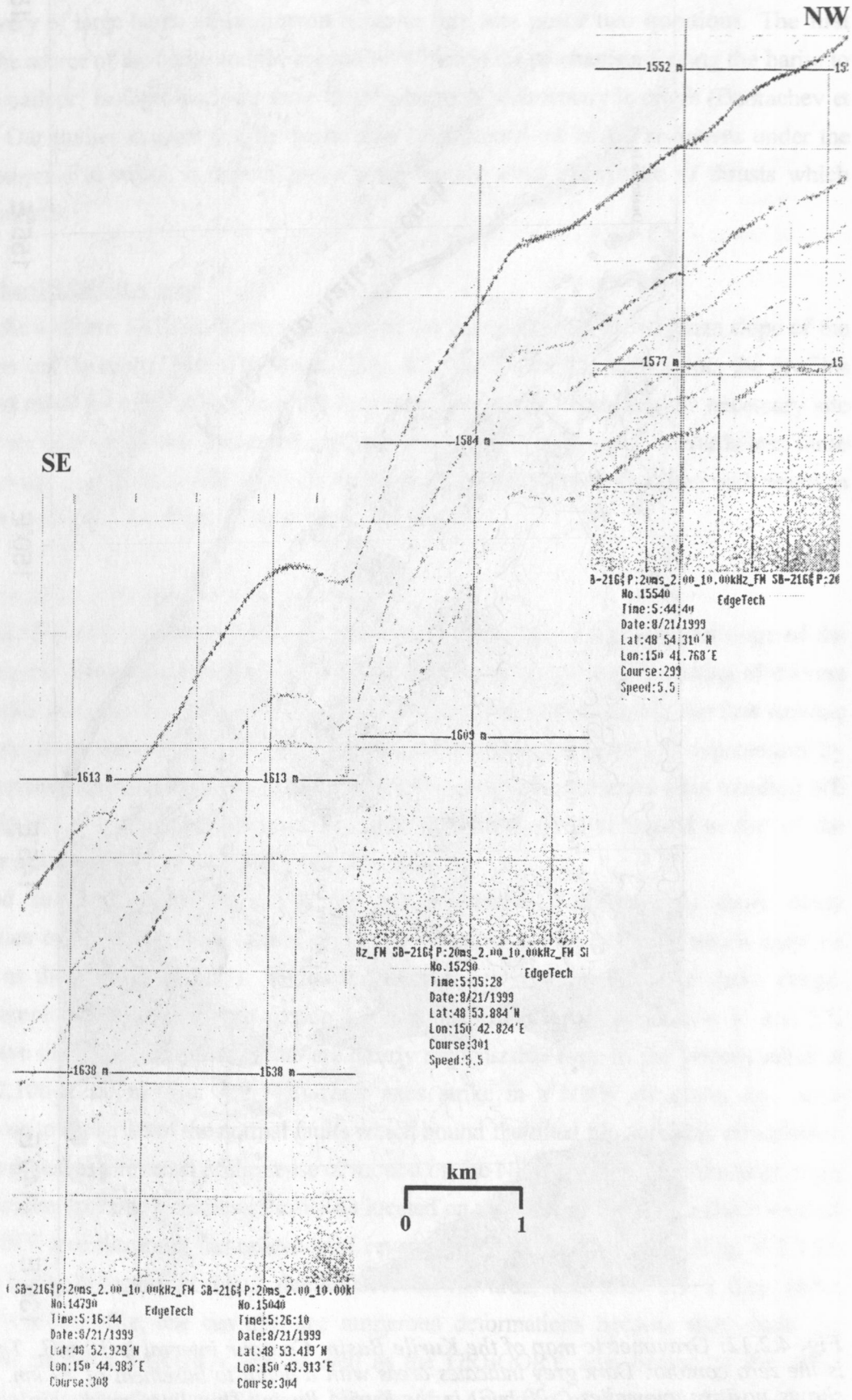

Fig. 4.2.13: Recent thrusts on the northern slope of the Kurile Basin. Chirp record, part of profile 32.

The central Kurile Basin

The geophysical survey carried out in the central part of the Kurile Basin was designed to study the nature of a specific basement rise. This rise is expressed in the bottom relief as a gentle swell oriented in the NW-SE direction and is the element separating two subbasins. The Kurile Basin is the only back-arc basin of the northwestern Pacific for which there are hitherto no data on age and spreading character. Our interest in this particular area is concentrated on a number of unsolved problems:

1. Although the Kurile Basin is underlain by oceanic crust (Bikkenina et al., 1987), the extent of spreading is not clear.
2. Dredge data show that the bedrock outcrops on the basin slopes are composed of rocks of a Mesozoic continental crust. Near the Kurile Island Arc, the increase in young island arc volcanism may influence the crustal composition. There are, however, no reliable data on crustal composition of the Kurile Basin itself.
3. The basement of the Kurile Basin is subdivided into several deeps by two NW-striking basement highs. While it has been suggested that these highs correspond to transform faults (Gnibidenko et al., 1995), there is no evidence of the existence of a spreading axis in the Kurile Basin.
4. The sedimentary sequence in the Kurile Basin is laterally continuous and stratified. Evidence for an extensional regime has not hitherto been found. It has been suggested that sediments in this basin were deposited after the basin formed and that this formation was completed within a very short time period. Thereafter, the Kurile Basin remained passive during its entire history of sedimentation.

Structure of the swell

Previous studies. The swell in the central part of the basin was investigated during a cruise of the Pacific expedition *Souzmorgeo* to select a deep-water drilling site planned in 1978. The survey consisted of a network of 6 N-S and 6 E-W tracks spaced 10 nautical miles apart. It showed that the swell has a complicated structure and consists of isometric basement highs (Zhuravlev, 1982). The depressions between them form fan-like, N-S striking systems that resemble river valleys. Over the top of the swell, the basement lies at a depth of about 5 km; in the depressions to the southwest and the northeast, it is found at depths of 8 and 7 km respectively. It was also noted that the swell is expressed neither in the gravity nor in the magnetic field.

The survey area was chosen on the basis of previous results and on analysis of the gravimetric map shown in Fig. 4.2.12. In general, this map correlates very well with the basement relief of the Okhotsk Sea except in the case below.

Negative gravimetric anomalies (up to -50 mG) which correspond to depressions are observed along the northern side of the Kurile Basin from Aniva Cape to the latitude of Onekotan Island. The largest two are located at the northwestern corner of the basin. They are divided by a high

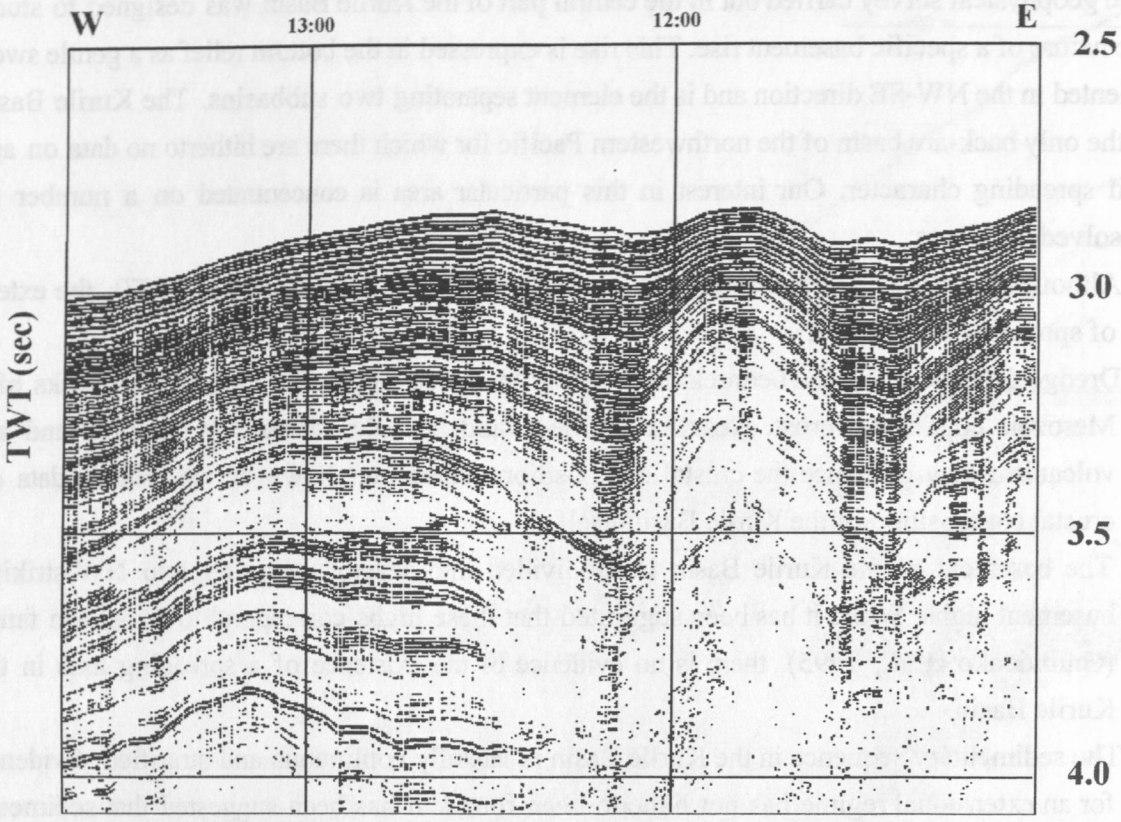

Fig. 4.2.14: *Folded sediments on the northern slope of the Kurile Basin suggestive of recent compression in this area. Part of seismic profile 36. One hour corresponds to about 4.5 nautical miles.*

which is the marine continuation of Terpeniya Cape. A series of small depressions is found near the Kurile Island Arc.

In the axial part of the Kurile Basin, there are positive gravity anomalies >20 mG in amplitude and isometric or linear in outline. The linear shape of the anomalies may be due to the existence of submarine volcanic chains of the Kurile Arc. A superposition of gravimetric and basement contour maps of the Kurile Basin (Zhuravlev, 1982; Gnibidenko et al., 1995; Kharakhinov, 1998) shows that only one of the basement depressions (with a depth up to 7 km) is located within the negative anomalies (Fig. 4.2.12). All the other depressions coincide with positive anomalies. Some (for instance that off Urup Is.) correspond to anomaly maxima >20 mG. Thus, denser oceanic crust must exist beneath the deeps and this crust is responsible for the anomalies. The basement rise under study is also located in the axial part of the basin with positive anomalies of >29 mG.

Structure of the rise

A general basement profile crossing the rise from southwest to northeast is shown in Fig. 4.2.16. The basement becomes shallower towards the top of the rise from 7 s depth below sea

level to 6 s in steps, with the steep side facing the northeast. The top of the basement rise is at 5 km below sea level (see this report).

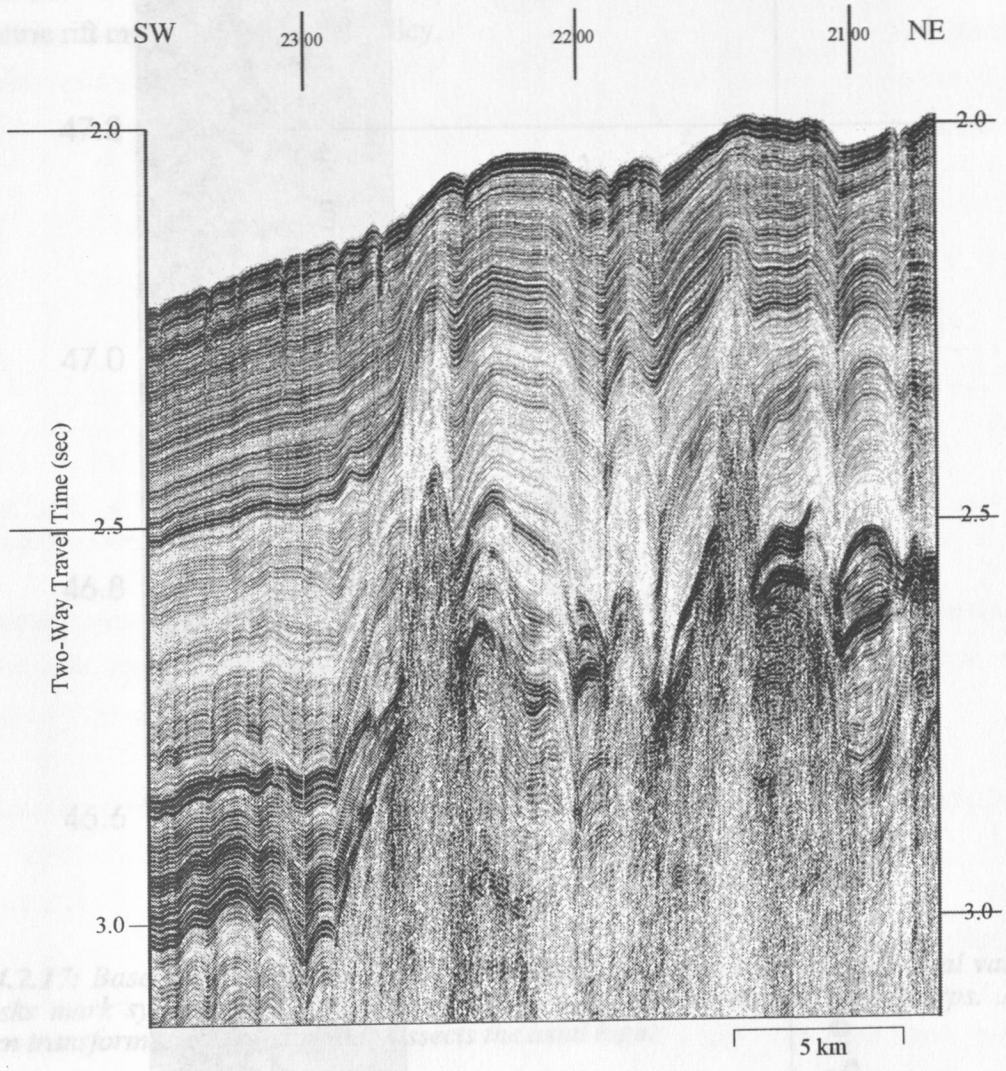

Fig. 4.2.15: *Part of profile 63 on the northern slope of the Kurile Basin west of the GREGORY area. Sediments are gently folded all the way to the seafloor.*

Northeast of the rise top, the basement also shows a step-like pattern, but here their steep sides face the southwest. Since the basement does not become lower after the top of the rise is passed, the rise must be asymmetric. This apparent asymmetry may be a result of a slight change in profile orientation: after 0600 h, profile 45 is oriented at a smaller angle to the strike of the structures (Fig. 4.2.17).

Despite some asymmetry, the profile of the rise is comparable to typical profiles of spreading ridges. Therefore, we will describe the rise morphology using terminology common for mid-ocean ridges.

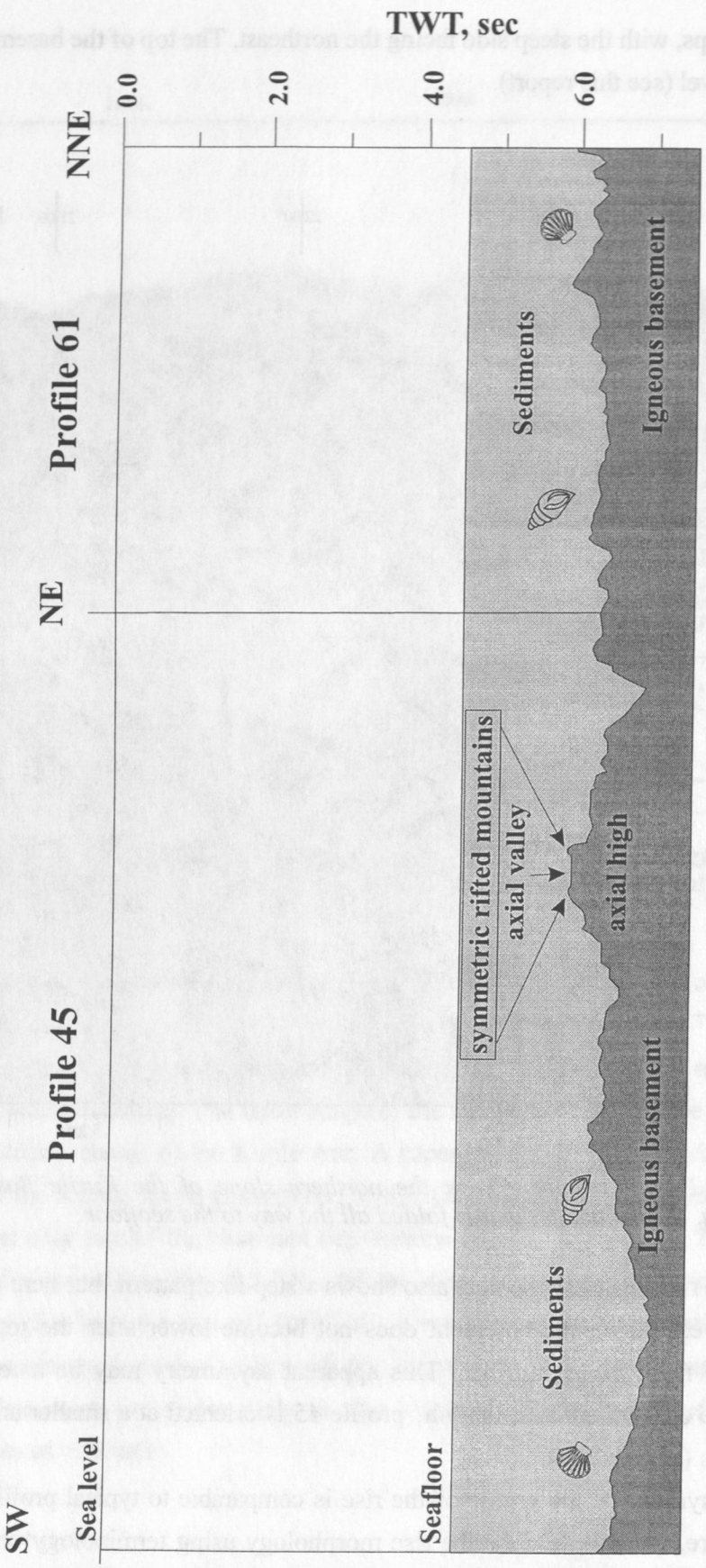

Fig. 4.2.16: Interpreted composite cross-section across the Kurile Basin. The rise which has the morphology of a spreading center is seen at the center.

A seismic survey with a regular track network having a 5 nm spacing was carried out around the axial part of the rise (Fig. 4.2.17). A first analysis of the data obtained allows the general morphology to be understood. This morphology will be compared with those of well-known spreading zones in detail. The following elements have been identified: axial high, axial zone, symmetric rift mountains and axial valley.

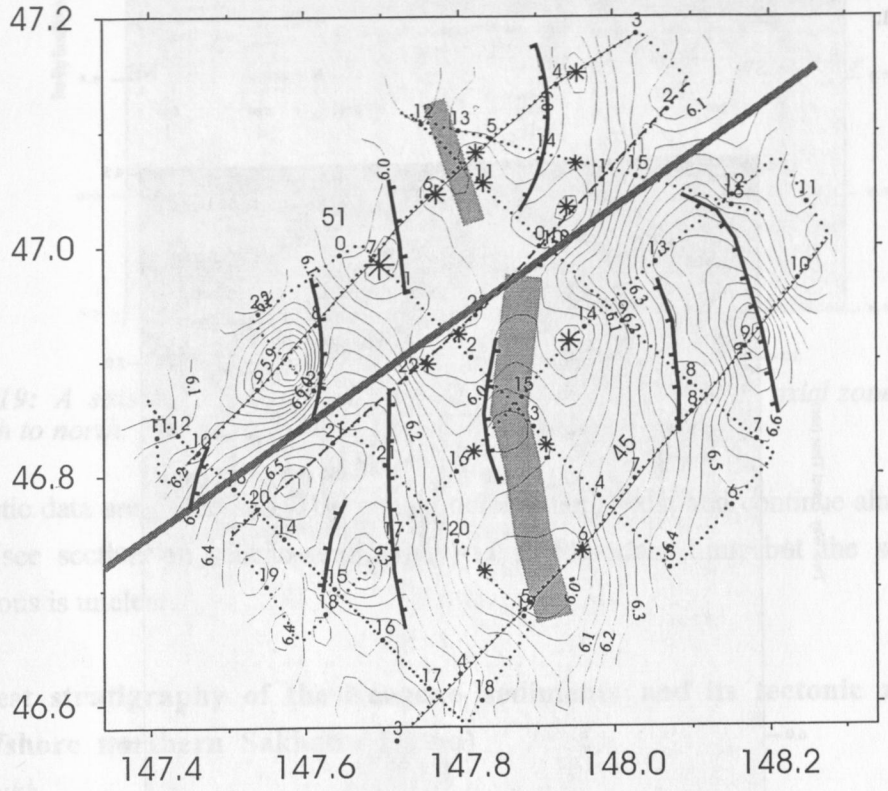

Fig. 4.2.17: *Basement morphology of the axial high. Grey line indicates the axial valley, and asterisks mark symmetric rift mountains. Lines with bars are normal fault scarps. A north-eastern transform or strike-slip fault dissects the axial high.*

The axial high strikes in a nearly N-S direction (350°), and has the form of a south-facing wedge. The width of the rise in the central part of our detailed study area is about 15 km, its height is about 1 km. From east to west, it is accompanied by depressions and conjugate asymmetric rift mountains bounded to one side by normal faults. The depressions terminate abruptly where the axial high widens, and is apparently cut by a NE-SW-striking fault. This fault is oriented oblique to the axial high and obviously has a transform or strike-slip nature.

The axial zone occupies the flat top of the axial high which is outlined by the 5.2 km basement depth contour and includes symmetric rift mountains and an axial valley. The symmetry of the rift mountains which according to their shape can be regarded as volcanic edifices can be seen distinctly on profile 45. On this profile, two mountains of about 0.1 s height (ca. 100-200 m) are located on the sides of the axial zone. Between the rift mountains is the flat, 5-7 km wide,

axial valley. This axial valley together with the accompanying rift mountains continue to where the axial high is cut by the strike-slip fault.

Farther to the north, the structure of the axial zone changes (compare Figs. 4.2.18 and 4.2.19, profile 45 and 51). Firstly, the axial valley becomes much wider (up to 17 km), though it is also accompanied by chains of volcanic mountains. Secondly, a new pair of volcanic mountains appears in the central part of the valley. A new, relatively symmetric axial valley originates between them.

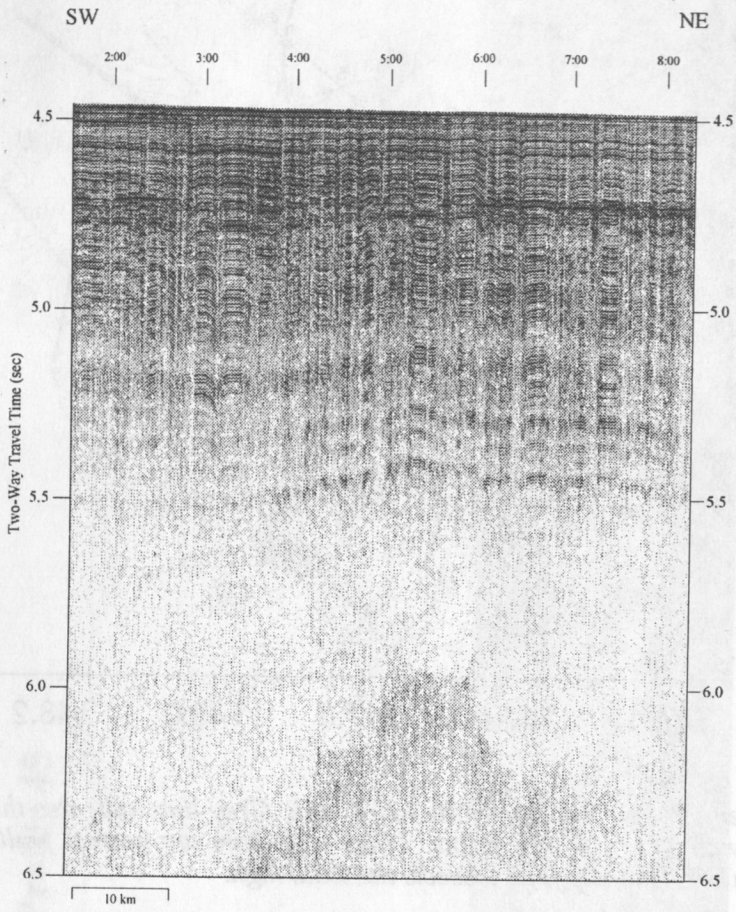

Fig. 4.2.18: *A seismic cross-section (profile 45) showing change in axial zone morphology from south to north. Profile location is shown in Fig.4.2.17.*

The morphology of the axial high suggests that it corresponds to a spreading axis. This axis (a spreading ridge) strikes N-S normal to the general strike of the Kurile Basin. We have mapped only one segment of it and do not know much about its northern and southern extensions. Obvious is only that it becomes wider to the north and is apparently bounded near the northern slope of the Kurile Basin by a strike-slip or transform fault, a situation similar to that within the detailed study area. To the south towards the Kurile Basin, it apparently becomes a rift with stretched continental crust.

One question must remain open: During which time period was this rise (hereby named the SAKURA spreading center) active? We may have an opportunity to answer this question after

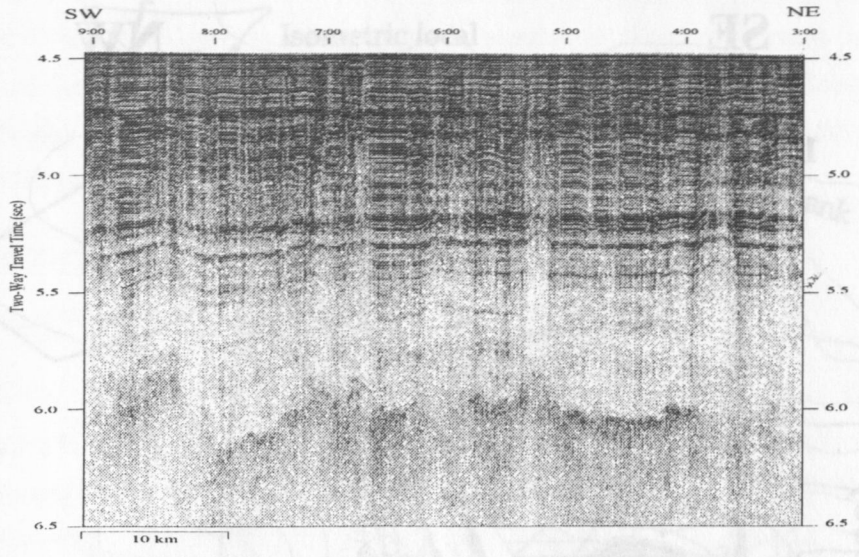

Fig. 4.2.19: *A seismic cross-section (profile 51) showing change in axial zone morphology from south to north. Profile location is shown in Fig.4.2.17.*

the magnetic data are processed. That certain deformations exist and continue almost up to the seafloor (see section on seismo-stratigraphy) is an important hint, but the style of these deformations is unclear.

4. 3 Latest stratigraphy of the Neogene sediments and its tectonic applications (area offshore northern Sakhalin Island)

V. Karnaukh

The area of study is located in the Staretsky Trough from 56°N southward to the Derugin Basin. The water depth of the Trough increases from 400 to 1,400 m in the southeastern direction. The northern slope of the Trough is complicated by two NE-SW striking depressions, called here the Northern and the Southern Depression. The sediment thickness in the Staretsky Trough is generally 1.5-2.0 s but can be more. The sedimentary cover is supposedly of Oligocene-Quaternary age (Gnibidenko & Khvedchuk, 1982). A regional unconformity exists within this cover (Fig. 4.3.1). Its depth distribution is shown in Fig. 4.3.2. Generally, this depth increases in the southeasterly direction from 1.0-1.5 to 3.0 s. An exception is given by the isometric local depression with a dimension of 30 x 25 km in the northwestern part of the Trough. This unconformity is located at a of depth more than 2.0 s (Fig. 4.3.3). We will call the sedimentary unit located above this interface unit A, and that located below, unit B. The maximum thickness of unit A (>1.2 s) is observed in the local depression at the northwestern part of the Trough and in the area where it joins the Derugin Basin. In the central part of the Trough, unit A has a thickness of about 0.8 s.

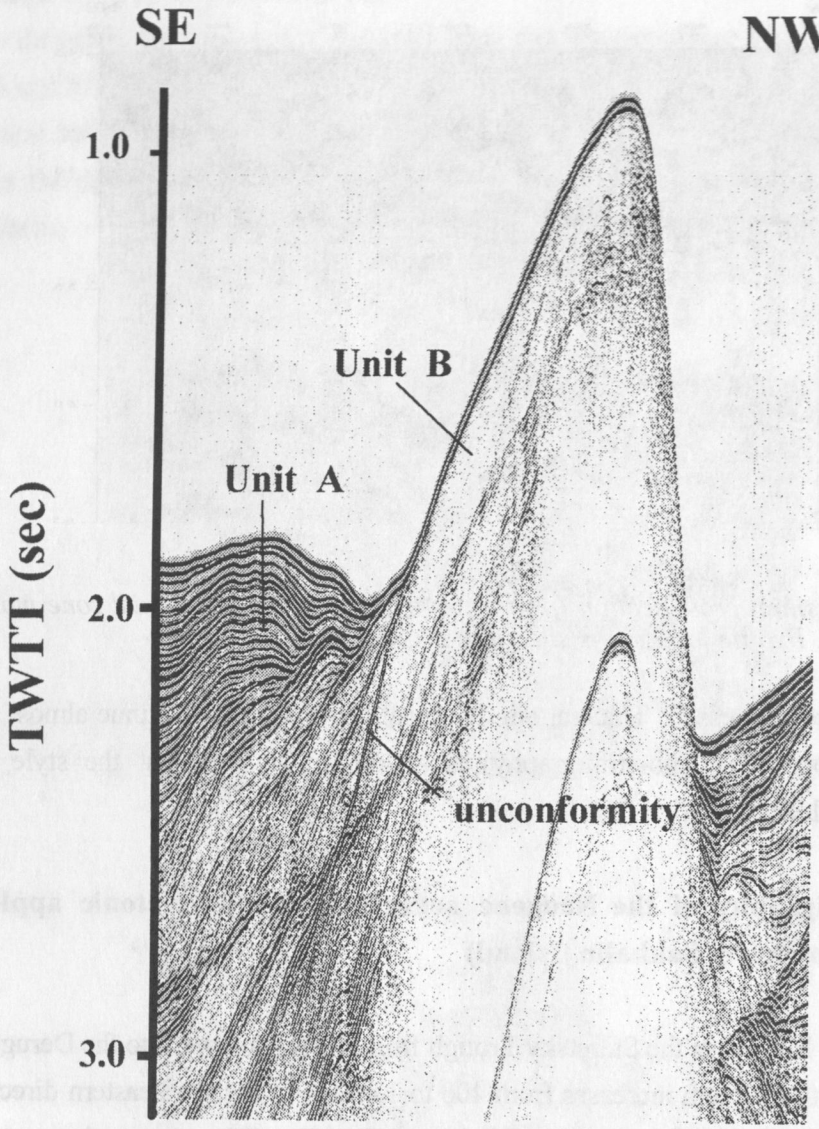

Fig.4.3.1: *Part of reflection seismic profile 7 showing the sedimentary structure of the southern part of Staretsky Trough. For location see Fig. 4.3.2.*

In the isometric local depression and in the Southern Depression, there is an acoustically transparent facies in the upper part of unit B. Since these depressions were areas of active terrigenous sedimentation in the Late Neogene (the thickness of the Plio-Pleistocene sediments on the shelf to the east off Northern Sakhalin is about 6,000 m; Zhuravlev, 1982), the seismically transparent characteristic of the upper unit B implies that the sedimentary material must have been well-sorted and homogeneous. In the local depressions, the unconformity dips towards their axes and is interrupted by faults with displacements of up to 0.12 s. This suggests rapid subsidence after the formation of the unconformity. In the Southern Depression, unit B onlaps the acoustic basement. Reflections here are rare but continuous and generally overlie the paleorelief. Thus, in this depression, sediments of unit B must have accumulated on an existing

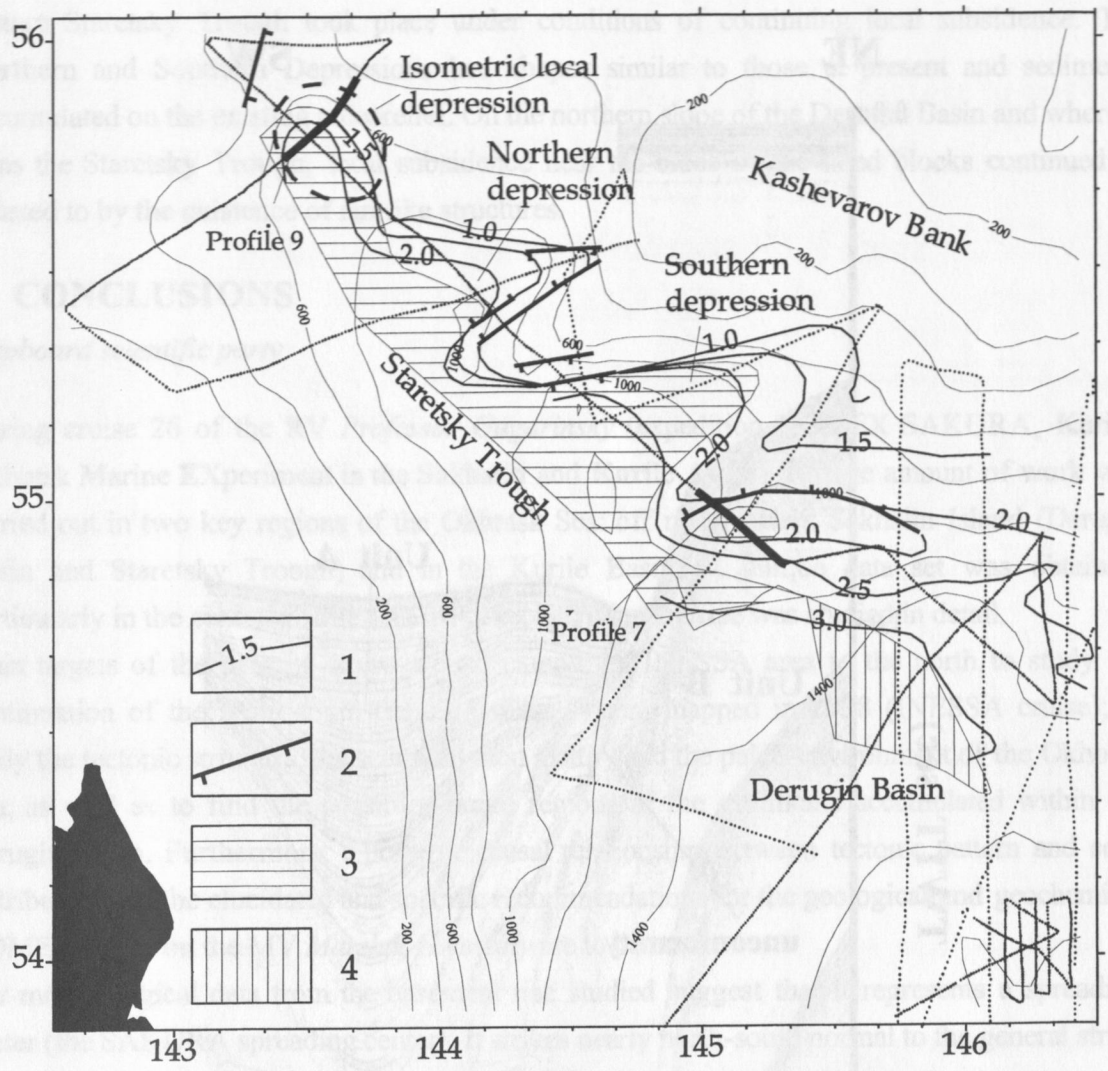

Fig. 4.3.2: *Structural pattern of the Staretsky Trough. 1: depth of regional unconformity surfaces; 2: faults; 3: areas of acoustically transparent facies at the top of layer B; 4: chaotic facies at the top of layer B.*

surface of paleorelief under tectonically quiescent conditions. On the northern slope of the Northern Depression, unit B is acoustically well-stratified and is interrupted by numerous faults with displacements of up to 0.15 s. Above the unconformity, faults are usually absent. The stratifications of unit B here dip towards the axis of the depression. On the southern slope of the Northern Depression, unit B is characterized by a chaotic facies and terminates onlap. Thus the Southern Depression was formed in a subsiding regime during the deposition of unit B. A horst which separates the Southern Depression from the Derugin Basin is covered by acoustically transparent sediments of unit B. The difference between the depths of the unconformity on the horst and in the adjacent depressions is about 1.0 s. We interpret this difference to be due to uplifting of the horst after accumulation of unit B.

In the area between Staretsky Trough and the Derugin Basin, the upper part of unit B is seismically chaotic. Its sedimentary nature is unclear. Towards the northern slope of the

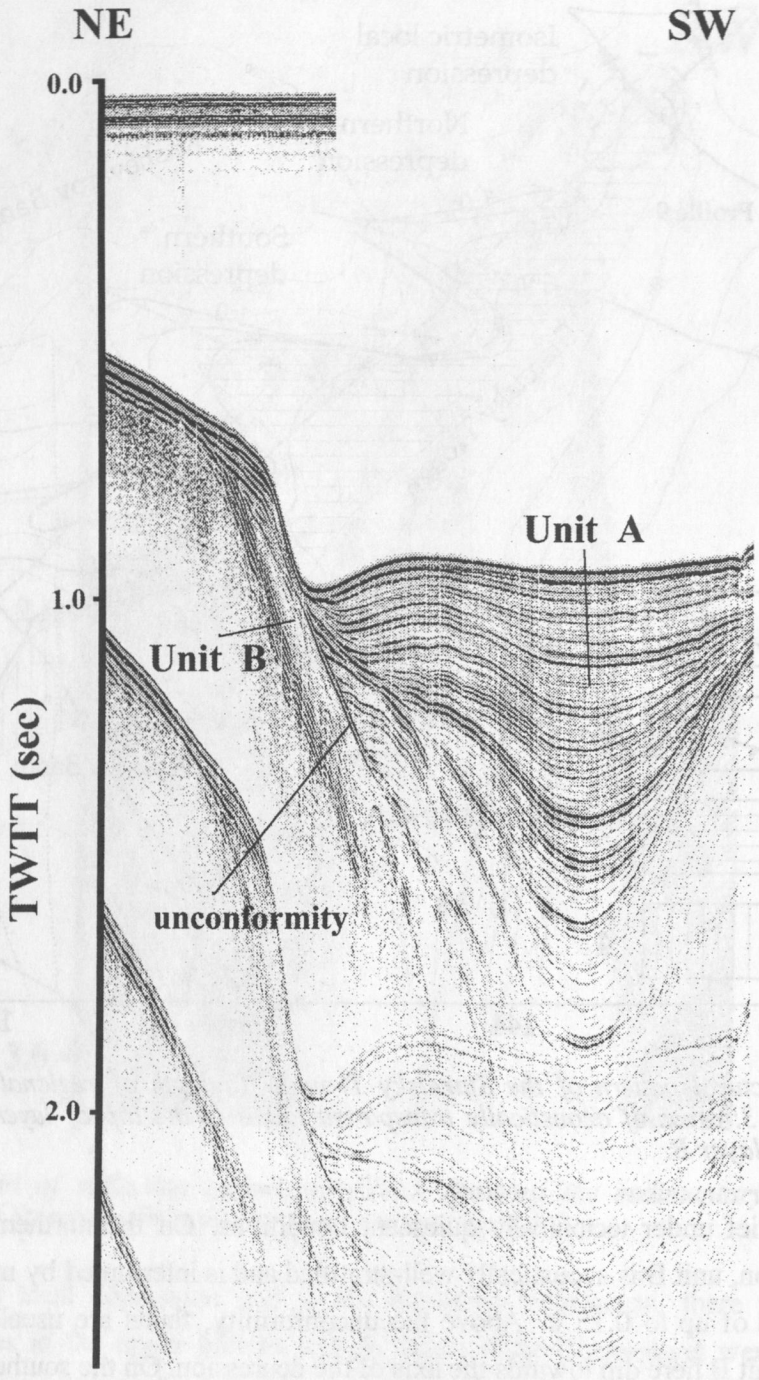

Fig. 4.3.3: *Part of reflection seismic profile 9 showing the sedimentary structure of the isometric local depression of the northern Staretsky Trough.*

Derugin Basin, the reflection pattern changes from chaotic to stratified (characteristic of turbiditic flows).

The regional unconformity in the Staretsky Trough formed in the Early Pliocene (Bondarenko et al., 1981). Thus, unit B must be pre-Early Pliocene and unit A Late Pliocene to Quaternary in age.

In the Late Plio-Pleistocene, sedimentation within the isometric local depression in the north-eastern Staretsky Trough took place under conditions of continuing local subsidence. The Northern and Southern Depressions had shapes similar to those at present and sediments accumulated on the existing paleorelief. On the northern slope of the Derugin Basin and where it joins the Staretsky Trough, local subsidence near the sides of the tilted blocks continued as attested to by the existence of fan-like structures.

5. CONCLUSIONS

Shipboard scientific party

During cruise 26 of the RV *Professor Gagarinsky* (expedition KOMEX SAKURA, **K**urile-**O**khotsk **M**arine **EX**periment in the **Sa**khalin and **Kur**ile **A**reas), a large amount of work was carried out in two key regions of the Okhotsk Sea: off northeastern Sakhalin Island (Derugin Basin and Staretsky Trough) and in the Kurile Basin. A unique data set was obtained, particularly in the central Kurile Basin in which a basement rise was studied in detail.

Main targets of the present cruise are: to extend the INESSA area to the north to study the continuation of the north-south trending shear system mapped in 1998 (INESSA cruise); to study the tectonic structure, the sedimentation history and the paleo-environment of the Okhotsk Sea; as well as to find the possible source regions of the sediments accumulated within the Derugin Basin. Furthermore, a possible causal relationship between tectonic pattern and seep distribution is to be elucidated and specific recommendations for the geological and geochemical KOMEX cruise on the MV *Marshal Gelovany* are to be made.

Our morphological data from the basement rise studied suggest that it represents a spreading center (the SAKURA spreading center). It strikes nearly north-south normal to the general strike of the Kurile Basin. Thus, the Kurile Basin must have opened in a NE-SW direction as a pull-apart basin. Such opening kinematics is in excellent agreement with the plate tectonic history of this region. Two tectonic regimes were distinguished in the areas investigated. The first, more ancient, was responsible for the formation of the basic structural pattern and is characterized by extension. During this period, a majority of the extensional structures, including the deep-water basin with stretched continental or oceanic crust, was created. It was succeeded by a compressional regime which inherited the existing structural pattern, but the sense of motion along corresponding faults reversed (reverse tectonics).

Today compressional conditions still prevail. Both tectonic regimes are governed by motions along vast shear zones which have a NW-SE strike in the northern part of the Okhotsk Sea and a NE-SW strike in its southern part. In Fig. 5.1, the Derugin Basin area is chosen to illustrate these ideas. To a first approximation, such motions can be explained by a clockwise rotation of the Okhotsk Plate as is assumed in the model.

The existence of a recent compressional regime in the Okhotsk Sea creates favorable conditions for the extrusion of dissolved fluids from sediments and for their migration to the surface. Our

Structural pattern of the northern SAKURA area as a result of a change in the tectonic regime

Stage I: Oligocene-Miocene - Pliocene(?)
Left-lateral shear and extension

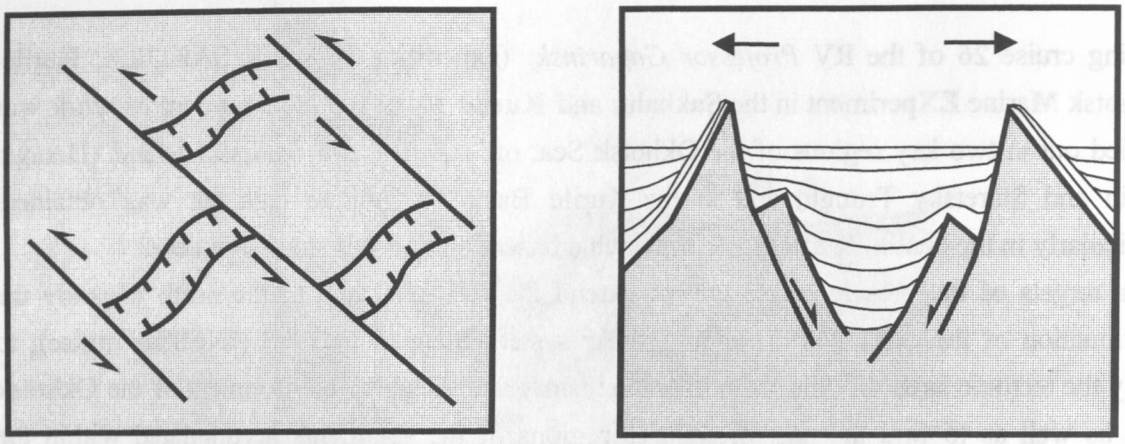

Stage II: Pliocene(?) - Present
Right-lateral shear and compression
(reverse tectonics)

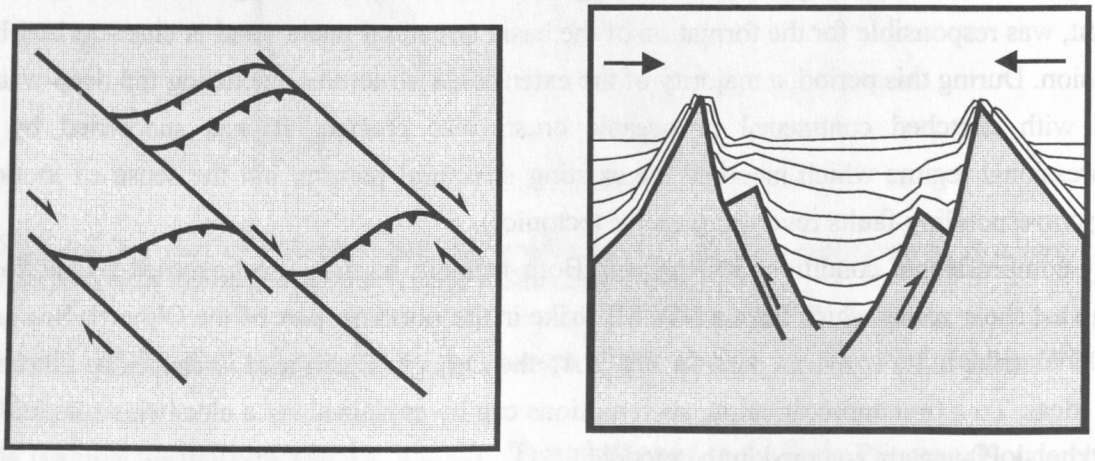

Fig. 5.1: *Tectonic history of the Okhotsk Sea: from extension to compression.*

survey results from the area of the barite mineralisation field in the Derugin Basin demonstrates clearly that recent compressional tectonics exists in this region. The barite fields are located near zones where the thrusts approach the seafloor and therefore function as fluid conduits (Fig. 5.2). Among the several newly discovered seep locations within the Staretsky Trough at water depths of 470-1,000 m, one site is unequivocally associated with recent tectonic movements within a thrust zone.

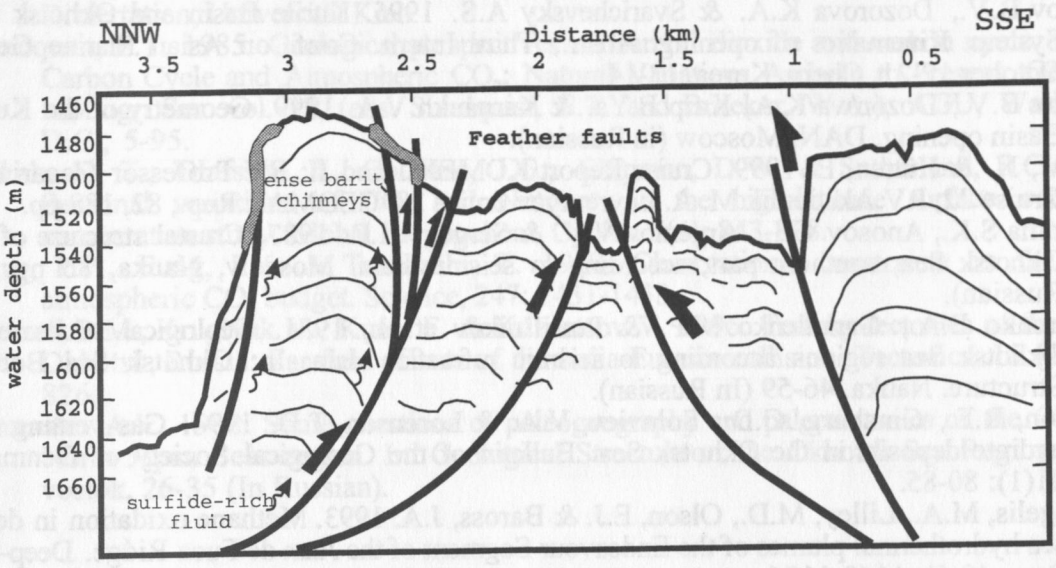

Fig. 5.2: *Interpreted cross-section of the giant barite field. Sulfide-rich fluid is extruded by compression and rises along the system of thrusts.*

Reflection seismic studies off northeastern Sakhalin led to 3 new facies areas in the Staretsky Trough and its transition zone to the northwestern Derugin Basin. The reflection pattern of two of these seismic facies types indicate that during the last sea level lowstand, glaciers advanced from the Siberian shelf into the Staretsky Trough at least up to a present water depth of ca. 1,000 m. U-shaped valleys and moraine-like sediment deposits provide evidence for this conclusion. The age of the lowstand deposits cannot be accurately estimated because of the lack of absolute ages from core samples, but these sediments might represent several Pleistocene glacial cycles. The basinward continuation of these facies units is a turbid facies which is almost ubiquitous within the northern Derugin Basin. However, the main source region of the turbid sediments was probably not surveyed during the present cruise. It is still uncertain whether the Amur River entered the Derugin Basin via the Staretsky Trough during the Pleistocene or whether it crossed the shelf off northern Sakhalin.

The Holocene depositional regime appears to be dominated by erosion and sediment reworking. The high-resolution *Chirp* records reveal that up to water depths of ca. 1,400 m, submarine erosion occurred. Bottom currents winnowed out the finer particles especially around topographic highs. The uppermost layers within the study area off northeastern Sakhalin are

dominated by silty to sandy sediments as the attenuation coefficient deduced from the *Chirp* system suggests.

6. REFERENCES

Bange, H.W., Bartell, U.H., Rapsomanikis, S. & Andreae, M.O. 1994. Methane in the Baltic and North Seas and a reassessment of marine emissions of methane. Global Biogeochem. Cycles, 8(4): 465-480.

Baranov B.V., Dozorova K.A. & Svarichevsky A.S. 1995. Kurile Basin and Okhotsk Rift System: Kinematics of opening. Abstr., Third Intern. Conf. on Asian Marine Geol., October 17-21, Cheju, Korea, 13-14.

Baranov B.V., Dozorova K.A, Karp B.Ya. & Karnaukh V.A. 1999. Geometry of the Kurile Basin opening. DAN, Moscow (in Russian).

Biebow, N. & Hütten, E. 1999. Cruise Report KOMEX I and II: RV Professor Gagarinsky Cruise 22, RV Akademik M. A. Lavrentyev cruise 28. GEOMAR Rep., 82, 188 pp.

Bikkenina S.K., Anosov G.I., Argentov V.V. & Sergeev K.F. 1987. Crustal structure of the Okhotsk Sea, southern part, according to seismic data. Moscow, Nauka, 86 pp. (in Russian).

Bondarenko B.A., Garkalenko M.P. & Pustil'nikov et al., 1981. Geological structure of Okhotsk Sea regions according to seismic refraction data. In: Okhotsk Sea Bottom Structure. Nauka, 46-59 (In Russian).

Cranston, R.E., Ginsburg, G.D., Soloviev, V.A. & Lorenson, T.D. 1994. Gas venting and hydrate deposits in the Okhotsk Sea. Bulletin of the Geological Society of Denmark, 41(1): 80-85.

De Angelis, M.A., Lilley, M.D., Olson, E.J. & Baross, J.A. 1993. Methane oxidation in deep-sea hydrothermal plumes of the Endeavour Segment of the Juan de Fuca Ridge. Deep-Sea Res., 40(6): 1169-1186.

Derkachev, A.N., Bohrmann, G. & Greinert, J. 1999. Mineralogical and morphological types of authigenic precipitates from Derugin Basin sediments. Second Workshop on Russian-German Cooperation in the Sea of Okhotsk - Kurile Island Arc System KOMEX. Program and Abstracts, Kiel, 31-32.

Dickens, G.R., Castillo, M.M. & Walker, J.C.G. 1997. A blast of gas in the latest Paleocene: Simulating first-order effects of massive dissociation of oceanic methane hydrate. Geology, 25(3): 259-262.

Dozorova K.A., Baranov B.V., Karp, B.Y. & Karnaukh V.A. 1998. Sakhalin Shear Zone and the origin of the Derugin Basin (Okhotsk Sea). Abstracts of the 6th Zonenshain Conference, Moscow.

GERDA, 1995. Report of RV Professor Gagarinskiy Cruise 16 „GERDA": Geophysical Research in the Derugin Basin Area (the Okhotsk Sea), 36 pp.

Gnibidenko H.S. 1985. The Sea of Okhotsk-Kurile island ridge and Kurile-Kamchatka trench. In: A.E.M. Nairn, F.G. Stehli and S. Uyeda, The Ocean Basin and Margins, Vol. 7A, Plenum Press: 377-418.

Gnibidenko G.S. & Khvedchuk I.I., 1982. Main features of the Okhotsk Sea tectonics. In: Geological Structure of the Okhotsk Sea Region. Vladivostok, 3-25 (in Russian).

Gnibidenko H.S., Hilde T.W.C., Gretskaya E.V. & Andreev A.A. 1995. Kurile (South Okhotsk) Backarc Basin. In: B. Taylor (ed.) Backarc Basins: Tectonics and Magmatism, New York, 421-449.

Honza E., Tamaki K. & Nishimura K. 1978. Sonobuoy refraction measurements. In: E. Honza (ed.) GH77-3 Cruise Report N11, Geological survey of Japan, 46-47.

Fournier M, Jolivet L., Huchson P., Sergeyev K.F. & Oscorbin L.S. 1994. Neogene strike-slip faulting in Sakhalin and Japan Sea, Journal of Geophys. Res., 99(B2), 2701-2725.

Jolivet L., Huchon P, Brun J.P., Chamot-Rooke N., Le Pichon X. & Thomas J.C. 1991. Arc deformation and marginal basin opening: Japan Sea - a case study. Journ. Geophys. Res., 96, 4367-4384.

Keeling, C.D., Bacastow, R.B., Carter, A.F., Piper, S.C., Whorf, T.P., Heinmann, M., Mook, W.G. & Roeloffzen, H. 1989. A three-dimensional model of atmospheric CO_2

transport based on observed winds, 1 Analysis of observational data. In: Aspects of Climate Variability in the Pacific and the Western Americas; Geophys. Monogr. Ser. vol. 55, (ed. Petersen, D.H.), AGU, Washington D.C., 165-236.
Kharakhinov V.V. 1998. Tectonics of the Okhotsk Sea Oil and Gas Potential Province. Okha, 77 pp. (in Russian).
Kimura G. & Tamaki K. 1986. Collision, rotation, and back-arc spreading in the region of the Okhotsk and Japan Seas. Tectonics, 5(3), 386-401.
Nürnberg, D,. Baranov, B.V. & Karp, B.Y. 1997, RV Akademik M.A. Lavrentyev cruise 27 - Cruise Report GREGORY, Geomar Rep., 60, 69 pp.
Rehder, G. 1996. Quellen und Senken marinen Methans zwischen Schelf und offenem Ozean. Dissertation, Universität Kiel.
Sundquist, E.T. 1985. Geological perspectives on carbon dioxide and carbon cycle. In: The Carbon Cycle and Atmospheric CO_2: Natural Variations Archean to Present; Geophys. Monogr. Ser. vol. 32, (eds. Sundquist, E.T. and Broeker, W.A.), AGU, Washington D.C., 5-95.
Takahashi, T., Olafsson, J., Goddard, J.G., Chipman, D.W. & Sutherland, S.C. 1993. Seasonal variations of CO_2 and Nutrients in the high-latitude surface oceans: a comparative study. Global Biogeochem. Cycles, 7(4): 843-878.
Tans, P.P., Fung, I.Y. & Takahashi, T. 1990. Observational constraints on the global atmospheric CO_2 budget. Science, 247: 1431-1438.
Worrall D.M., Kruglyak V., Kunst F. & Kuznetsov V. 1996. Tertiary tectonics of the Sea of Okhotsk, Russia: Far-field effects of the India-Eurasia collision. Tectonics, 15 (4), 813-826.
Zhuravlev A.V. 1982. Some questions of paleogeography and paleotectonics of the Okhotsk-North Japan Seas region. In: Geological Structure of the Okhotsk Sea Region. Vladivostok, 26-35 (In Russian).

Appendix I: List of participants

1. Dr. Boris Karp	Co-Chief Scientist, seismics (POI, FED RAS)
2. Dr. Thomas Lüdmann	Co-Chief Scientist, seismics (IfBM, UniHH)
3. Dr. Boris Baranov	Tectonics (IO, RAS)
4. Mrs. Karina Dozorova	Tectonics (IO, RAS)
5. Dr. Viktor Karnaukh	Seismics (POI, FED RAS)
6. Dr. Vladimir Prokudin	Seismics (POI, FED RAS)
7. Mr. Anatoly Sudakov	Seismics (POI, FED RAS)
8. Mrs. Tatyana Kolpashchikova	Gravity (POI, FED RAS)
9. Dr. Sergei Nikolaev	Gravity (POI, FED RAS)
10. Mr. Maksim Valitov	Gravity (POI, FED RAS)
11. Mr. Nikolay Tsovbun	Magnetics (POI, FED RAS)
12. Dr. Stefan Lammers	Geochemistry (GEOMAR)
13. Mr. Philipp Konerding	Seismics (IfBM, UniHH)
14. Mr. Martin Jovanovic	Seismics (IfBM, UniHH)
15. Mr. Matthias Spietz	Seismics (IfBM, UniHH)
16. Mr. Mark Heymann	Seismics (IfBM, UniHH)
17. Mr. Gabriel Ion	Seismics (GeoEcoMar)

GEOMAR: Research Center for Marine Geosciences, Christian-Albrechts-University, Kiel

GeoEcoMar: National Institute of Marine Geology and Geo-Ecology, Bucharest, Romania

IfBM, UniHH: Institute of Biogechemistry and Marine Chemistry, Hamburg University, Hamburg

IO RAS: P.P. Shirshov Institute of Oceanology, Russian Academy of Sciences, Moscow

POI FED RAS: Pacific Oceanology Institute, Far Eastern Division of the Russian Academy of Sciences, Vladivostok

Appendix II: List of profiles, KOMEX 99, Cruise 26 of the RV *Professor Gagarinsky*, Sea of Okhotsk, August-September 1999

Profile No.	Start				End				Course (°)	Duration (hh:min)	Distance	
	Date (d.mm.yy)	Time (hh:min)	Latitude (N)	Longitude (E)	Date (d.mm.yy)	Time (hh:min)	Latitude (N)	Longitude (E)			nm	km
3	11.08.99	21:02	53°04.55	144°02.42	13.08.99	02:01	54°54.99	146°17.79	75	27:59	118.67	219.77
4	13.08.99	02:23	54°53.92	146°17.20	13.08.99	07:30	54°32.84	146°20.00	178	29:07	21.47	39.77
5	13.08.99	07:38	54°32.78	146°20.00	13.08.99	13:37	54.53.41	145°41.12	317	06:59	30.25	56.02
6	13.08.99	13:41	54°53.52	145°40.65	13.08.99	16:46	54°51.27	145°19.79	315	04:05	13.18	24.41
7	13.08.99	16:58	54°51.28	145°18.10	14.08.99	14:32	55°59.38	143°08.01	318	21:34	103.08	190.91
8	14.08.99	14:42	56°00.30	143°07.91	14.08.99	18:46	56°00.07	143°48.83	90	04:22	23.87	44.21
9	14.08.99	18:53	55°59.79	143°49.24	15.08.99	09:18	55°25.39	142°35.50	220	14:25	53.61	99.29
10	15.08.99	09;22	55°25.09	142°35.44	15.08.99	12:13	55°14.30	142°59.56	129	02:09	17.45	32.32
11	15.08.99	12:18	55°14.20	143°00.55	15.08.99	23:20	55°33.64	144°45.72	5	11:02	64.47	119.40
12	16.08.99	00:36	55°39.95	144°43.55	16.08.99	05:38	55°09.93	144°25.45	350	05:02	35.93	66.54
13	16.08.99	05:39	55°09.79	144°35.66	16.08.99	10:43	55°24.74	145°39.44	50	05:04	40.12	74.30
14	16.08.99	10:55	55°25.03	145°40.83	16.08.99	20:23	54°24.80	144°26.06	8	09:28	74.14	137.31
15	16.08.99	20:31	54°24.08	144°25.16	17.08.99	01:43	54°13.12	145°26.62	105	05:12	31.16	57.71
16	17.08.99	05:18	54°04.81	146°01.82	17.08.99	05:53	54°03.40	146°05.62	130	00:35	15.79	28.24
17	17.08.99	08:56	53°55.47	146°23.70	17.08.99	12:49	54°06.98	146°23.66	3	03:53	11.15	20.66
18	17.08.99	12:50	54°07.04	146°23.61	17.08.99	13:24	54°06.91	146°19.03	6	10:33	2.77	93.7
19	17.08.99	13:27	54°06.77	143°18.65	17.08.99	15:35	53°55.04	146°19.01	179	02:07	10.31	19.09
20	17.08.99	15:36	53°54.95	146°19.03	17.08.99	16:03	53°54.91	146°16.02	280	00:27	1.38	2.56
21	17.08.99	16:04	53°54.94	146°15.94	17.08.99	19:23	54°07.03	146°15.94	355	03:19	11.56	21.41
22	17.08.99	19:24	54°07.08	146°15.89	17.08.99	19:50	54°06.84	146°12.39	270	00:26	1.60	2.97
23	17.08.99	19:51	54°06.79	146°12.38	17.08.99	22:38	53°54.54	146°13.08	180	02:47	11.43	21.17
24	17.08.99	22:40	53°54.47	146°13.09	17.08.99	23:35	53°55.01	146°09.06	310	00:55	2.43	4.34
25	17.08.99	23:36	53°55.10	146°09.00	18.08.99	02:30	54°07.01	146°09.12	360	02:54	11.52	21.34
26	18.08.99	02:31	54°07.05	146°09.14	18.08.99	04:08	54°03.02	146°20.93	120	01:37	7.50	13.88
27	18.08.99	04:08	54°03.00	146°20.97	18.08.99	09:34	53°51.90	145°43.35	240	05:26	24.04	44.52
28*	18.08.99	09:31	51°03.43	148°40.33	20.08.99	05:28	49°21.68	150°24.48	270	43:57	298.92	553.60
29	20.08.99	05:28	49°17.06	150°34.05	20.08.99	12:39	48°43.11	150°25.00	175	07:11	33.69	62.40
30	20.08.99	12:39	48°43.05	150°25.02	20.08.99	19:04	48°32.01	151°11.57	106	06:25	29.08	53.86

31	20.08.99	19:08	48.32.06	151°12.18	20.08.99	22:15	48°35.90	151°31.31	80	03:07	3.18	5.89
32	20.08.99	22:17	48°36.00	151°31.48	21.08.99	11:45	49°03.76	150°04.06	291	13:28	55.45	102.69
33	21.08.99	11:48	49°03.89	150°03.79	21.08.99	13:31	49°1204	150°05.28	356	01:43	7.07	13.09
34	21.08.99	13:33	49°12.17	150°05.33	21.08.99	22:09	48°58.73	151°01.78	100	08:36	34.81	64.47
35	22.08.99	03:07	48°51.64	151°25.74	22.08.99	04:28	48°48.68	151°30.65	250	01:21	2.79	5.17
36	22.08.99	04:35	48°48.55	151°30.13	22.08.99	13:48	48°32.73	150°28.02	250	09:13	40.47	74.94
37	22.08.99	13:52	48°32.57	150°27.78	22.08.99	21:32	48°43.15	151°33.44	65	07:40	39.25	72.69
38	22.08.99	21:33	48°43.23	151°33.61	23.08.99	01:00	48°29.16	151°16.75	230	03:27	13.78	25.52
39	23.08.99	19:32	48°05.80	150°49.45	23.08.99	22:13	47°13.28	149°55.90	230	02:41	54.29	100.55
40*	23.08.99	22.14	47°13.31	149°55.61	24.08.99	04:25	47°26.42	150°05.51	80	06:09	18.36	34.00
41	24.08.99	04:26	47°26.57	150°05.13	24.08.99	07:52	47°18.56	150°28.51	123	03:26	14.83	27.47
42*	24.08.99	07:53	47°18.65	150°28.29	24.08.99	23:13	46°09.93	148°01.07	235	15:20	96.27	178.30
43	24.08.99	23:14	46°09.96	148°01.14	25.08.99	11:30	45°41.90	146°43.58	240	12:16	50.76	94.00
44	25.08.99	11:32	45°41.85	146°4328	25.08.99	13:42	45°51.05	147°44.66	35	02:10	7,80	14.45
45	25.08.99	13:44	45°51.17	146°44.81	26.08.99	08:18	46°52.28	148°07.23	40	18:34	78.56	145.50
46	26.08.99	10:38	47°0051	148°16.59	26.08.99	11:30	47°04.39	148°12.07	320	00:52	4.19	7.76
47	26.08.99	11:31	47°04.33	148°12.00	26.08.99	15:00	46°52.05	147°5273	215	03:29	29.39	54.43
48	26.08.99	18:22	46°39.38	147°35.56	26.08.99	19:36	46°44.83	147°30.16	320	01:14	5.34	9.90
49	26.08.99	19:37	46°44.95	147°30.10	27.08.99	02:20	47°08.39	148°05.85	40	06:43	28.42	52.64
50	27.08.99	02:21	47°08.50	148°05.94	27.08.99	02:56	47°11.62	148°02.18	310	00:35	2.64	4.89
51	27.08.99	02:58	47°11.12	148°02.05	27.08.99	10:27	46°47.85	147°25.60	225	07:29	28.70	53.15
52	27.08.99	10:29	46°47.80	147°25.48	27.08.99	11:19	46°51.85	147°24.32	350	00:50	3,37	6,24
53	27.08.99	11:21	46°51.94	147°24.21	27.08.99	17:40	46°35.08	147°48.10	130	06:19	20.02	37.08
54	27.08.99	17:42	46°35.05	147°48.05	27.08.99	18:51	46°39.95	147°53.25	45	01:09	4.70	8.70
55	27.08.99	18:53	46°40.10	147°53.33	27.08.99	22:52	46°55.94	147°32.08	320	03:59	17.85	33.05
56	27.08.99	22:54	46°56.04	147°32.00	28.08.99	00:10	47°00.10	147°39.98	53	01:16	5.68	10.52
57	28.08.99	00:11	47.00.14	147°40.11	28.08.99	05:00	46°43.10	148°04.20	5	04:19	19,88	36.82
58	28.08.99	05:11	46°43.03	148°04.36	28.08.99	06:41	46°48.78	148°12.14	53	01:30	6.37	11.79
59	28.08.99	06:42	46°48.87	148°12.33	28.08.99	12:14	47°07.06	147°44.109	318	05:32	22.09	40.91
60	28.08.99	12:16	47°07.16	147°43.95	28.08.99	17:16	47°0009	148°18.34	103	05:00	21.02	38.93
61	28.08.99	17:19	47°00.29	148°18.45	29.08.99	06:10	47°48.26	148°36.67	4	12:51	42.41	78.54
62	29.08.99	06:12	47°48.34	148°36.86	29.08.99	17:36	48°29.24	147°58.35	320	11:24	42.97	79.59
63	29.08.99	17:39	48°29.34	147°57.98	30.08.99	01:01	48°04.28	147°13,76	225	07:22	33.50	62.04
								Total		475:04	1956.72	3623.85
								Total: air gun profiles		409:38	1543.17	2857.95

* no air gun profiles

PART II:

MV MARSHAL GELOVANY CRUISE 1

CRUISE REPORT KOMEX VI:

VLADIVOSTOK - PUSAN - SEA OF OKHOTSK - PUSAN - VLADIVOSTOK

AUGUST 22 - OCTOBER 5, 1999

1. INTRODUCTION

N. Biebow and R. Kulinich

The first scientific expedition of MV *Marshal Gelovany* (GE99-cruise) was organized as a continuation of the geophysical, geological, geochemical and hydrographical investigations in the Sea of Okhotsk which were begun in 1998 with the 22nd cruise of RV *Professor Gagarinsky* and the 28th cruise of RV *Akademik Lavrentyev* (Biebow & Hütten, 1999). On cruise GE99 these investigations should be continued and extended further. Within the framework of a continuous methane monitoring program, three short expeditions were carried out additionally in the area of active methane venting off east and northeastern Sakhalin and in the Derugin Basin (25th cruise of RV *Gagarinsky* 23.10 - 06.11.1998, ICE I- Expedition 22.03. -29.03.1999 and 1st cruise of MT *Utyos* 19.05. - 15.06. 1999). The data obtained during these expeditions served as a basis for formulating the tasks of the *Marshal Gelovany* cruise GE99.

As in 1998 a geophysical cruise aboard RV *Professor Gagarinsky* from 31.07. to 06.09. 1999 preceded GE99 cruise to gain basic geophysical data for the following geological cruise. The results of this cruise are described in the first part of this report.

The objectives of the *Gelovany* expedition GE99 comprise and contribute to the following research topics:

1) Detailed investigations of seasonal changes in the methane distribution in surface waters and in the water column (continuation of the methane monitoring program which was started on LV28 cruise in 1998 and was continued on several other expeditions (*Gagarinsky* 25 cruise, ICE I expedition and *Utyos* cruise Ut99).

2) Detailed investigations of gas and fluid venting sites in the two main areas which were discovered on cruise LV28 in 1998: off northeastern and northern Sakhalin (Piltunsky Flare area, Giselle Flare area, Obzhirov Flare area) and in the Derugin Basin (Biebow & Hütten, 1999).

3) Coring program for paleoceanological questions along two meridional (southern Sakhalin and Amour River mouth) and two latitudinal transects (northern part and central of the Sea of Okhotsk).

4) Dredging of volcanic rocks to assess volatile elements in Kurile Basin magmas and of basements rocks to gain information on the basement structure and the history of the Kurile Basin.

1) The study of seasonal changes in the methane distribution in the surface waters and in the water column is one central task of the KOMEX project. The interest in methane monitoring evolved from the study of natural methane sources releasing gas from the sea water into the atmosphere. Currently, a constant increase of the methane concentration in the atmosphere (1% per year) can be observed. In 1999, the methane concentration in the air layer above the sea surface was measured with 1.7-1.8 ppm; ten years ago it did not exceed 1.5 ppm. It is known that like carbon dioxide methane is a "greenhouse" gas which prevents the outflow of heat from the earth surface. As a result the air temperature increases, which leads to a global climate change and possibly to ecological changes.
   One central question of cruise GE99 therefore was to quantify the exchange rates of methane and CO_2 with the atmosphere and to determine the scale on which it influences the global climate. Another important task was to study the CH_4 and CO_2 distribution in the water column to quantify the outgassing rates of methane related to fluid or gas venting. To fulfill this task several expeditions in intervals of 3 to 4 month were carried out. On cruise GE99 these investigations were continued by sampling the reference stations in order to get the summer signal in the methane distribution. Several CTD castings along with water sampling and analyses of hydrographical parameters were carried out. These investigations were supported by flare observations with a 12 kHz echosounder system in order to find exact CTD sampling positions and discover new areas of methane venting.

2) The data obtained during several previous expeditions and particularly during the RV *Akademik Lavrentyev* cruise in 1998 constitute the basis for the continuation of the detailed study of gas and fluid venting near northeastern and northern Sakhalin Island and in the Derugin Basin.
   One of the tasks of the RV *Akademik Lavrentyev* 28th cruise was to map existing and locate new gas emission sites. The investigations were concentrated in two areas located on the shelf and upper slope of northeastern Sakhalin. These areas were studied before and recommended by the 22th expedition of RV *Professor Gagarinsky* and called "southern" and "northern" sectors (Biebow & Hütten, 1999).
   A 20 kHz-hydroacoustic survey was one of the most reliable and amazingly successful tools in detecting gas plumes in the water column. Up to 70 locations with features typical for gas emission were found. The use of OFOS represented the first attempt to actually see these gas emission sites on the seafloor of the Sakhalin shelf and slope. Of the two above-mentioned sectors the most productive was the "northern" one. Three areas with plume sites were discovered in this region: "Piltunsky Flare", "Giselle Flare" and "Obzhirov Flare". The last area is characterized by multiple gas manifestations and its detailed study is not yet completed. In the same area gas hydrates were found (Ginsburg et al., 1993). Up to now, the spatial extent and the geodynamic background of these venting sites are not clearly solved. The data obtained during previous expeditions aboard RV "*Professor*

Gagarinsky" indicate that these sites correlate with certain tectonic zones and are directly controlled by the tectonic regime. It is obvious that for the northern area all known seeps are located near reverse faults generated under conditions of NE-SW compression (Biebow & Hütten, 1999).

The second main area with gas or fluid venting which was studied in detail during the LV28 cruise was the Derugin Basin. Repeated findings of carbonate-barite mineral associations during previous expeditions to the Sea of Okhotsk (Astakhova et al., 1987; Astakhova et al., 1990) and the lacking knowledge of their origin, sources and tectonic position was one main reason to study this area again on GE99 cruise. One of the most significant results of the *Lavrentyev* expedition was the discovery of an area where hundreds of barite chimneys, edifices and blocks up to several meters high could be observed 2.5 miles along an OFOS track at a water depth of 1550 m. More than 1 ton of barite chimney fragments were dredged and 6 m of barite-turbidite sediment were cored in a small basin in the area of those chimney structures. Up to 2.000 nl/l of methane were measured in the deep water which fills the barite basin. The sediment between the barite edifices was populated by vent fauna.

Detailed petrographical, mineralogical, geochemical and isotopic investigations have shown that in the study area gas and fluid venting has existed since the last Glacial period, and has undergone several stages of activation. In accordance with the obtained data, an influence of hydrothermal processes on the barite-carbonate mineralization could not be discovered in the studied area.

At present, the sources of barite- and methane-containing fluids as well as the mechanism of their migration to the seafloor remain unclear. In this connection, one of the main tasks of GE99 expedition was to evaluate the spatial dimension of the barite mineralization area and to study the mineral formation processes and the nature of the geological basement of this area.

To solve these questions the work schedule of the "*Marshal Gelovany*" cruise included the continuation of the search for new gas flares as well as the detailed study of the bathymetry by means of a hydroacoustic system, a swath bathymetry system and an OFOS (Ocean Floor Observation System) to get information about their tectonical and structural origin and their spatial extent. After locating these venting sites a video-controlled sampling with a TV-grab should be carried out to sample the sediments and their biological communities directly on location.

3) The results of previous expeditions aboard RV *Akademik Lavrentyev* (cruises 27th and 28th) provide new data sets to elaborate a detailed sediment stratigraphy and reconstruct the paleoceanography of the Sea of Okhotsk during the Late Quaternary and Holocene. The shore-based laboratory analyses on magnetic susceptibility, tephrachronology, oxygen and carbon isotopes in foraminifera shells, sediment geochemistry and paleontology

allowed us to focus on special paleoceanographic topics during the "*Marshal Gelovany*" expedition in order to better understand regional paleoceanographic problems. The objects of the GE99 cruise were therefore to extend the east-west transect across the Sea of Okhotsk which were begun on the LV28 cruise towards the east (Kamchatka shelf), to extend the north-south transect along the Sakhalin continental margin further to the north and into the Amur River delta, to recover an east-west transect in the northern part of the Sea of Okhotsk and to complete the deep-water transect at the northwestern slope of the Kurile Basin. Thus the scientific targets were the following.

a) to receive long-time paleoceanography records covering oxygen isotope stage 11 (not studied in the Okhotsk Sea up to now) along the east-west transect. The eastern part of the profile represents the key area for the investigation of the influence of inflowing Pacific waters and the terrigenous input from the Kamchatka peninsula on the sedimentation and paleoproductivity in the Sea of Okhotsk.
b) to achieve high resolution sediment records of a time resolution scale of 100 years and less in the area off northeastern Sakhalin.
c) to study variations in paleoproductivity and surface paleoceanography that are related to Amur River inflow (one of biggest rivers in the world).
d) to investigate the influence of vent fields and gas emissions associated with gas hydrates that cause methane anomalies in the water column and the seafloor. Results of the 28th cruise of RV "*Akademik Lavrentyev*" (core LV28-2-4) show very light carbon isotope ratios in the benthic foraminifera *Cibicidoides kullenbergii* which are likely to be connected with methane fluxes in local sediments.
e) to study the paleoceanography in the northern part of the Sea of Okhotsk with a special focus on sea-ice distribution and sedimentation.
f) to study the deep water mass in the Derugin Basin. The bottom waters in the Derugin Basin show very low dissolved oxygen contents and therefore the sediment records in this basin are highly interesting for studying climatic variability and intermediate water formation changes because of their extremely good preservation under anoxic conditions.
g) to investigate the influence of the Soya current transport of warm and saline waters on the paleoproductivity and paleoecology of the Sea of Okhotsk.

4) The objective of the volcanological and petrological investigations carried out aboard *Marshal Gelovany* was to trace the origin and pre-eruptive evolution of magmatic volatiles (H_2O, SO_2, CO_2, Cl, F, B) in the region of the Kurile Island Arc. Interaction and dependencies between crustal and mantle sources, petrogenetic processes as well as the type and amount of volatiles in the eruptive products will be studied by applying geochemical and petrological methods. Another objective was to study the basement structure of the Kurile Basin, which is up to now only insufficiently known.

The planned dredging sites of cruise GE99 have mainly been selected on the basis of the results of the volcanological, petrological and geochemical analyses of the rocks gained during the cruises LV27 (Nürnberg et al., 1997) and LV28 and from the sample collection of the Institute of Volcanic Geology and Geochemistry in Petropavlovsk-Kamchatsky. During cruise LV28 bedrock dredging and subsequent petrological studies were completed in 3 areas located on the northern slope of the Kurile Basin and at the submarine volcano in the eastern part of the Kurile Basin (Tararin et al., 1999).

The initial objects of dredging on cruise GE99 were the following:

a) to study the interaction and dependencies between crustal and mantle sources, petrogenetic processes as well as the type and amount of volatiles in the eruptive products in different plate tectonic environments (e.g. rear arc/back arc vs. volcanic front). To solve these questions the northern, central (Bussol Strait) and southern transects across the Kurile Islands should be extended as far as possible into the Kurile Basin.

b) to reconstruct the origin and the evolution of volcanism, basement and structure of the Kurile Basin. Therefore additional samples from the seamount in the eastern part of the Kurile Basin (Tararin et al., 1999) should be sampled and further submarine volcanic edifices in the Kurile Basin should be identified and dredged as well.

c) to investigate the pillow-like structures identified on slides taken during OFOS profiles in the Derugin Basin on LV28-cruise.

2. CRUISE NARRATIVE

N. Biebow and R. Kulinich

MV *Marshal Gelovany* departed from Vladivostok on August 22nd 1999 with 31 scientists (14 Germans and 16 Russians) and 34 crew members on board. Modifications on two decks of the ship had been performed to accommodate a self-contained mobile deep-sea winch system (MobiWinch) with a 20 mm conducting cable and a hydrographical winch for work at sea. The MobiWinch was planned to be used for OFOS deployments, TV-grab sampling, coring and dredging after appropriately securing the electrical termination in the second half of the cruise. CTD castings and water sampling should be carried out with the hydrographical winch.
The vessel arrived at Pusan harbor in the night of August 24th, 1999. On the following morning, a pilot was taken aboard and the ship proceeded to a pier of the cargo port. During this day the German scientific equipment was loaded on board of the ship. At midnight of August 25th MV *Marshal Gelovany* left Pusan harbor and made its way to the Sea of Okhotsk. The complete cruise track is shown in Fig 2.1.

Transit to the first area of investigation took about 4 days. This period was used for preparing and testing the equipment and laboratories for the upcoming work. On August 26th already it became clear that the MobiWinch was not ready for work due to major faults in the electronical steering of the winch. Both German technicians started to do whatever possible to repair the winch resorting to the equipment aboard.
On August 27th the excellent weather favored a short stop to carry out a "sea bath" station at 41°01.224 N and 135°12.655 E which was enjoyed by everybody aboard. The water temperature at this spot was 20°C and the depth 3540 m.
On August 29th it became definitely clear that the MobiWinch could not be repaired with the equipment aboard, which meant that neither coring nor dredging nor the depolyment of any video-system would be possible during the cruise. Therefore the German owners of the winch were contacted and asked for technical support. On Monday, August 30th, a technician from the German service company was flown to Mombetsu in Japan. He was planned to be taken aboard *Marshal Gelovany* outside of the 12 mile zone the following day.

Nevertheless, *Marshal Gelovany* reached the area of investigations (Fig. 2.2, southern Sakhalin) on August 29th and the sampling program including CTD and minicorer (MIC) deployment was begun. Those devices were the only equipment aboard which could be used without the mobile deep-sea winch. In the night of August 30th to August 31st *Marshal Gelovany* departed from the investigation area to take the technician aboard near Mombetsu. Shortly after the arrival outside the 12 miles zone of Japan it turned out that the Japanese authorities would not allow the technician to leave Japan to enter a Russian military vessel.

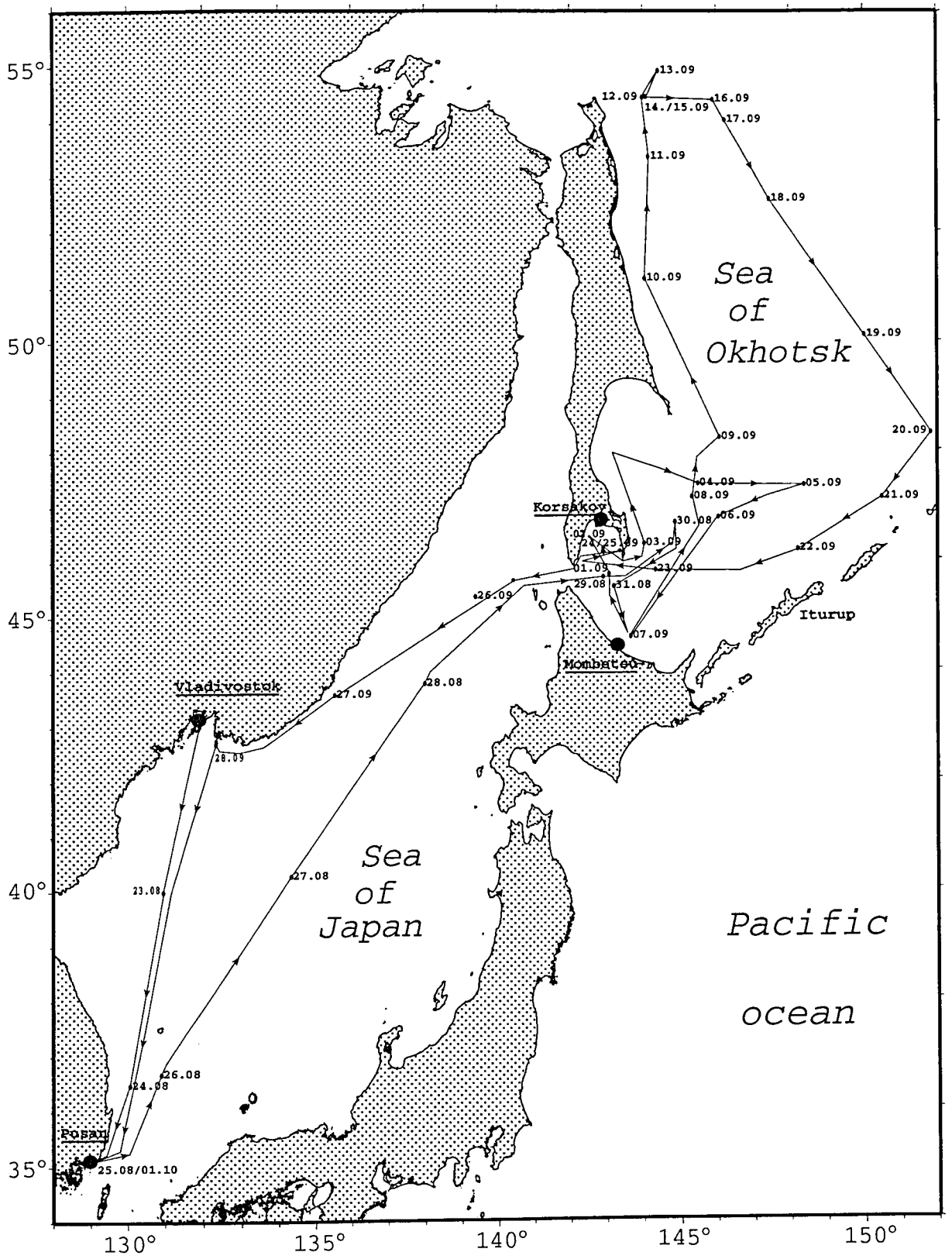

Fig. 2.1: Ships track of MV Marshall Gelovany, August - October 1999.

After several telephone calls to Germany and the intervention of the German embassy in Tokyo, Japanese authorities agreed to let the technician leave Japan to board *Marshal Gelovany* on September 7th. Thus the ship left Mombetsu to continue the scientific work with CTD and MIC deployments in the southern part of the Sea of Okhotsk in the meantime.
After leaving the vicinity of Mombetsu it was decided to save as much time for the remaining scientific work as possible and refill our water tanks in Aniva Bay first. This was done on 02.09.99 in front of Khorsakov harbor.

The period of August 31st to September 6th was mainly devoted to investigations along Profile 1 (southeastern Sakhalin), at the methane monitoring station (Terpenia Bay) and in the Kurile Basin (Fig. 2.2). CTD and MIC work was carried out at 8 stations. Additionally, the calibration of the swath echosounder was executed. The discovery of a new gas flare constituted a big surprise at the beginning of the expedition. It was discovered by a 12 kHz acoustic system on the upper slope of southeastern Sakhalin, where A. Obzhirov already had found a methane anomaly in 1988. Additionally, one CTD cast in the central part of the Kurile Basin showed very interesting bottom waters with unusually high salinity and oxygen concentrations not known before. Unfortunately, we were not successful in tracing these bottom waters over longer distances so that their distribution and origin remained unclear.

On Tuesday, 07.09.99, *Marshal Gelovany* arrived outside the 12 mile zone of Mombetsu; this time the technician could come aboard without problems. After several hours of work the MobiWinch could be put in working condition. The technician was brought back to Mombetsu by a tug boat. At the same evening bad weather came up and forced *Marshal Gelovany* to leave this area very quickly.
Unfortunately, a lot of the cruise time had been wasted on the necessary repair of the MobiWinch and the transit to and from Mombetsu. Therefore the initial working plan had to be changed significantly. The work on the Amur River transect, the northern paleoceanography transect and off the coast of Kamchatka and the eastern Kuriles had to be canceled because of the lack of time. The search for new seeps had to be cut short in order to carry out detailed work on the shelf and upper slope off northeastern Sakhalin (known gas and fluid venting fields) as well as in the area of fluid venting and carbonate-barite mineralization in the Derugin Basin.

During transit to northern Sakhalin, the paleoceanological work including German and Russian corers as well as MUC was begun at stations GE99-9 and -10. The core recoveries were 9,11 and 7,5 m. During the deployment of the coring equipment trouble with the deep-sea mobile winch again arose; one sensor of the bobbin rail broke down and the winch suddenly stopped working. It became clear that in spite of the repair work the winch would not work optimally and the deployment of all devices could become rather risky.

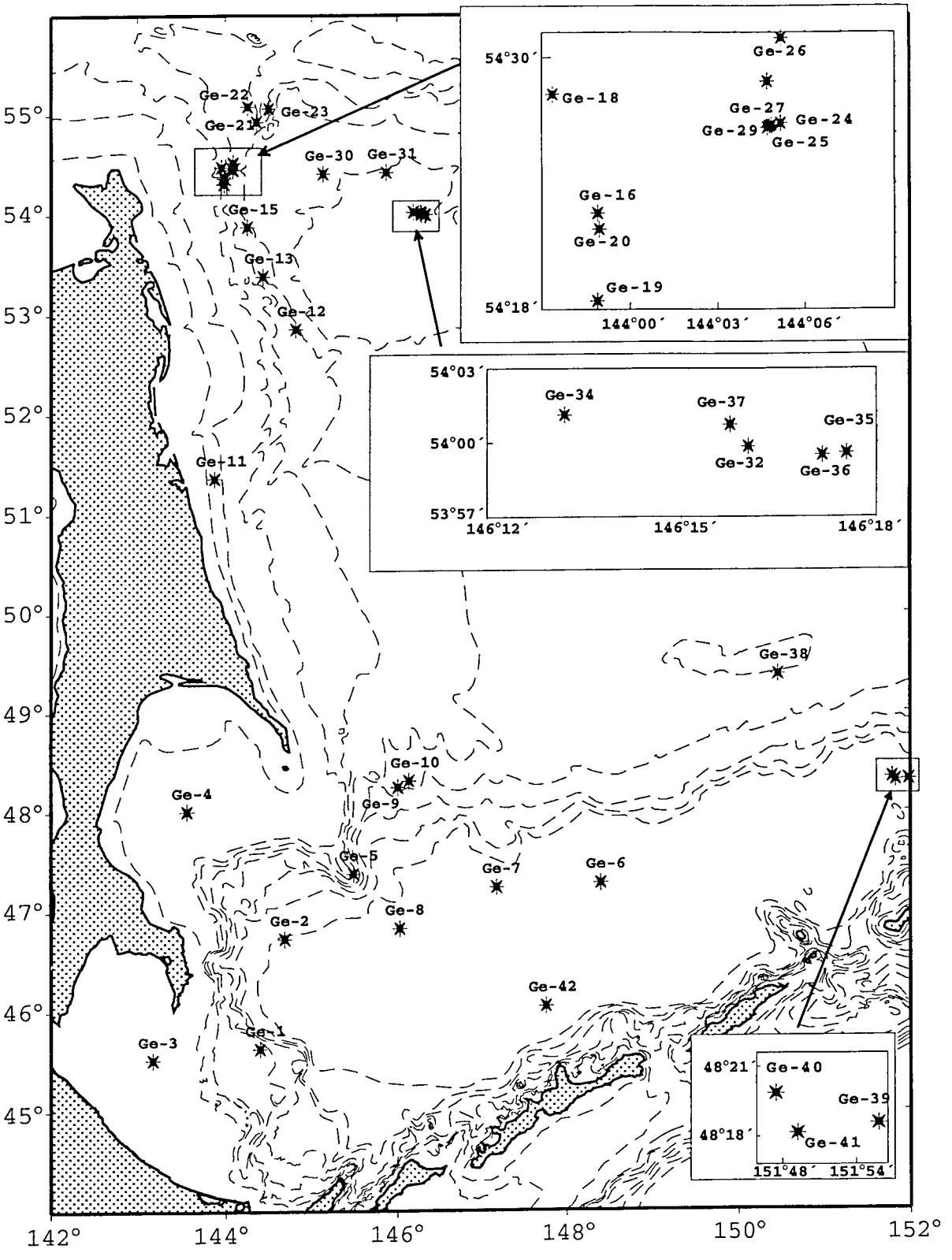

Fig. 2.2: *Map of working areas (shaded polygons) and stations (stars) during the first cruise of MV Marshal Gelovany, August - October 1999.*

On September 10th, before the arrival in the main venting investigation area, water column studies using a CTD-Rosette were carried out at a station situated on the shallow shelf (GE99-11). These surveys completed the annual cycle of methane monitoring started in summer 1998 during cruise LV28 and were repeated in the autumn, winter and spring of 1998 and 1999.

The following 5 days (September 11th to 15th) were devoted to the detailed study of methane venting fields in the "Giselle Flare" and "Obzhirov Flare" areas. During the whole week station work was hindered significantly by bad weather which culminated in the night from September 12th to 13th during which all work had to be stopped. The equipment and participants of the cruise suffered from severe shaking and rolling. OFOS- and TV-grab observations had to be canceled completely due to the rough sea and the bad performance of the mobile deep-sea winch. Also, the attempts to use the swath bathymetry system for detailed bottom relief mapping were more or less unsuccessful due to the bad weather. Therefore, only multicorer, minicorer, trawl, gravity corers, dredges, and hydroacoustic equipment could be used. Detailed work was carried out on 19 stations (GE99-12-30). The communication and cooperation between the German and Russian teams and the vessel's crew was excellent during this difficult time.
On Tuesday, September 14th our endurance was rewarded by the recovery of gas hydrates in two gravity cores (Station GE99-24-2, GE29-3) at "Obzhirov Flare". The following trawl contained a huge amount of vent organisms and one living specimen of the bivalve *Conchocele disjuncta* and *Calyptogena* sp.. Finally, a CTD could be deployed directly in a flare; here, the highest methane concentration, 23.000 nl/l, of this cruise was measured. (Station GE99-29-1).

During September 15th to 17th, investigations were carried out in the Derugin Basin mainly in the carbonate-barite mineralization area. Bad weather in this area hindered our work significantly again; thus video-systems could not be used. Up to then, 9 stations (GE99-30-37) had been carried out and completed. About 300 kg of barite boulders, pebbles and sediment were recovered by dredging (GE99-35-1). One of the interesting results was the discovery of barite crusts of unclear origin.

During our work in the northern Sakhalin area and in the Derugin Basin the master of *Marshal Gelovany* informed us that the ship would not have enough fuel left to continue station work as planned. Fuel consumption was higher than assumed because of the transits to and from Mombetsu and because of a miscalculation before our cruise. In order to bring the scientific crew back to Pusan without problems and to save some fuel for possible bad weather, we again had to change our working plan. The work in the Derugin Basin area was canceled in order to have at least 3 days for paleoceanology work on transit and dredging in the Kurile Basin.
Additionally, a sharp intensification of the wind and roughness of the sea forced us to stop work; on 18.09.99 we started on the transit to the paleoceanological station (GE99-38) situated

on the Academy of Sciences Rise. We tried to recover a 15m sedimentary record at this station with both Russian and German corers. Unfortunately, a stiff layer at about 6m sub-bottom depth prevented further penetration. As a result, the pipe of the GEOMAR corer broke. However, we were able to rescue a 529 cm record. This station was completed on September 19th. After that the ship made its way to the Kurile Islands for dredging.

The following three days (September 20th to 22th) were devoted to dredging on submarine volcanoes including the transit between stations. A single small submarine volcano located in the northeastern part of the Kurile Basin was the first object of study. This seamount had already been studied during the 28th cruise of RV "*Akademik Lavrentyev*". Shore-based isotope analyses of the recovered basalts had not provided an unambiguous answer yet concerning the geotectonic conditions of their formation. Repeated dredging at this site should yield additional information for solving this problem. To get an idea of the bathymetry of the seamount we made an attempt to map the seamount with the swath bathymetry system before dredging. This attempt was in part unsuccessful due to the big water depth. Dredging was nevertheless successful.
The submarine Obruchev volcano located near the Bussol Strait was the second dredging target. Two stations (GE99-42, -43) were carried out and completed there and approx. 150-200 kg of rock material was recovered. The samples contained boulders and pebbles of altered porphyritic basalts, porphyritic andesite and orthopyroxene-amphibole dacite.
In the meantime, we received information on typhoon BART which was approaching us. On September 20th it was located near the southern Japanese island. The forecast for its further motion was unfavorable to our expedition; therefore we decided to speed up our work and leave the Sea of Okhotsk to seek shelter. We made an attempt to study one more submarine mountain located in the Kurile Basin north of Iturup Island on the way. Dredging was not successful; the dredge came up empty.

In the night of September 22nd work had to be stopped and the ship steamed to La Peruse Strait in order to avoid contact with the typhoon and find shelter at the Primorye coastline. During the night of the following day the ship reached La Peruse Strait, but as time would not have sufficed to reach a safe place along the Primorye coast the captain got order from his headquarters in Vladivostok not to proceed in this direction but seek shelter in Aniva bay. The ship changed course and came into the bay for anchoring. It took one day of waiting for BART to pass by. In the night of September 25th the typhoon reached Hokkaido Island and Aniva Bay. The wind speed exceeded 100 km/h, but the ship was protected by the steep coasts of the bay and not damaged. During the afternoon the typhoon passed, but strong winds and huge waves made it impossible for the ship to leave the bay. Finally at midnight the ship could continue on its way to Pusan.

The passage through the Japan Sea was used to demobilize the heavy equipment, complete work on samples and run final analyses. In the early morning of September 28th *Marshal Gelovany* reached Askold Island near Vladivostok where additional fuel and water were bunkered as there was not enough fuel left to reach Pusan harbor. After this the vessel steamed towards Pusan where it arrived on the evening of September 30th. The next morning a pilot was taken aboard and we proceeded into the port of Pusan and tied up at pier at 6:00 am local time.

BATHYMETRY AND NAVIGATION

A. Koptev, A. Salyuk, and A. Svarichevsky

3.1 Goals and tasks

The goal of the bathymetric investigations was to receive detailed knowledge about the topography of the Okhotsk seafloor in the areas of extensive gas flares including the known area on the shelf and slope of North-East Sakhalin. New flares should be searched continuously during this cruise and investigations on their spatial distribution features should be done. Accordingly, the following topics constituted the main objectives:

1. Carrying out constant echosounding for bathymetric investigations over extensive areas and for observing hydroacoustic anomalies;
2. Searching new and verifying previously known flares;
3. Giving bathymetric and cartographic support for all work groups to carry out successful investigations;
4. Carrying out modifications in the bathymetric measuring system.

3.2 Equipment and methods

3.2.1 Echosounding

The bathymetric research was carried out with the deep-water narrow-beam echosounder GEL-3 made in USSR. GEL-3 has a working frequency of 12.4 kHz, the width of the beam is 10° x 10°, maximum sounding depth is as large as up to 10.000 m. The echograms were registered with a GEL-3 paper recorder on a paper tape and with a two-channel multi-frequency registration system (UDM). The UDM was successfully applied on LV28 cruise as an observation tool for finding vents in the northern Sakhalin shelf and slope area.

The UDM system also has a PC Pentium-166 and a global positioning/navigating system (GPS 31). The UDM provides real time reception, color display and hard disk records (with subsequent records on CD ROM) echosounding information, current time and coordinates.

The signal goes to the input channel of the UDM after arriving at the preliminary amplifier of the GEL-3 system; the pulse is synchronized. The second channel was not used. The frequency passband of the channel is 1 kHz. The time increment for signal sampling is 0.33 msec. The recorded time interval for traveling is 1.2 sec, which corresponds to the maximum sounding depth of 900 m.

For an expansion of the range, the UDM was modified during the cruise. Instead of using the adapter unit, the pulse synchronization was realized from the GEL- 3 system by computer with a PC-386 Programmed Synchronization System (PSS). PSS allowed real time top depth input for the echogram from the keyboard. The time of top depth change and the respective values were stored in a special file. This allowed to carry out bathymetry and vent observation in a 900

m window for the whole depth range of the Sea of Okhotsk, including the Derugin and Kurile Basins, and to digitize the maximal bottom depth from the UDM data.
Due to high noise in the Gel-3 data, signal filtration and image processing were carried out with MATLAB.
The signal from GPS 31 was transferred by the ship's high-frequency communication system from the mate's cabin to the main deck for the navigation maintenance during swath bathymetry, geological work and CTD deployments. For this purpose one computer constantly worked with WINGPS.

During drifting on several hydrological stations additional vent observations with a portable FURUNO acoustic station were carried out using frequencies of 50 and 200 kHz. The polar pattern was 60° and 11° for 50 kHz and 200 kHz, correspondingly. The maximum transmission power was about 300 W. This acoustic station allowed to register bottom depths up to 1500 m on the 50 kHz channel and up to 600 m on the 200 kHz channel. Gas expulsions and bottom layers were confidently registered up to 700 m depth.
During the cruise, the analog two-channel FURUNO signal was digitized and stored on a hard disk of a PC under the control of WINGPS by a standard soundcard input at the same time. The total volume of sound information exceeded 400 Mbytes.

3.2.2 Positioning

The positioning for bathymetric surveys, searches for flares and for all hydrological and geological stations was carried out by the vessel's global positioning system (GPS). The marine navigation receiver GPS 120 allows to recognize the position of the vessel, international time (UTC), the direction towards a specified location, the distance to it, the course and speed of the ship.
The receiver used was a differential MultiTrack 8 (traces up to 8 satellites). The GPS 120 by GARMIN worked autonomously with one measurement each second. The GPS was connected to a computer for averaging the incoming data. The deviation with which allocations were determined was not less than 15 m. The precision of the speed determination was 0.1 knot. The data from the GPS were mapped on the display for operational control by the vessel and logged for further manipulation.
The record was produced in the following manner:

- on stations with a spacing of 10 seconds;
- on tracks with a spacing of 10 seconds to 10 minutes.

The array of coordinates obtained was utilized for creating ship tracks on stations as well as during transits.

3.3 Description of the tasks involved

3.3.1 Bathymetric survey

The first bathymetric surveys were performed at geological stations. They were carried out in small areas as well as on tracks between stations, including paleoceanological transects. The depth data were stored on an analog echosounder line scan recorder. The total distance measured by echosounding amounts to 2486 miles.

The sea water sound velocity was considered to be 1500 m/s. Variations in sea-water temperature and ambient pressure were not taken into consideration. Relying on the bathymetric survey data, an electronic version of the Derugin Basin bathymetric map will be prepared by KOMEX.

The geographic names used in the following text correspond to the ones used in previous publications (Gnibidenko and Svarichevsky, 1984) and by the National Committee of Geographical Names.

3.3.2 Searching and observing hydroacoustic anomalies

Searching for and observing flare-connected anomalies was carried out by echosounding (GEL-3; 12 kHz) with the standard ship recorder; the computer-aided recording and imaging of the automatically measured information was carried out by UDM. We gained data on a new flare field, which showed hydroacoustic anomalies in the Basin of the Terpenia Gulf. Other gas sources were studied and added to the general list of vents achieved during LV28 cruise (Biebow & Hütten, 1999).

3.4 Results

3.4.1 Hydroacoustic observations

Echograms were recorded at 62 sites with hydroacoustic anomalies which are hypothetically coupled with gas seepages. Some flares are rooted in the seafloor, others have no bottom contact. The height of the flares vary from 40 m to 850 m. Some run vertically, some show straight upward-going features, some appear to have a reverse inclination, some extensive anomalies had the form of "stratus clouds" (Plates 1-3). The sites of these hydroacoustic anomalies usually are situated on the continental margin of North-East Sakhalin. We could not find any flares in the Derugin Basin this year, whereas there were at least some hints to flares existing there visible on the paper records of the 12 kHz echosounder on RV *Akademik Lavrentyev* last year.

The locations of the flares are shown in Fig. 3.1. The results of the searches of hydroacoustic anomalies are reflected in Appendix 2. It is important to mention that the table lists only the most gaseous sources. Using this new method of analyzing echograms, we can find evidence for a much greater amount of small flares in some areas.

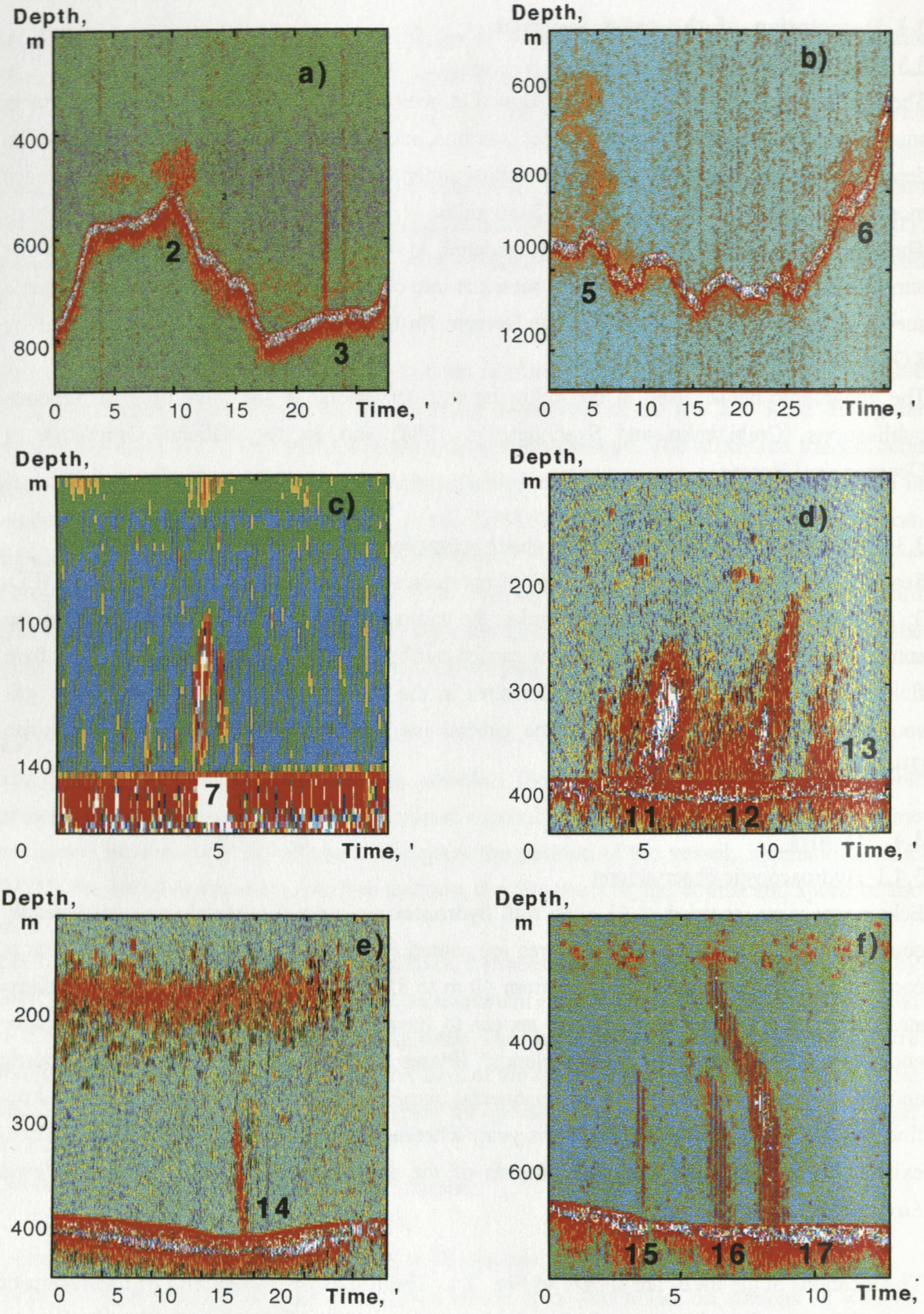

Plate 1: *Flare images, observed in the Sea of Okhotsk during the Komex 99 cruise MV "Marshal Gelovany", September 1999. Digits - numbers of acoustic anomalies according to Appendix 2.*

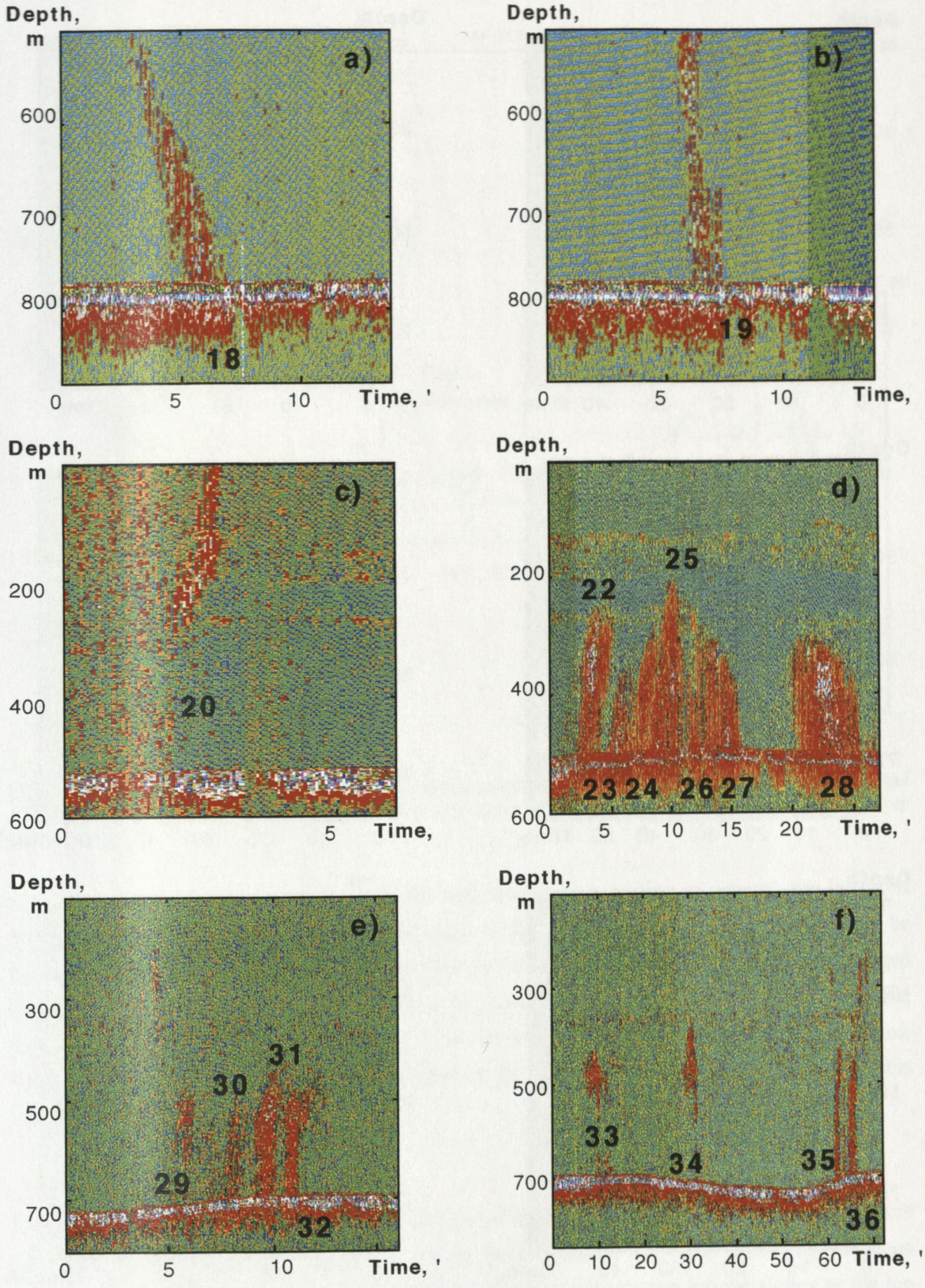

Plate 2: *Flare images, observed in the Sea of Okhotsk during the Komex 99 cruise MV "Marshal Gelovany", September 1999. Digits - numbers of acoustic anomalies according to Appendix 2.*

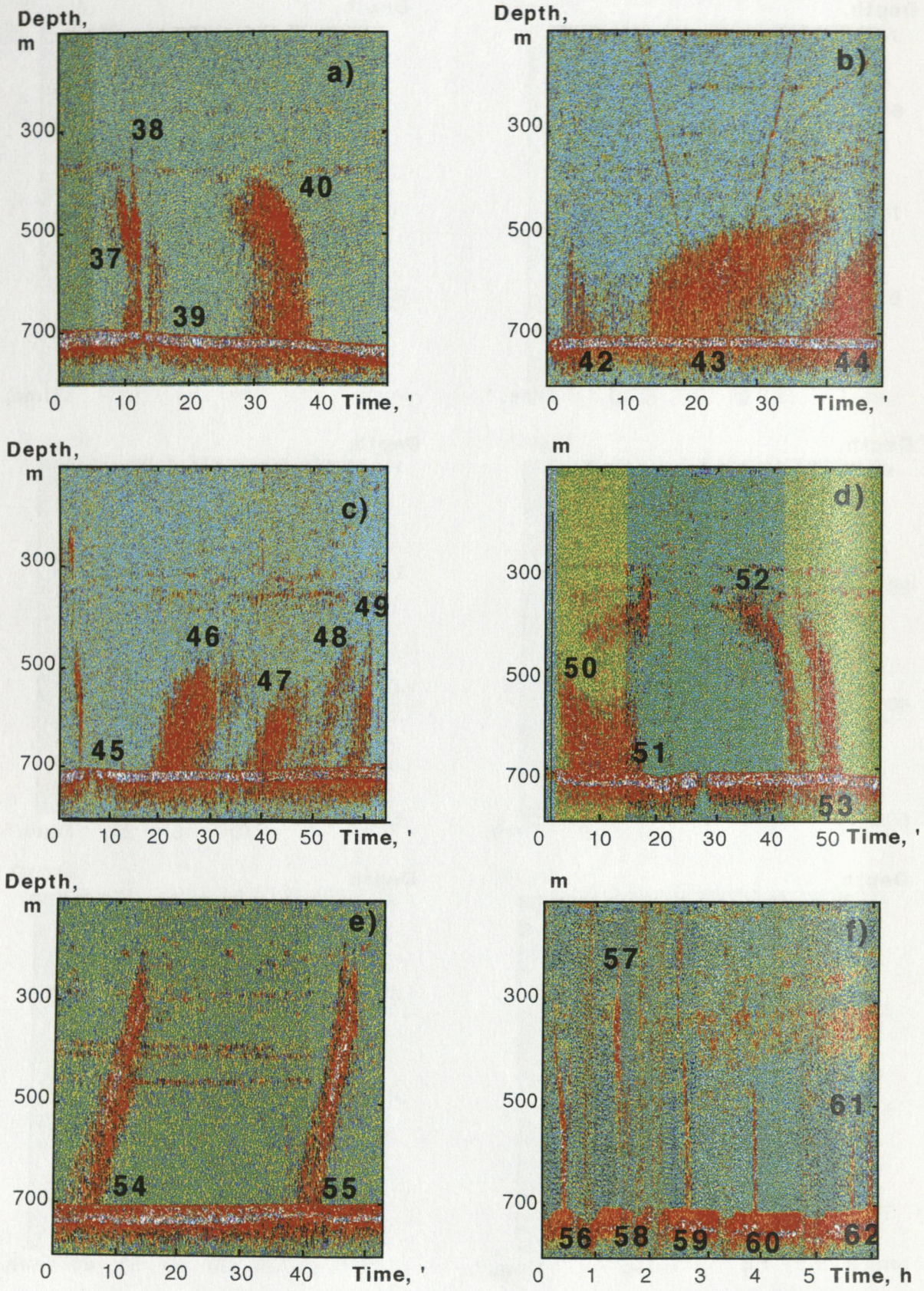

Plate 3: *Flare images, observed in the Sea of Okhotsk during the Komex 99 cruise MV "Marshal Gelovany", September 1999. Digits - numbers of acoustic anomalies according to Appendix 2.*

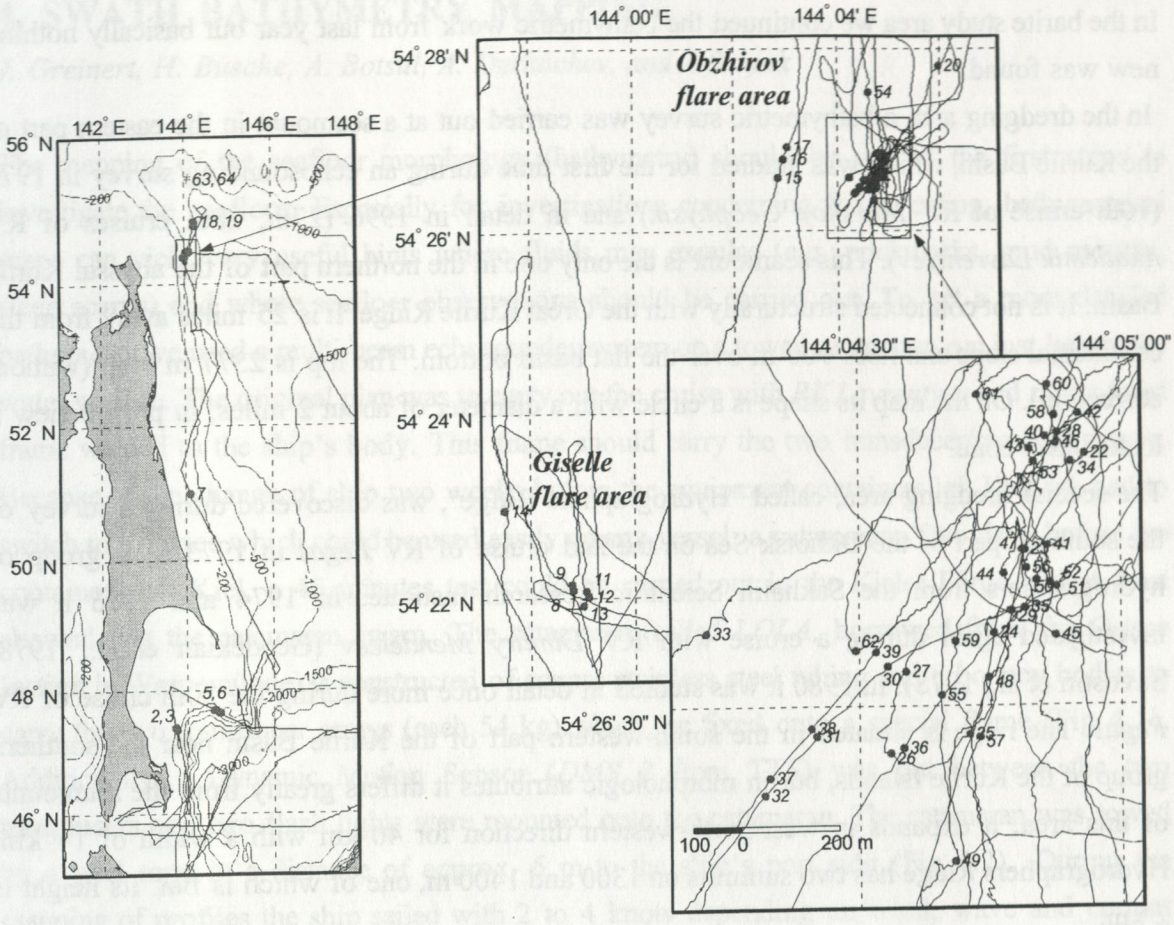

Fig. 3.1: *Location of hydroacoustic anomalies observed during GE99-cruise (filld dots) and GA26-cruise (crosses). Number of observed acoustic anomalies are given according to appendix 2.*

Fig. 3.1a shows the spatial positioning of the hydroacoustic anomalies; in general, the locations follow sublatitude lines, but not in the direction of the isobaths. The same directions can be found in fracture zones of the south-west slopes of the North-Okhotsk Rise less camouflaged by sediments. Considering the orientation of the flares in greater detail, one can observe that they follow a north-eastern direction (Fig. 3.1b) or west-north-western (Fig. 3.1c) directions. This perhaps mirrors the tectonic background of these gas sources. However, to prove this additional data is necessary.

3.4.2 Bathymetric investigations

With these echosounding surveys investigations of the study areas of previous cruises were continued. Near the North-East Sakhalin region, the bathymetry allows to distinguish between the Smidt' Peninsula's extensive circular slump depression with its precipitous slopes at the top and the convex body of the slide which constitutes the middle part of the slope. On the southern edge of the depression a small submarine canyon can be distinguished.

In the barite study area we continued the bathymetric work from last year but basically nothing new was found.

In the dredging area a bathymetric survey was carried out at a seamount in the eastern part of the Kurile Basin, which was studied for the first time during an echosounding survey in 1979 (10th cruise of *RV Morskoy Geophysik*) and in detail in 1996 (27th, 28th cruises of RV *Akademik Lavrentyev*). This seamount is the only one in the northern part of the abyssal Kurile Basin. It is not connected structurally with the Great Kurile Ridge. It is 25 miles away from the continental slope and rises 900 m over the flat basin bottom. The top is 2377 m high (without correction). On the map its shape is a circle with a diameter of about 2 miles, in profile view it looks like a cone.

The second dredging area, called "Hydrographers Ridge", was discovered during a survey of the southern part of the Okhotsk Sea on the 2nd cruise of RV *Pegas* in 1973 by a group of hydrographers from the Sakhalin Scientific Research Institute. In 1974 and 1976 it was investigated again during a cruise with RV *Dimitry Mendeleev* (Geodekian et al., 1978; Savostin et al., 1978). In 1980 it was studied in detail once more during the 20th cruise of RV *Pegas*. The ridge is situated in the south-western part of the Kurile Basin near the southern group of the Kurile Islands, but in morphologic attributes it differs greatly from the seamounts of this area. It expands in west-north-western direction for 40 km with a width of 14 km. Hydrographers Ridge has two summits on 1300 and 1400 m, one of which is flat. Its height is 2 km.

In the third dredging area the Obruchev Seamount is well-known in a group of submarine mountains from works by Bezrukov et al., 1958 and from the Japanese expedition *Hecateus* (Yasui et al., 1968). By an echosounding survey we could verify the existence of submarine mountains west to the Hydrographers' Ridge which were found on RV *Vitiaz* cruise in 1972 and on RV *Dimitry Mendeleev* cruise in 1976. They have a similar morphology as the Hydrographers' Ridge showing a west-north-western strike with a height of about 800 m.

4. SWATH BATHYMETRY MAPPING

J. Greinert, H. Busche, A. Botsul, A. Derkachev, and A.Salyuk

The mapping of the seafloor morphology (bathymetry) should be one of the first steps to investigate the seafloor. Especially for investigations concerning fluid venting, bathymetrical maps can yield very useful hints where fluids may expulse (e.g. pockmarks, mud mounts, steep scarps) and where seafloor observations should be carried out. To get a more detailed bathymetry we used a multi-beam echosounder system on a towed catamaran run just below the water surface. The original plan was to carry out the cruise with *RV Lavrentyev* and use a fixed frame welded to the ship's body. This frame should carry the two transducer/receiver arrays. Because of the change of ship two weeks before the equipment containers left Kiel we had to switch to a device which could be used easily on any vessel: a catamaran. Two days before the containers left Kiel, a 45 minutes test could be carried out in the Kieler Förde and at least showed that the catamaran swam. The catamaran (called *LOLA,* borrowed from the Ostsee Institut in Warnemünde) is constructed of square stainless steel tubing and 8 bouncy bodies to carry the two transducer arrays (each 54 kg) which are fixed onto a special frame (Fig 4.1). Additionally, a Dynamic Motion Sensor (*DMS 2* from TTS) was put between the two transducers and two flash lights were mounted onto the catamaran. The catamaran was towed by a steel rope in a distance of approx. 5 m to the ship's port side (Fig 4.2). During the mapping of profiles the ship sailed with 2 to 4 knots depending on wind, wave and current conditions.

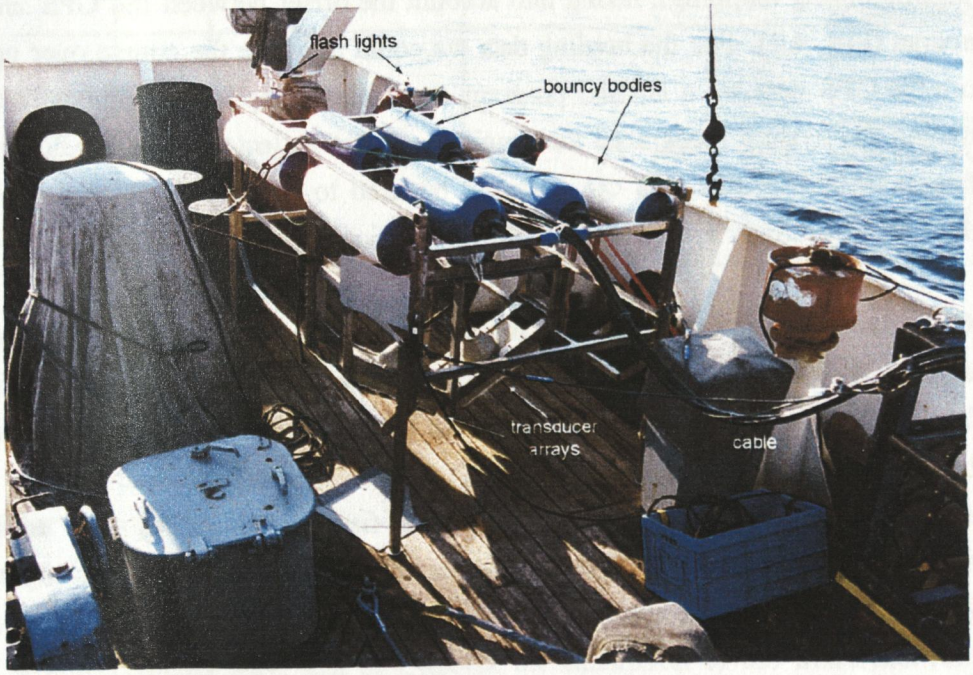

***Fig. 4.1**: The catamaran LOLA on board RV Marshal Gelovany.*

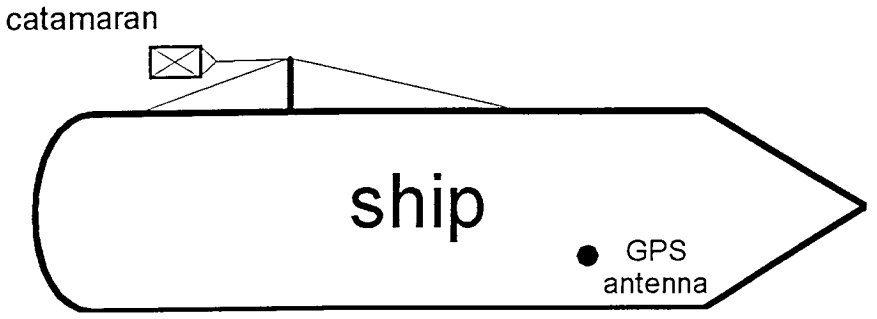

Fig. 4.2: Scheme of the towed catamaran.

4.1 Equipment and mapping procedure

The multi-beam equipment BOTTOM CHART MKII leased from ELAC in Kiel consists of two multi-beam transducer/receiver arrays (50 kHz) with 63 beams each. The beam angle can be varied from 120° down to 18° in discrete steps (100°, 80°, 60°, 40°) depending on the water depth (max. 3000 m). The power supply and beam forming is controlled by a SEE 30 deck's unit which is additionally connected to the motion sensor by a repeater link. The SEE 30 is controlled by a RS422/RS232 converter with *Hydrostar* software (ELAC) installed on a Windows NT computer. This computer was used for on-line data acquisition and connected to a HP UNIX computer for postprocessing (*HPedit* and *HPpost* software, ELAC). Unfortunately, the UNIX computer was damaged during transport and only worked temporarily. Because neither a separate GPS nor a compass could be mounted on the catamaran direct information on position and heading of the catamaran was not available. The position was taken from the ship's GPS (each second during mapping), taking into account the offset between the GPS antenna and the catamaran (Fig. 4.2). For the heading data we could only use the course over ground extracted from the GPS data by a BASIC program on a third computer. Additionally to the depth information the system recognized the amplitude of the reflected beams. After further postprocessing at GEOMAR this data can probably be used to get some information on the sediment composition similarly to side scan sonar investigations.

During the GE99 cruise five target areas were more or less successfully investigated after the calibration profiles (Tab. 4.1). Due to a lack of time the areas under investigation at Giselle and Obzhirov Flare as well as in the Derugin Basin were planned as small as possible with an overlap of the adjacent profiles of approx. 20%. As a rule the catamaran was put into the water approximately half a mile before the starting point for the first profile during slow sailing (1 knot) with a heading parallel to the profile. Before the first pinging, a sound velocity model were taken from a CTD in the respective area.

Tab. 4.1: Swath bathymetry profiles investigated during GE99.

area station	profile #	begin latitude N	begin longitude E	end latitude N	end longitude E	water depth m	remarks
calibration							
SBM 4-4	1	48°01.74'	143°35.52'	48°03.801'	143°35.88'	70 - 80	
	2	48°03,81'	143°35.295	48°01.734'	143°35.432	70 - 80	
	3	48°01.753'	143°35.295	48°03.788'	143°35.725	70 - 80	
Piltunski							
SBM 14-1	1	53°21.2'	144°07.44'	53°22.18'	144°15.57'	210 - 400	problems with heading input, data need to be reprocessed by ELAC
Giselle Flare							
SBM 17-1	1	54°25.10'	143°57.10'	54°18.43'	143°57.44'	275 - 400	
	2	54°18.43'	143°58.25	54°20.48'	143°58.25'	310 - 400	profile stopped because of bad weather
Obzhirov Flare							
SBM 28-2	1	54°29.07'	144°06.54'	54°24.45'	144°07.199	755 - 670	
	2	54°24.45'	144°07.19'	54°28.51'	144°05.46'	750 - 630	
	3	54°28.51'	144°05.46'	54°24.526'	144°03.13'	720 - 560	
	4	54°24.526'	144°04.381	54°28.49'	144°03.13'	680 - 520	last two westernmost profiles could not be mapped because of bad weather
Derugin Basin							
SBM 33-1	1	54°00.25'	146°15.62'	54°0.035'	146°12.256	1360 -1650	
	2	54°0.035'	146°12.256	53°59.915'	146°26.60'	1360 - 1500	southernmost 3rd profile could not be mapped because of bad weather
Kurile Basin Seamount							
SBM 39-1	1	48°20.0'	151°48.0'	48°17.5'	151°48.0'	2400 - 3400	mostly too deep, no reflections from seafloor areas deeper than 2900m, several small profiles during dredging

Data processing was carried out using the *HPedit* and *HPpost* software to create an xyz ASCII file which was further processed with *Surfer* to create the maps and 3D-images shown in this report.

4.2 First test and calibration

The work with the swath bathymetry system started with a successful test of the catamaran and echosounder unit on Aug. 31st, 1999, in Aniva Bay, Sea of Okhotsk (SBM 3-2). At station SBM 4-4 in Terpenia Bay, Sea of Okhotsk the calibration of the transducer/receiver arrays could be carried out in a flat smooth southward dipping area with 70 to 74 m water depth. Calibration is necessary because the position of and especially the angle between the two

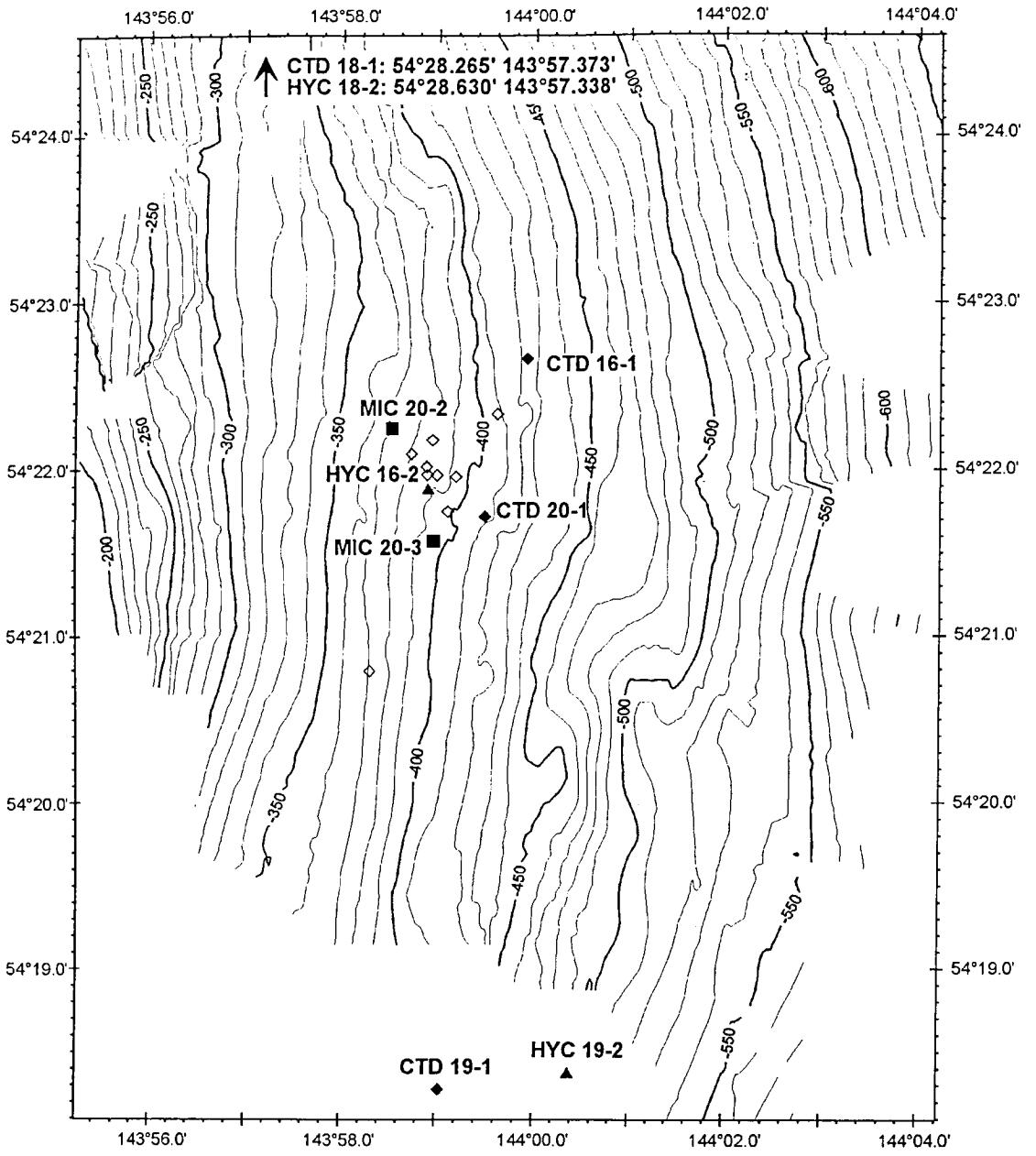

Fig 4.3: Positions of the stations taken in the Giselle Flare area (bathymetry taken from LV28 data). Open symbols are stations from Lavrentyev cruise LV28.

transducer arrays can not be fixed as accurate as necessary beforehand. Three profiles (each 1 - 2 Nm long) were carried out with the port and starboard array covering the same area; one was mapped south to north, the other the north to south. After the processing of the data (eliminating bad data points) the calibration values for the positioning were calculated using the *HPpost* software and the sound velocity model from CTD 4-1. In spite of the calibration values and a well-processed sound velocity model, each swath show a smooth 'w'-like form which could not be eliminated during the cruise. To correct the calibration values and therefore all other data, the data has to be reprocessed in Kiel together with experts of ELAC. Nevertheless, first

bathymetric maps of the Derugin Basin and a seamount in the eastern part of the Kurile Basin could be processed during GE99.

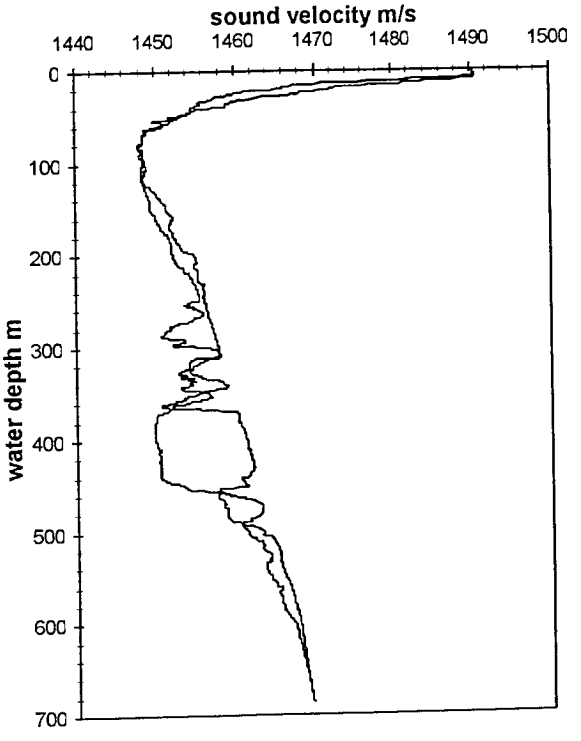

Fig. 4.4: Sound velocity profiles of CTD 24-1 and 26-1 taken at Obzhirov Flare show the typical, strong decrease below 10 m water depth with a minimum at around 70 m.

4.3 Results

4.3.1 Piltunsky area

In this area, a wave-like bottom morphology was observed during the 22th cruise of *RV Gagarinsky* in summer 1998. At the upper part of the Sakhalin shelf between 200 and 400 m the seafloor shows a relief of up to 10 m high and around 300 m width "mountains" (profiles 10 and 14; Biebow & Hütten, 1998) which might be small ridges, sediment waves or even mud mounts or pock marks. To get more information on the dimension, elongation and spatial distribution of this waves we followed line 14 from G22 cruise (Biebow & Hütten, 1999) during one profile covering a water depth between 210 and 400 m. Due to problems with the heading input from the GPS signal all swaths were shot in E-W direction although the profile inclines in ENE direction. These data have to be reprocessed in Kiel as well.

4.3.2 Giselle Flare

In the Giselle flare area, 10 profiles were planned orientated in N-S direction covering nearly the same area as in LV28. At station GE99-17-1, the easternmost profile could be mapped sailing north to south. During this track the already strong wind increased further and the second profile had to be canceled half way to the north to save the catamaran from damage.

Because of the lesser quantity these data are still unprocessed. To plot the stations at Giselle Flare taken during GE99, we used the bathymetric data of LV28 (Fig. 4.3).

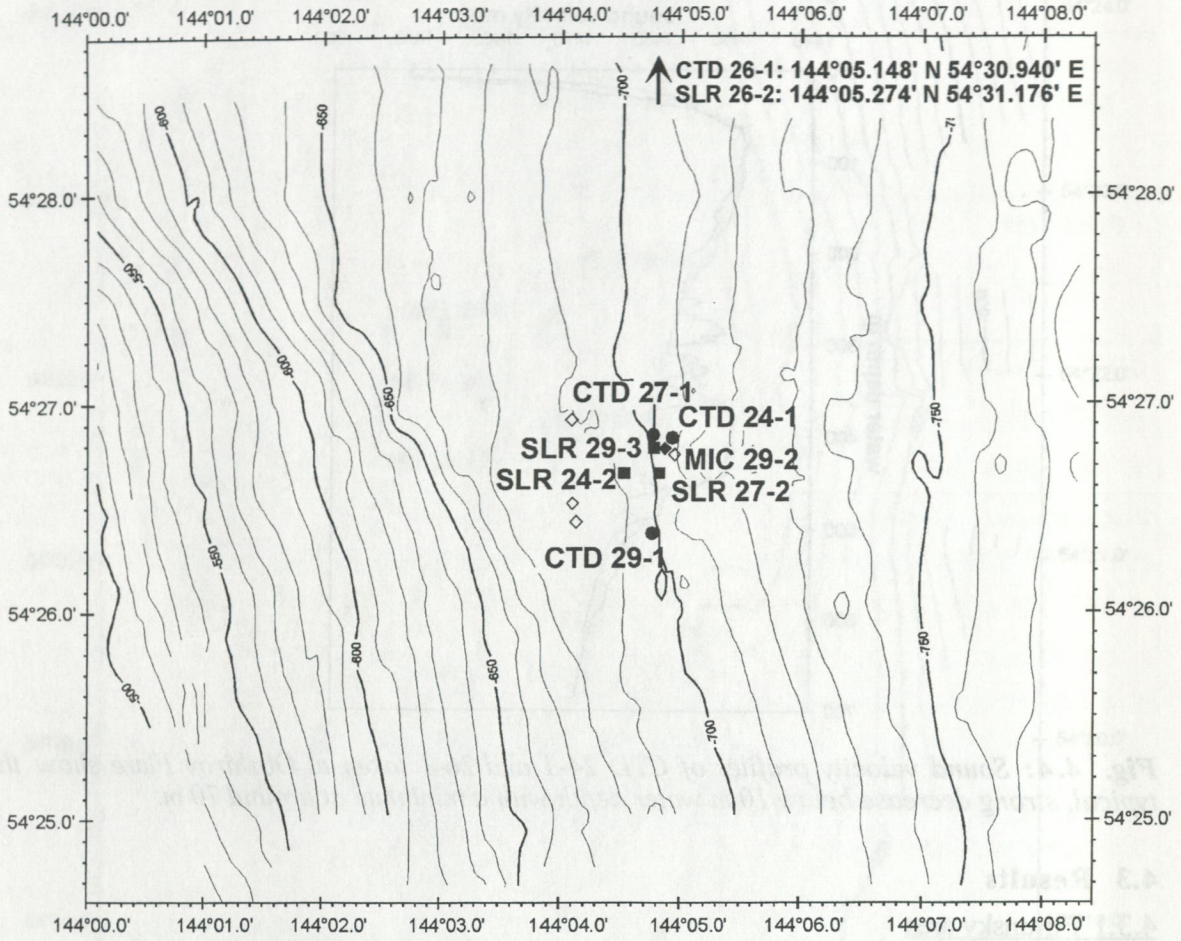

***Fig. 4.5**: Position of the stations taken during GE99 near Obzhirov Flare (bathymetric data of LV28 cruise). Open symbols are stations of Lavrentyev cruise LV28.*

4.3.3 Obzhirov Flare

Similarly to the mapping procedure at Giselle Flare the profiles were orientated in N-S direction. Due to the lack of time only the 4 easterly profiles of the seven ones planned could be carried out during station GE99-28-2. The sound velocity model was calculated from CTD GE99-24-1 and CTD GE99-26-1. Nevertheless, the cross sections of the mapped profiles show a smooth 'u'-like shape which was probably induced by the unusual sound velocity profiles common for the Sea of Okhotsk. Typically the sound velocity profiles show fast velocities of around 1500 m/s in the upper 10 to 20 m of the water column followed by a strong decrease down to 1440 to 1450 m/s in water depths around 50 to 80 m. Additionally so-called intrusions between 250 and 500 m disturb the increasing velocity and show fluctuations even between the two CTD stations which were used (Fig. 4.4). Thus, the collected data from Obzhirov Flare also have to be reprocessed in Kiel using ELAC expertise. To show the position of the stations

carried out in the Obzhirov Flare area in a bathymetric map, we again used the data of Lavrentyev cruise LV28 (Fig. 4.5).

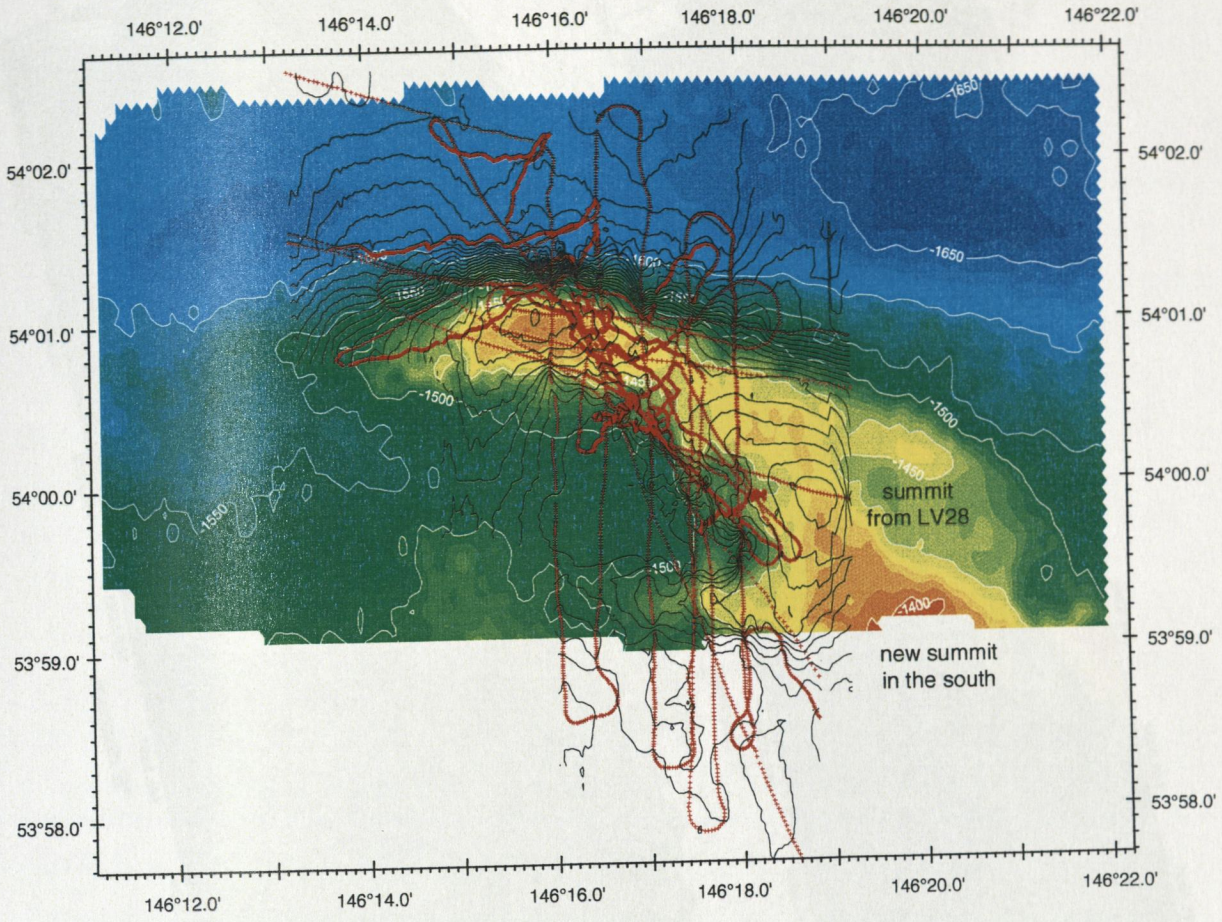

Fig 4.6: *The overlaid bathymetric map of the investigated Derugin Basin area mapped during LV28 (black isobaths) shows a summit in the east where the colored map processed during GE99 shows only a smooth ridge (yellow) connecting the E-W striking summit at 54°01.0' N and the new summit in the south. This wrongly mapped summit from LV28 was induced by the mapping procedure during the cruise. Here, the ridge was crossed only once (small red points are coordinates of LV28 data); thus no more data existed in the north and south which could be used for the calculation of the grid.*

4.3.4 Derugin Basin "Barite Mountains"

In contrast to the previous surveys we had good weather conditions during the first two (GE99-33-1) of the three profiles planned in the Derugin Basin area. These profiles should map the seafloor from the western border of the area mapped during LV28 to the east where higher heat flow values at three locations possibly hint to warmer fluids expulsing at the seafloor. To map these areas of 1350 and 1750 m water depth we used a swath angle of 100° and a sound velocity profile calculated from CTD GE99-32-1. Starting with the inner profile heading to the east the main working area of cruise LV28 was covered. Here, a smooth ridge striking NW - SE between the known summit in the north and a newly discovered summit in the south was mapped. This ridge area was formerly mapped as an isolated summit and was interpreted as a

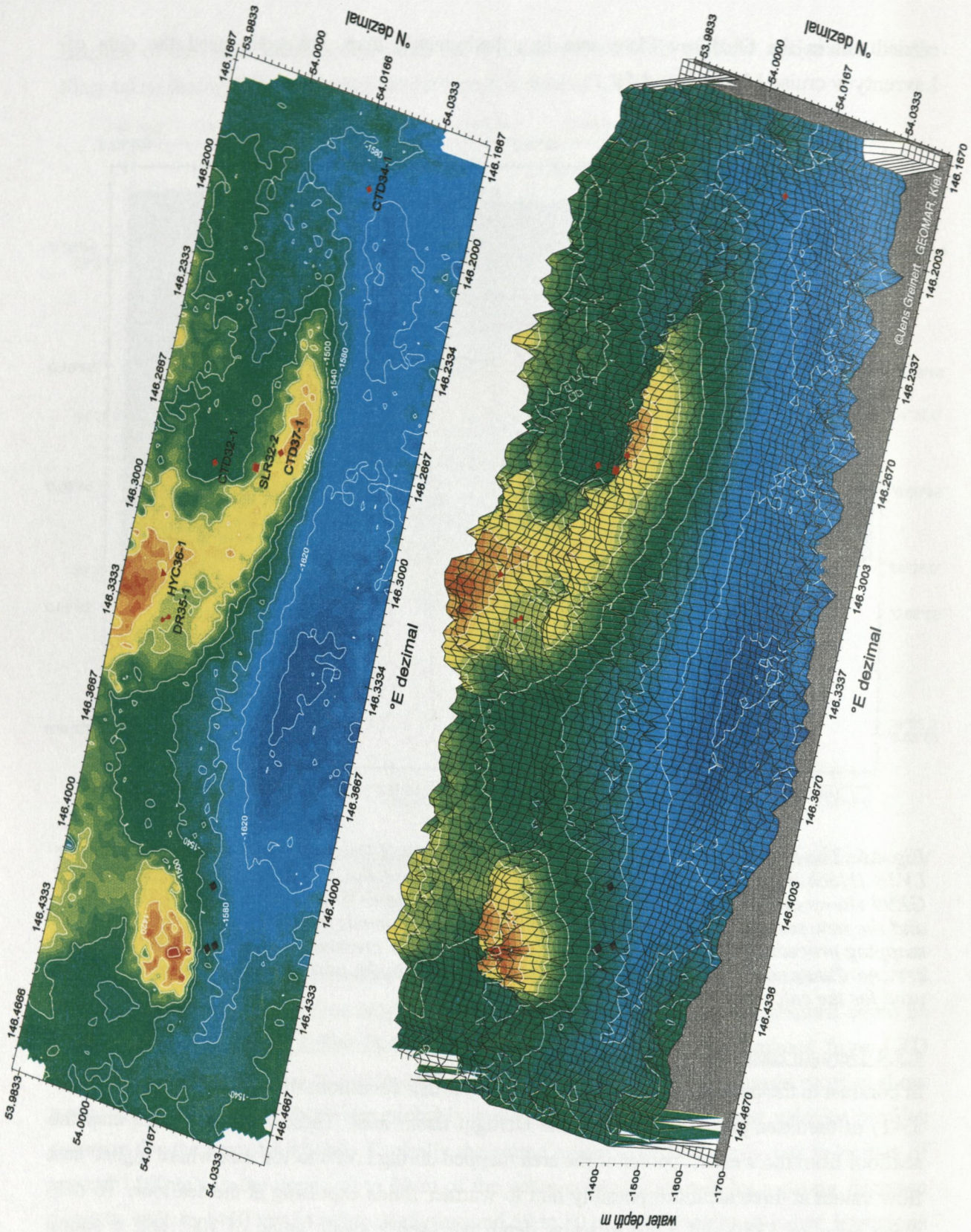

Fig 4.7: *3D-image seen from NW (345°; tilt 50°; vertical exaggeration 13) shows the mapped 'Barite Mountain' area in the Derugin Basin. Red symbols are stations carried out during GE99. Black symbols north of the eastern mountain are locations at which a higher heat flow was measured.*

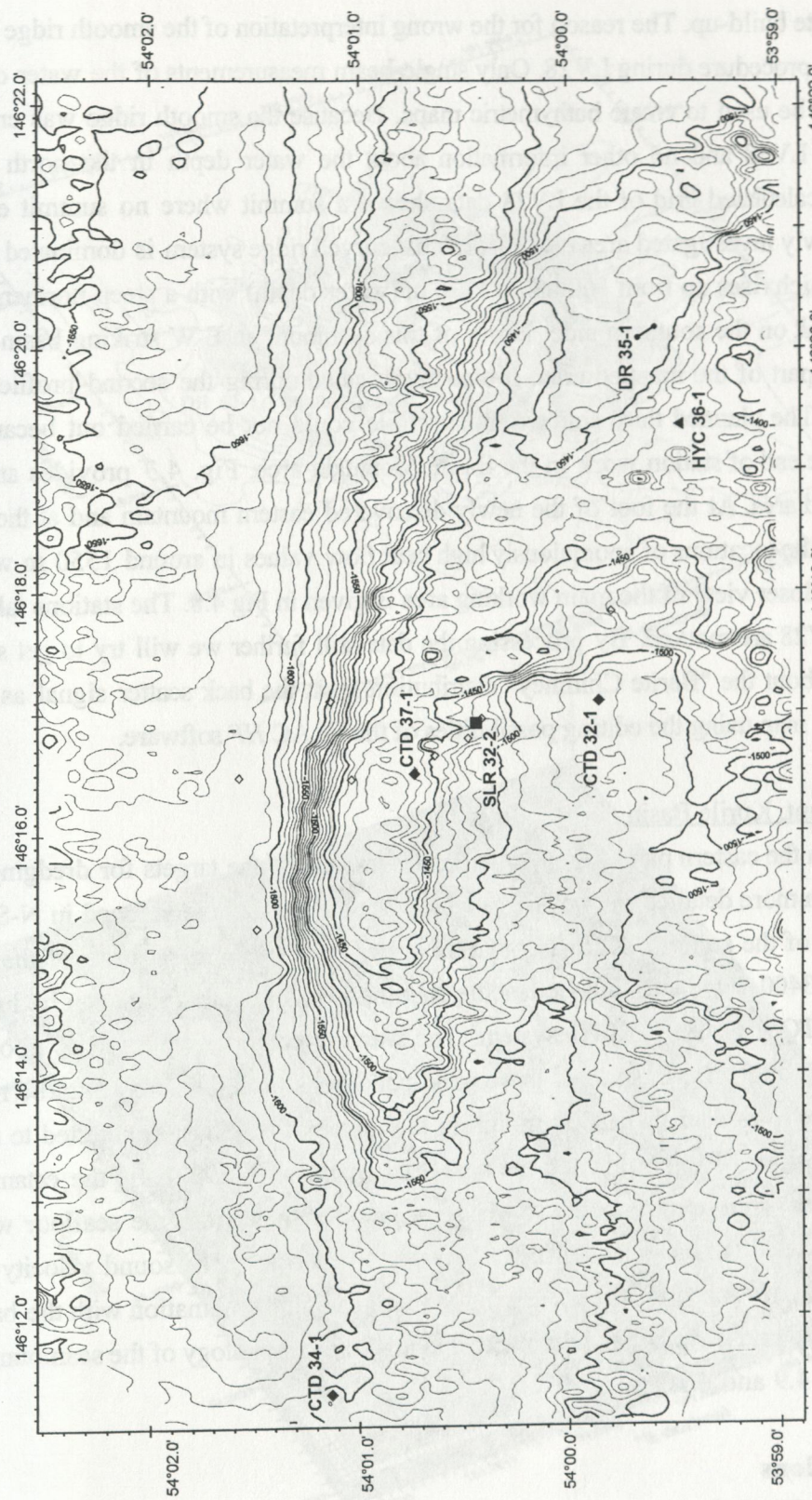

Fig. 4.8: *Map of the western part of the 'Barite Mountain' area in the Derugin Basin, view from. Stations of GE99 are plotted in black symbols. The positions of the stations taken during LV28 are marked as open diamonds.*

possible barite build-up. The reason for the wrong interpretation of the smooth ridge is given by the mapping procedure during LV28. Only single-beam measurements of the water depth every 10 sec could be used to create bathymetric maps. Because the smooth ridge was crossed only once during LV28 and no other information about the water depth in the north and south existed, the calculated grid of the LV28 data shows a summit where no summit exists (Fig. 4.6). The newly investigated area eastward of this curved ridge system is dominated by a small seamount which rises up from 1600 m to 1370 m (water depth) with a steep northern edge and a smooth flank on the southern side. North of this seamount an E-W striking basin dominates the northern part of the mapped area. It was investigated during the second profile of station GE99-33-1. The planned third southernmost profile could not be carried out because of bad weather at the end of station work in the Barite Mountain area. Fig. 4.7 provides an overview of the mapped area. At the foot of the newly discovered eastern mountain and at the border of the basin are the locations of anomalously high heat flow values in around 1550 m water depth (Fig 4.7). A closer view of the main working area is given in Fig 4.8. The stations taken during GE99 and LV28 are marked. By processing the data still further we will try to get some more information about the "Barite Chimney" distribution from the back scatter signal as well as a more detailed map using the editing possibilities of the ELAC *HP* software.

4.3.5 Seamount, Kurile Basin

A seamount in the eastern part of the Kurile Basin was one of the targets for dredging volcanic rocks. To get a more detailed map of this seamount, two tracks were planned in N-S direction east and west of the summit. Knowing that the water depth at the basal parts of the seamount goes down to 3400 m we were able to test the maximum water depth which can be investigated with the BOTTOM CHART MKII system. The weather conditions were very good without strong wind or rough sea. In spite of these good conditions no reflections could be recognized from water depths greater than 3000 m during the first profile. Thus, we started to sail to the first dredge position. During this and the next dredge station (GE99-40-1) the catamaran was left in the water. Thus we were able to get some good signals from the seafloor with water depths less than 3000 m using swath angles between 40° and 18°. The sound velocity model of CTD GE99-41-1 was used for the processing of these data. In combination with the bathymetry data of the LV28 cruise we got an acceptable image of the morphology of the seamount which is shown in Fig. 4.9 and 4.10.

4.4 Conclusions

The BOTTOM CHART equipment used is easy to handle and to install. The software for data acquisition as well as for postprocessing is easy to use too. Because of the catamaran and the mostly bad weather conditions the collected data are not as good as could be. If the system should be used again with the catamaran it certainly needs rebuilding so that it can be positioned 0.5 m below the wave surface. Probably a still better solution would be to fix the

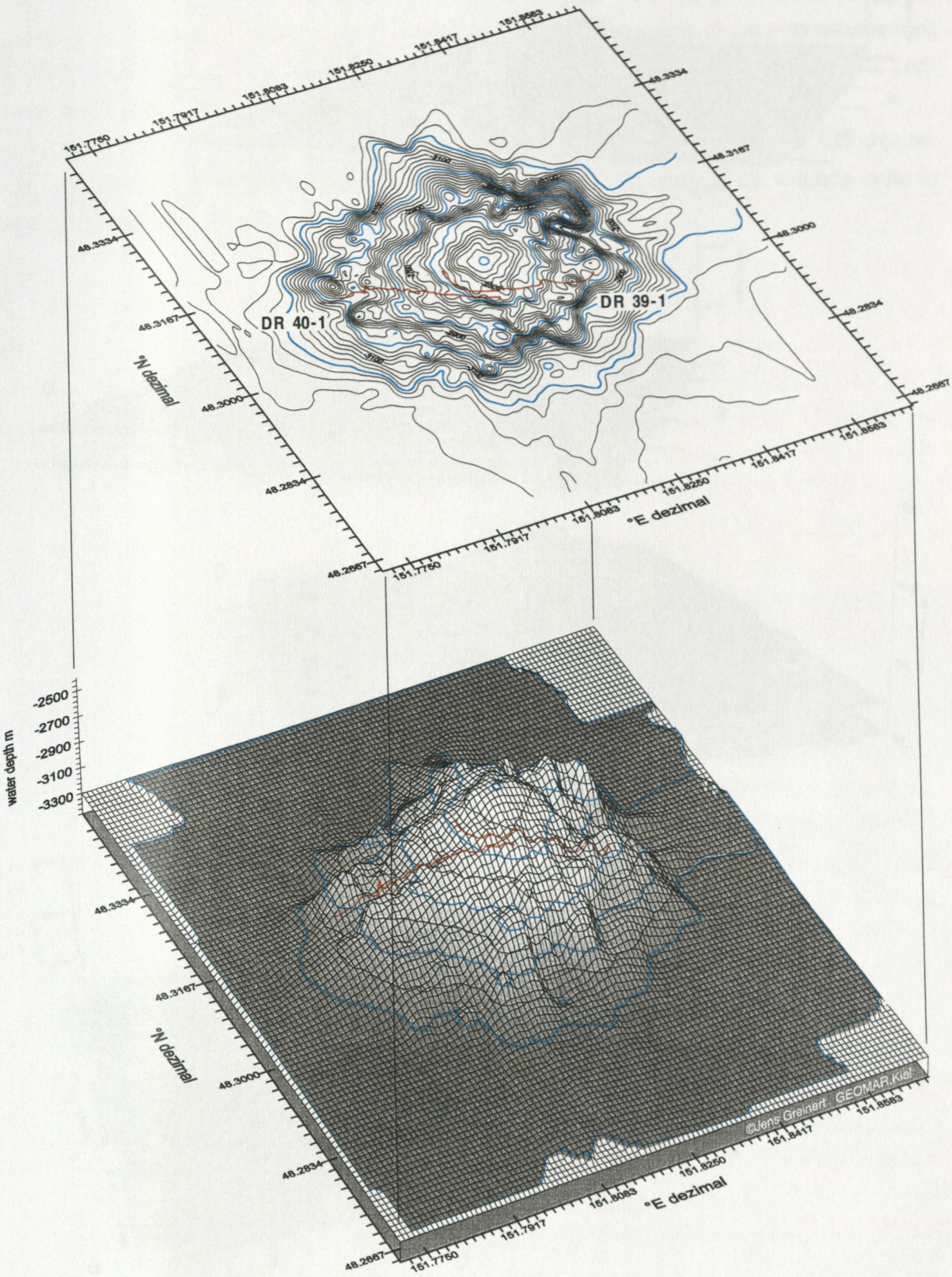

Fig. 4.9: *Kurile Basin seamount seen from SSW (205° ,tilt 40°, vertical exaggeration 2). The dark lines are the dredge tracks DR 39-1 and 40-1.*

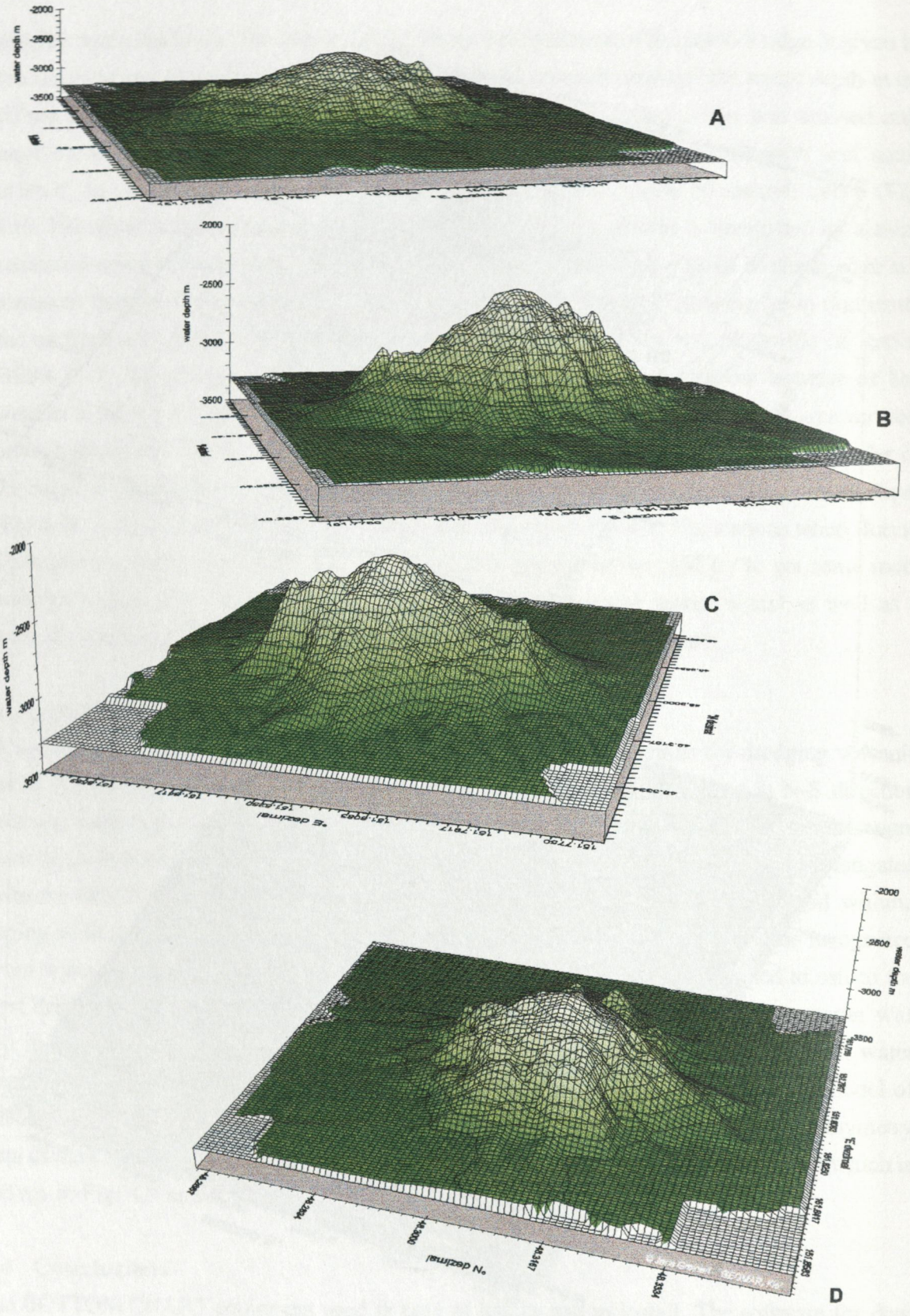

Fig 4.10: *3-D images of the seamount in the Kurile Basin. A: view from SSW (197°, tilt 7°) no vertical exaggeration; B: same like A but a vertical exaggeration of 2; C: view from NNW (345°, tilt 15°) vertical exaggeration 2; D: view from ENE (65°, tilt 32°) vertical exaggeration 2.*

transducer/receiver arrays outside the ship with a frame as had been planned for *Akademik Lavrentyev*. The best way to fix the transducer outside the ship seems to put a transducer each on both sides of the ship. Thus it would not be necessary to put the transducers below the keel; furthermore the frame does not need to be so heavy.

All in all the system worked surprisingly good and the collected data in spite of the bad weather are very useful and provided a new insight into the detailed bathymetry of the working areas in the Okhotsk Sea.

5. WATER COLUMN WORK

G. Winckler, A. Salyuk, and V. Sosnin

5.1 Introduction

The initial objective of GE99 cruise was to revisit the highlights investigated during LV28 cruise (e.g. the northern Sakhalin Shelf region, Derugin Basin etc.) and to further extend our data set of the Sea of Okhotsk, e.g. undertake a detailed investigation of new venting areas, the Amur delta region, an additional northern west-east transect and completion of the central west-east transect (started during LV28) to the Kamchatka region. Due to technical and fuel problems, these "new" objectives could only be marginally touched.

Thus, we focused on the first objective. The highest priority in the water column work was given to a detailed reinvestigation of the venting areas at the northern Sakhalin Shelf and Slope ("Giselle Flare", "Obzhirov Flare") and the Derugin Basin barite area, especially to methane studies. Our CTD strategy included two aspects. On the one hand, we used the echosounder data as flare indicator and placed CTD stations in the center of vents to get the vent signal as undiluted as possible (e.g. GE99-27-1, GE99-29-1 at "Obzhirov Flare"). On the other hand, we placed CTD transects across the known venting areas to compare the vent signal to the regional background concentrations to map the venting influence. The new data will provide further information regarding methane and vent distribution in the Sakhalin Shelf area. In the Derugin Basin, we revisited the barite field area discovered during LV28 and reproduced the findings of extremely high methane concentrations in the lower water column. We planned to map the methane plume to find out the extent of the plume, but due to time constraints we only finished this work partly.

Another goal in this region was the monitoring aspect. The GE99 cruise complements the annual cycle of water column investigations, which consists of observations in summer 98 (LV28), autumn 98 (G25), March 99 (ICE I), May 99 (Ut99). The data will provide new information regarding time variability of water column features as well as of vent-related features.

5.2 CTD - rosette

Water column sampling was carried out using a rosette water sampling system combined with a CTD probe. The rosette system used was a Sea-Bird 32 twelve position system with 10 l Niskin-type bottles. The probe used was a Seabird 911 plus CTD with standard temperature, pressure and conductivity sensors which also logged data from additional sensors for oxygen and transmission.

The rosette/CTD system was run using the HATLAPA hydrowinch. Downcasts were carried out continuously at 1m/sec until the bottom trigger alarm (10 m) sounded. The first sample was usually taken at maximum water depth, the others were collected on the up-cast. The only

exception was station GE99-29-1 ("Obzhirov Flare"), where three bottles were taken on the downcast. During the first part of the cruise (up to station GE99-8-1) some problems with the data transmission between the rosette system and the deck unit occurred: bottles closed arbitrarily without being triggered by the operator and an erroneous sequence report was sent. Erroneous data transmission could be avoided by stabilizing and filtering the ship's power supply using a transformator.

For each station, separate data files for down- and upcast were collected. The data processing was performed using the modular processing routines provided by the software package SEASOFT (version). The raw CTD data of the downcasts of each station were converted to 1m interval data files (*.cnv).

A total of 29 stations were carried out and are tabulated in Tab. 5.1. Water samples were collected for methane and higher hydrocarbons, oxygen concentration, Helium/Tritium, oxygen isotopes, carbon isotopes, nutrients and bioproductivity. Oxygen concentrations were determined by Winkler titration, nutrient analyses (silicate, phosphate) were performed on board by photometry. The data are tabulated and discussed below. Isotope data ($^{3}He/^{4}He$, ^{3}H, ^{18}O, ^{13}C) will follow after post-cruise laboratory analyses.

At several stations the station-keeping ability of the ship turned out to be a serious problem. For a detailed study of vent systems and associated water column features station-keeping is essential. Due to the motion of the ship at some stations it was difficult to determine the respective position of the CTD when deployed and to carefully sample vent features.

5.3 General hydrography

The general circulation within the Sea of Okhotsk consists of a broad cyclonic gyre. The Sea of Okhotsk is connected to the North Pacific Ocean through two deep straits: (1) Bussol Strait (sill depth 2300 m) and (2) Kruzenshterna Strait (sill depth 1900 m).

A flow of relatively warm and saline Pacific waters (NPW - North Pacific Water) into the Sea of Okhotsk occurs through the northern passages of the Kurile Islands, primarily through Kruzenshterna Strait and is fed by the East Kamchatka Current. A flow out of the Sea of Okhotsk occurs through the southern Kurile straits, primarily through Bussol Strait. Another flow also enters the Sea of Okhotsk from the Sea of Japan through La Peruse Strait (sill depth 40 m). The estimated gross exchange of water between the Sea of Okhotsk is 15 Sv.

The Sea of Okhotsk plays an important role in the ventilation processes of the North Pacific. The North Pacific is the one ocean basin in which very deep ventilation does not occur; its deep waters originate from the North Atlantic and around Antarctica. However, the North Pacific is ventilated to a depth of 1000 to 2000 m, mainly as a result of dense shelf water production in the northern Sea of Okhotsk. The ventilated water from the Sea of Okhotsk flows out into the North Pacific; some of it remains in the subarctic North Pacific, while another part flows southward into the subtropical region where the top of the water is characterized by a salinity

minimum. Thus, the northwestern North Pacific including the Sea of Okhotsk is connected to ocean circulation on a much larger scale.

Tab. 5.1: *CTD statistics - types of samples taken.*

Station	CH_4	O_2	δ^3He	nuts	$\delta^{13}C$ Paleo	$\delta^{13}C$ Vent	$\delta^{18}O$	^3H	earth alkali	bio
1-1	x	x	x	x			x	x	x	
2-3	x	x	x	x		x	x	x	x	
3-1	x	x		x		x	x		x	
4-1	x	x	x	x		x	x	x	x	
5-3	x	x	x	x		x	x	x	x	x
6-1	x						x			
6-2	x	x	x	x		x	x	x	x	
7-1	x	x	x	x		x	x	x	x	
8-1	x	x	x	x		x	x	x	x	
11-1	x	x	x	x		x	x	x	x	
12-2	x	x	x	x	x	x	x	x	x	
13-1	x	x	x	x		x	x	x	x	
15-1	x	x	x	x		x	x	x	x	
16-1	x	x	x	x		x	x	x	x	
18-1	x	x	x	x		x	x	x	x	
19-1	x	x	x	x		x	x	x	x	
20-1	x	x	x	x		x	x	x	x	
21-1	x	x	x	x	x	x	x	x	x	x
24-1	x	x	x	x		x	x	x	x	
26-1	x		x	x	x	x	x	x	x	
27-1	x	x	x	x		x	x	x	x	
29-1	x	x	x	x		x	x	x	x	
30-1	x		x	x		x	x	x	x	
31-1	x	x	x	x	x	x	x	x	x	
32-1	x	x	x	x		x	x	x	x	
34-1	x		x	x		x	x	x	x	
37-1	x	x	x	x		x	x	x	x	
38-1	x	x	x	x	x	x	x	x	x	x
41-1	x	x	x	x			x	x	x	

The surface layer of the Sea of Okhotsk contains very fresh water. The surface layer is separated by a sharp pycnocline from the deeper waters. The temperature of the surface layer decreases due to surface cooling in autumn and winter, but even when the temperature is lowered to the freezing point, the pycnocline is still maintained by the sharp salinity gradient. Thus, the winter convection occurs only within a thin surface layer. This peculiar situation allows sea ice formation at a very low latitude in comparison with other seas and oceans. About two thirds of the Sea of Okhotsk are covered by sea ice in winter; all sea ice in the Sea of Okhotsk is first year sea ice. The sea ice formation starts in November, the maximum sea ice extent usually occurs in March. Active sea ice formation generates dense shelf water. This water looses its high salinity character before it flows out to the central part of the sea. However, this water is believed to be important for the ventilation of the intermediate waters of the entire North Pacific.

The fresh surface water is thought to originate from fresh water discharge mainly from the Amur River (315 km^3) and from other areas from Siberia to the Kamchatka coast (148 km^3). However, the fresh water balance of the Sea of Okhotsk is still only insufficiently known and needs further consideration.

5.4 Main hydrographic features

The CTD stations investigated during GE99 cruise can be divided into four groups using the common structural features of vertical temperature distribution. Figures of hydrographic data (salinity, potential temperature, potential density, oxygen) are given in the Appendix 3.

5.4.1 Shelf region (< 120 m)
5.4.2 Slope region (370-1000 m)
5.4.3 Derugin Basin
5.4.4 Kurile Basin

5.4.1 Shelf stations

Three stations were carried out in the shelf region at water depths lower than 120 m (GE99-3-1, 4-1 and 11-1). The most common feature of these stations is the absence of a warm intermediate layer which is usually found beneath the cold subsurface layer. The temperature decreases continuously towards the bottom. The coldest water is found near the bottom and represents the remnant of the formerly homogeneous winter layer. At GE99-4-1 in Terpenia Bay the minimum temperature (-1.6°C) of the three profiles could be found. Here, the profiles still show significant gradients implying that the bottom water in the bay is only poorly ventilated. A comparison of GE99-4-1 with 3-1 and 11-1 supports the idea of the semi-closed nature of the bay in contrast to the open shelf position of stations GE99-3-1 and 11-1.
Summer heating at GE99-11-1 in the central part of the Sakhalin shelf is much less pronounced than at station 4 (13°C compared to 16°C). However, in contrast to GE99-4-1, GE99-11-1 shows a well-developed homogenous deep layer which implies effective mixing. In comparison with the spring season, the temperature of this layer increased by approximately 1°C. Apparently, this demonstrates tidal mixing with new warmer water which is transported from the north according to the general Sakhalin current.

5.4.2 Slope region (370-1000m)

This group contains GE99-12-2 to 30-1 and includes the stations at "Obzhirov and Giselle" Flares. The specific feature of the slope stations is the presence of multiple intrusions which points to strong dynamical activity and intensive vertical mixing processes in the water column.
At Giselle Flare we investigated four CTD stations during one day (GE99-16-1, 18-1, 19-1, 20-1). The temperature profiles at these stations differ from the typical subarctic structure. The warm intermediate layer is only weakly pronounced and highly variable in time. This is

probably related to a sequence of transport and mixing of waters along the slope. The temperature near the bottom is lower than in the subsurface cold layer but much higher than in winter. This supports the idea that water masses are advected from the north and mixed at the slope.

At "Obzhirov" Flare, four CTD stations were carried out (GE99-24-1, 26-1, 27-1, 28-1). These represent the maximum intensity of intrusive inter-layering. The characteristics of the intrusions at "Obzhirov Flare" (depth and temperature value) are similar to that of the near bottom layer at "Giselle Flare". We may conclude that both the bottom water at "Giselle Flare" as well as the intrusions at "Obzhirov Flare" are advected water masses.

Intrusion features were also observed at the southern slope stations GE99-12-2, 13-1 and 15-1. Obviously, mixing processes occur along the entire northern Sakhalin slope.

5.4.3 Derugin Basin

In the Derugin Basin, five CTD stations were investigated (GE99-30-1, 31-1, 32-1, 34-1, 37-1). A characteristic feature of this group is the presence of cold intrusions occurring at water depths between 150 and 400 m. However, these dynamical processes only occur in the upper 400 m. Below 400 m, all CTD profiles show a homogenous temperature distribution implying very low vertical mixing activity. This confirms the hypothesis that the Derugin Basin is the most stagnant zone of the Sea of Okhotsk.

5.4.4 Kurile Basin

GE99-2-1, 6-1, 7-1, 8-1 and 41-1 represent a transect across the deepest part of the Sea of Okhotsk, the Kurile Basin. They reflect the different levels of dynamic activity in that area. More conservative temperature profiles with relatively little structures in temperature could be observed at GE99-7-1 and 8-1 in the central part of the Kurile Basin. The stations show temperature and salinity profiles typical for the subarctic zone. Moreover, GE99-7-1 and 8-1 represent the only stations of the transect where negative temperatures were observed.

In contrast, GE99-2-1 being situated near the slope represents the maximum modification in the temperature profile. The cold subsurface layer in this region is almost completely destructed due to intensive mixing with slope waters and has positive temperatures. High mixing activity is also observed at GE99-6-1. Another type of vertical temperature distribution is found at GE99-41-1 which demonstrates the final stage of the mixing process without intrusions in an almost homogeneous layer.

5.4.5 Bottom waters of the Kurile Basin

The vertical distribution of hydrologic properties in the Kurile Basin shows some features which are connected to deep and bottom water formation in the Kurile Basin. One of these features is a slight, monotonous increase of oxygen concentration and salinity, which takes place from deep waters to the very bottom (from about 2500 to 3400 m). This raises the

question if the increase in oxygen concentration is the result of bottom water ventilation by fresh waters with a higher oxygen concentration, or if it is a relict water mass that has conserved higher density, salinity, oxygen concentration and lower temperature after some warming and freshening in the last period.

At station Ge99-6-2 carried out in the Kurile Basin, the positive anomaly of oxygen content (from 84 to 88 mM/kg) in a thin near-bottom layer (about 90m) could be observed (Fig. 5.1).

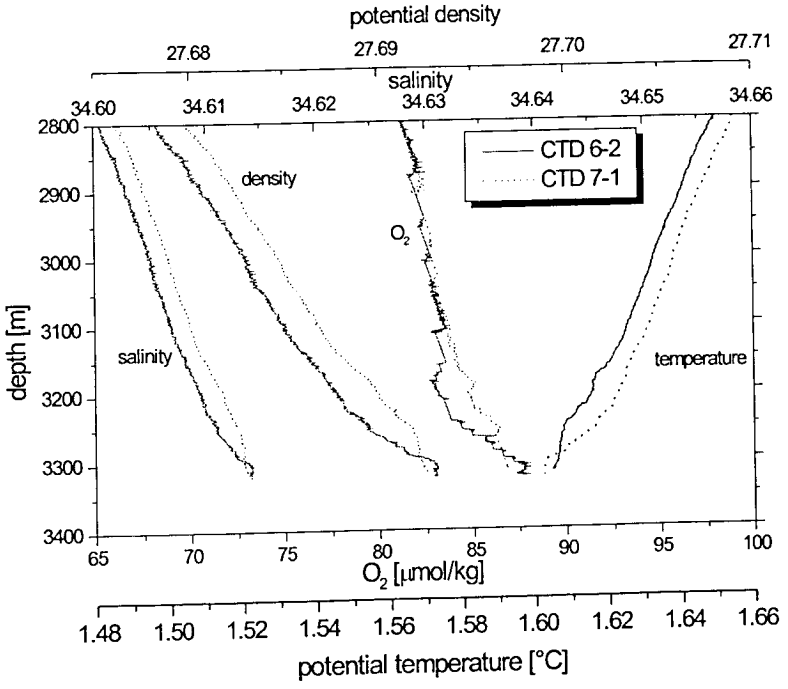

***Fig. 5.1**: Vertical distribution of potential temperature, salinity, potential density and oxygen concentration at GE99-6-2 and 7-1.*

This anomaly overlays the potential temperature anomaly; it is a mixed layer with a potential temperature 1.6025 °C (0.005 °C less then the potential temperature of the waters above) and a thickness of about 30 m.

Such thin layers with temperature anomalies are usually characterized by dissipation velocities values about one order faster than their salinity indicates; this layer is undoubtedly new and must disappear in time due to heat exchange and near bottom mixing.

The source of this new water anomaly is Pacific water with a higher density coming from approx. 2300 m of depth; this is the maximum sill depth of the Bussol Straight. A similar explanation has been proposed by Yasuoka (1967) who suggested that Pacific waters with a density of 27.7 flow through the Bussol Strait into the Sea of Okhotsk.

The revealed oxygen, temperature, density anomaly at GE99-1 shows that the process of supplying dense bottom waters with higher oxygen contents is continuing. This permanent supply of dense water seems to be a very effective renewal mechanism of bottom and deep waters in the whole Kurile Basin.

5.5 Nutrients and oxygen

Major nutrients were analyzed at most of the CTD stations (see table 5.1). Fig. 5.2 presents a comparison between the silicate concentrations obtained in the Derugin Basin and along the transect across the Kurile Basin.

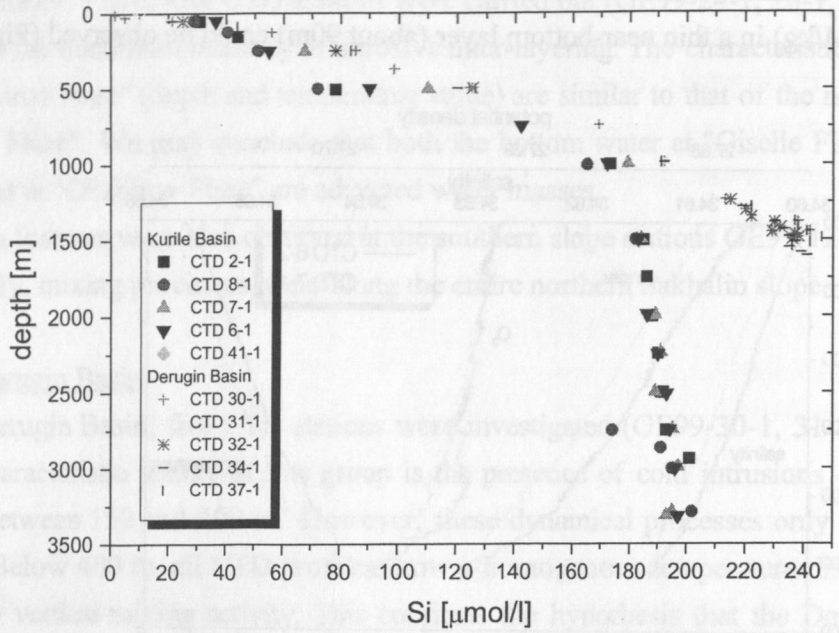

Fig. 5.2: Distributions of silicate concentrations in the Kurile and Derugin Basins.

The silicate distributions in the Derugin Basin stations differ significantly from those in the Kurile Basin and show extremely high levels, up to 240 mmol/l. In the Kurile Basin, the silicate concentrations are much lower, but still increase with depth, in contrast to the behavior known from the North Pacific Ocean. The distinct silicate distributions coincide with different oxygen profiles: oxygen concentrations in the Kurile Basin at 1500 m are higher than in the Derugin Basin by a factor of 2. The characteristics of the Derugin Basin, very high silicate and extremely low oxygen concentrations, are interpreted as indicator of an old water mass with only little exchange with the water column above.

5.6 Isotope tracers

Water samples for the analysis of the helium isotope ratio, helium and neon concentrations, tritium and oxygen isotopes were obtained from all CTD stations. The mass spectrometric isotope analyses will be carried out at the Institute of Environmental Physics (University of Heidelberg). Two different objectives will be studied using the isotope data:

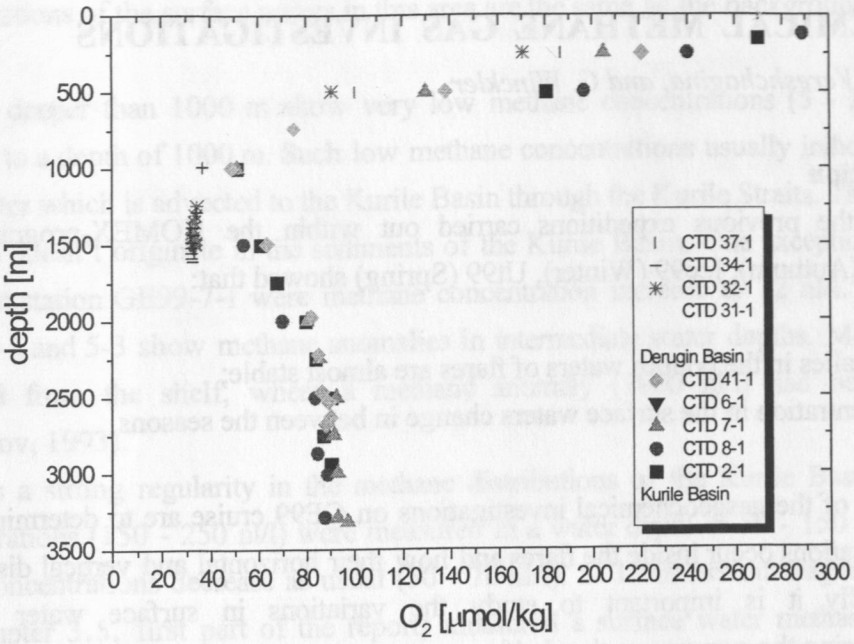

Fig. 5.3: *Distribution of oxygen concentrations in the Kurile and Derugin Basins.*

a) the geochemical information of the helium isotope data. In most of the studied areas (Sakhalin Shelf, Derugin Basin) the source of the gas and fluid venting carrying extreme methane anomalies is still an open question, e.g. if the basic process is limited to shallow or
b) deep sediment horizons. As the $^{3}He/^{4}He$ ratio depends on the geochemical reservoir the fluid is derived from, helium isotope analysis may help to identify the source of the methane signal emitted from the seafloor. This especially applies to Obzhirov Flare where gas hydrates could be recovered from two sediment cores. After pieces of hydrate had been extracted on board, gas samples were taken in copper tubes and will be analyzed for their noble gas composition in order to obtain new insights on the formation processes and the source of the hydrates.
c) the oceanographic tracer information. Isotope data of different tracers ($^{3}He/^{4}He$, $^{18}O/^{16}O$, ^{3}H) will be related to hydrographic parameters (salinity, temperature) and provide information on the regional water mass distribution. Knowledge on the current hydrographic situation, e.g. circulation processes, is crucial for understanding the vent distribution. Ventilation processes leading to the formation of intermediate water are very important in the Sea of Okhotsk. Combined, helium isotope and tritium data may be used to describe the evolution of the vertical age structure of the water column. The oxygen isotope data are of special interest as the ventilation processes are strongly related to fresh water components. Based on coupled tracer balances for ^{18}O and salinity the regional distribution of fresh water components will be obtained. The ^{18}O data are of special interest as they allow to distinguish between different fresh water components, the river run-off component mainly originating from the Amur River, and sea ice meltwater.

6. GEOCHEMICAL METHANE GAS INVESTIGATIONS

A. Obzhirov, O. Vereshchagina, and G. Winckler

6.1. Introduction

The results of the previous expeditions carried out within the KOMEX-program LV28 (Summer), G25 (Autumn), Ice99 (Winter), Ut99 (Spring) showed that:

1. methane anomalies in the bottom waters of flares are almost stable;
2. methane concentration in the surface waters change in between the seasons.

The main targets of the gasgeochemical investigations on GE99 cruise are to determine which methane concentrations occur inside the flares and how their horizontal and vertical distribution changes. Secondly it is important to study the variations in surface water methane concentrations during the summer on the shelf.
The gas investigations of the *Gelovany* expedition comprise the following research topics:

1) Detailed water column investigations of gas and fluid vent fields on the north-eastern shelf and upper slope of Sakhalin Island and their contribution to the air-sea exchange of methane;
2) Detailed investigations of the gas distribution in the bottom waters around the "Barite Mountains" of the Derugin Basin;
3) Investigation of the "methane monitoring" stations;
4) Water column investigation in the Kurile Basin.

6.2 Methods

Special soft bottles are used to take 0.5 l of water without air contact from the Niskin bottles. Gas is extracted from the water by a vacuum line and analyzed by gas chromatography aboard the ship (Obzhirov, 1993). The sensitivity of the hydrocarbon analysis is 0.00001%, 0.01% of other gases.

6.3 Results

Gas investigations were carried out at 28 CTD stations (Appendix 4). The methane concentrations of all stations in the water column are presented in Appendix 4.

6.3.1 Kurile Basin and Aniva Bay

In this region 9 stations were carried out: GE99-1-1, 2-3, 3-1, 5-3, 6-1, 6-2, 7-1, 8-1, 41-1. The methane concentrations in the bottom waters of the bay and slope stations (GE99-1-1, GE99-3-1) are by 1.5 times higher than the background (150 - 180 nl/l). The methane

concentrations of the surface waters in this area are the same as the background values (53 - 56 nl/l).

Stations deeper than 1000 m show very low methane concentrations (5 - 20 nl/l) from the seafloor to a depth of 1000 m. Such low methane concentrations usually indicate Pacific Ocean deep water which is advected to the Kurile Basin through the Kurile Straits. That means that the methane doesn't originate in the sediments of the Kurile Basin. One exception are the bottom waters at station GE99-7-1 were methane concentration increase to 72 nl/l. Besides, stations GE99-2-3 and 5-3 show methane anomalies in intermediate water depths. Methane is possibly advected from the shelf, where a methane anomaly (3900 nl/l) had been found before (Obzhirov, 1993).

There is a strong regularity in the methane distributions of the Kurile Basin. High methane concentrations (150 - 250 nl/l) were measured in a water depth of 50 - 150 m. In the surface water concentrations decrease as usual (50 - 70 nl/l). S. Lammers on Gagarinsky cruise G26 (see chapter 3.5, first part of the report) measured a surface water methane anomaly in the central part of the Kurile Basin. Those findings could not be reproduced at stations GE99-6-1 and 6-2. To verify those data, CTD and equilibrator measurements should be carried out simultaneously.

6.3.2 Terpenia Bay

Station GE99-4-1 was carried out in the monitoring area of Terpenia Bay. The methane anomaly (579 nl/l) in the bottom water is stable, values are approximately the same as the background concentrations on the surface.

6.3.3 Sakhalin shelf and slope

Methane anomalies (500 - 2500 nl/l) in the bottom waters could be found at all stations in this area: GE99-11-1, 12-2, 13-1, 15-1. The methane concentrations decrease towards the surface waters and equal the background concentrations on the surface. Perhaps methane emanates from oil-gas-bearing sediments into the water and is produced by methane-generating bacteria at the same time.

6.3.4 Giselle Flare

Stations GE99-16-1 and 20-1 were carried out inside "Giselle Flare" (Fig. 6.1). Station GE99-18-1 is located 6 miles to the north from "Giselle Flare" and station GE99-19-1 4 miles to the south from that flare. The bottom waters of the stations contained an anomaly from 9.080 nl/l inside the flare to 500 nl/l outside the flare. It means that methane migrates from the sediments to the water via the flare (fault zone) as well as via seepage (fissure zone). The methane concentrations in the surface waters are 60-70 nl/l similar to other stations.

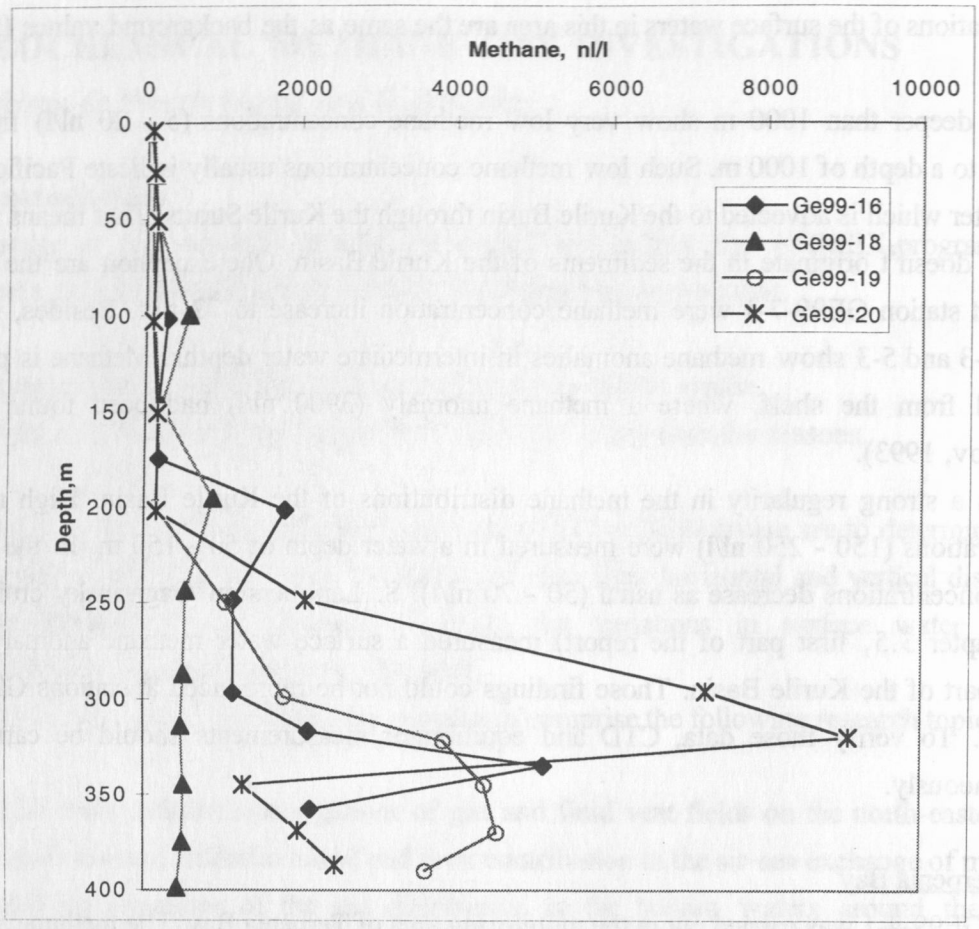

Fig. 6.1: *Comparison of methane concentrations derived from CTD-stations GE99-16,-18,-19,-20 carried out at "Giselle Flare".*

6.3.5 Obzhirov Flare

Stations were carried out in the following areas: GE99-27-1 - inside the flare (northern part), GE99-29-1 - inside the flare (southern part), GE99-24-1 - near the flare, GE99-26-1 - 5 miles to the north from the flare, GE99-30-1 - 4.5 miles to the south-east from the flare.

A significant anomaly (23.759 nl/l) was found in the near bottom waters inside "Obzhirov Flare" (GE99-29-1) (Fig. 6.2). Outside the flare the concentrations at a depth of about 50 - 100 m above the sea floor (see GE99-29-1) decrease about 5 times. The methane concentrations change distinctly between different sampling levels of the near bottom waters as well as in the water column. This is connected with differing bubble density. There are water layers with bubbles (looking like a cloud in the echogram, see plates 1-3) Those bubbles are forming as a result of gas hydrates destabilization. On some stations (GE99-29-1) these bubbles could be sampled by the CTD bottles, but this did not work always.

5 miles to the north of the flare, methane concentration in the bottom waters decrease to 229 nl/l (GE99-26-1), 34 miles to the north (GE99-21-1) to only 62 nl/l. To the south of the flare the

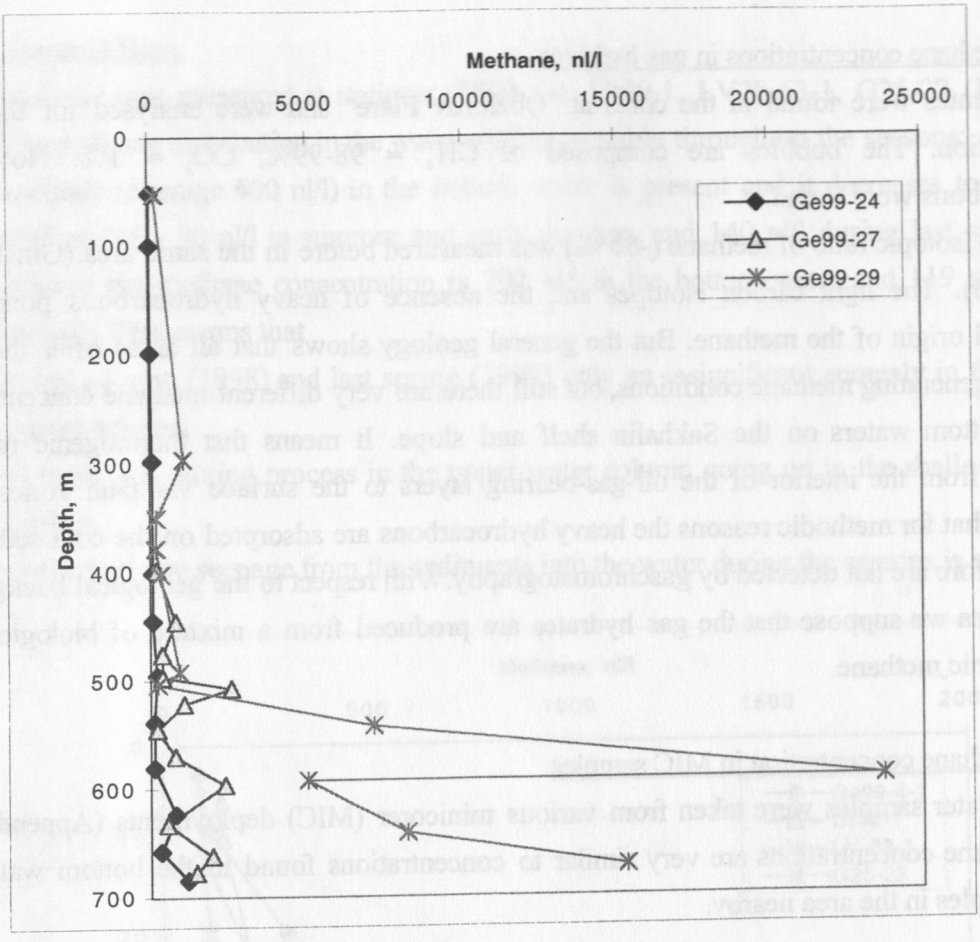

Fig. 6.2: *Comparison of methane concentrations derived from CTD-stations GE99-24,-27,-29 carried out at "Obzhirov Flare".*

methane concentrations show the same decrease in bottom waters (180 nl/l). The condition of methane-generating bacteria are almost everywhere the same in this area. It means that methane is emanating into the water mostly from oil-gas-bearing sediments and destabilizing gas hydrates in this area.

6.3.6 Derugin Basin "Barite Mountains"

A methane anomaly (5.723 nl/l) could be found in the bottom water layer (50 m thickness) in the "barite mountains" area (stations GE99-32-1, 37-1). Above the methane plume the water column contains low methane concentrations. The methane concentrations decrease to background values outside this area (GE99-31-1, 34-1).

6.3.7 Academy of Sciences Rise

Typical methane background values for the central part of the Sea of Okhotsk were obtained in this area (station GE99-38-1): 11 - 8 nl/l in the bottom water (water depth 1037-986 m), 101-97 nl/l at 100-50 m depth and 57 nl/l at 4 m depth.

6.3.8 Methane concentrations in gas hydrates

Gas hydrates were found in the cores at "Obzhirov Flare" and were analysed for their gas composition. The bubbles are composed of CH_4 ≈ 98-99%, CO_2 ≈ 1%. No heavy hydrocarbons were found.

A carbon isotopic ratio of methane (-60 ‰) was measured before in the same area (Ginsburg et al., 1993). The light carbon isotopes and the absence of heavy hydrocarbons point to a biological origin of the methane. But the general geology shows that all areas offer the same bacteria-generating methane conditions, but still there are very different methane concentrations in the bottom waters on the Sakhalin shelf and slope. It means that thermogenic methane migrates from the interior of the oil-gas-bearing layers to the surface via fault zones. It is possible that for methodic reasons the heavy hydrocarbons are adsorpted on the cold sediments and therefore are not detected by gaschromatography.With respect to the geological background of this area we suppose that the gas hydrates are produced from a mixture of biological and thermogenic methane.

6.3.9 Methane concentration in MIC samples

Bottom water samples were taken from various minicorer (MIC) deployments (Appendix 1). The methane concentrations are very similar to concentrations found in the bottom waters of CTD samples in the area nearby.

6.3.10 CO_2, O_2, and N_2 concentrations

The concentrations of these gases are presented in Appendix 3. Their distribution in the water column follows common patterns: the CO_2 concentration increases from the surface (0.1 - 0.2 ml/l) to a depth of about 1000 m (0.8 - 0.9 ml/l) and decreases a little towards the bottom water (0.6 - 0.7 ml/l).

The O_2 concentration shows the same regular distribution as methane at the background stations: 4 - 5 ml/l in the surface, 6 - 7 ml/l in a depth of 50-100 m, 0.5 - 1.0 ml/l in a depth of about 1000 m and 2-3 ml/l in the bottom waters. Inside the flare, the O_2 distribution does not change, whereas the methane concentrations inside the flare change significantly.

The N_2 concentration does not show any specific regularity with its 9 - 10 ml/l in the surface and 11 - 12 ml/l in the bottom waters.

6.4 Methane monitoring

Additionally methane measurements were carried out during all seasons (LV28 = summer 1998, G25 = autumn 1998, ICE I = winter 1999, Ut99 = spring 1999 and GE99 = early autumn 1999) in the following areas (Appendix 4):

6.4.1 Terpenia Bay.

Methane was measured at stations: GE99 4-1, Ut99-1, LV28-63-1, G25-22 (Fig. 6.3). The methane distribution in the water column is stable throughout the seasons: a methane anomaly (average 600 nl/l) in the bottom water is present and it decreases towards the surface (85 - 90 nl/l in summer and early autumn, and 140 nl/l during last spring). In autumn the methane concentration is 202 nl/l in the bottom water and 119 nl/l on the surface. This means that

a) last autumn (1998) and last spring (1999) only an insignificant anomaly in the surface waters existed,

b) there is a mixing process in the upper water column going on in the shallow areas in autumn,

c) the methane seepage from the sediments into the water during the seasons is constant.

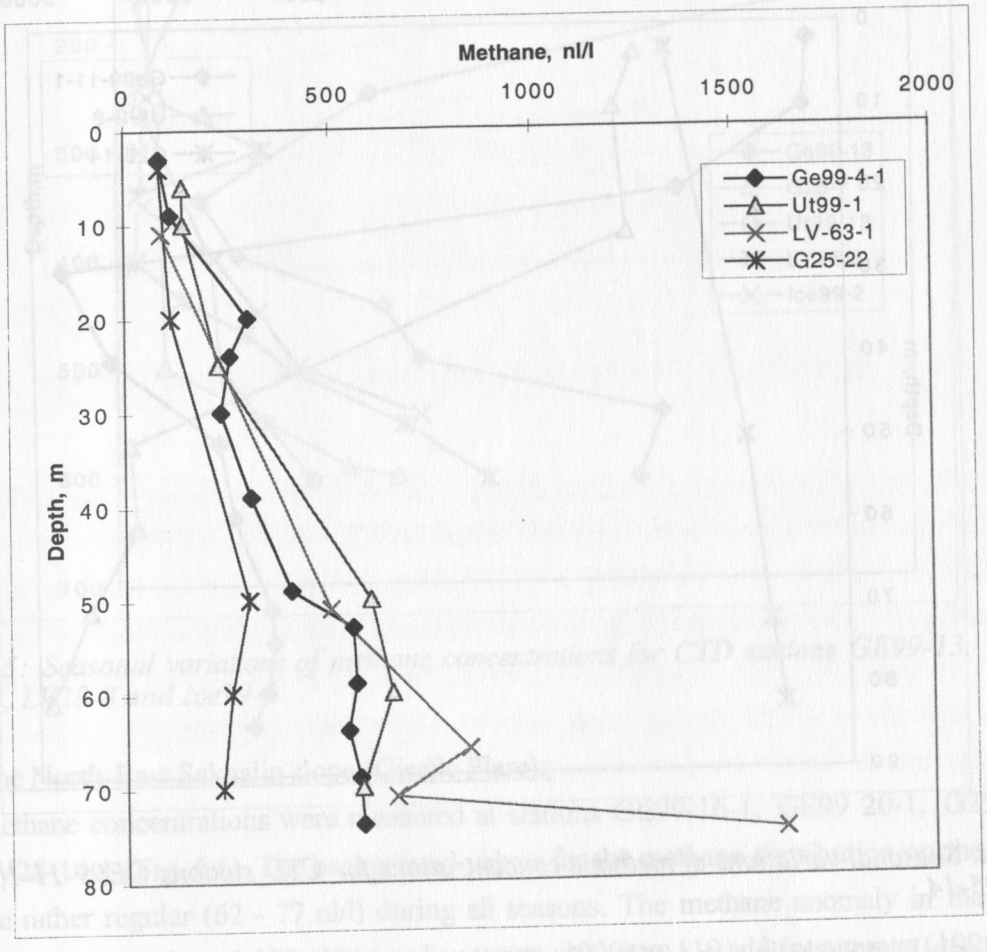

Fig. 6.3: *Seasonal variations of methane concentrations for CTD stations GE99-4-1, Ut99-1, LV28-63-1 and G25-22.*

6.4.2 East Sakhalin shelf (Lunsk oil-gas deposit):

methane concentrations were measured at stations GE99-11-1, Ut99-8 and G25-14 (Fig. 6.4). The methane anomaly (2.200-2.900 nl/l) observed in the lower part of the water

column in this year's early autumn was similar to that of last spring. There is a difference in the methane concentrations on the surface between last spring (761 nl/l) and early autumn (122 nl/l). Last autumn the methane concentration changed unusually sharply; methane concentrations decreased in the bottom water (243 nl/l) and increased in the surface waters (651 nl/l). It means that

a) during the cold season warm bottom water with methane anomalies wells up to the surface and cold water from the surface without methane wells down to the bottom,

b) during spring and autumn methane is oversaturated in the surface water and will emanate into the atmosphere.

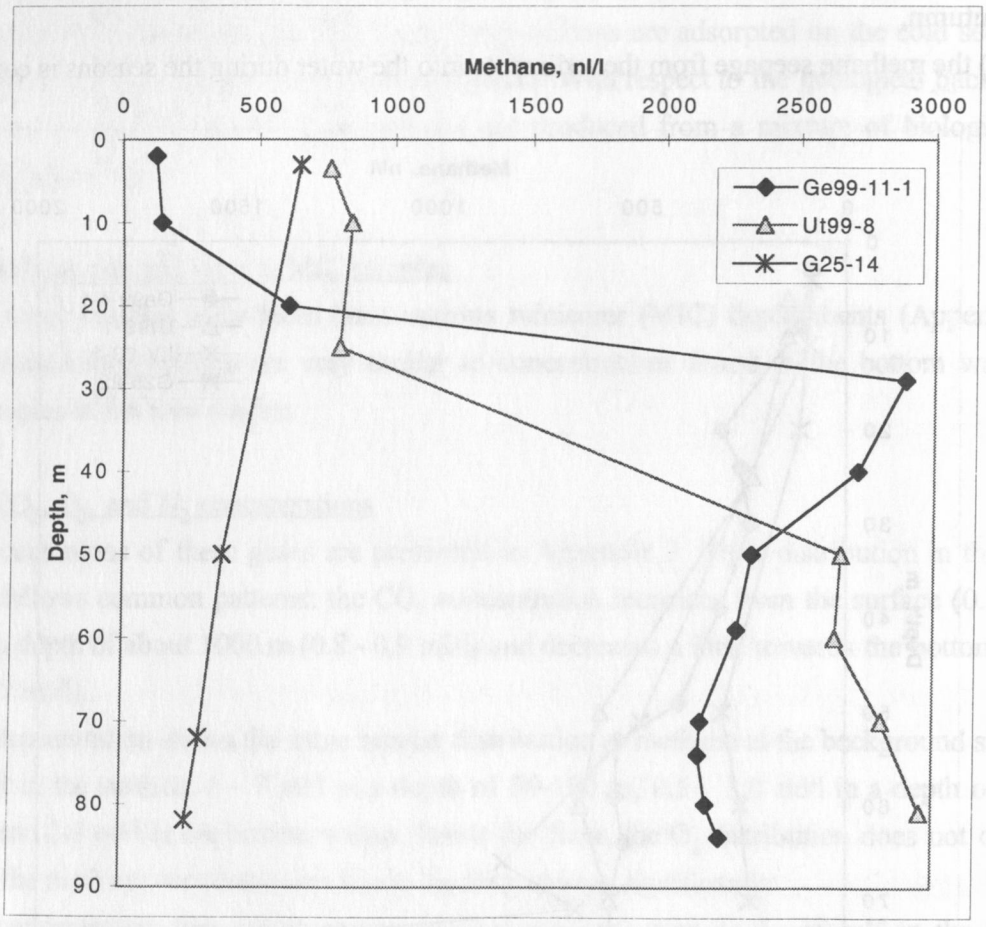

***Fig. 6.4**: Seasonal variations of methane concentrations for CTD stations GE99-11-1, Ut99-1 and G25-14.*

6.4.3 North-East Sakhalin slope (Piltunsky Flare):

Methane concentrations were measured at stations: GE99-13-1, G25-7, Ut-13, LV28-8 and Ice99-2 (Fig. 6.5). The methane distribution shows a very regular pattern throughout all seasons. There are certain differences, though:

a) the presence of methane anomalies at the surface during spring 1999 (531 nl/l) and in April (132 nl/l) and an insignificant anomaly in last autumn (113 nl/l);

b) a significant anomaly (1.905 nl/l) two times higher than usual occurs in intermediate water depth in early autumn.

This means that

a) methane emanations from the surface water to the atmosphere are likely;

b) "Piltunsky Flare" was more active in early autumn this year compared to other seasons.

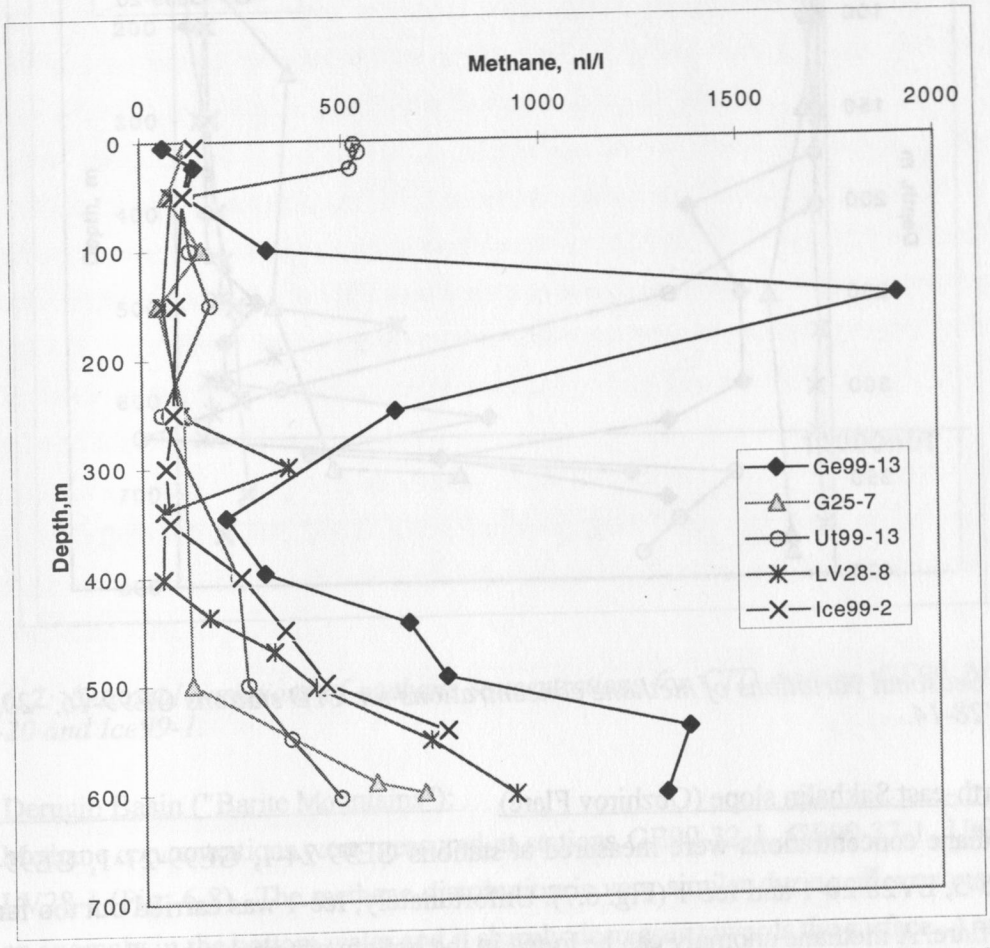

***Fig. 6.5**: Seasonal variations of methane concentrations for CTD stations GE99-13, G25-7, Ut99-13, LV28-8 and Ice99-2.*

6.4.4 The North-East Sakhalin slope (Giselle Flare):

Methane concentrations were measured at stations GE99-16-1, GE99 20-1, G25-4 and LV28-14-1 (Fig. 6.6). The background values for the methane distribution on the surface are rather regular (62 - 77 nl/l) during all seasons. The methane anomaly in the bottom water changes from 9.080 nl/l in early autumn (1999) to 119 nl/l in summer (1998). This means that

a) there was seismo-tectonic activation in this area 1998-1999,

b) the CTD was not always positioned into center of "Giselle Flare".

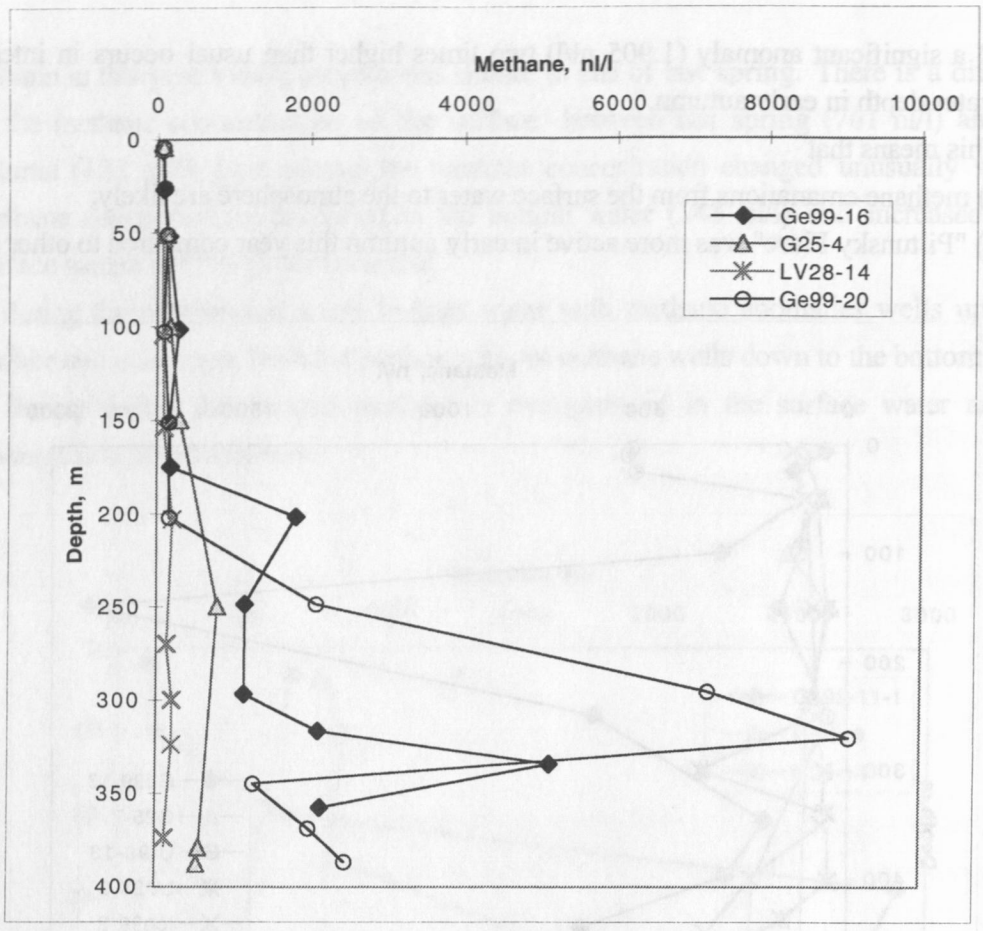

***Fig. 6.6**: Seasonal variations of methane concentrations for CTD stations GE99-16, -20, G25-4 and LV28-14.*

6.4.5 North-east Sakhalin slope (Obzhirov Flare)

Methane concentrations were measured at stations GE99-24-1, GE99-27-1, GE99-29-1, G25-5, LV28 20-1 and Ice-1 (Fig. 6.7). Unfortunately, Ice-1 was carried out too far from the flare. A methane anomaly can be found in the bottom waters during all seasons. A big anomaly (23.759 nl/l) is situated inside the flare. It is 2 - 30 times higher than the concentrations found during other seasons. A methane anomaly (309 nl/l) could be measured on the surface in summer. It means that

a) there was seismo-tectonic activation from 1998 to 1999,

b) it influences the sampling very much whether the CTD is positioned inside or outside the flare,

c) sometimes methane bubbles from the flare can reach the water surface.

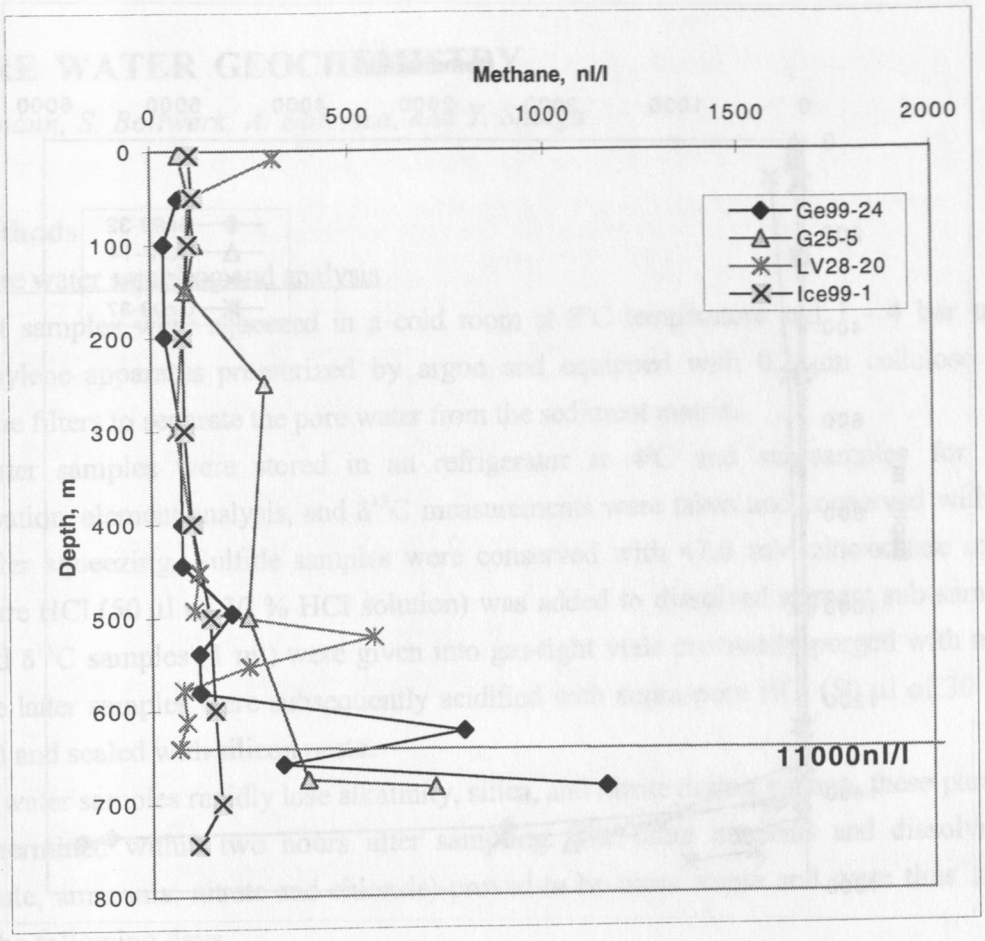

***Fig. 6.7**: Seasonal variations of methane concentrations for CTD stations GE99-24, G25-5, LV28-20 and Ice99-1.*

6.4.6 Derugin Basin ("Barite Mountains"):

Methane concentrations were measured at stations GE99-32-1, GE99-37-1, Ut99-14 and LV28-1 (Fig. 6.8). The methane distribution is very similar during all seasons. There is an anomaly in the bottom water and it sharply decreases towards the surface. A significant anomaly (5.723 nl/l) was found in early autumn in 1999.

6.5 Conclusions

1) Significant methane anomalies at "Giselle and Obzhirov Flare" were found that were 2 - 5 times higher than those values found during earlier cruises. Maybe these anomalous high values are connected with

a) the fact that sampling was carried out directly inside the flare only on GE99 cruise, which points to a high spatial variability of methane concentration inside and around one flare

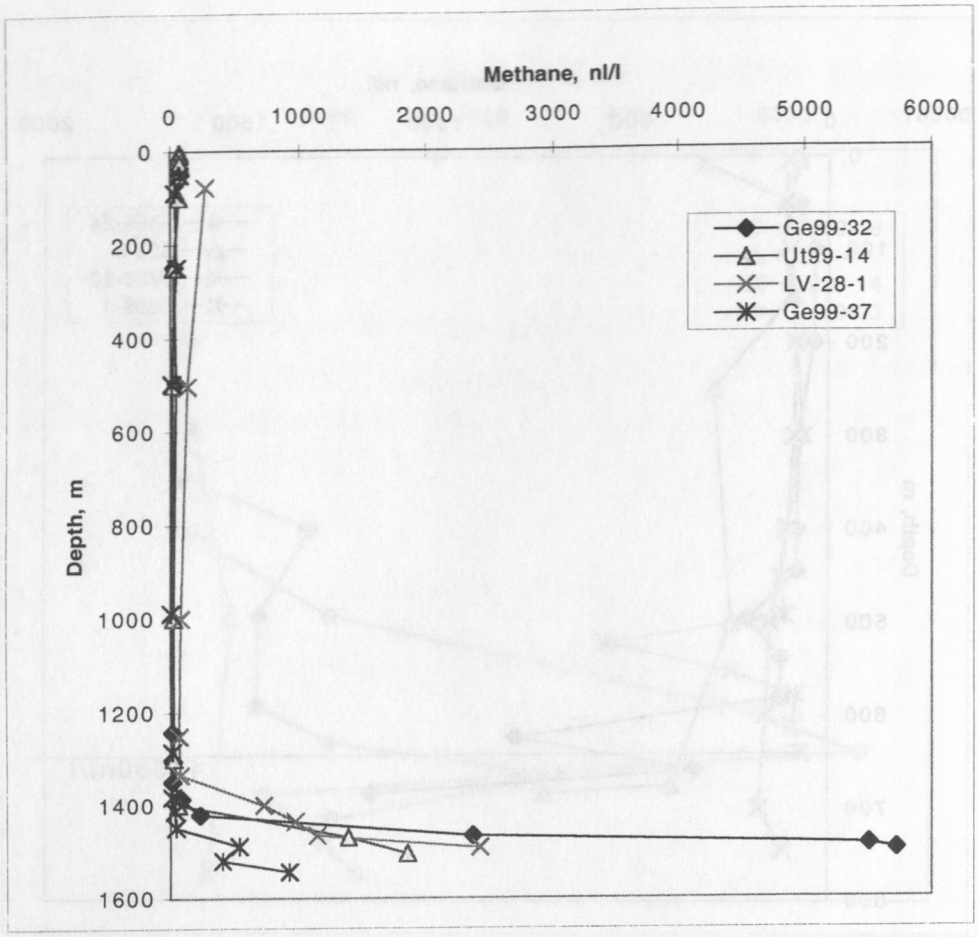

Fig. 6.8: *Seasonal variations of methane concentrations for CTD stations GE99-32, Ut99-14, LV28-1 and GE99-37.*

b) a seismo-tectonic activation in this period. This hypothesis could be supported by the occurrence of earthquakes with a magnitude of 6-7 near Paramushir area (Kurile Islands) and on Taiwan Island in September 1999.

2) Gas hydrates were found at "Obzhirov Flare". Their main component is methane.
3) Methane monitoring showed that the surface waters in shallow areas are oversaturated in autumn and spring. This means that in these seasons methane is emanating from the surface water to the atmosphere.
4) A new flare was found on the south-east Sakhalin slope.

The methane source on the Sakhalin shelf and slope is a mixture of biogenic and thermogenic methane (bacteria-generating, oil-gas, gas hydrate). In the Derugin Basin, biogenic methane is less significant and thermogenic methane is rising up from oil-gas-bearing sediments.

7. PORE WATER GEOCHEMISTRY

K. Wallmann, S. Bollwerk, A. Kolevica, and Y. Shulga

7.1 Methods

7.1.1 Pore water sampling and analysis

Sediment samples were squeezed in a cold room at 8°C temperature and 1 - 4 bar using a polypropylene apparatus pressurized by argon and equipped with 0,2 µm cellulose acetate membrane filters to separate the pore water from the sediment matrix.

Pore water samples were stored in an refrigerator at 4°C and sub-samples for sulfide determination, element analysis, and $\delta^{13}C$ measurements were taken and conserved within two hours after squeezing. Sulfide samples were conserved with 47.6 mM zinc-acetate solution, supra-pure HCl (50 µl of 30 % HCl solution) was added to dissolved element sub-samples (4 ml), and $\delta^{13}C$ samples (1 ml) were given into gas-tight vials previously purged with nitrogen gas. The latter samples were subsequently acidified with supra-pure HCl (50 µl of 30 % HCl solution) and sealed with silicon paste.

As pore water samples rapidly lose alkalinity, silica, and nitrite during storage, these parameters were determined within two hours after sampling. The other nutrients and dissolved ions (phosphate, ammonia, nitrate and chloride) proved to be more stable and were thus analyzed during the following days.

All vials used for pore water storage were previously washed with acid and Milli-Q water to prevent sample contamination.

7.1.2 Hydrogen ion activity (pH)

The pH value was measured in sediments which were retrieved with a hydro-corer and a gravity corer by pushing the electrode into the sediment cores at selected depths. Mini- and multi-corer sediments were first sectioned into slices and than analyzed by introducing the pH sensor into each of the sediment slices. During the pH measurements, sediment temperature was recorded with a small thermometer. The pH electrode was calibrated with BIS and AMPY seawater standards (Dickson, 1993). The temperature-dependent slope (s) and intercept (i) of the electrode were determined from the potential measurements (E) in the two standard buffer solutions:

$$E = s \cdot pH + i$$

and

$$s = \frac{E_{BIS} - E_{AMPY}}{pH_{BIS} - pH_{AMPY}} \qquad i = \frac{pH_{AMPY} \cdot E_{BIS} - pH_{BIS} \cdot E_{AMPY}}{pH_{AMPY} - pH_{BIS}}$$

The electrode parameters were determined for the sediment temperature range registered aboard MV *Marshal Gelovany* after core retrieval. The linear dependence of slope and intercept on temperature was used to calculate electrode parameters and pH values for the sediment temperatures recorded during the pH measurements (Fig. 7.1). These temperatures were considerably higher than the in-situ temperatures at the seafloor.

pH values, total alkalinity, total sulfide, boron, sulfate, silica, and phosphate concentrations will later be used to determine the total inorganic carbon concentrations in pore water samples. These conservative concentrations and the total alkalinity will then allow the calculation of pH values at in-situ temperatures and pressures.

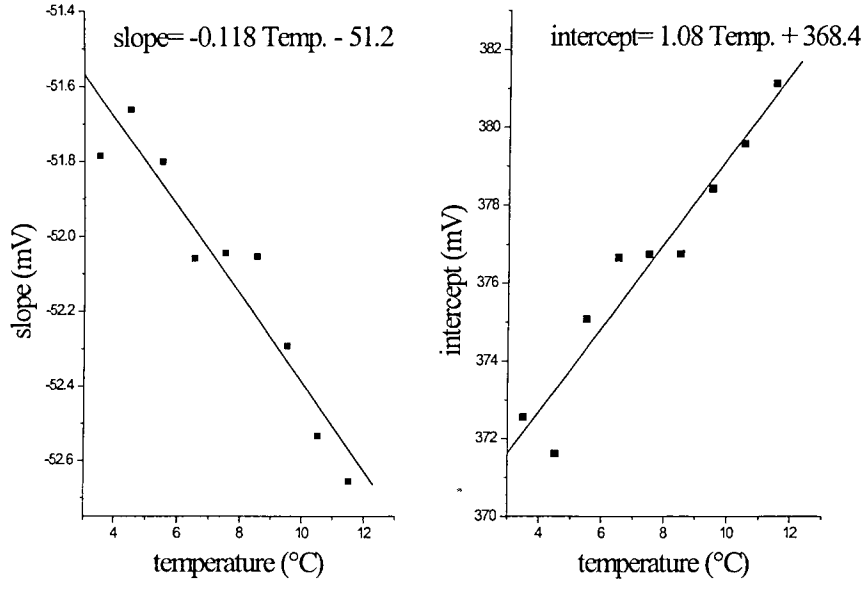

Fig. 7.1: *Temperature dependence of electrode parameters. Symbols indicate electrode calibrations at different temperatures and solid lines represent the linear correlation between electrode parameters and temperature.*

7.1.3 Oxidation - reduction potential (Eh)

The laboratory set for direct measurements of the oxidation-reduction potential (Eh) and the pH value consists of an electrochemical cell and pH-meter (OP-208). A smooth platinum redox-metric electrode (platinum wire), Ti-silicate glass (EO-021) and Fe-silicate glass EO-035) electrodes developed at the Research Institute of Chemistry of Glass, St. Petersburg University, served as electrode indicators. The glass electrode ESL-63-07 was used for measuring pH. The glass electrode was calibrated relative to the standard NBS-buffer solution with pH = 4.01 and

pH = 6.86 at 25°C. A removable chlorine- silver electrode was used for comparison. An electro-motive force (EMF) was measured by the pH-meter OP-208 with an accuracy of 0.1 mv.

The temperature of the samples was measured with a digital thermometer with an accuracy of 0.1°C. The temperature of 25°C of the measuring cell was supported by a thermostat U-8. For better contact, a sediment sample at the electrode-sediment boundary was diluted with seawater (sw) in proportion $V_{sediment}/V_{sw}$ = 5:1. Solutions of iron (Fe^{2+}, Fe^{3+}, $C=10^{-3}$ mol/l) with EDTA (ethylendiaminetetraacetic acid) were used as mediators for the reduced sediments of the Okhotsk Sea. The mediator interacts with the redox system of sediments very quickly and promotes the fast establishing of an equilibrium potential at the electrodes. The amount of the mediator introduced into the sediments must not alter the redox conditions of the sample. It was found that the volume of the mediator must provide a redox- buffer 50-100 times less than the redox-buffer of the samples: $\beta \times V_{sed}/C_{med} \times V_{med} \geq 50\text{-}100$, where β is the oxidation volume. The volume of the added mediator (V_{med}) is calculated from the above-mentioned formula. Eh of the mediator solution must be optimally close to the Eh of the sediments. The Fe^{3+}/Fe^{2+} ratio in the mediator is 1:10.

The oxidation volume (β) was determined potentiometrically by a Pt-electrode. As a redox system, the system $Fe(CN)_6^{3-,4-}$ with a concentration of C = 10^{-3}mol/l and a ratio 10:1 was used to determine β of the sediment sample. The β values were calculated by a formula deduced from Nernst's equation:

$$\beta = C_{ox} \times V_o \times C_{red} \times V_o(1 - A) / (C_{ox} \times V_o + C_{red} \times V_o \times A) \times V_{sed},$$

where V_o is the volume of $Fe(CN)_6^{3-}$ and $Fe(CN)_6^{4-}$ in the the mixed solution;

V_{sed} is the volume of sediment added;

C_{ox} is the concentration of $Fe(CN)_6^{3-}$, mol/l;

C_{red} is the concentration $Fe(CN)_6^{4-}$, mol/l;

A - antilog $(E_1 - E_2) / \theta$, θ = 59.16 mv;

E_1 is the potential of the solution free from sediment;

E_2 is the potential of the solution containing sediment.

The duration of β measurements is 10-30 minutes.

After β was determined, 30 ml of sediment were put into the cell and diluted with seawater (6 ml), then stirred, and 1 ml of mediator solution was added and stirred again. The cell containing the sediment was controlled thermostatically at 25°C; 30 min later the Eh value of the sediment was recorded with an accuracy of 1 mv according to the reading of Pt, Ti and Fe electrodes.

7.1.4 Total alkalinity

Total alkalinity was analyzed by direct titration with 0.02 N HCl solution of 1 ml pore water dispensed in 5 ml deionized water in an open cell (Ivanenkov & Lyakhin, 1978). The acid was standardized daily with Na_2CO_3 solution prepared from crystals dried at 280°C and dissolved in CO_2-free deionized water. To remove carbon dioxide during titration the samples and standards were flushed with a continuous stream of pure nitrogen. A mixture of methylene blue and methyl red was used as indicator; titration was completed when the green color of the solution turned to light pink (pH of the end point is equal to 5.4 - 5.5). A Metrohm Dosimat 665 motor-driven burette was used for the titration.

Replicate measurements of pore water samples over a time span of several hours revealed that the total alkalinity of anoxic pore water samples is not stable but decreases with time. The two most important reactions that cause alkalinity reduction are carbonate precipitation and sulfide oxidation. Carbonate precipitation is induced by a loss of CO_2 and H_2S from the pore waters to the atmosphere and the resulting shift in the dissolution/precipitation equilibrium:

$$Ca^{2+} + HCO_3^- \Rightarrow CaCO_3(s)\downarrow + CO_2(g)\uparrow + H_2O$$

In contact with air, sulfide is oxidized by molecular oxygen:

$$HS^- + 2O_2 \Rightarrow SO_4^{2-} + H^+$$

Both the decrease in dissolved HS^- and the production of H^+ significantly reduce the total alkalinity.

The sulfide oxidation rate and its impact on total alkalinity were tested under shipboard conditions using a 30 mM solution of Na_2S in 0.5 M NaCl . The initial pH was adjusted to 7.1 with concentrated HCl and the solution was titrated repeatedly at room temperature (24 - 25°C). The data depicted in Fig. 7.2 clearly show that the total alkalinity is significantly reduced within a few hours. The simultaneous increase in pH indicates that the H_2S loss to the atmosphere proceeds more rapidly than the oxidation reaction.

During the expedition, the total alkalinity of anoxic samples was determined within two hours after pore water retrieval. The data in Fig. 7.2 imply that up to 10 % of the total alkalinity might be lost during this short time span. As the samples were stored at 4°C, the oxidation reaction probably proceeded at a lower rate, so that the real loss was somewhat lower than implied by the experimental data obtained at room temperature. In future expeditions, the time lag between pore water squeezing and alkalinity determination should be shortened further.

Replicate measurements (n = 5) indicated stable values and an analytical precision of ± 10 µmol dm^{-3} for oxic and suboxic samples with low sulfide contents.

Concentrations of dissolved silicate, phosphate, nitrate, nitrite and ammonia were measured using standard photometric hand methods (Digital Photometer LP2W).

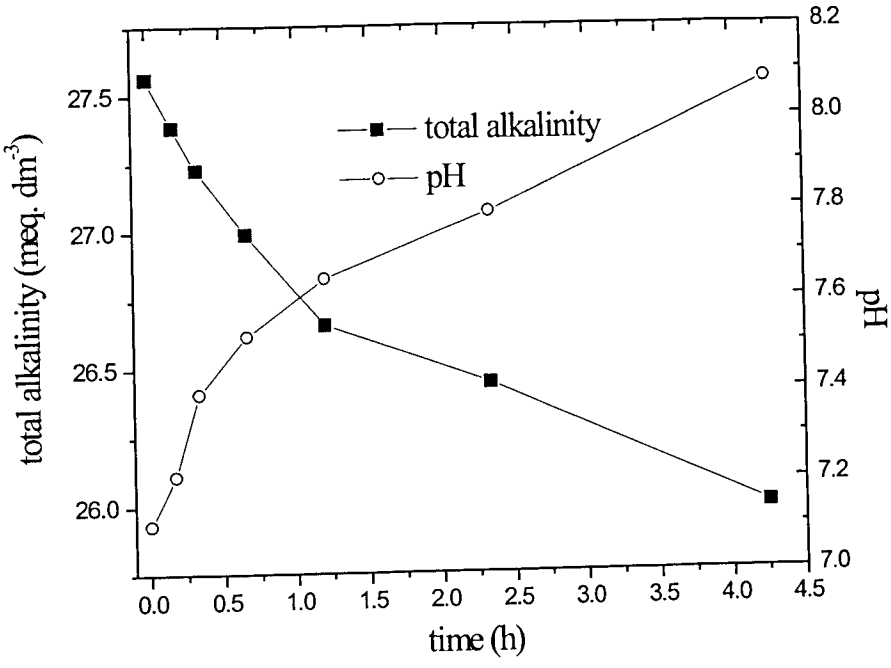

Fig. 7.2: *Oxidation of a sulfide solution (~30 mM ΣH_2S in 0.5 M NaCl) in contact with air at room temperature.*

7.1.5 Dissolved silica

A volume of 0.5 ml sample (pore water and seawater) or standard was diluted to 5.0 ml with deionized Milli-Q water and 0.2 ml heptamolybdate solution. After 30 minutes 0.2 ml oxalic acid solution and ascorbic acid were added. The blue-colored silicomolybdic complex takes another 30 minutes to develop before the absorbance can finally be measured at 810 nm.

The analysis of silicate concentrations was disturbed in anoxic samples with high ΣH_2S concentrations.

Fig. 7.3 shows the influence of ΣH_2S (0, 5, 10, 15 mMol/l) on the SiO_2 standards. As standards with ΣH_2S have a higher absorbance than standards without H_2S, milli-molare sulfide concentrations severely disturb the silica determination. The presence of H_2S can be recognized by the blue color that forms after the addition of the first reagent, heptamolybdate solution (normally the blue color forms only after the second and third reagent are added to the sample). The sulfide content of water samples decreases during storage due to sulfide oxidation and H_2S loss to the atmosphere so that reliable silica values can be determined in aged samples. During GE 99 cruise anoxic pore water samples were repeatedly analyzed over a time span of several weeks until a stable silica concentration was obtained. As precipitation of SiO_2 colloids can occur in water samples with a high dissolved silica content, a procedure that rapidly removes

H_2S without disturbing the determination of silica and other nutrients should be developed and applied in future cruises.

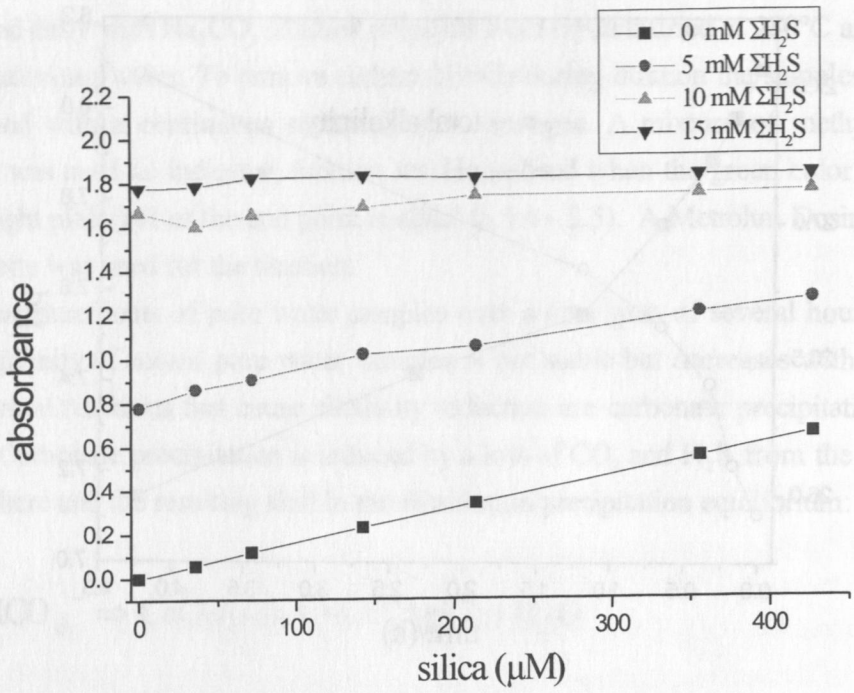

Fig. 7.3: *Impact of sulfide on the photometric determination of dissolved silica.*

7.1.6 Phosphate

For the analyses 2 ml of a pore water sample or standard were diluted with 4 ml pure water; subsequently 0.1 ml ascorbic acid and 0.1 ml heptamolybdate reagent were added and the absorbance was measured after 10 minutes at 880 nm. The analysis of seawater samples does not require dilution because of the low phosphate concentrations.

The H_2S in anoxic pore water samples also disturbs the phosphate determination (Fig. 7.4). The samples react with a red-brown color after the addition of the reagents. After a waiting time of some days the H_2S concentration decreases to a low level, so that phosphate can be determined accurately.

7.1.7 Nitrite and nitrate

For the determination of NO_2^-, 0.1 ml sulphanilamide and 0.1 ml NED were added to a 5 ml water sample or standard. The absorbance of the red azo dye was measured after 30 minutes at 540 nm. For NO_3^- determination, 4-10 ml of water sample or standard were diluted 1:2 with ammonium chloride buffer solution and passed through a reductor column at 5 ml/minute. The last 5 ml were taken and treated as described for nitrite. For the preparation of the reductor, cadmium granules were sieved and the 0.5-0.8 mm fractions were washed with 2 n HCl. After a thorough rinsing, the cadmium was allowed to react with 1 % $CuSO_4$ for 5-10 minutes and

rinsed again. A funnel was used to carefully pour the copperized granules into the reductor column, which was filled with water to prevent air inclusion. After both outlets were sealed with glass wool, 20-30 ml of ammonium chloride buffer solution containing about 100 µM $NaNO_3$ were passed through the column at about 5 ml/minute to activate the reductor. Once more rinsed with buffer solution, the reductor was ready for use. As the copperized granules of the reductor decomposed by dissolving sulfide, only sulfide-free samples were analyzed for dissolved nitrate.

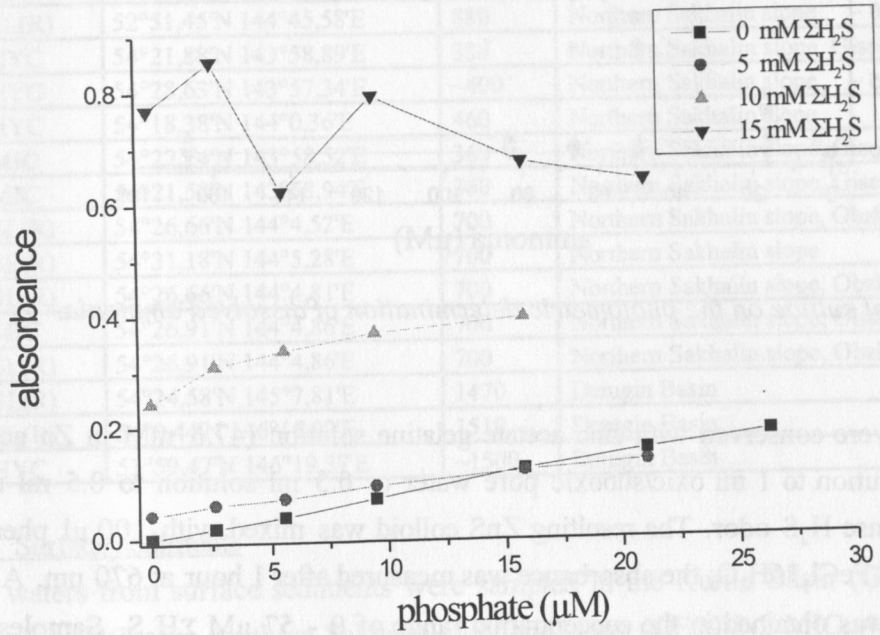

Fig. 7.4: *Impact of sulfide on the photometric determination of dissolved phosphate.*

7.1.8 Ammonium

For the ammonia determination, 1 ml water sample or standard were made up to 5 ml using 4.8 ml Milli-Q water and 0.2 ml phenol solution. After 2 minutes 0.1 ml citrate buffer and 0.2 ml DTT reagent were added. After mixing the samples were kept at room temperature protected from sunlight for about 24 hours before the absorbance was measured at 630 nm. As dissolved H_2S reacts with the DTT reagent, the ammonia analysis was severely disturbed in anoxic samples with high sulfide content (Fig. 7.5). We tried to remove sulfide by adding Zn-acetate solution to the samples, but control measurements showed that the absorbance of the standard solutions was diminished by this reagent (Fig. 7.5). Therefore, the Zn-acetate addition was abandoned and samples were stored until the sulfide content was sufficiently low for ammonia determination.

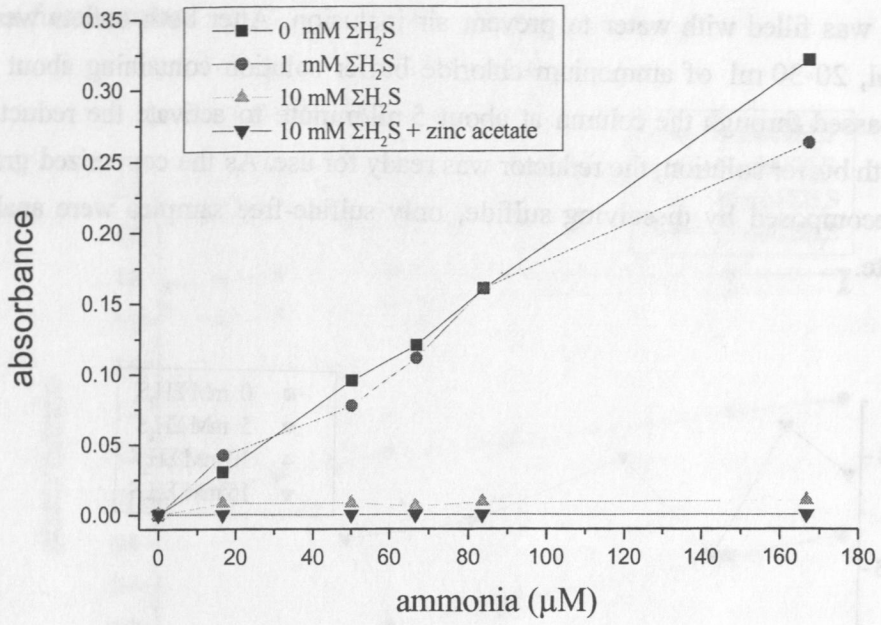

Fig. 7.5: *Impact of sulfide on the photometric determination of dissolved ammonia.*

7.1.9 Sulfide

Sulfide samples were conserved with zinc acetate gelatine solution (47.6 mM in Zn acetate), adding 0.1 ml solution to 1 ml oxic/suboxic pore water or 0.5 ml solution to 0.5 ml anoxic samples with intense H_2S odor. The resulting ZnS colloid was mixed with 100 µl phenylen-diamin and 100 µl $FeCl_3*6H_2O$; the absorbance was measured after 1 hour at 670 nm. A linear calibration curve was obtained in the concentration range of 0 - 57 µM ΣH_2S. Samples were diluted to calibration range before reagent addition. Tests showed that absorbance was not fully developed when only 10 µl reagents were added to the samples as suggested in the original instruction. The reagent volumes were increased to 100 µl to ensure complete decomposition of the ZnS colloids and sulfide turn-over.

7.1.10 Chloride

Dissolved chloride was determined by titrating 0.1 ml sample dispensed in 5 ml Milli-Q water with $AgNO_3$ solution. As dissolved sulfide reacts with Ag^+ ions to form an Ag_2S precipitate, the chloride titration was performed only in aged samples with low sulfide content.

7.2 Results and discussion

Pore waters were separated from surface sediments recovered in 9 mini-corer (MIC), 1 multi-corer (MUC), 4 hydro-corer (HYC), and 7 gravity corer (SL(R)) deployments (Tab. 7.1). They were analyzed for dissolved nutrients (nitrate, nitrite, ammonia, phosphate, silica), alkalinity, sulfide, chloride and pH as described in the methods section. A complete list of measured concentrations is given in the Appendix 5.

Tab. 7.1: *Pore water sampling sites in cruise GE99.*

Station	Location	Depth (m)	Working Area
1-2 MIC	45°35,79'N 144°21,57'E	790	Southern Sakhalin slope
2-1 MIC	46°40,74'N 144°50,60'E	3050	Kurile Basin
4-2 MIC	48°1,33'N 143°34,90'E	75	Southern Sakhalin shelf
5-1 MIC	47°24,53'N 145°22,72'E	515	Southern Sakhalin slope
6-3 MIC	47°19,09'N 148°23,09'E	3360	Kurile Basin
7-2 MIC	47°15,55'N 147°11,18'E	3340	Kurile Basin
12-3 MUC	52°51,45'N 144°45,58'E	880	Northern Sakhalin slope
12-4 SL(R)	52°51,45'N 144°45,58'E	880	Northern Sakhalin slope
16-2 HYC	54°21,88'N 143°58,89'E	386	Northern Sakhalin slope, Giselle Flare
18-2 HYC	54°28,63'N 143°57,34'E	~400	Northern Sakhalin slope
19-2 HYC	54°18,38'N 144°0,36'E	460	Northern Sakhalin slope
20-2 MIC	54°22,24'N 143°58,52'E	360	Northern Sakhalin slope, Giselle Flare
20-3 MIC	54°21,58'N 143°58,94'E	360	Northern Sakhalin slope, Giselle Flare
24-2 SL(R)	54°26,66'N 144°4,52'E	700	Northern Sakhalin slope, Obzhirov Flare
26-2 SL(R)	54°31,18'N 144°5,28'E	700	Northern Sakhalin slope
27-2 SL(R)	54°26,66'N 144°4,81'E	700	Northern Sakhalin slope, Obzhirov Flare
29-2 MIC	54°26,91'N 144°4,86'E	700	Northern Sakhalin slope, Obzhirov Flare
29-3 SL(R)	54°26,91'N 144°4,86'E	700	Northern Sakhalin slope, Obzhirov Flare
30-3 SL(R)	54°24,58'N 145°7,81'E	1470	Derugin Basin
32-2 SL(R)	54°0,44'N 146°16,92'E	1510	Derugin Basin
36-1 HYC	53°59,47'N 146°19,37'E	~1500	Derugin Basin

7.2.1 Surface sediments

Pore waters from surface sediments were sampled in the Kurile Basin (GE99-2-1 MIC, 6-3 MIC, 7-2 MIC), the southern Sakhalin shelf and slope (GE99-1-2 MIC, 4-2 MIC, 5-1 MIC) and the northern Sakhalin slope areas (GE99-12-3 MUC, 20-2 MIC, 20-3 MIC, 29-2 MIC). Dissolved silica, nitrate, ammonia, and alkalinity concentrations depicted in Fig. 7.6 - 7.8 reveal intense diagenesis at all sites.

Nitrate concentrations rapidly decrease in the sampled surface sediments due to denitrification (Fig. 7.6 - 7.8). The shallow nitrate penetration depth of only 4 cm recorded in Southern Sakhalin shelf and slope sediments documents a considerable input of degradable organic matter and intense degradation processes. In surface sediments from the Kurile Basin, nitrate penetrates to a depth of 4 - 8 cm. Concentration peaks recorded at 4 cm (GE99-2-1) and 6 cm (GE99-6-3) sediment depth are caused by the benthic fauna irrigating inhabited sediment layers and thereby enhancing nitrate penetration. In the northern slope sediments nitrate penetration further decreases to less than 1 cm in GE99-29-2. This extremely low value indicates enormous denitrification rates that may be caused by rising methane gas bubbles as core GE99-29-2 was taken within the "Obzhirov Flare" area where gas venting has previously been documented (Biebow & Hütten, 1999).

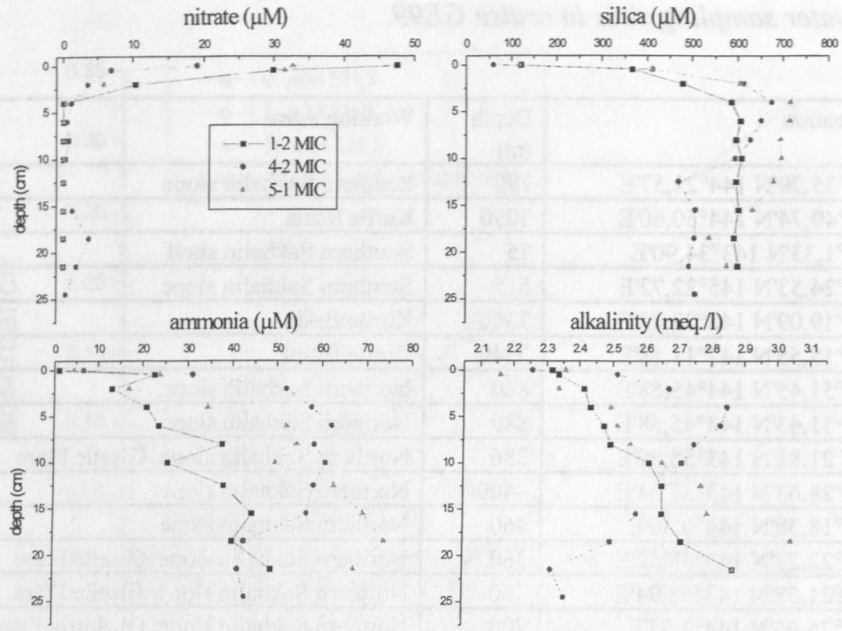

Fig. 7.6: *Dissolved nutrients (nitrate, silica, ammonia) and alkalinity in surface sediments from the Southern Sakhalin Shelf and Slope.*

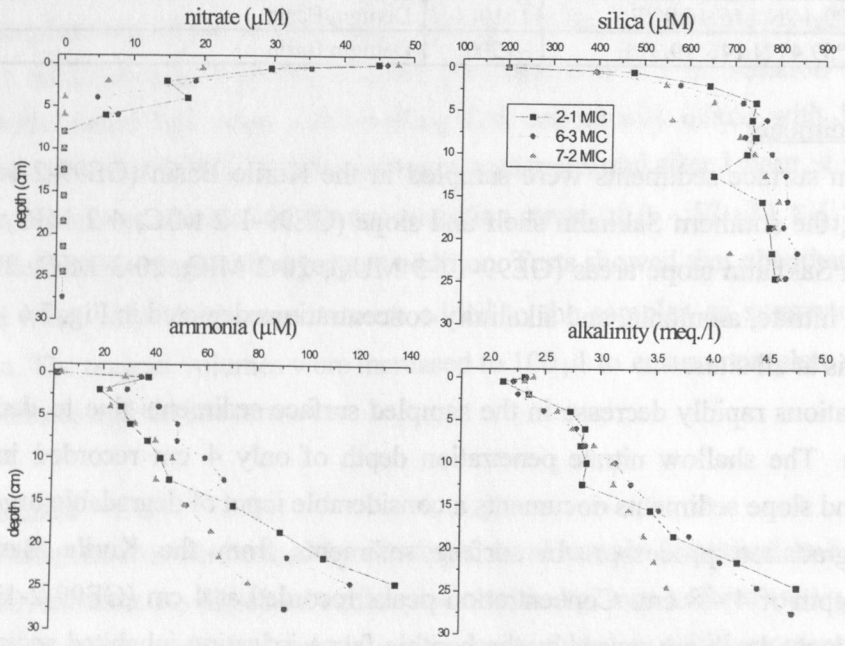

Fig. 7.7: *Dissolved nutrients (nitrate, silica, ammonia) and alkalinity in surface sediments from the Kurile Basin.*

Due to the dissolution of biogenic opal, dissolved silica rapidly increases with depth to a concentration level of about 750 µM in the Kurile Basin and Northern Sakhalin slope sediments and to a level of 600 - 700 µM in sediments from the Southern Sakhalin shelf and slope. The lower concentrations in the southern study area indicate that the deeper sediment layers are

depleted in biogenic opal. The gradient at the sediment water interface shows a clear dependence on water depth (Fig. 7.9). As expected the gradients and thus the diffusive fluxes are diminished with increasing water depth because opal is dissolved during its passage through the water column before it is deposited at the sediment surface.

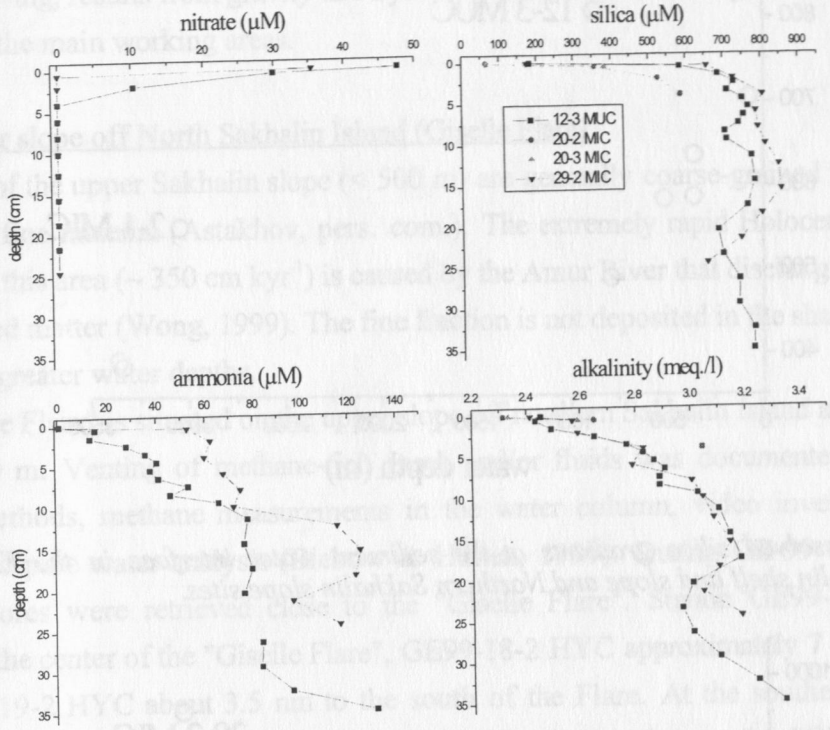

Fig. 7.8: *Dissolved nutrients (nitrate, silica, ammonia) and alkalinity in surface sediments from the Northern Sakhalin Slope.*

Only stations GE99-12-3 and 29-2 from the middle slope off Northern Sakhalin and station 2-1 in the western Kurile Basin deviate from the general trend. The enhanced mid-slope values indicate an extremely high rain rate of biogenic matter to the seafloor. Previously recovered sediment cores from the mid-slope of Sakhalin (LV27-2-4, LV28-32-1, LV28-4-4) confirm that the central and northern mid-slope (600 - 800 m water depth) is an area of intense biogenic sedimentation (Nürnberg et al., 1997, Biebow & Hütten, 1999). The western Kurile Basin site (GE99-2-1) is located close to the Sakhalin Slope and may receive lateral inputs from the adjacent productive continental margin. Fig. 7.10 demonstrates that the mid-slope silica gradients increase towards the north. This south-north gradient in biogenic opal sedimentation may be caused by the Amur River that enforces the primary and export production in the northern slope areas. The south - north productivity gradient is confirmed by remote sensing data (Biebow & Hütten, 1999) and the ammonia and alkalinity pore water concentrations that are also enhanced at the northern stations (Fig 7.6 versus Fig. 7.8).

A strong and almost linear increase in ammonia and alkalinity is observed in Kurile Basin sediments that is caused by anaerobic degradation processes in deeper sediment layers (Fig.

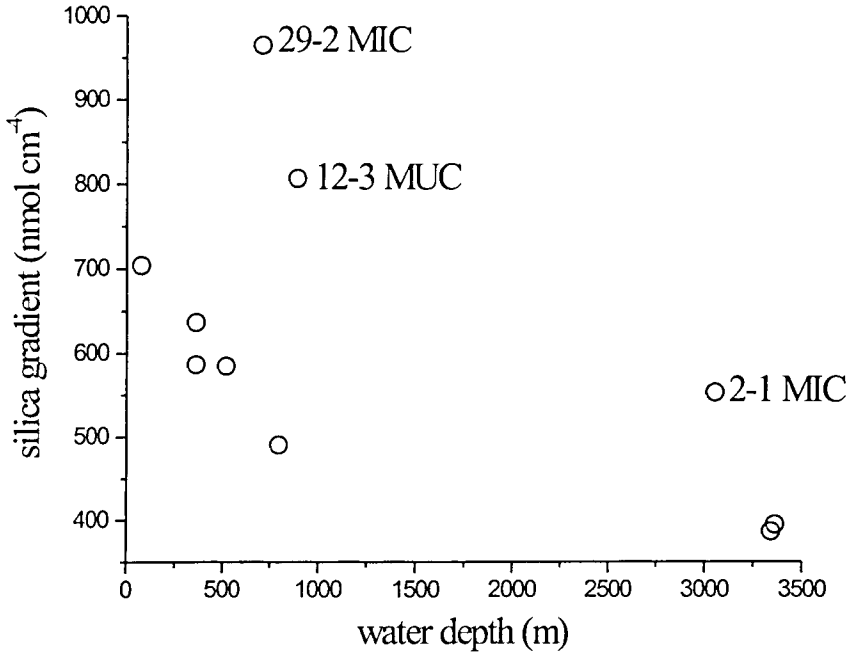

Fig. 7.9: Dissolved silica gradients at the sediment water interface in the Kurile Basin, Southern Sakhalin shelf and slope and Northern Sakhalin slope sites.

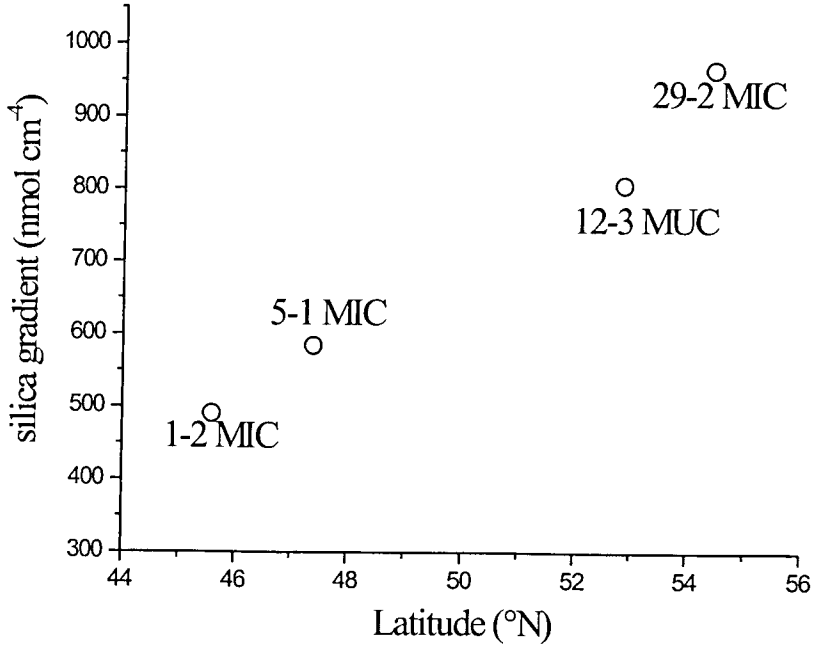

Fig. 7.10: Dissolved silica gradients at the sediment-water interface at mid-slope stations (500 - 800 m water depth) off Sakhalin Island.

7.7). This remarkable feature is not observed in Sakhalin shelf and slope sediments. It indicates organic carbon-bearing sediments at bigger depths that may be transported as turbidites from the productive Sakhalin shelf and slope to the Kurile Basin. The Basin possibly acts as a deposition center where organic matter accumulates at high rates and degrades to produce alkalinity, methane and other degradation products. This hypothesis is also supported by high

concentration levels of dissolved silica in the Kurile Basin sediments (Fig. 7.7). The Basin sediments should be further investigated in future cruises to the Sea of Okhotsk.

In the following, results from gravity and hydro-corer deployments are presented and discussed for each of the main working areas.

7.2.2 Upper slope off North Sakhalin Island (Giselle Flare)

Sediments of the upper Sakhalin slope (< 500 m) are generally coarse-grained with only minor amounts of fine material (Astakhov, pers. com.). The extremely rapid Holocene sedimentation recorded in this area (~ 350 cm kyr^{-1}) is caused by the Amur River that discharges large amounts of suspended matter (Wong, 1999). The fine fraction is not deposited in the shallow slope areas but only at greater water depths.

The "Giselle Flare" is situated on the upper slope off northern Sakhalin Island at water depths of 360 to 390 m. Venting of methane-rich gases and/or fluids was documented previously by acoustic methods, methane measurements in the water column, video investigations of the seafloor and pore water analysis (Biebow & Hütten, 1999). During GE-99 expedition, three sediment cores were retrieved close to the "Giselle Flare". Station GE99-16-2 HYC was situated in the center of the "Giselle Flare", GE99-18-2 HYC approximately 7 nm to the north, and GE99-19-2 HYC about 3.5 nm to the south of the Flare. At the southern station of the north-south transect the sediments were almost pure sands whereas the "Giselle Flare" and northern station sediments contained a considerable portion of silts and clays.

The pore water data plotted in Fig. 7.11 show that dissolved ammonia is low within the "Giselle Flare" (GE99-16-2) and at the northern reference location (GE99-18-2), whereas high concentrations occur at the southern station (GE99-19-2). In contrast, total alkalinity and sulfide are high at both the "Giselle Flare" and the southern site. The low ammonia/alkalinity and ammonia/sulfide ratios at the "Giselle Flare" can only be explained by anaerobic methane oxidation that produces sulfide and alkalinity without generating ammonia and other organic matter degradation products:

$$CH_4 + SO_4^{2-} \Rightarrow HCO_3^- + HS^- + H_2O$$

In contrast, anaerobic degradation of particulate organic matter (POM) with sulfate as terminal electron acceptor generates not only sulfide and alkalinity but also appreciable amounts of ammonia:

$$(C(H_2O))_{2n}(NH_3)_m + n\ SO_4^{2-} \Rightarrow (n+m)\ HCO_3^- + n\ HS^- + m\ NH_4^+ + (n-m)\ CO_2 + (n-m)\ H_2O$$

where the m/(2n+m) ratio that corresponds to the ammonia/alkalinity ratio is 0.07 - 0.04.

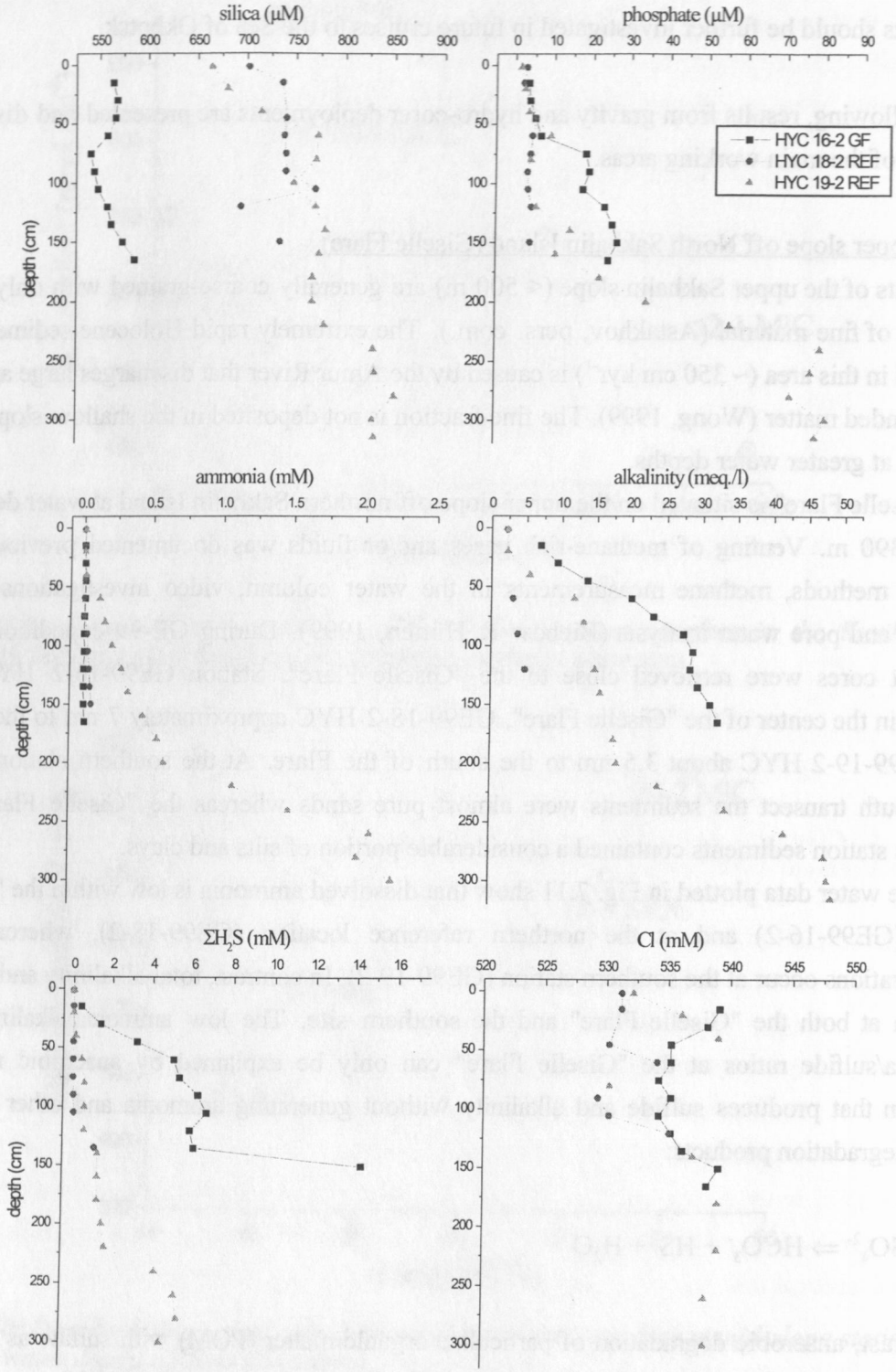

Fig. 7.11: *Dissolved nutrients (silica, phosphate, ammonia), sulfide, alkalinity, and chloride in sediments of the upper slope off Northern Sakhalin Island.*

The data plotted in Fig. 7.11 clearly show that anaerobic organic matter degradation is the main diagenetic process at the southern reference station (GE99-19-2), whereas anaerobic methane oxidation dominates at the "Giselle Flare" (GE99-16-2).

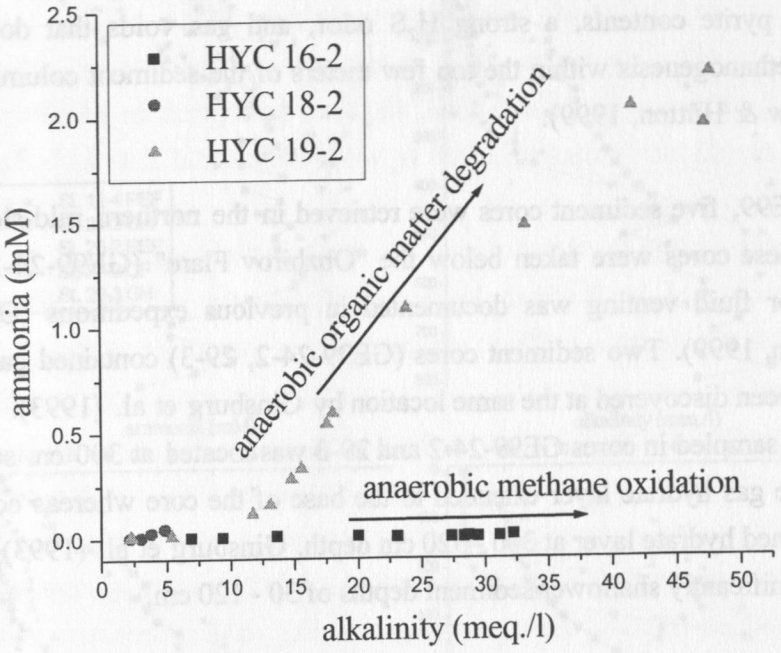

Fig. 7.12: *Ammonia concentrations versus alkalinity in pore waters from the upper slope off Northern Sakhalin Island.*

Fluids generated in methanogenic sediment layers contain not only methane but also POM degradation products such as ammonia and phosphate. Therefore, an upward advection of fluids from deeper methanogenic layers would bring both methane and dissolved degradation products to the surface. A separation of methane and degradation products as observed in HYC GE99-16-2 may either occur during gas-hydrate formation and dissociation or by free gas formation and gas bubble transport to the surface. As salt-free water is produced during gas hydrate dissociation, fluids with a gas hydrate component have a characteristically low salt contents and are thus easily detected. Fig. 7.11 shows a homogeneous chloride distribution throughout the studied surface sediments so that gas hydrate dissociation can be excluded as methane source. Therefore, rising methane gas bubbles are the most likely explanation for the unusual pore water composition observed at the "Giselle Flare" site. Gas bubbles are also suggested by the acoustic measurements in the water column that reveal a distinct structure (flare) of increased reflectivity above the studied surface sediments.

7.2.3 Middle slope off North Sakhalin Island (Obzhirov Flare)

Sediments of the northern mid-slope area (500 m - 800 m) are generally finely grained (Astakhov, pers. com.) and characterized by a high input of biogenic matter. Holocene

sedimentation as determined from seismic stratigraphy (Wong, 1999) is extremely rapid (~300 cm kyr^{-1}). Sediments are composed of a terrigenous fraction delivered by the Amur River and a biogenic fraction produced in the enormously fertile area off northern Sakhalin Island. Previously studied sediments from the northern mid-slope area (LV27-2-4, LV 28-4-4, LV28-32-1) have high pyrite contents, a strong H_2S odor, and gas voids that document sulfate reduction and methanogenesis within the top few meters of the sediment column (Nürnberg et al., 1997, Biebow & Hütten, 1999).

During cruise GE99, five sediment cores were retrieved in the northern mid-slope area (Tab. 7.1). Three of these cores were taken below the "Obzhirov Flare" (GE99-24-2, 27-2, 29-3) where gas and/or fluid venting was documented in previous expeditions (Obzhirov 1992, Biebow & Hütten, 1999). Two sediment cores (GE99-24-2, 29-3) contained gas hydrates that have previously been discovered at the same location by Ginsburg et al. (1993). The top of the gas hydrate layer sampled in cores GE99-24-2 and 29-3 was located at 300 cm sediment depth. At GE99-24-2 the gas hydrate layer extended to the base of the core whereas core GE99-29-3 contained a confined hydrate layer at 300 - 320 cm depth. Ginsburg et al. (1993) found the gas hydrate top at significantly shallower sediment depths of 30 - 120 cm.

The reference sediments taken southwards from "Obzhirov Flare" (GE99-12-4, 26-2) have high phosphate, ammonia, alkalinity, and sulfide values that document high rates of anaerobic organic matter degradation (Fig. 7.13). The slope of the alkalinity profiles shows a distinct change at 300 cm (GE99-26-2) and 600 cm (GE99-12-4) depth that is accompanied by a well-expressed sulfide maximum. These depths mark the lower boundary of the sulfate reduction zone and the upper boundary of the underlying methanogenic sediment column. Thus, methane production occurs at shallow depths in the northern mid-slope sediments.

In contrast to the reference cores, sediments from the "Obzhirov Flare" (GE99-24-2, 27-2, 29-3) have diminished silica, phosphate and ammonia concentrations in the upper 300 cm, whereas the sulfide concentrations are generally enhanced in the surface layers (Fig. 7.13). The resulting low ammonia/sulfide ratios indicate anaerobic methane oxidation. As the chloride concentrations are not diminished but slightly enhanced, gas hydrate dissociation can be excluded as methane source so that free methane gas can be postulated to supply methane to the surface sediments. The low chloride concentrations in the gas hydrate layers do not reflect the in-situ values but are artifacts produced by the dissociation of gas hydrates on board.

Gas bubble formation and transport through sediments can have a significant impact on the distribution of dissolved species. During bubble formation pore water is displaced from its original pore space to be replaced by a newly formed gas phase. The expelled pore water induces a vertical or lateral fluid displacement in adjacent sediment layers that may finally result

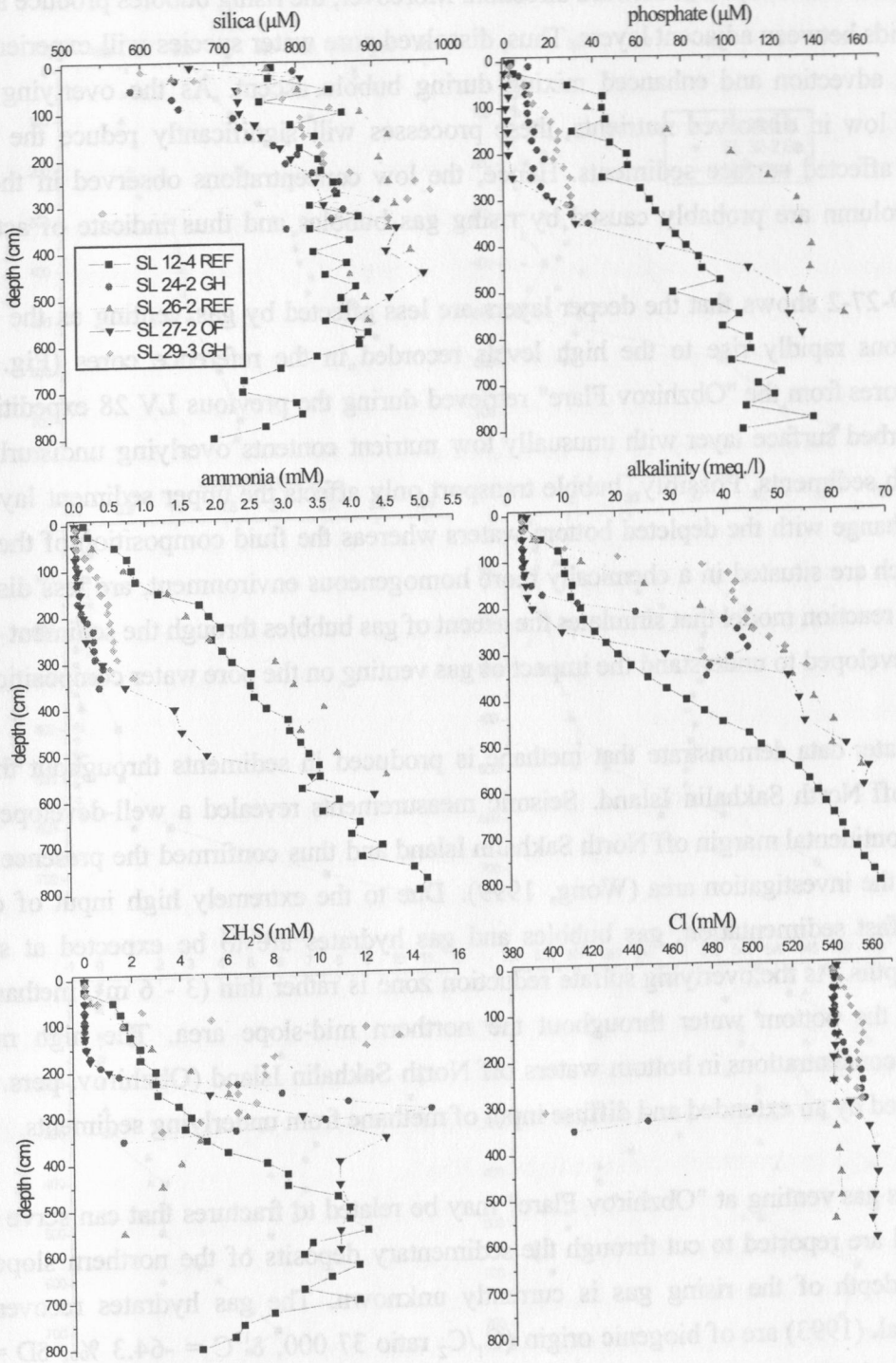

Fig. 7.13: *Dissolved nutrients (silica, phosphate, ammonia), sulfide, alkalinity, and chloride in sediments of the middle slope off Northern Sakhalin Island.*

in upward fluid advection. During the gas bubble ascent, authigenic pore waters are again expelled from their formation site. As the abandoned gas voids are refilled with pore waters, the replaced fluids will adopt a downward direction. Moreover, the rising bubbles produce a mixing of pore fluids between adjacent layers. Thus, dissolved pore water species will experience both downward advection and enhanced mixing during bubble ascent. As the overlying bottom waters are low in dissolved nutrients, these processes will significantly reduce the nutrient content in affected surface sediments. Hence, the low concentrations observed in the upper sediment column are probably caused by rising gas bubbles and thus indicate of active gas venting.

Core GE99-27-2 shows that the deeper layers are less affected by gas venting as the nutrient concentrations rapidly rise to the high levels recorded in the reference cores (Fig. 7.13). Sediment cores from the "Obzhirov Flare" retrieved during the previous LV 28 expedition also had a disturbed surface layer with unusually low nutrient contents overlying undisturbed and nutrient-rich sediments. Possibly, bubble transport only affects the upper sediment layers that rapidly exchange with the depleted bottom waters whereas the fluid composition of the deeper layers, which are situated in a chemically more homogeneous environment, are less disturbed. A transport reaction model that simulates the ascent of gas bubbles through the sediment column has to be developed to understand the impact of gas venting on the pore water composition.

The pore water data demonstrate that methane is produced in sediments throughout the mid-slope area off North Sakhalin Island. Seismic measurements revealed a well-developed BSR across the continental margin off North Sakhalin Island and thus confirmed the presence of gas hydrates in the investigation area (Wong, 1999). Due to the extremely high input of organic matter and fast sedimentation, gas bubbles and gas hydrates are to be expected at shallow sediment depths. As the overlying sulfate reduction zone is rather thin (3 - 6 m), methane may escape into the bottom water throughout the northern mid-slope area. The high methane background concentrations in bottom waters off North Sakhalin Island (Obzhirov, pers. com.) may be caused by an extended and diffuse input of methane from underlying sediments.

The vigorous gas venting at "Obzhirov Flare" may be related to fractures that can serve as gas conduits and are reported to cut through the sedimentary deposits of the northern slope area. The source depth of the rising gas is currently unknown. The gas hydrates recovered by Ginsburg et al. (1993) are of biogenic origin (C_1/C_2 ratio 37 000, $\delta^{13}C$ = -64.3 ‰, δD = -207 ‰) and are probably produced by bacterial carbonate reduction. Thus, it may be concluded that the oil/gas deposits off Sakhalin Island, which are presumably of thermogenic origin, are not the source of the venting methane gas. It is possible that the methane-bearing and extended Holocene sediment cover with a thickness of 30 - 80 m (Wong, 1999) is the shallow biogenic gas reservoir tapped in the "Obzhirov Flare" area.

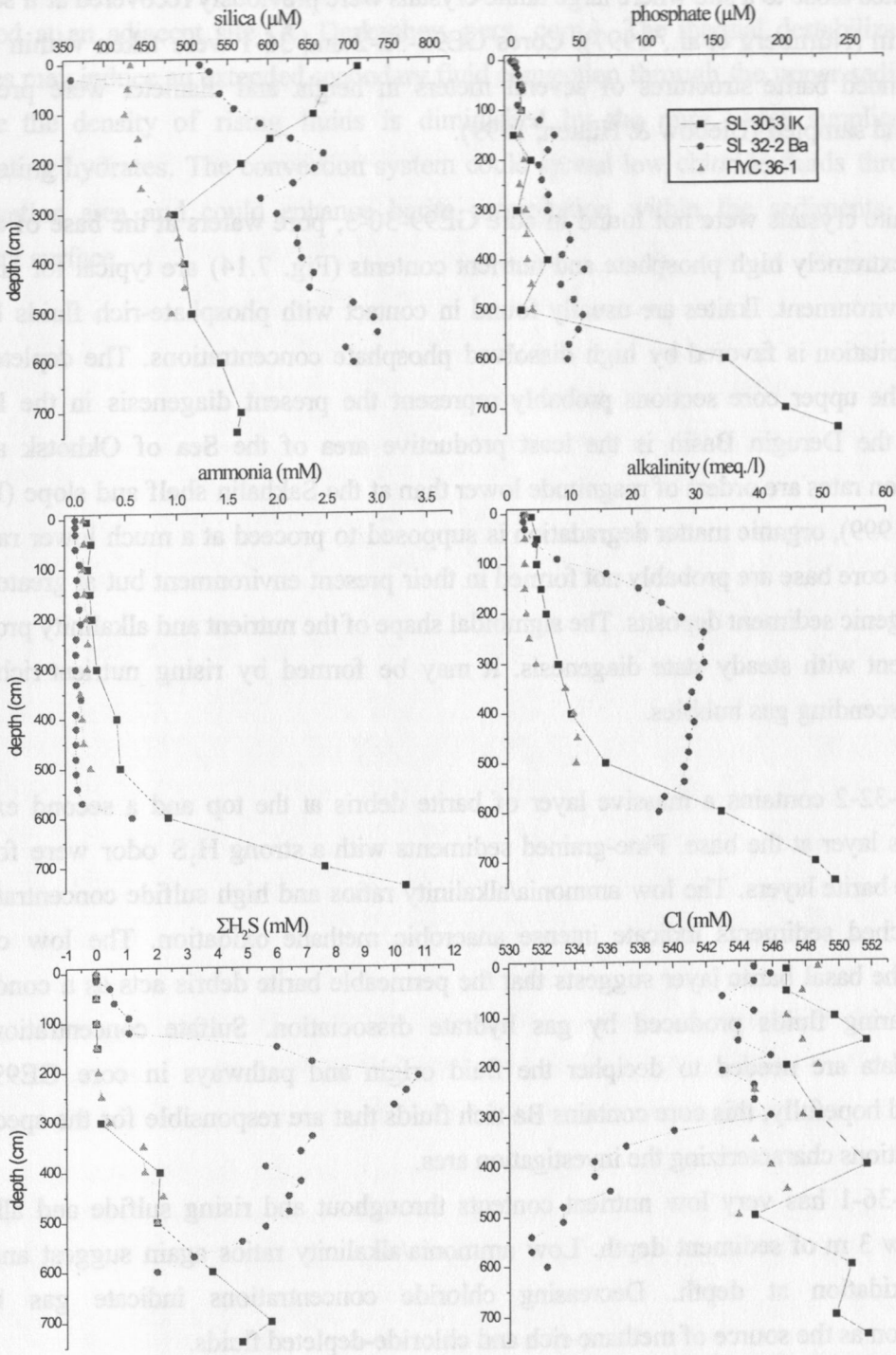

Fig. 7.14: *Dissolved nutrients (silica, phosphate, ammonia), sulfide, alkalinity, and chloride in sediments of the Derugin Basin.*

7.2.4 Derugin Basin

Three sediment cores were recovered from the Derugin Basin during cruise GE99. Core GE99-30-3 is located close to a site where large ikaite crystals were previously recovered at a sediment depth of 6 m (Nürnberg et al., 1997). Cores GE99-32-2 and 36-1 were taken within an area where extended barite structures of several meters in height and diameter were previously observed and sampled (Biebow & Hütten, 1999).

Though ikaite crystals were not found in core GE99-30-3, pore waters at the base of the core with their extremely high phosphate and nutrient contents (Fig. 7.14) are typical for an ikaite-forming environment. Ikaites are usually found in contact with phosphate-rich fluids because ikaite precipitation is favored by high dissolved phosphate concentrations. The depleted pore waters of the upper core sections probably represent the present diagenesis in the Derugin Basin. As the Derugin Basin is the least productive area of the Sea of Okhotsk and the sedimentation rates are orders of magnitude lower than at the Sakhalin shelf and slope (Biebow & Hütten, 1999), organic matter degradation is supposed to proceed at a much lower rate. The fluids at the core base are probably not formed in their present environment but at greater depth in methanogenic sediment deposits. The sigmoidal shape of the nutrient and alkalinity profiles is not consistent with steady state diagenesis. It may be formed by rising nutrient-rich fluids and/or by ascending gas bubbles.

Core GE99-32-2 contains a massive layer of barite debris at the top and a second extended barite debris layer at the base. Fine-grained sediments with a strong H_2S odor were found in between the barite layers. The low ammonia/alkalinity ratios and high sulfide concentrations in the sandwiched sediments indicate intense anaerobic methane oxidation. The low chloride content of the basal barite layer suggests that the permeable barite debris acts as a conduit for methane-bearing fluids produced by gas hydrate dissociation. Sulfate concentrations and additional data are needed to decipher the fluid origin and pathways in core GE99-32-2. Possibly and hopefully, this core contains Ba-rich fluids that are responsible for the spectacular barite formations characterizing the investigation area.
Core GE99-36-1 has very low nutrient contents throughout and rising sulfide and alkalinity values below 3 m of sediment depth. Low ammonia/alkalinity ratios again suggest anaerobic methane oxidation at depth. Decreasing chloride concentrations indicate gas hydrate destabilization as the source of methane-rich and chloride-depleted fluids.

Fluids from both cores retrieved in the barite area have low chloride values that indicate gas hydrate destabilization. Two more cores recovered during the previous LV28 cruise also contained layers of barite debris with slightly diminished chloride contents (Biebow & Hütten, 1999). Thus, the barite area in the Derugin Basin seems to be characterized by wide-spread gas hydrate destabilization. The barite chimneys that characterize the area can only be formed by a

fast and focused fluid flow. It is possible that warm fluids from greater depths rise to the surface to thermally erode the sedimentary gas hydrates and to form the barite landscape of the Derugin Basin. This hypothesis is supported by thermal anomalies that have previously been observed at an adjacent site (A. Derkachev, pers. com.). The thermal destabilization of gas hydrates may induce an extended secondary fluid convection through the upper sediment layers because the density of rising fluids is diminished by the pure water supplied from the dissociating hydrates. The convection system could spread low chloride fluids throughout the investigation area and could enhance barite precipitation within the sediments and at the sediment surface.

8. BIOLOGICAL COMMUNITIES AT VENTING SITES IN THE SEA OF OKHOTSK

S.Galkin

8.1 Introduction

Even though the benthic fauna of the Sea of Okhotsk has already been studied thoroughly, the influence of seeping processes on the biological communities is not well known yet. In general, the seepage of reduced chemical compounds has the potential of fuelling a complex trophic web based on chemoautotrophic microorganisms. The microorganisms can occur either as free-living bacteria or symbiotic species. Chemosynthesis can be regarded as primary production and dominates the biomass and flux of organic matter at the sites, but the spatial scale of this process is not known. Characteristic macrofauna sometimes is the only visual manifestation of recent venting. Most species dominating seep communities harbour bacterial symbionts (sulphide-, methane-oxidizing or both). The specific benthic community dominated by the symbiont-bearing bivalve *Conchocele sp.*, which is associated with gas seepage in the Sea of Okhotsk was first described at the Paramushir gas-hydrate site (Zonenshayn et al., 1987).

The KOMEX expedition on RV *Akademik Lavrentyev* in 1998 was the first attempt to discover seeps and associated fauna in the western part of the Sea of Okhotsk. During this expedition, several vent sites inhabited by specific fauna have been discovered by the video/camera sled OFOS (Ocean Floor Observation System). The taxonomic composition and diversity of the benthic fauna were determined by deploying a trawl (TWL) and several corer (MUC) deployments at the "Giselle Flare" and the Derugin Basin seep sites. The faunal microscale distribution and the seepage influence on non-vent fauna abundance were analysed using slides.

The main objectives of biological investigations aboard MV *Marshal Gelovany* were:

- mapping of seep communities in the studied area; defining the taxonomic composition and abundance of the benthic fauna (incl. meiofauna) more accurately;
- collecting and preparing symbiotrophic animals for analyses.
- investigating the trophic strategy of dominant animals, looking for evidence of their fluid dependence, determining the hydrogen sulfide- or methane-based chemoautotrophy by analysing stable nitrogen and carbon isotopes, by using light and transmission electron microscopy
- investigating the relationship of characteristic fauna to known vent and seep habitats by molecularbiological techniques;
- geochemical characterization of the seep habitat.

- estimation of the influence of seep processes on the background fauna abundance and its distribution.

Due to technical reasons (OFOS and TVG could not be used, MUC and trawl were deployed episodically), the complete set of investigations has not been possible. However, certain new data have been obtained in regions not thoroughly studied previously.

8.2 Methods

8.2.1 Recovery of seafloor samples

To collect benthic animals, a small biological bottom trawl was used. The steel frame (120 cm x 30 cm) was equipped with a triple-layered net 3 m long (outer net: 45 mm double 3,1 x 2 capron net; middle net: 7 mm knotty net; inner net: at the termination a 1 m long sieve net, cell 1,0 mm). The trawl was towed onto the ship's deck by wire and drawn over the seafloor for 10 - 20 min. Some organisms could be collected from the MUC and MIC cores, the geological dredge (DR) and the gravity corers (dead mollusks shells) as well.

Meiofaunal samples have been collected from MUC and MIC tubes (2 cm^3 from each 1 cm layer, three samples from one single tube).

8.2.2 Sample preservation

All samples were sieved immediately after recovery (re-suspending the light fraction) through a 1,0 mm sieve. The animals were extracted in the lab and sorted into taxonomic groups. After counting and determination of the wet weight of selected specimens with beam scales, these species were fixed. Specimens for taxonomic identification, anatomical and histological study were fixed in 70% ethanol or 4% buffered formaldehyde (stored in 70% ethanol). Selected specimens were prepared and their soft tissues for stable isotope analyses were dried by 50°C - 60°C or frozen by nitrogen liquid. The parts of tissues for transmission electron microscopy were fixed in 5% glutaraldehyde. For molecularbiological analyses the symbiont-bearing tissues of the selected animals were frozen in liquid nitrogen separately from the symbiont-free tissues. The meiofaunal samples recovered from the MIC and MUC cores were fixed totally in 6% buffered formaldehyde.

8.3 Results

The investigation area north Sakhalin shelf and slope first explored during the LV28 cruise combined four different target areas (Biebow & Hütten, 1999). These sites are very unevenly studied. A very thorough investigation was undertaken on a well defined flare site with the working title „Giselle flare", incl. detailed visual observations during three OFOS profiles combined with two trawl stations and four multicorer stations. The very shallow flares at a water depth of 200 m

were investigated only by two profiles, no samples were taken at this site or in the „Piltunski" area, where one OFOS station was deployed.

During the present *Marshal Gelovany* expedition the investigations concentrate on a target area with the working title "Obzhirov Flare". At this site in 1998, apart from numerous water anomalies recorded by CTD, two gravity corers yielded bivalve shells; observations at one OFOS-profile were made as well. Seepages occur at the base of the slope, where a small plateau could be seen. Visual seep occurences (clam clusters, bacterial mats, dark sediment) were observed at the background of an Ophiuroidea-Polychaeta-Gastropoda community.

No biological samples were taken previously at this site.

8.3.1 Trawl samples

Substratum characteristic:

Both trawl samples (GE99-25-1, GE99-28-1) were taken at the same site on approximately meridional (south to north) tracks at a depth of around 700 m. Both trawls (14 and 20 min. at seafloor) appeared to be taxonomically representative. The trawls collected nearly 50 to 80 m^3 of grayish sediment (silty-pelite with sand) with a slight smell of hydrogen sulfide. The samples contained various carbonate precipitates varying in form and size (up to 15 cm, 10-15 kg). Some precipitates contained pebbles and clam shells. The pebbles (up to 20 cm) were also abundant. A characteristic feature in these samples were several kg of shells and fragments of Thyasirids (pres. *Conchocele disjuncta)*, and Vesicomyids (pres. *Calyptogena sp.*), some of them were complete or slightly damaged. Fragments and entire shells of other bivalves and gastropods were less abundant although well represented.

Faunal composition :

The dominant animals in the samples were small Ophiuroidea (cf. *Ophiura leptoctenia*) and large Polychaets (cf. Maldanidae, up to 10 cm); up to thousand and up to several hundred specimens respectively. The polychaets in the second trawl were less abundant corresponding to their irregular distribution. Small polychaets, bivalves and gastropods are also rather diverse (at least 6, 7 and 5 species respectively). Among the large forms a single shrimp (10 cm), a crab *Chionoecetes opilio* (40 cm) and two species of Buccinid gastropods (up to 12 cm) could be found. The presence of *living* symbiont-bearing bivalves (Thyasiridae, Vesicomyidae and Solemyidae) is most peculiar.

Trophical specialization:

The animals dominating the community are mostly deposit feeders and scavengers. Suspension feeders (Hydrozoa, Actiniaria, small Sponges) are less abundant.

There are four or five species which are probably symbiotrophic. The symbiont-bearing Solemyid mollusc cf. *Acharax sp.* represented by two small specimens is well known from organic-rich and hypoxic sediments (as well as Pogonophora aff. *Siboglinum sp.*).
The Thyasirid mollusc *Conchocele disjuncta*, represented by a lot of shells and for the first time collected alive, showed important anatomical and physiological features connected with symbiotrophic nutrition. This mollusc is well known from the Paramushir gas-hydrate seep community. It harbours endosymbiotic bacteria which are able to oxidize both methane and sulphide. Experiments showed that a considerable amount of organic carbon derived from methane and carbon dioxide is incorporated in mollusc tissues (Galchenko et al., 1988).
Very interesting was the finding of Vesicomyid clam shells and living molluscs at "Obzhirov Flare" site. All vesicomyids investigated so far harbour sulphide-oxidizing endosymbionts. The occurrence of living molluscs combined with plenty of shells could suggest that sulphide plays an important role in the energy flux of the community. Furthermore it is the most shallow occurrence of Vesicomiidae in the Sea of Okhotsk.
The difference in relative abundance of dead thyasirids and vesicomyids shells in trawl samples taken at the same site is worth mentioning. At station GE99-25-1 24, whole or slightly damaged valves occurred, while at GE99-28-1 only 6 could be found. The number of *Calyptogena* valves was 34 and 65, respectively. Although the trawl samples could not be considered quantitative, such differences may reflect the patchiness in thyasirids and vesicomyids microscale distribution caused by their different environmental requirements.

8.3.2 Gravity corer data

Conchocele and *Calyptogena* shells and fragments could repeatedly be observed in the gravity core samples taken at vent sites. Vesicomyids were sometimes recorded in association with Thyasirids, sometimes without. The most peculiar finding is the occurrence of 6 complete vesicomyid shells at GE99-29-3 at horizon 167-174 cm suggesting the corer caught a former „cluster" of clams.

8.3.3 Multicorer samples

Macrofaunal samples collected on several stations could not be taken as quantitatively representative as the animals were only picked by hand when the cores were sliced for geological and geochemical analyses. The multicorers provided some additional information on the microscale distribution of some animals, though. The MIC samples confirmed that the small *Ophiura leptactenia* seems to constitute the most abundant and common group (they occured with up to 4 specimens in one tube which covered 23,7 cm^2).
Two representative samples (one was taken from the background station GE99-12-3, and one from the seep stationGE99-29-2) could be fixed quantitatively for meiofaunal investigations.

Those samples were firstly recovered by a standard method (three 2 cm tubes from each core).

8.3.4 Dredge samples

One dredge (GE99-35-1) was deployed in the region of presumably active seeps in the Derugin Basin. The dredge yielded nearly 100 m^3 of grayish sediment (silty-pelite), broken barites (incl. large blocks up to 40 cm), and a few pebbles; there was no H_2S smell.

The fauna collected was not abundant: apparently the dredge collected a big amount of sediment and then was blocked by barites rather soon and stopped to catch. The dominating animals were represented by suspension-feeding epifauna of old barite chimneys: Hydrozoa, small sponges, Bryozoa and Ascidiae (cf. *Boltenia echinata* - 8 specimens). No seep-specific fauna was recorded apart from 2 dead solemyids shells, though the OFOS observations and samples recovered during the LV28 cruise suggested a rather diverse symbiotrophic fauna in the Derugin Basin (at least 3 sp. of Vesicomyid bivalves, Provannid gastropods etc.). It seems the present dredge doesn't reach the area of recent active venting.

Two dredges deployed at Kurile Arc volcanoes (GE99-39-1, GE99-40-1) recovered ordinary deep sea suspension feeding epifaunal species associated with basalts and old (subfossil) sponges. These specimens could be used as "background" samples for analyses.

8.4 Conclusions

In the investigation area "Obzhirov Flare", ca. 25 species of bottom fauna have been recorded. Faunal composition and trophical orientation of dominant groups are common for the highly productive slopes of the Okhotsk Sea.

The total non-vent fauna diversity is lower compared to the previously studied "Giselle Flare", which could be caused by its deeper water depth. On the contrary, the specific symbiont bearing fauna seems to be more diverse.

A specific fauna associated with seeping is represented by the Thyasirid bivalve *Conchocele* sp. (cf. *C. disjuncta*), Vesicomyid bivalves cf. *Calyptogena* (1 or 2 spp.), Solemyid bivalves cf. *Acharax jonsoni* and Pogonophoran tube worms. In the western Sea of Okhotsk, the first two groups were collected alive for the first time. In the Sea of Okhotsk, "Obzhirov Flare" is the shallowest occurrence of Vesicomyids known so far.

The occurrence of these symbiotrophic animals suggests high recent activity of bacterial chemosynthesis in this area. The thyasirid bivalve *Conchocele cf. disjuncta* harbouring both methane and sulfide-oxidizing bacteria is the most striking feature at the seeps. These data is in agreement with the observed chemical environment at the North Sakhalin slope flares, where methane seems to be the dominant reduced chemical compound. The reliance on methane as a sole

energy source or as source of additional symbiotrophic nutrition indicates a very stable supply with methane and underlines the stability of the gas seepage at the North Sakhalin slope.

Very interesting and rather unexpected is the finding of numerous living Vesicomyids at "Obzhirov Flare" (the finding of a single complete shell on station LV28-21-1 by gravity core was considered out of character). No vesicomyids seem to inhabit the relatively well studied "Giselle Flare". Clusters and single specimen of *Calyptogena* have been observed by OFOS only at the isolated "Piltunski Flare" and furthermore have been recorded in the Derugin Basin.

All vesicomyids and solemyids investigated so far harbour sulphide-oxidized symbionts. The occurrence of sulphide-based bivalves *Calyptogena* and *Solemya* indicate a sulphide-rich fluid flow. Even though large methane anomalies near the bottom have been measured by CTD (and underlined by the occurrence of methane-based thyasirids and pogonophorans), sulphide seems to play a significant role in the recent energy flow. Even the occurrence of symbiotrophic species in the gravity cores suggests both methane and sulphide may have played an important role in the past history of the seep.

9. AUTHIGENIC MINERALS AND SEDIMENTS OF THE SAKHALIN ISLAND SLOPE

A. Derkachev, N. Nikolayeva, A. Botsul, and J. Greinert

In an area of recent gas venting, on the Sakhalin slope, sediments were sampled in 7 cores. Four cores were taken in direct proximity to gas emanations: GE99-16-2 ("Giselle Flare"), GE99-24-2, GE99-27-2, GE99-29-3 ("Obzhirov Flare"). Three cores (GE99-18-2, GE99-19-2, GE99-26-2) were taken as a background to estimate the gas seeping influence on the pore water geochemistry.

The sediments of background station GE99-18-2, situated in the north, are represented by well-sorted fine sand with minor admixtures of diatomaceous mud. They were formed under high hydrodynamic conditions.

The southern background station (GE99-19-2) contains Holocene sediments (325 cm) represented by bioturbated, weakly siliceous terrigenous silty sand. Signs of carbonatization are missing. In the upper part of the core a brecciated texture with dip joining was observed, which is typical for gas-saturated sediments.

Core GE99-26-2 is situated in a water depth of 700 m, north-east of "Obzhirov Flare". The sediments are mottled, strongly bioturbated, and signs of carbonate formation are missing as well. A brecciated texture could be traced in lower sections (314 - 582 cm).

The cores GE99-24-2, GE99-27-2, GE99-29-3 were taken in direct proximity to "Obzhirov Flare". All these cores are characterized by the same type of lithology and an intensive H_2S odor. They are represented by clayey-siliceous sediments (sandy silt, clayey silt, rarely silty clay) with a strong admixture of terrigenous silty-sandy particles. The sediments of the upper core parts are dark grayish green, mottled and strongly bioturbated and contain numerous burrows (empty or filled with sediment). In separate sections, black lenses and small interlayers of hydrotroilite could be found. The characteristic feature in the upper core part are numerous carbonate concretions of different morphological types and sizes. The thickness of this section is not constant and changes from 173 cm (GE99-24-2) up to 315 cm (GE99-27-2).

In the cores mentioned above all stages of carbonate formation are present. The initial stage can be observed in the upper sections and is expressed in mottled-lenticular concretions 0,5 - 4 cm in diameter. They differ from the surrounding sediment by both a lighter color (light gray, light grayish green) and a gradual density increase towards their center. Sometimes, similar concretions can be found around the burrows of bottom organisms (a prototype of tubular carbonate concretions). In some cases (GE99-27-2, GE99-29-3), they cement shell fragments or form crusts on large shells. Towards the lower part of the cores, these concretions become denser and sharply mark the beginning of the surrounding sediment. In lower sections with concretions, the sediments have a brecciated texture and show dip joining, which is typical for gas-saturated sediments. Within these sections (GE99-24-2, 310-360 cm; GE99-29-3, 305-312

cm), gas-hydrates were discovered in form of pure, thin (up to 2-5 mm), subparallel beds and lenses, intercalating the surrounding sediment. Carbonate concretions have not been found here, with the exception of core GE99-29-3, situated nearest to the seeping area. The intensity of the methane supply and the processes of its bacterial anaerobic oxidation are possibly expressed here to a very high degree. Authigenic carbonate formation practically started here on the sea floor. Soft carbonate concretions of small sizes were discovered even in section 1 - 3 cm. The occurrence of shell fragments and shells of *Bivalvia (Vesicomyidae), Thyasiridae,* typical for vent fauna (S. Galkin, pers. com) also confirm to the proximity of a gas source to this station. A fauna, typical for highly productive areas enriched by organic matter can be found here: *Macoma, Gastropoda, Buccinidae sp.* The increased quantity of shell fragments in some sections of the cores indicates spatial and temporal variations in their distribution, which are connected to local changes in the geochemical conditions and are probably caused by periods of increasing vent activation.

The trawling conducted in this area (GE99-25-1, GE99-28-1) provided about 20-30 kg of carbonate concretions from 1 to 20 cm in diameter of different morphological types: formless, uneven, smoothed, tabular, tubular bodies and crustified crusts on shells. All concretions are of greenish gray color, soft on the surface and dense in the center. The trawl also yielded mollusk fauna and numerous shell fragments.

Core GE99-16-2 taken in the area of "Giselle Flare" is essentially different from the cores mentioned above. The thickness of the Holocene sediments consisting of silty sand of different sorting degrees with admixtures of diatomaceous mud does not exceed 30 cm. Below, they sharply turn into viscous, dense and moderately dense, bioturbated clayey and silty clayey sediments of dark gray color, containing both small thin-valved shell fragments in separate sections and a large quantity of organic plant fragments. These sediments are different from Holocene sediments in their structure and lithology and probably represent deposits of a Pleistocene debris cone of the Amur River.

The characteristic feature of these sediments is the existence of numerous light gray lenses and mottles that have both indistinct boundaries and compactions in the center (the initial stage of carbonate concretion formation). They consist of a terrigenous silty clayey matrix, cemented by cryptocrystalline aragonite aggregates that distinguish these sediments from the ones of the "Obzhirov Flare" area. Dense, tabular concretions (90 cm, 157 cm) up to 9 cm in size are rarely found.

10. THE GEOMORPHOLOGY OF THE DERUGIN BASIN

A. Svarichevsky

The echosounding and seismo-acoustic profiling data of the Derugin Basin include those data gathered during several joint cruises within the KOMEX framework (GERDA cruise G16 in 1995, INESSA cruise G22 in 1998; LV27 (Nürnberg et al., 1997); LV28 (Biebow & Hütten, 1999)). A number of morphologic features were observed, which make the compilation of a new bathymetric map possible (Fig. 10.1).

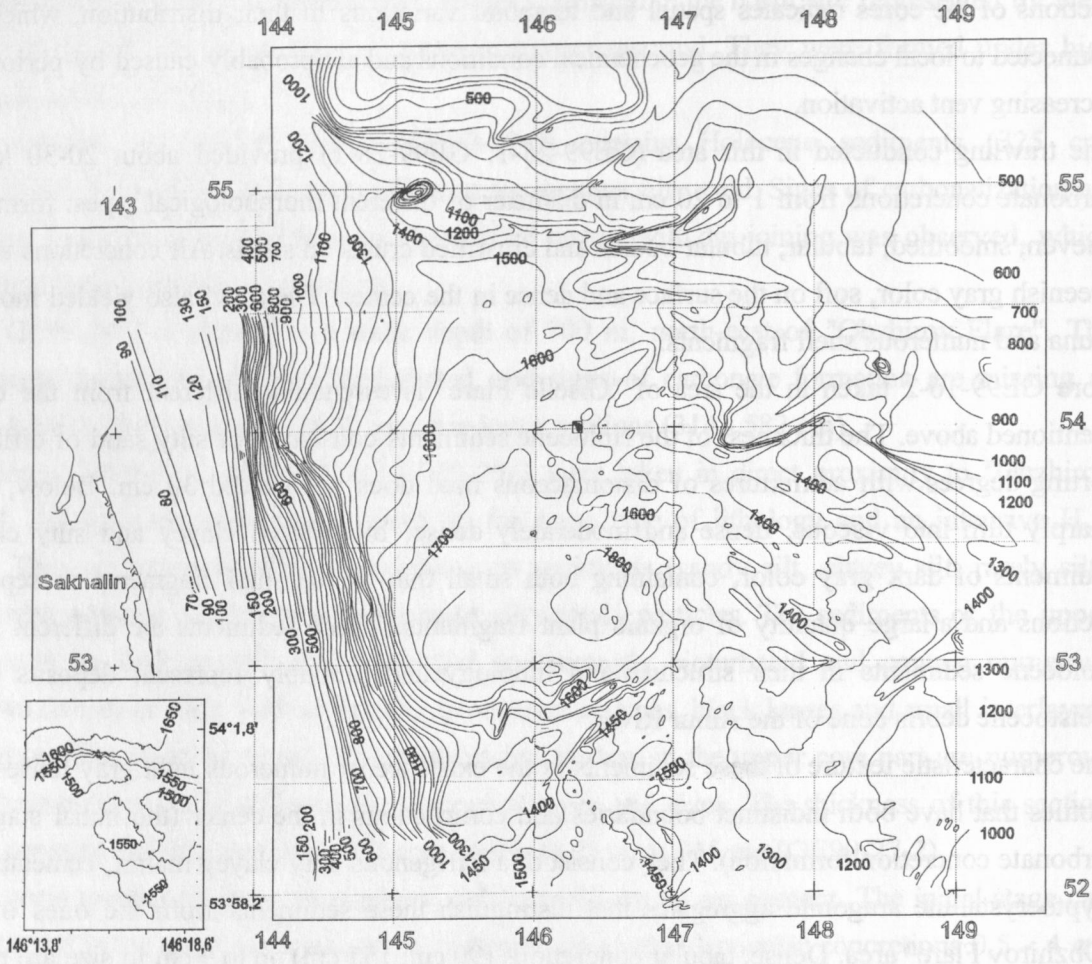

Fig. 10.1: *Bathymetry of the Derugin Basin.*

The Derugin Basin is the deepest region of the Central Okhotsk marginal plateau, its border lies at the 1400 m contours. The seafloor represents an abyssal plain and is situated at a depth of 1800 m. It has an asymmetric structure. To the west it is bordered by the accumulative continental margin of North-East Sakhalin. To the north and east its borders incise into the

slopes of the North-Okhotsk Rise, in the southern basin the Peter Shmidt Trough (at 1300 m depth) can be observed.

The slopes of North-East Sakhalin are an accumulative flexure gashing through all sediment layers (2 sec twt). At a depth of about 700 m the slopes are marked by terraces connected with the development of slumps.

The step-like slopes of the North-Okhotsk Rise are characterized by intensive fracturing of the acoustic basement, numerous outcrops of which act as dams for sediments. The dams can be grouped into three different units trending in north-south, north-eastern and north-western direction. The sediment is trapped behind the dams which fill up with sediment layers until they overflow. This leads then to the formation of extensive accumulative steps and hills.

In the south, the accumulative slopes are very gentle (1°) and reach a height of about 300 m. These extensive accumulative plains are situated in a depth of 1300-1400 m.

Small forms of relief in the Derugin Basin are represented in "submerged beach-ridges" (definition by Lisitsin & Udintsev, 1953), barite mounts, moats at the base of the bedrock outcrops and small gauges. Those gauges are abundant at the gentle southern slope of the Derugin Basin. The nature of those gauges is not very clear yet, but in their morphology they are similar with pockmarks. Their examination thus should have high priority. In most cases they are certainly erosional valleys, possibly of subaerial origin.

Thus at the borders of the Derugin Basin numerous features of subaerial development could be observed on the seafloor surface. This gives evidence of significant changes in the environmental conditions during the geological past. Their explanation demands special investigations.

11. SEDIMENTS AND CARBONATE-BARITE PRECIPITATES OF THE DERUGIN BASIN

A. Derkachev, N. Nikolayeva, J. Greinert, S. Bollwerk, and A. Botsul

Previous investigations of a rise (called "Barite Mountains") in the Derugin Basin showed a wide distribution of carbonate and barite mineralizations of various types (Astakhova, 1987, 1990; Derkachev et al., 1999 a, b; Derkachev et al., in press). In 1998 complex investigations in this area were conducted within the project KOMEX. They included sampling by cores, dredges and also trawling, the study of both pore water geochemistry and water masses, OFOS video surveys, and investigations of bottom organism communities (Biebow & Huetten, 1999).

In Holocene-Pleistocene sediments the following mineralogical and morphological types of authigenic-diagenetic precipitates were revealed by detailed mineralogical and petrographic researches:

a) calcite, barite, tubular calcite-barite bodies,

b) calcite concretions of various densities,

c) barite spherolites and their brushes (microconcretions),

d) thin, dense barite crusts,

e) crustified calcite and aragonite cement debris of barite chimneys.

Tubular bodies of various diameters and sizes prevail. They represent mainly burrows of benthic organisms in the sediment. These bodies consist of Mg-calcite and barite. Several show complicated build-ups with concentrically-zonal structures and differing types of mineralization (calcite and barite). The cross section of such a tubular body is shown in Fig. 11.1.

At the upper part of the rise outcrops of pure strongly porous travertine-like barite were recovered by OFOS surveys, dredging, trawling and core sampling (Biebow & Huetten, 1999). The chimneys up to 3-10 m high consist of similar barite.

During Ge99 cruise additional investigations of calcite and barite mineralization were conducted in the same area The sediment samples and authigenic precipitates were recovered by core sampling (GE99-32-2) in the area where methane anomalies in the near-bottom water layer had been discovered before (CTD LV28-28-1) (Biebow & Huetten, 1999). The core was taken on the southern slope of a submarine range trending in a sublatitudinal direction where outcrops of barite chimneys were discovered before (LV28-35-1, LV28-37-1). Core GE99-32-2 consists of terrigenous silty clayey and sandy silty clayey sediments, which contain debris of barite chimneys of various sizes (from 1 up to 10 cm in diameter) in differing quantities. The most considerable congestion could be found in the upper part of the core on section 23-64 cm. It consists of pure, very fragile barite debris of a white or light grey colour (a mixture of differently sized fragments: from silt to fragments of 5-10 cm in diameter). At 278 cm, 470 cm, 580 cm, 590 cm carbonatizations of barite chimneys debris were observed pointing to a cementation of pore space by Mg-calcite microcrystals in the debris. Several of the calcite crystal

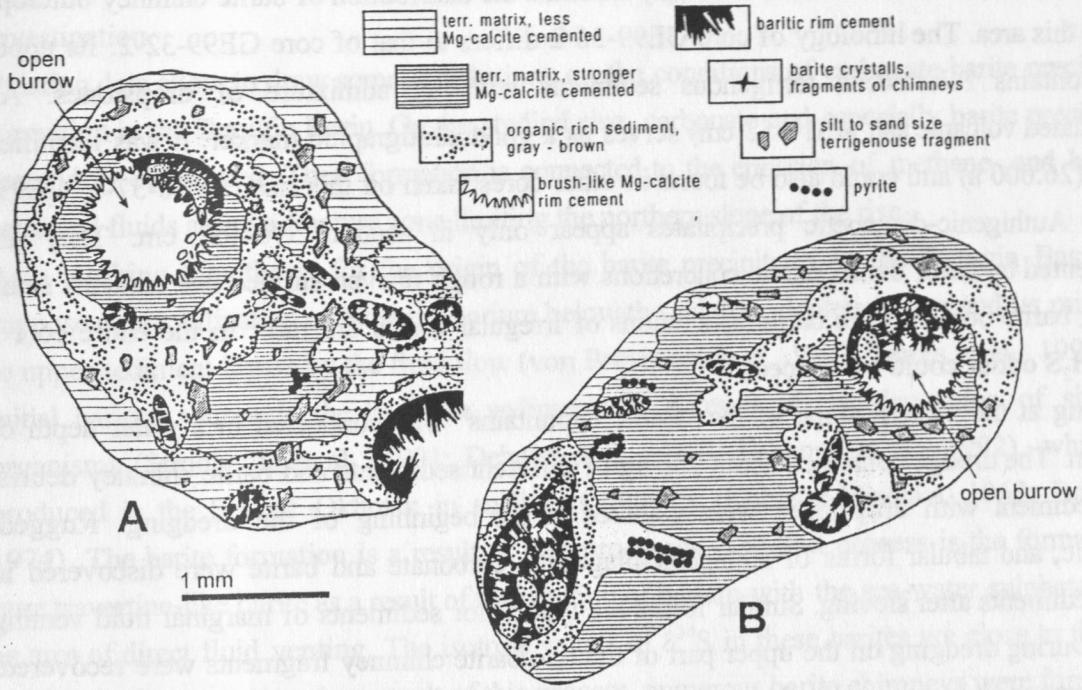

Fig. 11.1: *Cross section of tubular barite-calcite bodies. The empty central channel and numerous cross-cut burrows are incrusted by barite and Mg-calcite crystals.*

aggregates have characteristic forms (dumbbells) which are typical for bacterially induced calcite precipitates (Buczyinski & Chafets, 1991). Similar forms were also discovered in core LV28-37-1 and studied under an electron microscope.

The recovery of authigenic-diagenetic barite crusts and worm tubes cementing surrounding sediment or filling burrows of bottom organisms prove the existence of a diffusive inflow of barium and methane from deep sediment sections in the area of station GE99-32-2. Similar barite forms were found in sections 117-150 cm, 210 cm, 275 cm, 320 cm. They are present in large quantity, especially in section 117-150 cm. Partly they are covered by Mg-calcite crusts. This type of complicated carbonate-barite precipitates is characteristic for the studied area (Derkachev et al., 1999 a, b; Derkachev et al., in press). Large, hard tabular carbonate concretions were also discovered in sections 200-210 cm (3 x 3,5 cm in size) and 217 cm (13 x 1,5 cm in size). They cement both the terrigenous-clayey matrix of the surrounding sediment and the barite worm tubes in it.

The entire core is suffused by a H_2S odour; it shows a brecciated texture with dip joining typical for gas-saturated sediments, especially pronounced in its upper part. Similar textures could be traced in many cores from areas of gas-fluid venting activity on the Sakhalin Island slope (see chapter 9).

Core GE99-36-1 was taken on the isthmus between two ranges (Fig. 4.8), where carbonate-barite mineralization had not been known before. Core sampling (LV28-37-1) (Biebow &

Huetten, 1999; Derkachev et al., 1999 a,b) confirms the distribution of barite chimney outcrops within this area. The lithology of core GE99-36-2 differs to that of core GE99-32-2. Its upper part contains Pleistocene terrigenous sediments with an admixture of dropstones. An intercalated volcanic ash (151-152 cm) serves as a good stratigraphic marker. It was identified as K2 (26.000 a) and could also be found in other cores taken on this rise (LV28-37-1, GE99-32-2). Authigenic-diagenetic precipitates appear only in section 390-462 cm. They are represented by hard, dense calcite concretions with a rough uneven surface that contains small tubular barite bodies. Pure barite concretions of irregular forms are rare. In the entire core a weak H_2S odour could be noticed.

Dredging at the eastern slope of the "Barite Mountains" was conducted in a water depth of 1.600 m. The dredge contained about 300 kg of different sediments and barite chimney debris. Soft sediment with dropstones were gathered at the beginning of the dredging. Rugged, dendritic, and tabular forms of authigenic-diagenetic carbonate and barite were discovered in these sediments after sieving. Similar forms are typical for sediments of marginal fluid venting areas. During dredging on the upper part of the rise barite chimney fragments were recovered. Their upper part is oxidized and has a brownish black coating, which penetrates in the pores and cavities of the barite chimneys to a depth of 1-2 cm. As follows from research done on similar coatings of barite fragments on station LV28-36, they consist of amorphous flocculent-flaky manganese hydroxide precipitates forming spheroids. On the surface of these fragments an overgrowth of fauna was found, which is typical for this depth. Apart from pure barite chimney debris, complicated forms (up to 15 cm in size) were recovered in small quantities. They consist of travertine-like barite fragments with a vesicular-uneven surface, cemented with pebbles. The surface is covered by a thin coating of manganese hydroxides. The lower part of those fragments consists of a very dense, greenish dark-gray sediment, in which numerous burrows orientated in different directions were observed. They are cemented by cryptocrystalline authigenic barite. The outer side of these fragments is often tabular, crustated, with a rough surface; on this surface both dendritic carbonate tubular bodies and pebbles could be found. The formation of such crusts consisting of authigenic barite may be connected with the lateral breaching of barium-saturated fluids near the boundary of the barite chimney body and the sediment. As a result, new portions (fragments) of barite chimneys are formed on the surface of the water-sediment boundary; these fragments gradually cover the sediment. In this reduced environment authigenic-diagenetic barite crusts are formed.

In the same dredge carbonate fragments up to 3-8 cm in size were recovered, which were not found before. They represent dense, mushroom-shaped fragments of a light gray colour. Their upper part consists of densely packed calcite crystals with inclusion of terrigenous particles orientated without system. The interweaving of numerous vein-shaped thickenings up to 1-2 mm in diameter (it may be burrows of bottom organisms) are clearly visible on the surface. They are filled by well-crystallized calcite. The mushroom's "cap" consists of crusts up to 1-2 cm in thickness containing quite pure, well-crystallized, massive calcite of white colour. The

origin of this type of carbonate mineralization is not clear yet and it requires additional investigation.

Existing data allow to draw some conclusions on the conditions of carbonate-barite precipitates formation in the Derugin Basin. On the studied rise, carbonate and especially barite precipitates are widely distributed. Their formation is connected to the emission of methane- and barium-saturated fluids along a fracture zone limiting the northern slope of the rise.

As a working hypothesis for the origin of the barite precipitates in the Derugin Basin, we suppose a remobilization of biogenic barium below the sulphate-depleted zone and its migration to upper sediment layers by the fluid flow (von Breymann et al., 1992; Torres et al., 1996). An initial barium source is the barite in sediments as a result of the deposition of siliceous organisms (Stroobants et al., 1991; Dehairs et al., 1991; Dymond et al., 1992), which are produced in the Sea of Okhotsk in sufficient quantity (Koblenz-Mischke, 1967; Bogorov, 1974). The barite formation is a result of two processes. The first process is the formation of pure travertine-like barite as a result of the reaction of barium with the sea-water sulphate-ion in an area of direct fluid venting. The isotope values of $\delta^{34}S$ in these barites are close to those of sulphur in the sea-water. As a result of this process, numerous barite chimneys were formed.

The second process is the diagenetic reaction of barium in the sulphate reduction zone with the residual sulphate of the pore water, enriched in heavy sulphur isotopes. For the diagenetic barite samples represented mainly by tubular bodies (rarely by crusts), we received high $\delta\ ^{34}S$ values equal 57,4 - 80,1 ‰ CTD (Derkachev et al., 1999 b). As our investigations show, similar diagenetic barites form in the sediment as a result of diffusive barium seeping in the periphery of the main fluid venting fields.

The isotope data for carbon and oxygen in the carbonate precipitates ($\delta^{13}C$: -37,6 - 42,3 ‰ PDB; $\delta^{18}O$: 3,83 - 4,89 ‰ PDB) correlates well with values typical for cold vent carbonates in other regions of the World Ocean (Lein et al., 1989; Ginsburg & Soloviev, 1994; Ritger et al., 1987; Kulm & Suess, 1990; Paull et al., 1992; Sample et al., 1993; Roberts & Aharon, 1994; Von Rad et al., 1996; Bohrmann et al.,1998; Suess et al., 1998). This confirms that the carbonates were mainly formed as a result of anaerobic microbiological oxidation of methane supplied as a fluid component.

The investigated cores enriched in carbonate concretions and crusts, the crustified cement on the barite chimneys debris (LV28-37-1, GE99-32-2) and the increase in the quantity of authigenic barite may prove stages of different venting activation at the rise. Detailed investigations on core LV28-37-1 showed that authigenic-diagenetic carbonate and barite are usually confined to sections with strong bioturbation, which contain remains of specific vent fauna (*Calyptogena, Provanna*).

The mineralogical analysis of the sediment composition (the existence of both authigenic calcite and barite precipitates and also barite chimneys debris) testifies that in the studied area a long-existing cold seep centre with a several stages of activation exist. A good stratigraphic framework for the cores supported by the volcanic ash interlayer (K2) (see chapter 12.3.5),

allows to suppose that venting activity has been continuing about 100.000 years. The presence of authigenic-diagenetic carbonate and barite only in the lower part of core GE99-36-2 allows to suppose that the venting activity in the south-eastern part of the rise has stopped about 50 000 years ago (if taking into account the stratigraphical position of the volcanic ash interlayer K_2). But in the north it continued further. The methane anomalies discovered in the near-bottom water layer (see chapter 6) confirm its moderate activity at present.

Taking into consideration the large scale of carbonate-barite precipitates manifestation, it is possible to suppose the existence of a gigantic cold seep in the Derugin Basin whose origin has not finally been established yet. The main task is to determine both the barium source and the mechanism of its transportation to the sea floor.

At present, direct evidence of hydrothermal activity (including paragenetic associations of minerals characteristic for hydrothermal systems (Alt, 1988; Koski et al., 1985; Tufar et al., 1986; Gieskes et al., 1982; Lisitsin et al., 1991; Von Damm et al., 1985; Herzig et al., 1988 and see Derkachev et al. in chapter 15) does not exist. At the moment, the available data including the isotope data does not confirm that the carbonate-barite mineralization is a result of a direct influence of a hydrothermal processes. Nevertheless it is impossible to exclude hydrothermal fluids as a source of mineral-forming components in other areas of the Derugin Basin completely. Gravimetric data and heat flow anomalies (Hayachi, 1997) east of the studied area indicate such influence and should be investigated in the future. Unfortunately, due to time restrictions we were not able to sample sediments in this area on GE99 cruise to see whether there is a thermal anomaly.

12. PALEOCEANOGRAPHY AND SEDIMENTOLOGY

A. Astakhov, A. Botsul, N. Biebow, A. Derkachev, S. Fessler, S. Gorbarenko, A. Kaiser, N. Nikolayeva, R. Tiedemann, and R. Werner

12.1 Introduction

The initial object of this cruise was to extend our east-west transect across the central Sea of Okhotsk to the east (Kamchatka shelf), to extend our north-south transect along the Sakhalin continental margin further to the north and into the Amur River delta, to recover an east-west transect in the northern part of the Sea of Okhotsk, and to complete our deep water transect at the northwestern slope of the Kurile Basin (Fig. 2.2). However, due to technical, time, and fuel problems during this cruise our sphere of activity was restricted to the Sakhalin continental margin, the Derugin Basin and the Kurile Basin (Fig. 2.2). Thus, we had to reconsider our scientific targets and focused our interests on the following topics:

- To study variations in paleoproductivity and surface paleoceanography that are related to fluctuations in the nutrient supply and freshwater discharge of the Amur River, we decided to increase our data basis by two additional cores from the Sakhalin continental margin between 51°N and 55°N (GE 99-12-1 and GE 99-21-1; Fig. 1). At site GE 99-12-1 we retrieved a high resolution Holocene sediment record 11,31 m long. At site GE 99-21-1, unfortunately, the pipe of our gravity corer broke while pulling the gravity corer on deck. We lost about 8 m of pipe and were not able to rescue the sediment record. Due to our cruise schedule we had to skip a second effort.

- To investigate the influence of vent fields and gas emissions associated with gas hydrates that cause methane anomalies in the water column and in the seafloor we focused our coring on two areas, the southeastern and the northeastern slope of Sakhalin. Methane plumes in the lower water column along the western slope of the Sea of Okhotsk are a widespread phenomenon that has been recognized over the last 10 years. These gas emissions may effect the $\delta^{13}C$ ratio in the water column when biological oxidation rates of methane to CO_2 are high. Furthermore, several sediment records from cruise LV 28 recovered from the Sakhalin slope are characterized by traces of outgassing voids. First results from the LV-28-2 sediment record from the southeastern slope (Fig. 12.2) provide evidence for a nearby source of increased glacial methane outgassing. This is indicated by extremely low epibenthic $\delta^{13}C$ values (*C. kullenbergi*) of up to -3.6 ‰ compared to a typical glacial Okhotsk Sea Intermediate Water value of 0 to -0.5 ‰. The light carbon isotope signature implied that methane ($\delta^{13}C$ = up to -60 ‰) may play a role as a carbon source via oxidation. To estimate the area that can be effected by methane outgassing, we recovered two additional sediment records in the proximity of site LV-28-2. Site GE 99-9-1 was positioned 6 miles to the east at

the same water depth of core LV-28-2, whereas GE 99-10-3 was retrieved 200 m downslope to the south (Fig. 12.1).

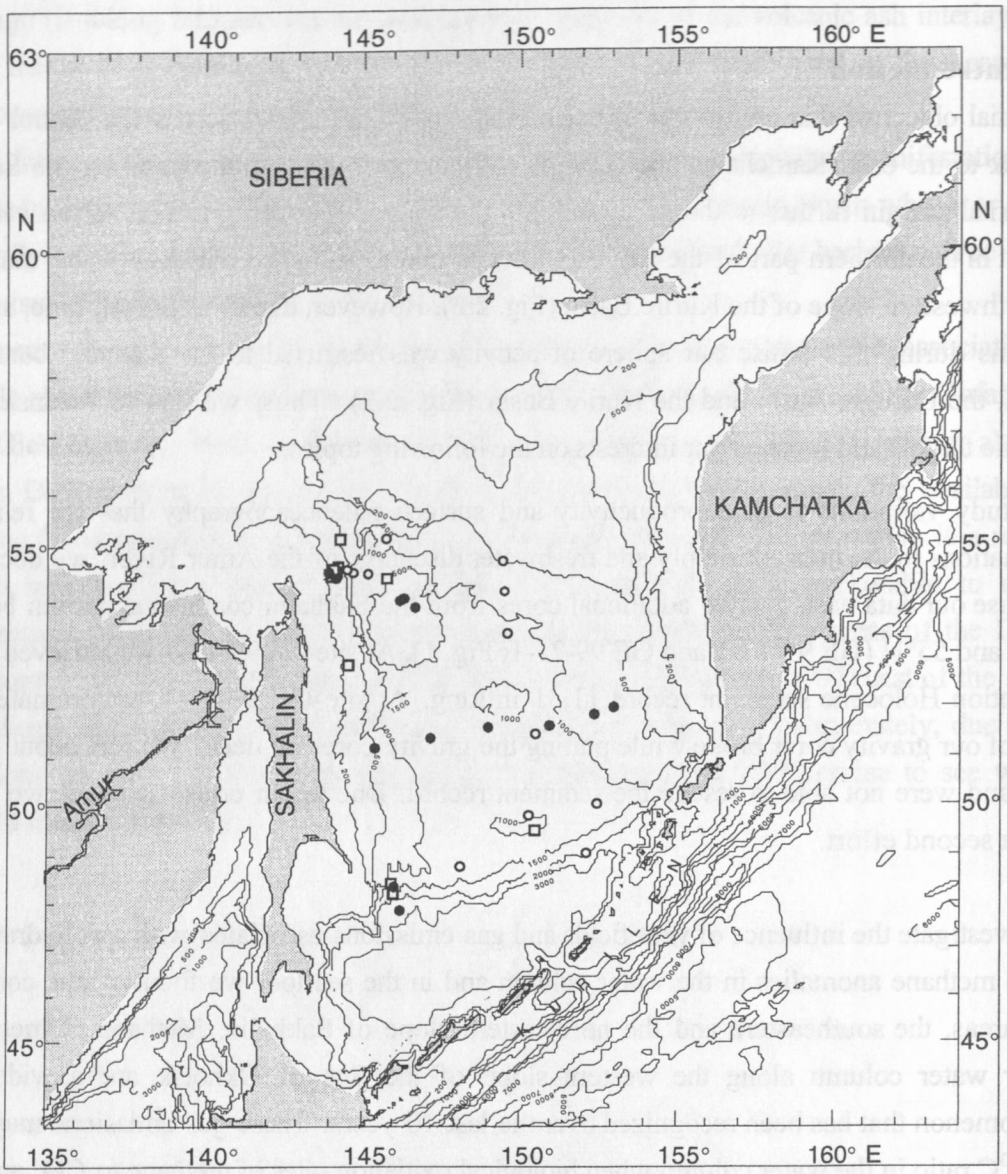

Fig. 12.1: Location map of paleoceanographic sites: Cores from cruise LV 27 (open circles), cruise LV 28 (filled circles), cruise GE99 (filled squares).

At the northeastern Sakhalin slope, we placed three cores (GE 99-24-2, GE 99-27-2, GE 99-29-3) into the center of the Obzhirov Flare (Fig. 12.1). This area of increased outgassing has already been observed during LV 28 and is characterized by methane concentrations of up to 1 - 2.5 µl/l. Two sediment records (GE 99-24-2 and GE 99-29-3) revealed considerable amounts of gas hydrates below 2 m sub-bottom depth. These records are expected to reflect the extent of modern $\delta^{13}C$ anomalies in the bottom water that is caused by methane oxidation. Another core (GE99-26-2) outside the gas hydrate field will be used to quantify the "normal

background signal" for methane in the water column. The frequent occurrence of the bivalves *Calyptogena* and *Solemya* throughout the sediment records will permit precise ^{14}C age control.

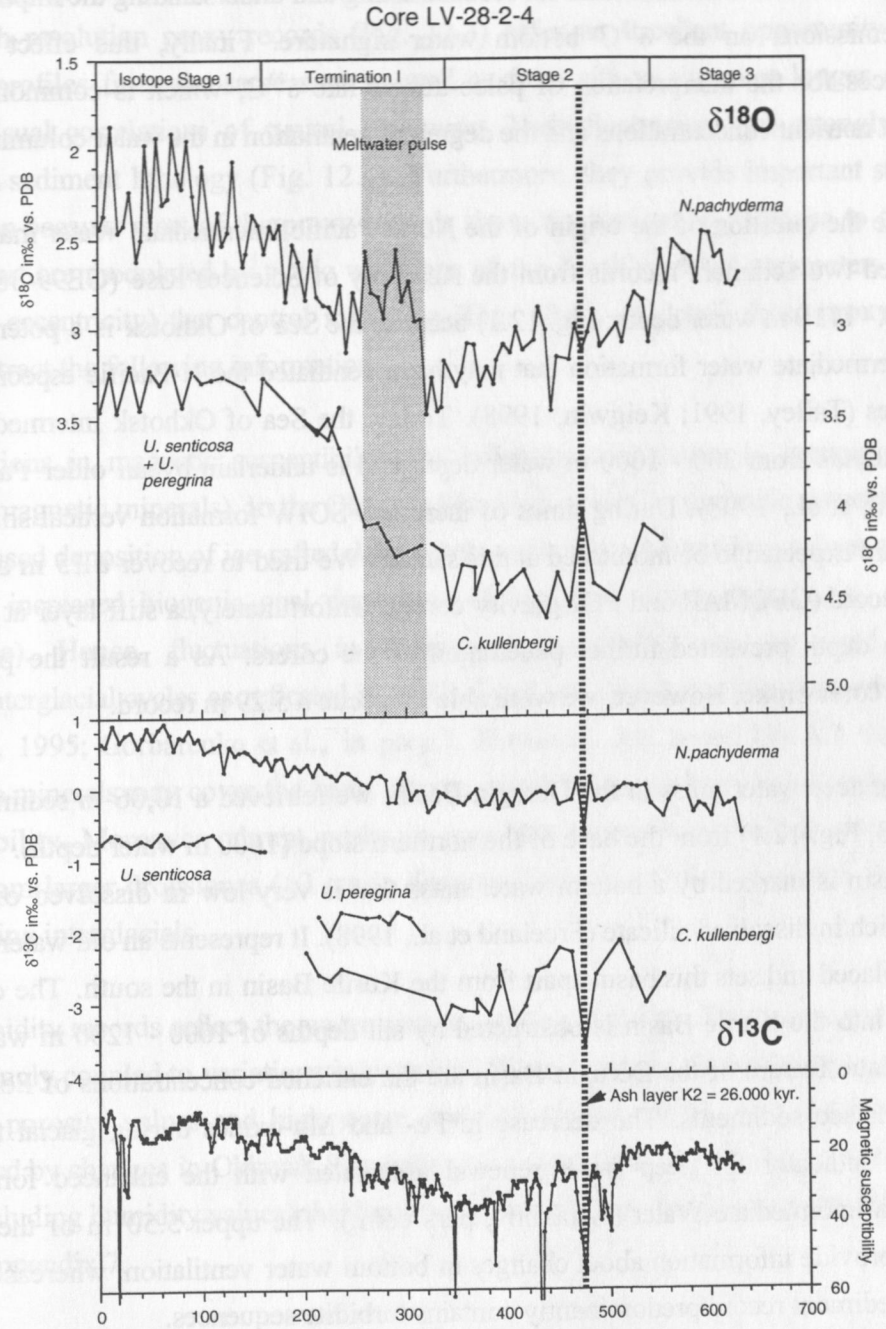

Fig. 12.2: *Summary of $\delta^{18}O$ and $\delta^{13}C$ records from planktonic (N. pachyderma), benthic (U. senticosa, U. peregrina) and epibenthic (C. kullenbergi) foraminifers. The structures of the $\delta^{18}O$ isotope records indicate isotope stages 1-3 as well as Termination I. The occurrence of ash layer K2 (26 ka) provides an additional age control point. The planktonic $\delta^{18}O$ record is marked by a $\delta^{18}O$ decrease of about 1 ‰ at the beginning of Termination I and suggests a meltwater pulse in the Sea of Okhotsk or an increased freshwater discharge of the Amur River. Extremely low epibenthic $\delta^{13}C$ values mark the last glacial and the beginning of Termination I. Such low values imply that methane ($\delta^{13}C$ = up to -60 ‰) may play a major role as a carbon source via oxidation.*

In summary, this set of sediment records from the southeastern and the northeastern Sakhalin slopes will provide an excellent opportunity to study the influence of modern outgassing into the water column and is fundamental for reconstructing and understanding the impact of paleo-methane emissions on the $\delta^{13}C$ bottom water signature. Finally, this effect may have consequences for the interpretation of paleo-tracers like $\delta^{13}C$, which is commonly used to reconstruct nutrient concentrations and the degree of ventilation in the water column.

- To examine the question of the origin of the North Pacific Intermediate Water mass (NPIW) we retrieved two sediment records from the Academy of Sciences Rise (GE99-38-2; GE99-38-5; 1080 - 1110 m water depth; Fig. 12.1) because the Sea of Okhotsk is a potential source area of intermediate water formation that may have ventilated the N-Pacific especially during glacial times (Talley, 1991; Keigwin, 1998). Today, the Sea of Okhotsk Intermediate Water (SOIW) extends from 200 - 1000 m water depth and is underlain by an older Pacific water mass (Wong et al., 1998). During times of increased SOIW formation vertical shifts of this boundary are expected to be monitored at this station. We tried to recover a 15 m and a 13 m sediment record (GEOMAR and POI gravity corer). Unfortunately, a stiff layer at about 6 m sub-bottom depth prevented further penetration of the corers. As a result the pipe of the GEOMAR corer broke. However, we were able to rescue a 5.29 m record.

- To study the deep water mass in the Derugin Basin, we retrieved a 10,06 m sediment record (GE99-31-3, Fig. 12.1) from the base of the northern slope (1600 m water depth). Today, the Derugin Basin is marked by a bottom water mass that is very low in dissolved oxygen and extremely rich in dissolved silicate (Freeland et al., 1998). It represents an old water mass that is rarely replaced and sets this basin apart from the Kurile Basin in the south. The outflow of deep water into the Kurile Basin is obstructed by sill depths of 1000 - 1200 m water depth. Another unique feature of the Derugin Basin are the enriched concentrations of Fe- and Mn-oxides in surface sediments. The decrease in Fe- and Mn-oxides during glacial times may serve as an indicator for deep water renewal associated with the enhanced formation of Okhotsk Sea Intermediate Water (Astakhov, pers com.). The upper 5.50 m of the sediment record will provide information about changes in bottom water ventilation, whereas the lower part of the sediment record predominantly contains turbidite sequences.

- To complement our set of surface sediment samples and to receive an undisturbed profile of the upper sediment record (0 - 30 cm) we used the minicorer or multicorer equipment at nearly each station.

For our paleoceanographic investigations, we successfully recovered 11 cores from 7 site locations. The total recovery of these sediments amounts to 76.59 m.

12.2. Core logging

The core logging includes the measurement of sediment color spectra (one data point every cm), magnetic susceptibility and humidity (one data point every second cm; see also Appendix 7. These high resolution proxy records (Fig. 12.3) offer an excellent opportunity to compare sediment profiles from the same sites as well as from site to site over longer distances by detailed visual correlations of typical structures. Their fluctuations are strongly coupled to changes in sediment lithology (Fig. 12.4). Furthermore, they provide important stratigraphical information because most of the proxy records show fluctuations in response to cyclic climate changes that are modulated by cyclic variations of the Earth's orbital parameters (precession, obliquity, eccentricity) that control insolation (Fig. 12.4). In detail, these proxy records are used to extract the following information:

- Fluctuations in magnetic susceptibility are indicative of changes in terrigenous sediment supply (magnetic minerals). In the Okhotsk Sea, high values in magnetic susceptibility reflect an increased deposition of ice-rafted debris during glacials, whereas low values are associated with an increased biogenic opal deposition during peak warm stages (e.g. stage 5.5 or Holocene). Hence, fluctuations in magnetic susceptibility can be used to identify glacial/interglacial cycles as reflected in $\delta^{18}O$ global and regional climate records (Tiedemann & Haug, 1995; Gorbarenko et al., in prep.). However, ash layers like K2 that are rich in magnetic minerals may cover the basic climate signal by generating strong peaks in magnetic susceptibility. Moreover, abrupt peaks in magnetic susceptibility values occasionally also result from larger dropstones (>3 cm in diameter), which are more common during glacials than during interglacials.

- The humidity records reflect the water content of the sediments. Fluctuations in humidity are also strongly coupled to variations in porosity. Biogenic opal-rich sediments e.g. are marked by high porosity values and high water contents. Hence, fluctuations in humidity are also controlled by changes in Okhotsk Sea sediment composition. Additionally, physical property data (including humidity values) that have been measured on discrete samples are summarized in the Appendix 7.

- The color spectra of Okhotsk Sea sediment records have been determined with a simple colorimeter and described in the second CIE 1976 color space (L*a*b* color space). In general, L* values (lightness ranging from 0-100 %) are indicative of calcium carbonate for whitish color and of organic matter and/or dark minerals for blackish color (Nago & Nakashima, 1992; Mix et al., 1995). The a* values reflect the red-green chromaticness, whereas positive values correspond to red and negative values to green. In general, positive a* values are indicative of iron oxides and hydroxides. Fig. 12.4 also demonstrates that

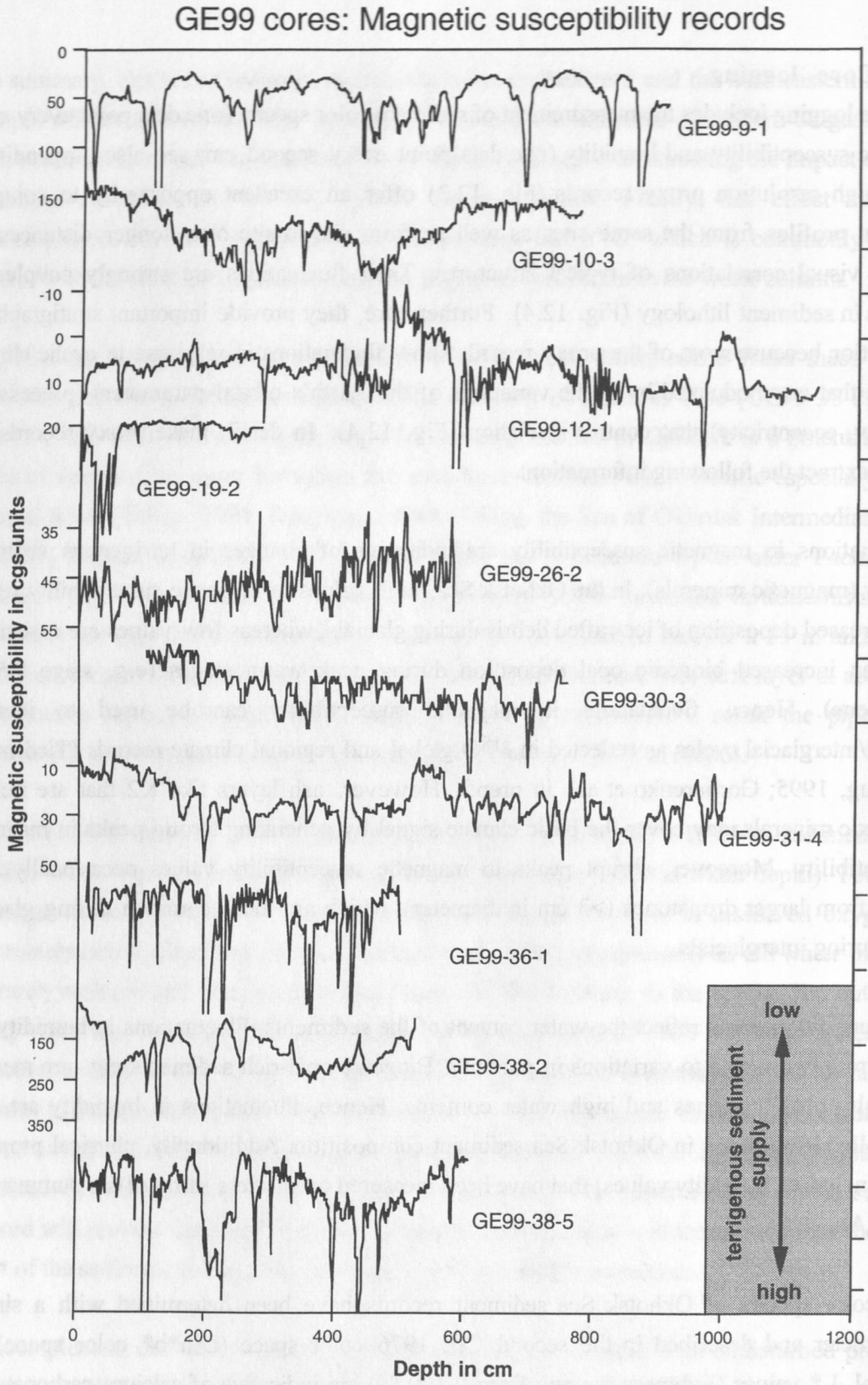

Fig. 12.3 (cont.): *Summary of core logging data: (A) magnetic susceptibility, (B) humidity, (C) lightness of reflectance spectra, (D) red-green chromaticness and (E) yellow-blue chromaticness of reflectance spectra.*

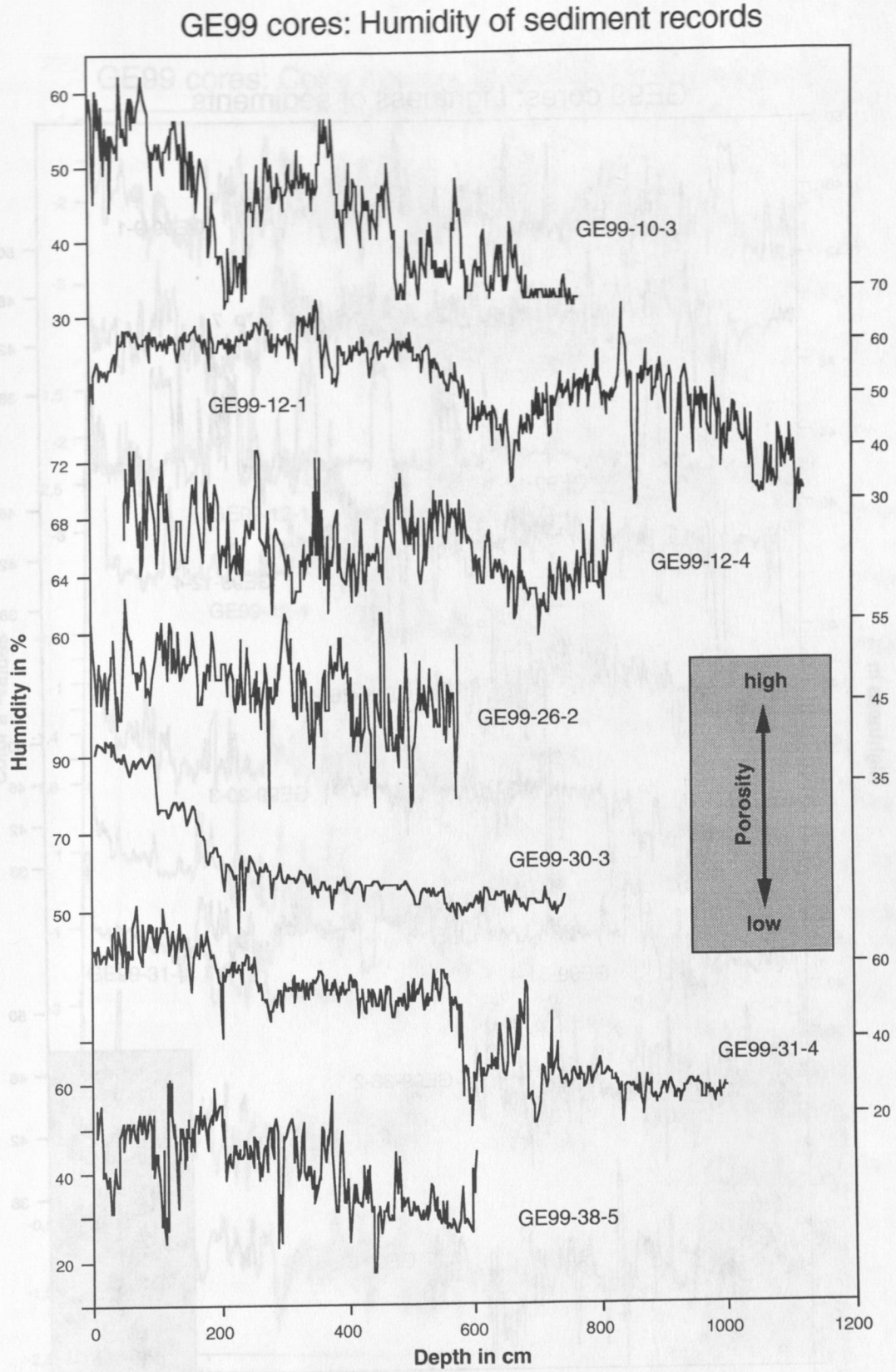

Fig. 12.3 (cont.): *Summary of core logging data: (A) magnetic susceptibility, (B) humidity, (C) lightness of reflectance spectra, (D) red-green chromaticness and (E) yellow-blue chromaticness of reflectance spectra.*

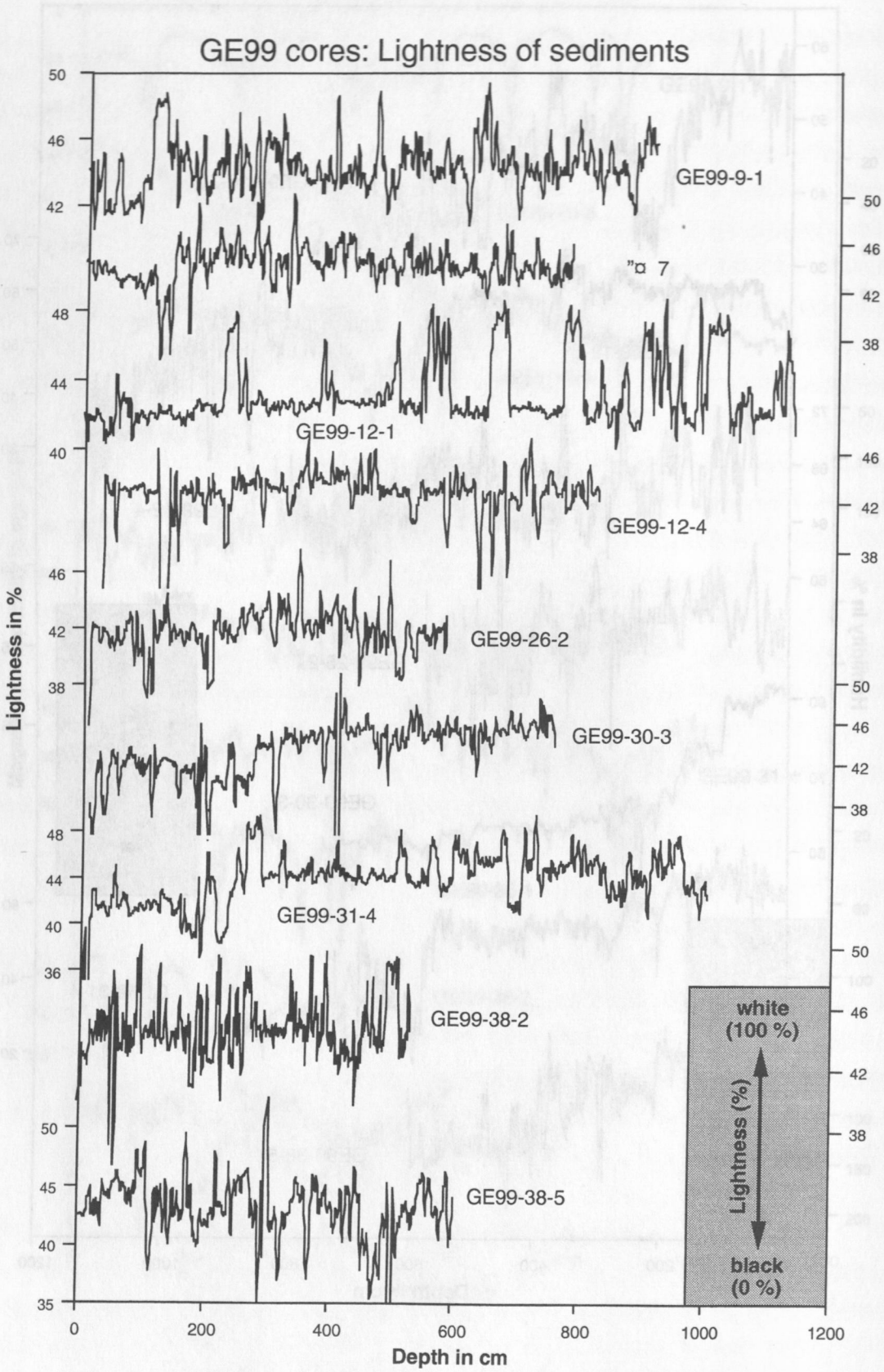

Fig. 12.3 (cont.): *Summary of core logging data: (A) magnetic susceptibility, (B) humidity, (C) lightness of reflectance spectra, (D) red-green chromaticness and (E) yellow-blue chromaticness of reflectance spectra.*

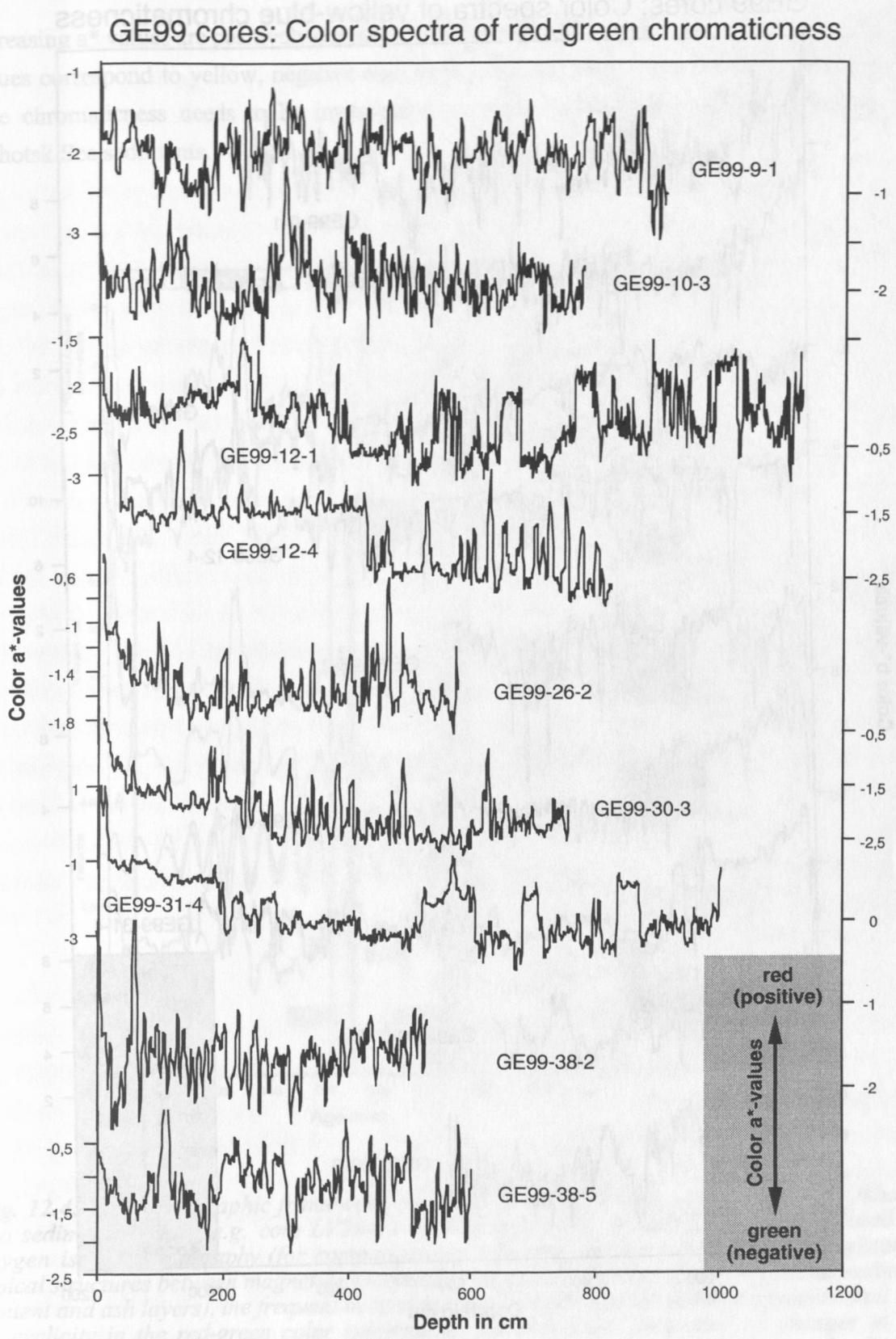

Fig. 12.3 (cont.): *Summary of core logging data: (A) magnetic susceptibility, (B) humidity, (C) lightness of reflectance spectra, (D) red-green chromaticness and (E) yellow-blue chromaticness of reflectance spectra.*

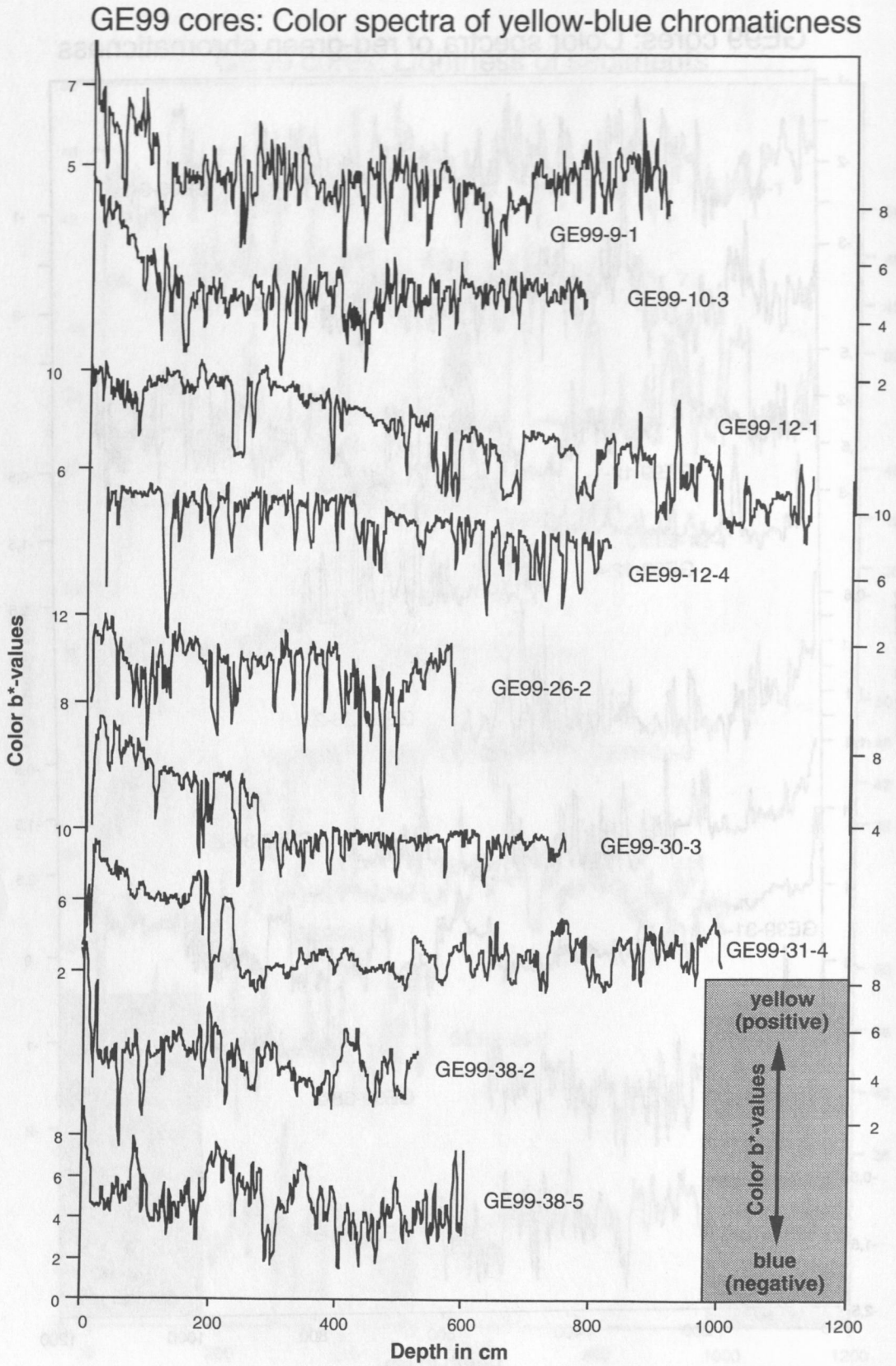

Fig. 12.3 (cont.): *Summary of core logging data: (A) magnetic susceptibility, (B) humidity, (C) lightness of reflectance spectra, (D) red-green chromaticness and (E) yellow-blue chromaticness of reflectance spectra.*

increasing a* values are positively correlated with increasing biogenic opal contents. Positive b* values correspond to yellow, negative ones to blue (Hunt, 1980). The validity of the yellow-blue chromaticness needs to be investigated by more detailed sedimentological studies on Okhotsk Sea sediments.

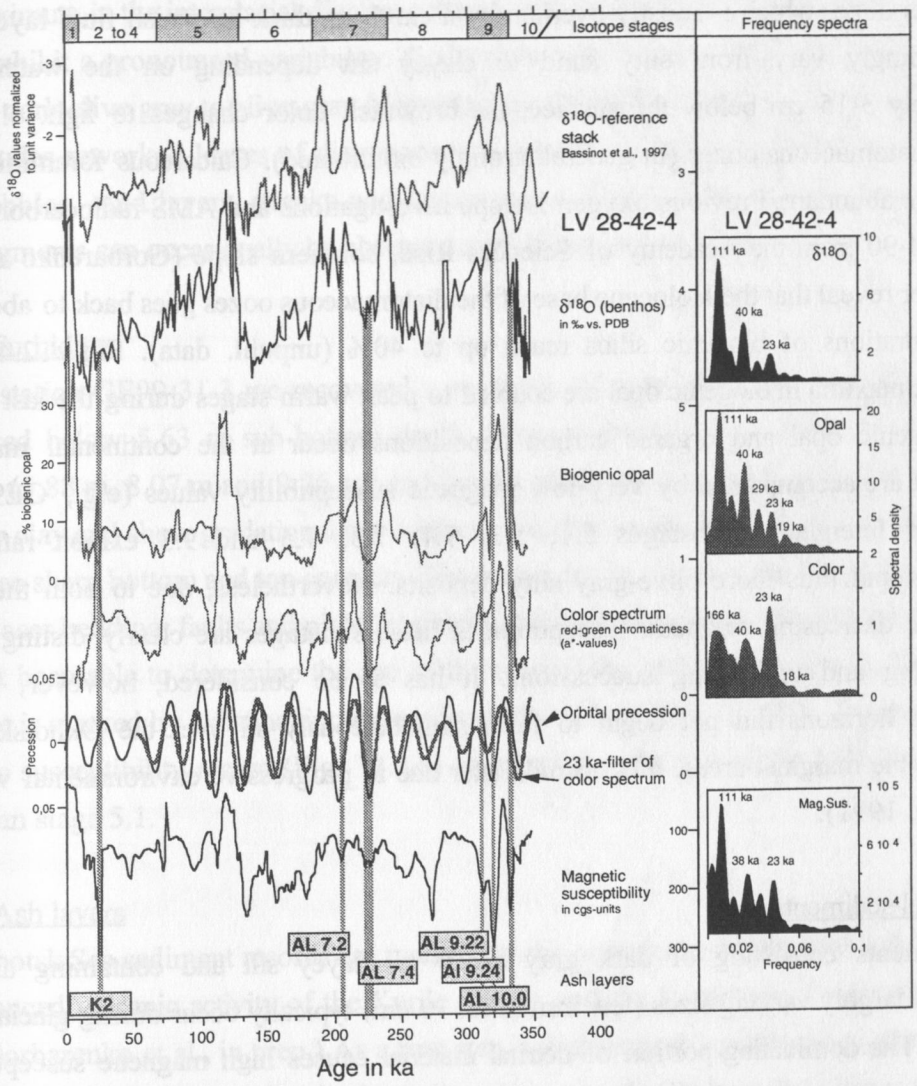

Fig. 12.4: *This stratigraphic framework covering the last 350 ka is used to date our Okhotsk Sea sediment records (e.g. core LV28-42-4). The age model of core LV28-42-4 is based on oxygen isotope stratigraphy (for comparison see reference isotope stack). The comparison of typical structures between magnetic susceptibility records (indicative of the terrigenous sediment content and ash layers), the frequent occurrence of ash layers and the dominant precessional 23-ka cyclicity in the red-green color spectrum of the sediments (indicative of changes in the biogenic opal content) allows a detailed correlation of sediment records across the Sea of Okhotsk, and thus, a transfer of age control points. The frequency spectra of the different proxy data indicate dominant cyclicities of 100 ka, 41 ka, 23 ka and 19 ka as a response to cyclic fluctuations in the Earth's orbital parameters eccentricity, obliquity and precession. This result corroborates the accuracy of the age model.*

12.3 Lithological classification of sediments

The lithological core descriptions are summarized in the Appendix 7. In general, changes in the sediment composition follow typical structures that are controlled by climate variability.

12.3.1 Interglacial sediments

Wide parts of the Okhotsk Sea surface deposits commonly consist of a soft, brown diatomaceous ooze, which is mostly overlain by a ca. 1 cm thick brownish fluff layer. Grain sizes accordingly vary from silty sand to clayey silt depending on the water depth. Approximately 3-15 cm below the surface, the brownish color changes to light olive gray typical for diatomaceous oozes (in general strongly bioturbated). Calcareous foraminifera and coccoliths are abundant. Previous oxygen isotope investigations and AMS-radiocarbon datings on Core B34-90 from the Academy of Sciences Rise, southern slope (Gorbarenko et al., in press), further reveal that the Holocene base of the diatomaceous oozes goes back to about 6 ky BP. Concentrations of biogenic silica reach up to 40% (unpubl. data). Fig. 12.4 clearly indicates that maxima in biogenic opal are coupled to peak warm stages during the last 350 ka. Highest biogenic opal and organic carbon depositions occur at the continental margin of Sakhalin and are accompanied by very low magnetic susceptibility values (e.g., GE99-12-1; Fig. 12.3A). Interglacial substages 5.1, 5.3, 7.1, 7.3, 7.5 and 9.3 exhibit rather less diatomaceous and thus more olive-gray silty deposits. Nevertheless, due to both their olive color and the decreasing magnetic susceptibilities these substages are clearly distinguishable from overlying and underlying successions. It has to be considered, however, that the diatomaceous horizons did not begin to form simultaneously all over the Okhotsk Basin. Especially in the marginal areas, they formed later due to progressive environmental warming (Gorbarenko, 1991).

12.3.2 Glacial sediments

Glacial sediments consisting of dark gray sandy to clayey silt and containing abundant dropstones of largely varying sizes (few mm to ca. 10 cm) typically occur during glacial stages 2, 6, and 8. The dominating portion of detrital material causes high magnetic susceptibilities partly enhanced by the significant influence of coarse ice-rafted dropstones. Calcareous shell fragments occur but are rare. Opal concentrations decline below 10% (unpubl. data). Greenish diagenetic horizons are characteristic for the glacial deposits and may be related to the formation of authigenic clays (hydrotroillite).

Distinct variations in the coarse fraction (sand, pebbles), magnetic susceptibility values, and slightly varying carbonate and opal concentrations in these deposits suggest short but severe environmental changes even during glacial times.

12.3.3 Transitional sediments

The transition from peak glacial to peak interglacial climatic conditions is reflected in a "transitional type" of sediment characteristic for oxygen isotope stages 3, 4, stadials and interstadials (best seen in cores GE99-9-1, GE99-10-3, GE99-38-5; see Appendix 7). It is dominated by terrigenous components, although the diatom concentrations may gradually increase from cool (poor to weakly diatomaceous) to warm periods (diatomaceous), reaching their maximum in the interglacial diatomaceous oozes. Accordingly, the magnetic susceptibility values exhibit a pronounced variability. Grain sizes vary between sandy silt and clayey sandy silt. The dark olive gray to olive-gray (dependent on the opal content) sediment is homogenous and includes reworked lenses of diatomaceous ooze due to strong bioturbation. Occasionally, small pebbles, sand layers, streaks and lenses occur. Foraminifers are common, and calcitic shell fragments can occasionally be observed even in deeper core segments.

12.3.4 Turbidites

Only at station GE99-31-3 we recovered a sequence of turbidites. Four turbidites have been recognized below 5.63 m sub-bottom depth. Three turbidites are marked by sharp bottom contacts (5.88 m, 8.07 m and 9.76 m) and have a sandy layer at the bottom that fines upward into silty clay and show gradational top contacts. Another sandy turbidite occurs at 8.06 - 8.07 m and has sharp bottom and top contacts. The sequences in between the turbidites contain mud clasts, flaser bedding, faults and plant fragments and thus seem also to be allochton. So far, we have not been able to determine the age of the base of the turbidite sequence. The top of the sequence is marked by a distinct increase in humidity values (Fig. 12.3B). The structure of the magnetic susceptibility record (Fig. 12.3A) suggests that the top of the turbidite sequence is older than stage 5.1.

12.3.5 Ash layers

The Okhotsk Sea sediment records are marked by the occurrence of different ash layers due to the enhanced volcanic activity of the Kurile Islands and the Kamchatka Peninsula (Braytseva, 1996; Gorbarenko et al., in prep.).As a first step, mineralogical investigations allow to identify and to distinguish volcanic ashes in the sedimentary records (Biebow & Hütten, 1999). Based on the results of radiocarbon dating (Gorbarenko et al., in press) and oxygen isotope stratigraphy (Fig. 12.4), reliable information on the stratigraphic position and the age of fresh volcanic ash layers already exist. So far, the KOMEX work group has been able to distinguish between the following ash layers:

- K0 and TR (8.3 ka), K2 (26 ka), Spfa (32- 35 ka), K3 (60 - 70 ka), AL 7.2A (ca. 201 ka), AL 7.2B (ca. 206 ka), AL 7.4 (ca. 229 ka), AL 9.22 (ca. 311 ka), AL 9.24 (ca. 316 ka) and AL 10.0 (ca. 330 ka).

Analyses of ash deposits (ashes TR, K2 and K3) that have been recovered on previous cruises were analyzed at GEOMAR for their major element composition and volatile contents using fresh glass particles. The most important results are plotted in Fig. 12.5. The TAS-Diagram according to Le Maitre (1989) suggests a rhyolitic composition for all ash layers. However, these ash layers can be clearly distinguished by their element composition. The most significant difference between these ashes is the varying concentration of the main element potassium (Fig. 12.5). The ash layer K2 has a potassium content between 2.42 - 2.84 wt % ("medium-K-series"). The highest potassium concentrations mark ash layer K3 ("high-K-series", about 5%). The TR ash has the lowest potassium contents ("low- K-series", about 1%). Other important components that can be used to distinguish between these ash layers are TiO_2 (Fig. 12.5) and FeO.

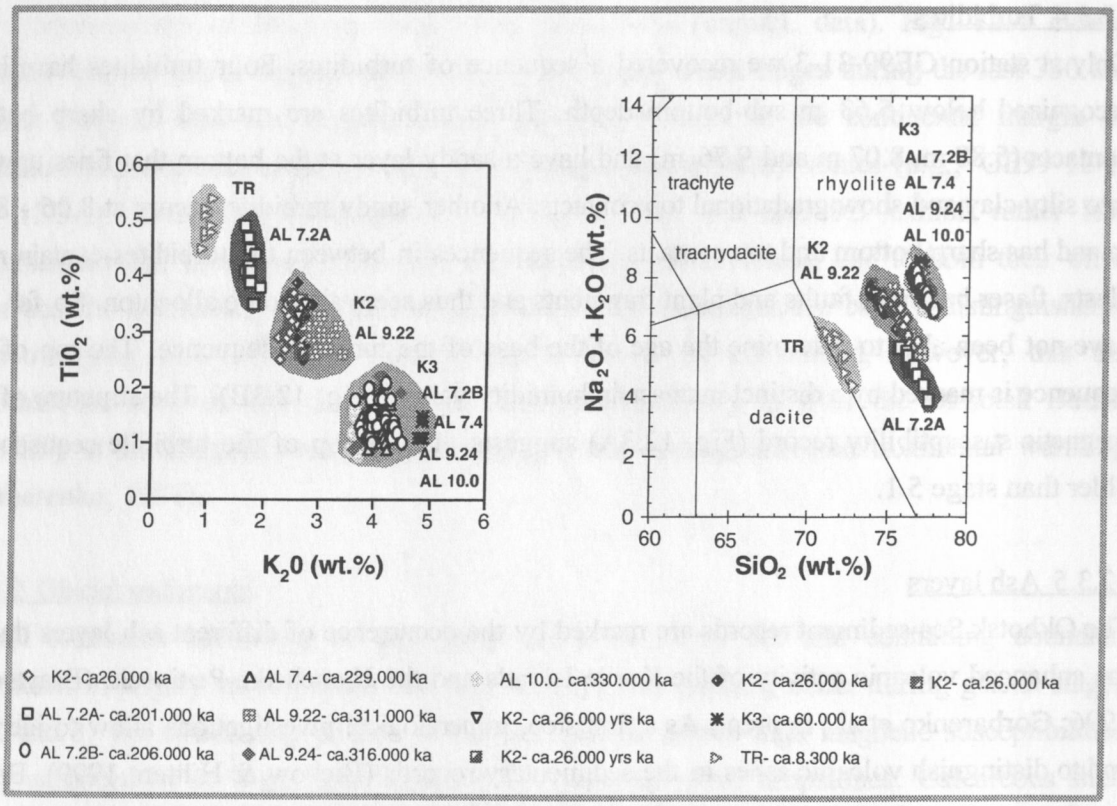

Fig. 12.5: Classification of the glass components of tephra from cores that were recovered during LV cruises 27 and 28 (right) and distribution pattern of TiO_2 vs. K_2O of the glass components (left).

All ash layers that have been found in the sediment records of Gelovany cruise are summarized in Table 12.1. So far, only a few ash layers have permitted reliable identification, especially the occurrence of K2 and K3.

Tab. 12.1: *Summary of ash layers found in GE99-sediment records.*

Core	Depth interval		Ash
	Ash layer	Lenses of ash	
GE99-9-1		784 cm (reddish-gray)	K2 ?
GE99-10-3		279 cm	K2 ?
		630 cm	?
GE99-32-2	371-372 cm (reddish-gray)		K2
GE99-36-1	151-152 cm		K2
GE99-38-2	52-61 cm (gray)		K3
	200-203 cm (reddish)		?
		298 (reddish)	?
GE99-38-5	104-120 cm (gray)		K 3
		225-226 cm	?
		272-274 cm	?
	402-405 cm (gray)		?

12.4. Stratigraphy

We combined the results from tephrachronology, lithostratigraphy, cyclic changes in magnetic susceptibility and color spectra and developed a stratigraphic framework of age control points to date our sediment records (Fig. 12.4). As a first step, typical structures in the magnetic susceptibility curves and typical patterns of lithological changes are used to construct a detailed depth correlation between the sediment records. This allows a quick transfer of age control points from dated reference records (LV28-2, LV28-42) to other records. Additional stratigraphic information is provided by identifying the major ash layers (Tab. 12.1) Their ages are based on present results from Okhotsk Sea sediment records that include ^{14}C-ages and oxygen isotope stratigraphy (Fig. 12.2 and 12.4) to date typical structures in the records of magnetic susceptibility and color spectra. Glacial-interglacial isotope stages are identified by cyclic changes in the magnetic susceptibility and color spectra records that result from 100 kyr, 41-kyr and 23-kyr-rhythms in climate due to changes in axial tilt and orbital precession, respectively. These glacial/interglacial changes are also characterized by distinct changes in lithology. This stratigraphic framework of age control points suggests that two sediment records (GE99-38-2 and GE99-38-5) from the Academy of Sciences Rise may extend back into stage 11 (ca. 400 kyr.) although the core recovery did not exceed 6.11 m. This region is marked by low sedimentation rates due to the elevated relief and low rates in terrigenous sediment supply. The proposed stratigraphy (Fig. 12.6) is based on changes in sediment composition, the occurrence of ash layers (Tab. 12.1) and the variability of magnetic susceptibility, humidity and color reflectance data. The changes in the sediment composition

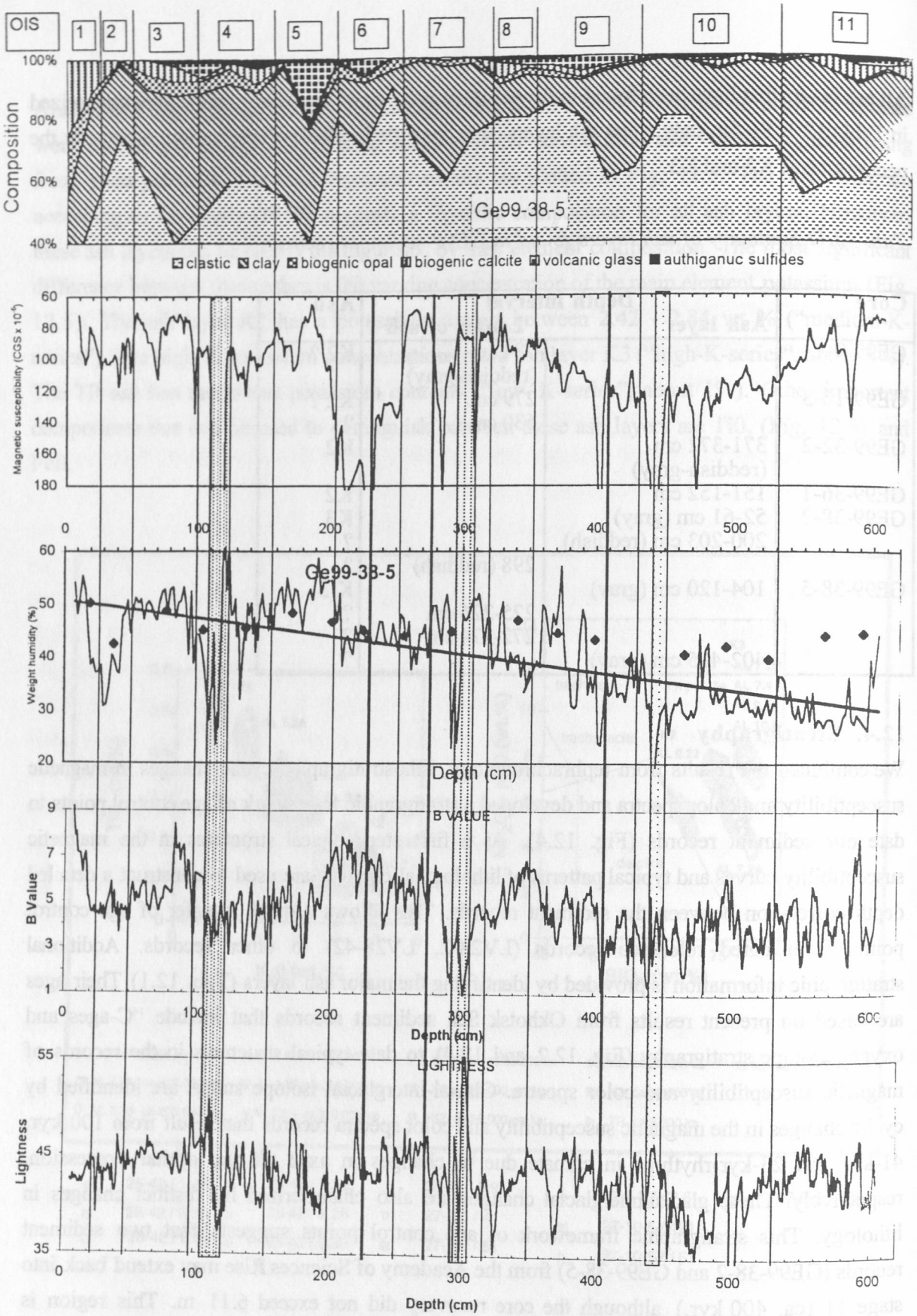

Fig. 12.6: *Proposed stratigraphy of core GE99-38-5. The figures from top to base represent: sediment composition (based on smear slide data, magnetic susceptibility, humidity, color b*value and lightness). Proposed boundaries of isotope stages are marked by thin lines. Thicker lines indicate ash layers. Stippled areas at 104-120 cm, 291-306 cm, 442-447 cm reflect ash layer K3, the diagenetic horizon and a sand layer, respectively.*

from biogenically enriched sediments (low magnetic susceptibility and high humidity values) to coarser and higher siliciclastic sediments (high magnetic susceptibility and low humidity values) are believed to reflect interglacial to glacial climate variations (Fig. 12.6). Moreover, diagenetic alterations that occur as stiff green layers enriched in smectite (47-49, 62-72, 77-79, 98, 133, 260-270, 425-427 and 454-456 cm) are marked by strong changes in color reflectance and decreases in magnetic susceptibility values. The strongest change occurs at 291-306 cm (Fig. 12.6). The decrease in magnetic susceptibility values may result from magnetic minerals that were diagenetically transformed into weak magnetic sulfides. The ash layer at 104 - 120 cm is characterized by coarse siliciclastic grain sizes of 0.1-3 mm and most likely reflects the ash layer K3 (60-70 ka). The most valid part of the stratigraphy is limited to the upper 200 cm clearly reflecting MIS 1-5. The oldest ashes may represent one of the known ash layers that occur in stage 7 (AL 7.2 or AL 7.4) and 9 (Al 9.22 or AL 9.24).

No detailed age model has been developed for the sediment profiles from sites GE99-12 at the upper slope off Sakhalin yet. In cores GE99-12-1 and GE99-12-4 the magnetic susceptibility record is characterized by extremely low values and small amplitude fluctuations (Fig. 12.3A). On the one hand, this may result from sulfate reduction. On the other hand, most of the sediment record consists of diamagnetic diatomaceous ooze. Hence, the persistently high biogenic opal contents suggest a high resolution Holocene record (younger than 10 kyr) with sedimentation rates higher than 1 m/kyr. According to Gorbarenko et al. (1998) and Gorbarenko et al. (in press), the Holocene variability in biogenic opal that can be monitored by changes in humidity can be used to develop a more detailed preliminary age model for the Holocene as shown in Fig. 12.7:

- 6 - 4.5 ka; beginning of strong diatom accumulation
- 4.5 - 3.5 ka; decrease in diatom accumulation
- 3.5 - 2.7 ka; maximum in opal accumulation
- 2.7.- 1.5 ka; decrease in opal accumulation
- 1.5 - present; increase in opal accumulation

According to Gorbarenko et al. (1998) and Gorbarenko et al. (in press), ^{14}C-dated records of magnetic susceptibility, humidity, biogenic opal and carbonate from the Sea of Okhotsk allow to provide a preliminary age model for the records from the Derugin Basin (GE99-30-3; GE99-31-4).
The carbonate peaks at 120 cm (GE99-30-3) and 180 cm (GE99-31-4) typically occur at Termination 1A at 12 ka. The following monotonous stiff clayey silt layer extends to approx. 600 cm in core GE99-30–3 (520 cm in core GE99-31-4) most likely reflects MIS 2-3 (Fig. 12.8, see core description). The high magnetic susceptibility values at 240 - 380 cm in core

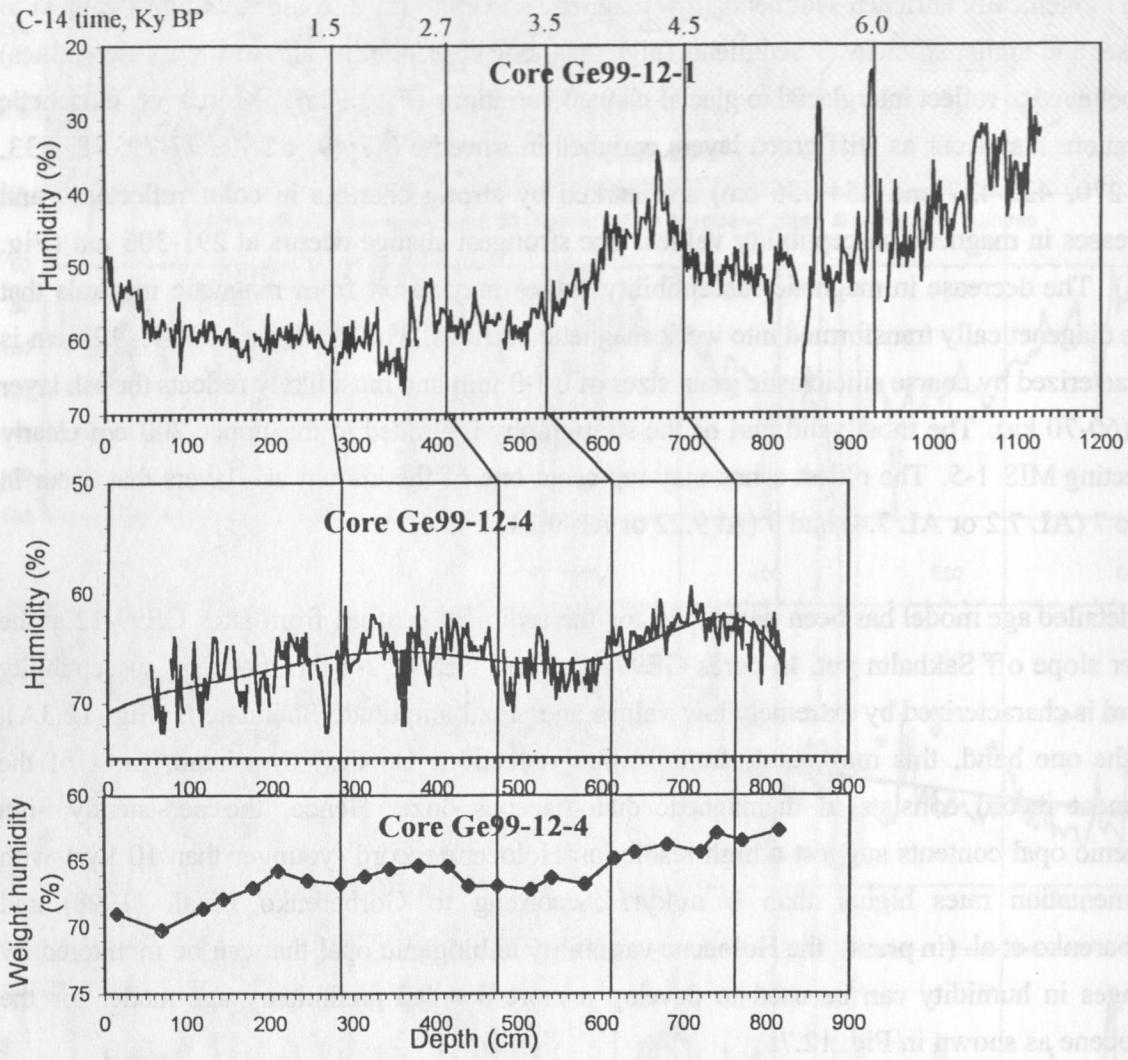

Fig. 12.7: *Proposed age model of core GE99-12-1 and its correlation to core GE99-12-4 using humidity records. The lower figure shows values of discrete samples for core GE99-12-4. Vertical lines give proposed ^{14}C age control points for changes in opal contents.*

GE99-30-3 reflect isotope stage 2. The low sea level during glacial stage 2 shifted the Amur delta more to the east and thus closer to the Derugin Basin; this may have resulted in an increased supply of terrigenous magnetic minerals to sites GE99-30-3 and GE99-31-4. The older sediment section is marked by the frequent occurrence of turbidites (see chapter 12.3.4) and prevents further age control.

So far no age model has been developed for the "gas hydrate stations" around the Obzhirov Flare (GE 99-24-2, GE 99-26-2, GE 99-27-2, GE 99-29-3) because ash layers are not present and our proxy records allow no clear identification of typical structures that can be dated.

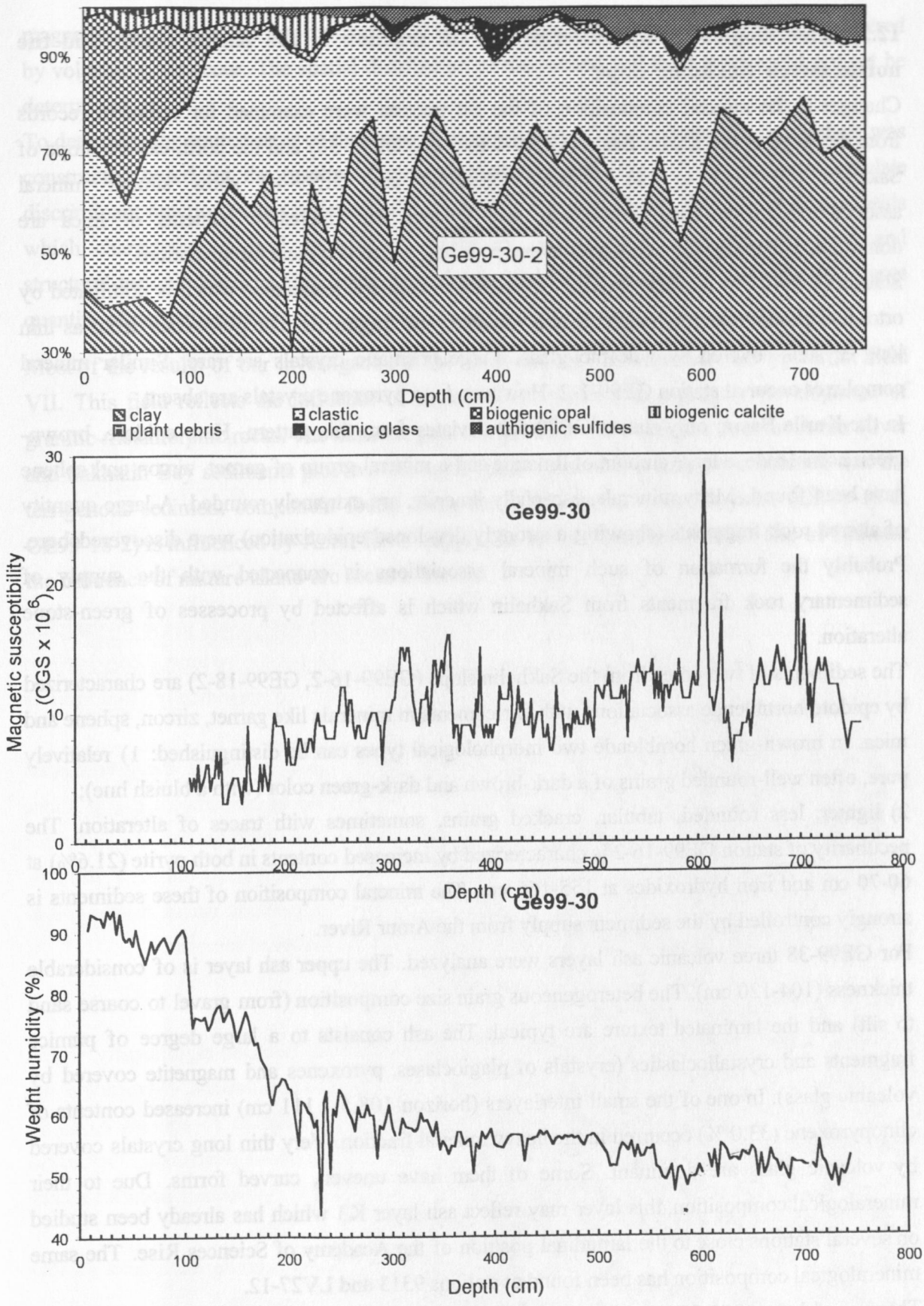

Fig. 12.8: *Records of changes in sediment composition, magnetic susceptibility and humidity in core GE99-30-3.*

12.5. Mineralogical composition of the silt fraction in the Kurile Basin and the northeastern Sakhalin slope

Changes in the mineral composition of the silt fraction were examined for sediment records from the slope of the Kurile Basin (GE99-1 to 6 and GE99-38) and the north-eastern slope of Sakhalin (GE99-12 to 18). Stations GE99-2-1 and GE99-4-1 show similar mineral associations: brown-green hornblende and epidote with increased contents of mica are dominant. The mica is severely altered and rounded, which is typical for all stations.

Station GE99-6-3 is characterized by a volcanogenic mineral association which is dominated by orto- and clinopyroxenes, magnetite and volcanic rock fragments. The pyroxenes occur as thin long crystals covered by volcanic glass. Large prismatic crystals are rare. Similar mineral complexes occur at station GE99-1-2. However, long pyroxene crystals are absent.

In the Kurile Basin, only station GE99-5-2 deviates from this pattern. Here epidote, brown-green hornblende, a large amount of ilmenite and a mineral group of garnet, zircon and sphene have been found. Many minerals, especially ilmenite, are extremely rounded. A large quantity of altered rock fragments (showing a strongly developed epidotization) were discovered here. Probably the formation of such mineral associations is connected with the supply of sedimentary rock fragments from Sakhalin which is affected by processes of green-stone alteration.

The sediments of two cores from the Sakhalin slope (GE99-16-2, GE99-18-2) are characterized by epidote-hornblende associations with enrichments in minerals like garnet, zircon, sphene and mica. In brown-green hornblende two morphological types can be distinguished: 1) relatively pure, often well-rounded grains of a dark-brown and dark-green color (with a bluish hue);

2) lighter, less rounded, tabular, cracked grains, sometimes with traces of alteration. The peculiarity of station GE99-16-2 is characterized by increased contents in both pyrite (21.6%) at 60-70 cm and iron hydroxides at 155-165 cm. The mineral composition of these sediments is strongly controlled by the sediment supply from the Amur River.

For GE99-38 three volcanic ash layers were analyzed. The upper ash layer is of considerable thickness (104-120 cm). The heterogeneous grain size composition (from gravel to coarse sand to silt) and the laminated texture are typical. The ash consists to a large degree of pumice fragments and crystalloclastics (crystals of plagioclases, pyroxenes and magnetite covered by volcanic glass). In one of the small interlayers (horizon 108.5 - 111 cm) increased contents of clinopyroxene (33.0 %) occurred in the heavy mineral fraction. Very thin long crystals covered by volcanic glass are dominant. Some of them have uneven, curved forms. Due to their mineralogical composition, this layer may reflect ash layer K3 which has already been studied on several stations close to the latitudinal position of the Academy of Sciences Rise. The same mineralogical composition has been found at stations 9313 and LV27-12.

The second layer (272-274 cm) is characterized by pyroxenes of other forms than mentioned above. It consists of large pure, angular grains or large prismatic long crystals, covered by volcanic glass. The third ash horizon (402-405 cm) is characterized by a dominance of

magnetite (41.85 %) and ortopyroxene (30.03 %). Large prismatic elongated crystals covered by volcanic glass occur. The spatial distribution of the second and third layer could not yet be determined.

To determine the source areas of the mineral supply a plot of discriminant function values was constructed based on the results of mineralogical analyses (Fig. 12.5). How to calculate discriminant function values is described in Biebow & Hütten (1999). This plot indicates fields which characterize mineral associations that mark provinces of different geological and structural-tectonic history. This fields were determined in the process of generalizing a large quantity of current material.

Most of the results of our investigation at the north-eastern Sakhalin coast are typical for field VII. This field reflects the influence of ancient folded belts with a primary development of granitic-metamorphic rocks. The mineralogical composition characteristics from the Amur River and Sakhalin Bay sediments plot into the same field. From this it may be concluded that the terrigenous sediment component found along the north-eastern Sakhalin coast (GE99-16-2, GE99-18-2) is influenced by Amur River supply. In the southern areas of the Sea of Okhotsk the influence of mature island-arc rocks is visible.

13 RADIOLARIANS IN SEDIMENT SURFACE LAYERS IN THE SEA OF OKHOTSK

D. Zasko

Surface sediments in the Okhotsk Sea contain a diverse fauna of radiolaria. The total radiolarian abundance corresponds to that in North Pacific sediments with relatively low radiolaria contents. Radiolarians from surface sediments (0-1 cm) have been studied at 10 stations.

13.1 Methods

Radiolarian assemblages were studied in surface sediment samples recovered from multicorer (MUC) and minicorer (MIC) deployments. All samples were sieved through a 50 micron sieve, organic particles were removed by hydrogen peroxide solution, and put on slides in Canada balsam. The slides were analyzed using a light microscope; 200-300 specimens per sample were counted.

13.2 Distribution of high rank taxa

More than 42 forms which belong to 9 groups (suborder, family) were found at the investigated stations, except for station GE99-4-2 (Appendix 8). At GE99-4-2 the sediment consisted of completely terrigenous material. Radiolarians and diatoms occurred episodically; foraminifers are lacking at this station.

Four groups (*Cyrtoidae*, *Spyroidae*, *Discoidea* and *Sphaeroidea)* dominate the investigated samples. The family *Cyrtoidae* is most abundant (33,3%-55,5%) in all samples except those from GE99-38-2. At this station the content of *Cyrtoidae* is low (6,8%) and the suborder *Discoidea* (fam. *Spongodiscidae*) constitutes the dominant group (67,6%). At the other stations, *Discoidea* are less abundant (6,7%-26,7%). The percentage of *Spyroidae* varies from 15% to 38,5% while *Sphaeroidea* - varies from 1,45% to 15,6% in the analyzed samples.

13.3 Species composition

The species composition of the radiolarian assemblages does not fluctuate significantly within the analyzed samples. Each assemblage contains 12 to 25 forms of radiolarians. *Cyrtoidae* is the most diverse group. 22 species of this family occur in the samples (6 to 15 species could be found at every station). The most abundant species are *Cycladophora davisiana, Pterocorys hirundo, Arachnocorys dubius, Pseudodictyophimus gracilipes. C. davisiana* occurs in each sample. The average percentage of this species varies from 21% to 35%.

The family *Spyroidae* is represented by only two species, *Acanthodesma micropora* (4,4%-25,3%) and *Tholospyris borealis* (5,9%-18,5%), but both occur frequently.

Five species of the suborder *Sphaeroidea* were recorded in all investigated samples. The most abundant species is *Cromyechinus borealis.*

The suborder *Discoidea* is represented by at least 6 species (fam. *Spongodiscidae*). *Spongotrochus gracialis* (3,3%-10,1%) and *Stilochlamidium venustum* (1,4%-9,7%) are most abundant.

Five different groups of radiolarians (*Larcoidea*, *Cannobotryoidae*, *Collosphaeridea*, *Prunoidea*, *Phaeodaria*) are less diverse. In each assemblage, only 1-2 species of these groups could be found.

It is known that some radiolarian species (*C. davisiana, T. borealis, Pseudocubus* spp., *Plagiacantha* spp., *Arachnocorys* spp.) from the Sea of Okhotsk show a very high morphological variability. In the investigated samples two forms of *C. davisiana*: „marine" and „typical" were recorded. *C. davisiana* forma "marina" occurs in all investigated samples. *C. davisiana* forma "typical" was found only at several stations.

13.4 Conclusions

1. In the investigated samples, three species (*Cycladophora davisiana, Tholospyris borealis, Acanthodesma micropora)* dominate the assemblage.
2. In terms of faunal composition, boreal species are the most significant. These species do not play a significant role in radiolarian assemblages of the North Pacific.
3. The relative abundance of radiolarians high taxa (suborder and family) in the Okhotsk Sea differs significantly from that in the Pacific Ocean. In the Pacific Ocean the predominant groups are *Cyrtoidae, Discoidea* and *Larcoidea*, while in the Okhotsk Sea *Cyrtoidae, Discoidea* and *Spyroidae* dominate the assemblages. A relative high abundance of *Spyroidae* is the most striking feature of the radiolarian assemblages in the Sea of Okhotsk.

14. PETROLOGY AND VOLCANOLOGY

R. Werner, I. Tararin, and E. Lelikov

14.1 Introduction

The aim of the volcanological and geochemical studies of volcanic rocks within the KOMEX project, analytical methods and an introduction to the regional geology (Kurile Basin, Kurile Island Arc) are given in Biebow & Hütten (1999), Tararin et al. (1999 b), Avdeiko & Volynets (1999) and Werner et al. (1999). The planned dredging sites on RV *Marshal Gelovany* comprised various submarine volcanic edifices mainly selected on the basis of the results of our volcanological, petrological and geochemical analyses of rocks collected on earlier KOMEX cruises (LV 27, LV 28) as well as from the sample collection of the Institute of Volcanic Geology and Geochemistry (Petropavlovsk-Kamchatsky). The initial objects of dredging during this cruise were

1) to extend our northern, central (Bussol Strait) and southern transects across the Kurile Island Arc as far as possible into the Kurile Basin in order to study the interaction and dependencies between crustal and mantle sources, petrogenetic processes as well as the type and amount of volatiles in the eruptive products in different plate tectonic environments (e.g., rear arc/back-arc vs. volcanic front). The dredging sites proposed were several submarine volcanoes west of Onekotan Island (northern transect), north-west of Simushir and Browton Islands (Bussol Strait transect) and north of Iturup Island (southern transect). These volcanoes are foothills of the Kurile Island Arc extending into the Kurile Basin and have not been sampled yet or the available material comprised predominantly rounded, most probably ice-rafted material.

2) to recover additional samples from the seamount in the eastern part in the Kurile Basin dredged on RV *Akademik Lavrentyev* cruises 27 and 28 (Tararin et al., 1999 a) and to identify and sample further submarine volcanic edifices in the Kurile Basin in order to reconstruct the origin and evolution of volcanism, basement and structure of the Kurile Basin.

3) to dredge and investigate pillow-like structures identified on slides taken during OFOS profiles in the Derugin Basin on LV28 cruise.

However, due to considerable time restrictions resulting among others from technical problems we had to omit the proposed sites north of the Bussol Strait and in the Derugin and Kurile Basins with exception of the seamount in the eastern part of the Kurile Basin. During dredging, fuel problems and weather conditions again forced us to significantly reduce our remaining program. We finally focused on the following sites:

* the seamount in the eastern part of the Kurile Basin in order to verify preliminary results of our volcanological, petrological and geochemical analyses of rocks from this volcano which may have important implications for the crustal structure and evolution of the Kurile Basin;

* the rear-arc volcano Obruchev south of the Bussol Strait to receive samples from the foothills of the Browton transverse zone which extends farthest to the north-west into the Kurile Basin. Obruchev volcano belongs to a group of three poorly known volcanoes which form a horse-shoe-shaped structure at the end of our Bussol Strait profile.
* the WNW-ESE trending Hydrographers Ridge north of Iturup Island to extend our southern transect further into the Kurile Basin.

14.2 Recovery of seafloor samples (dredging)

Sampling of volcanic and subvolcanic rocks in the Kurile Basin and of the Kurile Island Arc was carried out using a rectangular dredge (1.0 x 0.5 m) with a chain bag; barites in the Derugin Basin were sampled with a cylindrical dredge 50 cm in diameter. The dredges were operated with a steel by a stern winch and the A-frame. A RIKADENKI multi-pen recorder was used to detect bottom contact and bites of the dredge.

The dredge tracks were set in the areas where steep slopes with possible bedrock outcrops were identified by the detailed bathymetry and seismic reflection profiling obtained during RV *Akademik Lavrentyev* cruises 27 and 28 as well as by echosounding surveys during *Marshal Gelovany* cruise 99. Additionally, a detailed site survey was planned using swatch bathymetry mapping (see chapter 4). Due to bad weather conditions and time problems, however, swath bathymetry mapping was restricted to the seamount in the eastern part of the Kurile Basin. The location of dredge tracks was determined by the GPS system aboard the ship, the depth of the dredging sites was determined by the echosounder records.

Taking into account the widespread ice-rafted debris in the Sea of Okhotsk, detailed analysis of the obtained material was carried out to identify bedrocks. The criteria used for distinction include but are not restricted to a) shape of the samples (angular vs. well-rounded), b) existence of fresh surfaces formed by tearing away from the bedrock outcrops, c) homogeneity of the dredged material.

14.3 Results

Due to technical, fuel, weather and time problems dredging during *Marshal Gelovany* cruise 99 was restricted to five dredges and subsequent petrological analyses at 2 sites in the rear-arc region of the Kurile Island Arc (Iturup area, Browton transversal zone) and at the seamount in the eastern part of the Kurile Basin (Fig 14.1, see also chapter 2, Appendix 1). Additionally, dredging of barites was carried out at one site in the Derugin Basin.

14.3.1 The seamount in the eastern part of the Kurile Basin

An introduction to the geological setting of the Kurile Basin is given in Tararin et al. (1999 a). The seamount in the eastern part of the Kurile Basin has first been dredged on *Akademik Lavrentyev* cruises 27 and 28. Its structure and geology including mineralogical and

geochemical data available at this time (major and some trace elements) has been described in some detail in Tararin et al. (1999 a) and Nürnberg et al. (1997).

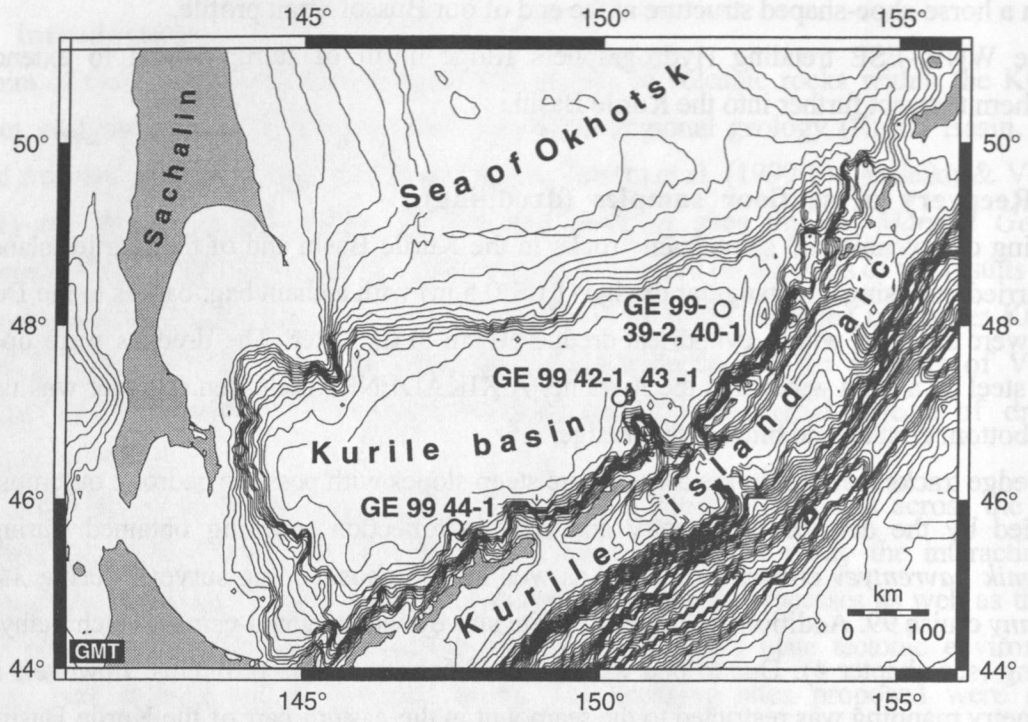

Fig. 14.1. Map showing sites dredged during Marshal Gelovany cruise 99 in the Kurile Basin and in the rear-arc region of the Kurile Island Arc.

Our preliminary results of the volcanological, petrological and geochemical analyses of the rocks gained on LV 28 indicate that this seamount shows some special features. For example, the high vesicularity of the dredged rocks as well as low sulfur concentrations in matrix glasses (< 400 ppm; Werner, unpublished data) compared to high sulfur contents of melt inclusions (> 2000 ppm; Doubik, unpublished data) indicate volcanic activity in shallow water (< ca. 500 m) or subaerial conditions. Considering the available data for age determination of the volcano (K-Ar age: 0.9 and 1.6 Ma; Tararin et al., 1999) and the recent position of its top in ca. 2200 m b.s.l. (below sea level), our data may imply extremely high subsidence rates for the eastern part of the Kurile Basin. The Sr-Nd-Pb isotope ratios of most samples from this seamount fall into the range of the Kurile Island Arc volcanoes. They are very homogeneous and indicate a MORB (mid ocean ridge basalt)-like source for these magmas in the mantle wedge (Werner et al., 1999, Werner and Hoernle, unpublished data). Some basalts, however, differ significantly in their isotopic composition (higher $^{87}Sr/^{86}Sr$ [despite intense leaching], lower $^{143}Nd/^{144}Nd$ and varying Pb isotope ratios; Werner and Hoernle, unpublished data). These data could point to a sediment component in the melts or, more probably, to crustal contamination. The latter would be in agreement with the model proposing a continental crustal basement for the eastern part of the Kurile Basin (Tararin et al., 1999 a,b; Tararin, unpublished data).

These preliminary results suggest that detailed studies of the seamount in the eastern part of the Kurile Basin may provide important information on the crustal structure and evolution of the Kurile Basin. Additional samples, however, are required to verify our results and to get a better understanding of its melt generation and paleo-environment. Therefore we gave this volcano high priority in our reduced dredging program on GE99 cruise despite the lack of time.

A site survey by swath bathymetry mapping was planned before dredging to get detailed information on the structure of the volcano and to select the most promising locations for the dredge tracks. High waves and the water depth of the volcano of up to 3200 m b.s.l., however, led to difficulties with the mapping system. Nevertheless, the swath mapping yielded excellent data for the top area and the upper slopes of the volcano. Combined with the GPS and echosounding data gained on LV28 cruise, the processing of these data provided detailed maps and 3D-illustrations of the structure of the seamount (Fig. 4.10, see chapter 4).

Following the swath bathymetry mapping, two dredge tracks were carried out: GE99-39-2 from the upper eastern slope to the top of the volcano and GE99-40-1 from the lower western slope to the top (Fig. 4.10 A). Dredge GE99-40-1 probably did not touch the seafloor which was caused by the strong southward drift of the vessel, whereas dredge GE99-39-2 yielded ca. 100 kg of rocks and marine fauna. Beside sponges (see chapter 8) and dropstones (granite etc.) the majority of the dredged material consisted of highly hydrothermally altered basaltic and/or andesitic lava fragments. These fragments were broken off the surface of a sheet lava flow as indicated by completely palagonized, up to 3 cm thick glassy rims, which are covered by up to 4 cm thick manganese layers on some pieces. Fresh rock fragments recovered by this dredge comprised andesites, among them amphibole-pyroxene andesites and a breccia fragment consisting of andesitic blocks covered by manganese, porphyric plagioclase basalt, fine-grained biotite-amphibole diorite or gabbro, dacite and possibly felsite. Among others, the angular shape, the fresh surfaces and the frequent occurrence of manganese crusts as well as the similarity of some rocks (basalt, andesite) to rocks dredged on earlier cruises at this volcano supply evidence for an *in situ*-origin of these rocks fragments at the volcano. In particular, the broad spectrum of different rock types gained from dredge GE99-39-2 possibly enables us to verify the preliminary results discussed above.

14.3.2 The submarine volcano Obruchev in the Browton transverse zone of the Kurile Island Arc

The seamount Obruchev, located ca. 105 km north of the volcanic front and 50 km north-west of Browton Island, is a typical volcano of the rear-arc zone of the Kurile Island Arc. Its conical edifice has a sharp top, steep upper slopes (up to 25°), and rises up to 2200 m over the bottom of the Kurile Basin. The base, located in 3200 m b.s.l., measures 20-24 km in diameter, the total volume of the edifice is ca. 400 km^3 (Avdeiko et al., 1992).

Obruchev volcano is characterized by slightly negative magnetic anomaly patterns. The minimum values are located under its north-eastern slope (220 nT, Avdeiko et al., 1992) and maximum values (300 nT) have been found under the top of the submarine mountain.

Recent geological and geophysical surveys in the Kurile Island Arc provide the tectonic and petrologic framework for our study (Avdeiko et al., 1992). Rocks collected from this volcano on expeditions of the Institute of Volcanology include plutonic, volcanic and sedimentary rocks (altered basalt, andesite, dacite, tuff of basalt and andesite, tuffaceous sandstone, tuffaceous siltstone, diorite, granodiorite, granite). Most of them have been interpreted as ice-rafted debris (Avdeiko et al., 1992). Beside these glacial dropstones some fragments of fresh olivine-orthopyroxene-clinopyroxene basalt have been sampled. The rocks show geochemical features typical for high-Al island arc volcanics of the frontal zone of the Kurile Island Arc (Avdeiko et al., 1992), although Obruchev volcano is clearly located in the rear arc zone.

Two dredge tracks have been carried out at Obruchev volcano on GE99 cruise. Dredge GE99-42-1 recovered about 80-100 kg rocks from its south-western slope comprising predominantly dropstones (boulders, pebbles and fragments of plutonic and volcanic rocks) and gialospongia. Some rock samples and gialospongia were covered by Mn-oxide coating (up to 0.5-1.0 cm thick). Furthermore, dredge GE99-42-1 contained two angular fragments up to 15-17 cm in size: a sparsely porphyric basalt altered in greenstone facies conditions and a porphyric andesite (maybe basaltic andesite). The shape, the fresh surfaces and type of these rocks supply evidence for an origin by magmatic activity of Obruchev volcano.

Dredge GE99-43-1 from the north-western slope of Obruchev volcano collected about 100 kg of rocks including boulders (up to 50 cm) and fragments of orthopyroxene-amphibole dacite (ca. 50% of dredged rocks) and gialospongia. Some of these boulders stem from outcrops, but most of the fragments originated from the large talus piles on the slope of the volcano. Most samples were completely covered by up to 2-4 cm thick Mn-oxide crusts. The dacites commonly show a fine-grained granoblastic microstructure. The most common dacite assemblage is orthopyroxene+amphibole+plagioclase and minor quartz. Common accessory minerals are Fe-Ti-oxides.

One of the most striking features of the dacites from Obruchev volcano is their similarity to rocks of an extrusive dome. The dacite from this dome probably penetrated the older basalt and form a dacite unit on the north-western flank of the volcano which causes the slight magnetic anomalies in this area.

14.3.3. Hydrographers Ridge

Dredging at Hydrographers Ridge north of Iturup island (Fig. 14.1) was restricted to one dredge track by the master of the vessel due to weather problems (typhoon was brewing). After a brief site survey by echosounding the dredge track GE99-44-1 was carried out from the north-western slope to the top region of the ridge to get fresh volcanic bedrock for detailed volcanological and geochemical analyses. Unfortunately, the dredge came up empty.

14.3.4. Derugin Basin

On the basis of data gained on LV28 cruise and after site surveys by swatch bathymetry mapping barites were dredged in 1600 m water depth at one site within an area of intensive hydrothermal activity in the Derugin Basin (GE99-35-1). Apart from dropstones and sediment, dredging at this site yielded numerous boulders and fragments of big barite chimneys (up to 300 kg) which are described in detail in chapter 11 of this report.

15. LOW-TEMPERATURE HYDROTHERMAL MINERALIZATION IN SUBMARINE VOLCANOES IN THE EASTERN PART OF THE KURILE BASIN

A. Derkachev, I. Tararin, E. Lelikov, J. Greinert, and R. Werner

Low-and high-temperature hydrothermal vents and deposits of hydrothermal oxides, nontronites and massive sulfides have been discovered and investigated on all major spreading ridges, in back-arc basins, and on hotspot volcanoes (Hoffet et al., 1978; Haymon & Kastner, 1981; Styrt et al., 1981; Malahoff et al., 1982; Kononov, 1989; Alt, 1988; Hannington & Scott, 1988; Herzig et al., 1988; Lisitzin et al., 1991; Urabe & Kusakabe, 1990; Fouquet et al., 1991; Puteanus et al., 1991; Koski et al., 1985; Stuben et al., 1992). These deposits are precipitations formed as the result of the interaction of hydrothermal vents with seawater. The chemistry of these solutions differs from vent area to vent area but in general is determined by the interaction of seawater and basalts (Edmonds et al., 1979; Michard et al., 1984; Von Damm et al., 1985).

Low-temperature hydrothermal deposits of hydrothermal oxides and sulfides on the crest of a Pleistocene submarine volcano in the eastern part of the Kurile Basin were discovered and investigated during RV "*Akademik Lavrentyev*" cruise 28 in 1998. The dredges LV28-45, LV28-48 and LV28-56 from the upper and middle slopes of the volcano sampled the most representative low-temperature hydrothermally altered basalts. Those basalts are vesicular, porphyric rocks with phenocrysts of olivine, pyroxene, amphibole, plagioclase and magnetite in a glassy matrix.

The correlation of the mean composition of hydrothermally altered basalts with unaltered samples testifies that altered basalts are considerably enriched by many minor elements, especially Cr, Ni and Mo.

The greatest alterations could be observed along fractures, where basalt easily breaks up in differently sized fragments. Along the fractures the main part of the rock and olivine and pyroxene phenocrysts are partly or completely replaced by a green, poorly double-refracting clay substance (illite-smectite). The thickness of the altered rocks along fractures does not exceed 0.3 - 0.5 mm, sometimes it increases up to 10 mm. Smectite mineralization is typical also for the holes, pores and cavities in the basalts. Often smectite incrusts cavities and pores or completely fills them.

Usually the pore surface or cavities are covered by a crustified mantle of microglobular and collomorphous pyrite. Electron microprobe investigations proved pure pyrite in the crystallized phases.

The succession and morphology of low-temperature hydrothermal mineralization is divided in different zones. From the surface to the inside of the cavities and fractures the thin pyrite layer (2-3 mm) was first replaced by crustifical-zonal smectite and then by globular cryptocrystal or amorphous smectite aggregates. Larger aggregates of octahedral pyrite crystals (up to 50-60

μm) are rarely observed. In these aggregates, minute holes (up to 3-5 μm in diameter) on the top of the octahedral crystal pyrite were found that suggested a microchannel for hydrothermal vent water (Fig. 15.1 a).

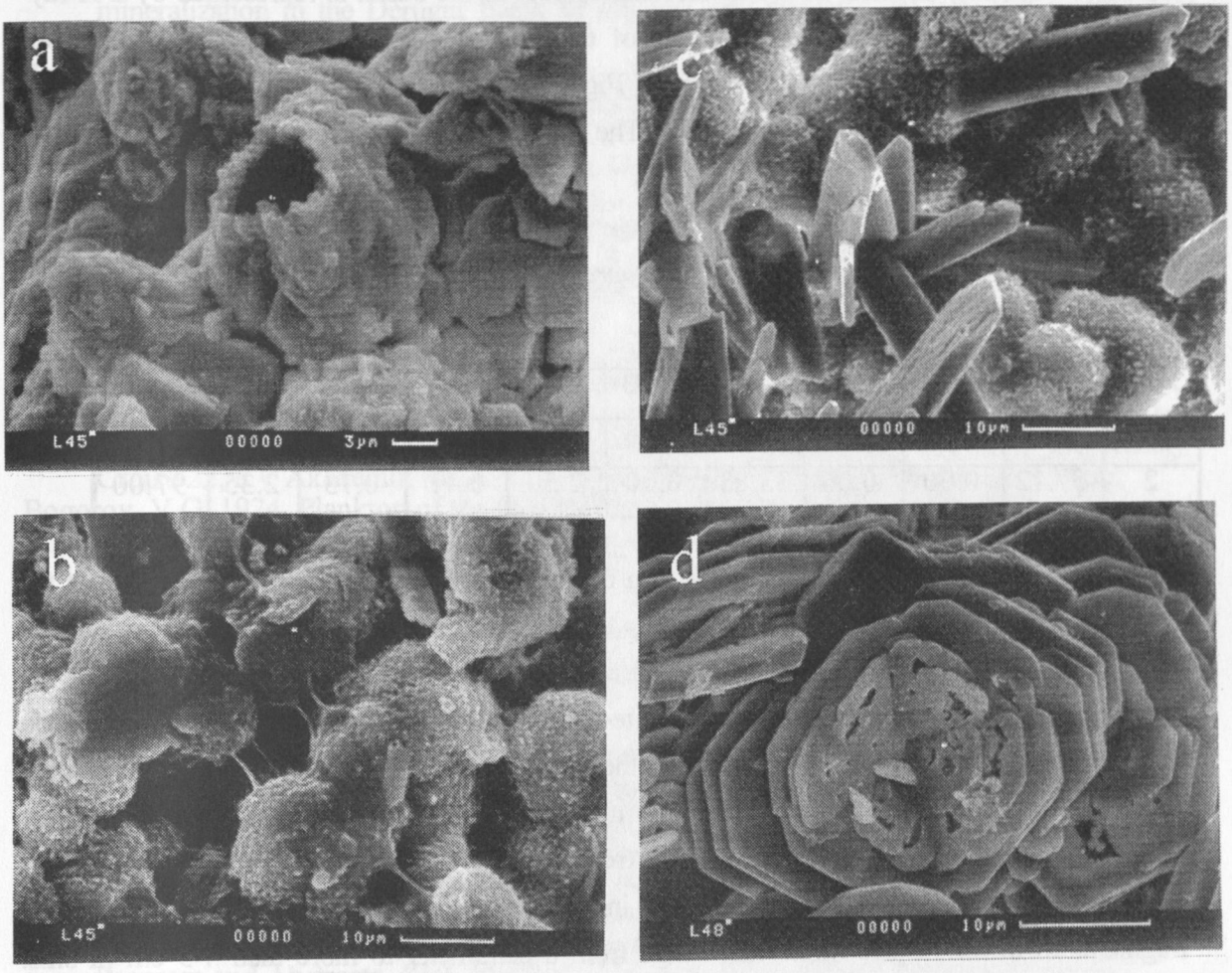

Fig. 15.1: (a) SEM images of octahedral pyrite crystals with a microchannel in central part, (b) SEM images of spherolite smectite aggregates, (c) the same, but with barite crystals, (d) SEM images of rose-shaped barite crystal aggregates.

In these hydrothermalites, pyrite is the dominant Fe-sulfide mineral. Neither Zn- nor Cu-sulfides were found, which corroborates the low-temperature hydrothermal activity. It is suggested that higher temperature precipitates like Zn-or Cu-sulfides do not outcrop on the recent surface of the submarine volcano but could perhaps be found in the deeper part of the volcano. The average chemical pyrite composition is given in Table 15.1.

Tab. 15.1: Average chemical pyrite composition (N = 29) from the submarine volcano in the eastern part of the Kurile Basin.

Fe	S	Mn	Ni	Co	Zn	Total
44.70	53.64	0.32	0.30	0.04	0.001	99.2

Investigations showed that the crystallized phases are composed of pure pyrite. Sulfide deposits of the submarine volcano show the same high content of pure pyrite as the Vai Liti sulfide mounts of the Lau back-arc Basin and the mid-ocean ridge deposits (Fouquet et al., 1991).
The light-green clay material from fractures and cavities in the basalt is represented by a X-ray-amorphous iron-silica phase and minerals of the smectite-nontronite series. The numerous spherolite aggregates are typical for smectite (Fig. 15.1 b,c). Smectite is sometimes associated with opal which is the main phase present. The chemical composition of smectite is given in Table 15.2.

Tab. 15.2: *Representative electron microprobe analyses of smectite (nontronite) from hydrothermally altered basalt.*

	SiO_2	TiO_2	Al_2O_3	FeO	MnO	MgO	CaO	Na_2O	K_2O	Total
1	52.86	0.10	0.00	36.74	0.06	1.79	0.39	0.49	1.63	93.97
2	57.12	0.00	0.06	33.83	0.00	2.50	0.41	0.73	2.35	97.00

Hydroxides of both iron and manganese form reddish goetite extractions in the fractures at the top of the lava flow and dark-brown crusts (up to 2-4 cm in size) cover the basalts. The rounded gravel and pebble fragments of dropstones are marked in the iron-manganese crusts.
Similar hydrothermal low-temperature smectite-nontronite assemblages with oxyhydroxide Mn and Fe occurrences were recovered during the GE99 cruise on the slopes of the submarine volcano in the Kurile Basin (GE99-39) and on the slopes of the Obruchev submarine volcano within the rear-arc zone of the Kurile Island Arc (GE99-42, -43).
Dredge collections from submarine volcanoes in the Kurile Basin include angular, white-yellow fragments of travertine-like barite that range from a centimeter to more than 4-5 cm in size. Microscopic investigations showed that the barite fragments are composed of homogeneous, loosely-packed aggregates of uniform barite spherolites or rose-shaped aggregates of barite crystals (Fig. 15.1 d). The $\delta^{34}S$-values of the barite from this volcano range from 22 to 28 ‰. Sulfur isotope values indicate a rather large-scale interaction of hydrothermal vents with seawater.
Both a distinct geochemical differentiation of chemical elements and the precipitation of ore components from hydrothermal fluids can be traced. This phenomenon is common for hydrothermal systems: sulfides (pyrite) → illite-smectite (nontronite) → opal → iron oxyhydroxides → manganese oxyhydroxides.

16. REFERENCES

Alt, J.C. 1988. Hydrothermal oxide and nontronite deposits on seamounts in the eastern Pacific. Marine Geol., 81, 227-139.

Astakhova, N.V., Lipkina, M.I. & Mel'nichenko, Yu.I. 1987. Hydrothermal barite mineralization in the Derugin Basin of the Sea of Okhotsk. Doklady Akademii Nauk USSR, 295, 1, 212-215 (in Russian).

Astakhova, N.V., Narnov, G.A. & Yakusheva, I.N. 1990. Carbonate-barite mineralization in the Derugin depresion (the Sea of Okhotsk). Tikhookeanskaya geologiya, 3, 37-42 (in Russian).

Avdeiko, G.A., Antonov, A.Yu. & Volynetz, O.N. 1992. Submarine volcanism and zonality of the Kuril Island Arc. Moscow, Nauka, 528 pp. (in Russian).

Avdeiko, G.P. & Volynets, O.N. 1999. Volatiles from the subducted slab and magma generation beneath the Kurile Island Arc. Second Workshop on Russian-German Cooperation in the Sea of Okhotsk - Kurile Island Arc System KOMEX. Program and Abstracts, Kiel, 13.

Bezrukov, P.L., Zenkevich, N.L., Kanaev, V.F. & Udintsev, G.B. 1958. Submarine mountains and volcanoes of the Kurile Island Ridge. In: Young volcanism of the USSR. Publ. AS USSR, Proceeding of the Laboratory of Volcanology, 13, 71 pp.(in Russian).

Biebow, N. & Hütten, E. 1999. Cruise Report KOMEX I and II: RV Professor Gagarinsky Cruise 22, RV Akademik M. A. Lavrentyev cruise 28. GEOMAR Rep., 82, 188 pp.

Bogorov, V.G. 1974. Plankton of the World Ocean. Moscow, Nauka (in Russian).

Bohrmann, G., Greinert, J., Suess, E. & Torres, M. 1998. Authigenic carbonates from the Cascadia subduction zone and their relation to gas hydrate stability. Geology, 26(7), 647-650.

Braytseva, O.A., Melekestsev, I.V., Ponomareva, V.V. & Kirianov, V.Yu. (1996). The caldera-forming eruption of Ksudach volcano about cal. AD 240, the greatest explosive event of our aera in Kamchatka. Journal of Volcanology and Geothermal Research, 70(1-2), 49-66.

Buczynski, C. & Chafets S. 1991. Habit of bacterially induced precipitates of calcium carbonate and the influence of medium vicosity on mineralogy. J. Sedim. Petrol., 61(2), 226-233.

Dehairs, F., Stroobants, N. & Goeyens, L. 1991. Suspended barite as a tracer of biological activity in the Southern Ocean. Mar. Chem., 1991, 35(1-4), 399-410.

Derkachev, A.N., Bohrmann, G. & Greinert, J. 1999 a. Mineralogical and morphological types of authigenic precipitates from Derugin Basin sediments. Second Workshop on Russian-German Cooperation in the Sea of Okhotsk - Kurile Island Arc System KOMEX. Program and Abstracts, Kiel, 31-32.

Derkachev, A.N., Bohrmann, G. & Greinert, J. 1999 b. Authigenic calcite and barite in sediments from the Derugin Basin, Sea of Okhotsk. AAPG- Convention Pacific Section: Fluid Seeps at Transform and Convergent Margins, 26.-30. March 1999, Monterey, California, Convention Program, 26-27.

Derkachev, A.N., Bohrmann, G., Greinert, J. & Mozherovsky, A.V. in prep. Mineralogy of diagenetic calcite and barite formation in sediments of the Derugin Basin, sea of Okhotsk. Facies.

Dickson, A.G. 1993. pH buffer for sea water media based on the total hydrogen ion concentration scale. Deep-Sea Res. I, 40, 107-118.

Dymond, J., Suess, E. & Lyle, M. 1992. Barium in deep sea sediments: a geochemical indicator of paleoproductivity. Paleoceanography, 7, 163-181.

Edmond, J.M., Measures, C.J. & Mangum, B. 1979. On the formation of metal-rich deposits at ridge crests. Earth Planet. Sci. Lett., 46, 19-30.

Fouquet, Y., Von Stackelberg, U. & Charlon, J.L. 1991. Hydrothermal activity in the Lau back-arc basin: Sulfides and water chemistry. Geology, 19, 303-306.

Freeland, H.J., Bychkov, A.S., Whitney, F., Taylor, C., Wong, C.S. &. Yurasoy G.I 1998. WOCE section P1W in the Sea of Okhotsk. 1. Oceanographic data description. J. Geophys. Res. 103(C8), 15, 613-15, 623.

Geodekian A.A., Mirlin E.G. & Trotzuk V.Y. 1978. About eventual dirty volcanic manifestations in Abyssal Basin of the Okhotsk sea. -In: The Genetic Prerequisites of the Oil and Gas Resources of the World ocean, 90-97 (in Russian).

Gieskes, J.M., Kelts, K. & Niemitz, J. 1982. Hydrothermal activity in the Guayamas Basin, Gulf of California: a synthesis. Init. Repts Deep Sea Drill. Proj., 64, 2, 1159-1167.

Ginsburg G.D., Soloviev V.A., Cranston R.E., Lorenson, T.D. & Kvenvolden, K.A. 1993. Gas hydrates from the continental slope, offshore Sakhalin Island, Okhotsk Sea. Geo-Marine Letters 13, 41-48.

Ginsburg, G.D. & Soloviev, V.A. 1994. Submarine gas hydrates. St. Petersburg, 5-200 (in Russian).

Gnibidenko H.S. & Svarichevsky A.S. 1984. Tectonics of the South Okhotsk Deep-sea Basin. Tectonophysics, 102, 225-244.

Galchenko, V.F., Lein, Yu.A. & Ivanov, M.V. 1988. Quantitative estimation of primary chemosynthesis production in the rift zones of modern oceans. In Schidlowski, M. (chairperson), Terra Cognita, 8(3), European Union of Geosciences, Strasbourg, 223 pp.

Gorbarenko, S.A. 1991. Stratigraphy of the upper Quaternary sediments from the central part of the Okhotsk Sea und its paleoceanology by the isotopic-oxygen method data und other methods. Oceanology, 31, 1036-1042 (in Russian).

Gorbarenko S.A., Chekhovskaya, M.P. & Southon, J.R. 1998. Detailed environmental changes in the Okhotsk Sea central part during the last glaciation-Holocene. Oceanology, 38, 305-308.

Gorbarenko, S.A., Derkachev, A.N., Southon, J.R. & Churupin-Shapovalov, V.V. in press. Lithostratigraphy and tephrachronology of the upper Quaternary sediments of the Okhotsk Sea using isotope-geochemical, physical properties and mineralogical results. Tikhookeanskaya geologiya (in Russian).

Gorbarenko S.A., Derkachev A.N., Southon J.R., Astakhov A.C. & Shapovalov V.B. Lithostratigraphy and tephrochronology of the Okhotsk Sea sediments (in prep.).

Hannington, M.D. & Scott, S.D. 1988. Mineralogy and geochemistry of a hydrothermal silica-sulfide-sulfate spire in the calderas of Axial Seamount, Juan de Fuca Ridge. Canad. Mineral., 26, 603-625.

Hayashi, T. 1997. The study of thermal structure and tectonic history of the Derugin Basin, Sea of Okhotsk. Master's thesis, Tokyo University, 39 pp.

Haymon, R.M. & Kastner, M. 1981. Hot spring deposits on the East Pacific Rise at 21°N: preliminary description on mineralogy and genesis. Earth Planet. Sci. Lett., 53, 363-381.

Herzig, P.M., Becker, K.P., Stoffers, P., Backer, H. & Blum, N. 1988. Hydrothermal silica chimney field in the Galapagos Spreading Center at 86°W. Earth Planet. Sci. Lett., 89, 261-272.

Hoffert, M., Perseil, A. & Hekinian, R. 1978. Hydrothermal deposit samples by diving saucer in Transform Fault "A" near 37°N on the Mid-Atlantic Ridge, FAMOUS area. Oceanol. Acta, 1, 73-86.

Hunt R.W.G. 1980. Color terms, symbols, and their usage. In Grum, F. & Bartleson, C.J. (eds.), Optical radiation measurement. Academic Press, New York, 11-31.

Ivanenkov, V.N. & Lyakhin, Yu.I. 1978. Determination of total alkalinity in seawater. In Bordovsky, O. K. & Ivanenkov, V. N. (eds.), Methods of hydrochemical investigations in the ocean. Nauka Publ. House, Moskow, 110-114 (in Russian).

Keigwin, L.D. 1998. Glacial-age hydrography of the far northwest Pacific Ocean. Paleoceanography, 13 (4), 323-339.

Koblenz-Mischke, O.J. 1967. Primary production of the Pacific Ocean. Biology of Pacific Ocean. Moscow, Nauka, pt. 1, 62-65 (in Russian).

Kononov, V.V. 1989. Ore mineralization from submarine volcanic zones of Iturup island. Geology of bottom in Pacific Ocean and zones of transit to Asian continent. Vladivostok, 135-138 (in Russian).

Koski, R.A., Lonsdale, P.F., Shanks, W.C., Berndt, M.E. & Howe, S.S. 1985. Mineralogy and geochemistry of a sediment-hosted hydrothermal sulfide deposit from the Southern Trough of Guaymas Basin, Gulf of California. J. Geophysical. Res., 90(B8), 6695-6707.

Kulm, L.D. & Suess, E., 1990. Relationship between carbonate deposits and fluid venting. Oregon accretionary prism. J. Geophysical. Res., 95, 8899-8915.

Lein, A.Y., Galchenko, V.F. & Pokrovskiy, B.G. 1989. Marine carbonate concretions as a result of processes of microbe oxidizing of gas-hydrate methane in the Sea of Okhotsk. Geochimiya, 10, 1396-1406 (in Russian).

LeMaitre, R.W. 1989. A Classification of Igneous Rocks and Glossary of Terms. Blackwell Scientific Publ., Oxford, London, Edinburgh, Boston, Melbourne, 1-193.

Lisitsin, A.P. & Udintsev, G.B. 1953. On ancient coastal lines on the sea. Izvestia. ÀS USSR. Ser. Geogr., 11, 23-31 (in Russian).

Lisitsin, A.P., Binns, P.A. & Bogdanov, Yu.A. 1991. Modern hydrothermal activity of a submarine mountain Franklin in the western part of Vudlark Sea (Papua-New Guinea). Isv. AN USSR, Ser. Geol., 8, 125-140 (in Russian).

Malahoff, A., McMurty, G.M., Wiltshire, J.C. & Yeh, H.-W. 1982. Geology and chemistry of hydrothermal deposits from active submarine volcano Loihi, Hawaii. Nature, 298, 234-239.

Michard, G., Albarede, F., Michard, A., Minster, J.-F., Charlou, J.L. & Tan, N. 1984. Chemistry and solutions from the 13°N hydrothermal site. Earth Planet. Sci. Lett., 67, 297-307.

Mix, A.C., Harris, S.E., & Janecek, T.R. 1995. Estimating lithology from nonintrusive reflectance spectra.- Proc. of the Ocean Drilling Program, Scientific Results, 138.413-427.

Nagao, S. & Nakashima, S. 1992. the factors controlling vertical color variations of North Atlantic Madeira Abyssal Plain sediments. Mar. Geol., 109,83-94.

Nürnberg, D,. Baranov, B.V. & Karp, B.Y. 1997, RV Akademik M.A. Lavrentyev cruise 27 - Cruise Report GREGORY, Geomar Rep., 60, 69 pp.

Obzhirov, A.I. 1992. Gas-geochemical manifestations of gas hydrates in the Sea of Okhotsk. Alaska Geology, 21(7), 1-7.

Obzhirov, A.I. 1993. Gas and geochemical fields of the benthic layer of seas and oceans. Moscow, Nauka, 131 pp.

Paull, C.K., Chanton, J.P. & Newmann, A.C. 1992. Indicators of methane-derived carbonates and chemosynthetic organic carbon deposits: Examples from the Florida Escarpment. Palaios., 7, 361-375.

Puteanus, D., Glasby, G.P., Stoffers, P. & Kunzendorf, H. 1991. Hydrothermal iron-rich deposits from the Teahitia-Mehetia and Macdonald hot spot areas, Southwest Pacific. Marine . Geol., 98, 389-409.

Ritger, S., Carson, B. & Suess, E. 1987. Methane-derived authigenic carbonates formed by subduction-induced pore water expulsion along the Oregon-Washington margin. Geol. Soc. Amer. Bull., 98, 147-156.

Roberts, H.H. & Aharon, P. 1994. Hydrocarbon-derived carbonate buildups of the northern Gulf of Mexico continental slope: A review of submersible investigations. Geol. Mar. Lett., 14, 135-148.

Sample, J.C., Reid, M.R., Tobin, H.J. & Moore, J. 1993. Carbonate deposits indicate channeled fluid flow along a zone of vertical faults at the deformation front of the Cascadia accretionary wedge (northwest U.S. coast). Geology, 21, 507-510.

Savostin, L.A., Baranov, B.V. & Zonenshain, L.P. 1978. About the eventual nature of the submarine mountains of Kurile abyssal Basin of the Okhotsk Sea. Proc. ÀS USSR, 242, 1 3, 676-679 (in Russian).

Stroobants, N., Dehairs, F., Goeyens, L., Vanderheiden, N. & Van Grieken, R. 1991. Barite formation in the Southern Ocean water column. Mar. Chem., 35, 1-4, 411-421.

Stuben, D., Bloomer, S.H. & Yaibi, N.E. 1992. First results of sulfide-rich hydrothermal activity from an island-arc environment: Esmeralda Bank in the Mariana Arc. Marine. Geol., 103, 521-528.

Styrt, M.M., Brackman, A.J., & Holland, H.D. 1981. The mineralogy and the isotopic composition of sulfur in hydrothermal sulfide/sulfate deposits in the EPR, 21°N latitude. Earth Planet. Sci. Lett., 53, 382-390.

Suess, E., Bohrmann, G., von Huene, R., Linke, P., Wallmann, K., Lammers, S., Sahling, H., Winckler, G., Lutz, R.A. & Orange, D. 1998. Fluid venting in the eastern Aleutian subduction zone. J. Geophys. Res., 103, B2, 2597-2614.

Talley, L.D. 1991. An Okhotsk Sea water anomaly: implications for ventilation in the North Pacific. Deep-Sea Res. Suppl. (1), 38, 171-190.

Tararin, I., Lelikov, E.P., Werner, R., Geldmacher, J., Terekhov, E.P. & Emelyanova, T.A. 1999 a. Petrology and Volcanology. In Biebow, N. & Hütten, E. (eds) Cruise Report KOMEX I and II: RV Professor Gagarinsky Cruise 22, RV Akademik M. A. Lavrentyev cruise 28. GEOMAR Rep., 82, 178 -184.

Tararin, I.A., Lelikov, E.P. & Karp, B.Ya. 1999 b. Volcanism of the Kurile Basin and the inner part of the Kurile Island Arc. Second Workshop on Russian-German Cooperation in the Sea of Okhotsk - Kurile Island Arc System KOMEX. Program and Abstracts, Kiel, 11-12.

Tiedemann, R. & Haug, G. 1995. Astronomical calibration of Site 882 cycle stratigraphy in the Northwest. Proc. ODP Sci. Res., 145, 283-293.

Torres, M.E, Brumsack, H.J., Bohrmann, G. & Emeis, K.C. 1996. Barite front in continental margin sediments: A new look at barium remobilization in the zone of sulfate reduction and formation of heavy barites in diagenetic fronts. Geochem. Geol., 127, 125-139.

Tufar, W., Tufar, E. & Lange, J. 1986. Ore paragenesis of recent hydrothermal deposits at the Cocos-Nazca plate boundary (Galapagos Rift) at 85°51'and 85°55'W: complex massive sulfide mineralizations, non-sulfidic mineralizations and mineralized basalts. Geol. Rundsch., 75, 829-961.

Urabe, T. & Kusakabe, M. 1990. Barite silica chimneys from the Sumisu rift, Izu-Bonin Arc: possible analog to hematitic chert associated with Kuroke deposits. Earth Planet. Sci. Lett., 100, 283-290.

Von Breymann, M.T., Brumsack, H. & Emeis, K.C. 1992. Depositional and diagenetic behaviour of barium in the Japan Sea. Proc. of the Ocean Drilling Program. Scientific Results, 127/128, 1, 651-665.

Von Damm, K.L., Edmond, J.M., Measures, C.I. & Grant, B. 1985. Chemistry of submarine hydrothermal solutions at Guyamas Basin, Gulf of California. Geochim. Cosmochim. Acta, 49, 2221-2237.

Von Rad, U., Rösch, H. & Berner, U.1996. Authigenic carbonates derived from oxidized methane vented from the Makran acretionary prism off Pakistan. Mar. Geol., 136, 55-77.

Werner, R., Hoernle, K., Volynets, O.N., Avdeiko, G., Tararin, I.A., Lelikov, E.P., Geldmacher, J. & Wenskowski, B. 1999. Second Workshop on Russian-German Cooperation in the Sea of Okhotsk - Kurile Island Arc System KOMEX. Program and Abstracts, Kiel, 14.

Wong, C.S., Matear, R.J., Freeland, H.J., Whitney, F.A. & Bychkov A.S. 1998. WOCE line P1W in the Sea of Okhotsk. 2. CFCs and the formation rate of intermediate water. J. Geophys. Res., 103, C8, 15625-15642.

Wong. H.K. 1999. TP7: Sedimentationsprozesse und strukturgeologische Entwicklung des Okhotskischen Meeres. In KOMEX-Zwischenbericht, Kiel, pp. 143.

Yasui M., Nagasaka K. & Hashimoto Y. 1968. Geomagnetic and bathymetric study of the Okhotsk sea. (2). - The Oceanogr. Mag., 20, N 1, 65-72.

Yasuoka, T. 1967. Hydrography in the Okhotsk Sea. Oceanogr. Mag. 198(7), 61-72.

Zonenshayn, L.P., Murdmaa, I.O., Baranov, B.V., Koznetsov, A.P., Kurin, V.S., Barash, M.S., Valyashirv, G.M. & Demiral, M. 1987. An underwater gas source in the Sea of Okhotsk. Oceanology, 27, 598.

APPENDIX 1

List of Stations

KOMEX 1999 : *Marshal Gelovany* GE 99

Date 1999	Stat. No	Instrument	Begin (UTC)	at seafloor max. depth	off seafloor	End (UTC)	Duration hh:mm	Latitude N° begin: at sf. / end: off sf	Longitude E° begin: at sf. / end: off sf	Water depth m	Recovery	Remarks
	West Kurile basin slope											
29. Aug	GE99 1-1	CTD	7:10	7:46		8:30	1:20	45°37.650'	144°23.560'	900	11 bottles	bottle 8 failed to close properly
29. Aug	GE99 1-2	MIC	9:30	10:08		10:40	1:10	45°35.786'	144°21.567'	790	4 cores	each core yielded 40 cm of sediment
29. Aug	GE99 1-3	MIC	10:55	11:20		12:00	1:05	45°34.893'	144°20.395'	795	4 cores	each core yielded approx. 40 cm of sediment
29. Aug	GE99 2-1	MIC	23:15	0:20		1:30	2:15	46°40.742'	144°50.600'	3050	4 cores	each core yielded approx. 35-40 cm of sediment
30. Aug	GE99 2-2	MIC	1:45	2:57		4:00	2:15	46°41.692'	144°47.519'	3040	4 cores	each core yielded approx 35-40 cm of sediment
30. Aug	GE99 2-3	CTD	6:22	7:32		9:20	2:58	46°43.700'	144°40.843'	2970	11 bottles	bottle 4 failed to close properly
	Aniva bay											
31. Aug	GE99 3-1	CTD	0:28	0:33		0:45	0:17	45°30.954'	143°10.609'	130	7 bottles	sound velocity profile for SBM; only 7 bottles fired
31. Aug	GE99 3-2	SBM	3:00			4:20	1:20	45°32.800'	143°11.000'	120		testing for calibration
	Terpenia bay											
03. Sep	GE99 4-1	CTD	11:45	11:48		11:58	0:13	48°00.520'	143°33.880'	76	12 bottles	
03. Sep	GE99 4-2	MIC	13:00	13:03		13:07	0:07	48°01.329'	143°34.900'	75	3 cores	
03. Sep	GE99 4-3	MIC	13:20	13:22		13:24	0:04	48°01.499'	143°35.170'	75	4 cores	
03. Sep	GE99 4-4	SBM	13:29			15:27	1:58	see seperate table		70 - 80	3 profiles	calibration
	North-West Kurile basin slope											
04. Sep	GE99 5-1	MIC	1:34	1:41		1:50	0:16	47°24.526'	145°22.720'	515	4 cores	each core yielded approx. 20 cm of sediment
04. Sep	GE99 5-2	MIC	1:57	2:05		2:12	0:15	47°24.747'	145°23.048'	495	3 cores	each core yielded approx 25 cm of sediment
04. Sep	GE99 5-3	CTD	3:24	3:51		4:23	0:59	47°22.640'	145°29.520'	1360	12 bottles	
	West Kurile basin											
04. Sep	GE99 6-1	CTD	18:47	18:50		18:56	0:09	47°15.580'	148°24.029'	3350	5 bottles	only the upper 50 m sampled (A. Obzhirov)
04. Sep	GE99 6-2	CTD	19:11	20:15		21:35	2:24	47°16.807'	148°23.615'	3350	12 bottles	
04. Sep	GE99 6-3	MIC	21:43	22:43		23:31	1:48	47°19.086'	148°23.035'	3360	4 cores	each core yielded approx. 25-35 cm of sediment
04. Sep	GE99 6-4	MIC	23:43	0:35		1:30	1:47	47°21.188'	148°22.627'	3350	4 cores	each core yielded approx 21-30 cm of sediment
04. Sep	GE99 6-5	HN	23:45			23:55	0:10	47°20.626'	148°22.639'	3350		
05. Sep	GE99 7-1	CTD	8:30	9:28		10:45	2:15	47°14.340'	147°09.860'	3350	12 bottles	bottles 11+12 fired at the same depths erroneously
05. Sep	GE99 7-2	MIC	10:45	11:37		12:35	1:50	47°15.547'	147°11.183'	3340	4 cores	each core yielded apporx. 30 cm of sediment
05. Sep	GE99 7-3	MIC	12:43	13:28		14:21	1:38	47°17.654'	147°12.914'	3350		cores empty
05. Sep	GE99 8-1	CTD	22:27	23:25		0:37	2:10	46°49.680'	146°01.790'	3300	12 bottles	
	North-West Kurile basin slope											
08. Sep	GE99 9-1	SL-G	23:30	23:52		0:45	1:15	48°14.537'	146°00.434'	1550	9.11m	12m core deployed: 9.11m of sediment gained
09. Sep	GE99 10-1	MUC	2:48	3:07		3:55	1:07	48°18.342'	146°08.107'	1380	no cores	empty, no cores
09. Sep	GE99 10-2	MUC	4:05	4:31		5:00	0:55	48°18.309'	146°08.148'	1390	6 cores	6 cores, each yielded approx. 26 cm of sediment; remaining cores: water
09. Sep	GE99 10-3	SL-R	6:08	6:28		7:00	0:52	48°18.666'	146°08.092'	1335	7.50m	7,50m core gained from 11m core deployment

KOMEX 1999 : *Marshal Gelovany* GE 99

Date 1999	Stat. No	Instrument	Begin (UTC)	at seafloor max. depth	off seafloor	End (UTC)	Duration hh:mm	Latitude N° begin: at sf. / end: off sf	Longitude E° begin: at sf. / end: off sf	Water depth m	Recovery	Remarks
	Sakhalin shelf											
10. Sep	GE99 11-1	CTD	2:40	2:44		2:53	0:13	51°21.243'	143°52.727	80	12 bottles	11 bottles for sampling, first bottle erroneously fired during downcast
10. Sep	GE99 12-1	SL-G	14:00	14:15		14:45	0:45	52°51.309'	144°48.662'	950	11.31m	12m coring equipment yielded 11.31m of sediment
10. Sep	GE99 12-2	CTD	14:55	15:12		15:38	0:43	52°50.984'	144°48.577'	940	12 bottles	11 bottles for sampling, first bottle fired during downcast
10. Sep	GE99 12-3	MUC	16:12	16:35		17:05	0:53	52°50.787'	144°47.626'	930	10 cores	each yielded approx. 0.30 - 0.45m of sediment
10. Sep	GE99 12-4	SL-R	18:12	18:20		18:45	0:33	52°51.455'	144°45.581'	880	8.25	11m coring equipment yielded 8.25m of sediment
	Piltunsky flare											
10. Sep	GE99 13-1	CTD	22:54	23:07		23:33	0:39	53°22.742'	144°25.672'	630	12 bottles	
10. Sep	GE99 13-2	BS	22:50			23:40	0:50	53°22.742'	144°25.672'	630		no signs of flares
11. Sep	GE99 14-1	SBM	1:42			23:24	0:50	see separate table			1 profile	problems with heading input
	Sakhalin shelf											
11. Sep	GE99 15-1	CTD	7:39	7:59		8:30	0:51	53°52.490'	144°14.867'	830	12 bottles	angle of cable considerable
	Giselle flare											
11. Sep	GE99 16-1	CTD	13:10	13:25		13:41	0:31	54°22.659'	143°59.902'	400	12 bottles	
11. Sep	GE99 16-2	HYC	2:15	2:21		3:40	1:25	54°21.884'	143°58.888'	386	2m	5m coring equipment yielded 2m of sediment, carbonates present from 1m depth downward
11. Sep	GE99 17-1	SBM	15:52			20:08	4:16	see separate table			2 profiles	mapping stopped during 2nd profile because of bad wether
11. Sep	GE99 18-1	CTD	22:49	22:58		23:10	0:21	54°28.265'	143°57.373'	380	12 bottles	strong wind; strong current pushed CTD under ship
11. Sep	GE99 18-2	HYC	23:25	23:35		23:45	0:20	54°28.630'	143°57.338'	380	1.70m	5m coring equipment yielded 1.70m of sediment
12. Sep	GE99 19-1	CTD	5:11	5:20		5:36	0:25	54°18.277'	143°59.014'	380	12 bottles	
12. Sep	GE99 19-2	HYC	5:35	5:43		6:23	0:48	54°18.376'	144°00.356'	460	3.25m	5m coring equipment yielded 3.25m of sediment
12. Sep	GE99 20-1	CTD	7:50	8:03		8:16	0:26	54°21.719'	143°59.469'	370	12 bottles	
12. Sep	GE99 20-2	MIC	9:34	9:39		9:47	0:13	54°22.243'	143°58.517'	360	1 core	1 core: 20cm of sediment, 3 cores empty
12. Sep	GE99 20-3	MIC	9:57	10:03		12:05	2:08	54°21.571'	143°58.945'	360	2 cores	core 1: 10 cm, core 2: 15 cm, 2 cores empty
	North Sakhalin 'Amur canyon'											
12. Sep	GE99 21-1	CTD	22:36	22:54		23:17	0:41	54°55.664'	144°21.105'	900	12 bottles	
12. Sep	GE99 21-2	MIC	23:26	23:44		0:04	0:38	54°55.590'	144°22.829'	960	2 cores	2 cores remained empty, each of the other 2 yielded approx. 10cm of sediment
13. Sep	GE99 22-1	SL-G	5:38	5:58		6:45	1:07	55°04.887'	144°15.083'	1050	no core	tube bent and broken, no sediment (due to sand); core weight could be recovered
13. Sep	GE99 23-1	MUC	8:40	9:03		9:21	0:41	55°03.750'	144°29.709'	1150	no cores	
	Obzhirov flare											
13. Sep	GE99 24-1	CTD	21:10	21:32		21:49	0:39	54°26.832'	144°04.917'	710	12 bottles	
13. Sep	GE99 24-2	SL-R	23:26	23:40		0:00	0:34	54°26.662'	144°04.517'	700	3.60m	gas hydrate in bottom part of core; 5m coring equipment yielded 3.50m of sediment
14. Sep	GE 99 25-1	TWL	0:57	1:06	1:36	2:04	1:07	54°26.741'/54°27.079'	144°04.820'/144°05.45(	700	70 kg	vent fauna (living specimens), big clams

KOMEX 1999 : *Marshal Gelovany* GE 99

Date 1999	Stat. No	Instrument	Begin (UTC)	at seafloor max. depth	off seafloor	End (UTC)	Duration hh:mm	Latitude N° begin: at sf. / end: off sf	Longitude E° begin: at sf. / end: off sf	Water depth m	Recovery	Remarks
14. Sep	GE99 26-1	CTD	2:55	3:11		3:29	0:34	54°30.940'	144°05.151'	700	12 bottles	very near a very big flare, almost in the center
14. Sep	GE99 26-2	SL-R	3:35	3:50		4:07	0:32	54°31.176'	144°05.276'	700	5.70m	H_2S smelling core
14. Sep	GE99 27-1	CTD	7:19	7:32		7:46	0:27	54°26.847'	144°04.761'	700	12 bottles	CTD completely inside Obzhirov flare
14. Sep	GE99 27-2	SL-R	8:22	8:37		8:50	0:28	54°26.663'	144°04.812'	700	5.90m	6m coring equipment yielded 5.90m of sediment, during last 2m strong H_2S smell
14. Sep	GE99 28-1	TWL	10:15	10:28	0.45625	11:26	1:11	54°26.576'/54°27.271'	44°04.877'/144°04.77	700		
14. Sep	GE99 28-2	SBM	12:30			19:15	6:45	see separate table			4 profiles	
15. Sep	GE99 29-1	CTD	2:05	2:22		2:40	0:35	54°26.375'	144°04.752'	700	12 bottles	near Obzhirov flare, almost in the centre; 3 bottles closed during down-cast
15. Sep	GE99 29-2	MIC		3:30				54°26.780'	144°04.860'	700	4 cores	
15. Sep	GE99 29-3	SL-R	4:58	5:17		5:35	0:37	54°26.784'	144°04.765'	700	2.50m	bottom part yielded gas hydratefragments, most 1-3cm in diameter, some layered pieces (1 cm thick, 4cm long, 2,5cm wide)
	North Derugin Basin											
15. Sep	GE99 30-1	CTD	13:16	13:42		14:20	1:04	54°24.471'	145°07.993'	1480	12 bottles	
15. Sep	GE99 30-2	MIC	14:19	14:44		15:15	0:56	54°24.323'	145°08.739'	1470	4 cores	each core yielded approx. 43 cm of sediment
15. Sep	GE99 30-3	SL-R	16:15	16:37		17:05	0:50	54°24.576'	145°07.811'	1480	7.40m	H_2S smell, no ikkait found
15. Sep	GE99 31-1	CTD	22:25	22:53		23:22	0:57	54°24.127'	145°52.313'	1570	12 bottles	
15. Sep	GE99 31-2	MUC	23:47	0:16		0:46	0:59	54°23.699'	145°52.917'	1480	no cores	cores came up empty
16. Sep	GE99 31-3	MUC	1:03	1:34		2:20	1:17	54°23.327'	145°54.979'	1600		
16. Sep	GE99 31-4	SL-G	16:02	16:30		17:10	1:08	54°23.492'	145°54.149'	1600	10.06m	11m coring equipment yielded 10.06m of sediment
	Derugin Basin 'barite mountains'											
16. Sep	GE99 32-1	CTD	9:31	10:00		10:34	1:03	53°59.854'	146°17.092'	1560	12 bottles	
16. Sep	GE99 32-2	SL-R	11:19	12:23		13:10	1:51	54°00.441'	146°16.916'	1510	6.25m	8m coring equipment provided 6.25m of sediment with barite fragments
16. Sep	GE99 33-1	SBM	13:05			22:05	9:00	see separate table		1350 -1750	2 profiles	
16. Sep	GE99 34-1	CTD	23:07	23:35		0:10	0:53	54°01.128'	146°11.367'	1640	12 bottles	
17. Sep	GE99 35-1	DR	4:40	5:25	5:45	6:45	2:05	53°59.586'/53°59.666'	46°20.170'/146°20.07	1600	300kg	mostly barite (big chimney fragments?) booulders, dropstones, pebbles, sediment
17. Sep	GE99 36-1	HYC	8:09	8:35		9:10	1:01	53°59.474'	146°19.369'	1520	5 m	5m coring equipment yielded 5m of sediment
17. Sep	GE99 37-1	CTD	11:32	12:03		12:44	1:12	54°00.739'	146°16.497'	1680	12 bottles	
	Academy of Science Rise											
19. Sep	GE 99 38-1	CTD	7:14	7:34		8:00	0:46	49°22.289'	150°28.088'	1050	12 bottles	
19. Sep	GE99 38-2	SL-G	8:01	8:19		8:50	0:49	49°21.653'	150°28.765'	1080	5,10m	bent tube, broken coring equipment, upper part of core could be saved
19. Sep	GE99 38-3	MIC	8:59	9:17		9:36	0:37	49°21.022'	150°29.418'	1080	4 cores	each core held approx. 30cm of sediment
19. Sep	GE99 38-4	MIC	9:46	10:02		10:25	0:39	49°20.491'	150°29.809'	1100	3 cores	each core held approx. 25-30cm of sediment
19. Sep	GE99 38-5	SL-R	10:41	11:03		11:35	0:54	49°19.805'	150°30.596'	1110		

KOMEX 1999 : *Marshal Gelovany* GE 99

Date 1999	Stat. No	Instrument	Begin (UTC)	at seafloor max. depth	off seafloor	End (UTC)	Duration hh:mm	Latitude N° Longitude E° begin: at sf. / end: off sf	Water depth m	Recovery	Remarks
	Kurile Basin										
19. Sep	GE99 39-1	SBM	22:10			11:08	12:58	see separate table	2400 - 3300		several profiles coverd during dredging, water depth mostly to deep
20. Sep	GE99 39-2	DR	2:49	3:34	3:40	4:45	1:56	48°18.570'/48°19.180'51°58.950'/151°49.10	2940/2740	20 kg	2 pieces of fresh basalt, approx. 10 kg of hydrothermally altered basalt, partly covered by manganese crusts on the surface; dropstones, 1 piece of breccia(?)
20. Sep	GE99 40-1	DR	5:50		7:40	8:50	3:00	48°19.900'/48°18.790'51°47.300'/151°48.89	3200/2670	empty	no recoveries as positioning of ship against strong drift could not be managed satisfyingly
20. Sep	GE99 41-1	CTD	9:31	10:21		11:20	1:49	48°18.093' 151°49.610'	2650	12 bottles	
21. Sep	GE99 42-1	DR	2:15	4:02	4:25	5:00	2:45	47°67.000'/47°67.300'50°29.700'/150°26.30	1200-1600	51 kg	fauna, several dropstones, 2 pieces of lava (andesit, basalt?), in situ?
21. Sep	GE99 43-1	DR	6:45	8:30	9:10	9:30	2:45	47°06.400'/47°06.560'50°28.520'/150°28.41	1850-1050	70 kg	5 pieces of tuff or grandiorite; dropstones, fauna, some hydrothermally altered (ex-basalt?) pieces
22. Sep	GE99 44-1	DR	16:00	17:45	18:10	18:40	2:40	46°02.880'/46°02.520'47°45.370'/147°45.93	1400-1600	empty	

Latitude/Longitude: trawl and dredge at seafloor and off seafloor
CTD at maximum depth
SBM see extra table

Sample devices : SL-G: gravity corer (German)
SL-R: gravity corer (Russian)
HYC: hydro-corer (Russian)
MIC: mini-corer
MUC: multi-corer

CTD : CTD sensors and hydrocasts
SBM: swath bathymetry mapping
DR: dredge
TWL: trawl

APPENDIX 2

Hydroacoustic anomalies

Table of hydroacoustic anomalies (flares), observed in the Sea of Okhotsk during the KOMEX 99 cruise MV *Marshal Gelovany*, September 1999, and the 26-th cruise of RV *Professor Gagarinsky*, August 1999.

No	Latitude, N	Longitude, E	Date (UTC)	Time (UTC)	Depth, m bottom	low edge	top edge	Description
Terpenia Bay								
1	47°12.167	143°47.381	03-Sep-1999	06:53:56	893			beg flare band
	47°27.597	143°42.519	03-Sep-1999	08:14:45	425			end flare band
2	47°21.602	143°44.366	03-Sep-1999	07:43:46	499	499	405	cloud on the hill
3	47°23.995	143°43.611	03-Sep-1999	07:56:19	740	744	425	stright peak
4	47°42.163	144°33.062	03-Sep-1999	20:30:36	477			beg flare band
	47°37.571	144°45.454	03-Sep-1999	21:22:47	758			end flare band
5	47°40.306	144°38.209	03-Sep-1999	20:52:23	994	994	596	smoke column
6	47°37.896	144°44.657	03-Sep-1999	21:19:32	923	923	771	smoke
Sakhalin shelf								
7	50°59.511	144° 5.268	10-Sep-1999	00:02:06	143	140	97	double flare
Giselle flare area								
8	54°22.075	143°58.802	11-Sep-1999	12:40:15	385	343	107	hanning flare
9	54°22.135	143°58.785	11-Sep-1999	12:41:32	385	385	265	cluster
10	54°22.512	143°58.200	11-Sep-1999	14:10:41	395			beg flare band
	54°22.558	143°58.128	11-Sep-1999	14:21:34	389			end flare band
11	54°22.072	143°58.185	11-Sep-1999	14:12:57	407	407	257	power inclined flare
12	54°22.009	143°58.156	11-Sep-1999	14:17:20	396	396	210	strong inclined flare
13	54°21.909	143°58.134	11-Sep-1999	14:20:39	392	392	270	cluster
14	54°22.955	143°57.510	11-Sep-1999	15:55:40	399	399	282	inclined column
Obzhirov flare area								
15	54°26.579	144° 2.850	12-Sep-1999	11:46:33	670	659	440	column
16	54°26.781	144° 2.941	12-Sep-1999	11:49:36	683	683	437	thick column
17	54°26.913	144° 3.022	12-Sep-1999	11:51:32	681	681	250	thick inclined column
18	54°48.491	144°12.650	12-Sep-1999	19:48:36	773	773	506	inclined column
19	54°51.789	144°12.352	12-Sep-1999	20:58:07	773	773	492	column
20	54°27.809	144° 5.972	13-Sep-1999	20:49:16	525	525	0	inclined pike
21	54°26.820	144° 4.991	13-Sep-1999	21:09:24	505			beg flare band
	54°26.844	144° 4.924	13-Sep-1999	21:35:55	516			end flare band
22	54°26.773	144° 4.934	13-Sep-1999	21:10:29	510	510	259	strong jet
23	54°26.670	144° 4.819	13-Sep-1999	21:12:52	512	512	360	cluster
24	54°26.579	144° 4.760	13-Sep-1999	21:14:47	501	501	295	jet
25	54°26.469	144° 4.713	13-Sep-1999	21:16:53	507	507	205	power inclined column
26	54°26.448	144° 4.559	13-Sep-1999	21:19:57	496	496	382	cluster

No	Latitude, N	Longitude, E	Date (UTC)	Time (UTC)	Depth, m bottom	low edge	top edge	Description
27	54°26.538	144° 4.589	13-Sep-1999	21:23:02	503	503	291	big cluster
28	54°26.796	144° 4.881	13-Sep-1999	21:32:58	517	517	297	giant cluster
29	54°26.604	144° 4.795	13-Sep-1999	23:00:51	702	702	472	cloud
30	54°26.543	144° 4.555	13-Sep-1999	23:03:04	698	698	498	column in fog
31	54°26.467	144° 4.419	13-Sep-1999	23:04:53	693	693	443	strong jet
32	54°26.404	144° 4.320	13-Sep-1999	23:06:09	696	696	486	jet
33	54°26.581	144° 4.211	13-Sep-1999	23:29:45	693	535	430	cloud
34	54°26.764	144° 4.905	13-Sep-1999	23:50:27	706	538	393	cloud
35	54°26.607	144° 4.818	14-Sep-1999	00:21:41	709	709	417	jet
36	54°26.454	144° 4.584	14-Sep-1999	00:24:41	693	693	451	thick jet
37	54°26.423	144° 4.330	14-Sep-1999	00:47:58	693	693	385	broken column
38	54°26.475	144° 4.408	14-Sep-1999	00:49:21	698	698	388	broken column
39	54°26.559	144° 4.532	14-Sep-1999	00:51:37	704	704	498	cluster
40	54°26.792	144° 4.858	14-Sep-1999	01:12:20	714	714	380	huge broken column
41	54°26.675	144° 4.862	14-Sep-1999	06:54:24	715	463	268	cloud
42	54°26.817	144° 4.921	14-Sep-1999	07:13:14	711	711	512	cluster
43	54°26.779	144° 4.830	14-Sep-1999	07:29:15	713	713	488	Huge inclined column
44	54°26.644	144° 4.780	14-Sep-1999	07:51:49	707	707	506	cluster
45	54°26.576	144° 4.877	14-Sep-1999	08:02:08	705	705	480	broken jet
46	54°26.785	144° 4.878	14-Sep-1999	08:20:47	705	705	485	thick inclined column
47	54°26.670	144° 4.814	14-Sep-1999	08:38:54	714	714	536	inclined column
48	54°26.531	144° 4.750	14-Sep-1999	08:50:51	701	701	453	inclined column in fog
49	54°26.331	144° 4.683	14-Sep-1999	09:03:30	697	697	473	inclined column
50	54°26.637	144° 4.841	14-Sep-1999	09:53:01	725	725	515	thick inclined column
51	54°26.630	144° 4.879	14-Sep-1999	09:59:26	722	722	564	cluster
52	54°26.634	144° 4.867	14-Sep-1999	10:30:15	711	711	344	inclined column
53	54°26.765	144° 4.837	14-Sep-1999	10:35:55	709	709	350	inclined column
54	54°27.517	144° 4.580	14-Sep-1999	17:51:37	712	712	231	inclined pike
55	54°26.512	144° 4.657	14-Sep-1999	18:26:37	696	696	215	inclined pike
56	54°26.650	144° 4.821	14-Sep-1999	23:58:54	707	707	419	huge broken column
57	54°26.466	144° 4.733	15-Sep-1999	01:02:44	698	599	213	huge dense cloud
58	54°26.815	144° 4.875	15-Sep-1999	01:12:24	704	704	413	jet
59	54°26.571	144° 4.686	15-Sep-1999	02:15:39	701	701	369	huge column
60	54°26.848	144° 4.863	15-Sep-1999	03:30:53	717	717	428	huge column
61	54°26.838	144° 4.731	15-Sep-1999	05:16:46	703	703	557	cluster in fog
62	54°26.560	144° 4.493	15-Sep-1999	05:36:48	694	694	533	cluster
Gagarinsky-26 flares								
63	55°28.31	144° 6.25	14-Aug-1999		950			profile P-7
64	55°25.60	144° 2.82	15-Aug-1999		1000			profile P-11

APPENDIX 3

Water column data

GE99 CTD: Water column analysis

Station	Bottle	Pressure	Depth	Salinity	Pot Temp	Pot Density	O_2 CTD	O_2 titr.	CH_4	CO_2(GC)	N_2(GC)	TA	Si	PO_4	NO_2	NO_3NO_2
		dbar	m		°C	kg/m³	µmol/kg	µmol/kg	nl/l	ml/l	ml/l	meq/l	µmol/l	µmol/l	µmol/l	µmol/l
CTD 1-1	1	844	835	34.237	2.286	27.338	40.2	51.7	117	0.81	9.7	2.36	175	3.29	0.01	47.3
	2	801	793	34.158	2.260	27.276	46.5	57.0	152			2.34	168	3.48	0.01	48.4
	3	753	745	34.103	2.228	27.235	53.4	45.6	38	0.90	10.5	2.30	161	3.53	0.01	48.6
	4	500	495	33.705	1.554	26.967	152.4	153.4	113	0.71	11.7	2.26	71.2	2.22	0.01	39.8
	5	376	373	33.510	0.965	26.849	188.5	159.7	134	0.72	12.0	2.24	58.5	2.79	0.01	32.3
	6	253	250	33.375	0.703	26.757	230.2	220.2	94	0.68	11.7	2.22	50.7	1.97	0.01	27.2
	7	100	100	33.089	-0.648	26.592	312.3	271.7	163	0.54	12.5	2.20	39.6	1.7	0.01	28.6
	8	52	51	32.907	-0.284	26.429	331.0	-	-	-	-	-	-	-	-	-
	9	52	51	32.906	-0.292	26.429	331.2	254.2	261	-	-	2.20	33.6	1.58	0.13	24.4
	10	25	25	32.644	1.943	26.089	413.7	276.0	158	-	-	2.18	5.88	0.68	0.21	0
	11	10	10	32.038	18.270	22.940	260.3	26.0	70	-	-	2.16	4.2	0.26	0.07	0
	12	1	1	32.041	18.327	22.929	250.6	182.4	56	0.22	9.0	2.16	6.62	0.53	0.05	0
CTD 2-3	1	2984	2939	34.611	1.628	27.689	80.5	90.5	21	0.54	10.7	-	201	3.09	0.01	45.9
	2	2794	2753	34.605	1.649	27.682	79.4	87.4	11	-	-	-	193	3.44	0.01	42.9
	3	2540	2504	34.595	1.686	27.671	75.8	90.5	11	0.55	9.7	-	192	3.24	0.01	43.6
	5	2279	2248	34.578	1.748	27.653	69.6	84.1	178	0.63	11.6	-	190	3.19	0.01	42.4
	6	2030	2004	34.554	1.835	27.628	61.7	79.8	27	0.58	10.8	-	188	3.24	0.01	42.9
	7	1769	1747	34.528	1.926	27.599	54.3	67.7	16	0.66	11.5	-	186	3.34	0.01	46.7
	8	1522	1504	34.491	2.031	27.561	46.6	61.0	7	0.67	10.7	-	185	3.39	0.01	48.6
	9	1014	1003	34.267	2.291	27.361	36.1	51.1	14	0.78	11.4	-	173	3.34	0.01	46.7
	10	510	506	33.658	1.569	26.928	174.4	180.4	113	0.63	11.9	-	78.1	2.65	0.01	31.4
	11	157	156	33.290	1.511	26.637	268.9	270.0	140	0.42	12.9	-	44.1	2.43	0.01	21.7
	12	53	53	33.091	2.773	26.381	301.2	309.7	138	0.29	12.2	-	30.7	1.82	0.21	17
CTD 3-1	1	109	108	33.298	0.537	26.704	300.5	250.7	181	0.54	11.9	-	-	-	-	-
	2	100	99	33.296	0.506	26.704	297.2	252.5	182	0.51	12.2	-	-	-	-	-
	3	75	74	33.144	0.005	26.607	331.9	290.8	160	0.39	11.6	-	-	-	-	-
	4	50	50	33.023	0.293	26.496	340.0	305.7	226	0.37	12.3	-	-	-	-	-
	5	26	26	32.716	1.093	26.204	408.1	367.7	187	0.24	12.3	-	-	-	-	-
	6	10	10	32.059	16.952	23.271	232.7	269.0	61	0.15	9.1	-	-	-	-	-
	7	3	3	32.050	17.935	23.031	180.4	246.1	53	0.16	9.0	-	-	-	-	-
	8	3	3	32.050	17.944	23.029	172.8	-	-	-	-	-	-	-	-	-
										-	-					
CTD 4-1	1	74	74	33.051	-1.474	26.588	258.5	238.3	579	0.54	11.1	-	61.9	2.38	-	-
	2	70	69	33.051	-1.475	26.588	257.8	241.2	572	0.56	11.1	-	59.6	2.35	-	-
	3	65	64	33.051	-1.472	26.588	257.8	241.4	543	0.58	11.3	-	60.2	2.4	-	-
	4	60	59	33.049	-1.461	26.586	258.3	245.5	563	0.56	11.1	-	59.1	2.27	-	-
	5	54	53	32.986	-1.146	26.526	305.3	281.5	556	-	-	-	50.9	2.1	-	-
	6	50	49	32.949	-0.954	26.490	331.5	294.3	403	0.37	14.0	-	49.8	1.48	-	-
	7	39	39	32.805	0.298	26.320	370.1	349.3	306	0.31	12.6	-	18.3	1.29	-	-
	8	30	30	32.727	1.924	26.157	407.3	374.1	231	-	-	-	16	0.97	-	-
	9	25	24	32.713	3.594	26.006	427.7	391.2	254	-	-	-	3.55	0.64	-	-
	10	20	20	32.553	5.380	25.693	392.1	389.6	298	-	-	-	3.55	0.57	-	-
	11	9	9	31.717	15.924	23.242	279.5	298.0	111	0.15	10.6	-	0	0.09	-	-
	12	3	3	31.735	15.999	23.239	279.8	274.5	85	0.15	12.8	-	0	0	-	-
CTD 5-3	1	1496	1479	34.488	2.077	27.555	50.3	50.5	9	-	-	-	189	3.4	-	-
	2	1465	1448	34.489	2.074	27.556	50.2	50.7	13	-	-	-	187	3.6	-	-
	3	1261	1247	34.438	2.163	27.509	43.5	43.5	15	-	-	-	186	3.6	-	-
	4	1011	1000	34.317	2.282	27.402	38.0	40.5	11	-	-	-	178	3.5	-	-
	5	757	750	34.130	2.245	27.256	50.1	54.0	21	-	-	-	162	3.4	-	-
	6	506	501	33.836	1.892	27.047	114.6	112.4	34	-	-	-	118	2.9	-	-
	7	378	375	33.444	0.812	26.805	207.6	237.5	143	-	-	-	70.6	2.5	-	-
	8	252	250	33.287	-0.041	26.725	236.3	225.9	31	-	-	-	61.8	2.6	-	-
	9	126	125	33.117	-0.736	26.618	296.9	262.0	37	-	-	-	-	-	-	-
	10	50	50	32.954	-0.151	26.462	330.3	321.1	158	-	-	-	33.1	1.7	-	-
	11	25	25	32.645	2.919	26.012	381.2	348.6	111	-	-	-	18	1.2	-	-
	12	2	2	32.210	16.432	23.506	275.4	264.5	43	-	-	-	3.9	0.1	-	-
CTD 6-1	1	51	50	33.086	3.300	26.331	357.4	-	63	0.27	10.5	-	-	-	-	-
	2	25	25	32.999	6.142	25.954	326.4	-	52	-	-	-	-	-	-	-
	3	10	10	32.690	12.858	24.632	312.0	-	37	0.15	9.0	-	-	-	-	-
	4	5	5	32.643	13.706	24.427	301.4	-	34	-	-	-	-	-	-	-
	5	1	1	32.645	13.710	24.428	298.8	-	35	0.16	9.2	-	-	-	-	-
CTD 6-2	1	3375	3321	34.614	1.603	27.693	87.4	93.0	14	-	-	-	197	3.35	-	40.9
	2	3051	3005	34.605	1.639	27.683	81.5	88.8	10	0.49	10.0	-	196	3.39	-	40.6
	3	2789	2748	34.599	1.662	27.676	79.4	87.0	10	-	-	-	194	3.35	-	37.2
	4	2550	2514	34.589	1.696	27.666	75.3	80.1	8	0.54	9.9	-	193	3.44	-	39.3
	5	2284	2253	34.574	1.751	27.650	70.3	75.8	6	0.55	9.9	-	190	3.35	-	40.4
	6	2021	1995	34.552	1.827	27.626	63.7	70.0	4	-	-	-	186	3.53	-	42.2
	7	1516	1499	34.479	2.063	27.549	46.2	54.1	7	0.74	10.7	-	183	3.49	-	46.1
	8	1010	999	34.258	2.315	27.352	38.0	46.8	7	0.79	11.1	-	172	3.44	-	45.1
	9	756	748	34.003	2.165	27.160	72.2	79.7	17	0.77	10.3	-	142	3.3	-	42.8
	10	507	502	33.619	1.803	26.880	157.2	154.7	64	0.58	12.2	-	89.9	2.89	-	33.3
	11	252	250	33.264	1.025	26.648	261.6	265.5	104	0.44	11.6	-	54.9	2.2	-	23.5
	12	50	50	33.115	3.217	26.361	286.0	277.5	100	0.39	12.1	-	36.2	1.77	-	20.5
CTD 7-1	1	3370	3317	34.614	1.604	27.693	86.9	97.2	72	0.47	10.9	-	193	2.64	-	-
	2	3343	3290	34.613	1.606	27.692	86.6	93.0	-	0.45	9.6	-	195	3	-	-
	3	3040	2994	34.606	1.633	27.685	82.2	93.1	67	0.48	9.8	-	197	3.1	-	-
	4	2786	2745	34.601	1.655	27.678	79.4	91.6	61	0.55	9.9	-	195	3.15	-	-
	5	2536	2500	34.592	1.691	27.668	76.4	92.5	22	-	-	-	189	3.2	-	-
	6	2272	2241	34.576	1.749	27.652	70.9	85.4	5	0.60	10.1	-	191	3.54	-	-
	7	2023	1997	34.555	1.821	27.629	63.7	80.3	11	0.61	9.8	-	189	3.25	-	-
	8	1515	1498	34.491	2.032	27.561	48.4	39.9	7	0.64	11.0	-	184	3.15	-	-
	9	1010	999	34.302	2.310	27.388	34.5	50.7	5	0.80	10.9	-	179	3.3	-	-
	10	507	502	33.775	1.858	27.001	120.4	129.6	40	0.73	11.4	-	110	3.1	-	-
	11	253	251	33.357	0.630	26.747	202.9	204.8	51	0.64	11.2	-	67.4	2.17	-	-
	12	244	242	33.336	0.473	26.738	212.3	-	60	0.60	11.8	-	-	-	-	-
CTD 8-1	1	3342	3288	34.611	1.623	27.689	80.2	87.8	26	0.52	10.7	-	202	3.64	-	-
	2	3053	3006	34.603	1.646	27.681	80.1	88.9	11	-	-	-	195	3.48	-	-
	3	2912	2868	34.599	1.660	27.677	78.9	84.6	15	0.51	9.9	-	191	3.48	-	-
	4	2792	2751	34.596	1.673	27.673	77.7	87.8	35	0.55	10.1	-	174	3.48	-	-
	5	2539	2504	34.585	1.713	27.661	73.3	83.7	7	0.59	10.5	-	190	3.43	-	-
	6	2029	2003	34.544	1.863	27.617	59.5	69.7	22	0.67	10.5	-	188	3.27	-	-
	7	1519	1501	34.467	2.089	27.538	43.3	53.7	11	0.72	10.6	-	182	3.53	-	-
	8	1015	1004	34.191	2.283	27.301	40.8	50.4	9	0.77	10.9	-	165	3.48	-	-
	9	505	500	33.558	1.404	26.860	197.7	196.5	123	0.55	11.0	-	71.9	2.53	-	-
	10	251	249	33.237	0.334	26.666	260.3	240.2	78	0.51	12.2	-	51	2.1	-	-

GE99 CTD: Water column analysis

Station	Bottle	Pressure	Depth	Salinity	Pot Temp	Pot Density	O_2CTD	O_2 titr.	CH_4	CO_2(GC)	N_2(GC)	TA	SI	PO_4	NO_2	NO_2NO_2
		dbar	m		°C	kg/m³	µmol/kg	µmol/kg	nl/l	ml/l	ml/l	meq/l	µmol/l	µmol/l	µmol/l	µmol/l
	11	125	124	33.073	0.397	26.531	301.8	288.8	108	0.39	11.0	-	40.5	1.83	-	-
	12	51	50	32.909	0.747	26.379	322.8	316.6	176	0.35	12.2	-	28.7	1.37	-	-
CTD 11-1	2	84	84	33.009	-0.608	26.525	276.0	255.0	2220	0.53	12.1	-	39.9	2.39	-	-
	3	80	80	33.008	-0.608	26.525	275.6	260.9	2169	0.59	12.2	-	41.1	2.43	-	-
	4	74	74	33.008	-0.608	26.525	274.9	255.2	2138	-	-	-	41.7	2.39	-	-
	5	70	70	33.005	-0.611	26.523	274.4	-	2145	0.54	11.7	-	-	-	-	-
	6	60	59	33.004	-0.612	26.522	272.8	255.5	2276	-	-	-	41.1	2.36	-	-
	7	50	50	33.000	-0.615	26.518	272.0	-	2329	0.57	11.8	-	-	-	-	-
	8	40	40	32.965	-0.608	26.490	273.5	257.7	2720	-	-	-	36.2	2.28	-	-
	9	29	29	32.686	0.155	26.231	302.2	-	2896	0.45	12.6	-	-	-	-	-
	10	20	20	30.266	9.213	23.382	322.9	302.5	610	-	-	-	3	0.653	-	-
	11	10	10	28.898	12.682	21.731	298.6	284.5	142	0.24	9.9	-	3.6	0.526	-	-
	12	2	2	28.870	13.062	21.638	297.5	281.6	122	0.15	9.8	-	3.6	0.484	-	-
CTD 12-2	1	614	609	34.016	2.195	27.168	65.7	-	409	-	-	-	-	-	-	-
	2	912	902	34.206	2.302	27.312	37.4	42.1	527	0.72	10.4	-	181	-	-	-
	3	851	842	34.190	2.292	27.299	39.4	43.1	657	0.74	10.2	-	179	-	-	-
	4	749	742	34.149	2.297	27.266	43.6	47.5	617	0.71		-	168	-	-	-
	5	624	618	34.030	2.214	27.178	58.6	59.4	189	0.80	11.2	-	152	-	-	-
	6	500	496	33.786	1.460	27.039	118.0	117.4	238	0.79	9.7	-	119	-	-	-
	7	374	371	33.609	1.190	26.914	146.4	150.1	254	0.81	11.4	-	97.7	-	-	-
	8	249	247	33.448	1.100	26.791	160.6	156.1	497	0.77	11.3	-	84.3	-	-	-
	9	125	124	33.116	-0.708	26.616	299.7	279.8	57	0.48	12.3	-	56.6	-	-	-
	10	50	50	32.818	-0.937	26.383	363.0	370.4	67	0.36	11.5	-	30.6	-	-	-
	11	25	25	32.621	3.729	25.920	402.3	382.7	74	0.26	11.8	-	4.41	-	-	-
	12	3	3	30.407	13.247	22.790	182.2	270.4	55	0.15	8.9	-	1.47	-	-	-
CTD 13-1	1	612	606	34.054	2.064	27.209	62.2	66.0	1311	-	-	-	161	-	-	-
	2	550	545	33.955	1.778	27.152	85.7	87.0	1369	0.65	10.0	-	146	-	-	-
	3	500	495	33.905	1.799	27.110	89.7	88.7	756	-	-	-	137	-	-	-
	4	449	445	33.852	1.678	27.076	100.5	103.2	663	0.60	9.1	-	126	-	-	-
	5	400	397	33.741	1.357	27.010	127.0	123.1	297	0.70	9.8	-	116	-	-	-
	6	349	346	33.667	1.441	26.945	128.0	127.8	202	0.78	11.3	-	108	-	-	-
	7	251	249	33.458	1.072	26.801	164.3	156.6	632	-	-	-	88.1	-	-	-
	8	149	148	33.262	0.491	26.678	231.8	216.0	1905	0.52	10.9	-	65.1	-	-	-
	9	100	100	33.034	-0.622	26.546	320.2	309.1	308	0.38	12.6	-	44.4	-	-	-
	10	50	50	32.732	0.785	26.235	364.6	348.5	109	0.38	12.4	-	14.4	-	-	-
	11	25	24	32.106	7.002	25.140	348.4	343.1	129	0.19	11.2	-	2.21	-	-	-
	12	5	5	29.846	13.145	22.377	283.1	276.0	55	0.14	9.0	-	0.735	-	-	-
CTD 15-1	1	856	847	34.170	2.225	27.289	44.0	50.0	950	-	-	-	177	-	-	-
	2	799	791	34.160	2.218	27.281	44.9	49.6	1894	-	-	-	178	-	-	-
	3	751	743	34.143	2.206	27.269	46.9	50.6	1524	0.70	10.0	-	174	-	-	-
	4	625	619	33.976	1.846	27.163	79.9	81.9	1394	0.69	10.1	-	148	-	-	-
	5	501	497	33.625	-0.138	27.003	208.4	203.1	361	-	-	-	81.7	-	-	-
	6	399	396	33.470	-0.472	26.893	233.8	226.9	840	-	-	-	70.6	-	-	-
	7	251	249	33.383	0.873	26.753	185.1	183.2	1234	0.66	11.0	-	66.7	-	-	-
	8	154	152	33.167	0.094	26.622	264.7	260.0	517	-	-	-	54.6	-	-	-
	9	103	102	32.993	-0.852	26.521	335.3	325.5	206	0.37	12.6	-	36.2	-	-	-
	10	51	50	32.850	0.802	26.328	379.2	395.8	91	0.29	12.6	-	7.59	-	-	-
	11	26	25	32.241	4.815	25.509	354.6	350.7	134	-	-	-	6.96	-	-	-
	12	4	4	29.686	12.886	22.302	286.9	277.3	78	-	-	-	2.53	-	-	-
CTD 16-1	1	361	358	33.433	-0.369	26.859	233.7	226.5	2156	0.56	12.1	-	60.5	-	-	-
	2	338	335	33.407	-0.351	26.836	233.4	226.9	5133	0.55	11.7	-	62.1	-	-	-
	3	320	317	33.405	-0.164	26.826	227.7	216.5	2126	0.58	11.3	-	63.6	-	-	-
	4	300	297	33.396	0.039	26.810	220.5	210.7	1152	-	-	-	62.6	-	-	-
	5	251	249	33.388	0.192	26.795	214.3	213.7	1163	0.59	11.3	-	63.1	-	-	-
	6	203	202	33.342	0.428	26.746	213.1	208.8	1826	0.68	12.2	-	62.6	-	-	-
	7	177	175	33.340	0.945	26.714	197.2	185.8	183	-	-	-	63.1	-	-	-
	8	152	151	33.292	0.692	26.690	216.0	212.0	163	0.58	11.6	-	61.5	-	-	-
	9	103	102	33.141	0.090	26.601	272.2	266.1	277	0.50	13.1	-	50.3	-	-	-
	10	52	52	32.844	0.254	26.354	345.8	343.2	145	0.34	12.8	-	21.9	-	-	-
	11	27	27	32.311	4.727	25.573	346.3	332.6	83	-	-	-	8.2	-	-	-
	12	6	6	29.666	12.609	22.339	289.1	275.5	62	0.15	9.6	-	3.04	-	-	-
CTD 18-1	1	402	399	33.434	-0.380	26.860	234.2	223.1	433	-	-	-	62.1	-	-	-
	2	378	375	33.413	-0.464	26.846	240.2	233.4	500	0.52	11.5	-	59.1	-	-	-
	3	348	345	33.412	-0.481	26.846	240.1	228.1	511	0.51	11.1	-	59.5	-	-	-
	4	316	314	33.412	-0.447	26.845	238.6	228.0	480	0.56	11.4	-	59.1	-	-	-
	5	290	287	33.403	-0.442	26.837	238.7	234.3	518	0.57	11.2	-	60	-	-	-
	6	246	244	33.388	0.042	26.803	219.2	214.8	544	0.63	11.9	-	62.6	-	-	-
	7	197	196	33.356	0.695	26.742	199.4	190.5	885	0.62	11.1	-	61.5	-	-	-
	8	148	147	33.243	0.465	26.664	233.6	224.2	209	0.54	11.8	-	55.9	-	-	-
	9	101	100	32.996	-0.274	26.501	315.8	316.9	558	-	-	-	36.1	-	-	-
	10	51	50	32.774	0.790	26.268	347.7	345.6	122	-	-	-	18.6	-	-	-
	11	27	27	32.278	4.165	25.605	347.5	347.3	104	0.24	11.8	-	6.78	-	-	-
	12	4	4	29.642	12.616	22.319	286.6	277.7	69	0.14	9.4	-	0.76	-	-	-
CTD 19-1	1	394	390	33.420	-0.336	26.847	234.1	-	3651	0.46	10.7	-	66.8	-	-	-
	2	373	370	33.415	-0.345	26.843	233.9	-	4545	-	-	-	73.8	-	-	-
	3	349	345	33.409	-0.309	26.836	233.4	-	4378	-	-	-	65.6	-	-	-
	4	325	322	33.404	-0.237	26.829	230.9	-	3864	0.50	11.1	-	73.8	-	-	-
	5	300	297	33.395	0.035	26.808	220.8	-	1808	0.53	11.0	-	81.7	-	-	-
	6	252	250	33.385	0.185	26.793	215.7	-	1048	0.62	12.0	-	83.6	-	-	-
	7	202	200	33.368	1.018	26.732	188.1	-	155	0.55	10.9	-	87.7	-	-	-
	8	151	150	33.271	0.627	26.678	222.9	-	181	-	-	-	65.6	-	-	-
	9	103	102	33.142	0.124	26.600	274.9	-	104	0.44	11.7	-	54.7	-	-	-
	10	53	52	32.839	0.835	26.318	342.7	-	75	0.30	11.3	-	23.5	-	-	-
	11	25	25	32.344	5.028	25.567	345.1	-	78	-	-	-	5.81	-	-	-
	12	4	4	29.803	12.815	22.406	286.0	-	60	0.15	9.5	-	1.94	-	-	-
CTD 20-1	1	391	387	33.424	-0.360	26.851	237.6	-	2483	0.54	11.9		69.3			
	2	372	369	33.427	-0.359	26.853	235.9	-	1997	0.57	11.6		66.8			
	3	348	345	33.418	-0.247	26.841	230.7	-	1276	0.56	11.5		70			
	4	323	321	33.389	-0.275	26.819	234.9	-	9080	-	-		68.7			
	5	298	296	33.384	-0.214	26.812	233.3	-	7233	0.57	11.2		68.1			
	6	251	249	33.381	0.740	26.759	194.1	-	2093	-	-		76.4			
	7	204	202	33.330	0.877	26.710	202.3	-	162	-	-		71.2			

GE99 CTD: Water column analysis

Station	Bottle	Pressure	Depth	Salinity	Pot Temp	Pot Density	O_2 CTD	O_2 titr.	CH_4	CO_2(GC)	N_2(GC)	TA	Si	PO_4	NO_2	NO_3NO_2
		dbar	m		°C	kg/m³	µmol/kg	µmol/kg	nl/l	ml/l	ml/l	meq/l	µmol/l	µmol/l	µmol/l	µmol/l
	8	153	151	33.213	0.386	26.644	246.1	-	158	0.52	12.1		58.5			
	9	104	103	33.072	0.037	26.548	294.3	-	91	0.43	12.7		47.6			
	10	52	51	32.758	1.125	26.235	342.2	-	125	-	-		23.5			
	11	26	26	31.936	6.004	25.132	339.7	-	87	0.20	11.7		4.52			
	12	4	4	29.718	12.785	22.346	286.1	-	65	0.15	-		5.17			
CTD 21-1	1	906	897	34.244	2.262	27.345	36.1	42.7	62	0.66	10.8	-	188	-	-	-
	2	848	839	34.237	2.260	27.340	37.1	41.9	23	0.69	10.3	-	184	-	-	-
	3	753	746	34.222	2.250	27.328	39.4	44.9	21	0.70	10.2	-	178	-	-	-
	4	625	619	34.144	2.194	27.271	49.0	52.3	37	0.71	10.5	-	165	-	-	-
	5	502	498	33.912	1.868	27.110	91.7	94.4	98	0.71	9.9	-	133	-	-	-
	6	400	396	33.623	1.508	26.904	128.2	128.0	127	0.76	11.6	-	104	-	-	-
	7	300	297	33.446	1.213	26.782	162.8	156.0	163	-	-	-	88.6	-	-	-
	8	200	198	33.282	0.781	26.677	222.0	214.7	44	-	-	-	76.2	-	-	-
	9	103	102	32.997	-0.160	26.497	327.2	323.0	78	0.40	13.2	-	32.4	-	-	-
	10	54	54	32.772	1.450	26.225	355.3	155.0	79	0.32	12.5	-	11.6	-	-	-
	11	28	27	32.525	3.928	25.825	348.8	346.5	79	0.26	12.3	-	7.13	-	-	-
	12	3	3	31.071	10.246	23.846	302.6	289.2	62	0.17	10.4	-	4.36	-	-	-
CTD 24-1	1	692	685	34.144	2.197	27.270	48.8	52.8	1160	0.73	11.3		165			
	2	665	658	34.131	2.184	27.261	49.9	54.7	330	-	-		162			
	3	630	624	34.076	2.116	27.222	57.9	61.2	791	0.75	10.7		142			
	4	587	581	33.984	1.847	27.169	78.6	81.7	119	-	-		141			
	5	544	539	33.875	1.531	27.105	102.7	103.4	117	0.74	10.3		128			
	6	500	496	33.771	1.179	27.046	126.5	129.9	200	-	-		114			
	7	450	445	33.498	-0.820	26.929	243.0	232.6	76	0.63	12.0		70.6			
	8	404	401	33.482	-0.773	26.915	243.3	240.4	77	0.62	11.9		70			
	9	301	298	33.476	1.262	26.803	154.2	154.4	73	0.72	12.1		71.8			
	10	200	199	33.332	1.038	26.702	198.5	197.1	35	0.63	11.6		66			
	11	101	100	33.043	0.183	26.518	308.2	307.7	33	0.38	11.6		39.3			
	12	52	52	32.800	0.651	26.297	347.2	*344.4*	70	0.34	12.6		15.8			
CTD 26-1	1	682	675	34.135	2.190	27.264	50.2	-	229	-	-		166			
	2	661	654	34.125	2.180	27.256	50.8	-	114	0.55	8.6		163			
	3	631	624	34.124	2.180	27.256	51.1	-	125	0.57	9.4		161			
	4	601	595	34.108	2.170	27.243	53.2	-	123	0.59	9.0		163			
	5	551	546	33.974	2.002	27.150	73.0	-	90	0.62	10.1		142			
	6	501	496	33.862	1.750	27.079	92.1	-	118	0.68	10.1		132			
	7	401	398	33.685	1.591	26.948	118.2	-	119	0.61	9.9		107			
	8	300	297	33.400	0.570	26.785	190.0	-	167	0.55	10.8		75.6			
	9	197	196	33.260	0.404	26.681	224.4	-	132	-	-		67.5			
	10	100	99	33.038	-0.025	26.524	309.4	-	85	0.36	12.0		40.5			
	11	49	48	32.844	0.947	26.315	342.7	-	82	-	-		18.4			
	12	5	5	29.776	11.787	22.574	296.8	-	83	0.13	9.2		0			
CTD 27-1	1	685	678	34.167	2.216	27.287	45.0	-	1426	0.58	9.7		169			
	2	670	663	34.153	2.208	27.276	46.1	50.7	1917	-	-		167			
	3	639	633	34.099	2.152	27.238	53.6	61.3	525	0.56	9.0		150			
	4	603	597	34.012	1.957	27.184	68.6	74.7	2329	0.57	9.4		136			
	5	575	570	33.927	1.760	27.130	87.9	88.5	762	0.59	9.9		137			
	6	550	545	33.852	1.302	27.103	114.1	114.6	197	-	-		127			
	7	527	522	33.824	1.412	27.073	114.0	*113.2*	1040	-	-		124			
	8	513	508	33.848	1.827	27.062	92.5	93.2	2537	-	-		129			
	9	501	497	33.835	1.805	27.053	94.4	96.8	354	-	-		126			
	10	481	476	33.738	1.023	27.029	117.5	124.1	364	0.63	10.7		115			
	11	450	446	33.610	-0.128	26.990	198.3	196.6	774	0.54	10.6		89.4			
	12	401	398	33.540	-0.139	26.934	206.1	190.5	203	0.58	11.2		80.6			
CTD 29-1	1	509	504	33.769	0.958	27.058	147.1	145.7	219	-	-		117			
	2	599	593	34.031	2.004	27.195	68.6	71.6	23759	-	-		164			
	3	680	674	34.131	2.184	27.261	49.6	53.7	15370	-	-		172			
	4	648	642	34.116	2.168	27.250	51.9	55.4	8215	-	-		171			
	5	599	593	34.033	2.011	27.196	66.0	69.6	4981	-	-		159			
	6	548	543	33.953	1.886	27.142	79.8	81.6	7128	-	-		164			
	7	498	493	33.747	0.831	27.049	146.6	-	907	-	-		115			
	8	406	402	33.578	0.231	26.947	189.2	197.9	322	-	-		93.2			
	9	382	378	33.529	0.208	26.908	194.2	177.5	179	-	-		93.2			
	10	353	350	33.452	-0.451	26.878	231.6	232.3	207	-	-		73.1			
	11	300	297	33.395	-0.378	26.828	231.6	226.9	1043	-	-		70			
	12	54	53	32.860	0.166	26.370	344.9	-	192	-	-		19.2			
CTD 30-1	1	1462	1445	34.419	2.253	27.486	20.2	-	180	-	-		242	*3*		
	2	1400	1384	34.415	2.256	27.482	21.2	-	18	-	-		238	*2.1*		
	3	1250	1236	34.388	2.286	27.458	25.8	-	14	-	-		213	*2.05*		
	4	1000	990	34.296	2.345	27.380	28.6	-	37	-	-		192	*1.91*		
	5	749	742	34.138	2.304	27.257	43.0	-	255	-	-		169	*1.72*		
	6	500	495	33.812	2.105	27.012	90.8	-	57	-	-		124	*1.17*		
	7	374	371	33.577	1.468	26.870	129.4	-	46	-	-		98.3	*1.27*		
	8	250	248	33.441	1.705	26.745	170.3	-	40	-	-		85	*1.03*		
	9	125	124	33.104	-0.195	26.585	308.6	-	70	-	-		55.8	*0.708*		
	10	49	49	32.870	0.038	26.385	365.2	-	79	-	-		21.2	*0.665*		
	11	25	25	32.655	1.547	26.125	376.6	-	127	-	-		4.88	*0.078*		
	12	5	5	30.752	13.362	23.035	276.3	-	59	-	-		1.39	*0*		
CTD 31-1	1	1562	1544	34.423	2.248	27.490	20.9	30.0	18	-	-		238	*2.79*		
	2	1500	1482	34.418	2.250	27.486	22.8	31.2	8	-	-		230	*2.3*		
	3	1249	1235	34.390	2.283	27.461	24.4	35.0	117	0.61	9.8		210	*2.51*		
	4	1000	990	34.302	2.357	27.384	26.4	37.2	132	0.73	10.5		193	*1.64*		
	5	775	767	34.162	2.337	27.274	39.3	47.1	34	0.77	11.3		173	*1.64*		
	6	624	618	34.002	2.218	27.155	61.4	69.3	94	-	-		148	*1.34*		
	7	499	495	33.760	1.851	26.990	102.4	112.0	52	0.65	10.2		118	*2.3*		
	8	249	247	33.376	1.097	26.734	182.4	182.3	46	0.51	9.9		80.6	*1.24*		
	9	100	99	32.995	-0.755	26.520	345.3	337.0	74	0.35	12.2		47.4	*0.898*		
	10	50	50	32.872	0.185	26.379	355.7	335.1	62	0.25	10.2		19.2	*0.862*		
	11	25	24	32.723	2.746	26.089	371.5	365.0	75	0.24	11.8		10.4	*0.22*		
	12	5	5	30.799	13.119	23.118	272.6	270.7	53	0.13	8.9		8.32	*0.078*		
CTD 32-1	1	1515	1498	34.427	2.243	27.493	21.7	*40.3*	5723	-	-		236	*2.79*		
	2	1505	1487	34.427	2.243	27.493	21.3	*35.6*	5507	-	-		238	*2.29*		
	3	1485	1468	34.427	2.243	27.493	21.0	*38.2*	2375	-	-		237	*1.82*		
	4	1466	1449	34.426	2.242	27.493	20.3	*41.6*		-	-		229	*2.33*		

GE99 CTD: Water column analysis

Station	Bottle	Pressure	Depth	Salinity	Pot Temp	Pot Density	O_2 CTD	O_2 titr.	CH_4	CO_2(GC)	N_2(GC)	TA	Si	PO_4	NO_2	NO_3NO_2
		dbar	m		°C	kg/m³	µmol/kg	µmol/kg	nl/l	ml/l	ml/l	meq/l	µmol/l	µmol/l	µmol/l	µmol/l
	5	1438	1422	34.424	2.244	27.491	19.9	*35.8*	225	-	-		232	*2.29*		
	6	1402	1386	34.423	2.245	27.490	20.0	*39.1*	85	-	-		230	*2.05*		
	7	1365	1350	34.419	2.246	27.487	21.0	*39.6*	12	-	-		222	*2.1*		
	8	1320	1306	34.416	2.251	27.484	21.3	*42.5*	21	-	-		220	*1.67*		
	9	1258	1244	34.409	2.257	27.478	22.0	*40.0*	14	-	-		215	*2.1*		
	10	499	495	33.850	2.243	27.032	80.3	*90.8*	47	-	-		125	*1.42*		
	11	250	248	33.409	1.044	26.763	170.8	*170.4*	30	-	-		78.1	*1.21*		
	12	51	50	32.878	0.108	26.388	359.6	*344.9*	77	-	-		24.8	*0.471*		
CTD 34-1	1	1627	1607	34.425	2.245	27.492	20.0	-	7	-	-		241	*2.65*		
	2	1605	1586	34.425	2.245	27.492	19.6	-	10	-	-		239	*2.24*		
	3	1570	1551	34.425	2.244	27.492	19.7	-	16	0.60	10.1		235	*2.5*		
	4	1534	1516	34.425	2.244	27.491	19.5	-	11	0.55	9.7		237	*2.4*		
	5	1500	1483	34.424	2.244	27.491	19.4	-	13	0.65	10.4		235	*2.35*		
	6	1450	1433	34.423	2.245	27.490	20.0	-	12	0.67	10.4		233	*2.33*		
	7	1400	1384	34.421	2.246	27.488	20.2	-	9	0.62	9.5		230	*2.15*		
	8	1299	1285	34.413	2.256	27.481	21.9	-	7	0.63	10.3		219	*1.67*		
	9	999	988	34.345	2.355	27.419	24.6	-	3	0.66	10.6		192	*1.67*		
	10	501	496	33.837	2.219	27.023	85.4	-	10	0.79	12.5		120	*1.58*		
	11	251	249	33.407	1.156	26.755	173.2	-	39	0.59	11.0		77.5	*1.23*		
	12	50	50	32.828	0.150	26.346	374.4	-	33	0.30	12.3		20.9	*0.235*		
CTD 37-1	1	1563	1545	34.424	2.245	27.491	20.8	*41.5*	933	-	-		236	*2.74*		
	2	1539	1521	34.425	2.245	27.491	20.4	*42.0*	402	0.53	8.6		242	*2.4*		
	3	1507	1489	34.425	2.245	27.491	19.7	*45.0*	533	0.55	9.7		246	*2.79*		
	4	1466	1449	34.425	2.245	27.491	19.1	*40.8*	42	-	-		241	*2.84*		
	5	1431	1414	34.424	2.245	27.491	19.1	*42.4*	33	0.61	10.2		238	*3.09*		
	6	1398	1382	34.424	2.245	27.490	19.0	*41.6*	14	0.68	10.8		237	*2.33*		
	7	1299	1285	34.413	2.255	27.481	22.0	*41.2*	14	0.58	9.8		222	*2.6*		
	8	1001	990	34.347	2.355	27.420	24.6	*53.2*	4	0.63	10.1		191	*2.15*		
	9	502	497	33.837	2.219	27.023	85.5	*100.5*	10	0.67	10.9		126	*2.3*		
	10	252	250	33.415	1.155	26.761	170.8	*186.4*	49	0.60	11.0		83.3	*2.4*		
	11	90	89	32.991	-1.176	26.531	346.1	*356.2*	33	0.34	11.9		43.8	*1.53*		
	12	52	51	32.848	-0.688	26.398	364.6	*358.6*	74	-	-		28.6	*1.02*		
CTD 38-1	1	1048	1037	34.347	2.357	27.420	30.7	37.8	11	-	-					
	2	996	986	34.344	2.357	27.417	30.8	38.1	8	0.59	9.7					
	3	873	864	34.269	2.375	27.356	38.7	43.9	7	0.59	10.0					
	4	750	743	34.172	2.433	27.273	34.5	62.4	12	0.61	9.9					
	5	627	621	34.047	2.314	27.183	64.8	71.0	16	0.64	10.5					
	6	502	498	33.840	2.086	27.036	108.8	109.8	33	0.67	11.1					
	7	401	397	33.652	1.891	26.900	149.1	153.5	51	0.57	11.0					
	8	250	248	33.405	1.353	26.740	208.3	207.6	62	0.48	11.0					
	9	101	100	33.096	-0.066	26.572	306.3	307.2	97	0.36	11.9					
	10	50	50	32.913	0.176	26.413	340.8	329.2	101	0.32	12.5					
	11	24	23	32.699	6.612	25.658	326.1	316.5	76	0.19	10.4					
	12	4	4	32.435	11.432	24.702	290.3	290.8	57	0.15	9.4					
CTD 41-1	1	2716	2677	34.595	1.671	27.673	80.7	88.2	4	0.39	9.3			3.32		
	2	2669	2630	34.596	1.670	27.673	80.5	90.2	3	0.44	9.9			3.03		
	3	2568	2532	34.595	1.674	27.672	79.7	89.3	4	-	-			3.18		
	4	2499	2464	34.504	1.676	27.671	79.4	86.6	4	0.48	10.3			3.13		
	5	2249	2218	34.584	1.713	27.661	75.5	85.0	4	0.46	10.5			3.46		
	6	1999	1973	34.563	1.796	27.637	67.5	81.9	4	0.55	10.9			2.76		
	7	1516	1498	34.496	2.037	27.565	49.1	63.4	6	0.59	10.4			3.22		
	8	1010	999	34.320	2.322	27.401	36.1	48.6	8	0.63	10.0			3.37		
	9	747	739	34.100	2.291	27.228	53.9	74.7	9	0.67	10.5			3.37		
	10	503	498	33.723	2.020	26.947	130.0	138.1	39	0.60	11.4			2.8		
	11	254	252	33.397	1.482	26.725	207.7	220.9	53	0.49	10.8			2.54		
	12	53	52	32.962	1.518	26.373	316.4	329.9	96	0.30	11.5			1.64		

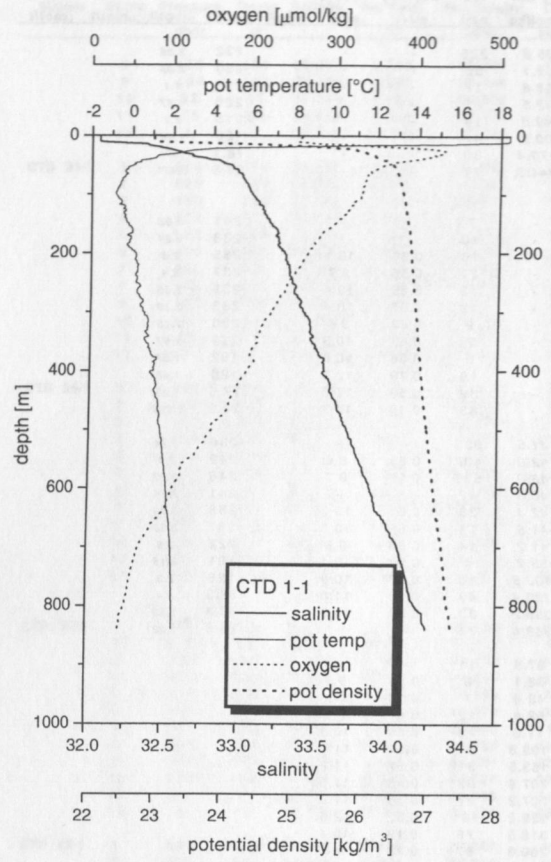
oxygen [µmol/kg]
pot temperature [°C]
depth [m]
CTD 1-1
salinity
pot temp
oxygen
pot density
salinity
potential density [kg/m³]

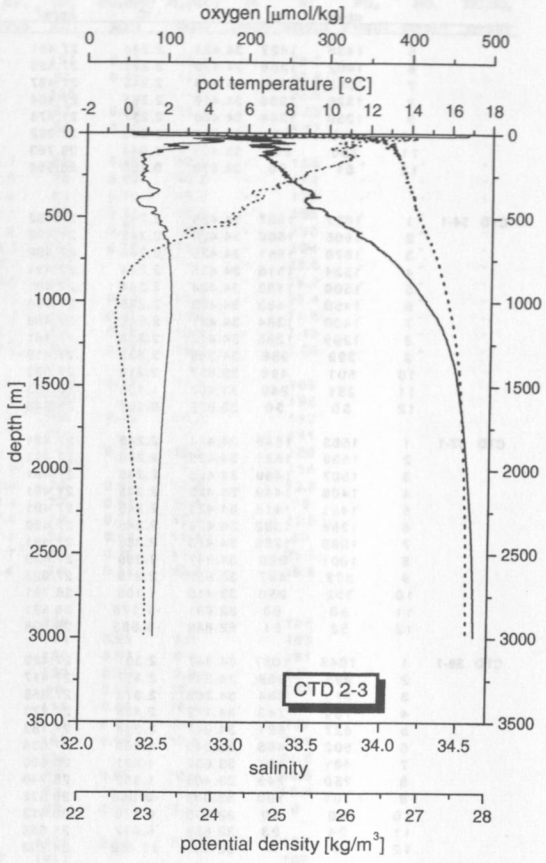
oxygen [µmol/kg]
pot temperature [°C]
depth [m]
CTD 2-3
salinity
potential density [kg/m³]

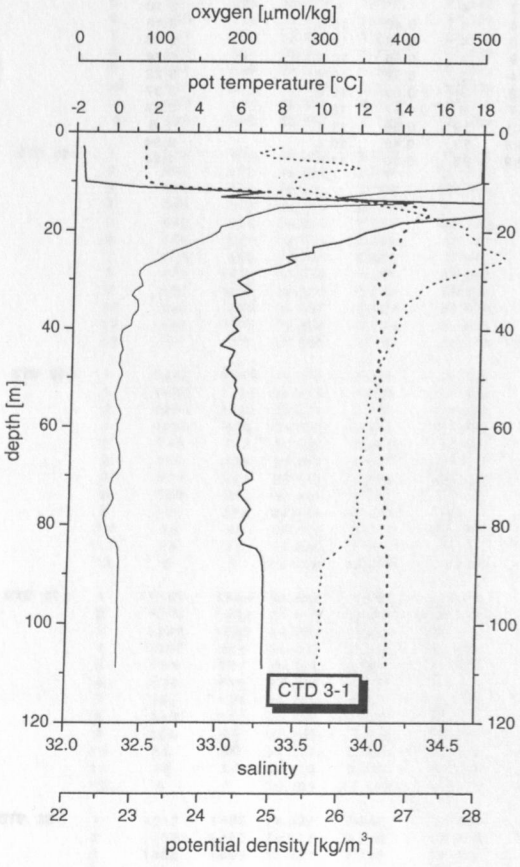
oxygen [µmol/kg]
pot temperature [°C]
depth [m]
CTD 3-1
salinity
potential density [kg/m³]

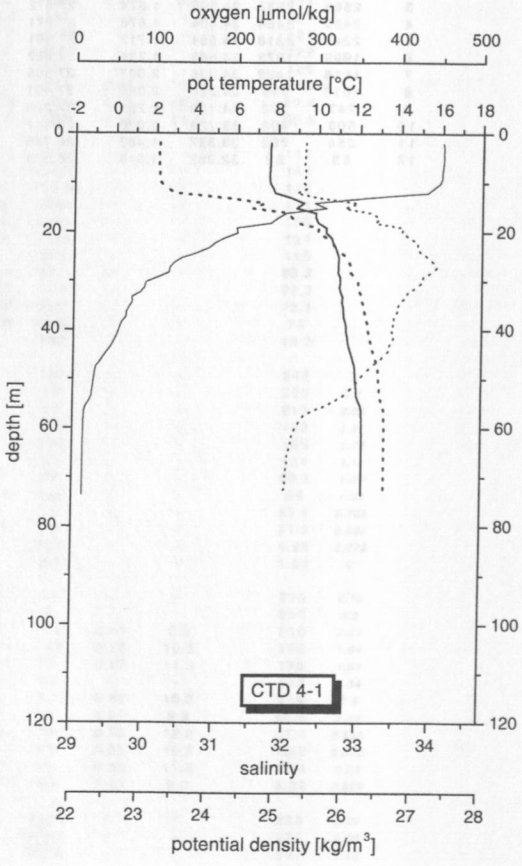
oxygen [µmol/kg]
pot temperature [°C]
depth [m]
CTD 4-1
salinity
potential density [kg/m³]

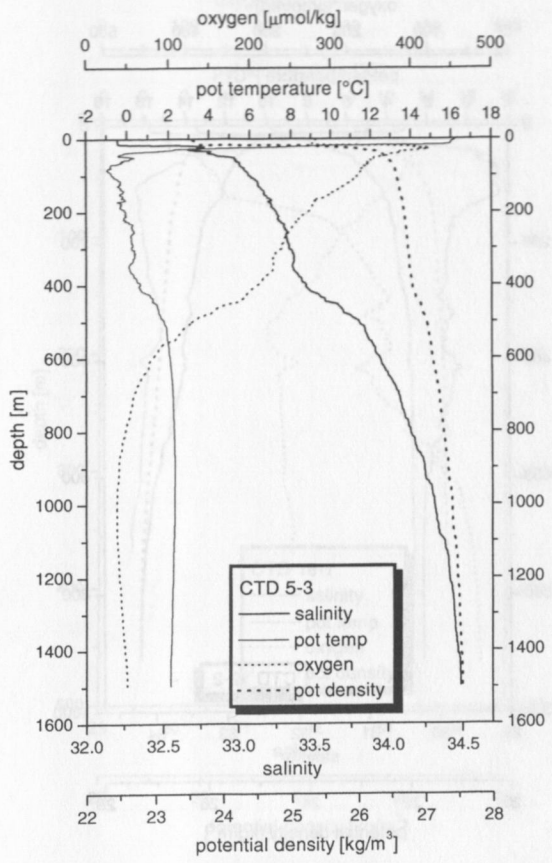
oxygen [µmol/kg]
pot temperature [°C]
depth [m]
CTD 5-3
salinity
pot temp
oxygen
pot density
salinity
potential density [kg/m³]

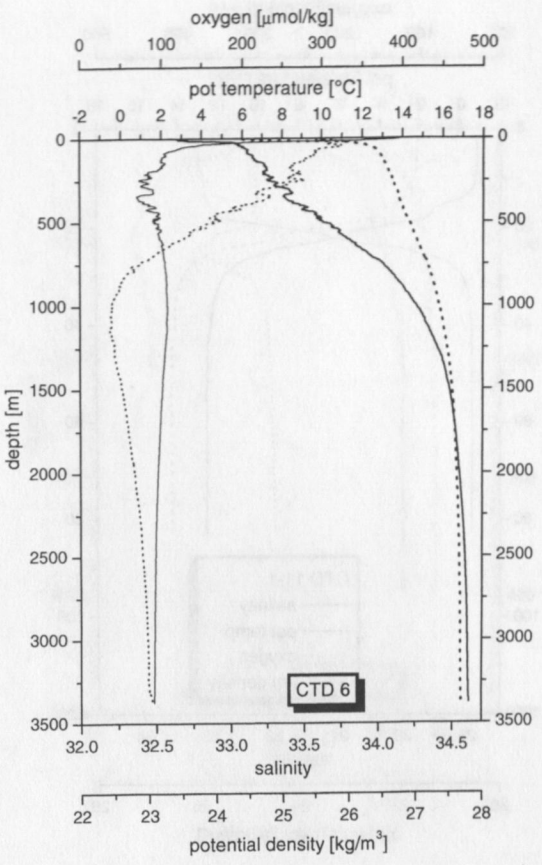
oxygen [µmol/kg]
pot temperature [°C]
depth [m]
CTD 6
salinity
potential density [kg/m³]

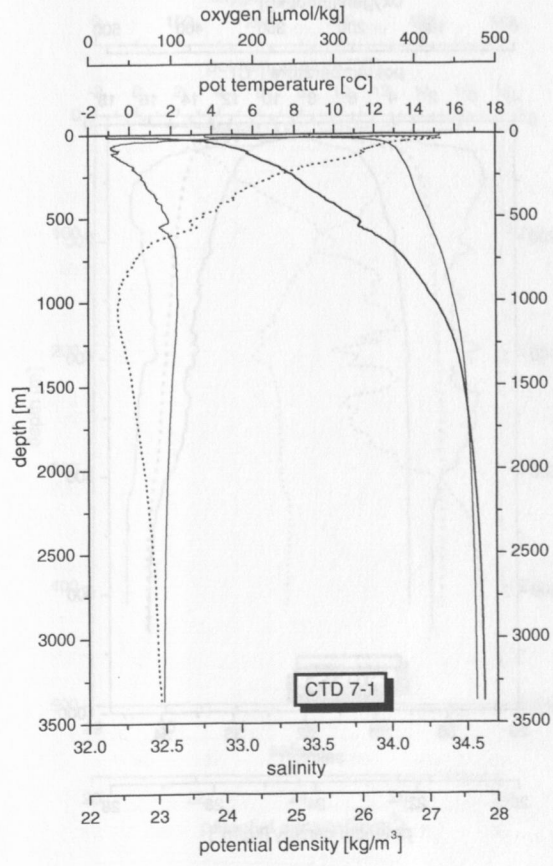
oxygen [µmol/kg]
pot temperature [°C]
depth [m]
CTD 7-1
salinity
potential density [kg/m³]

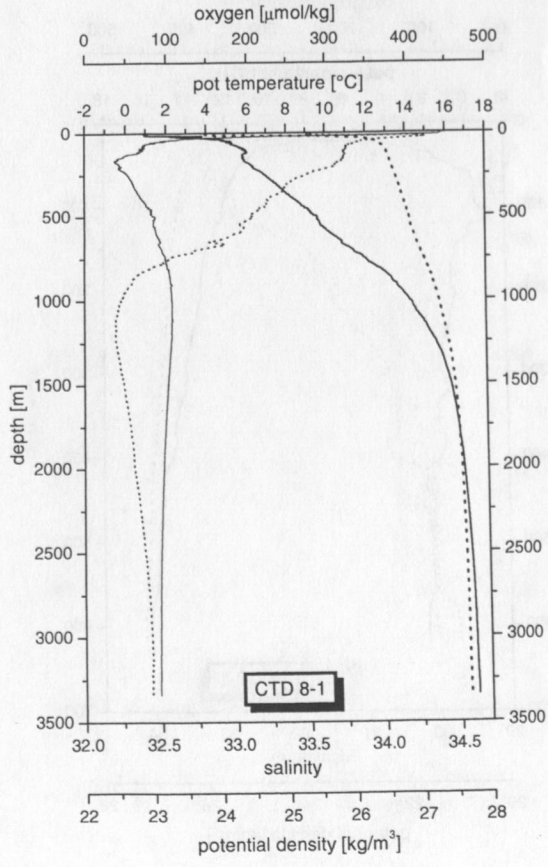
oxygen [µmol/kg]
pot temperature [°C]
depth [m]
CTD 8-1
salinity
potential density [kg/m³]

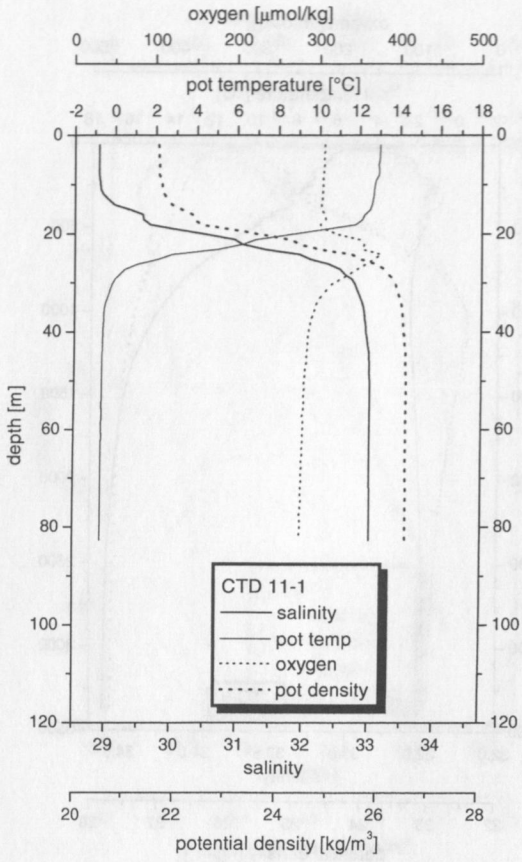
oxygen [µmol/kg]
pot temperature [°C]
depth [m]
CTD 11-1
salinity
pot temp
oxygen
pot density
salinity
potential density [kg/m³]

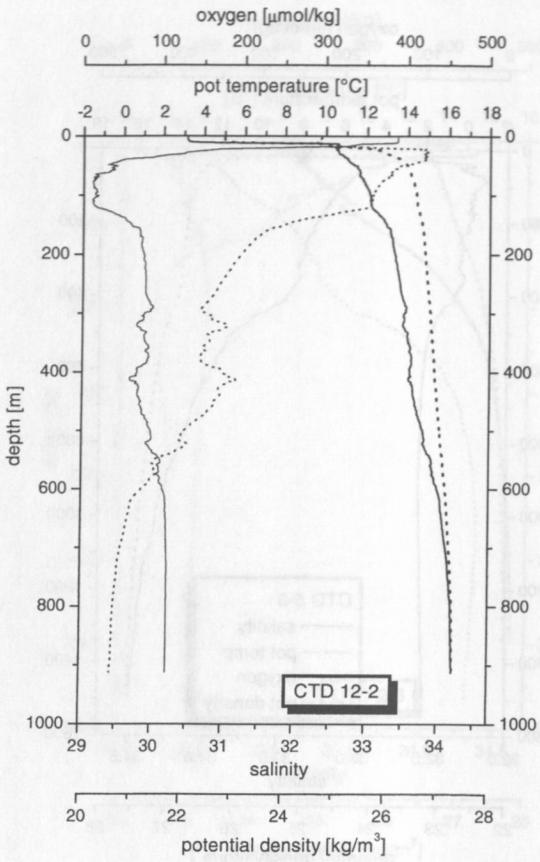
oxygen [µmol/kg]
pot temperature [°C]
depth [m]
CTD 12-2
salinity
potential density [kg/m³]

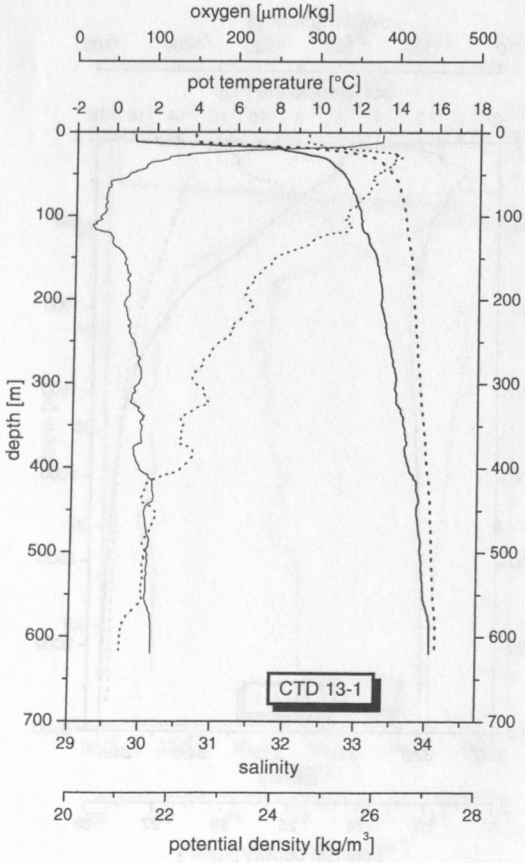
oxygen [µmol/kg]
pot temperature [°C]
depth [m]
CTD 13-1
salinity
potential density [kg/m³]

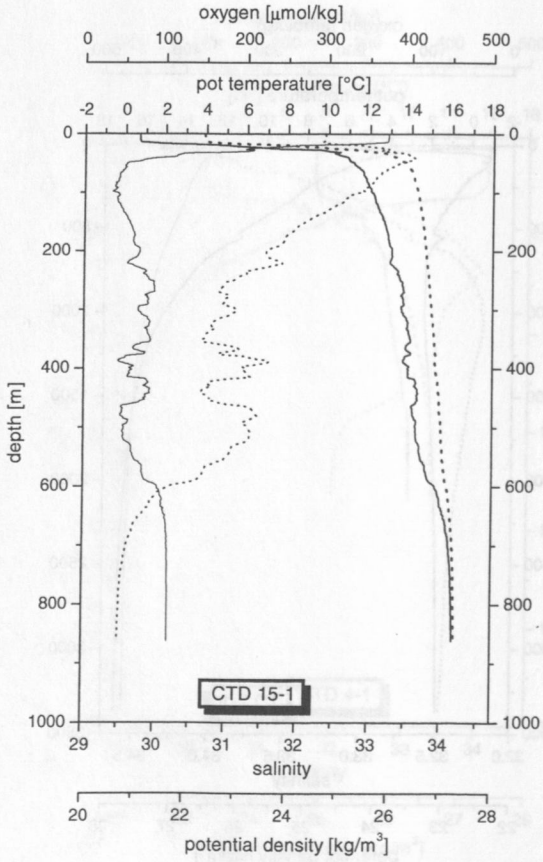
oxygen [µmol/kg]
pot temperature [°C]
depth [m]
CTD 15-1
salinity
potential density [kg/m³]

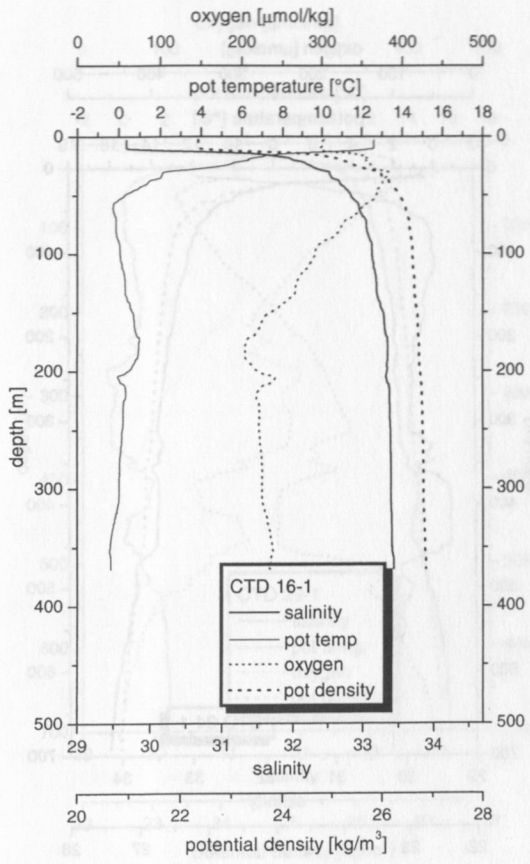
oxygen [µmol/kg]
0 100 200 300 400 500
pot temperature [°C]
-2 0 2 4 6 8 10 12 14 16 18
depth [m]
0 100 200 300 400 500
CTD 16-1
salinity
pot temp
oxygen
pot density
29 30 31 32 33 34
salinity
20 22 24 26 28
potential density [kg/m3]

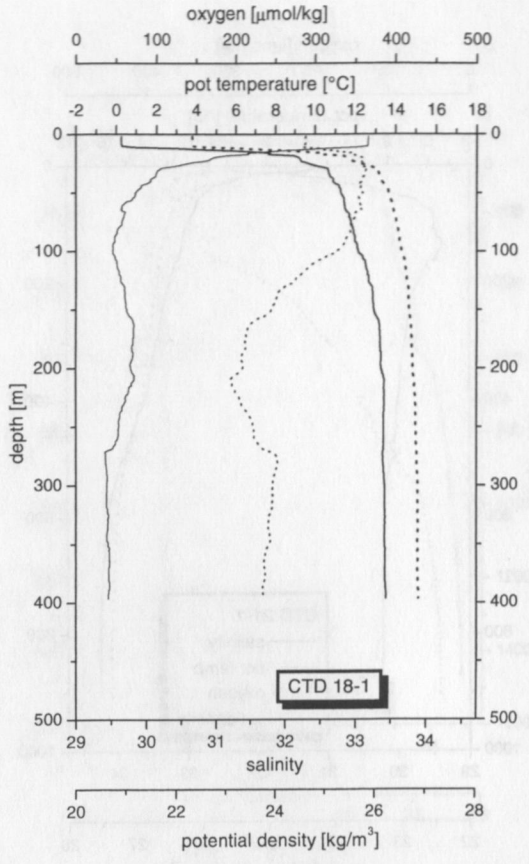
oxygen [µmol/kg]
0 100 200 300 400 500
pot temperature [°C]
-2 0 2 4 6 8 10 12 14 16 18
depth [m]
0 100 200 300 400 500
CTD 18-1
29 30 31 32 33 34
salinity
20 22 24 26 28
potential density [kg/m3]

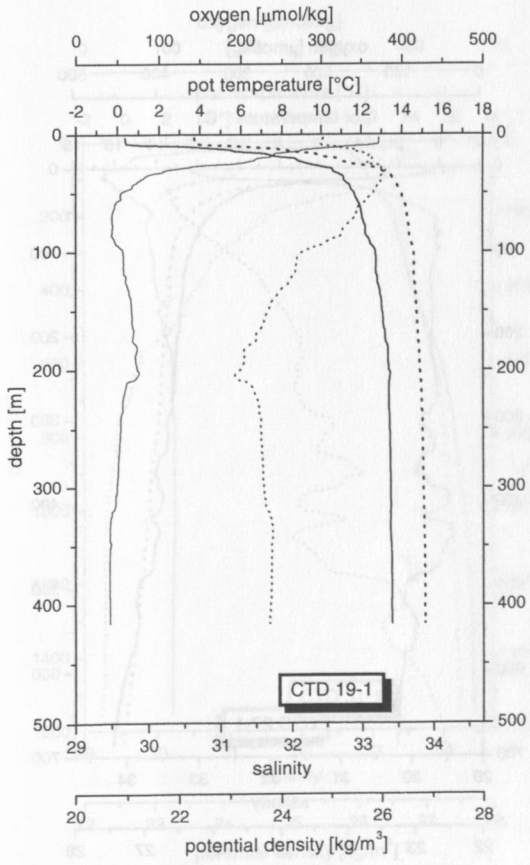
oxygen [µmol/kg]
0 100 200 300 400 500
pot temperature [°C]
-2 0 2 4 6 8 10 12 14 16 18
depth [m]
0 100 200 300 400 500
CTD 19-1
29 30 31 32 33 34
salinity
20 22 24 26 28
potential density [kg/m3]

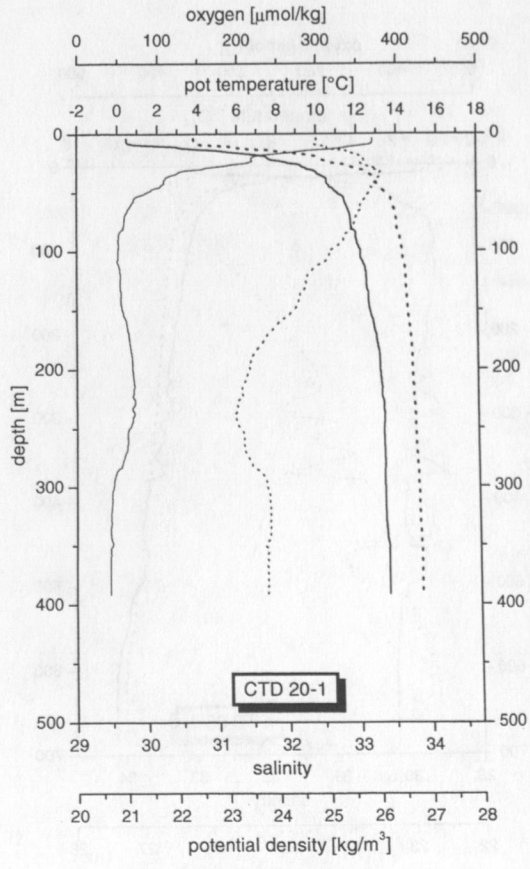
oxygen [µmol/kg]
0 100 200 300 400 500
pot temperature [°C]
-2 0 2 4 6 8 10 12 14 16 18
depth [m]
0 100 200 300 400 500
CTD 20-1
29 30 31 32 33 34
salinity
20 21 22 23 24 25 26 27 28
potential density [kg/m3]

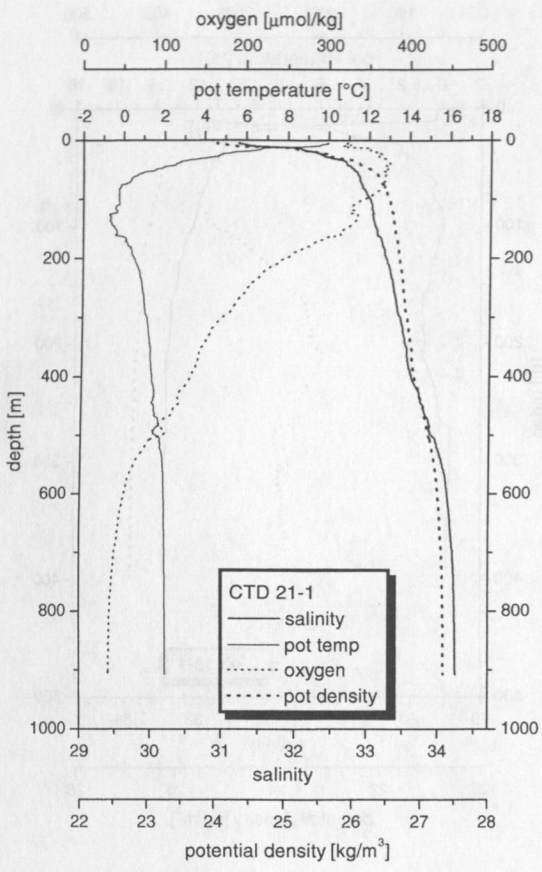
oxygen [µmol/kg]
pot temperature [°C]
depth [m]
CTD 21-1
salinity
pot temp
oxygen
pot density
salinity
potential density [kg/m3]

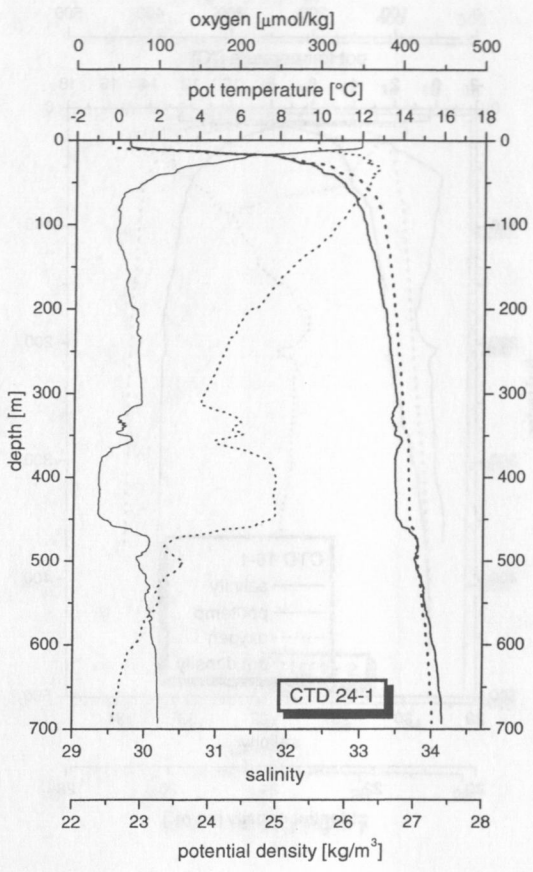
oxygen [µmol/kg]
pot temperature [°C]
depth [m]
CTD 24-1
salinity
potential density [kg/m3]

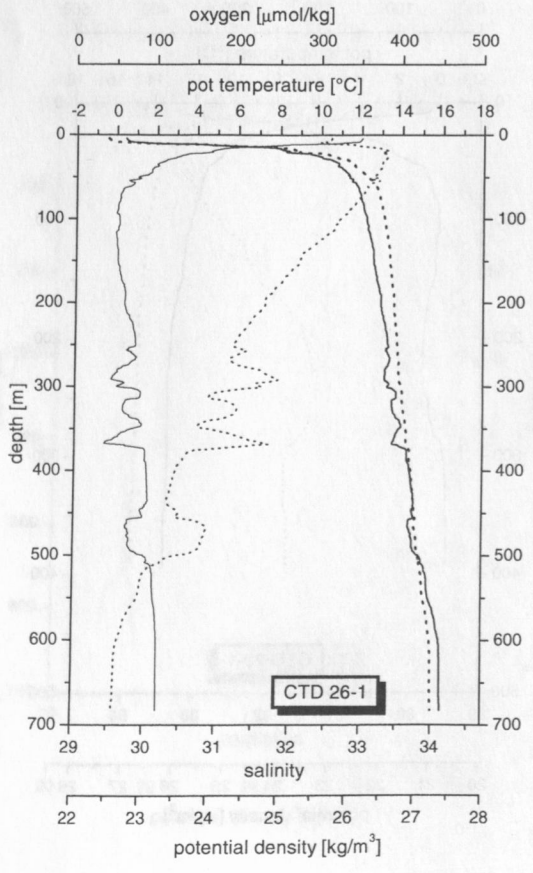
oxygen [µmol/kg]
pot temperature [°C]
depth [m]
CTD 26-1
salinity
potential density [kg/m3]

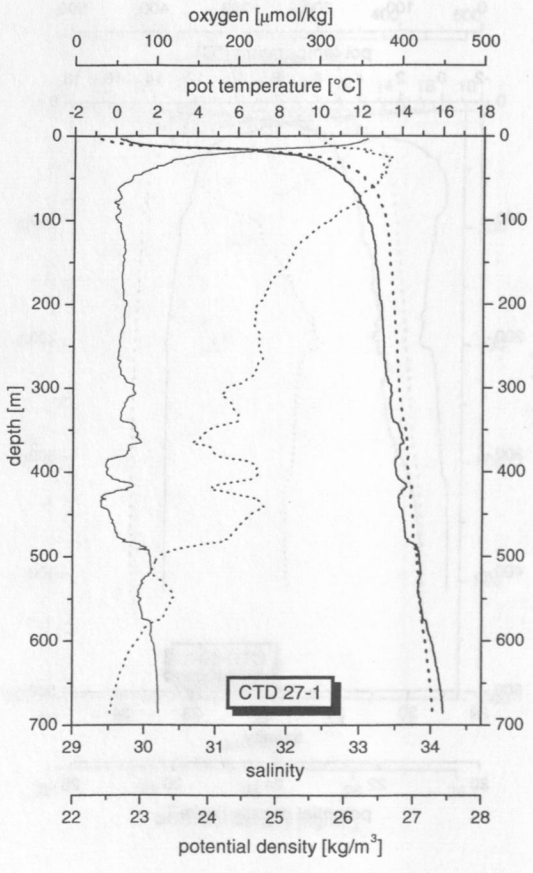
oxygen [µmol/kg]
pot temperature [°C]
depth [m]
CTD 27-1
salinity
potential density [kg/m3]

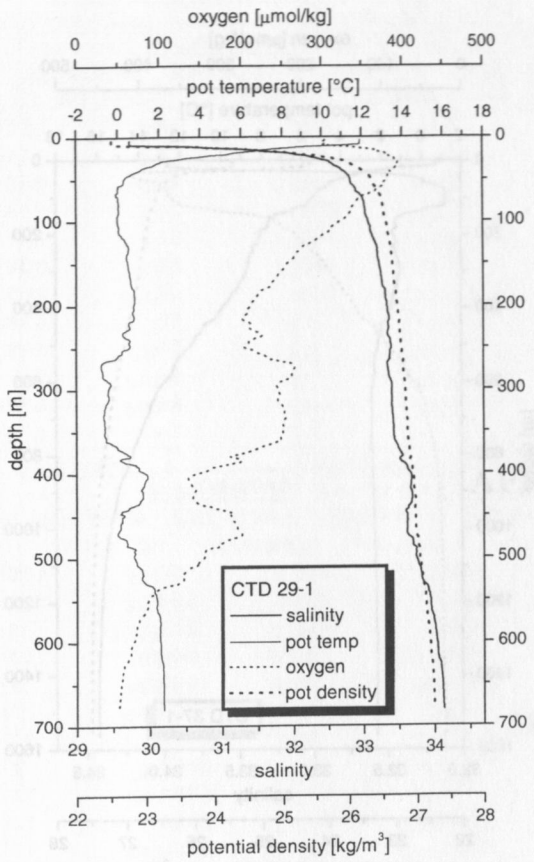
oxygen [µmol/kg]
pot temperature [°C]
depth [m]
CTD 29-1
salinity
pot temp
oxygen
pot density
salinity
potential density [kg/m³]

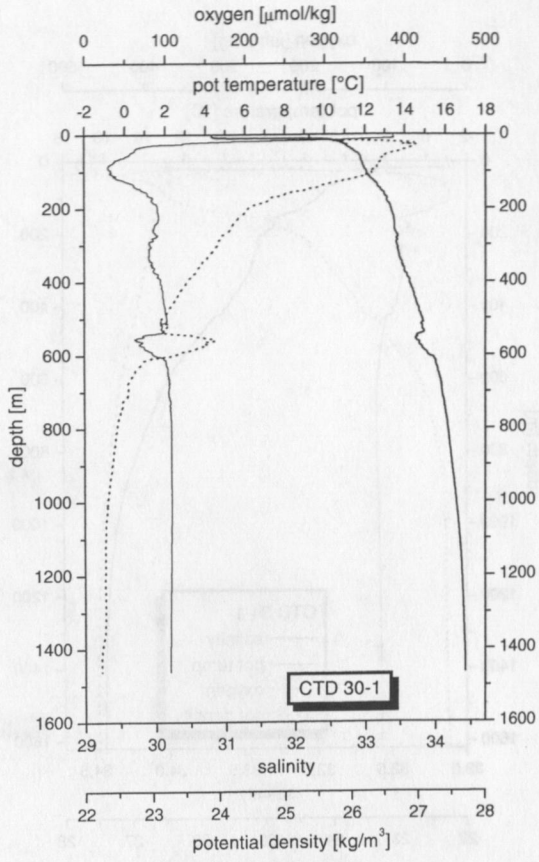
oxygen [µmol/kg]
pot temperature [°C]
depth [m]
CTD 30-1
salinity
potential density [kg/m³]

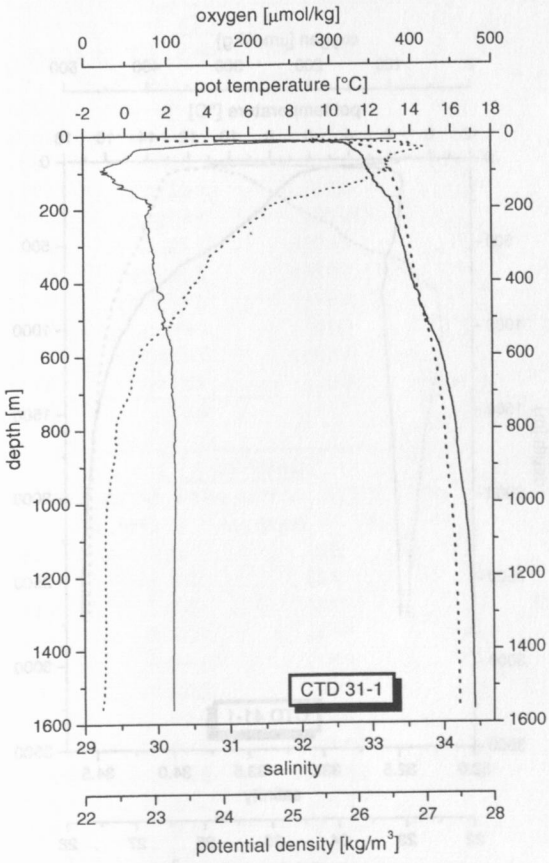
oxygen [µmol/kg]
pot temperature [°C]
depth [m]
CTD 31-1
salinity
potential density [kg/m³]

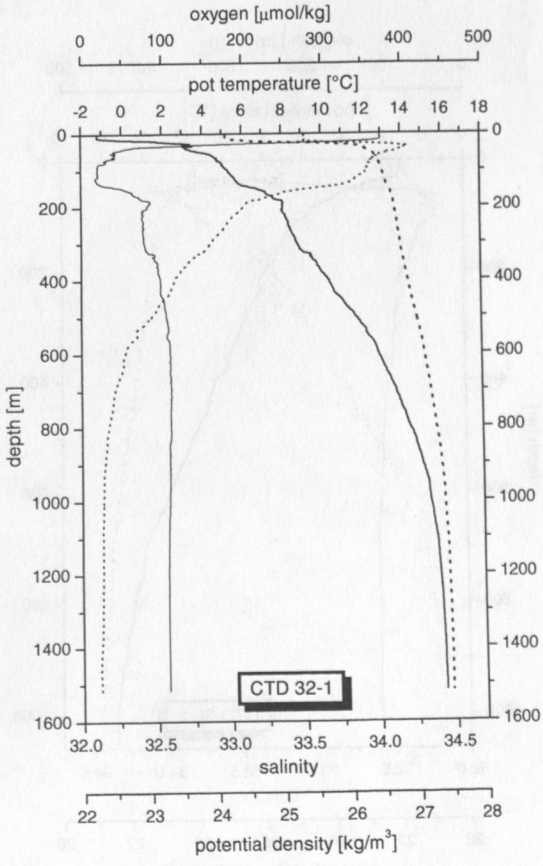
oxygen [µmol/kg]
pot temperature [°C]
depth [m]
CTD 32-1
salinity
potential density [kg/m³]

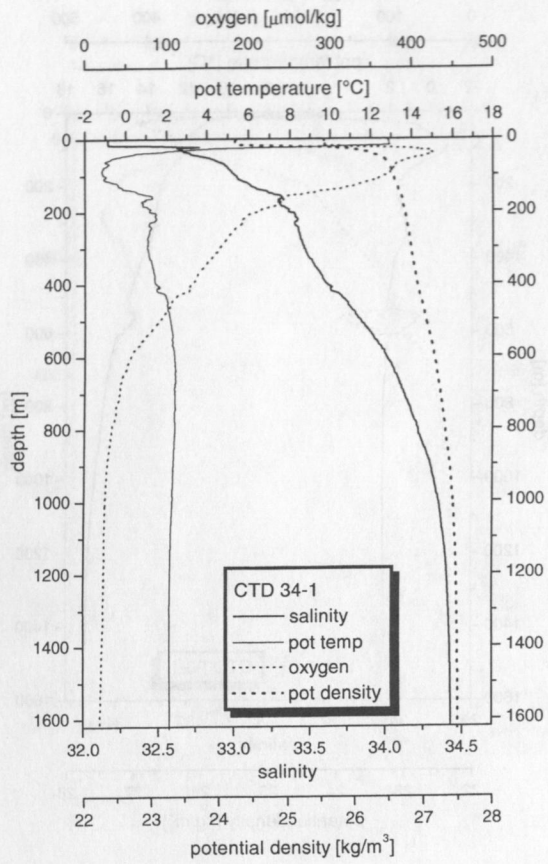
oxygen [µmol/kg]
pot temperature [°C]
depth [m]
salinity
potential density [kg/m³]
CTD 34-1
salinity
pot temp
oxygen
pot density

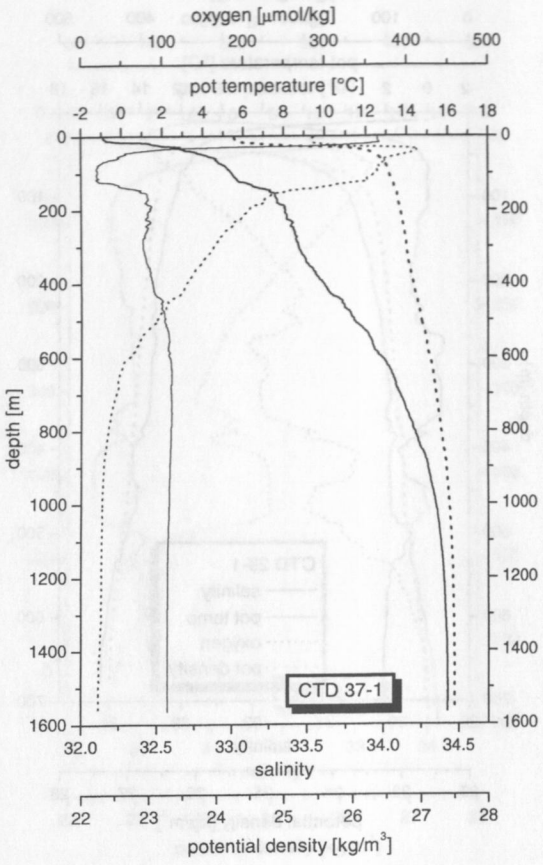
oxygen [µmol/kg]
pot temperature [°C]
depth [m]
salinity
potential density [kg/m³]
CTD 37-1

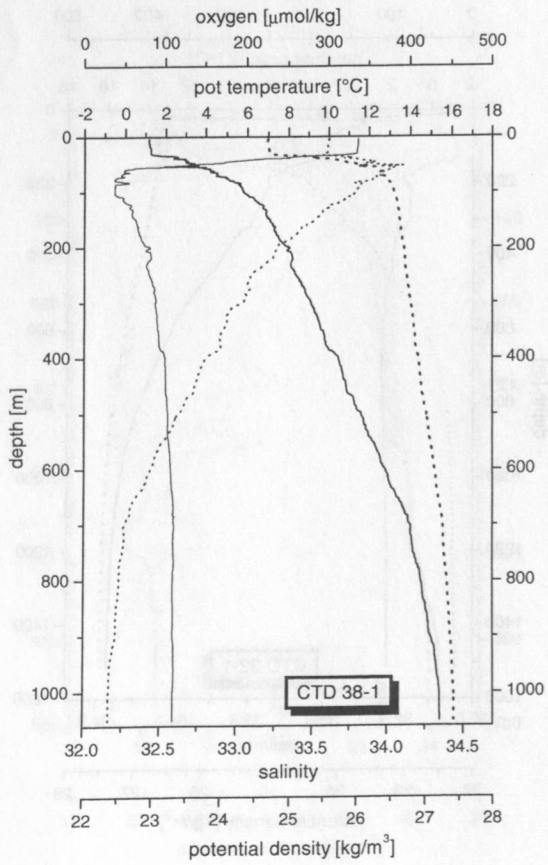
oxygen [µmol/kg]
pot temperature [°C]
depth [m]
salinity
potential density [kg/m³]
CTD 38-1

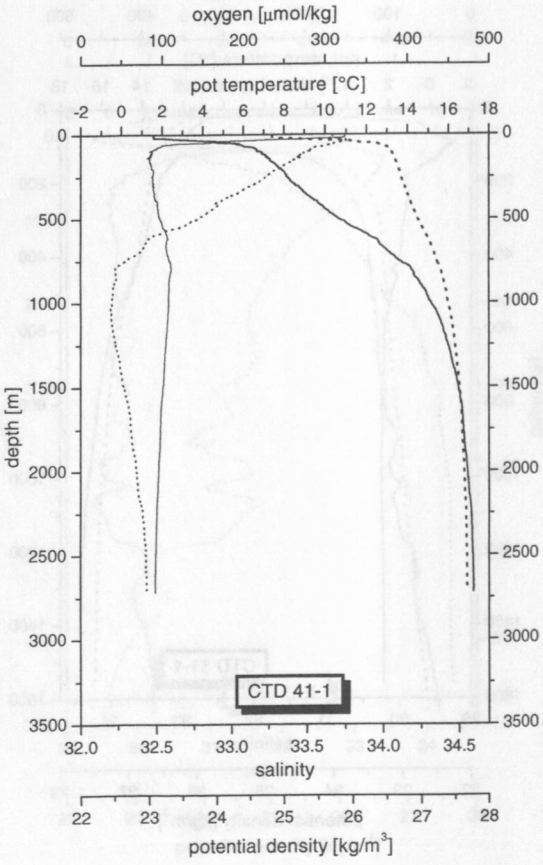
oxygen [µmol/kg]
pot temperature [°C]
depth [m]
salinity
potential density [kg/m³]
CTD 41-1

APPENDIX 4

Methane data

Ge99-1-1		Ge99-2-3		Ge99-3-1		Ge99-4-1	
144°23.56'E	45°37.65'N	144°40.843'E	46°43.7'N	143°10.609'E	45°30.954'N	143°33.88'E	48°00.52'N
depth, m	CH4, nl/l	depth, m	CH4, nl/l	depth, m	CH4, nl/l	depth, m	CH4, nl/l
1.5	56	53	138	3	53	3	85
10	70	156	140	10	61	9	111
25	158	506	113	26	187	20	298
52	261	1003	14	50	226	24	254
100	163	1504	7	74	160	30	231
250	94	1747	16	99	182	39	306
373	134	2004	27	108	181	49	403
495	113	2248	178			53	556
745	38	2504	11			59	563
793	152	2753	11			64	543
835	117	2939	21			69	572
						74	579

Ge99-5-3		Ge99-6-2		Ge99-7-1		Ge99-8-1	
145°29.52'E	47°22.64'N	148°23.615'E	47°16.807'N	147°09.86'E	47°14.34'N	146°01.79'E	46°49.68'N
depth, m	CH4, nl/l	depth, m	CH4, nl/l	depth, m	CH4, nl/l	depth, m	CH4, nl/l
2	43	50	100	242	60	50	176
25	111	250	104	251	51	124	108
50	158	502	64	502	40	249	78
126	37	748	17	999	5	500	123
252	31	999	7	1498	7	1004	9
378	143	1498	7	1997	11	1501	11
506	34	1995	4	2241	5	2003	22
757	21	2253	6	2500	22	2504	7
1011	11	2514	8	2745	61	2751	35
1261	15	2748	10	2994	67	2868	15
1465	13	3005	10	3317	72	3006	11
1496	9	3321	14			3288	26

Ge99-11-1		Ge99-12-2		Ge99-13-1		Ge99-15-1	
143°52.639'E	51°21.202'N	144°48.577'E	52°50.984'N	144°25.672'E	53°22.742'N	144°14.867'E	53°52.490'N
depth, m	CH4, nl/l	depth, m	CH4, nl/l	depth, m	CH4, nl/l	depth, m	CH4, nl/l
2	122	3	55	5	55	4	78
10	142	25	74	24	129	25	134
20	610	50	67	50	109	50	91
29	2896	124	57	100	308	102	206
40	2720	247	497	148	1905	152	517
50	2329	371	254	249	632	249	1234
59	2276	496	238	346	202	396	840
70	2145	609	409	397	297	497	361
74	2138	618	189	445	663	619	1394
80	2169	742	617	495	756	743	1524
84	2220	842	657	545	1369	791	1894
		902	527	606	1311	847	950

Ge99-16-1		Ge99-18-1		Ge99-19-1		Ge99-20-1	
143°58.902'E	54°22.639'N	143°57.373'E	54°28.265'N	143°59.014'E	54°18.277'N	143°58.947'E	54°21.813'N
depth, m	CH4, nl/l	depth, m	CH4, nl/l	depth, m	CH4, nl/l	depth, m	CH4, nl/l
6	62	4	69	4	60	4	65
27	83	27	104	25	78	26	87
52	145	50	122	52	75	51	125
102	277	100	558	102	104	103	91
151	163	147	209	150	181	151	158
175	183	196	885	200	155	202	162
202	1826	244	544	250	1048	249	2093
249	1163	287	518	297	1808	296	7233
297	1152	314	480	322	3864	321	9080
317	2126	345	511	345	4378	345	1276
335	5133	375	500	370	4545	369	1997
358	2156	399	433	390	3651	387	2483

Ge99-21-1		Ge99-24-1		Ge99-26-1		Ge99-27-1	
144°21.105'E	54°55.664'N	144°05.159'E	54°26.876'N	144°05.152'E	54°30.940'N	144°04.832'E	54°26.775'N
depth, m	CH4, nl/l	depth, m	CH4, nl/l	depth, m	CH4, nl/l	depth, m	CH4, nl/l
3	62	52	70	5	83	398	203
27	79	100	33	48	82	446	774
54	79	199	35	99	85	476	364
102	78	298	73	196	132	497	354
198	44	401	77	297	167	508	2537
297	163	445	76	398	119	522	1040
396	127	496	200	496	118	545	197
498	98	539	117	546	90	570	762
619	37	581	119	595	123	597	2329
746	21	624	791	624	125	633	525
839	23	658	330	654	114	663	1917
897	62	685	1160	675	229	678	1426

Ge99-29-1		Ge99-30-1		Ge99-31-1		Ge99-32-1	
144°04.728'E	54°26.674'N	144°07.993'E	54°24.471'N	145°52.313'E	54°24.127'N	146°17.092'E	53°59.854'N
depth, m	CH4, nl/l	depth, m	CH4, nl/l	depth, m	CH4, nl/l	depth, m	CH4, nl/l
53	192	5	59	5	53	50	77
297	1043	25	127	24	75	248	30
350	207	49	79	50	62	495	47
378	179	124	70	99	74	1244	14
402	322	248	40	247	46	1306	21
493	907	371	46	495	52	1350	12
504	219	495	57	618	94	1386	85
543	7128	742	255	767	34	1422	225
593	23759	990	37	990	132	1468	2375
593	4981	1236	14	1235	117	1487	5507
642	8215	1384	18	1482	8	1498	5723
673	15370	1445	180	1544	18		

Ge99-34-1		Ge99-37-1		Ge99-38-1		Ge99-41-1	
146°11.367'E	54°01.128'N	146°16.497'E	54°00.739'N	150°28.088'E	49°22.289'N	151°49.610'E	48°18.093'N
depth, m	CH4, nl/l	depth, m	CH4, nl/l	depth, m	CH4, nl/l	depth, m	CH4, nl/l
50	33	51	74	4	57	52	96
249	39	89	33	23	76	252	53
496	10	250	49	50	101	498	39
988	3	497	10	100	97	739	9
1285	7	990	4	248	62	999	8
1384	9	1285	14	397	51	1498	6
1433	12	1382	14	498	33	1973	4
1483	13	1414	33	621	16	2218	4
1516	11	1449	42	743	12	2464	4
1551	16	1489	533	864	7	2532	4
1586	10	1521	402	986	8	2630	3
1607	7	1545	933	1037	11	2677	4

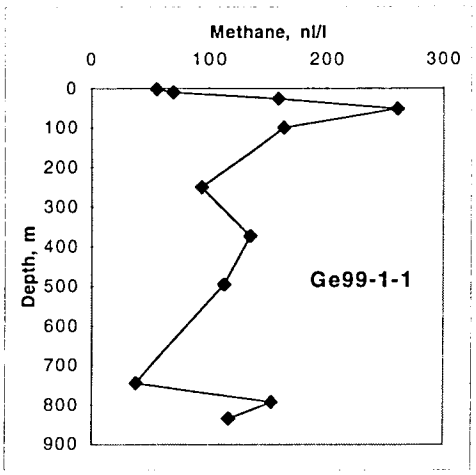
Methane, nl/l
0
100
200
300
Depth, m
0
100
200
300
400
500
600
700
800
900
Ge99-1-1

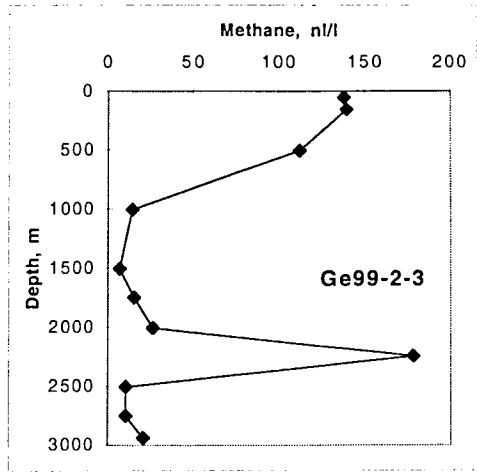
Methane, nl/l
0
50
100
150
200
Depth, m
0
500
1000
1500
2000
2500
3000
Ge99-2-3

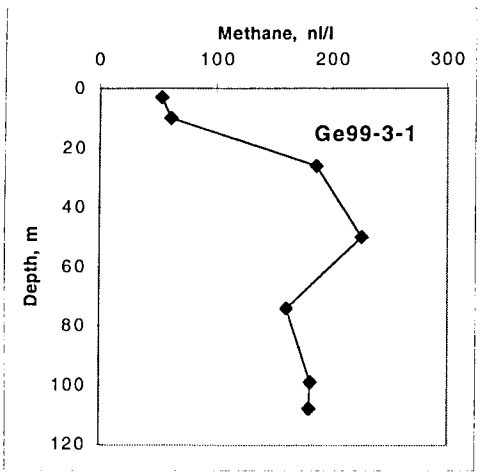
Methane, nl/l
0
100
200
300
Depth, m
0
20
40
60
80
100
120
Ge99-3-1

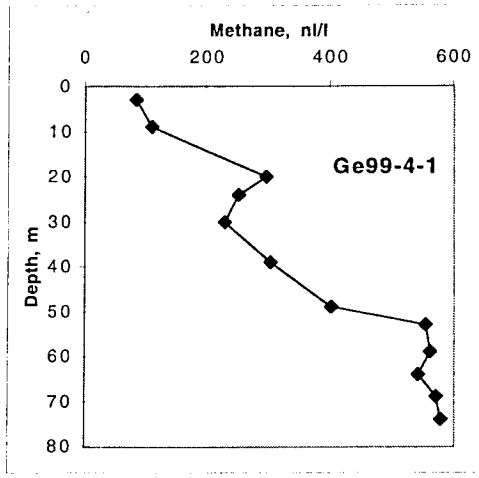
Methane, nl/l
0
200
400
600
Depth, m
0
10
20
30
40
50
60
70
80
Ge99-4-1

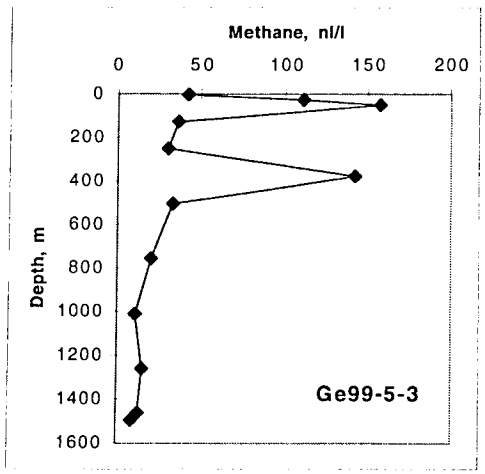
Methane, nl/l
0
50
100
150
200
Depth, m
0
200
400
600
800
1000
1200
1400
1600
Ge99-5-3

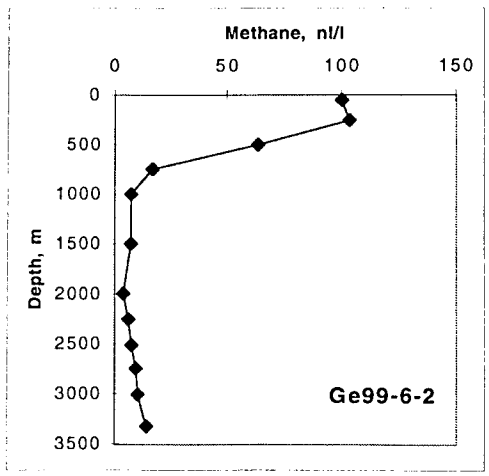
Methane, nl/l
0
50
100
150
Depth, m
0
500
1000
1500
2000
2500
3000
3500
Ge99-6-2

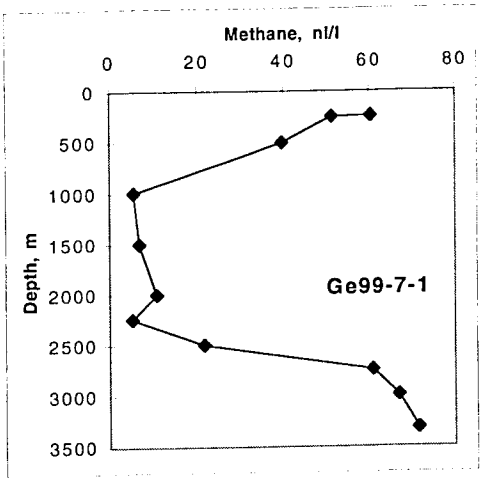
Methane, nl/l
0
20
40
60
80
Depth, m
0
500
1000
1500
2000
2500
3000
3500
Ge99-7-1

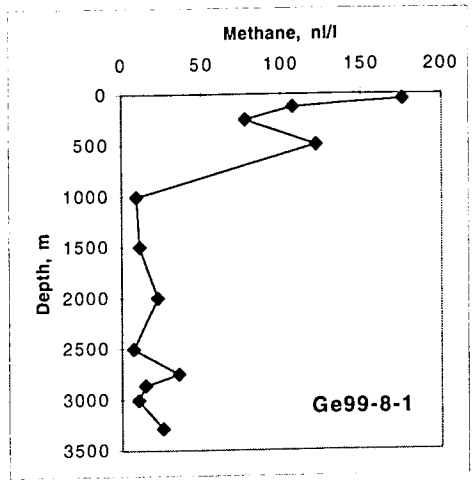
Methane, nl/l
0
50
100
150
200
Depth, m
0
500
1000
1500
2000
2500
3000
3500
Ge99-8-1

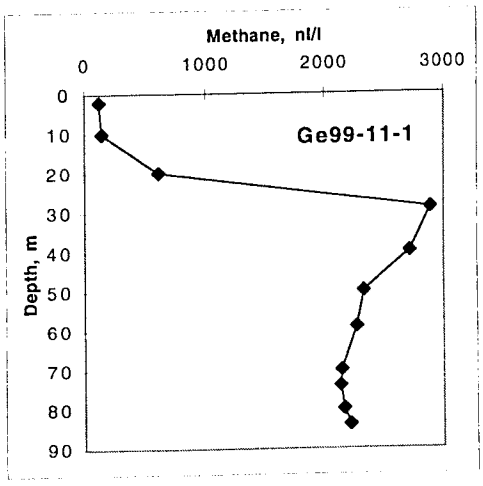
Methane, nl/l
0
1000
2000
3000
Depth, m
0
10
20
30
40
50
60
70
80
90
Ge99-11-1

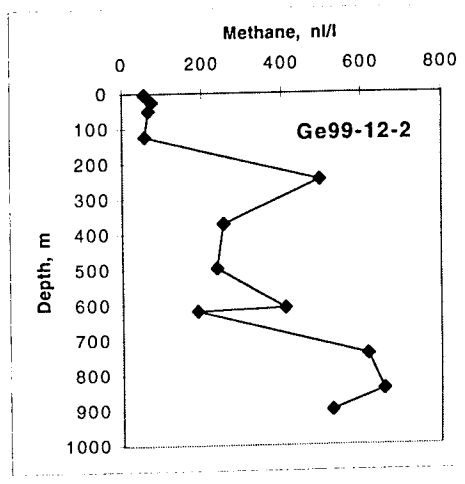
Methane, nl/l
0
200
400
600
800
Depth, m
0
100
200
300
400
500
600
700
800
900
1000
Ge99-12-2

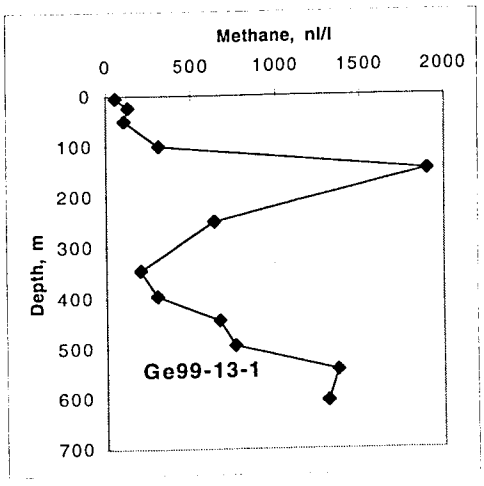
Methane, nl/l
0
500
1000
1500
2000
Depth, m
0
100
200
300
400
500
600
700
Ge99-13-1

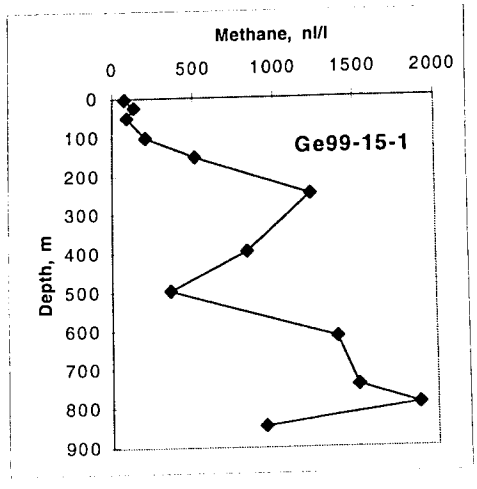
Methane, nl/l
0
500
1000
1500
2000
Depth, m
0
100
200
300
400
500
600
700
800
900
Ge99-15-1

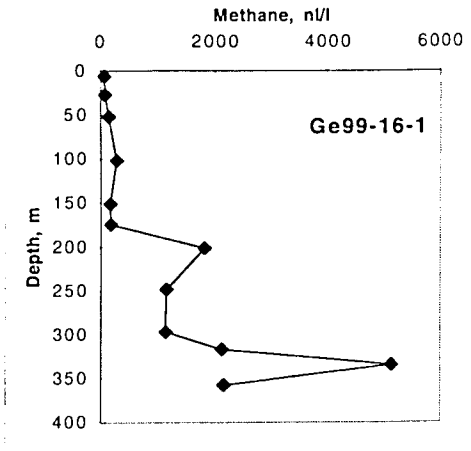
Methane, nl/l
0
2000
4000
6000
Depth, m
0
50
100
150
200
250
300
350
400
Ge99-16-1

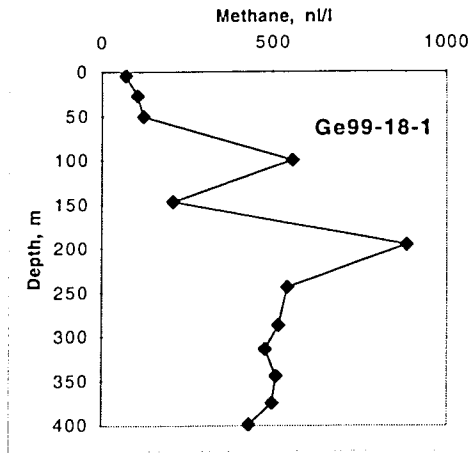
Methane, nl/l
0
500
1000
Depth, m
0
50
100
150
200
250
300
350
400
Ge99-18-1

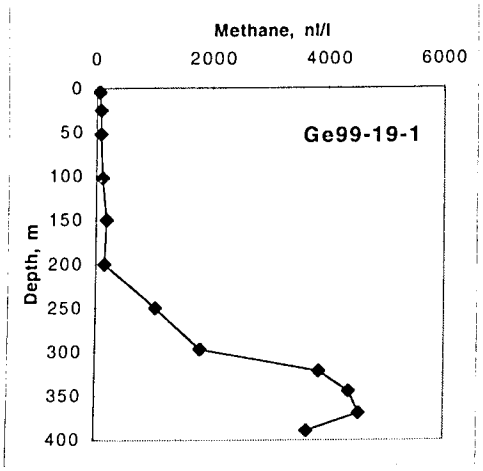
Methane, nl/l
0
2000
4000
6000
Depth, m
0
50
100
150
200
250
300
350
400
Ge99-19-1

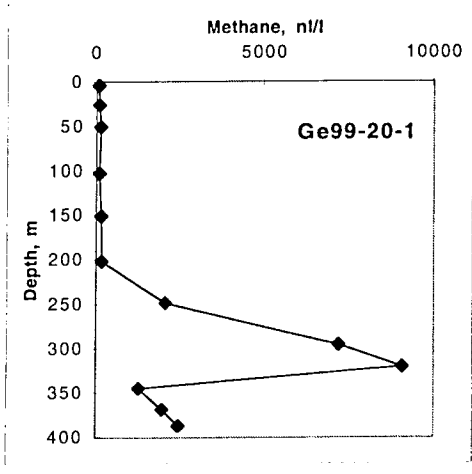
Methane, nl/l
0
5000
10000
Depth, m
0
50
100
150
200
250
300
350
400
Ge99-20-1

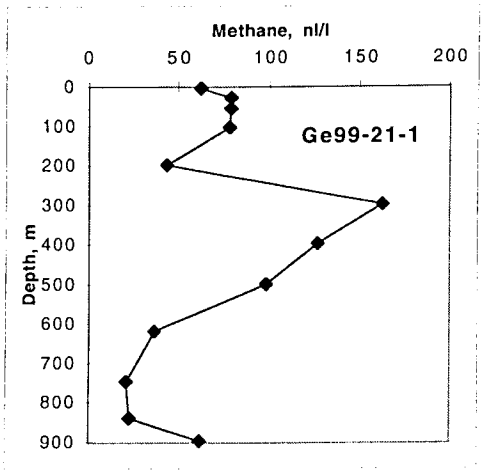
Methane, nl/l
0
50
100
150
200
Depth, m
0
100
200
300
400
500
600
700
800
900
Ge99-21-1

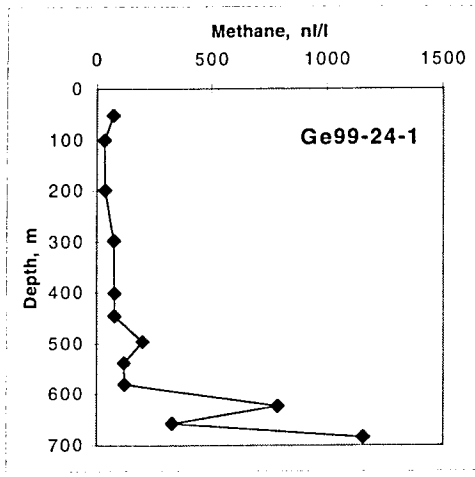
Methane, nl/l
0
500
1000
1500
Depth, m
0
100
200
300
400
500
600
700
Ge99-24-1

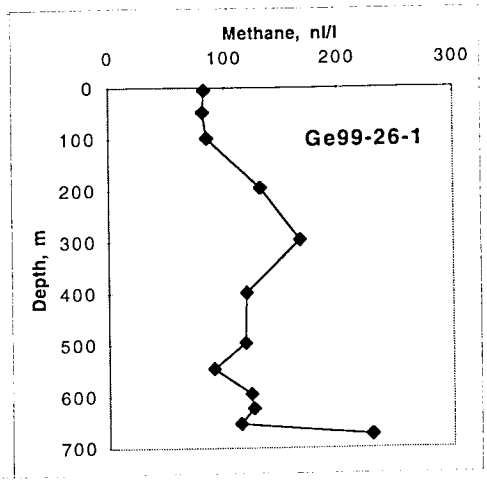
Methane, nl/l
0
100
200
300
Depth, m
0
100
200
300
400
500
600
700
Ge99-26-1

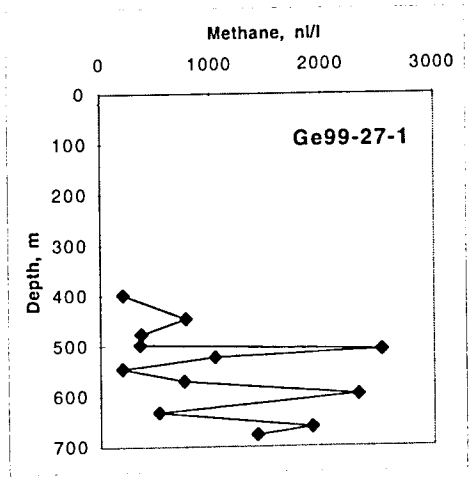
Methane, nl/l
0
1000
2000
3000
Depth, m
0
100
200
300
400
500
600
700
Ge99-27-1

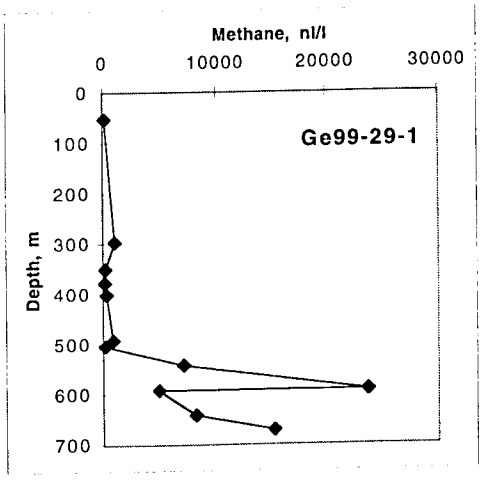
Methane, nl/l
0
10000
20000
30000
Depth, m
0
100
200
300
400
500
600
700
Ge99-29-1

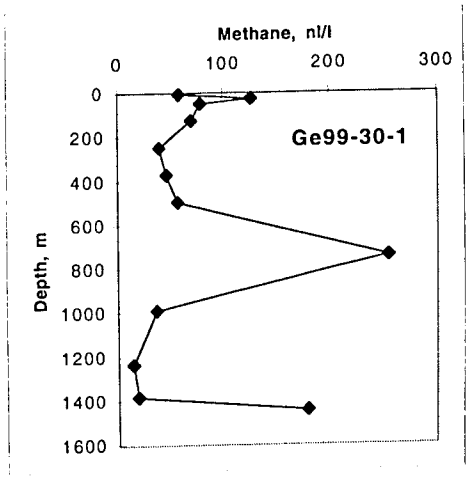
Methane, nl/l
0
100
200
300
Depth, m
0
200
400
600
800
1000
1200
1400
1600
Ge99-30-1

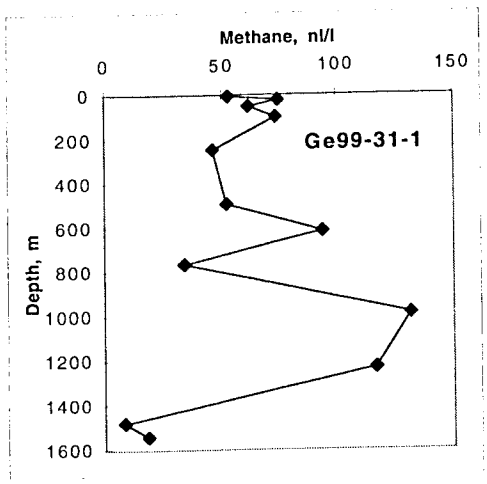
Methane, nl/l
0
50
100
150
Depth, m
0
200
400
600
800
1000
1200
1400
1600
Ge99-31-1

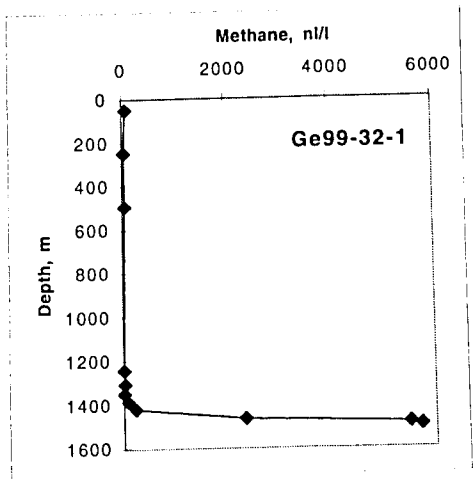
Methane, nl/l
0
2000
4000
6000
Depth, m
0
200
400
600
800
1000
1200
1400
1600
Ge99-32-1

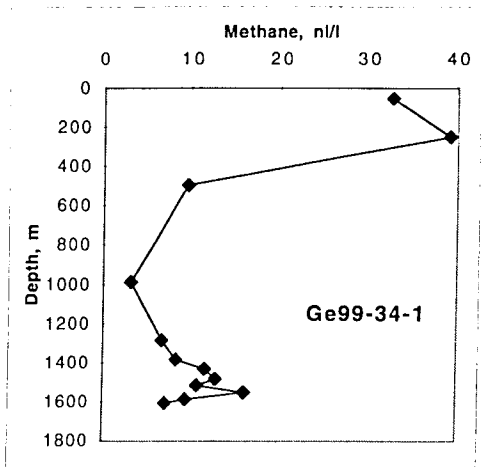
Methane, nl/l
0
10
20
30
40
Depth, m
0
200
400
600
800
1000
1200
1400
1600
1800
Ge99-34-1

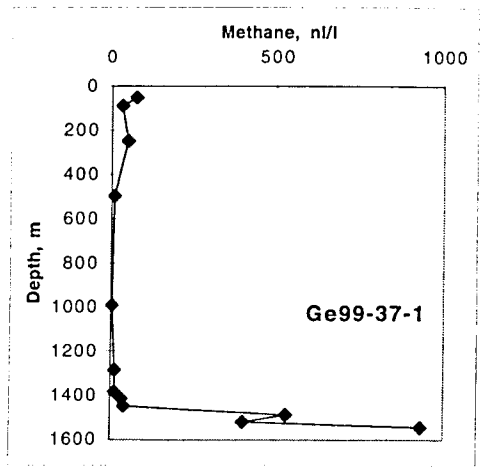
Methane, nl/l
0
500
1000
Depth, m
0
200
400
600
800
1000
1200
1400
1600
Ge99-37-1

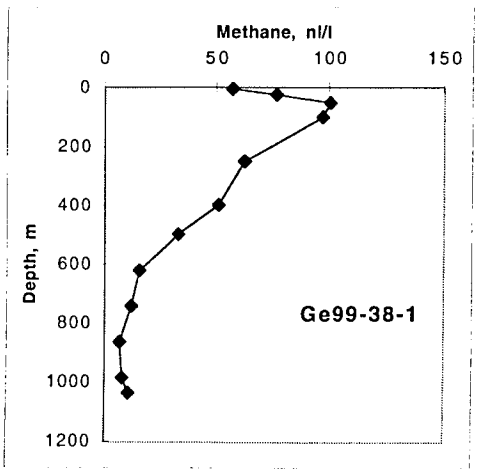
Methane, nl/l
0
50
100
150
Depth, m
0
200
400
600
800
1000
1200
Ge99-38-1

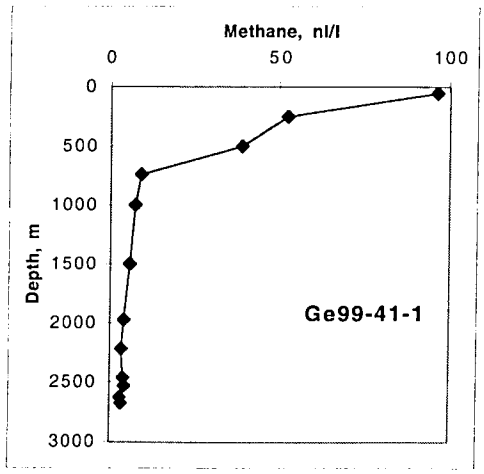
Methane, nl/l
0
50
100
Depth, m
0
500
1000
1500
2000
2500
3000
Ge99-41-1

APPENDIX 5

Pore water data

Pore Water Data Ge99

sample	depth cm	SiO_2 µM	ΣH_3PO_4 µM	$NO_3^-+NO_2^-$ µM	NO_2^- µM	NH_4^+ µM	ΣH_2S µM	alkal. meq./l	Cl^-+Br^- mM	T °C	pH
1-2 MIC											
BW	0	121	4.66	47.6	0.11	1.06	0	2.32			
0-1	0.5	366	6.65	29.9	0.19	22.6	0	2.34			
1-3	2	478	8.84	10.4	0.07	13.2	0	2.41			
3-5	4	586	7.75	0	0.11	20.9	0	2.43			
5-7	6	606	6.49	0	0.09	23.6	0	2.47			
7-9	8	596	4.51	0	0.11	37.8	0	2.49			
9-11	10	608	3.96	0	0.13	25.7	0	2.61			
11-14	12.5	596	4.1	0	0.09	38.1	0	2.65			
14-17	15.5	602	3.96	0	0.05	44.5	0	2.65			
17-20	18.5	592	3.96	0	0.19	40.2	0	2.71			
20-23	21.5	600	4.23	0	0.03	48.9	0	2.87			
2-1 MIC											
BW	0	200	3.41	45	0.13	1.39	0	2.32	554		
0-1	0.5	476	5.86	29.6	1.07	37.45	0	2.12	552		
1-3	2	644	7.65	14.7	1.42	18.58	0	2.36	553		
3-5	4	746	11.7	17.7	1.44	27	0	2.73	552		
5-7	6	738	10.7	6.06	0.82	30.7	0	2.87	550		
7-9	8	746	12.1	0	0.42	37.5	0	2.83	550		
9-11	10	728	9.94	0	0.35	42.5	0	2.89	549		
11-14	12.5	656	8.4	0	0.25	46.2	0	2.85	551		
14-17	15.5	762	12.3	0	0.07	71.2	0	3.46	550		
17-20	18.5	778	16.9	0	0.31	89.8	0	3.67	548		
20-23	21.5	784	19.7	0	0.07	106.8	0	4.24	546		
23-26	24.5	792	23.4	0	0.42	135.5	0	4.77	550		
4-2 MIC											
BW	0	60	2.8	19	0.195	6.66	–	2.26	525		
0-1	0.5	412	8.5	6.92	0.367	31	0.1	2.51	527		
1-3	2	612	7.3	3.54	0.751	52.1	0.342	2.67	533		
3-5	4	674	6.4	1.15	0.13	57.7	0	2.85	532		
5-7	6	650	6.6	0.576	0	62.2	0	2.83	527		
7-9	8	628	5.3	0.768	0	58.4	0	2.75	526		
9-11	10	594	2.8	0.348	0	60.9	0	2.71	529		
11-14	12.5	468	2.5	–	–	58.3	–	–	–		
14-17	15.5	506	3.2	1.34	0.687	56.8	0.066	2.57	530		
17-20	18.5	504	2.4	3.75	1.27	42.8	0	2.49	530		
20-23	21.5	492	1.9	1.94		41.4	0	2.32	531		
23-26	24.5	506	2.1	0.384		43		2.36	533		
5-1 MIC											
BW	0	118	3.2	32.7	0.324	4.55	0	2.36	546	–	–
0-1	0.5	410	5.5	31.5	–	23.8	0	2.16	537	7.6	7.35
1-3	2	604	7.8	5.87	0.238	17	0.352	2.34	545	7.2	7.27
3-5	4	716	10.4	0.3	0.324	34.3	0	2.49	546	7.6	7.38
5-7	6	714	8.5	0	0.602	52.1	1.248	2.51	546	7.6	7.40

sample	depth cm	SiO_2 µM	ΣH_3PO_4 µM	$NO_3^-+NO_2^-$ µM	NO_2^- µM	NH_4^+ µM	ΣH_2S µM	alkal. meq./l	Cl^-+Br^- mM	T °C	pH
7-9	8	694	7	0	–	54.4	0	2.55	544	7.5	7.46
9-11	10	696	6.6	0	–	49.6	0	2.65	545	7.6	7.38
11-14	12.5	678	8.8	0	–	62.7	0	2.77	545	7.8	7.31
14-17	15.5	632	6	0	–	69.3	0	2.79	545	7.6	7.46
17-20	18.5	536	4.1	0	–	74.2	0	3.04	546	8.1	7.63
20-23	21.5	576	6	0	–	67.4	0	2.87	543	7.1	7.33
6-3 MIC											
BW	0	199	3.01	46.3	0.231	1.45	0.374	2.34	551		
0-1	0.5	396	3.14	35.3	1.13	34.7	0.163	2.22	548	5.7	7.55
1-3	2	580	3.51	18.8	1	29.4	0.082	2.26	549	5.9	7.34
3-5	4	718	4.48	4.82	0.68	41.7	0.122	2.49	552	6.1	7.66
5-7	6	770	7.76	7.8	0.725	49.2	0.248	2.79	552	6.1	7.93
7-9	8	724	7.62	0	0.502	49.2	0.163	2.87	550	6.2	7.91
9-11	10	782	15.2	0	0.48	59.8	0.122	3.14	549	6.4	7.94
11-14	12.5	814	19	0	0.322	67.5	0.205	3.28	550	6.3	8.02
14-17	15.5	818	25	0	0.116	53	0.46	3.53	551	6.1	7.95
17-20	18.5	810	28.2	0	0.186	–	0.374	3.81	550	6.3	7.89
20-23	21.5	842	29.6	0	0.093	92.8	0.503	4.08	550	6	7.81
23-26	24.5	816	31.8	0	0.045	117.6	0.861	4.42	549	5.9	7.81
26-29	27.5		31.2	0	0.046	92	0.723	4.73	551	6	7.79
29-32	30.5		30.2	0	0.05	118.4	0.29	4.85	549		
7-2 MIC											
BW	0	199	3.87	47.8	0.484	3.14	0.374	2.40	556		–
0-1	0.5	392	3.43	19.7	1.36	28.5	0.205	2.32	555	6.9	7.31
1-3	2	548	4.62	6.38	0.858	22.5	0.248	2.36	555	6.1	7.28
3-5	4	654	7.1	0	0.574	22.9	0.205	2.61	556	6.5	7.39
5-7	6	562	8.79	0	0.394	32.6	0.205	2.75	553	6.7	7.52
7-9	8	712	9.98	0	0.507	40.4	0.122	2.94	556	6.4	7.62
9-11	10	744	11.4	0	0.28	47.4	0.163	3.12	555	6.4	7.60
11-14	12.5	768	13.8	0	0.234	40.9	0.205	3.12	554	6.7	7.68
14-17	15.5	798	12.1	0	0.165	52.2	0.163	3.26	553	6.8	7.67
17-20	18.5	788	11.5	0	0.188	62.5	0.163	3.40	554	6.7	7.71
20-23	21.5	692	12.2	0	–	65.8	0.248	3.49	552	6.7	7.69
23-26	24.5	800	12.5	0	0.165	77.4	0.374	3.61	552	6.7	7.69
12-3 MUC											
BW	0	181	2.07	38.5		0.893	0	2.45			–
0 -1	0.5	584	8.91	0		15.4	0	2.43		5.8	7.36
1 - 2	1.5	686	14.1	0		13.4	0	2.49		5.9	7.36
2 -3	2.5	728	19.2	0		28	0	2.65		5.6	7.43
3 - 4	3.5	710	17.2	0		35.7	0	2.77		5.6	7.43
4 - 5	4.5	750	18.8	0		40.3	0	2.83		5.6	7.38
5 - 6	5.5	766	10.2	0		37.6	0	2.87		5.5	7.36
6 - 7	6.5	754	18.6	0		40.9	0	2.91		5.4	7.32
7 - 8	7.5	740	17.7	0		53	0	2.89		5.4	7.32
8 - 9	8.5	704	14.5	0		45.6	0	2.89		5.4	7.30
9 - 10	9.5	708	14.1	0		65.7	0	3.02		5.3	7.34
10 -13	11.5	774	13	0		77.6	0	3.10		4.7	7.34

sample	depth cm	SiO_2 µM	ΣH_3PO_4 µM	$NO_3^-+NO_2^-$ µM	NO_2^- µM	NH_4^+ µM	ΣH_2S µM	alkal. meq./l	Cl^-+Br^- mM	T °C	pH
13 - 16	14.5	782	10.5			76.1	0	3.14		5.9	7.45
16 - 19	17.5	762	13			79.4	0	3.18		5.7	7.40
19 - 22	20.5	684	8.91			76.1	2	3.00		5.8	7.22
22 - 25	23.5	696	10.1			–	4	2.96		5.6	7.28
25 - 28	26.5	738	10.3			83.6	20	3.00		5.4	7.32
28 - 31	29.5	736	10.1			83.4	29	3.10		5.9	7.28
31 - 34	32.5	776	11.6			96.2	53	3.24		6.3	7.28
34 - 36	35	774	12.4			131.4	43	3.34		6.6	7.31
20-2 MIC											
BW	0	64.8	1.88	24.7			0	2.32		–	–
0-1	0.5	358	1.06	–			0	2.65		4.9	7.02
1-3	2	526	–	–			0	–		4.7	7.19
3-5	4	586	2.42	–			0	3.04		4.7	7.21
5-7	6	–	–	–			–	–		4.8	7.23
7-9	8	–	–	–			–	–		5	7.30
20-3 MIC											
BW	0	66	2.42	19.3			0	2.34		–	–
0-1	0.5	384	0.53	–			0	2.59		5.7	6.86
1-3	2	470	0.53	–			0	–		5.8	6.95
3-5	4	670	–	–			0	2.87		6	7.24
5-7	6	662	1.34	–			–	–		5.9	7.36
7-9	8	604	–	–			–	–		5.9	7.37
29-2 MIC											
BW	0	174	3.23	35.4		0	0	2.41		–	–
0-1	0.5	656	19.3	0		52.7	0	2.57		4.1	7.35
1-3	2	726	15.8	0		62.4	0	2.59		4	7.19
3-5	4	804	14.4	0		59.8	0	2.83		4	7.25
5-7	6	786	17	0		67.7	0	2.79		4.1	7.23
7-9	8	792	16.2	0		74.8	0	3.00		4.1	7.23
9-11	10	810	16.9	0		72.1	0	3.04		4.1	7.25
11-14	12.5	846	25	0		115.3	0	3.08		4.1	7.21
14-17	15.5	852	30.8	0		125	0	3.14		4	7.17
17-20	18.5	800	28.2	0		123	0	3.10		4	7.16
20-23	21.5	744	15.5	0		96.6	0	3.04		4	7.19
23-26	24.5	654	13.8	0		116.4	0	3.18		4.1	7.23

sample	depth cm	SiO_2 µM	ΣH_3PO_4 µM	$NO_3^-+NO_2^-$ µM	NH_4^+ mM	ΣH_2S mM	alkal. meq./l	Cl^-+Br^- mM	T °C	pH
12-4 SL(R)										
0-3	1.5	768	3.24		0.13	0.00	2.71		8.5	7.53
23.5-26.5	25	764	4.16		0.198	0.00	3.14		6.1	7.62
48.5-51.5	50	844	28.6		0.576	1.20	6.03		9.1	7.62
73.5-76.5	75	752	44.4		0.753	1.52	9.29		6.6	7.62
98.5-101.5	100	860	44.2		0.811	1.68	10.48		6.1	7.62
123.5-126.5	125	792	45.6		0.866	1.92	10.48		6.1	7.58
148.5-151.5	150	824	30.5		1.186	2.32	11.92		5.3	7.55
173.5-176.5	175	804	47.6		1.766	2.32	11.62		6.4	7.52
198.5-201.5	200	828	55.2		1.9	2.96	13.43		6	7.51
223.5-226.5	225	832	55.6		2.067	2.96	13.92		5.2	7.49
248.5-251.5	250	848	44		1.935	3.04	16.00		5.4	7.45
273.5-276.5	275	852	61.2		2.089	3.90	18.04		5.7	7.41
298.5-301.5	300	816	65.2		2.232	4.42	20.28		5.9	7.41
323.5-326.5	325	880	68		2.508	4.16	22.69		6	7.41
348.5-351.5	350	816	72.4		2.498	5.06	25.72		6.8	7.39
373.5-376.5	375	868	76.8		2.552	5.96	29.13		6	7.37
398.5-401.5	400	820	81.6		2.728	7.66	32.78		6.2	7.35
423.5-426.5	425	864	87.2		3.037	8.54	36.12		6.4	7.31
448.5-451.5	450	836	88.8		3.059	8.54	39.48		6.4	7.31
473.5-476.5	475	876	96.8		3.218	10.7	44.31		6.6	7.29
498.5-501.5	500	856	75.2		3.343	11.2	46.49		6.4	7.30
523.5-526.5	525	860	94		3.499	11.2	50.26		6.5	7.29
548.5-551.5	550	836	105.2		3.51	12.0	53.36		7	7.27
573.5-576.5	575	892	97.6		3.235	9.60	55.34		7.1	7.23
598.5-601.5	600	880	109.6		3.786	9.20	56.93		7.2	7.23
623.5-626.5	625	824	110.4		3.54	11.6	58.34		7.3	7.20
648.5-651.5	650	776	101.6		4.088	10.4	59.82		7.5	7.21
673.5-676.5	675	728	124		3.962	9.20	61.35		7.5	7.19
698.5-701.5	700	726	113.6		4.416	11.6	61.94		7.5	7.18
723.5-726.5	725	796	120.8		4.12	7.90	64.00		7.6	7.16
748.5-751.5	750	804	108		4.873	6.60	65.21		7.6	7.14
773.5-776.5	775	756	138.2		5.063	6.20	67.12		7.8	7.12
798.5-801.5	800	688	106.4		4.953	4.80	68.16		7.8	7.12
16-2 HYC										
13.5-16.5	15	564	3.38	–	0.003	0.38	6.93	539	6.6	7.29
28.5-31.5	30	568	3.62	0	0.004	1.4	9.36	538	5.7	7.30
43.5-46.5	45	566	4.96	0	0.008	3.2	13.62	535	5.1	7.21
58.5-61.5	60	558	6.48	0	0.007	5.0	20.02	535	5.1	7.21
73.5-76.5	75	540	18.2	–	0.002	5.3	23.11	534	5.6	7.22
88.5-91.5	90	544	19	–	0.002	6.2	27.39	535	7	7.22
103.5-106.5	105	548	17.4	–	0.006	6.6	28.70	534	7.3	7.27
118.5-121.5	120	558	23	–	0.002	5.8	28.37	535	7.2	7.22
133.5-136.5	135	562	25	–	0.002	6.0	29.45	536	7.8	7.21
148.5-151.5	150	574	26.3	–	0.005	14.2	31.17	539	8.4	7.19
163.5-166.5	165	586	24	–	0.012		32.27	538	9	7.15

sample	depth cm	SiO_2 µM	ΣH_3PO_4 µM	$NO_3^-+NO_2^-$ µM	NH_4^+ mM	ΣH_2S mM	alkal. meq./l	Cl^-+Br^- mM	T °C	pH
18-2 HYC										
0-3	1.5	702	2.76		0.002	0	2.20	531	8.4	7.30
13.5-16.5	15	736	2.05		0.003	0	–	531	5.3	7.23
43.5-46.5	45	740	5.01		0.004	0	–	530	9.3	6.86
58.5-61.5	60	738	4.29		0.003	0	3.04	534	9.5	6.84
73.5-76.5	75	740	3.8		0.002	0	–	–	8.9	6.88
88.5-91.5	90	740	3.02		0.025	0.01	3.81	529	9.9	6.86
103.5-106.5	105	770	3.26		0.034	0.03	–	530	10.3	6.90
118.5-121.5	120	695	4.1		0.043	–	4.87	535	10.6	6.88
133.5-136.5	135	–	–		0.052	1.12	–	–	–	–
148.5-151.5	150	735	3.8		0.062			–	12.3	6.98
19-2 HYC										
0-3	1.5	664	1.41	0	0.005	0	2.26	532	10.4	6.99
18.5-21.5	20	680	2.35	0	0.003	0	2.30	536	8.5	7.00
38.5-41.5	40	714	3.39	0	0.01	0.096	5.40	539	9.3	6.96
58.5-61.5	60	772	9.1		0.115	0.432	11.74	–	9.4	6.94
78.5-81.5	80	770	3.8		0.157	0.56	13.11	530	8.7	6.89
98.5-101.5	100	748	–		0.21	0.56	–	–	9	6.96
118.5-121.5	120	770	5.26		0.28	0.56	14.76	–	9.9	6.96
138.5-141.5	140	780	14.1		0.328	1.28	15.57	537	9.6	6.98
158.5-161.5	160	774	10.5		0.437	1.28	–	–	10.1	7.07
178.5-181.5	180	768	21.7		0.539	1.28	17.53	539	10.7	7.05
198.5-201.5	200	768	33.9		0.59	1.52	18.02	–	10.4	7.10
218.5-221.5	220	780	55.2		1.082	1.68	23.87	539	10.8	7.16
238.5-241.5	240	830	78.5		1.479	4.16	33.33	–	10.6	7.18
258.5-261.5	260	832	76		2.045	5.12	41.74	538	10.8	7.18
278.5-281.5	280	852	70.8		1.957	5.28	47.41	–	11.1	7.18
298.5-301.5	300	830	79.8		2.2	4.46	47.88	538	11.9	7.13
313.5-316.5	315	832	77.2				48.49	–	13.1	7.17
24-2 SL(R)										
8.5-11.5	10	796	11.06	0	0.041	0	2.67	540	8.8	6.98
28.5-31.5	30	644	6.64	0	0.035	0	2.71	541	6.9	7.31
48.5-51.5	50	588	10.52	0	0.03	0	2.57	540	6.2	7.35
68.5-71.5	70	640	9.42	0	0.034	0	2.63	541	6	7.39
88.5-91.5	90	648	10.24	0	0.028	0	2.65	541	6.3	7.39
108.5-111.5	110	718	10.52	0	0.03	0	2.69	541	5.8	7.43
128.5-131.5	130	726	11.06	0	0.039	0	2.98	540	5.2	7.38
148.5-151.5	150	738	13.24	0	0.076	0.06	4.30	541	4.7	7.34
168.5-171.5	170	770	12.1	0	0.051	0.24	6.24	545	4.4	7.29
188.5-191.5	190	801	14.3	0	0.1	0.68	12.88	546	4.4	7.25
208.5-211.5	210	785	17.8		0.183	1.44	23.58	548	4.2	7.27
228.5-231.5	230	820	12.7		0.266	6.4	39.89	554	4.3	7.29
248.5-251.5	250	855	11.6		0.268	8.3	42.36	555	4	7.25
268.5-271.5	270	850	15.9		0.277	11.2	43.35	554	4	7.27
288.5-291.5	290	905	18.4		0.29	14.8	44.27	556	3.6	7.25
308.5-311.5	310	860	29.4		0.398	10.2	40.97	500	-2.3	7.23
328.5-331.5	330	845	29.6		0.37	6.3	37.16	447	-2.3	7.29
348.5-351.5	350	785	37.6		0.341	1.6	36.59	410	-2.3	7.56

sample	depth cm	SiO_2 µM	ΣH_3PO_4 µM	$NO_3^-+NO_2^-$ µM	NH_4^+ mM	ΣH_2S mM	alkal. meq./l	Cl^-+Br^- mM	T °C	pH
26-2 SL(R)										
3.5-6.5	5	762	2.96	0	0	0	2.75	542	3.2	7.43
23.5-27.5	25	640	0.6	0	0.019	0	2.71	542	4.8	7.48
48.5-51.5	50	802	1.5	0	0.262	0.24	4.79	542	3.2	7.56
98.5-101.5	100	884	37.6		0.7	1.6	13.57	541	3	7.57
148.5-151.5	150	920	73.6		1.315	2.8	25.15	543	3.1	7.57
198.5-201.5	200	908	102.4		1.576	4.4	35.57	542	3.7	7.54
248.5-251.5	250	920	119.2		1.902	6	44.94	540	3.1	7.53
298.5-301.5	300	928	132		2.863	6.8	50.88	541	4.8	7.46
348.5-351.5	350	920	132.8		3.134	4.8	52.43	541	4.5	7.44
398.5-401.5	400	948	138.4		3.575	4	56.32	542	4.2	7.46
448.5-451.5	450	868	137.6		3.218	3.2	59.93	543	4.4	7.35
498.5-501.5	500	888	134.4		3.755	–	59.64	543	4.5	7.42
548.5-551.5	550	892	152.8		4.478	1.6	64.92	540	5.8	7.45
27-2 SL(R)										
0-3	1.5	662	1.6	0	0.004	0	3.44	542	3	7.43
23.5-26.5	25	806	0	0	0.006	0	2.81	541	2.3	7.51
48.5-51.5	50	722	0.3	0	0.005	0	2.77	541	2.8	7.49
73.5-76.5	75	724	1.9	0	0.008	0	2.75	540	3.3	7.56
98.5-101.5	100	726	0.5	0	0.057	0	3.04	540	2.9	7.55
123.5-126.5	125	746	0.8	0	0.054	0	3.14	541	3.4	7.54
148.5-151.5	150	754	1.4	0	0.09	0.07	3.28	542	3.6	7.54
173.5-176.5	175	778	1.6	0	0.083	0.22	3.49	541	3.4	7.52
198.5-201.5	200	792	1.6	0	0.127	1	4.40	540	3.9	7.46
248.5-251.5	250	824	3.28		0.158	5.2	9.87	540	4.1	7.37
298.5-301.5	300	835	21.2		0.39	9.2	28.94	548	3.9	7.37
348.5-351.5	350	930	31.6		0.714	12.8	51.61	557	4.6	7.31
398.5-401.5	400	916	70		1.397	10.8	53.61	560	4.1	7.29
448.5-451.5	450	965	109.6		1.5	10.8	54.57	561	4.5	7.25
498.5-501.5	500	920	127.2		1.847	11.2	62.17	559	3.6	7.29
548.5-551.5	550	870	128		3.381	10.8	66.26	558	4.7	7.27
588.5-591.5	590	880	133.6		4.3	10.8	65.39	560	4	7.64
29-3 SL(R)										
8.5-11.5	10	600	2.77	0	0.008	0.018	2.61	540	3.5	7.49
28.5-31.5	30	668	2.04	0	0.011	0.054	3.06	544	2.5	7.45
48.5-51.5	50	726	8.71	0	0.026	0.528	5.22	546	3.7	7.37
68.5-71.5	70	782	11.5		0.15	2.4	10.52	548	3.8	7.31
88.5-91.5	90	844	12.8		0.218	5.3	20.38	549	3.1	7.29
108.5-111.5	110	805	18.4		0.323	12	35.87	552	2.9	7.30
128.5-131.5	130	806	20.6		0.354	13.4	40.70	555	4.3	7.21
148.5-151.5	150	810	24		0.378	12	41.97	555	3.3	7.20
168.5-171.5	170	830	23.8		0.48	8	41.42	554	3.8	7.12
188.5-191.5	190	835	23.4		0.466	7.6	41.78	552	4.8	7.23
208.5-211.5	210	835	21.8		0.504	7.6	44.58	553	3.9	7.16
228.5-231.5	230	870	26.4		0.519	6	44.05	548	4.3	7.10
248.5-251.5	250	955	29.2		0.554	6.4	45.31	547	5.2	7.13
268.5-271.5	270	975	28		0.545	7.2	48.14	552	6.9	7.08
288.5-291.5	290	945	29.4		0.6	6.4	51.02	554	5.9	7.01

sample	depth cm	SiO_2 µM	ΣH_3PO_4 µM	$NO_3^-+NO_2^-$ µM	NH_4^+ mM	ΣH_2S mM	alkal. meq./l	Cl^-+Br^- mM	T °C	pH
308.5-311.5	310	550	27.5		0.5	4.8	36.24	395	-12	7.28
328.5-331.5	330	920	40.8		0.828	3.2	55.07	553	4.1	7.27
gashydrate						0.38	8.91	103		
30-3 SL(R)										
3.5-6.5	5	712	2.34	0	0.122	0	3.93	547	4	7.81
48.5-51.5	50	670	6.44	0	0.163	0.004	4.81	547	2.9	7.74
98.5-101.5	100	656	7.48		0.13	0.008	4.75	550	3.3	7.68
148.5-151.5	150	602	1.46		0.15	0.046	5.48	552	3.5	7.62
198.5-201.5	200	566	14.12		0.171	–	6.26	547	3	7.60
298.5-301.5	300	484	3.5		0.215	0.138	8.13	549	3.5	7.43
398.5-401.5	400	496	26.24		0.412	2.1	10.15	552	3.8	7.46
498.5-501.5	500	505	6.28		0.447	2	15.65	545	4.4	7.42
598.5-601.5	600	540	157.6		0.907	3.8	33.82	551	4.5	7.42
698.5-701.5	700	565	201.6		2.466	5.8	48.69	550	4.5	7.38
738.5-741.5	740	560	240		3.279	4.8	51.73	552	4.8	7.32
32-2 SL(R)										
0-3	1.5	516	0	0	0.005	0	2.61	545	19.1	7.31
13.5-17.5	15	528	4	0	0.006	0.002	2.59	546	19.5	7.47
28.5-31.5	30	360	5.28	0	0.007	0.46	2.85	545	19.2	7.62
58.5-61.5	60	540	8.28		0.006	0.6	4.50	543	19.4	8.07
88.5-91.5	90	558	4.64		0.046	1.1	8.03	545	19.5	8.24
118.5-121.5	120	590	21.04		0.022	1.1	15.88	544	19.3	8.13
148.5-151.5	150	628	31.8		0.018	6	20.99	544	19.2	8.11
178.5-181.5	180	668	27.12		0.045	7.2	24.68	546	19.7	8.13
218.5-211.5	210	657	20		0.057	10.8	27.82	543	–	–
238.5-241.5	240	630	22.12		0.016	10.4	31.19	545	19.5	8.09
268.5-271.5	270	590	27.12		0.011	10	30.78	545	19.6	8.13
298.5-301.5	300	610	26.52		0.004	–	31.33	546	19.6	7.94
328.5-331.5	330	635	42		0.013	7.2	30.49	540	19.6	8.20
358.5-361.5	360	635	42.8		0.061	6.8	29.31	537	20	8.40
388.5-391.5	390	640	36.8		0.006	5.6	28.56	535	19.6	8.25
418.5-421.5	420	655	53.2		0.01	6.8	29.64	535	19.5	8.18
448.5-451.5	450	650	35.72		0.005	6.4	28.84	536	19.5	8.22
478.5-481.5	480	705	45.2		0.007	6.4	28.74	533	19.6	8.20
508.5-511.5	510	730	52		0.007	5.6	28.11	533	19.6	8.18
538-5-541.5	540	735	48.8		0.022	4.8	28.07	531	19.5	8.16
568.5-571.5	570	695	41.6		0.066	3.2	24.97	531	19.5	8.16
598.5-601.5	600	705	40.4		0.562	2	24.07	532	19.6	8.24
36-1 HYC										
0-3	1.5	433	3.15	0	0.086	0	3.08	549	4	7.85
48.5-51.5	50	430	8.12	0	0.089	0	2.85	548	3.8	7.75
98.5-101.5	100	426	6.88		0.084	0	2.83	547	4.2	7.67
148.5-151.5	150	442	6.28		0.099	0	2.87	548	4.3	7.62
198.5-201.5	200	436	8.72		0.118	0.07	3.06	549	5.3	7.55
248.5-251.5	250	446	5.64		0.13	0.17	3.51	545	5.8	7.60
298.5-301.5	300	478	9.92		0.12	0.44	4.55	548	5.9	7.45
348.5-351.5	350	490	10.52		0.049	1.55	9.21	545	5.6	7.20
398.5-401.5	400	494	11.12		0.066	1.6	10.44	546	5.5	7.24

sample	depth cm	SiO_2 µM	ΣH_3PO_4 µM	$NO_3^-+NO_2^-$ µM	NH_4^+ mM	ΣH_2S mM	alkal. meq./l	Cl^-+Br^- mM	T °C	pH
448.5-451.5	450	497	14.12		0.082	2.2	11.11	547	6	7.16
498.5-501.5	500	481	14.72		0.151	2	10.88	544	7.4	7.18

Oxidation-reduction potential (Eh), pH(25) and oxidation volume (β) in sediments from the Sea of Okhotsk

St. No	Depth,cm	Eh(25), mv			$Ph_{NBS}(25)$	β, g-eqv/l·100
		Pt-electrode	Ti-electrode	Fe-electrode		
1	2	3	4	5	6	7
Ge99-12-4	0	82	93	89	7.441	-1.099
	50	48	67	66	7.372	-1.125
	100	31	61	59	7.492	-1.346
	150	18	51	51	7.492	-1.446
	200	16	43	41	7.561	-1.493
	300	-9	41	38	7.578	-1.494
	500	-89	17	14	7.578	-1.496
	700	-89	18	13	7.527	-1.497
	800	-91	19	19	7.458	-1.498
Ge99-24-2	10	69	75	73		-2.118
	30	66	74	75	7.148	-1.638
	50	66	66	70	7.200	-2.497
	90	65	61	66	7.492	-1.945
	130	61	70	65	7.475	-2.566
	210	1	11	7	7.355	-3.441
	250	-4	5	7	7.544	-3.386
	290	-117	-105	-107	7.510	-2.556
	310	-191	-189	-190	7.348	-2.450
	333	-199	-194	-196	7.355	-3.137
	360	-198	-192	-196	7.613	-2.645
Ge99-29-3	10	66	79	76	7.372	-2.497
	30	61	65	66	7.41	-2.244
	50	48	68	66	7.286	-2.432
	90	-28	37	33	7.527	-2.063
	150	-67	11	8	7.200	-4.472
	190	-71	-35	-34	7.596	-1.935
	270	-95	-85	-79	7.355	-2.946
	290	-155	-144	-149	7.148	-2.823
	310	-172	-165	-166	7.080	-2.626
	330	-175	-171	-169	7.183	-2.758
GE99-36-1	0	3	22	17	7.585	-1.498
	50	-18	17	9	7.682	-1.498
	100	-23	11	4	7.527	-1.498
	200	-7	8	3	7.768	-1.48
	300	-9	3	-5	7.451	-1.499
	500	-72	-136	-146	7.248	-1.497

APPENDIX 6

Biological objects prepared for analysis

Instrument/ Sta. No. 1	Object 2	Short description 3	Documentation Foto 4	Fixed in		frozen		TEM 9	Dried 10
				Formol 5	Ethanol 6	No. ind. 7	Sample 8		
MUC GE99-1-2	***Polychaeta***	Maldanidae-like		1 ind.					
		Chaetopteridae tube		1 ind.					
MUC GE99-12-3	**meiofauna**	quantitative		ok					
SL-R GE99-12-4 30-31 cm	*Thyasiridae* shell	complete shell (0,8 cm)							ok
130 cm	*Macoma* shell	complete 2,5 cm							ok
MIC GE99-20-3	***Polychaeta***	*Errantia*		1 ind.					
	meiofauna	qualitative		ok					
SL-R GE99-24-2 28 cm	*Thyasiridae* shells	fragms.							ok
40-50 cm	*Thyasiridae* shells	fragms.							ok
70 cm	*Thyasiridae shells*	fragms.							ok
325 cm	*Thyasiridae* shells	fragms.							ok
TWL GE99-25-1	***Hydrozoa***	2-3 sp. 1		ok					
		black, most abundant	ok	ok		several colonies	total		
		yellow tubes	ok	ok		2 colonies	total		
	Spongia	roundish	ok		ok	0,5	total		
	Actiniaria								
	sp. 1	small (1 cm)		5 ind.		10 ind.	total		
	sp. 2	orange, associated with *Buccinidae* (3 cm)		1 ind.		1 ind.	body wall		
	sp. 3	pink, (2,5 cm)		1 ind.		1 ind.	body wall		
	Polychaeta								
	sp. 1	large, most abundant		8 ind.		30	total		100 ind.
	sp. 2	*Nephtis* -like		2 ind.		2 fragm.			
	sp. 3	*Aphroditidae* -type		2 ind.					
	tubes	*Maladanidae* -type		ok					

Instrument/ Sta. No. 1	Object 2	Short description 3	Documentation Foto 4	Fixed in		frozen		TEM 9	Dried 10
				Formol 5	Ethanol 6	No. ind. 7	Sample 8		
	tubes	*Chaetopteridae* -type		ok		ok			
	Gastropoda								
	small (1-2 cm):								
	sp. 1	smooth shell	ok	1 ind. + shell		1 ind.	body total		
	sp. 2	ribbed shell	ok	1 ind.					
	sp. 3	*Muricidae* -like	ok	1 ind. + shell					
	juv. (3 mm)	white		3 ind.					
	large:								
	Buccinidae 1	smooth shell (7,57 cm)	ok	1 ind. head		1 ind.	foot rest of body		
	Buccinidae 2	ribbed shell (10,8 cm)	ok	1 ind. head		1 ind.	foot rest of body		
	Bivalvia								
	sp. 1	*Yoldia* -type	ok	11 ind.		10 ind.	total		
	sp. 2	*Nuchla* -type, small	ok	3 ind.		2 ind.	total	1 ind., total	
	sp. 3	*Macoma*	ok	2 ind.		0,5 ind.	gills mantle adductor foot gland	gills mantle gland foot	gills mantle adductor foot gland
	Thyasiridae	*Conchocele* large 1 ind. 114 x 80 mm	ok	0,5 ind. + shell					
	Vesicomyidae								
	Calytogena 1								
	ind. A	68,1 x 31,5 mm	ok			1 ind.	gills foot mantle adductor rest	mantle gill (outer part) gill (inner part) foot	shell
	ind. B	57,2 x 30,0 mm	ok	ok					
	ind. C	53,1 x 26,1 mm	ok			1 ind.	total		
	ind. D	41,0 x 25,6 mm	ok	ok					
	Calyptogena 2?	50,9 x 28,2 mm	ok					gill mantle	
	Amphipoda	2 spp. samll		ok, 10 ind.					
	Decapoda	large, 10 cm	ok	1 ind.,		1 ind.	abdomen		

Instrument/ Sta. No. 1	Object 2	Short description 3	Documentation Foto 4	Fixed in		frozen		TEM 9	Dried 10
				Formol 5	Ethanol 6	No. ind. 7	Sample 8		
	Macrura natantia			cephalo-thorax			muscle chitin		
	Ophiuroidae								
	sp. 1	small, abundant	ok		15 ind.	105 ind.	total		100 ind.
	sp. 2	*Ophiopholis* -like	ok		2 ind.	2 ind.	total		
	sp. 3	smooth disk			1 ind.	1 ind.	total		
SL-R GE99-27-2 380 cm	***Bivalvia*** shell *(Vescicomyidae ?)*	fragment							ok
515 cm	***Gastropoda*** shell	*Naticidae* 1 complete							ok
TWL GE99-28-1	***Hydrozoa***	3-4 spp.	ok	ok					
		"white"		ok		several colonies	total		
		"yellow"	ok	ok					
	Actinaria	small		1 ind.					
	Polychaeta	6-7 spp.		ok					
		Spionidae -type		ok		1 ind.	part of body total		
	Scaphopoda			1 ind. + 4 shells		1 ind. 2 ind.	total fragm. of shells		
	Gastropoda								
	small:								
	sp. 1	vertical rows		4 ind.					
	sp. 2	horizontal rows		3 ind.					
	sp. 3	smooth		2 ind.					
	sp. 4	"hairy snail"		1 ind. + shell		1 ind.	body total		
	large: *Buccinidae* 2	"ribbed"							
		ind. A (92 mm)	ok			1 ind.	siphon + rest of body		shell foot
		ind. B (75 mm)	ok			1 ind.	total		
	Bivalvia								
	sp. 1	*Yoldia* -like	ok	15 ind.		4 ind.	soft body		
		Leda -like	ok	2 ind.		2 ind.	total		
		Macoma	ok	13 ind.		2 ind.	soft body		
	sp. 2	*Nucula* -like		8 ind.					

Instrument/ Sta. No. 1	Object 2	Short description 3	Documentation Foto 4	Fixed in		frozen		TEM 9	Dried 10
				Formol 5	Ethanol 6	No. ind. 7	Sample 8		
	Solemyidae	*Acharax* sp. (?)	ok	1 ind.				total	
	Thyasiridae	*Conchocele* small, 2,5 cm	ok	2 ind.					shells fragm.
	Calyptogena (= sp.1?)								
	ind. A	57,7 x 30,1 mm	ok			0,5 ind.	gills mantle foot adductor rest	gill	gills mantle foot adductor rest shell
	ind. B	51,0 x 28,5 mm	ok	shell		0,5 ind.	gill adductor mantle foot rest	gill	gill adductor mantle foot rest
	ind. C	46,5 x 24,8 mm	ok			1 ind.	total		
	ind. D	43,6 x 23,5 mm	ok	total					
	Copepoda			ok					
	Amphipoda	small		ok					
	Decapoda ***Macura natantia***	small, pelagic		4 ind., fragm.					
	Decapoda Brachiura	*Chionoecetes opilio*	ok			1 ind.	chitin muscle		total
	Ophiuroidea	3 spp.			ok				
MIC Ge99-29-2	*Ophiuroidea*	*O. leptoctenia*			4 ind.				
	meiofauna	quantitative		ok					
	meiofauna	qualitative		ok					
	Ophiuroidea	*O. leptoctenia*			1 ind.				
SL-R GE99-29-3 12 cm	*Thyasiridae* shell	1 complete							ok
35 cm	*Thyasiridae* shell	fragm.							
	Vesicomyidae shells	1 complete							ok
?60 cm	*Buccinidae* sp. 2	complete							ok
124-132 cm	*Thyasiridae* shell	fragm. +1 complete							ok

Instrument/ Sta. No. 1	Object 2	Short description 3	Documentation Foto 4	Fixed in		frozen		TEM 9	Dried 10
				Formol 5	Ethanol 6	No. ind. 7	Sample 8		
	Vesicomyidae shells	1 complete 5 cm 1 damaged + fragm.							ok
167-174 cm	*Vesicomyidae* shells	7 complete + fragm.							ok
188-198 cm	*Thyasiridae* shell	(large) fragm.							ok
	Vesicomyidae shells	fragm. + 2 compl.							ok
280 cm	*Thyasiridae* shell	1 complete 3,3 cm							ok
DR GE99-35-1	***Hydroidea***	3-4 spp.	ok	ok		colonies	total		
		"black"	ok	ok					
	Polychaeta	*Serpulidae* tubes		ok					
		small sp.		ok					
	Bivalvia	*Solemya* 2 shells	ok	ok					ok
		Vesicomyidae ??	fragm. shell	ok					
	Ascidiae	aff. *Boltenia echinata*	ok	4 ind.		5 ind.	total		
	Incerta Sedis	colonial *Ascidiae* ?	ok	fragms.		fragm.	total		
DR GE99-39-1	***Hydrozoa***			ok					
	Hyalospongia				ok	fragm.	total		
	Polychaeta	*Errantia*		ok		fragm.	total		
	Actiniaria			ok			body wall		
	Brachiopoda			3 ind.					
DR GE99-40-1	***Hydroidea***			ok		colonies	total		
	Alcyonaria	red		1 colonie		1 colonie	total		
	Spongia	spheric small		1 ind.		1 fragm.	total		

APPENDIX 7

Core descriptions and sediment physical properties

Symbols used in graphical core descriptions

Lithology


clay


silt


sand


silty clay


sandy silty clay


sandy silt


sandy silt with greenish diagenetic alteration


diatomaceous ooze


diatomaceous sediment


weakly diatomaceous sediment


barite debris with coarse sand


coarse sand with barite debris


volcanic ash, glass


lenses of volcanic ash

ss smear slide

Texture

sharp boundary

weak boundary

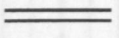
stratification

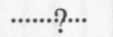
gradational boundary

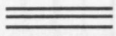
lamination


fining upwards


fining downwards

erosive surface


degassing voids / fissures


breccied texture

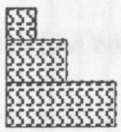
slight bioturbation
moderate bioturbation
strong bioturbation


lense (filled)


dropstone


sponge spicules


wormtube


plant fragments


shell fragments


authigenic carbonaceous concretions


gradational color changes

xxx diagenetic horizont (often with authigenic clay minerals, dominantly smectite)

KOMEX cruise 1999 (Marshal Gelovany)

GE 99-9-1

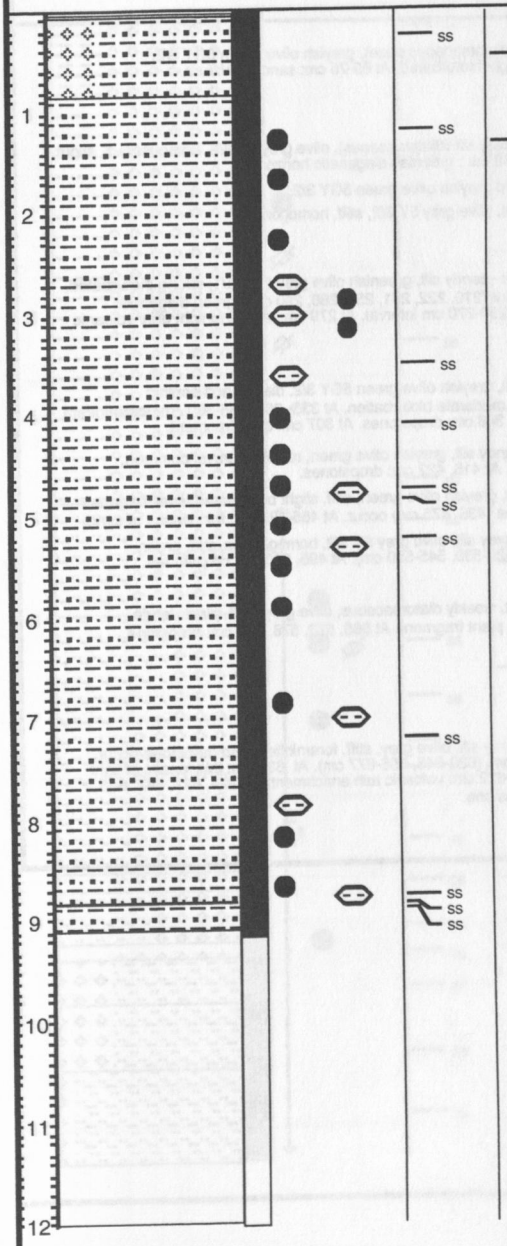

Lat: 48°14,537 N
Long: 146°00,434 E
Water depth: 1550 m
Length of tube: 1200 cm
Core recovery: 911 cm

REMARKS

0-87 cm: This interval contains olive gray (10Y4/1) sandy silty clay with diatoms and has a brown oxidized surface layer of only 1 cm. This implies a loss of surface sediment.

87-911 cm: This interval consist of olive-green (3GY4/1) sandy silty clay. A color change occurs at 880 to dusky yellow green (7GY5/1) although no change in lithology is observed.

Dropstones occur at 128-133, 210-240, 286, 312, 400, 400-580 (frequent), 684-689, and 811-830 cm.

Black sandy lenses that are dominated by quarz occur at 269, 302, 362-365, 478, 490, 526-535, 545 (pumice), 695-708, 720-731, 811-830 and 872-879 cm.

Reddish-white lenses of ash occur at 784 cm.

Small layers of greenish diagenetic alterations are disseminated throughout the core.

KOMEX cruise 1999 (Marshall Gelovani)

GE 99-10-3

Lat: 48° 18.666 N
Long: 146° 08.092 E
Water depth: 1335m
Recovery: 750

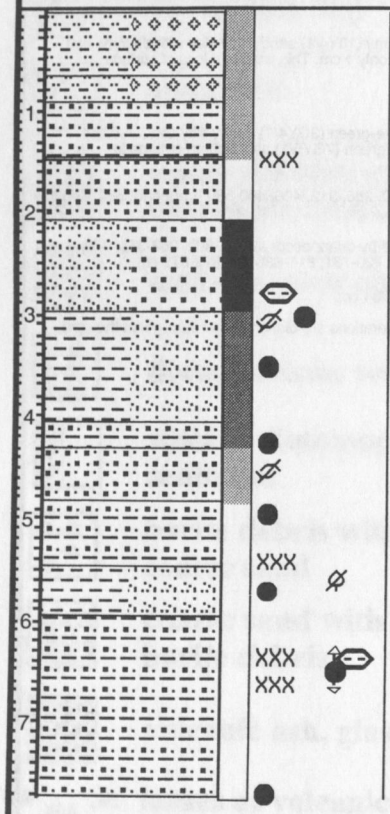

0-95 cm: Clayey silt (diatomaceous ooze), greyish olive green 5GY 3/2, homogenous, soft, slight bioturbated. At 60-75 cm: sand admixture.

95- 148 cm: sandy clayey silt (diatomaceous), olive grey 5Y 3/2, homogenous, slight bioturbated. At 145-148 cm : greenish diagenetic horizon.

148- 152 cm: silty sand greyish olive green 5GY 3/2.

152-210 cm: sandy silt, olive grey 5Y 3/2, stiff, homogenous.

210-298 cm: silty sand - sandy silt, greenish olive grey 5GY 4/1, strong bioturbated, pebble and gravel occur (210, 222, 251, 259, 286, 290 cm), green diagenetic horizons and spots in 230-270 cm interval. At 279 cm: lenses of light grey volcanic ash.

298-407 cm: clayey silt, greyish olive green 5GY 3/2, diatom and benthic foraminifera common, moderate bioturbation. At 335- 350, 365-380 cm: foraminifera increase. At 300, 305, 348 cm: dropstones. At 307 cm: shell fragment.

407-435 cm: clayey sandy silt, greyish olive green, rounded gravel common, moderate bioturbation. At 415, 422 cm: dropstones.

435-485 cm: sandy silt, greyish olive green, stiff, slight bioturbated, shell fragment (455 cm) and dropstone (436, 475 cm) occur. At 465-485 cm: thin lenses of sand.

485-550 cm: sandy clayey silt, olive grey 5Y 3/2, homogenous, stiff, green diagenetic horizons (520-530, 545-550 cm). At 495, 510 cm: dropstones.

550-595 cm: clayey silt, weakly diatomaceous, olive grey, soft, plant debris admixture. At 559 cm: plant fragment. At 565, 573, 578, 585 cm: dropstone.

595-775 cm: clayey sandy silt, olive grey, stiff, foraminifera and dropstone occur, green diagenetic horizons (620-645, 655-677 cm). At 630 cm: thin lenses of light grey volcanic ash, 617-622 cm: volcanic ash enrichment. At 624, 627, 642, 665, 668, 673, 773 cm: dropstone.

KOMEX cruise 1999 (Marshall Gelovani)

GE 99-12-1

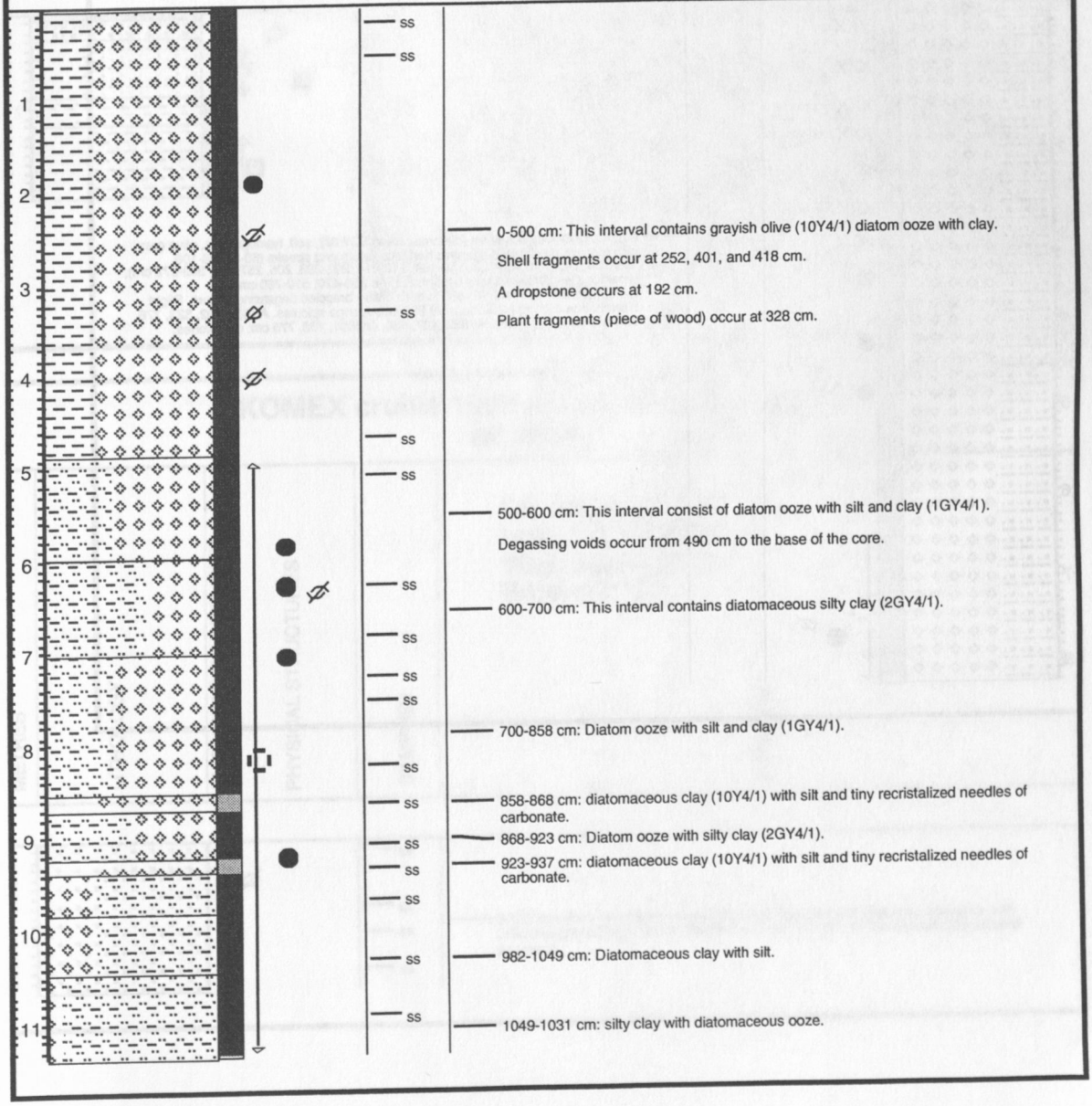

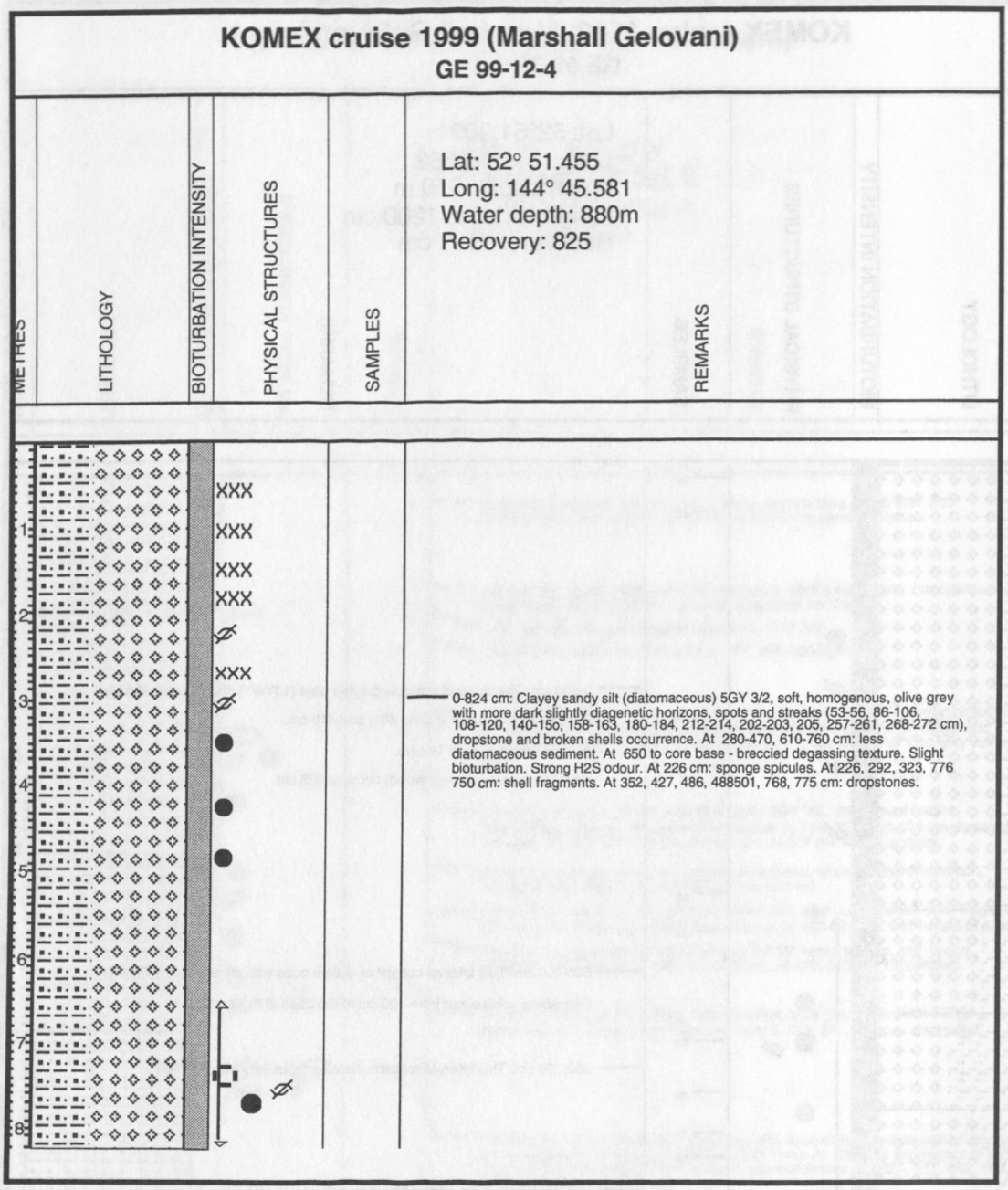
KOMEX cruise 1999 (Marshall Gelovani)
GE 99-12-4
METRES
LITHOLOGY
BIOTURBATION INTENSITY
PHYSICAL STRUCTURES
SAMPLES
REMARKS
Lat: 52° 51.455
Long: 144° 45.581
Water depth: 880m
Recovery: 825
0-824 cm: Clayey sandy silt (diatomaceous) 5GY 3/2, soft, homogenous, olive grey with more dark slightly diagenetic horizons, spots and streaks (53-56, 86-106, 108-120, 140-15o, 158-163, 180-184, 212-214, 202-203, 205, 257-261, 268-272 cm), dropstone and broken shells occurrence. At 280-470, 610-760 cm: less diatomaceous sediment. At 650 to core base - breccied degassing texture. Slight bioturbation. Strong H2S odour. At 226 cm: sponge spicules. At 226, 292, 323, 776 750 cm: shell fragments. At 352, 427, 486, 488501, 768, 775 cm: dropstones.

KOMEX cruise 1999 (Marshall Gelovani)
GE 99-16-2

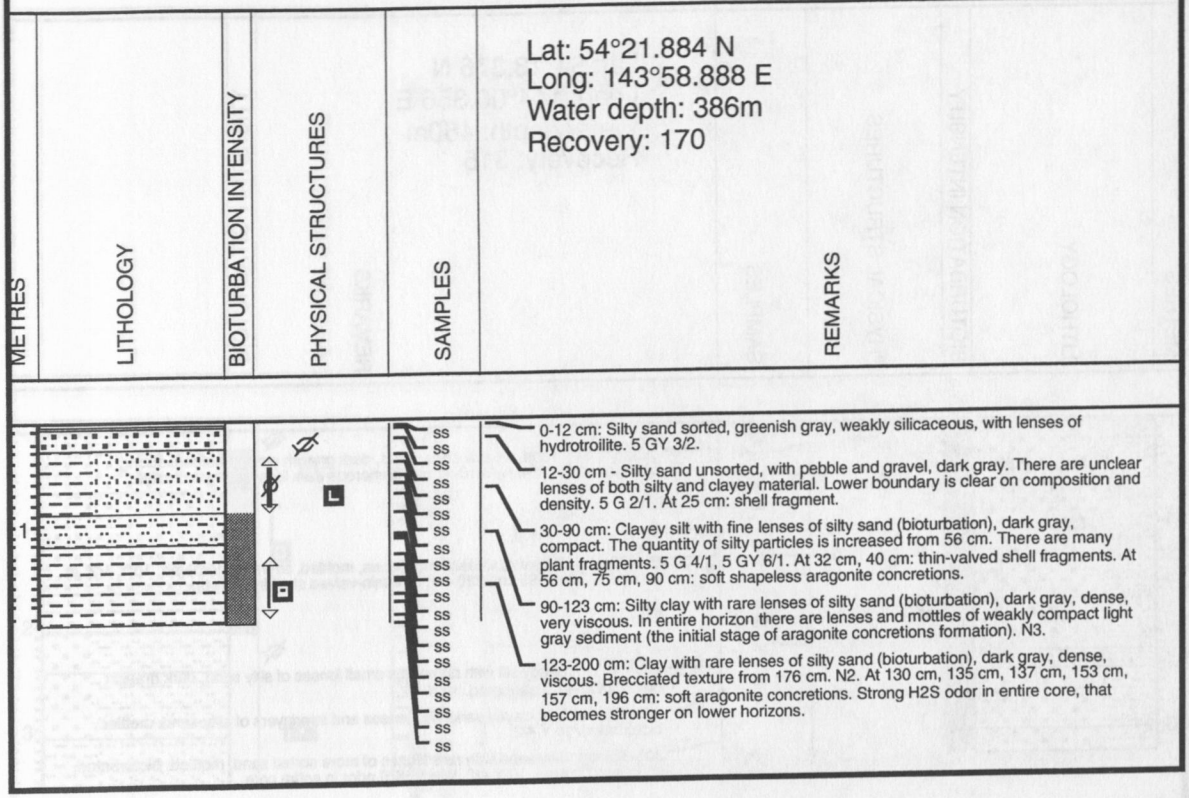

KOMEX cruise 1999 (Marshall Gelovani)
GE 99-18-2

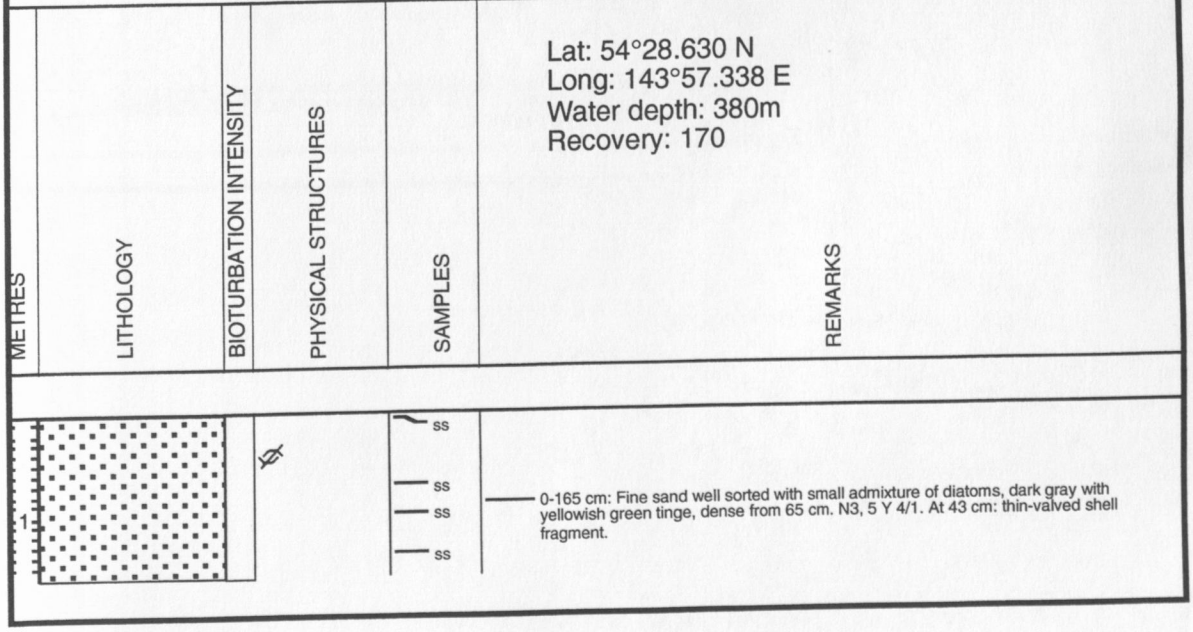

KOMEX cruise 1999 (Marshall Gelovani)
GE 99-19-2

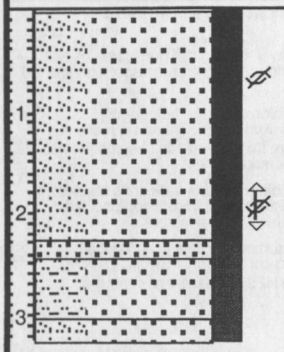

Lat: 54°18.376 N
Long: 144°00.356 E
Water depth: 460m
Recovery: 315

REMARKS

0-56 cm: Silty sand, weakly silicaceous, dark grayish green, mottled, strong bioturbated. 5 GY 4/1. At 10-41 cm: numerous dark lenses of hydrotroilite.

56-230 cm: Silty sand, weakly silicaceous, mottled, strong bioturbated. 10 Y 4/2. At 66 cm, 170 cm, 195 cm, 220 cm: rare thin-valved shell fragments.

230-245 cm: Sandy silt with numerous small lenses of silty sand, dark grayish green, mottled, bioturbated. 10 Y 4/2.

245-305 cm: Silty clayey sand with lenses and interlayers of silty sand, mottled, bioturbated. 10 Y 4/2.

305-325 cm: Silty sand with rare lenses of more sorted sand, mottled, bioturbated, brecciated texture. 10 Y 4/2. Weak H2S odor in entire core.

KOMEX cruise 1999 (Marshall Gelovani)

GE 99-24-2

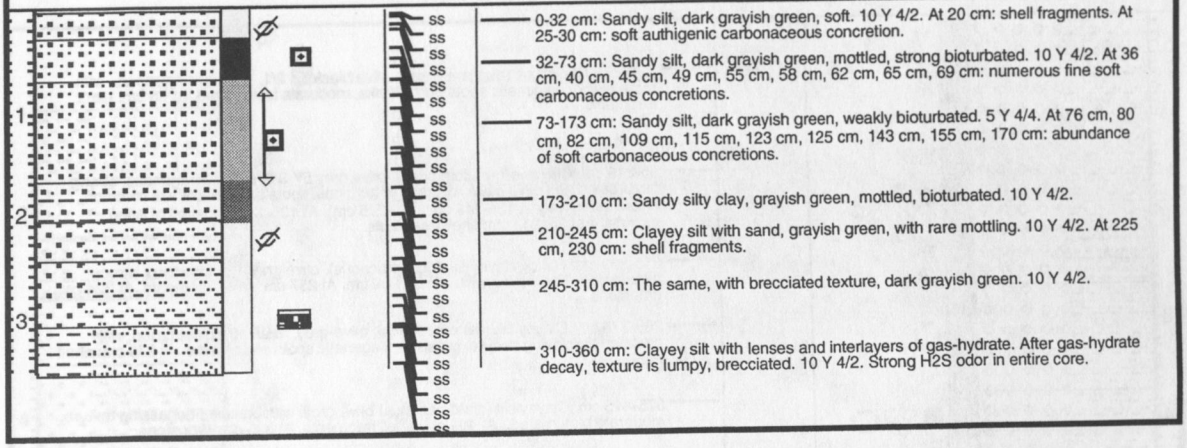

KOMEX cruise 1999 (Marshall Gelovani)

GE 99-26-2

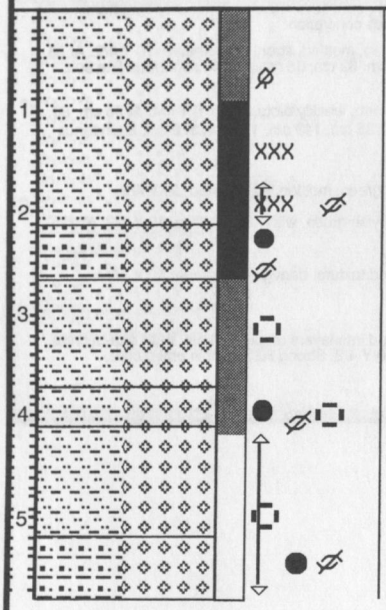

Lat: 54° 31.176
Long: 144° 05.276
Water depth: 700m
Recovery: 570

REMARKS

0-95 cm: Clayey silt (diatomaceous), olive black 5Y 2/1, soft, homogenous, with more blacky diagenetic spots and streaks, moderate bioturbated. At 68 cm: plant fragments.

95-215 cm: Clayey silt (diatom ooze), olive grey 5Y 3/2, soft, homogenous, strong bioturbated, the olive black diagenetic horizons, spots and streaks are common (more intensively at 136-146 and 165-215 cm). At 135-137 cm: shell of living mollusc. At 195, 212 cm: shell fragments.

215-269 cm: Sandy clayey silt (diatomaceous), olive grey, homogenous, strong bioturbated. The sand enrich at 262-269 cm. At 257 cm: shell fragments. At 224 cm: dropstone.

269-375 cm: Clayey silt (diatomaceous), olive-grey, moderate bioturbated, with breccied degassing texture, greenish diagenetic spots and streaks. At 279 cm: shell fragments.

375-415 cm: Clayey silt (diatomaceous) olive grey, with breccied degassing texture, moderate bioturbated. At 404 cm: shell fragments. At 395 cm: dropstone.

415-520cm: Clayey silt (diatomaceous), olive grey, intensively degassing breccied, black diagenetic spots and streaks (470-472, 482-484). At 436 cm: sand lens. At 430 cm: shell fragment.

520-582 cm: Sandy clayey silt (diatomaceous ooze), olive grey, intensively degassing breccied. At 540, 557 cm: dropstone. At 542, 557 cm: shell fragments. All core - strong H2S odour.

KOMEX cruise 1999 (Marshall Gelovani)

GE 99-27-2

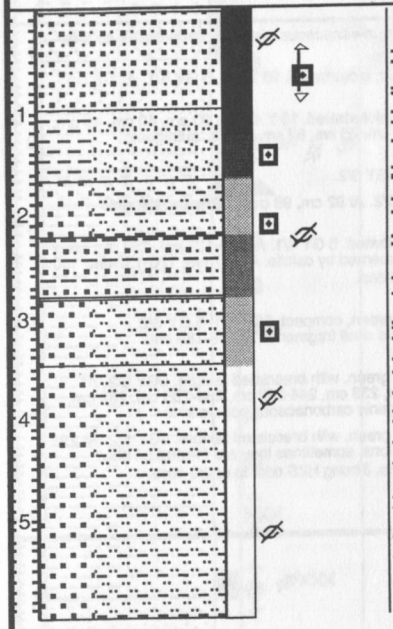

Lat: 54°26.663 N
Long: 144°04.812 E
Water depth: 700m
Recovery: 590

REMARKS

0-100 cm: Sandy silt, dark grayish green, mottled, strong bioturbated. 10 Y 4/2 (5 G 2/1). At 34 cm: shell fragments. At 35 cm, 47 cm, 55 cm, 73 cm, 78 cm, 85-90 cm: soft authigenic carbonaceous concretions.

100-170 cm: Clayey silt, dark grayish green, mottled, bioturbated. Degree of bioturbation is decreased from 127 cm. 10 Y 4/2. At 118 cm, 127 cm, 130 cm, 135-137 cm, 142 cm, 145 cm, 162 cm, 165 cm: soft carbonaceous concretions.

170-222 cm: Clayey silt with sand, dark grayish green, mottled, weakly bioturbated. 10 Y 4/2. At 210 cm: carbonaceous concretion.

222-281 cm: Silty clayey sand, dark grayish green, bioturbated. 10 Y 4/2. At 225 cm: soft carbonaceous concretions, cementing shell fragments.

281-285 cm: Dense, carbonaceous horizon. 10 Y 5/4.

285-350 cm: Clayey silt with sand, dark grayish green, weakly bioturbated. 10 Y 4/2. At 315 cm: soft carbonaceous concretion.

350-600 cm: Clayey silt with sand, dark grayish green, with brecciated texture. 10 y 4/2. At 380 cm, 515 cm: shell fragments. H_2S odor in entire core.

KOMEX cruise 1999 (Marshall Gelovani)

GE 99-29-3

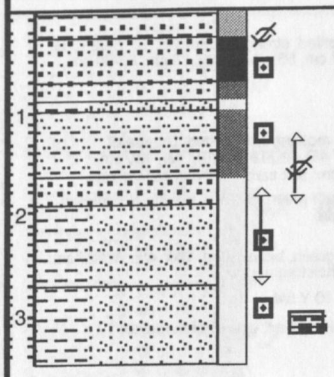

Lat: 54° 26.784
Long: 144° 04.765
Water depth: 700m
Recovery: 250

REMARKS

SS

0-1cm: Clayey silt with sand, terrigenous-silicaceous (diatomaceous ooze), soft. 5 GY 4/1.

1-32 cm: Clayey silt with sand, mottled, bioturbated. 10 Y 4/2, 5 GY 4/1. At 1-3 cm: shell fragments.

32-76 cm: Sandy silt, mottled, strong bioturbated. 10 Y 4/2. At 33 cm, 40 cm, 49 cm: shell fragments. At 46 cm, 54 cm, 60 cm, 65 cm, 67 cm, 72 cm: authigenic carbonaceous concretions.

76-92 cm: Sandy silt, bioturbated. 10 GY 3/2.

92-105 cm: Clayey silt, mottled. 5 G 5/2. At 92 cm, 98 cm, 100 cm: authigenic carbonaceous concretions.

105-167 cm: Silty clay, mottled, bioturbated. 5 GY 4/1. At 120-132 cm, 153 cm: shell fragments; the part of the shells is cemented by calcite. At 117 cm, 120-132 cm, 140 cm: authigenic carbonaceous concretions.

167-197 cm: Sandy silt, dark grayish green, compact. 5GY 4/1, 5 GY 3/2. At 167-174 cm, 186-197 cm: numerous shell fragments. At 176-186 cm: authigenic carbonaceous concretions.

197-274 cm: Clayey silt, dark grayish green, with brecciated texture. 5GY 5/2. At 205-215 cm, 218 cm, 225 cm, 235 cm, 238 cm, 244-248 cm, 254-258 cm, 269 cm, 270 cm, 274 cm: Abundance of authigenic carbonaceous concretions.

274-350 cm: Clayey silt, dark grayish green, with brecciated texture. 5GY 5/2. At 295 cm: authigenic carbonaceous concretions, sometimes they are formed on shell fragments. At 305-312 cm: gas-hydrate. Strong H2S odor in entire core.

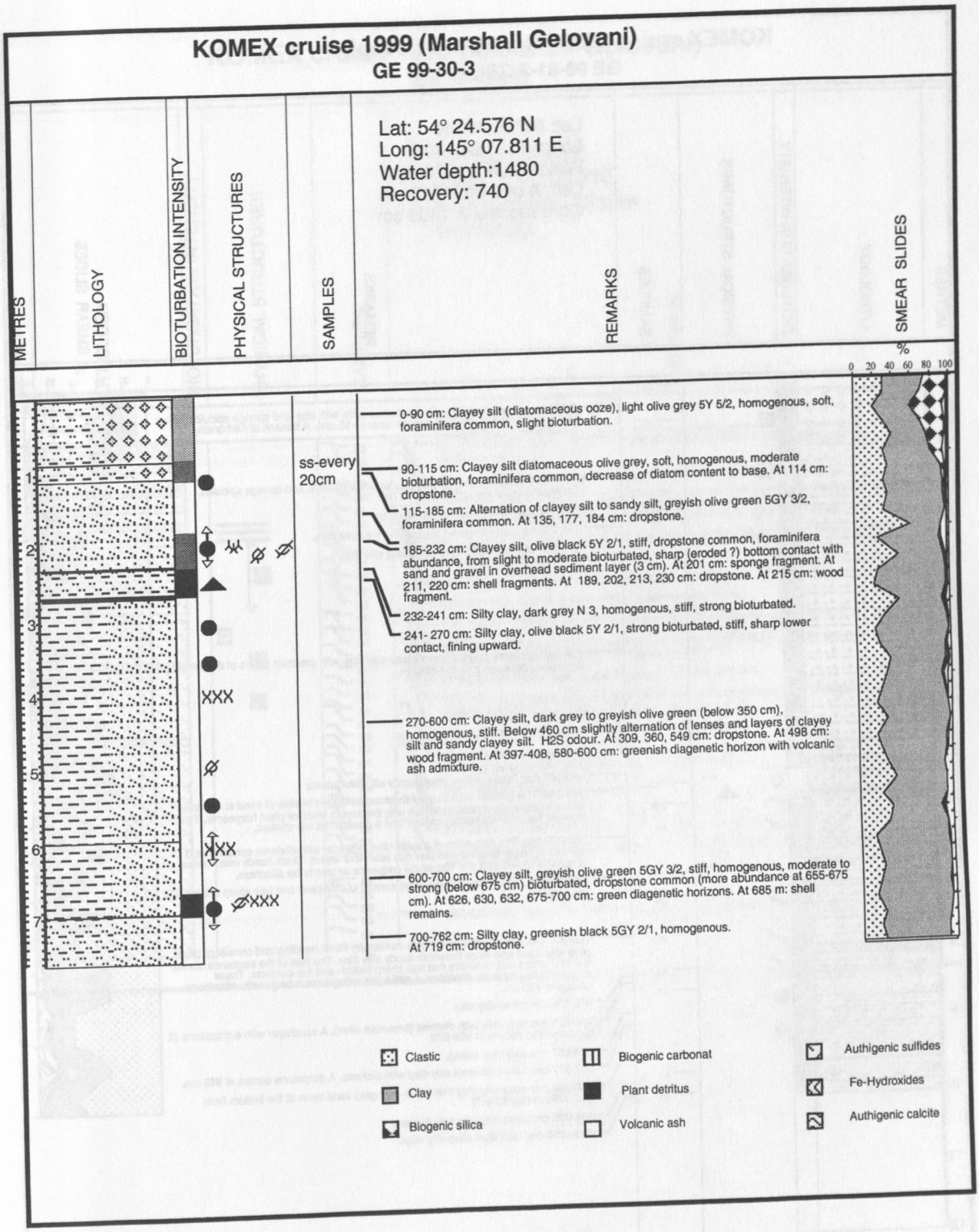
KOMEX cruise 1999 (Marshall Gelovani)
GE 99-30-3
METRES
LITHOLOGY
BIOTURBATION INTENSITY
PHYSICAL STRUCTURES
SAMPLES
REMARKS
SMEAR SLIDES
%
0 20 40 60 80 100
Lat: 54° 24.576 N
Long: 145° 07.811 E
Water depth:1480
Recovery: 740
ss-every 20cm
0-90 cm: Clayey silt (diatomaceous ooze), light olive grey 5Y 5/2, homogenous, soft, foraminifera common, slight bioturbation.
90-115 cm: Clayey silt diatomaceous olive grey, soft, homogenous, moderate bioturbation, foraminifera common, decrease of diatom content to base. At 114 cm: dropstone.
115-185 cm: Alternation of clayey silt to sandy silt, greyish olive green 5GY 3/2, foraminifera common. At 135, 177, 184 cm: dropstone.
185-232 cm: Clayey silt, olive black 5Y 2/1, stiff, dropstone common, foraminifera abundance, from slight to moderate bioturbated, sharp (eroded ?) bottom contact with sand and gravel in overhead sediment layer (3 cm). At 201 cm: sponge fragment. At 211, 220 cm: shell fragments. At 189, 202, 213, 230 cm: dropstone. At 215 cm: wood fragment.
232-241 cm: Silty clay, dark grey N 3, homogenous, stiff, strong bioturbated.
241- 270 cm: Silty clay, olive black 5Y 2/1, strong bioturbated, stiff, sharp lower contact, fining upward.
270-600 cm: Clayey silt, dark grey to greyish olive green (below 350 cm), homogenous, stiff. Below 460 cm slightly alternation of lenses and layers of clayey silt and sandy clayey silt. H2S odour. At 309, 360, 549 cm: dropstone. At 498 cm: wood fragment. At 397-408, 580-600 cm: greenish diagenetic horizon with volcanic ash admixture.
600-700 cm: Clayey silt, greyish olive green 5GY 3/2, stiff, homogenous, moderate to strong (below 675 cm) bioturbated, dropstone common (more abundance at 655-675 cm). At 626, 630, 632, 675-700 cm: green diagenetic horizons. At 685 m: shell remains.
700-762 cm: Silty clay, greenish black 5GY 2/1, homogenous. At 719 cm: dropstone.
1
2
3
4
5
6
7
Clastic
Clay
Biogenic silica
Biogenic carbonat
Plant detritus
Volcanic ash
Authigenic sulfides
Fe-Hydroxides
Authigenic calcite

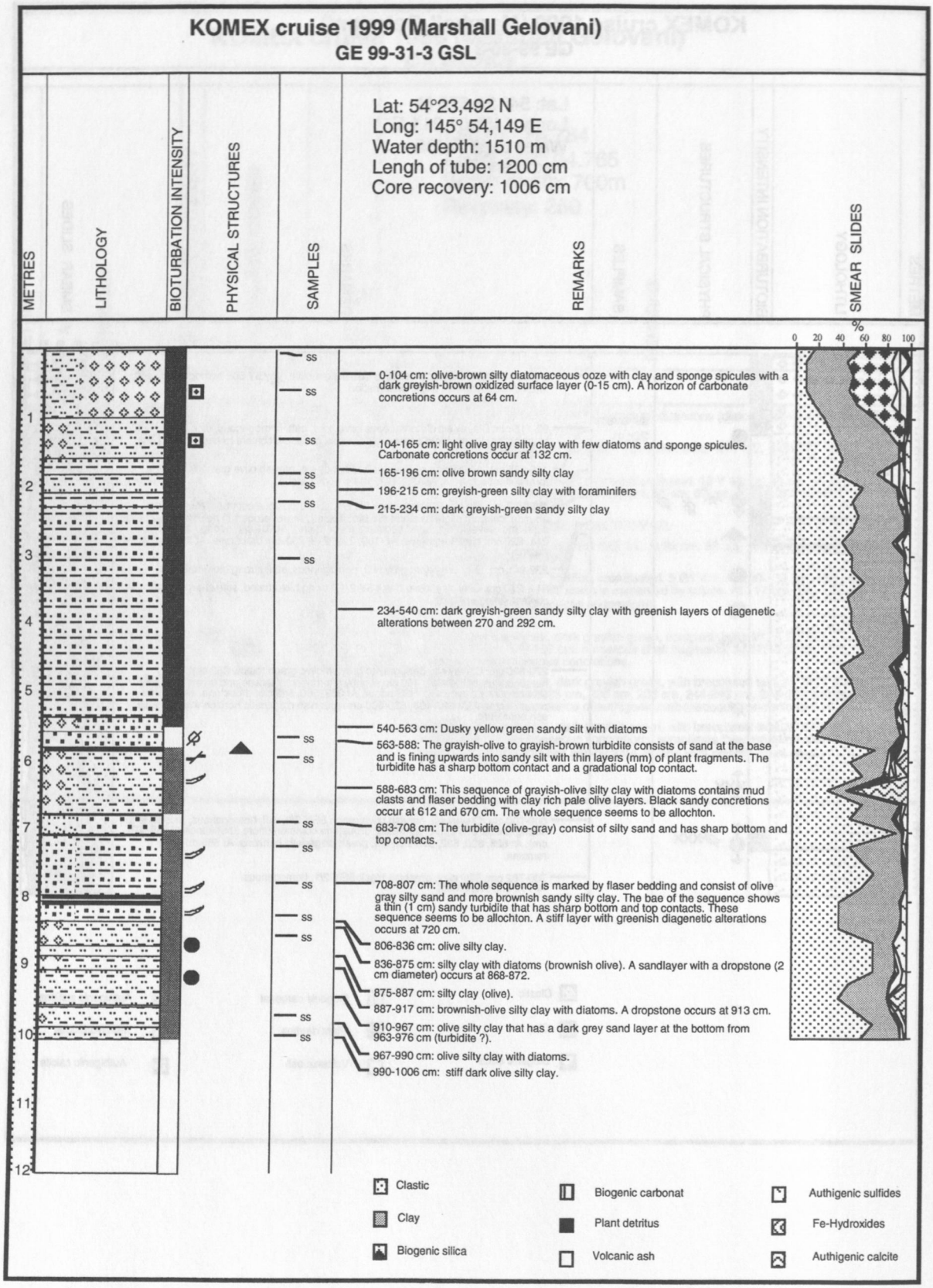
KOMEX cruise 1999 (Marshall Gelovani)
GE 99-31-3 GSL
Lat: 54°23,492 N
Long: 145° 54,149 E
Water depth: 1510 m
Lengh of tube: 1200 cm
Core recovery: 1006 cm
METRES
LITHOLOGY
BIOTURBATION INTENSITY
PHYSICAL STRUCTURES
SAMPLES
REMARKS
SMEAR SLIDES
%
0 20 40 60 80 100
1
2
3
4
5
6
7
8
9
10
11
12
SS
0-104 cm: olive-brown silty diatomaceous ooze with clay and sponge spicules with a dark greyish-brown oxidized surface layer (0-15 cm). A horizon of carbonate concretions occurs at 64 cm.
104-165 cm: light olive gray silty clay with few diatoms and sponge spicules. Carbonate concretions occur at 132 cm.
165-196 cm: olive brown sandy silty clay
196-215 cm: greyish-green silty clay with foraminifers
215-234 cm: dark greyish-green sandy silty clay
234-540 cm: dark greyish-green sandy silty clay with greenish layers of diagenetic alterations between 270 and 292 cm.
540-563 cm: Dusky yellow green sandy silt with diatoms
563-588: The grayish-olive to grayish-brown turbidite consists of sand at the base and is fining upwards into sandy silt with thin layers (mm) of plant fragments. The turbidite has a sharp bottom contact and a gradational top contact.
588-683 cm: This sequence of grayish-olive silty clay with diatoms contains mud clasts and flaser bedding with clay rich pale olive layers. Black sandy concretions occur at 612 and 670 cm. The whole sequence seems to be allochton.
683-708 cm: The turbidite (olive-gray) consist of silty sand and has sharp bottom and top contacts.
708-807 cm: The whole sequence is marked by flaser bedding and consist of olive gray silty sand and more brownish sandy silty clay. The bae of the sequence shows a thin (1 cm) sandy turbidite that has sharp bottom and top contacts. These sequence seems to be allochton. A stiff layer with greenish diagenetic alterations occurs at 720 cm.
806-836 cm: olive silty clay.
836-875 cm: silty clay with diatoms (brownish olive). A sandlayer with a dropstone (2 cm diameter) occurs at 868-872.
875-887 cm: silty clay (olive).
887-917 cm: brownish-olive silty clay with diatoms. A dropstone occurs at 913 cm.
910-967 cm: olive silty clay that has a dark grey sand layer at the bottom from 963-976 cm (turbidite ?).
967-990 cm: olive silty clay with diatoms.
990-1006 cm: stiff dark olive silty clay.
Clastic
Clay
Biogenic silica
Biogenic carbonat
Plant detritus
Volcanic ash
Authigenic sulfides
Fe-Hydroxides
Authigenic calcite

KOMEX cruise 1999 (Marshall Gelovani)

GE 99-32-2

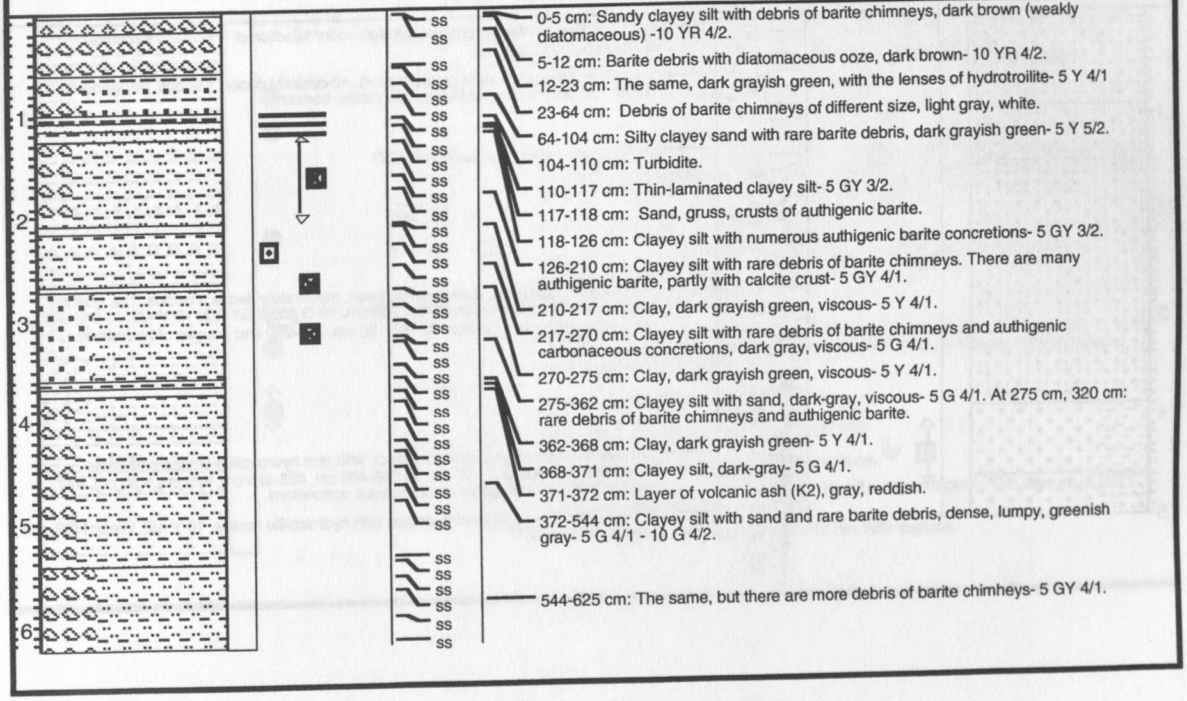

KOMEX cruise 1999 (Marshall Gelovani)

GE 99-36-1

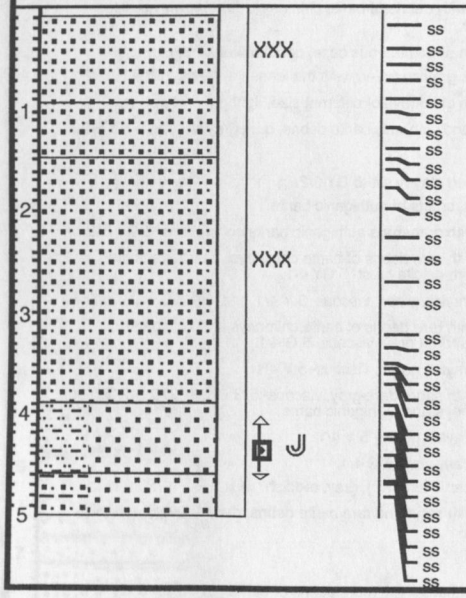

Lat: 53° 59.474 N
Long: 146° 20.170 E
Water depth: 1520m
Recovery:

REMARKS

0-13 cm: Horizon was strong deformated under injection of HYC, and structural features are not clear.

13-151cm: Silty sand, dark grayish green, moderately dense, viscous, terrigenous- 5 GY 4/1. At 38 cm: compact lumpy diagenetic horizon.

151-152 cm: Layer of volcanic ash (K2).

152-390 cm: Sandy silt, dark grayish green, moderately dense, viscous. The quantity of sandy particles is increased from 308 cm. 10 G 3/2, 5 GY 5/2, 10 Y 4/2. At 244-246 cm: lumpy diagenetic horizon. At 180-190 cm, 265-280 cm: gouges of hydrotroilite.

390-462 cm: Silty clayey sand, compact, with rare hydrotroilite lenses and barite authigenic wormtubes. 5 GY 4/1. At 395-400 cm, 405-420 cm, 425 cm, 435 cm, 447 cm, 455-460 cm: authigenic carbonaceous concretions.

462-503 cm: Clayey silty sand, dense, with hydrotroilite lenses. 10 Y 4/2. Weak H2S odor in entire core.

KOMEX cruise 1999 (Marshall Gelovani)

GE 99-38-2

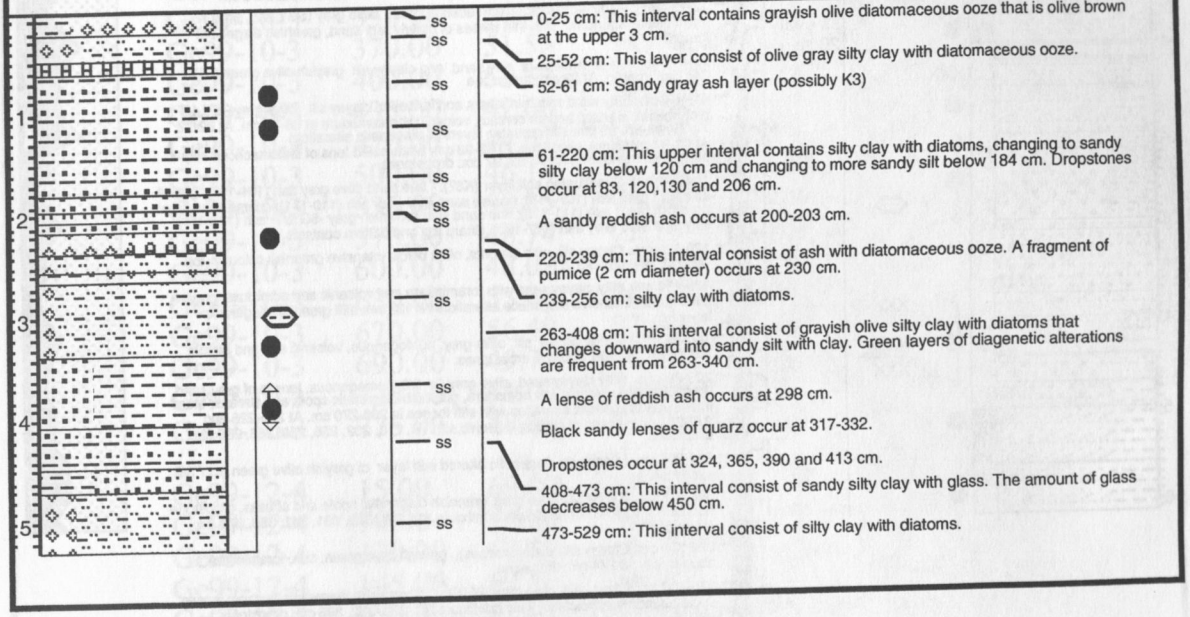

KOMEX cruise 1999 (Marshall Gelovani)

GE 99-38-5

Lat: 49°19.805 N
Long: 150°30.596 E
Water depth: 1110 m
Length of tube: 13 m
Recovery: 611

METRES | LITHOLOGY | BIOTURBATION INTENSITY | PHYSICAL STRUCTURES | SAMPLES | REMARKS | SMEAR SLIDES

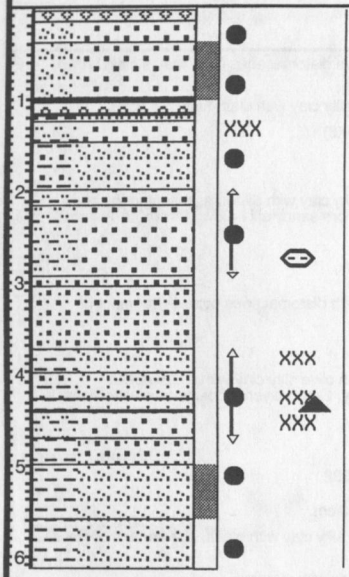

ss-every 20cm

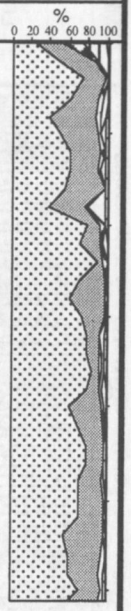

0-12 cm: Lens of brownish grey -5YR 4/1 -silty sand (foraminifera-diatomaceous ooze), homogenous, erosive bottom contact. At 3 cm: rounded pebble 3 cm

12-19 cm: Clayey sandy silt (diatomaceous ooze) olive grey (5GY 3/2), soft, foraminifera abundant, with thin lenses of clayey silty sand, greenish diagenetic lumps.

19-41 cm: Thin alternation of silty sand and clayey silt greyish olive green 5GY 3/2, bioturbated. At 32 cm: dropstone

41-104 cm: Silty sand with thin layers and lenses of clayey silt, olive grey - 5Y 4/1-, bioturbated, a sharp bottom contact, volcanic ash admixture at 60-70 cm. At 62-72, 77-79, 86-88, 98 cm: stiff greenish layers of diagenetic alteration. At 90-93 cm: black sand lens. At 86-93 cm: bioturbated lens of diatomaceous silty sand from top layers. At 84, 93, 97 cm: dropstones.

104-120 cm: Stratificated ash layer (K3?): - fine sand olive grey ash (104-107); gravel size light grey ash (107-110); coarse sand light grey ash (110-111); coarse sand size greenish black ash (111-113); fine sand size brownish grey -5G 2/1- ash (113-117); silty size olive grey ash (117-120). Sharp top and bottom contacts.

120-128 cm: Clayey silt with diatoms, olive black, intensive greenish colour in top contact with ash-5G 2/1-

128-150 cm: Silty clayey sand with foraminifera and volcanic ash admixture, greyish olive green, intensive diagenetic alteration. At 133 cm: stiff greenish diagenetic layer.

150-203 cm: Sandy clayey silt, olive grey, homogenous, volcanic ash and diatom admixture. At 165, 200 cm: dropstones.

203-291 cm: Silty clayey sand, olive grey 5Y 3/2, homogenous, lenses of grey sand, dropstone and volcanic ash admixture, greenish diagenetic spots and streaks. More intensively diagenetic alteration with stiff lenses in 260-270 cm. At 225-226 and 272-274 cm: lenses of silt size volcanic ash. At 210, 232, 256, 289, 283, 299 cm: dropstone.

291-306 cm: Intensively diagenetic altered stiff layer of greyish olive green 5GY 3/2 sandy silt.

306-372 cm: Sandy silt, olive grey, greenish diagenetic spots and streaks, dropstone common. At 360-372 cm: diatom admixture. At 308, 323, 331, 341, 353, 371 cm: dropstone.

372-375 cm: Clayey silt (diatomaceous), greyish olive green, soft, foraminifera abundance. At 274 cm: dropstone.

375-402 cm: Clayey silt, olive grey 5Y 3/2, stiff, greenish diagenetic horizon, lenses, spots abundance, volcanic glass admixture. At 372, 382, 398 cm: dropstone.

402-405 cm: Volcanic ash, fine sand size, dark grey-N2-. At 402-404 cm: sediment admixture.

405-430 cm: Sandy clayey silt, olive grey 5Y 3/2, stiff, homogenous. At 425-427 cm: green diagenetic horizon. At 420 cm: dropstone.

430-447 cm: The turbidite (olive grey - black) consist of coarse sand in the base (442-447 cm) and is fining upwards into sandy clayey silt. Sharp bottom contact with intensive green diagenetic alteration.

447-475 cm: Clayey silty sand, dark grey N 4, stiff. At 454-456 cm: green diagenetic horizon. At 446, 458 cm: dropstone.

475-502 cm: Clayey sandy silt, olive grey, stiff, with foraminifera admixture. At 478 cm: dropstone.

502-560 cm: Clayey silt, olive black 5Y 2/1 , stiff, gravel and foraminifera admixture, moderate bioturbated, greenish diagenetic spots and streaks. At 510 cm: dropstone.

560-611 cm: Clayey silt, greyish olive green 5GY 3/2, diagenetic alteration, foraminifera admixture, stiff. At 587, 593 cm: dropstone.

Clastic
Clay
Biogenic silica
Biogenic carbonat
Plant detritus
Volcanic ash
Authigenic sulfides
Fe-Hydroxides
Authigenic calcite

Appendix 7: Physical property data from different GE99-cores

Core	Depth (cm)	Weight water (%)	Volume water (%)	Wet density (g/cm^3)	Dry density (g/cm^3)	Porosity (%)
Ge99-10-3	18.00	67.20	88.60	1.32	0.43	65.92
Ge99-10-3	53.00	66.80	87.10	1.30	0.43	65.19
Ge99-10-3	100.00	61.73	82.90	1.34	0.51	67.15
Ge99-10-3	140.00	55.96	77.70	1.39	0.61	69.42
Ge99-10-3	175.00	50.39	73.10	1.45	0.72	72.53
Ge99-10-3	195.00	50.18	74.40	1.48	0.74	74.13
Ge99-10-3	235.00	49.10	72.80	1.48	0.75	74.13
Ge99-10-3	270.00	52.27	76.80	1.47	0.70	73.47
Ge99-10-3	300.00	50.63	74.70	1.48	0.73	73.77
Ge99-10-3	330.00	51.43	74.60	1.45	0.70	72.53
Ge99-10-3	370.00	51.55	74.70	1.45	0.70	72.46
Ge99-10-3	400.00	52.82	78.10	1.48	0.70	73.93
Ge99-10-3	435.00	42.66	68.90	1.62	0.93	80.75
Ge99-10-3	470.00	44.61	71.30	1.60	0.89	79.91
Ge99-10-3	500.00	46.14	70.70	1.53	0.83	76.61
Ge99-10-3	535.00	50.35	74.20	1.47	0.73	73.68
Ge99-10-3	570.00	48.74	72.10	1.48	0.76	73.96
Ge99-10-3	600.00	48.02	67.30	1.40	0.73	70.07
Ge99-10-3	630.00	53.06	76.10	1.43	0.67	71.71
Ge99-10-3	670.00	56.49	83.00	1.47	0.64	73.47
Ge99-10-3	690.00	49.71	74.00	1.49	0.75	74.43
Ge99-10-3	725.00	51.00	74.00	1.45	0.71	72.55
Ge99-10-3	775.00	48.66	73.20	1.50	0.77	75.21
Ge99-12-4	15.00	69.00	89.80	1.30	0.40	65.07
Ge99-12-4	70.00	70.22	88.30	1.26	0.37	62.87
Ge99-12-4	120.00	68.59	86.20	1.26	0.39	62.84
Ge99-12-4	145.00	67.86	85.50	1.26	0.41	63.00
Ge99-12-4	180.00	67.01	86.40	1.29	0.43	64.47
Ge99-12-4	210.00	65.72	84.60	1.29	0.44	64.36
Ge99-12-4	245.00	66.44	88.70	1.34	0.45	66.75
Ge99-12-4	285.00	66.70	88.50	1.33	0.44	66.34
Ge99-12-4	315.00	65.17	86.80	1.33	0.46	66.59
Ge99-12-4	345.00	65.59	84.80	1.29	0.44	64.64
Ge99-12-4	380.00	65.34	85.30	1.31	0.45	65.27
Ge99-12-4	415.00	65.40	87.20	1.33	0.46	66.67
Ge99-12-4	440.00	66.88	85.80	1.28	0.42	64.14
Ge99-12-4	475.00	66.89	88.40	1.32	0.44	66.08
Ge99-12-4	515.00	67.15	87.00	1.30	0.43	64.78
Ge99-12-4	540.00	66.26	84.20	1.27	0.43	63.54
Ge99-12-4	580.00	66.72	88.80	1.33	0.44	66.55
Ge99-12-4	615.00	64.82	88.60	1.37	0.48	68.34
Ge99-12-4	640.00	64.34	87.70	1.36	0.49	68.15
Ge99-12-4	680.00	63.75	87.00	1.36	0.49	68.23
Ge99-12-4	720.00	64.35	84.60	1.31	0.47	65.73
Ge99-12-4	740.00	62.90	83.50	1.33	0.49	66.38
Ge99-12-4	770.00	63.51	83.60	1.32	0.48	65.82
Ge99-12-4	815.00	62.73	84.80	1.35	0.50	67.59
Ge99-26-2	30.00	63.96	85.60	1.34	0.48	66.92
Ge99-26-2	55.00	61.95	82.20	1.33	0.50	66.34
Ge99-26-2	85.00	61.19	83.00	1.36	0.53	67.82

Core	Depth (cm)	Weight water (%)	Volume water (%)	Wet density (g/cm^3)	Dry density (g/cm^3)	Porosity (%)
Ge99-26-2	120.00	60.31	81.60	1.35	0.54	67.65
Ge99-26-2	155.00	60.97	84.40	1.38	0.54	69.22
Ge99-26-2	190.00	60.11	83.80	1.39	0.56	69.71
Ge99-26-2	220.00	57.50	81.40	1.42	0.60	70.78
Ge99-26-2	250.00	62.58	83.40	1.33	0.50	66.64
Ge99-26-2	290.00	58.59	80.60	1.38	0.57	68.78
Ge99-26-2	315.00	62.78	82.00	1.31	0.49	65.31
Ge99-26-2	355.00	60.42	81.80	1.35	0.54	67.69
Ge99-26-2	395.00	61.53	86.00	1.40	0.54	69.89
Ge99-26-2	415.00	57.25	78.80	1.38	0.59	68.82
Ge99-26-2	455.00	55.10	76.00	1.38	0.62	68.96
Ge99-26-2	495.00	55.81	78.60	1.41	0.62	70.42
Ge99-26-2	505.00	55.52	76.80	1.38	0.62	69.17
Ge99-26-2	535.00	57.11	77.80	1.36	0.58	68.11
Ge99-26-2	570.00	59.84	80.80	1.35	0.54	67.51
Ge99-27-2	15.00	63.00	83.40	1.32	0.49	66.19
Ge99-27-2	40.00	58.02	80.30	1.38	0.58	69.20
Ge99-27-2	85.00	59.20	82.80	1.40	0.57	69.93
Ge99-27-2	115.00	60.14	80.00	1.33	0.53	66.51
Ge99-27-2	155.00	60.12	80.00	1.33	0.53	66.53
Ge99-27-2	175.00	55.15	77.80	1.41	0.63	70.54
Ge99-27-2	220.00	53.29	75.00	1.41	0.66	70.37
Ge99-27-2	245.00	55.34	78.50	1.42	0.63	70.93
Ge99-27-2	275.00	59.60	82.20	1.38	0.56	68.96
Ge99-27-2	310.00	57.05	78.30	1.37	0.59	68.63
Ge99-27-2	345.00	60.73	82.60	1.36	0.53	68.01
Ge99-27-2	385.00	60.43	81.50	1.35	0.53	67.43
Ge99-27-2	415.00	61.80	84.60	1.37	0.52	68.45
Ge99-27-2	455.00	57.34	77.40	1.35	0.58	67.49
Ge99-27-2	495.00	59.77	80.20	1.34	0.54	67.09
Ge99-27-2	510.00	59.36	80.00	1.35	0.55	67.38
Ge99-27-2	545.00	54.29	74.40	1.37	0.63	68.52
Ge99-27-2	580.00	54.50	75.60	1.39	0.63	69.36
Ge99-29-3	25.00	61.22	79.60	1.30	0.50	65.01
Ge99-29-3	45.00	58.14	78.00	1.34	0.56	67.08
Ge99-29-3	80.00	57.71	81.80	1.42	0.60	70.87
Ge99-29-3	120.00	59.75	82.00	1.37	0.55	68.62
Ge99-29-3	145.00	61.41	82.60	1.35	0.52	67.25
Ge99-29-3	180.00	55.30	76.20	1.38	0.62	68.90
Ge99-29-3	220.00	55.07	72.20	1.31	0.59	65.55
Ge99-29-3	240.00	56.30	71.30	1.27	0.55	63.32
Ge99-29-3	275.00	58.80	79.30	1.35	0.56	67.43
Ge99-29-3	315.00	57.02	78.20	1.37	0.59	68.57
Ge99-30-3	30.00	77.42	93.80	1.21	0.27	60.58
Ge99-30-3	60.00	62.86	82.00	1.30	0.48	65.22
Ge99-30-3	90.00	71.81	89.30	1.24	0.35	62.18
Ge99-30-3	120.00	69.27	87.60	1.26	0.39	63.23
Ge99-30-3	150.00	68.42	88.40	1.29	0.41	64.60
Ge99-30-3	180.00	51.13	67.20	1.31	0.64	65.72
Ge99-30-3	220.00	59.38	81.10	1.37	0.55	68.29
Ge99-30-3	255.00	57.93	81.30	1.40	0.59	70.17
Ge99-30-3	295.00	55.11	78.40	1.42	0.64	71.13

Core	Depth (cm)	Weight water (%)	Volume water (%)	Wet density (g/cm^3)	Dry density (g/cm^3)	Porosity (%)
Ge99-30-3	320.00	53.82	77.60	1.44	0.67	72.09
Ge99-30-3	350.00	57.42	83.20	1.45	0.62	72.45
Ge99-30-3	395.00	53.55	78.40	1.46	0.68	73.20
Ge99-30-3	425.00	49.93	74.00	1.48	0.74	74.11
Ge99-30-3	455.00	52.54	74.60	1.42	0.67	71.00
Ge99-30-3	495.00	50.78	73.80	1.45	0.72	72.67
Ge99-30-3	515.00	49.81	74.90	1.50	0.75	75.18
Ge99-30-3	545.00	47.35	70.00	1.48	0.78	73.91
Ge99-30-3	585.00	49.13	74.00	1.51	0.77	75.31
Ge99-30-3	615.00	49.13	74.60	1.52	0.77	75.92
Ge99-30-3	650.00	49.65	74.60	1.50	0.76	75.12
Ge99-30-3	695.00	49.21	73.20	1.49	0.76	74.38
Ge99-30-3	730.00	48.63	72.40	1.49	0.76	74.44
Ge99-32-2	35.00	38.10	71.00	1.86	1.15	93.17
Ge99-32-2	135.00	46.32	68.80	1.49	0.80	74.27
Ge99-32-2	160.00	47.04	68.60	1.46	0.77	72.92
Ge99-32-2	205.00	47.17	71.40	1.51	0.80	75.69
Ge99-32-2	245.00	47.15	70.80	1.50	0.79	75.08
Ge99-32-2	280.00	47.14	70.40	1.49	0.79	74.67
Ge99-32-2	325.00	51.47	75.00	1.46	0.71	72.86
Ge99-32-2	360.00	48.47	73.00	1.51	0.78	75.31
Ge99-32-2	390.00	55.64	73.60	1.32	0.59	66.14
Ge99-32-2	415.00	57.32	76.80	1.34	0.57	66.99
Ge99-32-2	480.00	54.35	75.40	1.39	0.63	69.37
Ge99-36-1	50.00	48.51	73.80	1.52	0.78	76.06
Ge99-36-1	100.00	48.54	74.80	1.54	0.79	77.05
Ge99-36-1	120.00	52.54	77.20	1.47	0.70	73.47
Ge99-36-1	180.00	49.15	74.60	1.52	0.77	75.89
Ge99-36-1	220.00	49.97	75.60	1.51	0.76	75.65
Ge99-36-1	255.00	45.60	70.40	1.54	0.84	77.20
Ge99-36-1	290.00	47.25	72.40	1.53	0.81	76.62
Ge99-36-1	320.00	48.92	72.80	1.49	0.76	74.41
Ge99-36-1	345.00	37.95	61.20	1.61	1.00	80.64
Ge99-36-1	380.00	36.05	62.20	1.73	1.10	86.28
Ge99-36-1	405.00	32.18	57.00	1.77	1.20	88.57
Ge99-36-1	450.00	38.86	63.40	1.63	1.00	81.58
Ge99-36-1	475.00	41.88	67.20	1.60	0.93	80.22
Ge99-38-5	12.00	58.43	82.60	1.41	0.59	70.68
Ge99-38-5	30.00	49.64	75.40	1.52	0.76	75.94
Ge99-38-5	70.00	56.90	81.00	1.42	0.61	71.18
Ge99-38-5	98.00	52.65	78.80	1.50	0.71	74.83
Ge99-38-5	130.00	52.98	77.40	1.46	0.69	73.05
Ge99-38-5	165.00	56.34	80.00	1.42	0.62	71.00
Ge99-38-5	195.00	54.36	78.20	1.44	0.66	71.93
Ge99-38-5	220.00	52.51	76.60	1.46	0.69	72.94
Ge99-38-5	250.00	51.40	76.40	1.49	0.72	74.32
Ge99-38-5	285.00	52.37	74.80	1.43	0.68	71.42
Ge99-38-5	335.00	54.70	77.80	1.42	0.64	71.12
Ge99-38-5	365.00	51.97	75.20	1.45	0.70	72.35
Ge99-38-5	393.00	50.54	75.20	1.49	0.74	74.40
Ge99-38-5	420.00	45.98	70.80	1.54	0.83	76.99
Ge99-38-5	460.00	47.37	71.80	1.52	0.80	75.78

Core	Depth (cm)	Weight water (%)	Volume water (%)	Wet density (g/cm^3)	Dry density (g/cm^3)	Porosity (%)
Ge99-38-5	490.00	48.98	73.80	1.51	0.77	75.34
Ge99-38-5	520.00	46.32	71.40	1.54	0.83	77.08
Ge99-38-5	560.00	51.37	75.20	1.46	0.71	73.19
Ge99-38-5	590.00	51.75	70.80	1.37	0.66	68.41

APPENDIX 8

Radiolarian distribution in surface sediments

Group/ N st.	Ge99	1-2	Ge99	2-1	Ge99	5-2	Ge99	6-2	Ge99	10-2	Ge99	12-3	Ge99	27-2	Ge99	30-2	Ge99	31-3	Ge99	38-3
	%	spp	%	spp	%	spp	%	spp	%	spp	%	spp	%	spp	%	spp	%	spp	%	spp
Cyrtoidae	53	6	33	7	41	7	44	15	55	10	54	8	53	6	55	8	40	7	6.8	1
Discoidea	16	3	6.7	2	11	3	19	3	8.1	2	6.8	2	27	4	4.2	2	14	4	68	3
Larcoidea	4.4	1	11	2	1.1	1	7.2	1	4.9	1	6.8	1			2.8	1			5.4	3
Sphaeroidea			16	5	6.6	2	15	3	9.8	4	8.5	4	3.3	1	1.4	1	3.9	2	4.1	3
Spyroidae	24	2	29	2	38	2	12	2	20	2	22	2	17	1	37	2	40	2	15	1
Cannobotryoidae	1.5	1							0.8	1	1.7	1					1.3	1		
Collosphaeridea	1.5	1																	1.4	1
Prunoidea			4.4	1			2.2	1	0.8	1										
Phaeodaria					2.2	1														

N st.	Ge99 1-2	Ge99 2-1	Ge99 5-2	Ge99 6-2	Ge99 10-2	Ge99 12-3	Ge99 27-2	Ge99 30-2	Ge99 31-3	Ge99 38-3
Acanthodesmia micropora	21.6	4.4	15.7	21.7	11.0	13.1	13.3		21.6	25.3
Acrosphaera sp.		1.5								
Arachnocorys dubius	1.4	5.9		4.3		0.8			1.4	
Arachnocorys sp.	1.4					1.6	1.7	3.2	1.4	
Botryocampe inflata						0.8	1.7			1.3
Callimitra sp.						0.8				
Ceratocyrtis histricosa		1.5	2.0	1.1		0.8		3.2		
Collosphaera sp.										
Cornutella bimarginata					0.9					
Cromyechinus borealis	1.4		3.9		4.6	1.6			1.4	
Cycladophora davisiana	33.8	35.3	21.6	27.2	29.4	31.1	33.3	32.3	33.8	29.1
C. cornuta					0.9					
Echinomma delictulum					0.9	3.3				1.3
Litharachnium tentarium	1.4	1.5			0.9		1.7	3.2	1.4	1.3
Lithelidae fam.							1.7			
Lithelilius spiralis			3.9							
Lithomelissa setosa					2.8					
Lithomitra lineata		5.9	3.9		0.9					2.5
Lithomitra arachnea					0.9					
Lithomphora platicephala					0.9					
Plagiacantidae fam.	5.4	1.5	7.8			4.9	6.7	9.7	5.4	3.8
Plectocanta					1.8					
Pseudocubus sp.	1.4		2.0	2.2		1.6	1.7		1.4	
Pseudodictyophimus gracilipes	2.7		9.8	2.2	6.4	5.7	5.0		2.7	2.5
Pterocanium sp.		1.5								
Pterocorys hirundo	5.4		2.0		0.9	3.3	1.7	3.2	5.4	
Rhizoplegma boreale			3.9	4.3		2.5	5.0	3.2		
Sagosphaeridae fam.				1.1						
Schizodiscus stylotrochoides				1.1						
Sethoconus tubulatus					1.8	0.8	3.3			1.3
Sphaeroidea ordo					1.8	0.8	1.7			
Spongodiscidae fam.	2.7					0.8		6.5	2.7	1.3
Spongodiscus osculosus		8.8				0.0				
Spongotrochus glacialis		5.9		8.7	6.4	3.3	3.3	6.5		10.1
Stylochlamidium venustum	1.4	4.4	3.9	2.2	8.3	1.6	3.3	9.7	1.4	1.3
Srylacontarium aquilonium			2.0		2.8	0.8				
Stylodictya stella			3.9		0.9	2.5		3.2		1.3
Tolospira sp.		16.2	3.9	1.1	1.8	4.9	6.7			
Tholospyris borealis	14.9	5.9	7.8	18.5	8.3	7.4	8.3	16.1	14.9	13.9
Tricolocapsa papillosa					1.8					
Trisulcus sp	2.7			2.2		4.9			2.7	1.3
Indetermined rads	2.7		2.0	2.2	1.8				2.7	2.5

APPENDIX 8

List of participants

List of participants

Scientists

1. Kulinich, Ruslan	chief of expedition
2. Obzhirov, Anatoliy	scientist
3. Lelikov, Yevgeniy	scientist
4. Botsul, Anatoliy	scientist
5. Gorbarenko, Sergey	scientist
6. Derkachev, Alexandr	scientist
7. Tararin, Igor	scientist
8. Svarichevskiy, Aleksandr	scientist
9. Vereshchagina, Olga	scientist
10. Sosnin, Valeriy	scientist
11. Salyuk, Anatoliy	scientist
12. Nikolaeva, Natalya	scientist
13. Astakhov, Anatoliy	scientist
14. Galkin, Sergey	scientist
15. Zasko, Darya	scientist
16. Shulga, Yuriy	engineer
17. Koptev, Andrey	engineer
18. Biebow, Nicole	co-chief of expedition
19. Hütten, Edna	foreighn language assistant
20. Wallmann, Klaus	scientist
21. Bollwerk, Sandra	scientist
22. Winckler, Gisela	scientist
23. Greinert, Jens	scientist
24. Busche, Holger	scientist
25. Tiedemann, Ralf	scientist
26. Werner, Reinhard	scientist
27. Kaiser, Andre	scientist
28. Fessler, Sebastian	technician
29. Kolevica, Ana	technician
30. Kulescha, Friedhelm	technician
31. Nöske, Karl	technician

Ship's crew

1. Poroshin, Andrey	captain
2. Komirenko, Vitaliy	chief mate
3. Maevskiy, Denis	navigator
4. Krasnikov, Anatoliy	1rst mate
5. Kraskovskiy, Vyacheslav	2nd mate
6. Chumalo, Miroslav	engineer
7. Nikitin, Vladimir	chief engineer
8. Serba, Boris	2nd mechanic
9. Egorov, Nikolay	4th engineer
10. Repka, Sergey	electric engineer
11. Mokritskiy, Roman	2nd electric engineer
12. Tkachenko, Sergey	chief radio-operator
13. Nikulin, Victor	1rst radio-operator
14. Lubenko, Valeriy	2nd radio-operator
15. Rusinov, Andrey	electro-radio navigator
16. Karaganov, Vyacheslav	engineer
17. Zhitkov, Sergey	engineer
18. Lyashko, Nionila	doctor
19. Firsov, Valeriy	boatsman
20. Vladimirov, Ramil'	sailor
21. Bylkov, Sergey	sailor
22. Grigorov, Victor	sailor
23. Chuvilev, Vladimir	sailor
24. Khmel'nitskaya, Galina	sailor
25. Voloshchyak, Alexey	sailor
26. Smirnov, Vitaliy	chief motorman
27. Kozlov, Dimitriy	motorman
28. Borodin, German	chief electric welder
29. Petrykina, Tatyana	cook
30. Travina, Natalya	cook
31. Kachura, Oksana	cook
32. Kalinina, Galina	cook
33. Shinkevich, Nina	stewardess